Light Driven Hydrogen Generation by Ruthenium(II) – Palladium(II) / Platinum(II) Supramolecular Photocatalysts Using Water

Syntheses, Characterization and Photophysical Properties

by Gurmeet Singh Bindra

A Thesis presented to Dublin City University

for the

Degree of Doctor of Philosophy

under the supervision of Professor Johannes G. Vos

And

Dr. Mary T. Pryce

School of Chemical Sciences

Dublin City University

2012

Dedicated to the God "Waheguru Ji"

My parents and my sister "Manmeet Kaur",

My sweet loving wife "Pavneet Kaur" and my child "Gurbaani Kaur".

Authors Declaration

I hereby certify that this material, which I now submit for assessment on the programme of study leading to the award of Doctor of Philosophy by research and thesis, is entirely my own work, that I have exercised reasonable care to ensure that the work is original, and does not to the best of my knowledge breach any law of copyright, and has not been taken from the work of others save and to the extent that such work has been cited and acknowledged within the text of my work.

Signed: _____

(Gurmeet Singh Bindra)

ID No.: 58124713

Date: _____

Acknowledgements

ੴ

ਵਾਹਿਗੁਰੂ

aadh sach jugaadh sach ||, hai bh sach naanak hosee bh sach ||1||

True in the beginning, True throughout the ages True here and now. O Nanak, God shall forever be True. ||1||

With due respect and devotion, I would thank my God, “Waheguru Ji” to give me this opportunity to have knowledge, strength to do my work and always show me the right path to go and right way to do.

I would like to give my special thank to Prof. Han Vos and Dr. Mary T. Pryce for invaluable support and guidance throughout the work.

My Parents Satinderpal Singh Bindra (Dad) and Harjeet Kaur Bindra (Mom) without their love, support and blessings this would have been impossible. My sister (Manmeet Kaur), whose eyes were always looking towards my success and prosperity. I would give them my million thanks for there invaluable support. My wife (Pavneet Kaur), her great support and unconditional love, for giving me great inspiration and passion to become a scientist. I sincerely thank to my parents in law, sister in law (Kamalpreet Kaur), brother in law (Gurpreet Singh Kanwal and Prabhsimran Singh) and to my little niece’s Avi and Jot. I dedicated this thesis to my sweetheart my daughter “Gurbaani”.

My sincere thanks to Dr. Martine Schulz, Dr. Brian Maclean, Dr. Robert Groarke, Damien, Vinnie and John for their great support. Special thanks and appreciation to all members of our group, both past and present, for there help and back up. I would like to thanks to my “DCU” friends, both past and present, who made this experience unforgettable. Specially “Suraj Soman” who was often the one who had listed to my ups and downs, but who made it with lots of fun and happiness. My sincere thanks to my colleagues Dr. Harry Kelly, Dr. Rob J. Young and Mr. Simon Gaines from GlaxoSmithKline (Stevenage, UK) and all my respectable teachers of my life who has their great contribution in my journey of knowledge and study.

Abstract

Chapter 1 is an introductory chapter and is primarily concerned with presenting the main topic of this thesis, the use of diverse synthetic methods in the development and design of supramolecular metal complexes. It begins with an introduction to the concept of supramolecular chemistry and some of the most important features of supramolecular systems. The basic concepts regarding Ru(II) polypyridine chemistry are introduced and explained; as such complexes often serve as building blocks in supramolecules. This is followed by an extensive discussion on the using of ruthenium polypyridine complexes for the production of hydrogen as light absorbing units. The area of solar hydrogen production through the use of supramolecular photocatalysts that collect and deliver reducing equivalents in an active area of current research in inorganic and organic photochemistry.

The chapter 2 deals with the background of the different physical measurements used for an elucidation of the properties of ruthenium complexes and the experimental details of the several physical measurements are given. This chapter also described the synthesis and characterisation of the bridging ligands used in this thesis.

The chapter 3 deals with syntheses and characterisation of ruthenium(II) complexes containing 2,5-dpp as a bridging ligand are presented. The syntheses of ruthenium(II) complexes containing dceb as a peripheral ligand are also presented. The heterodinuclear complexes were synthesised from mononuclear complexes using $[Pd(CH_3CN)_2Cl_2]$ / $[Pt(DMSO)_2Cl_2]$ complexes. Deuteriated complexes were also synthesised. These complexes are fully characterisation via NMR and CHN with a discussion of their electronic properties included. These complexes also produced hydrogen using visible light irradiation in the presences of triethylamine (TEA). The production of hydrogen depends on the electron withdrawing substituent present on the bpy peripheral ligand. The intermolecular reactions were studies for the production of hydrogen.

The chapter 4 investigations into syntheses and characterisation of ruthenium(II) complexes containing 2,5-bpp and 2,6-bpp as bridging ligand are presented. The cyclometallated heterodinuclear complexes were synthesised from mononuclear

complexes using $(NH_4)_2[PdCl_4]$ but using $K_2[PtCl_4]$ complexes, heterodinuclear did not form. Deuteriated complexes were also synthesised. These complexes are fully characterisation via NMR and CHN with a discussion of their electronic properties. These complexes produced hydrogen using visible light irradiation in the presences of triethylamine (TEA). The intermolecular reactions were studies for the production of hydrogen. The complexes containing 2,6-bpp were not produced hydrogen.

The chapter 5 investigations into syntheses and characterisation of ruthenium(II) complexes containing bisbpy as a bridging ligand are presented. The cyclometallated heterodinuclear complexes were synthesised from mononuclear complexes using $[Pd(CH_3CN)_2Cl_2]$ / $[Pt(dmso)_2Cl_2]$ complexes. These complexes are fully characterisation via NMR and CHN with a discussion of their electronic properties. These complexes produced hydrogen using visible light irradiation in the presences of triethylamine (TEA). The intermolecular reactions were studies for the production of hydrogen.

Chapter 6 sees the conclusion on the discussion of the photocatalytic properties with an extensive examination of all the results found in chapter 3, 4 and 5.

Finally we conclude with a summary of the work completed in this thesis and possible future work in chapter 7.

Abbreviations and Symbols

CH_2Cl_2	dichloromethane
CHN	carbon, hydrogen, nitrogen analysis
COSY	correlated spectroscopy
CT	charge transfer
δ	chemical shift (NMR)
DMF	dimethylformamide
DMSO	dimethylsulphoxide
ε	extinction coefficient
$E_{½}$	half-wave potential
EDTA	ethylenediaminetetraacetic acid
Et_3N	triethylamine
EtOH	ethanol
Fc/Fc^+	ferrocene/ferricinium redox couple
GS	ground state
HOMO	highest occupied molecular orbital
IR	infrared
isc	intersystem crossing
J	coupling constant (NMR)
k_{nr}	non-radiative decay
k_r	radiative decay
λ	absorption wavelength
λ_{em}	emission wavelength
L	ligand
LC	ligand centred
LMCT	ligand to metal charge transfer
LUMO	lowest occupied molecular orbital
MC	metal centred
MeCN	acetonitrile
MeOH	methanol
^{1}MLCT	singlet metal to ligand charge transfer
^{3}MLCT	triplet metal to ligand charge transfer
NMR	nuclear magnetic spectroscopy
PET	petroleum ether
PS	photosensitiser
PV	photovoltaic
py	pyridine

SCE	standard calomel electrode
τ	lifetime
TLC	thin layer chromatography
UV/Vis	ultraviolet/visible
ν	stretching vibration (IR)

Table of Contents

Chapter 1: Introduction

Abstract:

Chapter 1 serves as a means to introduce many of the topics discussed within this thesis. The chapter begins with a discussion of the importance of ruthenium based metal complexes in supramolecular chemistry and their properties, electronic, photophysical, and photochemical, which have attracted great interest over the last four decades. The "parent" complexes of many of the compound synthesized in this thesis, $[Ru(bpy)_3]^{+3}$ *and their importance to the area of inorganic chemistry is then highlighted.*

The chapter continues with a discussion on the primary concern of this thesis, the photocatalytic generation of hydrogen from water using ruthenium(II) based light absorber as a photocatalysts. The photo-generating hydrogen catalysts based on ruthenium as a light absorber coordinated with a bridging ligand and another metal centre (e.g. Palladium and Platinum) as a catalytic centre was reviewed. Also complexes for the generation of hydrogen such as complexes of rhodium, cobalt, iridium and iron are also discussed.

1.1 Introduction

1.1.1 Supramolecular chemistry and light.

In nature, photons (sunlight) are utilised by living organisms for energy, for example sunlight is harnessed in photosynthesis. An important aim of photochemistry is to design and construct artificial energy conversion devices capable of delivering and controlling the great variety of machines which sustain our civilization.

The answers that can be obtained from the interaction of light with matter depend on the degree of orientation of the receiving matter.[1] The simplest form of orientation is that of small number of atoms in a molecule. The interaction of photons with molecules can cause changes in the molecular structure (electronic properties), which is useful, in principle, for both energy and information purposes. For example, solar energy can be converted and stored as chemical energy by transforming a molecule into its higher energy state by absorbing sun light.[2, 3] The latest technologies for photocatalytic production of hydrogen by splitting water molecules to hydrogen gas is based on photoelectrochemical process using semiconductors,[4] photo-biological processes[5] and photochemical molecular devices (PMD).[6, 7]

A higher level of association is the assembly of a discrete number of molecular components to yield supramolecular species.[1, 8, 9, 10, 11] The supramolecular association can be achieved by various types of intermolecular forces (for example - columbic forces, hydrogen bonding, etc.) or by combining molecular systems by coordination or covalent bonds (see section 1.1.2). In this manner it is possible to design molecular components with the desired light related properties: absorption, emission, excited state redox and photo-catalytic properties. Photochemical molecular devices (PMD))[12, 13] capable of performing complex functions (light harvesting, charge separation, conversion of light into electrical energy and fuel, data processing storage, etc.)

1.1.2 Supramolecular photochemistry: Basic concepts

The most applicable and widely accepted definition of supramolecular chemistry is "the chemistry beyond the molecule, bearing on the organized entities of higher complexity that result from the association of two or more chemical species held together by intermolecular forces".[8] When the interaction energy between subunits is small compared to other relevant parameters, the system can be consider a supramolecular species. Therefore, also species made of covalently linked (but weakly interacting) components can be taken as belonging to the supramolecular field.[14]

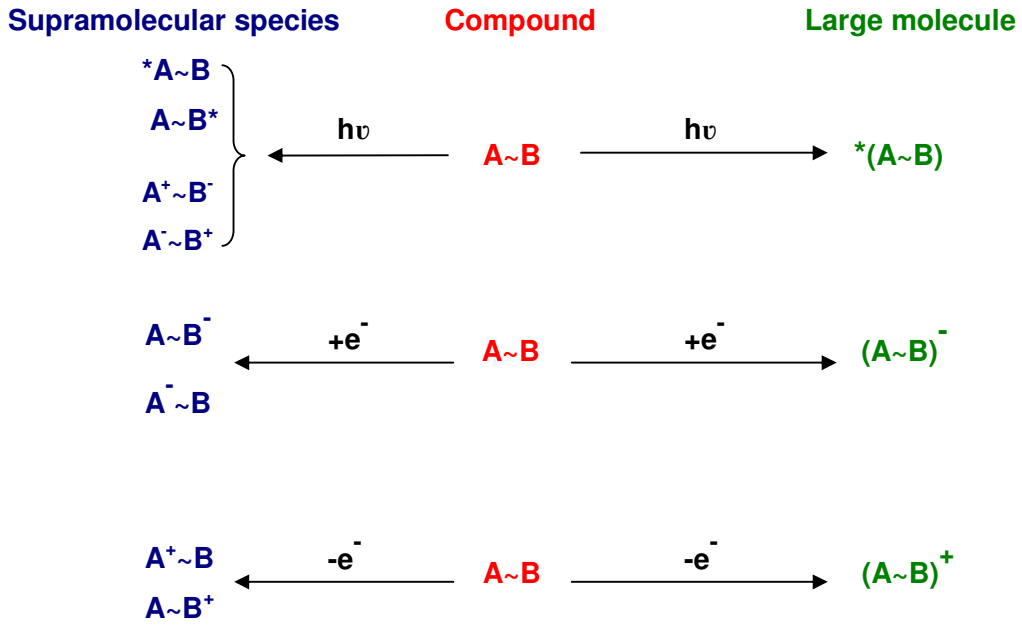

Scheme 1.1: *Light excitation of a compound A~B.*

As shown in Scheme 1.1,[13] light excitation of a supramolecular species A~B leads to excited states that are substantially localized on A or B. When the excited states are delocalised on both A and B, the species is considered as a large molecule rather than a supramolecular system. The oxidation and reduction of a supramolecular species can be described as oxidation and reduction of specific components, whereas oxidation and reduction of a large molecule lead to a species where the hole or the electrons are delocalized over the entire system.

The photochemical processes of supramolecular species are those taking place between the components (molecular subunits). Particularly important for the topics discussed in this thesis are inter-component energy and electron transfer processes as in Equation (1.1)-(1.3):

$$A \sim B + h\upsilon \longrightarrow {}^{*}A \sim B \quad \text{photo excitation} \qquad \text{Eq. (1.1)}$$

$$^{*}A \sim B \longrightarrow A \sim {}^{*}B \quad \text{electron transfer} \qquad \text{Eq. (1.2)}$$

$$^{*}A \sim B \longrightarrow A^{+} \sim B^{-} \quad \text{electron transfer} \qquad \text{Eq. (1.3)}$$

Where ~ indicates any type of "bond" that keep A and B subunits together; only one of the two possible electron-transfer is indicated. The thermodynamic ability of an excited state to participate in energy transfer processes is related to its zero-zero spectroscopy energy, $E^{0\text{-}0}$. For the electron-transfer processes, the relevant thermodynamic parameter is the reduction potential of an excited state that is both a stronger reductant and a stronger oxidant than the corresponding ground state. To a first approximation, the redox potentials for the excited state couples may be calculated from the potentials of the ground state couples and the zero-zero excitation energy, as shown in Equation (1.4) and (1.5).[15]

$$E(A^{+}/{}^{*}A) = E(A^{+}/A) - E^{0\text{-}0} \qquad \text{Eq. (1.4)}$$

$$E({}^{*}A/A^{-}) = E(A/A^{-}) - E^{0\text{-}0} \qquad \text{Eq. (1.5)}$$

As a consequence, the feasibility of an excited state electron-transfer process can be assessed by mean of the well-known Weller equation.[16] For the process of Equation (1.3) it is given by Equation (1.6).

$$\Delta G_{ET} \approx - E^{0\text{-}0} - E(B/B^{-})' + E(A^{+}/A)' - E_{IP} \qquad \text{Eq. (1.6)}$$

Where ΔG_{ET} is the free energy change of the quenching process, $E^{0\text{-}0}$ is the spectroscopy energy of the excited state, $E(B/B^{-})'$ and $E(A^{+}/A)'$ are corresponding to the potentials of the two species involved in one electron the process, and E_{IP} is the

coulombic stabilization energy of the products. In supramolecular species constituted by several molecular components, successive energy or electron-transfer steps may lead to energy migration or charge separation over long distances.

Another important event that can take place upon light excitation of supramolecular species is optical electron transfer process, which leads to the direct formation of an intranuclear charge transfer state, as shown in Equation (1.3). Both photoinduced electron transfer (Equation (1.1) plus Equation (1.3)) and optical electron transfer may be followed by a thermal back electron transfer process (Equation (1.7)):

$$A^{+} \sim B^{-} \longrightarrow A \sim B \qquad \text{Eq. (1.7)}$$

The relationships between optical, photoinduced, and back electron transfer processes in a supramolecular species are schematized in Figure (1.1). Several examples of energy and electron transfer process in supramolecular species have been discussed in a number of books and review articles.[1, 3, 13, 17, 18, 19, 20, 21, 22, 23, 24.]

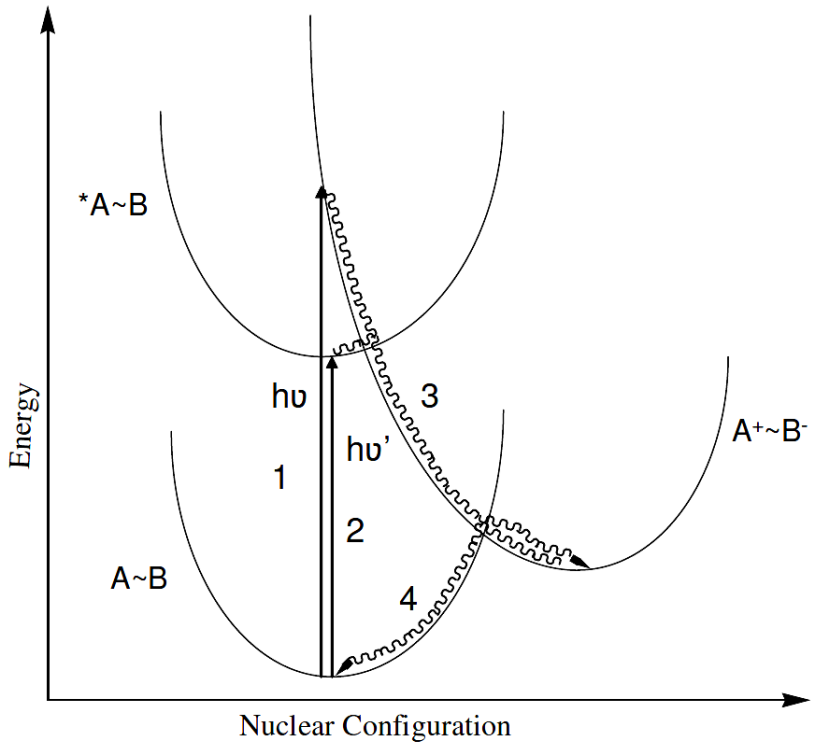

Figure 1.1: *Relationship between Optical (1), photoinduced (2 + 3), thermal (4) electron transfer processes in a supramolecular system.*

For the supramolecular system discussed above section, as a result of photoinduced charge separation, part of the absorbed light is transiently stored as redox energy. This energy can be converted in various ways. One is into electrical energy [25, 26], for example by using high surface area polycrystalline TiO_2 anatase films together with tris(2,2'-bipyridyl-4,4'-dicarboxylate)ruthenium(II), RuL_3^{4-}, L = $(bpy(COO)_2^{2-}$ = 4,4'-dicarboxy-2,2'-bipyridine), as a sensitizer, achieved high visible-light to electric current conversion efficiencies in regenerative photo-electrochemical cells are obtained. Incident photon to current conversion efficiencies of 73% have been obtained at the wavelength of maximum absorption of the dye in the presence of iodide as an electron donor. Bromide is oxidized under the same conditions with an efficiency of 56%.[27] An alternative, possibility is that followed by nature in photosynthesis, that is, the use of this energy for the production of high energy chemical products. Energy conversion by artificial photosynthesis is certainly one of the most challenging goals in chemistry. The requirement for the construction of supramolecular species suggests the use of building blocks [28] which have well understood properties and may be exploited for energy conversion function. For this reason transition metal complexes such as ruthenium, osmium, platinum and palladium have become ideal candidates as they possess interesting photophysical, photocatalytical and photochemical properties which have been well studied.[28] These photophysical and photochemical properties will be examined in more detail in later sections.

1.2 The photophysical properties of ruthenium complexes

1.2.1 Evaluation of ruthenium based light absorption and photophysical properties of supramolecular complexes.

Ruthenium polypyridyl chromophores absorb light with a widen spectral coverage have emissive charge transfer excited states and long excited state lifetimes.[29, 30, 31] Ruthenium polypyridyl light absorption display $\pi \rightarrow \pi^*$ ligand based transition with high extinction coefficients in the UV region of the electronic absorption spectrum. They also possess lower energy ^{1}MLCT (metal to ligand charge transfer) transitions

involving charge transfer from a ruthenium based highest occupied molecular orbital (HOMO) to a ligand based lowest unoccupied molecular orbital (LUMO). The absorption maximum is located in the visible region of the spectrum. The orbitals involved in an electronic transition must be electronic coupled to allow for the observation of an intense electronic transition. The symmetry selection rule for the intensity of an electronic transition is expressed in Equation 1.8:

$$f \propto |\int {}_{el}\psi^{ES}\ \mu\ {}_{el}\psi^{GS}\, dv|^2 \qquad \text{Eq. (1.8)}$$

The oscillator strength, *f*, is represent of the predicted integrated intensity and is proportional to the integral of the product of the ground state and excited state wavefunctions, ψ, and the electric dipole moment operator, μ. The spin selection rule predicts that an electronic transition is allowed only if the spin multiplicity of the ground state and excited state are the same. For ruthenium polypyridyl light absorption systems, the ^{1}MLCT state shows rapidly intersystem crossing (k_{isc} is the rate constant for intersystem crossing) to populate a ^{3}MLCT state. This state can undergo a radiative (k_r is the rate constant for radiative decay) or non-radiative (k_{nr} is the rate constant for non-radiative decay) decay to the ground state (GS) or undergo energy / electron transfer quenching. The emission from the ^{3}MLCT state provides a probe into the photoreactivity of the molecules, transition between ground state and electronic excited state are typically represented in a jablonski diagram (Figure 1.2). Radiative processes are typically represented as straight arrows (→) and non-radiative processes are presented as wavy arrows (~~>). Radiative decay with a change in spin state is phosphorescence, while radiative decay without change in spin is fluorescence. Typically ruthenium(II) polypyridyl chromophores display phospho-rescence from their emitting ^{3}MLCT states.

The quantum yield, **Φ**, of an excited state process provides a means to understand the efficiencies of a particular pathway to decay to the ground state for example, **Φ** for emission resulting from radiative decay from the ^{3}MLCT, represented in Equation (1.9) is defined as k_{τ} divided by the sum of the rate constant of all pathways

depopulating that state, $\sum k$ ($\sum k = k_r + k_{nr} + k_{rxn}$; Equation 1.9) times the quantum yield for population of that state $\mathbf{\Phi}\,^{3}_{MLCT}$.

$$\mathbf{\Phi} = \mathbf{\Phi}\,^{3}_{MLCT}\,(k_{\tau} / \sum k) \qquad \text{Eq. (1.9)}$$

For many ruthenium polypyridyl complexes, the $\mathbf{\Phi}\,^{3}_{MLCT}$ is unity and omitted from these equations. The excited state lifetime of the ^{3}MLCT state, τ, is the inverse of the sum of the rate constant of all pathways depopulating that state, $\sum k^{-1}$ (Equation 1.10):

$$\tau = \{1 / (k_r + k_{nr} + k_{rxn})\} \qquad \text{Eq. (1.10)}$$

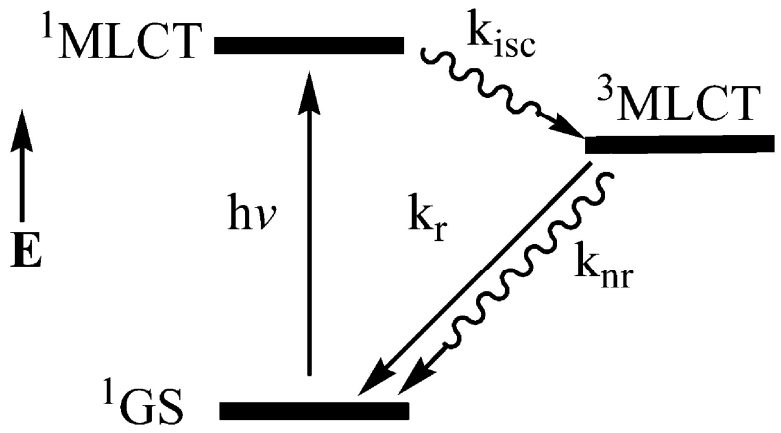

Figure 1.2: *Representative state diagram for ruthenium polypyridyl complexes of the type $[Ru(L)_3]^{2+}$ (L, polypyridyl ligand); GS = ground state, MLCT = metal-to-ligand charge-transfer, k_r = rate constant for radiative decay, k_{nr} = rate constant for non-radiative decay, k_{isc} = rate constant for intersystem crossing.*

The efficiency of excited state reactions can be described by probing $\mathbf{\Phi}$ for that reaction as a function of quencher concentrate using the Stern-Volmer kinetic relationship. There are two types of quenching processes usually encountered namely dynamic (collisional) quenching and static (complex formation) quenching. Collisional quenching occurs when the excited fluorophore experiences contact with an atom or molecule that can facilitate non-radiative transitions to the ground state. Common dynamic quenchers include O_2, I^-, Cs^+ and acrylamide (Equation 1.11). $\mathbf{\Phi^o}$

and Φ are quantum yields in the absence and presence of quencher, Q, respectively; k_q is the overall quenching rate constant (bimolecular quenching rate) and τ excited state lifetime of the ^{3}MLCT state. The Stern-Volmer relationship, which plot Φ^o/Φ as a function of the quencher concentration, provides a linear relationship with slope of τk_q. The value of K_q provides the rate of quenching by Q.

$$(\Phi^o/\Phi) = 1 + \tau\, k_q\, [Q] \qquad \text{Eq. (1.11)}$$

In static quenching, the fluorophore forms a stable complex with the quencher. If this assembly is non-fluorescent then the fluorophore is statically quenched. In such a case, the dependence of the fluorescence or phosphorescence as a function of the quencher concentration follows the relation (Equation 1.12):

$$(\Phi^o/\Phi) = 1 + k_a\, [Q] \qquad (1.12)$$

Where k_a is the association constant of the complex. Such cases of quenching via complex formation were first described by Weber.[32] In the case of static quenching the lifetime of the sample will not be reduced since those fluorophores which are not complexed and hence are able to emit after excitation will have normal excited state properties. The fluorescence of the sample is reduced since the quencher is essentially reducing the number of fluorophores which can emit.

1.2.2 Photophysical properties $[Ru(bpy)_3]^{2+}$

The complex $[Ru(bpy)_3]^{2+}$ (see Figure 1.3),[29] has been studied to a great extent by many research groups and therefore its physical properties are well understood. It is used as a reference for many different ruthenium(II) polypyridyl compounds, such as hetero-dinuclear derivatives developed in this project.

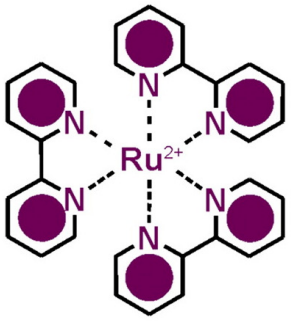

Figure 1.3: *Chemical structure of $[Ru(bpy)_3]^{2+}$*

The metal centre in the complex $[Ru(bpy)_3]^{2+}$ has a stable low-spin d^6 configuration, is octahedrally surrounded by six nitrogen donor atoms present in the 2,2'-bipyridine (bpy) ligands and shows reversible redox chemistry.[30, 31] Its absorption and emission properties are controlled by the electronic nature of the three coordinated bipyridine ligands. Polypyridyl ligands in general have the ability to donate a lone pair of electrons to the ruthenium cation in order to form an σ bond (see in Figure 1.4). The resulting metal complex is stabilized by a π-back-bonding between the empty π* orbitals of the ligand by accepting electron density from the d-orbitals of the ruthenium metal.[33]

For the free bipyridine ligand both nitrogen atoms have one free electron pair (called as non-bonding electrons (n)). By absorption of light those electrons can be excited to an antibonding π* orbital of the aromatic ring. This transition is known as $n \rightarrow \pi^*$, and is usually the lowest energy transition. By increasing the energy of the photon the next possible transition is a $\pi \rightarrow \pi^*$ transition, which is typical for aromatic rings.

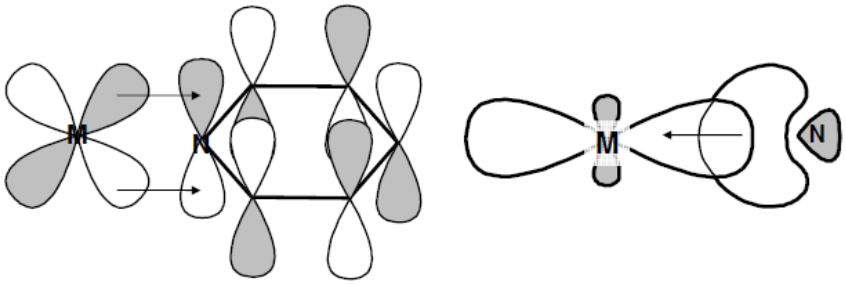

Figure 1.4: *Schematic description of σ bond between a free electron pair of nitrogen (depicted as N) and a metal (depicted as M, right) and a π back-bonding (left).*

When the bipyridine molecules are coordinated to the ruthenium cation the energy level of the free electron pairs is changed due to the formation of an σ-bond with the metal e_g orbitals. Therefore, the energy of the n electrons is lowered compared to the energy of the ligand π-orbitals, which are almost not effected by the complexation. Therefore, the lowest ligand centred (LC) transition is the $\pi \rightarrow \pi^*$ transition. This transition can be observed by measuring the absorption spectrum of $[Ru(bpy)_3]^{2+}$ in the ultraviolet region see figure 1.5. However, another broad peak occurs in the absorption spectrum. This peak does not belong to any ligand or metal centered transition, but was assigned as a metal to ligand charge transfer (MLCT) transition.[34] Hereby an electron from the fully occupied metal t_{2g} orbital is excited to an empty π* orbital of the ligand.

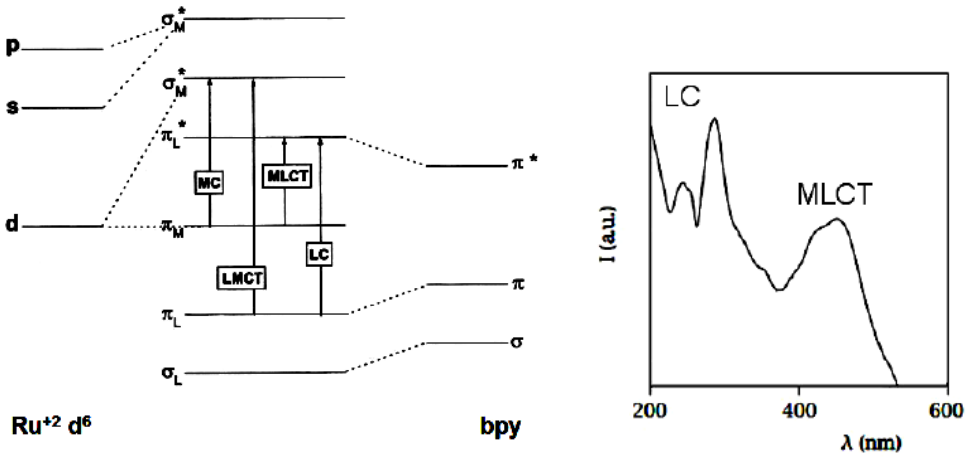

Figure I.5: *Left: molecular orbital energy diagram of $[Ru(bpy)_3]^{2+}$. The arrow indicates a MLCT and the LC transition. Right: absorption spectrum of $[Ru(bpy)_3]^{2+}$ in acetonitrile solution* [29]

MLCT transitions can be seen for many other polypyridyl complexes. Amongst others, they are responsible for their intense colour, because the absorption normally lies in the visible region of light. Furthermore, $[Ru(bpy)_3]^{2+}$ exhibits fluorescence. The emission is caused by a ^{3}MLCT → d-transition.[30, 31, 33 – 35]

Calculations have been carried out to understand the nature of the emitting state of $[Ru(bpy)_3]^{2+}$. After photoexcitation the electron resides in a singlet ^{1}MLCT state, but

it is rapidly transferred to a lower lying triplet ^{3}MLCT state by inter-system crossing.[35] This is the primary radiationless decay pathway at room temperature.[36] Originating from this state the electron can easily be transferred to a metal centered triplet (^{3}MC) excited state by internal conversion. The occupation of this ^{3}MC state, which is anti-bonding in character, as a result the Ru – nitrogen bonding is weakened. This can result in the loss of a ligand.[37, 38] The photophysical processes are depicted in Figure 1.6.

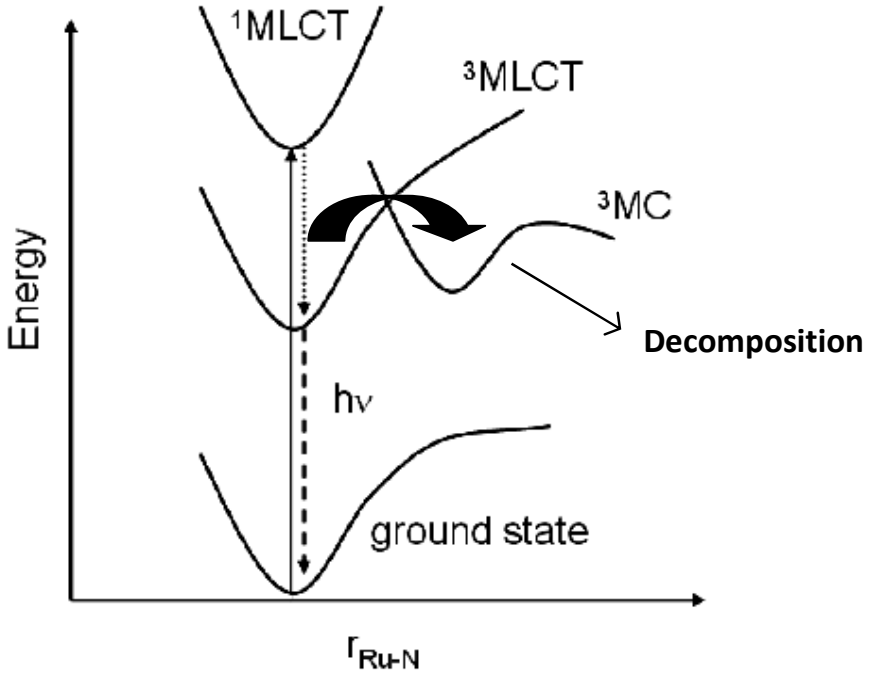

Figure 1.6: *Scheme of the photophysical properties of $[Ru(bpy)_3]^{2+}$. Straight arrows are excitation, dashed arrows indicate radiationless decay, and dotted arrows stand for emission of light.*

Furthermore, due to the weak absorption band at 452 nm for $[Ru(bpy)_3]^{2+}$, only a small part of solar energy spectrum can be used. By changing the ligand systems around the ruthenium(II) centre it is hoped that the ground state and excited state properties of the complexes can be tuned.[30] In order to prevent the photodecomposition much effort has been made to stabilize the dissociative ^{3}MC state. Two different approaches can be followed to prevent photodecomposition. One is to replace one bipyridine ligand by a strong σ donating ligand. The stronger ligand field would shift the ^{3}MC state to higher energies and thus make it difficult to

populate. Another possibility would be to make the ^{3}MC state non dissociative, i.e. by building a ligand cage around the metal centre.[39]

The properties of the ruthenium(II) complexes are governed by the σ-donor and π-acceptor properties of ligands. The σ-donor capacities of the ligands can be estimated by measuring the pK_a of the free ligands,[30, 40] whilst the π-acceptor properties are related to the reduction potential of the ligand. [30, 40] Complexes containing strong σ-donor ligands donate much electron density into the d-orbitals, causing lower oxidation potentials and more negative reduction potentials.[40] On the other hand, strong π-acceptor ligands stabilise the filled metal orbitals, giving rise to high oxidation potentials and low reduction potentials.[40, 41, 42] The difference in energy between the filled d-orbitals and the lowest empty ligand based orbital is related to the absorption and emission energy of the complexes. By changing the nature of the ligands, not only the redox potentials are altered, but also the energies of the absorption and emission bands.[30, 40, 41, 42]

Polynuclear complexes already have found application as molecular sensors, switches and motors.[31] By replacing one of the bpy ligands by a bridging ligand, the synthesis of polynuclear compounds is possibe.[31] Especially by using ruthenium(II) as the first metal centre, hundreds of bpy-type complexes have been prepared and characterized, thereby giving access to a big variety of photosensitizer components for the design of supramolecular assemblies based on intramolecular photoinduced charge separation or energy migration.[29]

Keeping this in mind, therefore, a number of ruthenium(II) supramolecular entities were developed. For this reason, the importance of intramolecular hetero-dinuclear photocatalyst assemblies will be discussed next and some important model systems based on intramolecular photoinduced charge separation and energy migration.

1.3 Photo-induced hydrogen generation

1.3.1 Development of photocatalyst

The inorganic assemblies discussed in this section contain a light absorbing unit, a catalyst and a bridge in between these units (bridging ligand), (see figure 1.7). One of the big advantages of these intramolecular systems is the opportunity to study light induced electron or energy transfer processes by means of spectroscopy.[43]

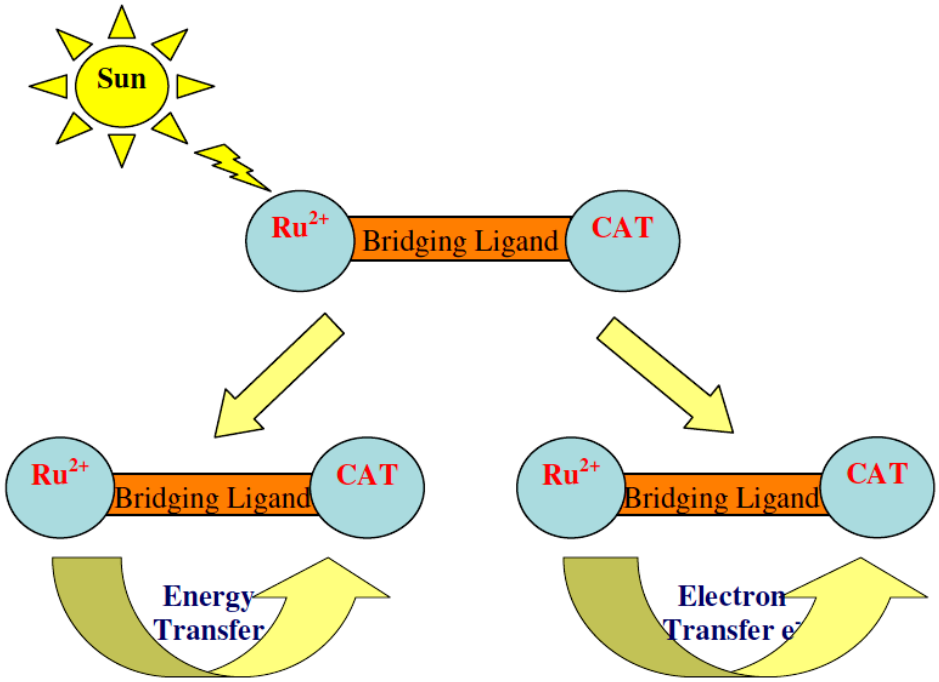

Figure 1.7: *General structure of a hetero-dinuclear photocatalytic intramolecular system. Ruthenium acts as a light harvesting unit and CAT: catalyst. After excitation, intramolecular energy or electron transfer to a catalytic subunit can take place.*

For the type of intramolecular photocatalytic systems described in figure 1.7, the efficiency for hydrogen formation is expected to be higher because the mechanism does not depend on collisional induced process between the involved species. However, electron donating species are still required to complete the catalytic cycle.

In intramolecular system, the complexed ruthenium moiety normally acts as the light harvesting unit or light absorbing unit. Its excited state is deactivated again by transferring energy or electrons to the second metal centre (Figure 1.7). The other metal centre can, for example, be a highly catalytically active metal e.g. Pt, Pd, Rh, Re [44, 45] and Co. Moreover both units are commonly linked by a bridging ligand which defines the extent of electron or energy transfer between both the neighbours (see Figure 1.7).

In hetero-bimetallic complexes a key role is played by the bridging ligand, because any kind of intramolecular interaction between the two different metallic moieties depends on the geometry, size and electronic nature of the bridge.[46] On changing these attributes and the type of the peripheral ligands it is possible to tailor the supramolecular devices with desired photophysical and photochemical properties. Supramolecular assemblies have already found applications in area such as dye sensitised solar cells,[47] as multi electron storage systems,[36] in the development of new materials,[48, 49] in medicine,[31] or as catalysts.[50] The well recognized bridging ligands are e.g.: bipyrimidine, substituted pyrazines, substituted bipyridines, biimidazoles and triazoles.[51, 52] All those dinuclear chelating bridging ligands mentioned above provide two binding sites with almost identical coordination properties which will be discussed next.

Much attention has focussed on systems containing strong π-accepting ligands apart from 2,2'-bipyridine (bpy) e.g. 2,2'-bipyrazine (bpz), 2,2'-bipyrimidine (bpm), 2,2'-biquinoline (biq), and derivatives. The mixed ligand complexes $[Ru(bpy)_2(LL)]^{2+}$ (LL = bpz, bpm, biq) display a red shift in absorption and emission energies. Due to the lower energies of the absorption bands, a larger portion of the solar energy can be harvested. A disadvantage, however, is that often the strong π-accepting ligands are weak σ-donor ligands. As a result the ligand field splitting of ruthenium(II) is much smaller and after excitation of the complex, the ^{3}MC state becomes very easily populated and the emission yield is diminished. The effect of population of the ^{3}MC state is that those complexes are often less photostable than the parent $[Ru(bpy)_3]^{2+}$. On the other hand, the π* levels of the LL ligands are stabilised compared to those of $[Ru(bpy)_3]^{2+}$. In some cases the energy gap between the ^{3}MLCT states and ^{3}MC states

is then larger than in $[Ru(bpy)_3]^{2+}$ and photostable complexes have been obtain.[53, 54] The second class of compounds are ruthenium complexes containing ligands with strong σ-donor properties, like imidazole (Him), pyrazole (Hpz), and 1,2,4-triazole (Htrz). The strong σ-donor capacities of these ligands may result in larger ligand field splitting, thus preventing photodecomposition. The empty π* levels of imidazole, pyrazole, or triazoles containing complexes are much higher in energy than those of bpy, because they are weaker π-acceptor ligands. This can be a disadvantage, because the energy difference between the filled d-orbitals and empty π* levels is then larger, which causes a blue shift in the absorption and emission spectra.

An important theoretical approach to define the metal-metal interaction is the superexchange theory [55] (Figure 1.8). It defines the overlap of the metal orbitals which is facilitated by the orbitals of the bridging ligand. Depending on the bridge electronic properties, electron or hole transfer can take place. The mechanism mainly relies on the energy of the metal d-(t_{2g}) orbital relative to the HOMO (highest occupied molecular orbital) and LUMO (lowest unoccupied molecular orbital) of the bridge. When the two metals are linked by an electron deficient bridging ligand, (low lying π* orbital), the energy difference relative to the metal d orbitals is very low. A small energy gap suggested that a LUMO mediated electron transfer mechanism, through which an electron is transported to the accepting metal moiety via transfer through the π* of the bridging ligand (see in Figure 1.8a), many electron deficient bidentate pyrazine based bridging ligands have been played an excellent role.[30]

On the contrary, for an electron rich bridge, with energetically highest lying π* orbitals, results in a HOMO mediated hole transfer interaction, due to the impassable energy gap between the involved metal d-orbitals and the π* of the bridging ligand.[56] Therefore, charge is transferred to the neighbouring unit by transferring electron holes via the highest occupied π orbitals of the bridge (figure 1.8b), for this many bidentate heterocyclic electron rich bridging linkers have been developed.[31]

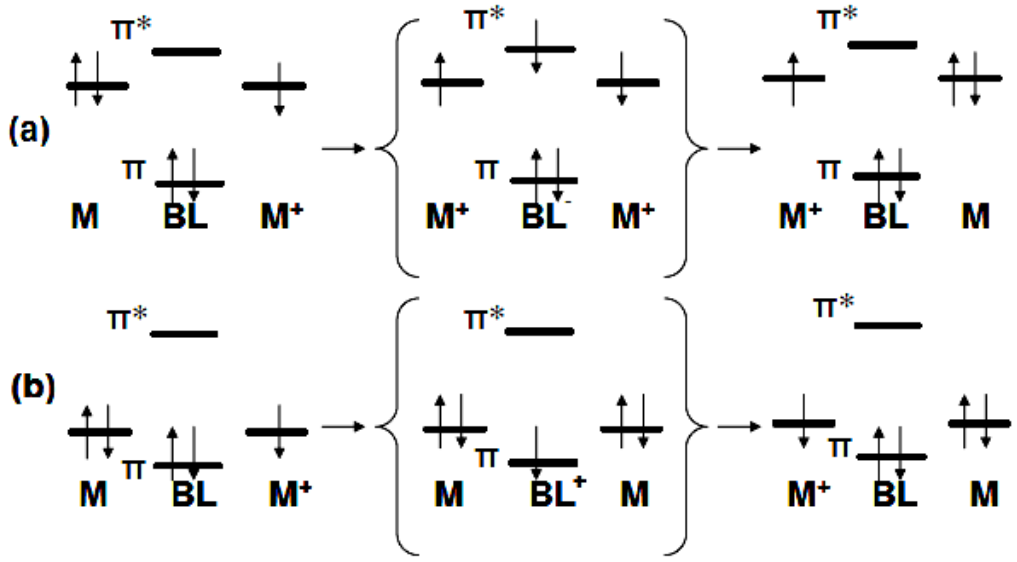

Figure 1.8: *(a) LUMO mediated electron transfer, (b) HOMO mediated hole transfer mechanism. The metal centres are abbreviated as M, and the bridging ligand as BL. The intermediate states are depicted in curly brackets.*

1.3.2 Ruthenium based photocatalytic systems for photo-induced hydrogen generation.

In an intramolecular process, a directional light driven electron transfer from the photocentre to the catalytic centre may be designed by manipulating the molecular components. These species may be viewed as photochemical molecular devices (PMD) consisting of a photoactive centre, a bridging unit and a catalytically active moiety. Figure 1.9, a typical ruthenium(II) based photocatalyst represents in a schematic diagram for a general structure of intramolecular bimetallic complexes is shown for the generation of hydrogen.

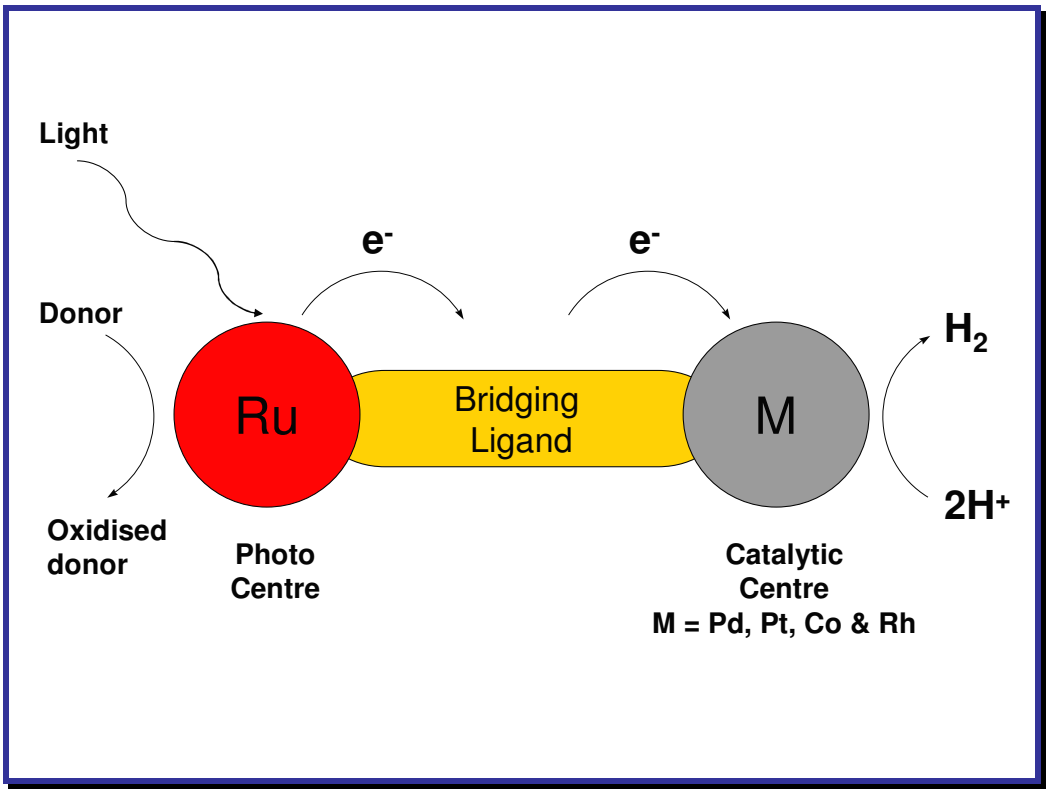

Figure 1.9: *General Structure of intramolecular bimetallic complexes reduced protons under visible light irradiation*

In 1977, Lehn and Sauvage succeeded to generate hydrogen with $[Ru(bpy)_3]^{2+}$ as a photocatalyst.[57] In this system after absorption of visible light, light induced electron transfer from the excited ruthenium compound to a rhodium(III) complex took place. This was followed by a further electron transfer to a platinum centre, where the catalytic cleavage of water took place. The initial redox state of the ruthenium complex was recovered by reduction with triethanolamine.[57] One year later, Grätzel and co-workers,[58] reported another approach to generate hydrogen by using $[Ru(bpy)_3]^{2+}$ as a light absorber. In this system methylviologen was used as electron relay, colloidal platinum used as a catalytic centre and triethanolamine as sacrificial donor.[58] These intermolecular systems were improved continuously. However, as usual in the case of intermolecular processes, the efficiency depends on collision between the involved components and therefore is limited due to many redox processes involved.

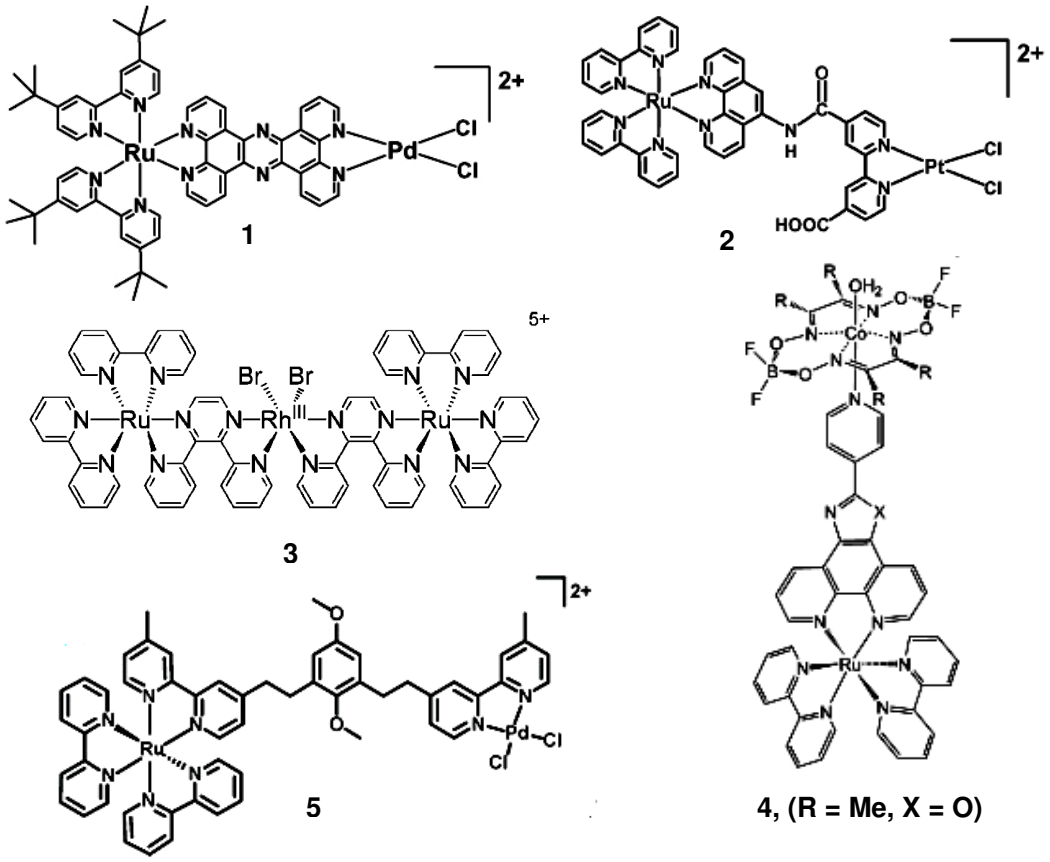

Figure 1.10: *Ruthenium(II) based photocatalysts for hydrogen generation.*

Rau *et al*. recently reported on their success in the development of an active model of a photohydrogen-evolving molecular device, compound 1, a bimetallic system of Ru-Pd, $[(^{t}Bu_2bpy)_2Ru(tppz)PdCl_2]^{2+}$, $^{t}Bu_2bpy$ = 4,4'-tertiary butyl derivative of 2,2'-bipyridine and tppz = tetrapyridophenazine (in Figure 1.10). [28(a), 59(a)] In that report, they used a photocatalyst consisting of the following three components:

1. A photoactive ruthenium(II) fragment acting as a light absorber.[60]
2. A $PdCl_2$ unit which, when coordinated at the other end of the assembly, acts as a catalytic centre.
3. A bridging unit connecting the two metal centres through a conjugated reducible π-electron system.[45]

For the $[(^tBu_2bpy)_2Ru(tppz)PdCl_2]^{2+}$, compound 1, electrochemical investigations have shown a reduction wave at -0.63 V Vs SCE assign to a reversible phenazine based reduction and an irreversible Pd^{2+} reduction at -0.82 V Vs SCE, which is a slightly less negative reduction potential than for the monomer $[(^tBu_2bpy)_2Ru(tppz)]^{2+}$ (-0.65 V Vs SCE) and indicates stabilisation of the tppz(π^*) orbital upon palladium coordination. Quasi-reversible bpy-based reduction potentials were observed between -1.09 V and -1.43 V Vs SCE. The oxidation potential wave of ruthenium in both compound 1 and monomer $[(^tBu_2bpy)_2Ru(tppz)]^{2+}$ were observed at 1.56 V Vs SCE. Compound 1 shows ligand based transitions in the UV and a MLCT transition in the visible regions in the electronic absorption spectrum with lowest energy MLCT transition at λ_{max}(abs) = 445 nm in acetonitrile. A weak emission of compound 1 at λ_{max}(em) = 650 nm with lifetime τ = 27 ns that is quenched relative to the monomer $[(^tBu_2bpy)_2Ru(tppz)]^{2+}$ at λ_{max}(abs) = 445 nm, λ_{max}(em) = 638 nm and τ = 154 ns in air-saturated acetonitrile.[59(a)] The amount of photocatalytically formed hydrogen depends strongly on the TEA concentration and the exposure time in the absence of water. So for 1, turnover numbers of 56 mol hydrogen per mol catalyst were achieved after 30 hours irradiation at λ = 470 nm. EPR examinations show that upon irradiation of 1 at 436 nm in CH_3CN/TEA mixtures, an EPR signal was detected and assigned to a pyrazine-based radical anion. This becomes evident by a comparison with electrochemically generated data reported by Fees *et al.*[61] The authors therefore suggest that the Ru^{2+}—phenazine^{-}—Pd^{2+} radical anion is involved in the photochemical production of hydrogen. The radical species initiates loss of chloride from the palladium site and intramolecular electron transfer from Pd^{2+} to Pd^0. It is suggested that the palladium centre acts as an electron collector and catalyst site, leading to hydrogen production from the photochemical reaction. The assembly was also active for the hydrogenation of tolane to cis-stilbene without added hydrogen, leading the authors to suggest that hydrogen production proceeds through a palladium hydride species.

In 2010, Rau and co-workers reported the amount of hydrogen produced as a function of irradiation wavelength. [59(b)] Resonance Raman (rR) spectroscopy revealed that when the excitation wavelength was shifted to lower energy, the electron density of

the excited state shifts from the terminal $^{t}Bu_2bpy$ (4,4'-tertiary butyl derivative of 2,2'-bipyridine) to the tpphz (tetrapyridophenazine) bridging ligand. [59(c)] The maximum TON of 161 is obtained for $[(^{t}Bu_2bpy)_2Ru(tppz)PdCl_2]^{2+}$ close to the absorption maximum at λ = 458 nm. This TON, which is significantly higher than that in previous investigations, [59(a)] is associated with the addition of a 10 volume % of water. The activating effect of water might be the result of altered solvent polarity, increased proton mobility, or the ability of water molecules to act as ligands at the Pd centre.

Another publication by Sakai *et. al*. describes a heterodinuclear ruthenium platinum photocatalyst, compound 2, $[(bpy)_2Ru(phenNHCO(COOHbpy))PtCl_2]^{2+}$. The platinum component is linked to the ruthenium light absorber through a amide bond on the phenanthroline ligand (Figure 1.10)[62] and is capable of producing hydrogen. Compound 2, shows ligand based transitions in the UV region and MLCT transitions in the visible regions of the electronic absorption spectrum with the lowest energy ^{3}MLCT transition at λ_{max}(abs) = 450nm and displays emission at λ_{max}(em) = 610 nm in water. The emission intensity is quenched by 67% relative to the parent mono-nuclear complex $[(bpy)_2Ru\text{-}(phenNHCO(COOHbpy))]^{2+}$. The redox potentials for the electrochemical processes observed for $[(bpy)_2Ru\text{-}(phenNHCO(COOHbpy))PtCl_2]^{2+}$ (compound 2) display a redox couple at ~ $E_{1/2}$ = 0.89 V vs. Fc/Fc^+, which correspond to a Ru(II)/Ru(III) couple and is slightly shifted to the negative side compared to mononuclear complex $[(bpy)_2Ru(phenNHCO(COOHbpy))]^{2+}$ at $E_{1/2}$ = 0.90 V vs. Fc/Fc^+. On the other hand, the first reduction potential undergoes a significantly positive shift upon the platination for $[(bpy)_2Ru\text{-}(phenNHCO(COOHbpy))PtCl_2]^{2+}$ compound 2 at $E_{1/2}$ (1^{st}) = -1.20 V vs. Fc/Fc^+ relative to the mononuclear complex $[(bpy)_2Ru\text{-}(phenNHCO(COOHbpy))]^{2+}$ with $E_{1/2}$ (1^{st}) = -1.63 V vs. Fc/Fc^+, indicating that the first reduction of compound 2 occurs at the bpy moiety coordinated to the Pt(II) ion, as reported for the Pt(bpy) complexes.[63] The corresponding second reduction potential for $[(bpy)_2Ru\text{-}(phenNHCO(COOHbpy))PtCl_2]^{2+}$ compound 2 at $E_{1/2}$ (2^{nd}) = -1.76 V vs. Fc/Fc^+ relative to the mononuclear complex $[(bpy)_2Ru\text{-}(phenNHCO(COOHbpy))]^{2+}$ at $E_{1/2}$ (2^{nd}) = -1.81 V vs. Fc/Fc^+, indicating bipyridine based reduction. The most important finding is that the visible light induced the reduction of water using EDTA as a sacrificial donor into molecular hydrogen which

was promoted by $[(bpy)_2Ru\text{-}(phenNHCO(COOHbpy))PtCl_2]^{2+}$ (compound 2), (Φ (1/2 H_2) = ca. 1%). Relatively low turnovers (4.8) were estimated on the basis of the total amount of H_2 evolved after 10 hours (2.4 μmol). It was also confirmed that H_2 formation was higher when ultraviolet light was eliminated by use of a suitable interference filter, presumably due to the decrease in the degree of photodegradation of the system.

It is important to note that $[(bpy)_2Ru\text{-}(phenNHCO(COOHbpy))PtCl_2]^{2+}$ (compound 2) evolves H_2 in aqueous media at pH 5 while $[(^tBu_2bpy)_2Ru(tppz)PdCl_2]^{2+}$ (compound 1) evolves H_2 in acetonitrile in the absence or presence of water. Importantly, 1 and 2 possess three common features. In both systems, (i) the bridging spacer preserves aromaticity, (ii) the charge transferred at the ^{3}MLCT excited state seems localized on the bridge unit, which can be judged by estimating the LUMO using DFT MO calculations, and (iii) the electronic coupling between the two metal centres seems relatively weak, presumably allowing the molecule to have an excited state life time sufficiently long to conduct the H_2-evolving process.

The supramolecular complexes of the general form LA-BL-RhX_2-BL-LA structural motif (LA. light absorber = Ru^{2+} polyazine chromophores, BL. bridging ligand = 2,3-dpp, X. halide = Cl^-, Br^-) have been evaluated as photoinitiated electron collectors (PEC) by Brewer and co-workers.[64, 65, 66, 67] These systems separate two Ru^{2+} light absorbers through a single Rh^{3+} acceptors. The metal components are connected to each other through a polyazine bridging ligands (2,3-dpp). These systems have a rhodium centre with potentially labile monodentate halide ligands that allow photoreactivity within the molecule. Visible light irradiation affords photoinitiated electron collectors resulting in rhodium reduction, followed by loss of the labile halide ligands.[68] Compound 3, $[\{(bpy)_2Ru(2,3\text{-}dpp)\}_2RhBr_2]^{5+}$ (see Figure I.10) act as a photocatalyst for solar energy driven hydrogen production from water with a hydrogen quantum yield of Φ = 0.01.[64-68] The compound shows ligand based transitions in the UV region and MLCT transitions in the visible region in the electronic absorption spectrum with a lowest energy MLCT transition at λ_{max}(abs) = 525 nm in deoxygenated acetonitrile. A weak emission at λ_{max}(em) = 760 nm

observed with a lifetime τ = 26 ns is quenched relative to the $[\{(bpy)_2Ru\}_2(2,3\text{-}dpp)]^{4+}$ (λ_{max}(em) = 744 nm and τ = 140 ns in deoxygenated acetonitrile). Photolysis of compound 3 in acetonitrile solution in the presence of DMA (N,N-dimethylaniline) and water at λ = 470 nm leads to water reduction to produce hydrogen with a quantum yield with Φ = 0.01 with ca. 38 turnover numbers in 4h.[68] The type of halide atom attached to the rhodium centre also impacts on higher turnover number for hydrogen. The increased ease of Br^- loss due to its weaker ligating ability may account for the enhanced photocatalytic activity of $[\{(bpy)_2Ru(2,3\text{-}dpp)\}_2RhBr_2]^{5+}$ compound 3. Electrochemically, overlapping of $Ru^{2+/3+}$ based oxidation process for both Ru centres is seen for $[\{(bpy)_2Ru(2,3\text{-}dpp)\}_2RhBr_2]^{5+}$ compound 3 at +1.60 V Vs SCE. The reductive side consists of a first reduction at -0.33 V due to sequential one electron irreversible reduction of rhodium centre from Rh^{3+} to Rh^{2+} to Rh^{1+}. At more negative potentials, two reversible reduction at -0.72 V and -1.02 V due to the two 2,3-$dpp^{0/-}$ reduction process. Reduction of the bpy ligands occurs at more negative potentials.

This system has a rhodium localized LUMO for electron collection and a ^{3}MLCT or ^{3}MMCT states/state with sufficient driving force for excited state reduction by an electron donor. The photochemistry of $[\{(bpy)_2Ru(2,3\text{-}dpp)\}_2RhBr_2]^{5+}$ compound 3 in the presence of DMA (electron donor) suggests the formation of Rh^{1+} following bromide ligand loss. The Rh^{1+} coordination geometry is d^8, square planar, and co-ordinately unsaturated, make it reactive and susceptible to interaction with substrate such as water.

The impact of the sacrificial agents on the $[\{(bpy)_2Ru(2,3\text{-}dpp)\}_2RhBr_2]^{5+}$ compound 3 was investigated. Photocatalysis was seen using the electron donors DMA, TEA and TEOA.[64] The hydrogen production efficiency varied in the order DMA > TEA > TEOH.[64] TEOA has a slightly higher driving forces for reductive quenching than TEA, but results in the lower hydrogen yields. An important factor to be considered is the solution pH. The effective pH values for the photolysis solution using DMA, TEA and TEOA were estimated to be ~ 9.1, 14.7 and 11.8, respectively, on the assumption that the pK_a values for their conjugate acids remain unchanged in the photocatalytic solution relative to aqueous conditions {pK_a = 5.07 ($DMAH^+$), 10.75 ($TEAH^+$), 7.76 ($TEOAH^+$)}.[69] It is known that water reduction is pH dependent and energetically

more feasible at lower pH. Thus the lower catalyst efficiencies, when TEOA is the electron donor may be attributing to the higher effective pH of the solution rendering water reduction energetically more difficult. In addition the ability of DMA to form donor-chromophore π-stacking interaction may be advantageous for more efficient reductive quenching of the excited states, affording the highest hydrogen yield compared to that of the aliphatic electron donors.

Photocatalytic hydrogen generation of compound 3 in an aqueous medium have also been investigated.[68] The first system shown to display this function in aqueous medium. The $[\{(bpy)_2Ru(2,3\text{-}dpp)\}_2RhBr_2]^{5+}$ compound 3 functions as a photocatalyst for the production of hydrogen in the presence of TEOA with added triflic acid, hydrobromic acid, or phosphoric acid in aqueous media. The photocatalytic efficiency (TON = 1) was lower in the aqueous medium possibly because of the lower lifetimes of the excited states of the ruthenium polyazine chromophores in water and additional quenching mechanisms.

The use of $[Co(bpy)_3]^{2+}$ as a catalyst in intermolecular photochemical hydrogen production schemes has inspired research on the use of cobaloximes.[70, 71] Recent efforts have been directed towards the construction of supramolecular complexes that couple light absorbing properties of Ru^{2+} and Ir^{3+} chromophores to the reactive properties of cobaloximes catalysts in solar hydrogen production schemes.[72, 73] Fontecave and co-workers have constructed a series of dyads and compound 4, $[(bpy)_2Ru(L\text{-}pyr)Co(dmgBF_2)_2(OH_2)]^{2+}$, (L-pyr = [(4-pyridine)oxazolo-(4,5-f)-phenanthroline, $dmgBF_2$ = (difluoroboryl)dimethylglyoximate, is one of the cobalt photocatalyst used for solar hydrogen production.[72, 73] The ability of cobalt to access the Co^{3+}, Co^{2+} and Co^{1+} oxidation states provides a pathway for multielectron catalysis. The compound 4 (see Figure 1.10) is a potent light absorber in the UV and visible region of the spectrum, with the lowest energy transition being MLCT in nature with λ_{max} (abs) = 450 nm in dimethyl-formamide (DMF). Compound 4 displays emission from ^{3}MLCT state with excited state lifetimes of 1.63 μs in deaerated acetone at room temperature. The emission from the ^{3}MLCT state of the dyad is slightly quenched relative to the Ru monomer (without cobaloximes unit) (τ = 1.72

μs).[72] In the compound 4, the $Co^{2+/1+}$ reduction was observed at -0.51 V Vs SCE as reversible couples in DMF using 0.1 M Bu_4NBF_4 as electrolyte.

The photolysis of compound 4, $[(bpy)_2Ru(L\text{-}pyr)Co(dmgBF_2)_2(OH_2)]^{2+}$ in acetone, using a CdI-doped Hg light source, in the presence of 100 fold excess of electron donor (Et_3N = TEA) and 100 fold excess of proton source (Et_3NH^+), resulted in photochemical hydrogen production. A turnover numbers of 56 over 4 hours was observed in acetone. The impact of solvent on photocatalytic efficiency of compound 4 was investigated.[72] Lower turnover number in acetonitrile (TON = 10), methanol (TON = 9), DMF (TON = 3) and 1,2-dichloroethane (TON = 0) were observed. The lower turnover number in DMF and 1,2-dichloroethane is attributed to decomplexation of the photocatalyst in these solvents. When the proton source was changed to water, a lower turnover numbers of 22 in 4 hours was obtained. The lower turn over number is attributed to the high pH (~14) of the solution under the conditions investigated.[72] Photocatalyst function was maintained under visible light by placing a UV cut-off filter between the lamp and photocatalytic solution with 103 turnover numbers of 15 hours of photolysis. Higher turnover numbers were obtained when a UV cut-off filter was used which suggests that both UV and visible light impact on the catalyst function. The ruthenium based dyads demonstrate superior photocatalytic efficiency to the multi component $[Ru(bpy)_3]^{2+}$/ cobaloximes system (Eu^{2+} as electron donor, visible light excitation at λ = 450 nm afforded hydrogen production, providing 10 turnovers with respect to $[Ru(bpy)_3]^{2+}$and 1 turnover with respect to $Co^{2+}L$ ($Co^{2+}(Me_6[14]dieneN_4)(H_2O)_2^{2+}$).[72, 73] It is proposed that in compound 4 intramolecular electron transfer affords a Co^{1+} species, which is protonated to yield a Co^{3+}– H intermediate that can be further protonated to generate hydrogen. A favourable driving force for oxidative quenching of the chromophore by the attached Co^{2+} site is predicted as the observed electrocatalytic potentials are more positive than the standard potentials of the excited state reduction potential for $[Ru(bpy)_3]^{2+}$.[74] The resistivity of the cobaloximes catalyst to acid hydrolysis and hydrogenation reactions, the presence of a more reducible Co^{2+} species in systems that incorporate a BF_2 to bridge, and the supramolecular nature of the dyads that favour more efficient intramolecular electron transfer events have been suggested as a means for higher photocatalytic efficiency.[72]

The photoinduced hydrogen production in a CH_3CN/ TEA solution for $[Ru(bpy)_2(DMB)PdCl_2]^{2+}$ (bpy = 2,2'-bipyridine and DMB = 2,6-bis(ethane)-(4-(bis(4'-methyl-2,2'-bipyridine))-1,4-dimethoxybenzene) (Compound 5) was investigated by Hammerström and co-workers,[75] (see Figure 1.10). Photoinduced hydrogen production with compound 5 was studied under continuous illumination with visible light from a tungsten filament lamp. A cut-off filter ($\lambda \geq 475$ nm) allowed for excitation into the MLCT band of the Ru unit while avoiding excitation of Pd^{II} unit. The illumination experiments were performed in deaerated solutions of compound 5 (50 μM) in CH_3CN/TEA (2:1 v/v), and H_2 formation was monitored online by Gas Chromatography analysis of the headspace above the reaction mixture. The maximum turnover numbers of 30 was obtained after 6 hours of continuous irradiation. The difference from the other compounds shown in Figure 1.10 is that the bridge is not a complete aromatic system (non conjugated reducible π-electron system). As metal colloids of group 10 are active as H_2 production catalysts,[76] this study focused on the potential formation of Pd colloids by photodegradation of the complex and their possible role in H_2 evolution. For this purpose the reaction mixture of compound 5 was analyzed at different stages of the H_2 formation reaction by transmission electron microscopy (TEM) and X-ray photoelectron spectroscopy (XPS).[75] In the TEM measurements of solutions cast on copper grids, small Pd nanoparticles (40 nm) appeared already at the catalysis start point, while after 45 min of irradiation in the same experimental run resulted in much larger Pd nanoparticles (150 nm) colloids were appeared and at the end stage, even more colloids were detected, suggesting further dissociation of Pd colloids (300 nm) from compound 5. As evidenced by XPS and TEM measurements, Pd is released from the complex upon illumination and the appearance of Pd^0/ colloids strongly correlates in time with the formation of H_2. The authors suggest that heterogeneous catalysis on the Pd colloids has a major contribution to the observed H_2 formation. These results emphasize that the mechanistic interpretation of H_2 production with supramolecular systems in general requires careful consideration of alternative mechanisms.

1.4 Miscellaneous systems for photo-induced hydrogen generation.

1.4.1 Photobiological water splitting

Photobiological water splitting employs sunlight and microorganism such as microalgae and cyanobacteria to produce hydrogen from water (Figure 1.11).[5] In these systems, electron and protons generated through solar water splitting are transported to the hydrogen producing enzymes, hydrogenase or nitrogenase, which catalyze the production of hydrogen fuel. Hydrogenase activity is impeded by the sensitivity to oxygen generated, limiting the efficiency of this systems.[5] Photobiological water splitting is still at its infancy and research on enhancing hydrogen production efficiency through modification of the microorganisms and identifying other naturally occurring microbes is ongoing. Despite often low efficiencies, hydrogenase engineering efforts show much promise as analysis projects to show that overcoming oxygen inhibition could leads to hydrogen production with 10 % efficiency in the conversion of solar energy. A recent report introduces the concept of using carbon nanotubes as electron relays to electrically wire hydrogenase[77] to be used in the hydrogen production technologies.[78] This method provides a facile way of incorporating an electrical connection between the hydrogenase and a single walled carbon nanotube that displays excellent electronic conductivity without compromising the catalytically activity of the hydrogenase site.

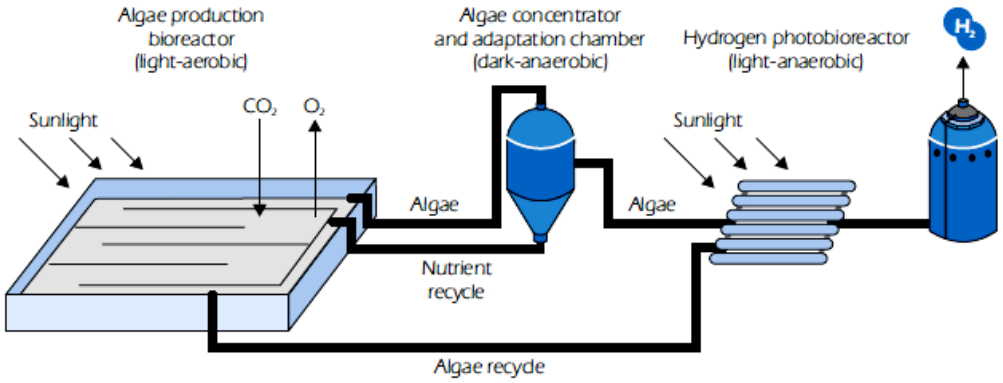

Figure 1.11: *Principle of photobiological hydrogen generation.*

Reisner and coworkers [79a, 79b] reported on the stable electrochemistry of a [NiFeSe]-hydrogenase from *Desulfomicrobium baculatum* (*Db* [NiFeSe]-H) on a TiO2 electrode. This observation led to a prototype solar H_2 production system consisting of this hydrogenase and a synthetic ruthenium photosensitizer {[$Ru(bpy)_2(H_4dpbpy)]Br_2$, RuP, bpy = 2,2′-bipyridine, H_4dpbpy = 2,2′-bipyridine 4,4′-diylbis(phosphonicacid)}, co-attached to colloidal TiO2 nanoparticles.[79a, 79b] Enzyme-modified nanoparticles were produced H_2 using visible light under ambient conditions. The optimized system consisting of *Db* [NiFeSe]-H attached to Ru dye-sensitized RuP-TiO_2 (see Figure 1.12), with triethanolamine as a sacrificial electron donor, produces H_2 at a turnover frequency of ~ 50 (mol H_2) s^{-1} (mol total hydrogenase)$^{-1}$ at pH 7 and 25 °C, under the solar irradiation. The system shows high electrocatalytic stability not only under anaerobic conditions but also after prolonged exposure to air. Erwin *et. al.* [79c] also reported a self-assembled system comprising of a molecular H_2 production cobalt catalyst attached on a ruthenium dye sensitised (Ru-P) TiO2 nanoparticles. Visible light irradiation of the dispersed nanoparticles in the presence of the sacrificial electron donor triethanolamine produces H_2 photocatalytically in pH neutral water and at room temperature.[79c]

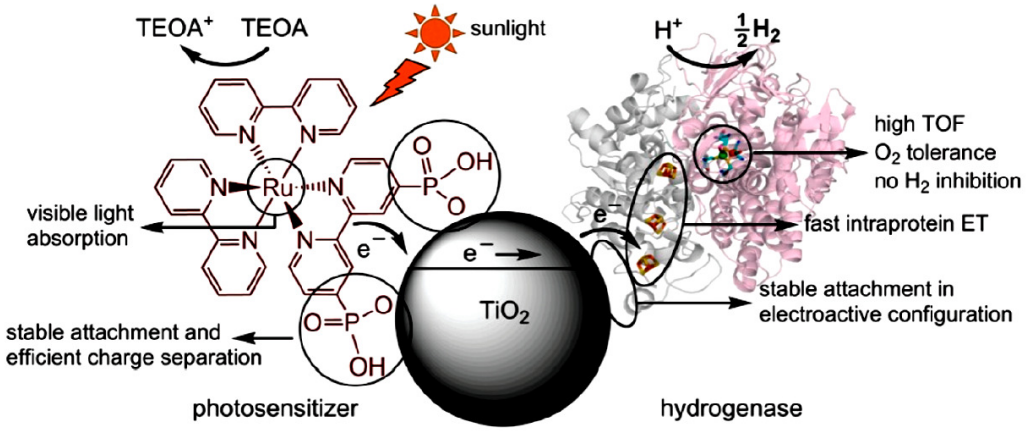

Figure 1.12: The system is shown with a hydrogenase (*Db* [NiFeSe]-H) as catalyst and the complex (RuP) as light absorbing unit attached to TiO_2 nanoparticles for the production of hydrogen using sunlight.[79]

1.4.2 Photoelectrochemical water splitting

Photoelectrochemical water splitting employs light and semiconductors to split water. This area has been recently reviewed.[4] These systems typically employed semiconductors, catalysts and more recently light absorbers.[4, 80, 81, 82, 83, 84, 85a, 85b, 86, 87]

The type of semiconductor, the nature of catalyst, as well as interfacial electron transfer processes impact the efficiency of water splitting to produce fuel. TiO_2 was used a semiconductor for UV based Photoelectrochemical water splitting in 1972 by Honda and Fujishima.[81] This system used UV light at wavelengths < 415 nm. Irradiation of the surface of a TiO_2 electrode coupled to a platinum black electrode through an external load resulted in hydrogen production at the platinum electrode. In the presence of more reducing species, for example Fe^{3+}, at the platinum compartment, hydrogen production occurred with quantum efficiency of 0.1.[81] There is recent focus on the development of efficient photoelectrochemical systems that utilize visible light to split water for fuel production.[4, 71]

The electronic structure of the semiconductor is key to efficient photocatalysis. An ideal semiconductor should have a band gap, E_g, that constitutes the energy difference between the conduction band (CB) and the valence band (VB) with sufficient energy to drive the water splitting reaction. For the production of hydrogen, the CB should be more negative than the redox potential of H^+/H_2 (0 V vs. NHE). For the production of oxygen, VB should be more positive than O_2/H_2O (1.23 V vs. NHE). Thus, the semiconductor should have an E_g minimum of 1.23 eV. Optical excitation promotes an electron from the VB to the CB to create an electron-hole pair. The water is reduced by promoted electron to form hydrogen and oxidized by the holes to produce oxygen. Figure 1.13 (a) represents the principle of water splitting using semiconductor photocatalysts and principle involved in photoelectrochemical device for hydrogen generation using Nocera's model; showing in Figure 1.13 (b).

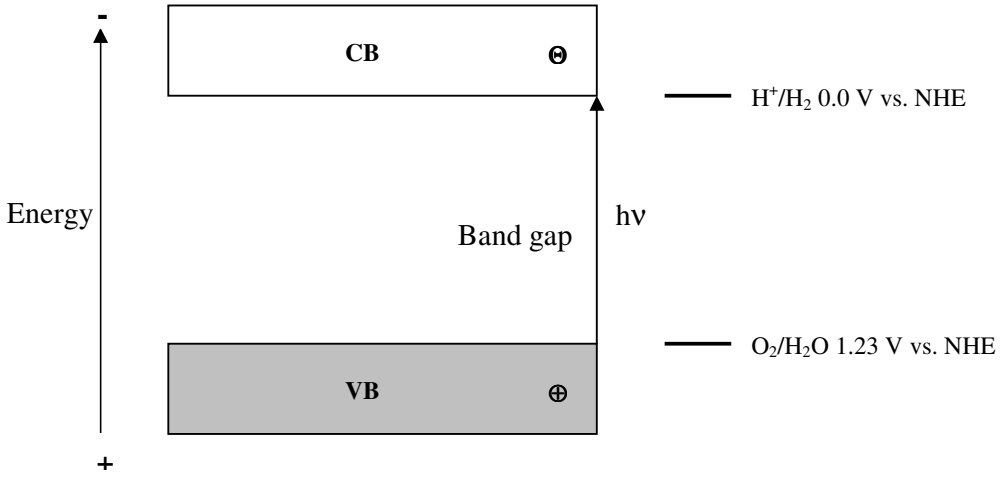

Figure 1.13 (a): *Schematic representing photocatalytic water splitting using semiconductor.*

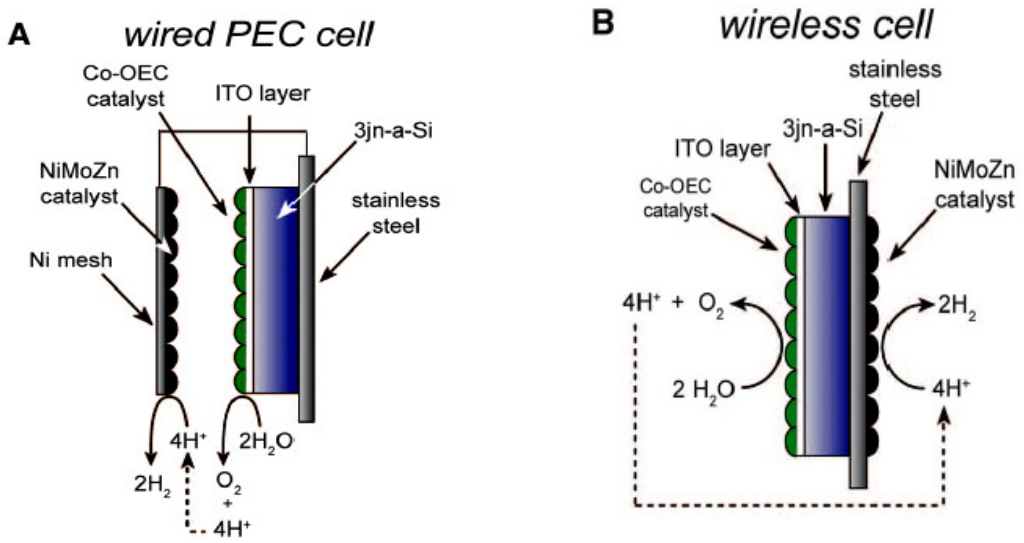

Figure 1.13 (b): *Principle involved in photoelectrochemical device for hydrogen Generation Nocera's model (a) Wired and (b) Wireless PEC cell.*

Many factors are critical for efficient light to fuel conversion in this semiconductor promoted water splitting. Rapid charge recombination in the electron hole pair is a serious concern, which impedes catalytic activity. In this regard, suitable band engineering is required when a designing systems that would be catalytically active in the visible region that do not rapid electron hole recombination. The addition of sacrificial agents has been studied and provides a method to evaluate whether the photocatalyst satisfies the thermodynamic and kinetic potential for hydrogen and

oxygen production.[4, 82] The level of crystallinity and particle size are factors that are considered during the engineering process. Enhancement of photocatalytical efficiency has been achieved through metal ion doping, anion doping and dye sensitization.[4, 82] A recent report describes the use of metal free polymeric carbon nitride that produces hydrogen from water under visible irradiation in the presence of sacrificial electron donor.[83] This system provides a promising first step toward water reduction by using commonly available materials in the absence of metals.

Nocera's and coworkers [85a] has describe the development of solar water-splitting cells comprising earth-abundant elements that operate in near-neutral pH conditions, both with and without connecting wires, see figure 1.13. The cells consist of a triple junction, amorphous silicon photovoltaic interfaced to hydrogen- and oxygen-evolving catalysts made from an alloy of earth-abundant metals NiMoZn alloy and a cobalt borate catalyst, respectively. The devices described here carry out the solar-driven water-splitting reaction at efficiencies of 4.7% for a wired configuration and 2.5% for a wireless configuration when illuminated with 1 sun (100 milliwatts per square centimeter) of air mass 1.5 simulated sunlight. Fuel-forming catalysts interfaced with light-harvesting semiconductors afford a pathway to direct solar to-fuels conversion that captures many of the basic functional elements of a leaf.[85a] The use of dye-sensitized colloidal semiconductor films is an attractive solar energy conversion method. The Grätzel cell employing this technology was first reported in 1991 and attracted much attention because of its stability, low cost and device efficiency.[85b] In this system, an optically transparent film of nanometre scale TiO_2 particles were coated with dye, $[(CN)(bpy)_2Ru\text{-}CN\text{-}Ru(L)_2\text{-}NC\text{-}Ru(bpy)_2(CN)]$, (L = 2'2-bipyridine-4,4'-carboxylic acid). The high surface area of the TiO_2 film and the favorable light absorbing properties of the dye allow a high proportion of the incident light to be absorbed. Optical excitation of the dye at $\lambda > 400$ nm affords an electron injection in to CB of the semiconductor. The dye is regenerated by electron transfer from a species in solution that regenerated at the counter electrode. Overall light to electric energy conversion efficiencies of 12% in diffused solar light has been achieved in this system.[85b] Studies are in progress to enhance system efficiency and focus on the impact by the essential components within the system including the conductivity mechanical support, semiconductor film, sensitizer, electrolyte, counter

electrode.[86] A system consisting of ruthenium dye sensitized TiO_2 nanoparticles loaded with a thin coating of Al_2O_3 and platinum ($Al_2O_3/TiO_2/Pt$) has been prepared.[87] This dye sensitized $Al_2O_3/TiO_2/Pt$ systems shows enhanced hydrogen production activity to the corresponding dye sensitized TiO_2/Pt system when an aqueous solution was irradiated at $\lambda > 420$ nm in the presence of the ethylenediaminetetraacetic acid (EDTA) as electron donor. Up to 390 turnovers in 3 hours was achieved with respect to dye. No hydrogen was produced in the absence of the dye or platinum loading. The enhanced photocatalytic efficiency in the dye sensitized $Al_2O_3/TiO_2/Pt$ system is attributed to the impact of platinum, which completely scavenges the electrons to reduces protons, and Al_2O_3 barrier, showing down the charge recombination processes.

1.4.3 Iron-based biomimetic supramolecular photocatalysts

Biomimetic systems that mimic the iron hydrogenase active site for photochemical water reduction to produce hydrogen have been a topic of interest.[77] The active site of the iron hydrogenase is known to consist of two iron atoms linked by a dithiolate bridge.[88] The biomimetic diiron model, $[Fe_2\{\mu\text{-}S_2(CH_2)_3\}(CN)(CO)_4(PMe_3)]^-$ (Figure 1.14), has been shown to serve as a catalyst for electrochemical hydrogen production.[89]

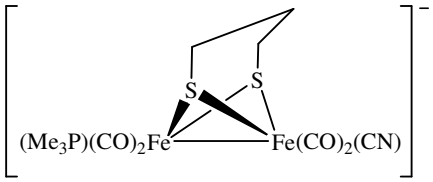

Figure 1.14: *Biomimetic model for $[Fe_2\{\mu\text{-}S_2(CH_2)_3\}(CN)(CO)_4(PMe_3)]^-$*

Sun and co-workers recently used a pyridyl functionalized hydrogenase active site model complex bound to a zinc tetraphenylporphyrin [ZnTPP] unit for photo-chemical hydrogen production, Figure 1.15, $[ZnTPP(pyridylCOO(CH_2)_2(Fe_2\{\mu\text{-}S_2(CH_2)_2N\}(CO)_6))]^{2+}$.[90] Two main strategies were employed in system design. The first strategy is to take advantage of the weak coordination of pyridine to zinc to limit

back electron transfer through complex dissociation after the reduction of the diiron centre. The second strategy is to make use of the ability of the system to self assemble to mediate intramolecular electron transfer. The mechanism for electron transfer was studied by transient absorption spectroscopy in the presence of ZnTPP and [pyridylCOO$(CH_2)_2$(Fe_2{μ-$S_2(CH_2)_2$N}$(CO)_6$)] (Figure 1.15). ZnTPP display a strong emission from the singlet state (^{1}ZnTPP*), providing a probe to excited state dynamics. The emission form ZnTPP is quenched by 50–60% in the presence of a 20 fold excess of [pyridylCOO$(CH_2)_2$(Fe_2{μ-$S_2(CH_2)_2$N}$(CO)_6$)] with a reduction in the singlet excited state lifetime. This emission quenching is consistent with a static absorption titration measurement under similar conditions.

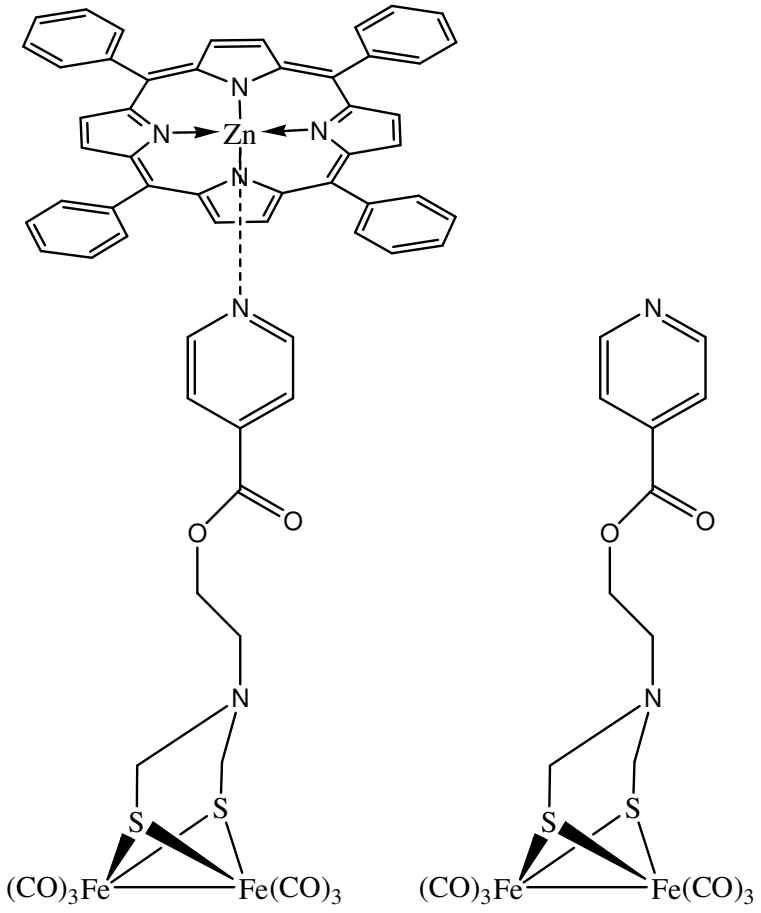

[ZnTPP(pyridylCOO$(CH_2)_2$-(Fe_2{μ-$S_2(CH_2)_2$N}$(CO)_6$))]$^{+2}$

[pyridylCOO$(CH_2)_2$(Fe_2{μ-$S_2(CH_2)_2$N}$(CO)_6$)]

Figure 1.15: *Representing of ZnFe self assembling system and FeFe subunit*

These both suggest the necessity for the formation of a supramolecular species through zinc coordination to pyridine, coupling the ^{1}ZnTPP* and the diiron moiety, which promotes excited state electron quenching. The high energy of ^{1}ZnTPP* singlet excited state allows electron or energy transfer to the diiron unit. Photoexcitation of ZnTPP using a nanosecond flash photolysis technique in the presence of [pyridylCOO$(CH_2)_2$(Fe_2{μ-$S_2(CH_2)_2$N}$(CO)_6$)], a new species is observed using transient absorption spectroscopy.[89] This is attributed to intramolecular electron transfer to form a charge separated species, ([ZnTPP$^{\bullet+}$ pyridylCOO$(CH_2)_2$(Fe_2{μ-$S_2(CH_2)_2$N}$(CO)_6)^{\bullet-}$]), which could dissociate to ZnTPP$^{\bullet+}$ and [pyridylCOO-$(CH_2)_2$(Fe_2{μ-$S_2(CH_2)_2$N}$(CO)_6$)]$^{\bullet-}$. Photolysis of ZnTPP, [pyridylCOO$(CH_2)_2$(Fe_2-{μ-$S_2(CH_2)_2$N}$(CO)_6$)] and the electron donor (2-mercaptobenzoic acid) in the presence of CF_3COOH as proton source in methylene chloride at $\lambda > 400$ nm resulted in photochemical hydrogen production with 0.16 turnovers based on [pyridylCOO-$(CH_2)_2$(Fe_2{μ-$S_2(CH_2)_2$N}$(CO)_6$)] and 16 turnovers based on ZnTPP. It is proposed that ([ZnTPP$^{\bullet+}$ pyridylCOO$(CH_2)_2$(Fe_2{μ-$S_2(CH_2)_2$N}$(CO)_6)^{\bullet-}$]) may undergo dissociation to form ([ZnTPP$^{\bullet+}$], which is reductively quenched by the electron donor and [pyridylCOO$(CH_2)_2$(Fe_2{μ-$S_2(CH_2)_2$N}$(CO)_6$)]$^{\bullet-}$, which gets protonated. Protonation of the radical anion renders the reduction potential more positive, facilitating the second electron transfer event which is followed by further protonation and hydrogen release. This represents an interesting system for hydrogen production using intramolecular excited state electron transfer in a self assembled system.[89]

1.4.4 Osmium – rhodium supramolecular photocatalysts for generation of hydrogen

Nishibayashi and co-workers have used diphosphine ligands attached to an $[Os(tpy)_2]^{2+}$ moiety to coordinate a rhodium centre (Figure 1.16) and used this system for photochemical hydrogen production.[91] The approach allows the use of a $Os(tpy)_2$-based chromophore in photocatalytic schemes. The OsRh dyad has been synthesized and analyzed in situ by treatment to osmium based chromophore with $[RhCl(CO)_2]_2$. The electrochemistry displays a reversible $Os^{II/III}$ couple at 0.92 V vs. SCE and $tpy^{0/-}$ reductions at -1.11 and -1.34 V vs. SCE.[90] The dyad absorb in the UV and visible

regions of the spectrum displaying ^{1}MLCT and ^{3}MLCT absorption at 482 nm and 655 nm, respectively.[90] An emission is observed at 728 nm (Φ_{em} = 0.52 in an acetonitrile/ water mixture) with reduced intensity than the parent chromophore (Φ_{em} = 0.73 in an acetonitrile/ water mixture).[90] Irradiation of catalytical amounts of the OsRh dyad generated in situ at λ > 380 nm in a trifluoromethanesulfonic acid/sodium ascorbate mixture at Ph = 5.2 for 18 hours affords hydrogen with 36 turnovers. The use of $RhCl_3$ instead of $[RhCl(CO)_2]_2$ yielded turnovers of 87 with Φ = 0.007. It is suggested that intramolecular electron transfer to rhodium upon optical excitation by two electrons leads to a reduced rhodium that can react with a proton to form a rhodium hydride, which generates hydrogen.

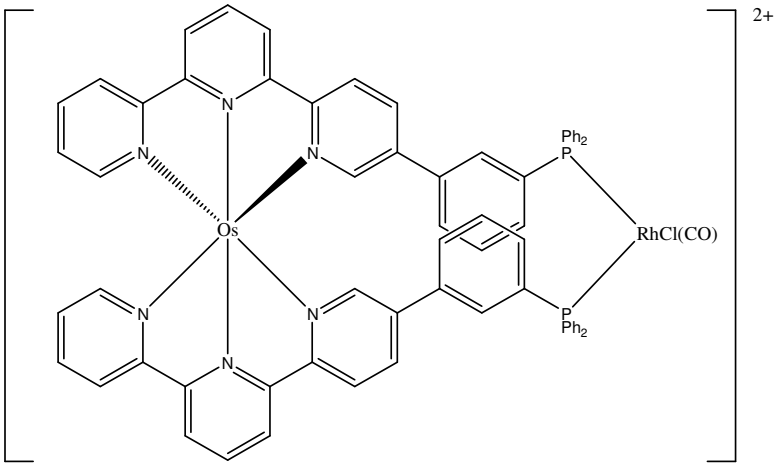

[{(tpyPh(PPh2))2Os}RhCl(CO)]$^{2+}$

Figure 1.16: *OsRh dyad for solar hydrogen generation.*

1.4.5 Mixed-valence systems for multielectron photo-chemistry to generate hydrogen.

Dinuclear mixed valence complexes for multielectron photochemistry are capable of reducing hydrohalic acid (HX) to hydrogen, with Φ = 0.01, in the presence of a halogen trap have been reported by Nocera and co-workers,[7, 92, 93] Mixed valence compounds of the form $M^{n+}\cdots M^{n+2}$ are employed to drive multielectron chemistry. Rhodium bimetallics, $[Rh_2(dfpma)_3X_4]$, when ligated by three dfpma ligands, transform to a two electron mixed valence state, $[Rh_2^{0,II}(dfpma)_3X_2(L)]$ (dfpma =

$MeN(PF_2)_2$, X = Cl or Br, L = CO, PR_3 or CNR) when irradiated at excitation wavelength between 300 and 400 nm in the presence of excess L and a halogen atom trap. At 20 °C in 0.1 M HCl in THF, the catalyst $[Rh_2^{0,0}(dfpma)_3(PPh_3)(CO)]$ was able to achieve turnovers of ~ 80 of H_2 with (λ_{exc} > 338 nm). The dfpma ligand is unique, the fact is that it can act as both a π-acceptor and a π-donor, stabilizing the mixed valence oxidation state of $[Rh_2^{0,II}(dfpma)_3X_2(L)]$. Further irradiation activates a Rh^{II} – X to generate a doubly reduced form, $[Rh_2^{0,0}(dfpma)_3(L_2)]$ (see Figure 1.17 for the proposed photocycle reaction mechanism). This Rh^{II} – X bond activation is the rate determining step in the hydrogen production scheme. Photolysis of $[Rh_2^{0,0}(dfpma)_3(L_2)]$ in the presence of HCl results in an intermediate Rh^{II},Rh^{II} dihydride,dihalide, $[Rh_2^{II,\ II}(dfpma)_3Cl_2H_2]$, which on photolysis, produces hydrogen with the generation of $[Rh_2^{I,\ I}(dfpma)_3Cl_2]$. This $Rh_2^{I,\ I}$ species undergoes internal disproportionation which is leading to regeneration of $[Rh_2^{0,\ II}(dfpma)_3X_2(L)]$. Since activation of the Rh – X bond is the rate determining step for solar hydrogen production, studies had focused on the systems that undergo more efficient rate of M–X bond activation. In this regard, heterobimetallic complexes, $[Rh^IAu^I(tfepma)_2(CN^tBu)_2]^{2+}$ and $[Pt^{II}Au^I(dppm)_2PhCl]^+$ (tfepma = $MeN(P(OCH_2CF_3)_2)_2$ and dppm = $CH2(PPh_2)_2$), have been synthesized.[94, 95] The Pt^{III} – Au^{II} species, $[Pt^{III}Au^{II}(dppm)_2PhCl_3]^+$, formed by photooxidation displays enhanced efficiency of metal halide bond activation with respect to the dirhodium complexes.[93]

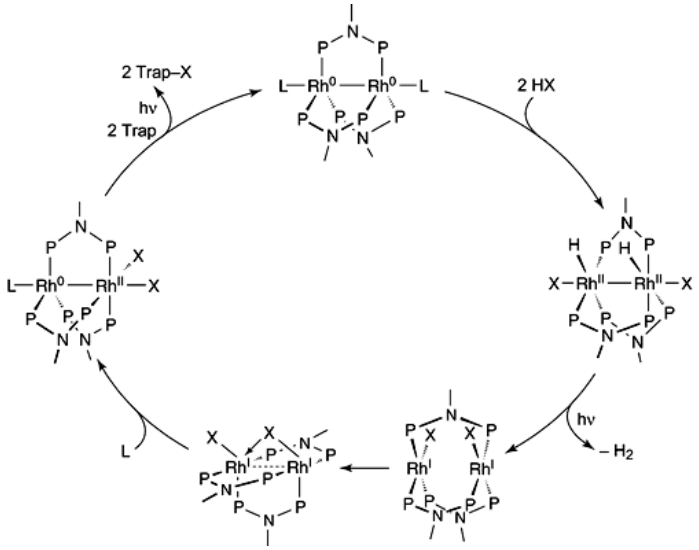

Figure 1.17: *Proposed photocycle for hydrogen generation from HCl solutions in THF as solvent.* [96]

1.4.6 Nickel catalysts for the photo-generation of hydrogen

Eisenberg and co-workers described a homogenous system for photocatalytic hydrogen generation that uses a nickel(II) molecular catalyst (1) in combination with a photo-sensitizer (PS) (1 or 2) and the sacrificial electron donor (ascorbate), see figure 1.18.[97] DuBois and co-workers described the nickel(II) complex 1 shown in figure 1.18, which also functions as an efficient and stable electrocatalyst for the generation of H_2 from acidic non-aqueous solutions with low overpotentials (TOF > 350 s^{-1}, 0.30 V).[98, 99, 100] Complex 1 is employed in conjunction with eosin Y (2) an organic dye that has been shown to act as a PS in a light-driven system for the generation of H_2 from water.[101] The system functions in 1 : 1 H_2O : CH_3CN with a pH range of 1–5 and maximum activity at pH 2.25. Eosin Y is only moderately stable under photocatalytic conditions when using light with $\lambda > 410$ nm and decomposes between 8 and 48 h depending on the catalyst concentration and irradiation power. The catalyst may also be paired with $[Ru(bpy)_3]Cl_2$ (3) as the PS, to evaluate the long-term stability of 1 as the catalyst. This system is inactive in the absence of any of the three components (catalyst, PS, or sacrificial donor).

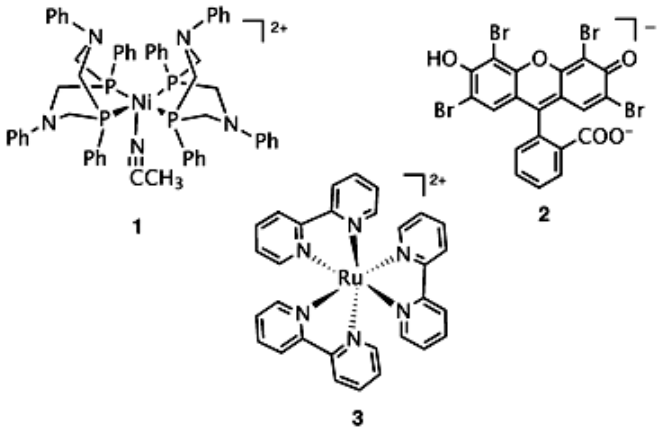

Figure 1.18: *Complexes in the photocatalytic system: (**1**) = Nickel (II) complex, (**2**) = Eosin Y, (**3**) = $[Ru(bpy)_3]^{2+}$.*[97]

The initial rate of H_2 production varies little (maximum TOF by catalyst = 20 h^{-1}) using various concentrations of either **2** or **3** as the PS. However, the rate decreases after longer irradiation times (>1 h) indicating the degradation of at least one system

component. Following total bleaching of the PS, the system's activity is completely restored by the addition of either **2** or **3** as the PS. The reconstitution of the system activity in this way indicates that the catalyst component is stable during irradiation, and that the system's photo-instability is due to PS decomposition. The stability of the catalyst is evident from $^{31}P\{^{1}H\}$ and ^{1}H NMR data; after photodegradation in a reaction mixture with deuterated solvents, the peaks in the NMR spectra associated with the catalyst are identical to those in the starting material. Through the addition of ascorbic acid and $[Ru(bpy)_3]Cl_2$ (3) during the course of photolysis, it is possible to obtain turnovers of 2700 which related to catalyst over 150 hours (see Figure 1.19). According to author, this is the highest TON (based on catalyst) yet reported for a photocatalytic system which employs a molecular catalyst consisting of earth abundant elements such as nickle.[71, 83, 101, 102, 103, 104, 105, 106, 107, 108, 109, 110, 111]

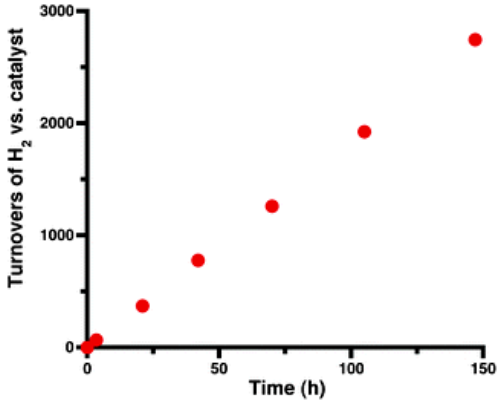

Figure 1.19: *Turnovers of H_2 generation from a system composed of 0.14 mM catalyst Ni(II) catalyst (**1**), 500 mM ascorbic acid (pH = 2.25), and 0.40 mM PS $[Ru(bpy)_3]^{2+}$ (**3**) in 1 : 1 H_2O : CH_3CN irradiated with a 410 nm cut-off filter. Aliquots of the PS $[Ru(bpy)_3]^{2+}$ (**3**) (400 µmol) and ascorbic acid (320 nmol) were added after each measurement to restore activity.*[97]

1.4.7 Iridium based photocatalyst for hydrogen generation.

The photophysical properties of iridium(III) compounds, which may be altered within the ligand sphere makes them particularly interesting candidates for photocatalytic water reduction experiments. Bernhard and co-workers,[112] carried out thorough studies by parallel screening of a library of $[Ir(C^{\wedge}N)_2(N^{\wedge}N)]^+$ complexes.[113] The

utility of those compounds for the light-driven water reduction and optimization of catalyst and solvent systems resulted in turnovers greater than 2000.[114] These optimum conditions included the use of a Pt or Pd precursor that formed a catalytically active metal colloid upon irradiation. As it is common to stabilize metal colloids by the addition of vinyl-derived polymers,[115] Ir(III) complexes containing one or more vinyl groups at the ligand backbone seemed to be promising candidates for improving the interaction between photosensitizer and catalyst. The beneficial effects of this approach include a stabilization of the Pt colloid as well as a faster electron transfer from the Ir photosensitizer to the Pt catalyst, which will result in higher stabilities of the reaction system and improved turn-over numbers. Various C^N ligands with electron-withdrawing or electron-donating substituents were used for these experiments. The N^N ligands 4-vinyl-4′-methyl-2,2′-bipyridine (mVbpy), 4,4′-dimethyl-2,2′-bipyridined (dMebpy) and 4,4′-divinyl-2,2′-bipyridine (dVbpy) incorporated one or two polymerizable vinyl moieties (see Figure 1.20).

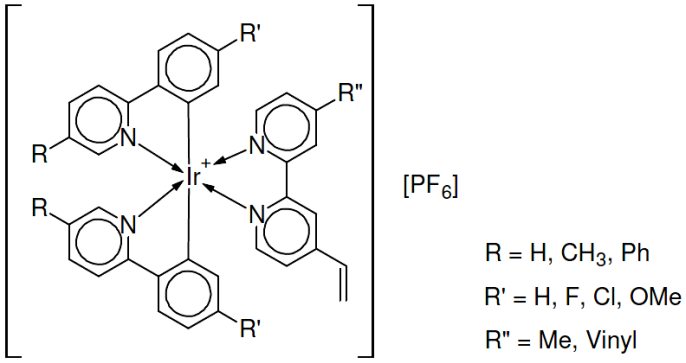

Figure 1.20: *Chemical structure of synthesized [Ir(C^N)$_2$(N^N)][PF$_6$] complexes.* [112]

These new compounds were compared to the [Ir(C^N)$_2$(N^N)]$^+$ analogs with N^N = 4,4′-dimethyl-2,2′-bipyridine (dMebpy). As the only difference is the substitution of methyl groups by one or two vinyl groups, changes in the properties should be a consequence of the vinyl group's presence. The photophysical properties of the iridium compounds described here are summarized in Table (1.1). All synthesized Ir(III) complexes are luminescent in the solid state and in solution. However, compared to their respective parent dMebpy species, the emission quantum yields of the mVbpy and dVbpy complexes are significantly decreased. This especially holds true for complexes with halide substituted C^N ligands (F–mppy and Cl–mppy). In

contrast, the lifetimes of the mVbpy complexes are only somewhat shorter than those of the dMebpy parent complexes. The lifetimes of the dVbpy compounds, on the other hand, are shorter than those of the dMebpy and mVbpy complexes, with a particular dramatic decrease for the Cl –mppy series. As expected, the substitution of one or two methyl groups by vinyl moieties leads to a small red-shift of the emission maximum.

The hydrogen evolution experiments were performed in sealed vials with a 16-well LED photoreactor (λ_{em} = 460 nm) on an orbital shaker with a thermostated block (25°C). Each sample contained *0.5 µmol* of the respective Ir(III) photosensitizer and *0.375 µmol* catalyst (K_2PtCl_4) in THF (8 mL), triethylamine (sacrificial reductant, 1 mL), and H_2O (1 mL). The solutions were degassed and then purged with argon at atmospheric pressure. Pressure transducers were used to obtain kinetic data, and the head-space was analyzed for H_2 by mass spectrometry. All iridium compounds studied functioned as photosensitizer for the reduction of water (Figure 1.21). The turn-over numbers (TONs) of the dMebpy derivatives ranged from 925 to 1625, whereas the mVbpy and dVbpy compounds exhibited dramatically increased stabilities with 5700–8500 turn-overs (Table 1.2).

Table 1.1: *Photophysical properties of the Ir(III) complexes. Data obtained from deaerated 20 µM solutions of the Ir(III) complexes in THF/water (8/1)* [112]

C^N[a]	N^N	λ_{em}[b]/nm	τ/µs	Φ_{em}[c]
F–mppy	dMebpy	546	1.280	0.299
F–mppy	mVbpy	556	1.167	0.011
Cl–mppy	dMebpy	541	1.465	0.327
Cl–mppy	mVbpy	547	1.383	0.014
Cl–mppy	dVbpy	571	0.080	0.014
MeO–mppy	dMebpy	583	0.383	0.048
MeO–mppy	mVbpy	606	0.296	0.025
mppy	dMebpy	581	0.422	0.071
mppy	mVbpy	601	0.332	0.044
mppy	dVbpy	612	0.268	0.028
ppy	dMebpy	583	0.430	0.077
ppy	mVbpy	596	0.349	0.053
Ph–ppy	dMebpy	575	0.610	0.085
Ph–ppy	mVbpy	599	0.389	0.049

[a] Abbreviation of N^N and deprotonated C^N ligands: 5-methyl-2-(4-fluorophenyl)pyridine (F–mppy), 5-methyl-2-(4-chlorophenyl)pyridine (Cl–mppy), 5-methyl-2-(4-methoxyphenyl)pyridine (MeO–mppy), 5-methyl-2-phenylpyridine (mppy), 2-phenylpyridine (ppy), 2,5-diphenyl-pyridine (Ph–ppy), 4,4′-dimethyl-2,2′-bipyridine (dMebpy), 4-vinyl-4′-methyl-2,2′-bipyridine (mVbpy), 4,4′-divinyl-2,2′-bipyridine (dVbpy). [b] Excitation at 400 nm. [c] Reference compound: $[Ir(ppy)_2(bpy)]PF_6$ (Φ_{CH_3CN} = 0.0622).

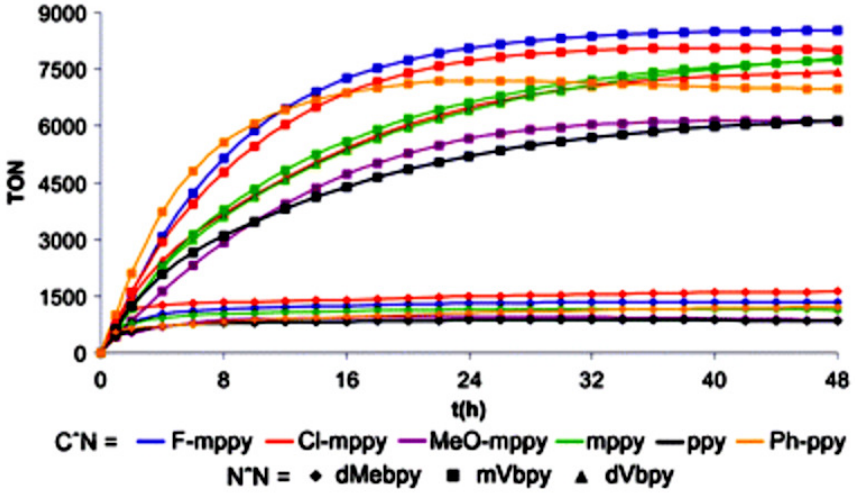

Figure 1.21: *Photocatalytic hydrogen production of the $[Ir(C^N)_2(N^N)]^+$ photosensitizers with in situ generated colloidal Pt.* [112]

In addition, cyclic voltammetry with $[Ir(Cl–mppy)_2(mVbpy)]^+$ was performed on a Pt electrode, indicating the formation of a polymeric film on the Pt electrode.[116] This further supports the existence of an interaction of the vinyl moieties with the Pt catalyst during the photocatalytic water reduction experiments.

Table 1.2: *Photocatalytic water reduction experiments. Data obtained from deaerated 50 μM solutions of the Ir(III) complexes in THF/water/triethylamine (8/1/1)* [112]

C^N	N^N	TON_{Pt} [a,b]
F–mppy	dMebpy	1300
F–mppy	mVbpy	8500
Cl–mppy	dMebpy	1625
Cl–mppy	mVbpy	7950
Cl–mppy	dVbpy	7225
MeO–mppy	dMebpy	925
MeO–mppy	mVbpy	5700
mppy	dMebpy	1175
mppy	mVbpy	7950
mppy	dVbpy	7925
ppy	dMebpy	925
ppy	mVbpy	5800
Ph–ppy	dMebpy	1325
Ph–ppy	mVbpy	7025

[a] 48 h irradiation. [b] TON = $2n(H_2)/n(PS)$.

In an another studies by Beller and co-workers, synthesis of novel, mono-cationic iridium(III) photosensitisers (Ir-PS) with the general formula $[Ir^{III}(C^N)_2(N^N)]^+$ (C^N: cyclometallating phenylpyridine ligand, N^N: neutral bidentate ligand) was

described in Figure 1.22.[117] All iridium complexes were tested for their ability as photosensitisers to promote homogeneously catalysed hydrogen generation from water under visible light irradiation.

In the presence of $[HNEt_3][HFe_3(CO)_{11}]$ as a water-reduction catalyst (WRC) and triethylamine as a sacrificial donor (SD), maximum turnover numbers of 4550 for the Ir-PS1 and 2770 for the Fe – WRC [118, 119] generated in situ from $[HNEt_3][HFe_3(CO)_{11}]$ and tris[3,5-bis(trifluoromethyl)phenyl]phosphine (PR_3) were obtained under visible light (see Table 1.3). These are the highest overall efficiencies for any Ir/Fe water-reduction system reported. The incident photon to hydrogen yield reaches 16.4 % with the best system. They developed an active three-component system based on simple iron carbonyls.[120, 121] More specifically, they showed that the activity of inexpensive $[Fe_3(CO)_{12}]$ was comparable to well-established cobalt oxime catalysts. The iron hydride $[HNEt_3][HFe_3(CO)_{11}]$ was identified as an active species by using in situ FTIR techniques and DFT calculations.[121]

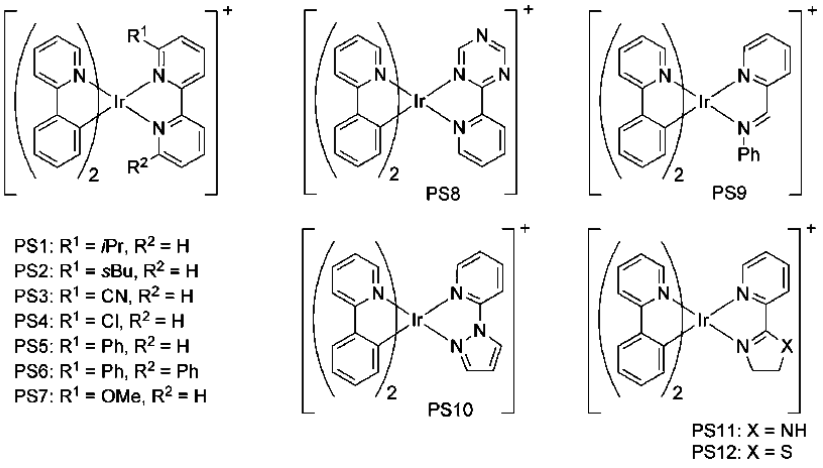

Figure 1.22: *Chemical Structures of Ir-PSs (PS1 – PS12).* [117]

Table 1.3: *Performance of the catalytic system comprising PS1 and the Fe-WRC/PR_3 catalytic system.*[117]

Entry[a]	PS1 [µmol]	H_2 [mL] 20 h	TON Ir-PS[b] 20 h	TON WRC[c] 20 h
1	15.0	225	1220	2770
2	0.5	28	4550	345

[a] Reaction conditions: $[HNEt_3][HFe_3(CO)_{11}]$ (3.3 µmol), $P[C_6H_3\text{-}3\text{-}5\text{-}(CF_3)_2]_3$ (5.0 µmol), 440 nm irradiation 1.5 W, $THF/NEt_3/H_2O$ (3/2/1; 20 mL), 25°C, gas volumes measured with an automatic gas burette, gas analysis by GC. [b] TON Ir-PS = $n(H)/n$(Ir-PS) [c] TON Fe = $n(H_2)/n$(Fe trimer).

For successful application of PS1–PS12 as photosensitisers in light-driven hydrogen generation from water, three prerequisites have to be fulfilled: 1) absorption of the visible part of the spectrum, 2) photoluminescence that can be quenched by the sacrificial reductant and 3) a sufficient reduction potential of the reduced state to transfer an electron into the Fe-WRC. UV/Vis absorption measurements were carried out to characterise the absorption properties of PS1–PS7, PS13 (top) and PS8 – PS12 (bottom) (see Figure 1.23). All complexes show a strong absorption in the UV region that can be attributed to π–π* transitions. In the visible range of the spectrum (> 390 nm) all complexes show absorptions that level off at longer wavelengths.

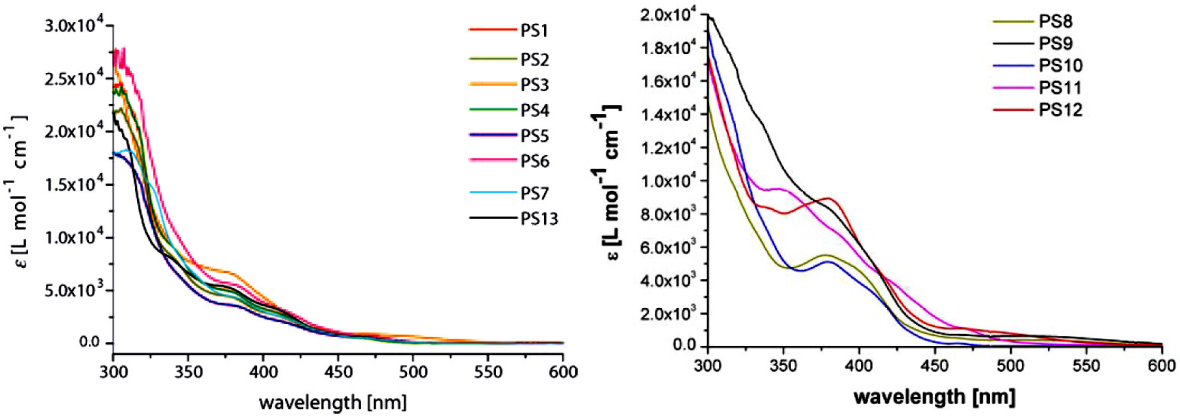

Figure 1.23: *UV/Vis spectra of all catalytically active iridium photosensitizers (PS1–PS7, PS13 (top) & PS1–PS12 (bottom)). Conditions: 0.1 mmolL^{-1} degassed solutions in acetonitrile.* [117]

No absorption was observed at > 500 nm. The luminescence behaviour of PS1–PS13 can be divided into three groups: (1) all complexes with 6- or 6,6′-substituted bpy ligands (PS1–PS7) which shows strong photoluminescence in the range of 570–640

nm that can be quenched with triethylamine,[117] (2) PS8, PS9, PS12 and PS11 give weak or no emission and (3) complex PS10 exhibits emission at 479 and 505 nm, but only negligible quenching is observed in the presence of NEt_3.[117] Furthermore, electrochemical measurements were carried out to determine the reduction and oxidation potentials of the respective complexes (Table 1.4). For PS1–PS13, the oxidation potentials are in the same range, showing that the first oxidation (Ir^{III}/Ir^{IV}) is only slightly influenced by the substitution of the N^N ligand (entries 1–13). Among the reduction potentials within the 6,6′-substituted bpy complexes, only PS3 has a relatively positively shifted reduction potential than PS13, PS1, PS2 and PS4–PS7 (Table 1.4, entries 1–8). This may be due to the electron-withdrawing and mesomeric effect of the nitrile moiety in PS3. Other iridium(III) complexes with 6- and 6,6′-substituted bpy ligands show comparable or more negative reduction potentials than the basic structure PS13, ranging from −1.25 to −1.30 V (Table 1.4). Notably, the triazine ligand in PS8 can be reduced in two independent steps (−0.68 and −1.44 V). Complexes PS9 and PS12 also possess more positive reduction potentials than PS13. In the case of PS10 and PS11, an irreversible reduction at a much more negative potential is observed (−1.66 V for PS10 and −1.43 for PS11).

Table 1.4: *Oxidation and reduction potentials of all Ir-PS.*[117]

entry	Structure	1^{st} (2^{nd}) E^{red} [V] [a]	1^{st} E^{ox} [a]
1	$[Ir(ppy)_2$(6-*iP*r-bpy)$]PF_6$ (**PS1**)	-1.30	+1.47
2	$[Ir(ppy)_2$(6-*sBu*-bpy)$]PF_6$ (**PS2**)	-1.30	+1.45
3	$[Ir(ppy)_2$(6-Cl-bpy)$]PF_6$(**PS4**)	-1.25	+1.47
4	$[Ir(ppy)_2$(bpy)$]PF_6$ (**PS13**)	-1.23	+1.40
5	$[Ir(ppy)_2$(6,6´-Ph_2bpy)$]PF_6$ (**PS6**)	-1.26	+1.40
6	$[Ir(ppy)_2$(6-Ph-bpy)$]PF_6$ (**PS5**)	-1.25	+1.39
7	$[Ir(ppy)_2$(6-CN-bpy)$]PF_6$ (**PS3**)	-1.00	+1.47
8	$[Ir(ppy)_2$(6-OMe)$]PF_6$ (**PS7**)	-1.27	+1.40
9	$[Ir(ppy)_2$(py-triazine)$]PF_6$ (**PS8**)	-0.68 (-1.44)	+1.47
10	**PS9**	-0.85 (-1.48)	+1.43
11	**PS12**	-1.09	+1.44
12	**PS10**	-1.66[b]	+1.40
13	**PS11**	-1.43[b]	+1.27

[a] conditions: acetonitrile solutions, 0.1 M NBu4BF4, working electrode: glassy carbon, Reference electrode: Ag/AgCl, counter electrode: Pt. [b] Irreversible.

1.5 Scope of thesis

The area of solar hydrogen production through the use of photocatalysts that collect and deliver reducing equivalents in an active area of current research in inorganic and organic photochemistry. The aim of this thesis deals with the syntheses, characterisation, photocatalysis and the photophysical properties of Ru(II) mononuclear and Ru(II)-Pd(II) / Ru(II)-Pt(II) hetero-dinuclear complexes based on the polypyridyl bridging ligands. Three main polypyridyl bridging ligands used were, 2,5-di(pyridin-2-yl)pyrazine (2,5-dpp), 2,5-di(pyridin-2-yl)pyridine (2,5-bpp), 2,6-di(pyridin-2-yl)pyridine (2,6-bpp) and 2-(pyridin-2-yl)-5-(6-(pyridin-2-yl)pyridin-3-yl)pyridine (bis-bpy). The structures of these complexes were determined by using one and two dimensional ^{1}H-NMR spectroscopy and elemental analysis. The photophysical properties were studied by UV/Vis absorption and emission spectroscopy. The lifetimes were determined using time correlated single photon count (TCSPC) at room temperature in aerated and deaerated fluorescence measurements. Using partially and fully synthesised deuteriated compounds and measuring their lifetimes it should be possible to determine the location of the excited states. Photocatalytic hydrogen generation experiments were performed e.g. variation in the amount of water and time dependent studies will be discussed next.

1.6 Bibliography

[1] V. Balzani and F. Scandola, "Supramolecular Photochemistry", Ellis Horwood, Chichester, 1991.

[2] R. R. Hautala, R. B. King and C. Kutal, eds. "Solar Energy Chemical Conversion and Storage", Humana Press, Clifton, NJ, 1979.

[3] V. Balzani and F. Scandola, Chapter 23, Photochemical and Photophysical Devices, "Comprehensive Supramolecular Chemistry, Vol. 10, Supramolecular Technology", Elsevier Science, 1996.

[4] A. Kudo and Y. Miseki, Chem. Soc. Rev., 2009, 38, 253.

[5] M. L. Ghirardi, A. Dubini, J. Yu and P.-C. Maness, Chem. Soc. Rev., 2009, 38, 52.

[6] M. Wang, Y. Na, M. Gorlov and L. Sun, Dalton Trans., 2009, 6458.

[7] A. J. Esswein and D. Nocera, Chem. Rev., 2007, 107, 4022.

[8] J.-M. Lehn, Angew. Chem., Int. Ed. Engl., 1998, 27, 89; 1990, 29, 1304.

[9] H. J. Schneider and H. Dürr (eds.) "Frontiers in Supramolecular Organic Chemistry and Photochemistry", VCH, Weinheim, 1991.

[10] F. Vögtle, "Supramolecular Photochemistry", Wiley, Chichester, 1991.

[11] V. Balzani and L. De Cola (eds.) "Supramolecular Photochemistry", Kluwer, Dordrecht, 1992.

[12] V. Balzani and F. Scandola, "Supramolecular Photochemistry", Ellis Horwood, Chichester, 1991, Chapt. 12.

[13] V. Balzani, Tetrahedron, 1992, 48, 10443.

[14] J.-M. Lehn, in "Organic Chemistry: Its Language and Its State of the Art", ed. M. V. Kisakürek, VCH, Weinheim, 1993, p.77.

[15] V. Balzani, F. Bolletta, M. T. Gandolfi and M. Maesteri, Top. Curr. Chem., 1978, 75, 1.

[16] D. Rehm and J. R. Miller, Science, 1988, 240, 440.

[17] R. A. Bissel, A. P. de Silava, H. Q. N. Gunaratne, P. L. M. Lynch, G. E.M. Maguire and K. R. A. S. Sandanayake, Chem. Soc. Rev. 1992, 21, 187.

[18] A. P. de Silva, H. Q. N. Gunaratne and C. P. McCoy, Nature, 1993, 364, 42.

[19] R. A. Bissel, A. P. de Silava, H. Q. N. Gunaratne, P. L. M. Lynch, G. E.M. Maguire, C. P. McCoy and K. R. A. S. Sandanayake, Top. Curr. Chem., 1993, 21, 187.

[20] J. S. Connolly and J. R. Bolton in "Photoinduced Electron Transfer," eds. M. A. Fox and M. Chanon, Part D, Elsevier, New York, 1988, p. 303.

[21] G. L. Closs and J. R. Miller, Science, 1988, 240, 440.

[22] D. Gust and T. A. Moore, Top. Curr. Chem., 1991, 159, 103.

[23] F. Scandola, C. A. Bignozzi and M. T. Indelli, in "Photosensitization and Photocatalysis using Inorganic and Organometallic Compounds," eds. K. Kalyanasundaram and M. Grätzel, Kluwer, Dordrecht, 1993, p. 161.

[24] (a) M. R. Wasielewski, Chem. Rev., 1992, 92, 435; (b) M. R. Wasielewski, in "Photoinduced Electron Transfer," eds. M. A. Fox and M. Chanon, Part, Elsevier, New York, 1988, p. 123.

[25] (a) M. Grätzel, Comments Inorg. Chem., 1991, 12, 93; (b) M. Grätzel and K. Kalyanasundaram, in "Photosensitization and Photocatalysis using Inorganic and Organometallic Compounds," eds. K. Kalyanasundaram and M. Grätzel, Kluwer, Dordrecht, 1993, p. 247.

[26] R. Amadelli, R. Argazzi, C. A. Bignozzi and F. Scandola, J. Am. Chem. Soc., 1990, 112, 7099.

[27] N. Vlachopoulos, P. Liska, J. Augustynski and M. Grätzel, J. Am. Chem. Soc., 1988, 110, 1216.

[28] (a) S. Rau, D. Walther, J. G. Vos, Dalton Trans., 2007, p. 915; (b) J. G. Vos, J. M. Kelly, Dalton Trans., 2006, 41, 2, 4869.

[29] K. Kalyanasundaram, Coord. Chem. Rev., 1982, 46, 159.

[30] A. Juris, V. Balzani, F. Barigelletti, S. Campagna, P. Belser, A. Von. Zelewsky, Coord. Chem. Rev., 1988, 84, 85.

[31] V. Balzani, A. Juris, M. Venturi, S. Campagna, S. Serroni, Chem. Rev., 1996, 96, 759.

[32] J. R. Barrio, G. L. Tolman, N. J. Leonard, R. D. Spencer and G. Weber, Proc Natl. Acad. Sci. USA, 1973, 70, 3, 941.

[33] W. R. Browne, R. Hage, J. G. Vos, Coord. Chem. Rev., 2006, 250, 1653.

[34] E. M. Kober, T. J. Meyer, Inorg. Chem., 1982, 21, 3967.

[35] R. Hage, Ph. D. Thesis, 1991, Leiden University.

[36] J. P. Sauvage, J. P. Collin, J. C. Chambron, S. Guillerez, C. Coudret, V. Balzani, F. Barigelletti, L. De Cola, L. Flamigni, Chem. Rev., 1994, 94, 993.

[37] E.M. Kober, T.J. Meyer, Inorg. Chem., 1983, 22, 1614.

[38] E.M. Kober, T.J. Meyer, Inorg. Chem., 1984, 23, 2098.

[39] A. Von Zelewsky, P. Belser, P. Hayoz, R. Dux, X. Hua, A. Suckling, H. Stoeckli Evans, Coord. Chem. Rev., 1994, 132, 75.

[40] S. D. Ernst, W. Kaim, Inorg. Chem. 1989, 28, 1520.

[41] F. Barigelleti, A. Juris, V. Balzani, P. Belser, A. Von Zelewsky, Inorg. Chem., 1987, 26, 4115.

[42] A. Juris, S. Campagna, V. Balzani, G. Gremaud, A. von Zelewsky, Inorg. Chem., 1988, 27, 3652.

[43] S. Tschierlei, M. Karnahl, M. Presselt, B. Dietzek, J. Guthmuller, L. Gonzalez, M. Schmitt, S. Rau, J. Popp, Angew. Chem., 2010, 49, 1.

[44] B. Gholamkhass, H. Mametsuka, K. Koike, T. Tanabe, M. Furue, O. Ishitani, Inorg. Chem., 2005, 44, 2326.

[45] C. Chiorboli, M. A. J. Rodgers, F. Scandola, J. Am. Chem. Soc., 2003, 125, 483.

[46] F. Barigelletti, L. De Cola, V. Balzani, R. Hage, J. G. Haasnot, J. Reedijk, J. G. Vos, Inorg. Chem., 1989, 28, 4344.

[47] A. Hagfeldt, M. Grätzel, Acc. Chem. Res. 2000, 33, 269.

[48] J. M. Lehn, Chem. Eur. J., 2000, 6, 2097.

[49] D. P. Funeriu, J. M. Lehn, K. M. Fromm, D. Fenske, Chem. Eur. J., 2000, 6, 2103.

[50] L. A. Worl, G. F. Strouse, J. N. Younathan, S. M. Baxter, T. J. Meyer, J. Am. Chem. Soc., 1990, 112, 7571.

[51] S. Rau, M. Ruben, T. Buttner, C. Temme, S. Dautz, H. Gorls, M. Rudolph, D. Walther, A. Brodkorb, M. Duati, C. O'Connor, J. G. Vos, J. Chem. Soc., Dalton Trans., 2000, 3649.

[52] R. Hage, J. G. Haasnoot, J. Reedijk, J. G. Vos, Inorg. Chim. Acta, 1986, 118, 73.

[53] Y. Kawanishi, N. Kitamura, S. Tazuke, Inorg. Chem., 1989, 28, 2968.

[54] G. H. Allan, R. P. White, D. P. Rillema, T. J. Meyer, J. Am. Chem. Soc., 1984, 106, 2613.

[55] E. Simanek and M. Tachiki, Physics Let., 1966, 21, 6, 625.

[56] G. Giuffrida, S. Campagna, Coord. Chem. Rev., 1994, 135/136, 517.

[57] J. M. Lehn; J. P. Sauvage, Nouv. J. Chim., 1977, 1, 449.

[58] K. Kalyanasundaram, J. Kiwi, M. Gratzel, Helv. Chim. Acta., 1978, 61, 2720.

[59] (a) S. Rau, B. Schäfer, D. Gleich, E. Anders, M. Rudolph, M. Friedrich, H. Görls, W. Henry, J.G. Vos, Angew. Chem. Int. Ed., 45, 2006, 6215: (b) S. Tschierlei, M. Karnahl, M. Presselt, B. Dietzek, J. Guthmuller, L. González, M. Schmitt, S. Rau and Jürgen Popp, Angew. Chem. Int. Ed. 2010, 49, 3981: (c) W. R. Browne, J. J. McGarvey, Coord. Chem. Rev. 2006, 250, 1696.

[60] B. Dietzek, W. Kiefer, J. Blumhoff, L. Böttcher, S. Rau, D. Walther,U. Uhlemann, M. Schmitt, J. Popp, Chem. Eur. J., 2006, 12, 5105.

[61] J. Fees, W. Kaim, M. Moscherosch, W. Matheis, J. Klíma, M. Krejčík, S. Záliš, Inorg. Chem. 1993, 32, 166.

[62] H. Ozawa, M. Haga, K. Sakai, J. Am. Chem. Soc., 2006, 128, 4926.

[63] (a) J. A. Weinstein, D. C. Grills, M. Towrie, P. Matousek, A. W. Parkerc and M. W. George, Chem. Commun., 2002, 382; (b) E. J. L. McInnes, R. D. Farley, C. C. Rowlands, A. J. Welch, L. Rovatti and L. J. Yellowlees, J. Chem. Soc., Dalton Trans., 1999, 4203.

[64] S. M. Arachchige, J. R. Brown, E. Chang, A. Jain, D. F. Zigler, K. Rangan and K. J. Brewer, Inorg. Chem., 2009, 48, 1989.

[65] M. Elvington and K. J. Brewer, Inorg. Chem., 2006, 45, 5242.

[66] M. Elvington, J. R. Brown, S. M. Arachchige and K. J. Brewer, J. Am. Chem. Soc. , 2007, 129, 1639.

[67] S. M. Arachchige, J. R. Brown and K. J. Brewer, J. Photochem. Photobiol. A: Chem., 2008, 197, 13.

[68] K. Rangan, S. M. Arachchige, J. R. Brown, K. J. Brewer, J. Energy Environ. Sci, 2009, 2, 410.

[69] D. R. Lide, ed., 'CRC Handbook of Chemistry and Physics, 88th edition (Internet Version 2008), CRC press/ Taylor and Francis, Boca Raton, 2008.

[70] G. M. Brown, B. S. Brunschwig, C. Creutz, J. F. Endicott and N. Sutin, J. Am. Chem. Soc., 1979, 101, 1298.

[71] P. Du, K. Knowles and R. Eisenberg, J. Am. Chem. Soc., 2008, 130, 12576.

[72] A. Fihri, V. Artero, M. Razavet, C. Baffert, W. Leibl and M. Fontecave, Angew. Chem. Int. Ed., 2008, 47, 564.

[73] A. Fihri, V. Artero, A. Pereira and M. Fontecave, Dalton Trans., 2008. 5567.

[74] U. Kölle, New J. Chem., 1992, 16, 157.

[75] P. Lei, M. Hedlund, R. Lomoth, H. Rensmo, O. Johansson and L. Hammerström, J. Am. Chem. Soc., 2008, 130, 26.

[76] E. Amouyal, Sol. Energy Mater. Sol. Cells, 1995, 38, 249.

[77] M. Y. Darensbourg. E. J. Lyon and J. J. Smee, Coord. Chem. Rev., 2000, 206-207, 533.

[78] T. J. McDonald, D. Svedruzic, Y, -H, Kim, J. L. Blackburn, S. B. Zhang, P. W. King, and M. J. Heben, Nano Lett., 2007, 7, 3528.

[79] (a) E. Reisner, J. C. Fontecilla-Camps, F. A. Armstrong, Chem. Commun., 2009, 550; (b) E. Reisner, D. J. Powell, C. Cavazza, J. C. Fontecilla-Camps, F. A. Armstrong, J. Am. Chem. Soc., 2009, 131, 18457; (c) F. Lakadamyali and E. Reisner, Chem. Commun., 2011, 47, 1695.

[80] S. Ardo and G. J. Meyer, Chem. Soc. Rev., 2009, 38, 115.

[81] A. Fujishima and K. Honda, Nature, 1972, 238, 37.

[82] M. Ni, M. K. H. Leung, D. Y. C. Leung and K. Sumathy, Renwable and Sustainable Energy Rev., 2007, 11, 401.

[83] X. Wang, K. Maeda, A. Thomas, K. Takanabe, G. Xin, J. M. Carlsson, K. Domen and M. Antonietti, Nat. Mater., 2009, 8, 76.

[84] N. S. Lewis, Inorg. Chem., 2005, 44, 6900.

[85] (a) S. Y. Reece, J. A. Hamel, K. Sung, T. D. Jarvi, A. J. Esswein, J. J. H. Pijpers, D. G. Nocera, Science, 2011, 334, 645; (b) B. O'Regan, M. Grätzel, Nature, 1991, 353, 737.

[86] J.-H, Yum, P. Chen, M. Grätzel, M. K. Nazeeruddin, ChemSusChem., 2008, 1, 699.

[87] W. Kim, T. Tachikawa, T. Majima, W. Choi, J. Phys. Chem. C, 2009, 113, 10603.

[88] J. W. Peters, W. N. Lanzilotta, B. J. Lemon, L. C. Seefeldt, Science, 1998, 282, 1853.

[89] F. Gloaguen, J. D. Lawrence, T. B. Rauchfuss, J. Am. Chem. Soc., 2001, 123, 1853.

[90] X. Li, M. Wang, S. Zhang, J. Pan, Y. Na, J. Liu, B. Akermark and L. Sun, J. Phys. Chem. B., 2008, 112, 8198.

[91] Y. Miyake, K. Nakajima, K. Sasaki, R. Saito, H. Nakanishi and Y. Nishibayashi, Organometallics, 2009, 28, 5240.

[92] A. F. Heyduk and D. G. Nocera, Science, 2001, 293, 1639.

[93] A. J. Esswein, A. S. Veige and D. G. Nocera, J. Am. Chem. Soc., 2005, 127, 16641.

[94] A. J. Esswein, J. L. Dempsey and D. G. Nocera, Inorg. Chem., 2007, 46, 2362.

[95] T. R. Cook, A. J. Esswein and D. G. Nocera, J. Am. Chem. Soc., 2007, 129, 10094.

[96] A. J. Esswein and D. G. Nocera, Chem. Rev. 2007**,** 107, 4022.

[97] Matthew P. McLaughlin, Theresa M. McCormick, Richard Eisenberg and Patrick L. Holland, Chem. Comm., 2011, Advance Article DOI: 10.1039/C1CC12347E.

[98] M. Rakowski DuBois and D. L. DuBois, Acc. Chem. Res., 2009, 42, 1974.

[99] M. Rakowski DuBois and D. L. DuBois, Chem. Soc. Rev., 2009, 38, 62.

[100] A. D. Wilson, R. H. Newell, M. J. McNevin, J. T. Muckerman, M. DuBois and D. L. DuBois, J. Am. Chem. Soc., 2005, 128, 358.

[101] T. Lazarides, T. McCormick, P. Du, G. Luo, B. Lindley and R. Eisenberg, J. Am. Chem. Soc., 2009, 131, 9192.

[102] E. Zahavy and I. Willner, J. Am. Chem. Soc., 1995, 117, 10581.

[103] B. Girginer, G. Galli, E. Chiellini and N. Bicak, Int. J. Hydrogen Energy, 2009, 34, 1176.

[104] K. Maeda, M. Higashi, D. Lu, R. Abe and K. Domen, J. Am. Chem. Soc., 2010, 132, 5858.

[105] T. Nann, S. K. Ibrahim, P.-M. Woi, S. Xu, J. Ziegler and C. J. Pickett, Angew. Chem., Int. Ed., 2010, 49, 1574.

[106] F. Zuo, L. Wang, T. Wu, Z. Zhang, D. Borchardt and P. Feng, J. Am. Chem. Soc., 2010, 132, 11856.

[107] L. Sun, B. Åkermark and S. Ott, Coord. Chem. Rev., 2005, 249, 1653.

[108] C. E. Lubner, R. Grimme, D. A. Bryant and J. H. Golbeck, Biochemistry, 2009, 49, 404.

[109] T. M. McCormick, B. D. Calitree, A. Orchard, N. D. Kraut, F. V. Bright, M. R. Detty and R. Eisenberg, J. Am. Chem. Soc., 2010, 132, 15480.

[110] P. Zhang, M. Wang, Y. Na, X. Li, Y. Jiang and L. Sun, Dalton Trans., 2010, 39, 1204.

[111] P. Du, J. Schneider, G. Luo, W. W. Brennessel and R. Eisenberg, Inorg. Chem., 2009, 48, 4952.

[112] S. Metz and S. Bernhard, Chem. Comm.., 2010, 46, 7551.

[113] M. S. Lowry, W. R. Hudson, R. A. Pascal, Jr. and S. Bernhard, J. Am. Chem. Soc., 2004, 126, 14129.

[114] P. N. Curtin, L. L. Tinker, C. M. Burgess, E. D. Cline and S. Bernhard, Inorg. Chem., 2009, 48, 10498–11506

[115] C.-W. Chen, D. Tano and M. Akashi, Colloid Polym. Sci., 1999, 277, 488.

[116] H. D. Abruña, P. Denisevich, M. Umaña, T. J. Meyer and R. W. Murray, J. Am. Chem. Soc., 1981, 103, 1 ; J. M. Calvert, R. H. Schmehl, B. P. Sullivan, J. S. Facci, T. J. Meyer and R. W. Murray, Inorg. Chem., 1983, 22, 2151.

[117] F. Gärtner, D. Cozzula, S. Losse, A. Boddien, G. Anilkumar, H. Junge, T. Schulz, N. Marquet, A. Spannenberg, S. Gladiali, and M. Beller, Chem. Eur. J. 2011, 17, 6998.

[118] M. Wang, L. Sun, ChemSusChem, 2010, 3, 551.

[119] Y. Na, M. Wang, J. Pan, P. Zhang, B. Åkermark, L. Sun, Inorg. Chem. 2008, 47, 2805–2810; D. Streich, Y. Astuti, M. Orlandi, L. Schwartz, R. Lomoth, L. Hammarström, S. Ott, Chem. Eur. J. 2010, 16, 60.

[120] F. Gärtner, B. Sundararaju, A.-E. Surkus, A. Boddien, B. Loges, H. Junge, P. H. Dixneuf, M. Beller, Angew. Chem., 2009, 121, 10147.

[121] F. Gärtner, A. Boddien, D. Hollmann, E. Barsch, K. Fumino, H. Junge, R. Ludwig, A. Brückner, M. Beller, Chem. Eur. J., 2011, 17, 6425.

Chapter 2: Instrumental & Experimental Techniques

Abstract:

This chapter introduces the instrumental methods used throughout this thesis for the identification of the compounds synthesised. The methods of characterisation were ^{1}H-NMR and elemental analysis while UV-Visible absorption, emission, luminescence lifetimes, photocatalytic experiments, gas chromatography headspace analysis and electrochemistry were recorded to detail the properties of these compounds. The synthesis of starting materials used in further chapters is also detailed.

2.1 Instrumental Methods.

2.1.1 Structural Characterization.

Proton Nuclear Magnetic Resonance Spectroscopy (^{1}H-NMR)

^{1}H-NMR (400 MHz) spectra were obtained on a Bruker Advance 400 NMR Spectrometer in deuteriated solvents with either TMS (trimethylsilane) or residual solvents peaks as reference. Free induction decay (FID) profiles were processed using a TOPSPIN-NMR and ACD-1D/2D NMR processor software packages. The 2D correlated spectroscopy (^{1}H-NMR COSY) experiments involved the accumulation of 128 FIDs of 16 Scans. The solvents used for the ruthenium complexes were deuteriated acetonitrile and for the ligands were deuteriated chloroform / dimethyl sulphoxide.

Elemental Analysis

Carbon, Hydrogen and Nitrogen (CHN) elemental analyses were carried out on an Exador Analytical CE440 by Microanalytical Department, University College Dublin, Ireland.

When calculating the percentage of Hydrogen for deuterium containing compounds, the mass of the whole compound including deuterium is calculated. The mass of hydrogen (M = 1 a.m.u) atom and where as deuterium (M = 2 a.m.u) atom counts as one hydrogen atomic mass unit, are added together and divided by the overall mass of the compound. The percentage of hydrogen in deuterium containing compounds will be generally little lower than in their non-deuterium containing analogues.

Ultra-Violet/ Visible Spectroscopy (UV/Vis)

UV/vis absorption spectra in the region between 200 and 800 nm were obtained by using a Varian Cary 50 spectrophotometer. The spectra were recorded in spectrophotometric grade acetonitrile solution at room temperature. The error associated with the absorption spectra is ± 2 nm with molar absorptivities ± 10 %. The extinction coefficients were determined by preparing a dilution series from a stock solution with a known concentration. The stock solutions were prepared by diluting 10.00 mg of the particular compounds in 25 ml of acetonitrile in a volumetric flask.

2.1.2 Photophysical and Electrochemical Characterizations.

Emission Spectra

Emission spectra at room temperature were recorded in spectroscopy grade solvents on a Perkin-Elmer LS50B luminescence spectrometer equipped with a red sensitive Hamamatsu R928 detector: this was interfaced with an Elonex-466 PC using windows based fluorescence software. Measurements at room temperature were carried out in 1 cm quartz cells. The error associated with the emission spectra is ± 5 nm.

Measurements at 77 K, were recorded in a rigid matrix of ethanol and methanol (4:1 volume ratio). Due to the range of the detector it was not possible to record emission above 850 nm. The spectroscopy grade ethanol and methanol were used. The error associated with the emission spectra is ± 5 nm. The emission quantum yields were measured in de-aerated acetonitrile solution by absorbance matching at the wavelength of excitation respectively to the $[Ru(bpy)_3]^{2+}$ standard with quantum yield, $\Phi = 0.06$.[1]

Electrochemistry

All cyclic voltammetry experiments were carried out by Ms. Jane Inglis and reported in her thesis at Dublin City University, Dublin, Ireland. Cyclic voltammetry was carried out in CH_3CN with a 0.1 M $TBABF_4$ using a CH instruments CHI Versions 2.07 software controlled potentiostat (CH instrument Memphis 660). A conventional 3-electrode cell was used. A 2 mm Pt electrode was used as the working electrode, the counter electrode was coiled Pt wire and a Ag/ Ag^+ was used as a reference electrode. The solutions were degassed with an argon gas (Ar) and a blanket of argon was kept over the electrolyte during the experiment. All glassware was dried in a vacuum oven at 70^0C. The electrode were polished on a soft polishing pad with aqueous slurry of 0.3 micron alumina and sonicated for 5 minutes in Mill-Q water to remove any remaining of polishing material from the surface of the electrode. Redox potentials are ± 10 mV. The reference electrode was calibrated externally by carrying out cyclic voltammetry in solutions of ferrocene of the same concentration as that of the complexes in the same electrolyte. The results obtained were compared with the

previous studies on similar complexes using different electrodes by using conversion values obtained from the literature.[2]

Luminescent Lifetime Measurements

Lifetime measurements were performed on an Edinburgh Analytical Instrument single photon counter with a T setting, using a lamp (nF900, in a nitrogen setting), monochromators, with a single photo photomultiplier detection system (model S 300), an MCA card (Norland N500) and PC interface (Cd900 serial). Data correlation and manipulation was carried out using the program F900, Version 5.13. The samples were excited using 360 nm as the excitation wavelength and the lifetime were collected at the maxima of the emission. The uncertainty associated with the luminescence lifetime is ± 10 %.

2.2 Gas chromatography & Photocatalysis Analysis.

Gas Chromatography

The hydrogen evolved was measured by headspace gas chromatogram on a Varian CP3800 chromatograph, with a thermal conductivity detector (TCD) and a CP7536 Plot Fused Silica 25 MX 0.32 MMID column (length 25 m, layer thickness 30 μm) with nitrogen as carrier gas (purity 99.999 %). The GC was calibrated by 100 ppm, 1000 ppm and 10,000 ppm hydrogen gas standard mixture in a sealed container were injecting (20μl) into GC by using a gas tight syringe (50 μl volume, bevel shaped needle from SGE Co.). After irradiation of reaction vials, 20 μl gas samples were drawn from the headspace and injected immediately into the GC apparatus. The obtained signal (retention time of H_2 = 1.59 min) was plotted against the calibration curve and multiplied accordingly to receive the total produced hydrogen content in the headspace (see figure 2.1 (a) calibration curve containing 100 ppm, 1000 ppm and 10,000 ppm gas mixture of Hydrogen gas (b) For Area calculation, 99.999 % hydrogen (20 μl) gas sample). Irradiation experiments and hydrogen measurements were repeated several times for an average value of every other photocatalysts.

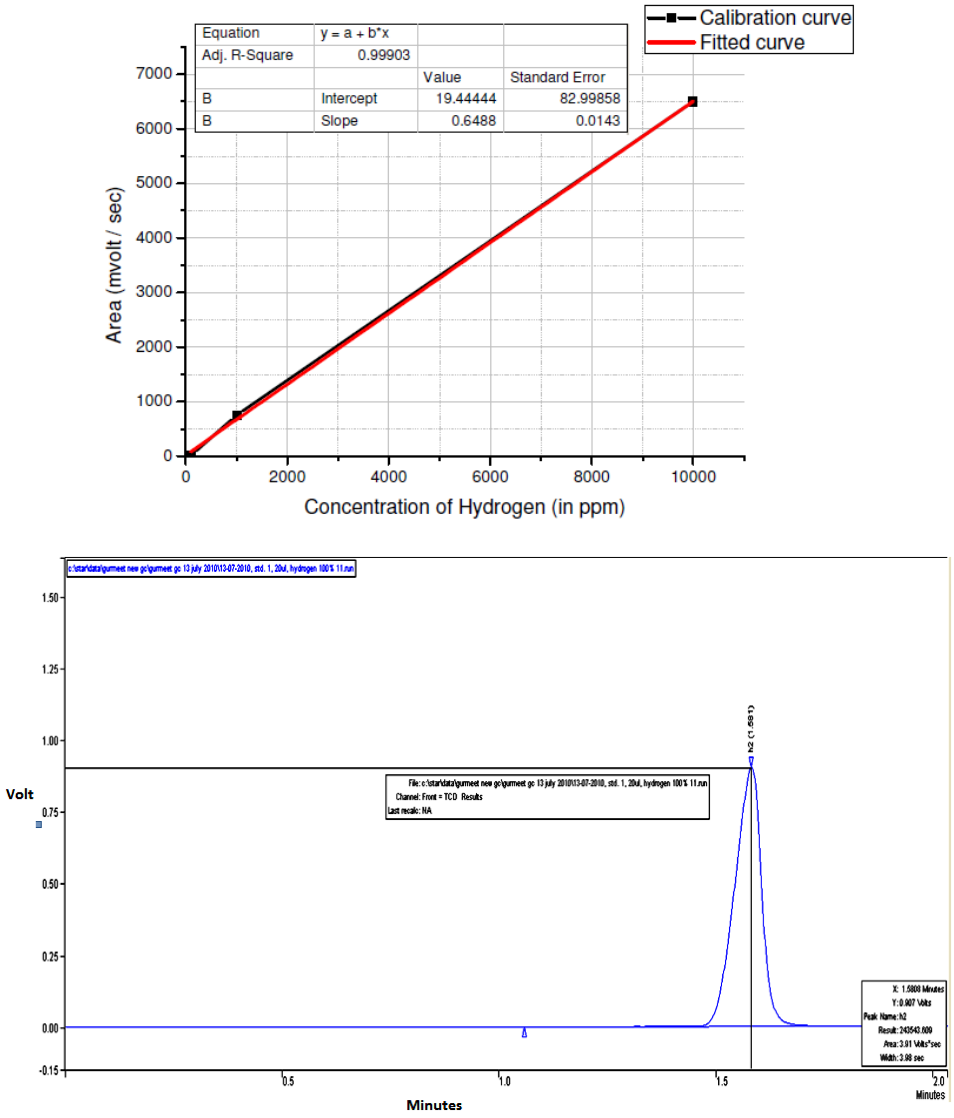

Figure 2.1: *(a) Calibration curve containing 100 ppm, 1000 ppm and 10,000 ppm of hydrogen gas (above) (b) For Area calculation of 99.999 % hydrogen gas, 20µl sample injected (below).*

Photolcatalytic experiments

Photocatalytic hydrogen production experiments were carried out using a home-built air-cooling apparatus for maintaining room temperature (22°C) under constant irradiation of the sample shown in figure 2.2. The acetonitrile used was dried over calcium hydride and the triethylamine dried over sodium before being freshly distilled under nitrogen. The samples for the laser irradiation experiments were prepared in GC vials (diameter = 13 mm, 5 cm^3 volume with Teflon/PTFE septa cap from VWR Co.)

with a known headspace of 3 cm^3 and a headspace-solution ratio of 3/2. Furthermore the GC vials were charged in the dark and under nitrogen stream. A typical sample solution was prepared by mixing 0.1 ml of a $8.16 \cdot 10^{-4}$ M ($1.2 \cdot 10^{-3}$ M) catalyst solution in acetonitrile, 0.6 ml of triethylamine, 0.1 ml (5 vol. %) or {(0.2 ml for 10 vol. %), (0.3 ml for 15 vol. %)} of thoroughly degased water and 1.2 ml (5 vol. %) or {(1.1 ml for 10 vol. %), (1.0 ml for 15 vol. %)} of anhydrous acetonitrile. Final Concentration of photocatalysts is $4.08 \cdot 10^{-5}$ M ($6.0 \cdot 10^{-5}$ M). Subsequently, the GC vials were irradiated with 470 nm wavelength LED'S for 18 hours.

LED-Torch

The LED-torch consists of a stick-shaped printed board (length 19 cm, breadth 1 cm). At its end, 30 LEDs (manufacturer: Kingbright, type L-7113PBC-G blue, light emission: 470 ± 20 nm, luminous efficiency: 2000 mcd per LED) are soldered on front and backside in a range of 9 cm (see figure 2.2). The torch can be placed within the home built reactor.

Figure 2.2: *Equipment for the examination of the Photocatalysis; on the left, the photo reactor with air ventilation; on the right, the blue LED-torch.*

2.3 General Synthetic Materials.

The $Pd(PPh_3)_4$ and nickel catalyst along with anhydrous solvents were purchased from Aldrich. Column chromatography was performed using neutral activated aluminium oxide (150 mesh) or silicone oxide (35-70 µm). All synthetic reagents

were of commercial grade and no further purification was employed. The compounds 2,2'-bipyridine (bpy), $RuCl_3.xH_2O$, 2-pyridylzinc bromide, 2,5-dibromobipyridine and 2,2':6',2''-Terpyridine (2,6-bpp) were purchased from Aldrich and used without further purification. The compounds $Pd(CH_3CN)Cl_2$, $Pt(CH_3CN)Cl_2$, K_2PtCl_4 and $(NH_4)_2PdCl_4$ were purchased from Aldrich. The compound $Pt(DMSO)_2Cl_2$ was synthesized by dissolving K_2PtCl_4 in excess of dimethyl sulphoxide (DMSO) and stirred for 1 hour at room temperature. The complex was precipitated as a white crystalline solid. The ligand 4,4'-carboxy-ethylester-2,2'-bipyridine (dceb) was prepared as described in the literature using ethanol instead of methanol as a solvent.[3, 4]

2.3.1 Synthesis of Starting Materials.

Cis-[Ru(bpy)$_2$Cl$_2$]·2H$_2$O

This procedure has been modified slightly to that described by Meyer et al.[5]

2,2'-bipyridine ($3x10^{-2}$ mol, 4.68 g), $RuCl_3·3H_2O$ ($1.5x10^{-2}$ mol, 3.90 g) and LiCl (0.10 mol, 4.30 g) were placed in 20 ml of anhydrous DMF and refluxed for 8 hours under a nitrogen atmosphere. The deep purple solution was then cooled down to room temperature and poured into 125 ml of acetone and left overnight at – 4°C. The violet crystals were recovered by vacuum filtration, washed with a small amount of cold water and diethyl-ether and air dried.

Yield: 6.77 g, $1.3x10^{-2}$ mol, 87%.

^{1}H-NMR (DMSO-d^6): 9.97 (d, 2H, J = 4.8 Hz), 8.64 (d, 2H, J = 8.4 Hz), 8.49 (d, 2H, J = 8.0 Hz), 8.07 (t, 2H, J = 7.8 Hz), 7.77 (t, 2H, J = 6.4 Hz), 7.68 (t, 2H, J = 7.8 Hz), 7.51 (d, 2H, J = 5.6 Hz), 7.10 (t, 2H, J = 6.4 Hz).

Cis-[Ru(dceb)$_2$Cl$_2$]·2H$_2$O

This procedure has been modified to that described by rau and brewer et al.[6]

4,4'-carboxy-ethylester-2,2'-bipyridine ($3x10^{-2}$ mol, 9.02 g), $RuCl_3·3H_2O$ ($1.5x10^{-2}$ mol, 3.90 g) and LiCl (0.10 mol, 4.30 g) were placed in 20 ml of anhydrous DMF and refluxed for 8 hours under a nitrogen atmosphere. The dark green solution was then cooled down to room temperature and poured into 125 ml of acetone and left overnight at – 4°C. The dark green crystals were recovered by vacuum filtration, washed with a small amount of cold water and diethyl-ether and air dried.

Yield: 11.4 g, $1.4x10^{-2}$ mol, 93%.

^{1}H-NMR (CD_2Cl_2): 10.17 (d, 2H, J = 5.7 Hz), 8.75 (d, 2H, J = 1.8 Hz), 8.59 (d, 2H, J = 1.8 Hz), 8.05 (d, 2H, J = 5.7 Hz), 7.56 (d, 2 H, J = 5.7 Hz), 7.37 (d, 2H, J = 5.7 Hz), 4.45 (8H, m), 1.38 (12H, m).

Cis-[Ru(d_8-bpy)$_2$Cl$_2$]·2H$_2$O

This procedure has been modified slightly to that described for the non-deuteriated analogue, by Meyer et al.[5]

Deuteriated d_8-2,2'-bipyridine ($3x10^{-2}$ mol, 4.86 g), commercial $RuCl_3 \cdot 3H_2O$ ($1.5 x10^{-2}$ mol, 3.90 g) and LiCl (0.10 mol, 4.30 g) were placed in 25 ml of anhydrous DMF and refluxed for 8 hours under a nitrogen atmosphere. The deep purple solution was then cooled down to room temperature and poured into 125 ml of acetone was added and left overnight at – 4°C. The violet crystals were recovered by vacuum filtration, washed with a small amount of cold water and diethyl-ether and air dried.

Yield: 5.79 g, $1.0x10^{-2}$ mol, 67%. ^{1}H-NMR (DMSO-d6): 9.97 (s, 2H), 8.64 (s, 2H), 8.49 (s, 2H), 8.07 (s, 2H), 7.77 (s, 1H), 7.68 (s, 2H), 7.51 (s, 2H), 7.10 (s, 2H).

2.3.2 Synthesis of Bridging Ligands.

1). 2,5-di(pyridine-2-yl)pyrazine (2,5-dpp). This ligand was prepared in three steps.[7, 8]

Step 1: Synthesis of 2-acetylpyridine oxime.

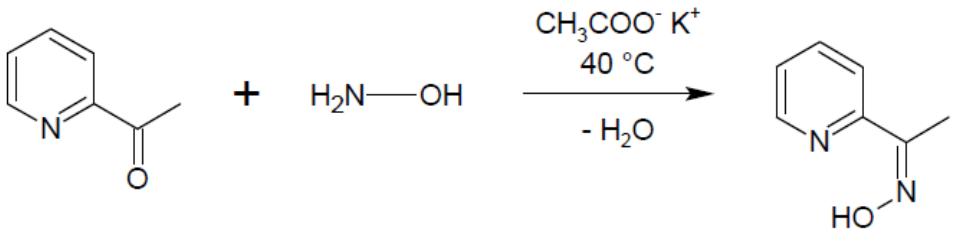

To a solution of NH_2OH (2.86g, 0.0412mol) dissolved in distilled water, excess of potassium acetate (4.0g, 0.0412mol) and 2-acetylpyridine (5.0g, 0.0412mol) was added. The reaction mixture was stirred for 1 hour at room temperature. The crude product was precipitated as a white solid and recrystallised from ethanol/ water (3:1) as colourless needle shape crystals. Yield= 5.53g, 0.0406 mol, 98%. NMR ($CDCl_3$,

400MHz) =2.43 (3H, s, CH_3), 7.29 (1H, t, J = 4.96, 6.28 Hz, ArH), 7.73 (1H, t, J = 6.40, 7.64 Hz, ArH), 7.88 (1H, d, J = 7.84 Hz, ArH), 8.68 (1H, d, J = 4.72 Hz, ArH), 9.91 (1H, s, C=N-OH).

Step 2: Synthesis of 2-acetylpyridine-oxime-O-(p-toluenesulphonyl ester).

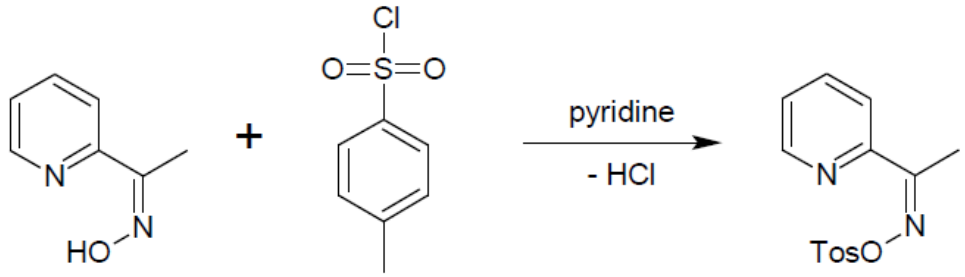

2-Acetylpyridine-oxime (10.0g, 0.073 mol) was dissolved in pyridine (10ml), kept in an ice bath and treated with finely powdered p-toluenesulphonyl chloride (15.3g, 0.081mol). The mixture was kept for 3 hours at room temperature and then poured into a mixture of ice and water. The 2-acetylpyridine-oxime-O-(p-toluenesulphonyl ester was precipitated out as a white solid, filtered off, vacuum dried and crystallised from ethyl alcohol / water (3:1). Yield= 18.8g, 0.064mol, 88.8%. ^{1}H-NMR ($CDCl_3$, 400MHz) = 2.46 (6H, s, $2CH_3$), 7.34 (1H, t, J = 4.96, 6.28 Hz, ArH), 7.37 (2H, J=6.30 Hz), 7.71 (1H, t, J = 6.40, 7.64 Hz, ArH), 7.95 (2H, J=6.30 Hz), 8.62 (1H, d, J = 4.72 Hz, ArH).

Step 3: Synthesis of 2,5-di(pyridine-2-yl)pyrazine (2,5-dpp).

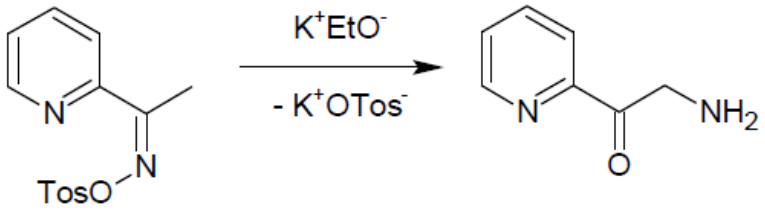

The mixture was shaken for 1 hour, and the precipitate of potassium p-toluenesulphonate removed. The filtrate was diluted with excess of dry ether, and a further precipitate of the potassium p-toluenesulphonate salt filtered off. The filtrate was extracted three times with 2M hydrochloric acid (3 x 50 ml). The aqueous layer became yellow and separated from the organic layer.

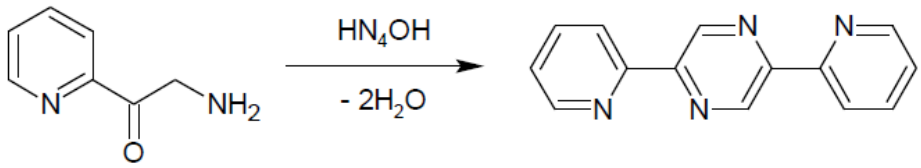

To the aqueous acid yellow layer was added an excess of conc. ammonium hydroxide solution (200 ml). The reaction mixture was stirred for 24 hours at room temperature. The crude product was precipitated out as a orange coloured compound 2,5-di(pyridine-2-yl)pyrazine (2,5-dpp) and recrystallised from ethanol / water (3:1). Yield= 1.9g, 0.0081mol, 13 %. ^{1}H-NMR ($CDCl_3$, 400MHz) = 7.31 (2H, t, J = 4.96, 6.28 Hz, ArH), 7.81 (2H, t, J = 6.40, 7.64 Hz, ArH), 8.38 (2H, d, J = 7.84 Hz, ArH), 8.68 (2H, d, J = 4.72 Hz, ArH), 9.59 (2H, s, ArH).

2). Synthesis of 2,2':5',5":2",2"'-quaterpyridine (bisbpy) [9, 10, 11] (see Scheme 1)

Step 1: Synthesis of 5-bromo-2,2'-bipyridine (5-brbpy).[11]

In a dried two neck round bottom flask $Pd(PPh_3)_4$ (0.3 gm, 0.26 mmol) and 2,5-dibromobipyridine (2.0 gm, 8.44 mmol) were added under a nitrogen atmosphere. During the addition of 2-pyridylzinc bromide (19.4 ml, 8.44 mmol) to the reaction mixture, the temperature was kept at 0^0C. The reaction mixture was then stirred over night at room temperature under a nitrogen atmosphere and a white precipitate was formed. The reaction mixture was poured in 200 ml of a saturated aqueous solution of equimolar EDTA and Na_2CO_3 and stirred until the white precipitate dissolved and a yellow precipitate formed. The aqueous solution and the precipitate were extracted with dichloromethane (3 x 50 ml) and the combined organic phase was dried over $MgSO_4$. The dichloromethane was allowed to evaporate off and the crude product was purified by column chromatography (neutral alumina, hexane/ethyl acetate (9.5 : 0.5 v/v), TLC: R_f = 0.2). The second spot in TLC was the desired product. Yield: 1.6 gm (6.80 mmol, 81%). ^{1}H-NMR (DMSO-d_6, 400 MHz): δ = 7.49 (t, 1H), 7.97 (t, 1H, J = 7.8 Hz), 8.21 (d, 1H, J = 8.3 Hz), 8.37 – 8.33 (m, 2H), 8.70 (d, 1H, J = 7.6 Hz), 8.82 (s, 1H).

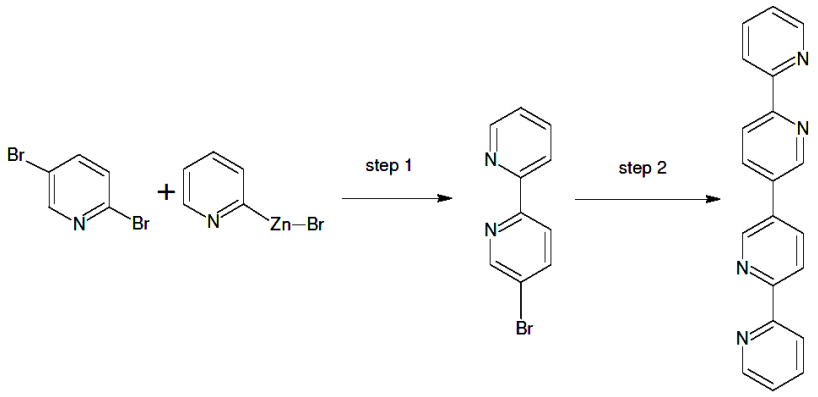

Scheme 1: *Step wise synthesis of 2,2':5',5":2",2"'-quaterpyridine (bisbpy).*

Step 2: Synthesis of 2,2':5',5":2",2"'-quaterpyridine (bisbpy).

A solid $[Ni(PPh_3)_2Cl_2]$ (0.557 g, 0.85 mmol) was taken in 10 ml of anhydrous DMF and stirred for few minutes at 20°C degassing nitrogen through the solution until the blue reaction mixture was formed. Then into the blue reaction mixture zinc powder (Zn) (0.056 g, 0.85 mmol) was added and stirred at 20°C degassing nitrogen through the solution. The reaction mixture was turned green from blue and then ultimately the solution was turned deep brown from green solution after 30 to 45 minutes. Now 5-bromo-2,2'-bipyridine (5-brbpy) (0.200 g, 0.85 mmol) was added and the reaction mixture was stirred at room temperature under nitrogen atmosphere for 10 hours. The completion of the reaction was checked by TLC (neutral alumina, hexane/ethyl acetate (9 : 1 v/v). The reaction mixture was poured in 150 ml of 3 molar aqueous NH_4OH solutions. A greyish white product was precipitated out. The aqueous solution and the precipitate were extracted with ethyl acetate (3 x 50 ml) and the combined organic phase was dried over $MgSO_4$. Removal of the solvent in vacuo yielded the crude product which purified by column chromatography (neutral alumina, hexane/ethyl acetate (9 : 1 v/v), TLC: $R_f = 0.1$).

Yield: 0.205 g (0.66 mmol, 78%).

^{1}H-NMR (DMSO-d_6, 400 MHz): δ = 7.50 (ddd, 2H, J = 7.6 Hz, J = 4.80 Hz, J = 1.77 Hz, J = 1.01 Hz), 8.00 (ddd, 2H, J = 7.83, J = 1.77 Hz), 8.43 (dd, 2H, J = 8.34, J = 2.53 Hz), 8.46 (dd, 2H, J = 7.83, J = 1.01 Hz), 8.54 (dd, 2H, J = 8.08, J = 0.76 Hz), 8.72 (dd, 2H, J = 4.80, J = 0.76 Hz), 9.18 (d, 2H, J = 2.53 Hz).

2). *Synthesis of bridging ligand (2,2':5',2''-terpyridine) (2,5-bpp), (see Scheme 2).*

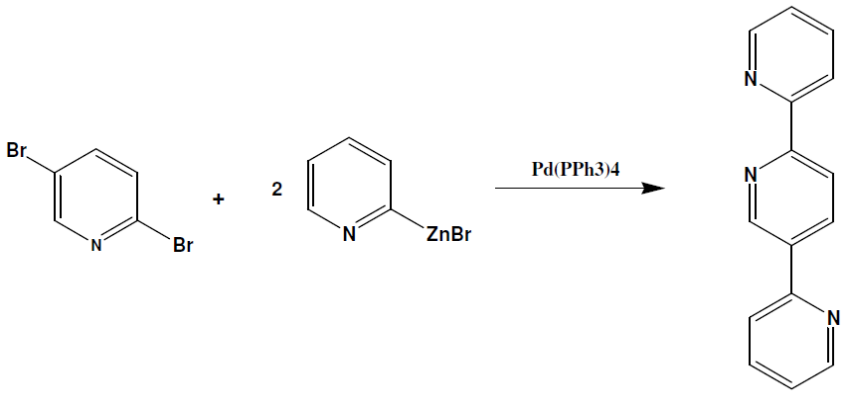

Scheme 2: *Synthesis of bridging ligand (2,2':5',2''-terpyridine) (2,5-bpp).*

The bridging ligand was synthesised differently from that reported by V. N. Kozhevnikov et al.[12, 13] In a dried two neck round bottom flask was added $Pd(PPh_3)_4$ (0.299 gm, 0.258 mmol) and 2,5-dibromobipyridine (1.0 gm, 4.22 mmol) under a nitrogen atmosphere at 0°C. To the reaction flask was added 2-pyridylzinc bromide (19.35 ml, 8.44 mmol) and the temperature was kept constant at 0°C during addition. The reaction mixture was stirred for 12 hours at room temperature under a nitrogen atmosphere and a white precipitate formed. The reaction mixture was poured in a saturated aqueous solution of EDTA and Na_2CO_3 until the precipitate dissolved and a yellow precipitate formed. The aqueous solution and the precipitate were extracted with dichloro-methane, dried over solid $MgSO_4$ and evaporated under vacuum. The crude product was purified on a neutral alumina column using hexane/ethyl acetate (9.5 : 0.5). The second spot in TLC (R_f = 0.15) shown was the desired product.

Yield: 505 mg (2.15 mmol, 51%). Anal. Calcd. for $C_{15}H_{11}N_3.(0.1\ C_2H_5OOCCH_3)$: C, 76.41; H, 4.91; N, 17.36%. Found: C, 76.60; H, 4.91; N, 17.31%.

^{1}H-NMR (DMSO-d_6, 400MHz) δ: 7.48 (m, 2H), 7.98 (m, 2H), 8.15 (d, J = 8.1 Hz, 1H), 8.47 (d, J = 7.8 Hz, 1H), 8.52 (d, J = 8.3 Hz, 1H), 8.62 (dd, J = 8.5 Hz, J = 2.1 Hz, 1H), 8.74 (m, 2H), 9.40 (d, J = 2.3 Hz, 1H).

2.3.3 Synthesis of Deuteriated Ligands.

Calculation of the Percentage Deuteriation Amount Percenatge

To estimate the relative deuteriated amount % of one sample, the ^{1}H-NMR spectra of both the deuteriated and the protonated species were compared. Hereby it is very

important that the spectra of both samples are recorded by using the same amount of substance and solvent. First the ^{1}H-NMR spectrum of the protonated sample is examined. The integral of the solvent peak is set as 1, whereas the resonances of the substance get the emanating values. Thus the ratio of the relative number of hydrogen of the compound to that of the deuteriated solvent is determined. Afterwards the same step is repeated in the spectrum of the deuteriated species. However the signals are only caused by the small amount of hydrogen remaining in the sample. Therefore by subtraction of the ratio estimated for the deuterated species from the ratio of the protonated sample results in the ratio of deuterated species. The amount of deuterated species in percent is easily calculated by dividing the ratio of deuteriated species by the ratio determined in the spectrum of the protonated sample. All the deuteriation experiments were carried out in a steel container with a Teflon liner.

Deuteriation of 2,2'-bipyridine

This procedure has been modified to that described for the deuteriated analogue, by Browne *et. al.*[14]

2,2'-bipyridine (1.5 g, 9.6 mmol) was reacted with 20 ml of 1 M NaOD/D_2O at 200° C in a sealed chamber for 6 days. The 1.0 M NaOD/D_2O solution was prepared by slowly adding (460 mg, 0.02 mol) of metallic sodium to 20 ml of D_2O. After cooling the reaction mixture was neutralized with aqueous HCl, extracted with CH_2Cl_2, and the organic phase was evaporated yielding a white solid.

Yield: 1.33 g (8.16 mmol, 85 %), deuteriated amount 98%.

^{1}H-NMR (400 MHz, $CDCl_3$): 8.63 (s, 2H), 8.36 (s, 2H), 7.77 (s, 2H), 7.26 (s, 2H).

Deuteriation of 2,5-bis(2-pyridyl)pyrazine (2,5-dpp)

2,5-bis(2-pyridyl)pyrazine (2,5-dpp) (150 mg, 6.4 mmol) was reacted with 20 ml of 1 M NaOD/D_2O at 200° C in a sealed chamber for 6 days. The 1 M NaOD/D2O solution was prepared by slowly adding (460 mg, 0.02 mol) of metallic sodium to 20 ml of D_2O. After cooling the reaction mixture was neutralized with aqueous HCl, extracted with CH_2Cl_2, and the organic phase was evaporated yielding yellow solid.

Yield: 66 mg (2.7 mmol, 42 %), deuteriated amount 99%.

Elemental analysis (CHN): calculated C = 68.85, H = 4.09, N = 22.95, found C = 68.71, H = 4.32, N = 22.64. ^{1}H-NMR (400 MHz, $CDCl_3$): 9.59 (s, 2H), 8.68 (s, 2H), 8.38 (s, 2H), 7.80 (s, 2H), 7.31 (s, 2H).

2.4 Bibliography.

[1] M. Montalti, A. Credi, L. Prodi, M. T. Gandolfi, Handbook of Photochemistry, 2006, CRC Press (Taylor and Francis group), 10, 574.

[2] V. V. Pavlishchuk, A. W. Addison, Inorg. Chim. Acta, 2000, 298, 97.

[3] A. R. Oki, R. J. Morgan, Synth. Commun. 1995, 25, 4093.

[4] K. Wiederholt, L. W. McLaughlin, Nucleic Acids Res. 1999, 27, 2487–2493.

[5] B. P. Sullivan, D. J. Salmon, T. J. Meyer, Inorg. Chem., 1978, 17, 3334.

[6] (a) M. Schwalbe, B. Schäfer, H. Görls, S. Rau, S. Tschierlei, M. Schmitt, J. Popp, G. Vaughan, W. Henry and Johannes G. Vos, Eur. J. Inorg. Chem., 2008, 3310; (b) J. M. D. Zapiter, B. M. Tissue, K. J. Brewer, Inorg. Chem. Comm., 2008, 11, 51.

[7] G. R. Clemo, T. Holmes and G. C. Leitch, J. Chem. Soc., 1938, 753.

[8] O. Vallat, A. Neels, and H. Stoeckli-Evans, Journal of Chemical Crystallography, Vol. 33, 2003, 39.

[9] L. Cassidy, S. Horne, L. Cleary, W. R. Browne, J. G. Vos, Dalton, 2009, 3923.

[10] Y. Halpin, L. Cleary, L. Cassidy, S. Horne, D. Dini, W. R. Browne and J. G. Vos, Dalton Trans., 2009, 21, 4146.

[11] Y. Q. Fang and G. S. Hanan, Synlett, 2003, 6, 852.

[12] V. N. Kozhevnikov, D. N. Kozhevnikov, O. V. Shabunina, V. L. Rusinov and O. N. Chupakhin, Tetrahedron Letters, 2005, 46, 1791.

[13] V. N. Kozhevnikov, O. V. Shabunina, D. S. Kopchuk, M. M. Ustinova, B. König, D. N. Kozhevnikov, Tetrahedron, 2008, 64, 8963.

[14] W. R. Browne, C. M. O'Connor, J. S. Killeen, A. L. Guckian, M. Burke, P. James, M. Burke and J. G. Vos, Inorg. Chem., 2002, 41, 4245.

Chapter 3: Ruthenium(II) and Palladium(II) / Platinum(II) Containing Hetero-Bimetallic Photocatalysts with 2,5-dipyridylpyrazine (2,5-dpp) for the Solar Energy Generation of Hydrogen from Water.

Abstract:

This chapter describes the synthesis of novel hetero-bimetallic complexes using the conventional "complexes as metal / complexes as ligands" strategy. The complexes synthesised in this chapter were designed for photocatalytic generation of hydrogen from water. 2,5-Dipyridylpyrazine ligand (2,5-dpp) has been used as a bridging ligand between the two metal centers. The advantages and problems associated with the development of larger metal complexes were investigated. This chapter includes the characterisation of the complexes synthesized using nuclear magnetic resonance, deuteriation of peripheral / bridging ligand and elemental analysis. The electronic and electrochemical properties are also reported. The photocatalytical production of hydrogen from water was investigated by using sacrificial agents and varies the amount of water in the photocatalytic solution.

3.1 Introduction

Ruthenium(II) polypyridine complexes have been extensively studied in the past two decades, because of their excited states[1, 2, 3] and electrochemical properties.[4, 5, 6, 7] More recently, much interest has focused on their use as building blocks to synthesise polynuclear complexes, which behave as supramolecular species.[8, 9, 10] Photoinduced energy and electron transfer [8 – 10] and multielectron redox[11] processes in polynuclear complexes are currently being investigated to design molecular devices [9, 12, 13, 14] that can perform useful functions, such as information processing, [15] conversion of light into chemical energy,[16, 17] and multielectron catalysis (Scheme 3.1).[18, 19, 20] $[Ru(bpy)_2Cl_2].2H_2O$ and its analogues are well-known precursors and many thousands of complexes have been prepared[21] including optically pure compounds.[22] The preparation of tris-heteroleptic compounds is substantially more challenging but there are now a number of methods available that have opened the path to extend the size to multinuclear systems.[23, 24] A number of approaches are discussed in a review by Kelly et. al.[17]

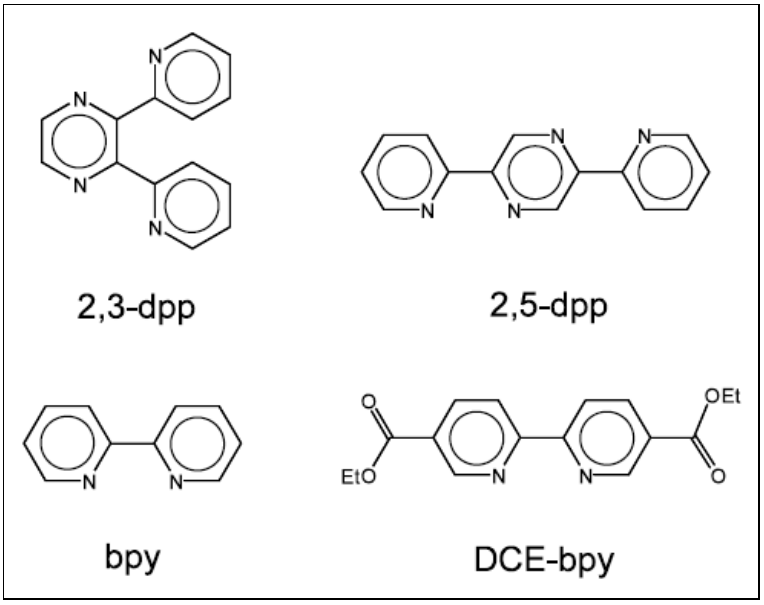

Scheme 3.1: *Chemical structures of bridging ligands and peripheral ligands.*

A convenient method to obtain hetero or polynuclear metal complexes is based on the use of bridging ligands (BL) like 2,3- and 2,5-bis(2-pyridyl)pyrazine (2,3-dpp and

2,5-dpp) which can connect mononuclear building blocks, and 2,2'-bypyridine (bpy) or its derivatives as the peripheral ligands (L).[25, 26] Using this method, polynuclear Ru(II) complexes containing two, three, four, six, seven, ten, thirteen and twenty two metal atoms, as well as a large number of BL (up to 21) and peripheral ligands (up to 24), have been obtained.[10, 25, 26] A detailed description have been reported on the complexes electrochemical and spectroelectrochemical behavior based on bridging ligands 2,3-dpp and 2,5-dpp of Ru(II) complexes containing bpy and DCE-bpy as the peripheral ligands.[27, 28] Furthermore, the effects on the voltammetric pattern brought about by the perturbation in the energy of the bpy-centred redox orbital has been appraised, by studying the complex $[Ru(2,3\text{-dpp})(DCE\text{-bpy})_2]^{2+}$ (DCE-bpy is 5,5'-dicarboxyethyl-2,2'-bipyridine). This is the precursor to polynuclear complexes with mixed terminal ligands that may be anchored (as carboxylate species) to metal-oxide semiconductors. The fact that the $Ru(DCE\text{-bpy})_2$ fragment possesses MLCT states at energies notably lower than $Ru(bpy)_2$, might in fact, allow intramolecular energy transfer paths within the polynuclear species based on these units and 2,3- and 2,5-dpp (BL), resulting in an effective antenna effect in the sensitization of large band-gap semiconductors.[29, 30]

It is well known that for Ru(II) polypyridine complexes the reduction processes involve the ligands. The analysis of the electrochemical behavior of the uncoordinated ligands is, therefore, instrumental in understanding the pattern of the ligand based redox series of the complexes. The electrochemistry of free bpy,[31] DCE-bpy[32] and 2,3-dpp[33] have previously been studied. The cyclic voltammetric curve (CV curve) for 2,5-dpp in DMF at – 54°C shows two reduction peaks which correspond to two one electron diffusion-controlled reversible processes. The $E_{1/2}$ potential values of the redox processes shown in Table 3.1, are for 2,3-dpp, bpy and DCE-bpy. Whereas both 2,5-dpp and bpy-type ligands (i.e. bpy and DCE-bpy, the latter being easier to reduce due to the presence of the ethyl carboxy groups) show two reduction processes, 2,3-dpp exhibits three reductions.

The 2,3- and 2,5-isomers of bis-(2-pyridy1)pyrazine (shown in scheme 3.1) are quite interesting bridging units, since they can coordinate luminescent and redox-reactive ML_2 building blocks (M = Ru(II), Os(II); L = bipyridine-type ligands).[34, 35, 36, 37, 38, 39]

Furthermore, coordination of dpp to Ru^{2+} and Os^{2+} gives rise to additional chromophoric and redox centers and the homo- and heterooligometallic complexes so obtained can be used as building blocks to design larger supramolecular species.[40, 41] Among the great variety of polypyridine ligands that can be used to obtain ML_2 units,[2] 2,2'-bipyridine (bpy) and 2,2'-biquinoline (biq) are quite valuable, since their Ru(II) complexes are both luminescent and redox reactive. Furthermore, the $[Ru(bpy)]^{2+}$ and $[Ru(biq)]^{2+}$ (biq = 2,2'-biquinoline) units exhibit sufficiently different excited-state energies and redox potentials to allow specific assignment of their spectral bands and redox waves in the supramolecular species. $E_{1/2}$

Ligands	**$E_{1/2}$ / V**		
	1	**2**	**3**
2,3-dpp	**- 1.93**	**- 2.55**	**- 2.74**
2,5-dpp	**- 1.53**	**- 2.12**	
bpy	**- 2.09**	**- 2.69**	
DCE-bpy	**- 1.37**	**- 1.78**	

Table 3.1: *Reduction potentials (vs. SCE) of the free ligands in DMF containing 0.1 M Tetraethyl ammonium tetrafluoborate (TEATFB) at* – 54°C.[28]

Denti et al.,[42] synthesised of mononuclear complexes containing one dpp and two bpy / biq ligands, according to Scheme 3.2 (i). In comparison with its bpy analogue, the precursor complex $[Ru(biq)_2C1_2]$ was less reactive toward both 2,3-dpp and 2,5-dpp. Furthermore, in contrast with previous observations, the latter ligand exhibited a lower reactivity than its isomer. In the preparations of mononuclear complexes the

best yields and purities were obtained by adding the bridging ligands only after a rather long reflux time, in order to allow the metal precursor to undergo till aquation (formation of aquo complex) in the absence of the bridging ligand. For oligonuclear compounds it was necessary to raise the reaction temperature to that of refluxing ethylene glycol. Due to the light sensitivity of all derivatives containing biq, their purification was accomplished by recrystallization.

The most convenient general route to dinuclear homoleptic complexes (Scheme 3.2 (ii)) consisted of two separate steps. This was obviously compulsory for the preparation of the heteroligated complexes (Scheme 3.2 (iii)). In order to prepare the trinuclear complexes (Scheme 3.2 (iv)), these were obtained in satisfactory yields by reacting $[Ru(bpy)Cl_3]_n$ with the appropriate bridging ligand in the presence of trifluoroacetic acid (1:2:2). This procedure prevented the massive formation of polymeric species by deactivating a chelating site of the BL through protonation. The subsequent reactions were then carried out by using purified intermediates. The tetranuclear complexes were synthesised (Scheme 3.2 (v)) by reacting $[Ru(dpp)_3]^{2+}$ with the appropriate counterpart $[RuL_2Cl_2]$ has been limited (limiting reagent) to the derivatives of 2,3-dpp. Up to now, attempts to prepare the analogous 2,5-dpp precursor were unsuccessful, due to the tendency of this ligand to behave as a bis-chelating agent toward $[Ru(bpy)Cl_2]$, irrespective of the reaction conditions and molar ratios employed.[42]

In the past few years, Balzani and coworkers have synthesized a variety of dendritic polynuclear transition metal complexes based on the 2,3- and 2,5-dpp bridging ligands (dpp) bis(2-pyridyl)pyrazine), exhibiting interesting photophysical and electrochemical properties. Until now, many metal units have been used in the assembly of dpp-based polynuclear complexes, namely, Re(I), Fe(II), Ru(II), Os(II), Rh(III), Ir(III), Pd(II), Pt(II), Pt(IV), and Cu(I),[10, 43] but so far, no more than two different metals have been introduced in a single compound. The compound RuPt with 2,3-dpp and bpy was previously reported.[44, 45]

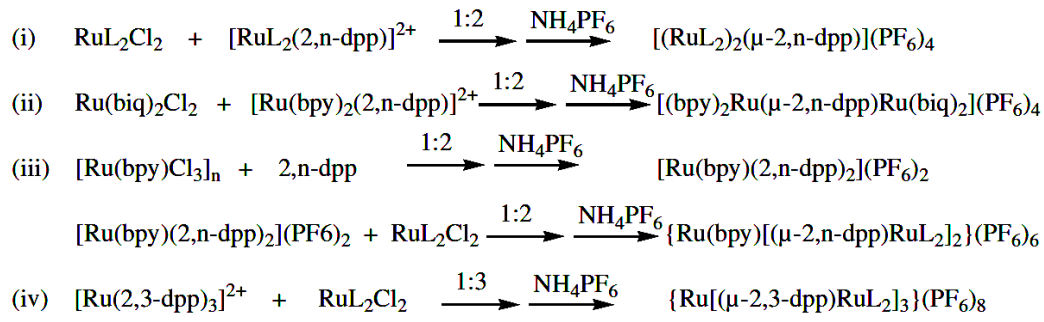

Scheme 3.2: *Synthetic strategies of complexation, where n = 3 or 5.*[28]

In 2001, Sommovigo and coworkers, synthesized $OsRuPt_2$ and $OsRu_3Pt_6$ which were the first examples of polynuclear complexes based on the 2,3-dpp/ 2,5-dpp bridging ligand containing three different metals. The interest in these dendrimeric species was related to the presence of many chemically different units since each unit introduces into the supramolecular structure its own piece of information (in the form of specific properties such as excited states, redox levels, etc.), thus making available more complex functions. Indeed, in the complexes $OsRuPt_2$ and $OsRu_3Pt_6$, a clear antenna effect is observed; the latter was the first decanuclear species where all the energy absorbed was efficiently transferred to a single unit. The molecular model of the compound $OsRu_3Pt_6$ displayed in Figure 3.1 gives an idea of the shape of one of the many possible isomers. The diameter of the molecule is ~ 3 nm.[10]

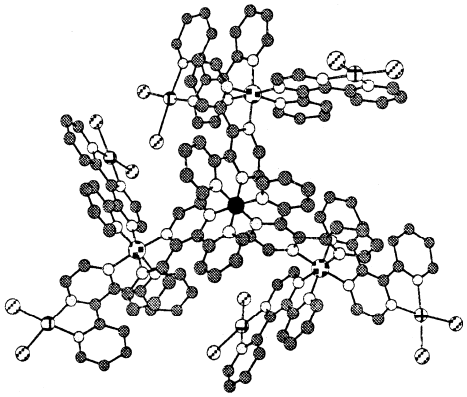

Figure 3.1: *Molecular model of one of the possible isomers of $OsRu_3Pt_6$.*[10]

The ligand 2,5-dpp was prepared by the literature method [46] in which the oxime of the 2-acetylpyridine was converted to its *O*-tosyl derivative [47] and subsequently treated with sodium ethoxide to give 2-(α-aminoacetyl)pyridine. The cyclization of 2-(α-aminoacetyl)pyridine with concentrated aqueous ammonia solution gave the desired ligand 2,5-dpp in acceptable yield. The reaction of $[Ru(bpy)_2Cl_2]$ with a slight excess

of 2,5-dpp gave a deep red solution from which the complex $[Ru(bpy)_2(2,5\text{-}dpp)][PF_6]_2$ was isolated, and purified used chromatography and precipitated using ammonium hexafluorophosphate (Scheme 3.3).[48] The X-ray structure for $[Ru(bpy)_2(2,5\text{-}dpp)][PF_6]_2$ was obtained from a cooled methanolic solution containing equimolar amounts of $[Ru(bpy)_2(2,5\text{-}dpp)][PF_6]_2$ and manganese(II) nitrate (Figure 3.2).[40]

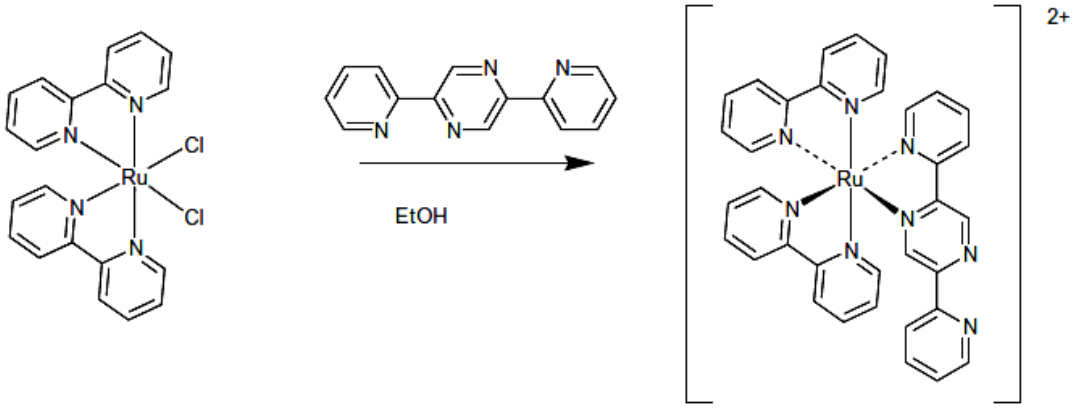

Scheme 3.3: *Synthetic procedure of complexation with 2,5-dpp.*[48]

The solid state structure of the $[Ru(bpy)_2(2,5\text{-}dpp)]^{2+}$ cation present in $[Ru(bpy)_2(2,5\text{-}dpp)][PF_6]_2$ is shown in Fig. 3.2. The structure of the cation confirms the expected features in which one bpy domain is coordinated to the ruthenium and the other is vacant. Both Δ and Λ enantiomers of the chiral trischelate cation are present in the lattice. The non-coordinated pyridine ligand is disordered over the two possible cisoid and transoid conformations with respect to the pyrazine ring and only the cisoid conformer is presented in Fig. 3.2. In contrast to other complexes containing hypodentate ligands that were described,[49] there is remarkably little distortion of the coordination sphere in the $[Ru(bpy)_2(2,5\text{-}dpp)][PF_6]_2$ cation. All three of the coordinated bpy domains exhibit bite angles between 77° and 82°, typical of a 2,2′-bipyridine coordinated to a second or third row transition metal centre.[50] The non-coordinated pyridine ring is twisted about the interannular bond to the pyrazine ring and makes a torsion angle of 32.5°. The majority of the Ru–N bond distances are typical and lie in the expected range 2.0–2.1 Å. There were no stacking interactions

between adjacent cations and no particularly short contacts between cations and anions.

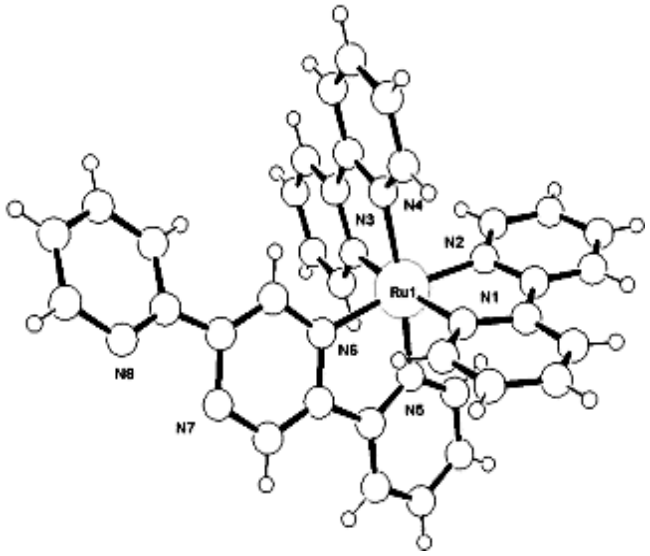

Figure 3.2*: The structure of the Λ-$[Ru(bpy)_2(2,5\text{-}dpp)]^{2+}$ cation present in rac-$[Ru(bpy)_2(2,5\text{-}dpp)][PF_6]_2$ showing only the cisoid conformation of the disordered non coordinated pyridine ring.*[45]

The primary interest in this type of complex is to utilise the vacant metal-binding domain for coordination to an additional metal centre to build heteropolynuclear systems. Recently, photophysical and photochemical properties of copper(I) have attracted attention,[51] due to the long lifetime of the MLCT excited state.[52] Potential applications of these complexes are photovoltaic cells or electroluminescent displays.[53] Some polynuclear metal complexes containing copper(I) which are mainly designed for supramolecular photoactive systems have been proposed. Several reports on Ru(II)-Cu(I) supramolecular complexes have been reported.[54] Although Ru(II)-Cu(I) complexes bridged by 2,3-bis(2-pyridyl)pyrazine (2,3-dpp) were reported,[55] copper(I) complexes containing 2,5-dpp have not been published yet. As a part of a study on luminescent d^{10} metal complexes,[56] the photophysical properties of Cu(I) complexes was examined.[57] In Tsubomura et al. reported that Cu(I) -Cu(I) homodinuclear and Cu(I)-Ru(II) heteromultinuclear complexes bridged by the 2,5-

dpp ligand were prepared for the first time (see Figure 3.3) and their photophysical and photochemical properties had been studied.[58]

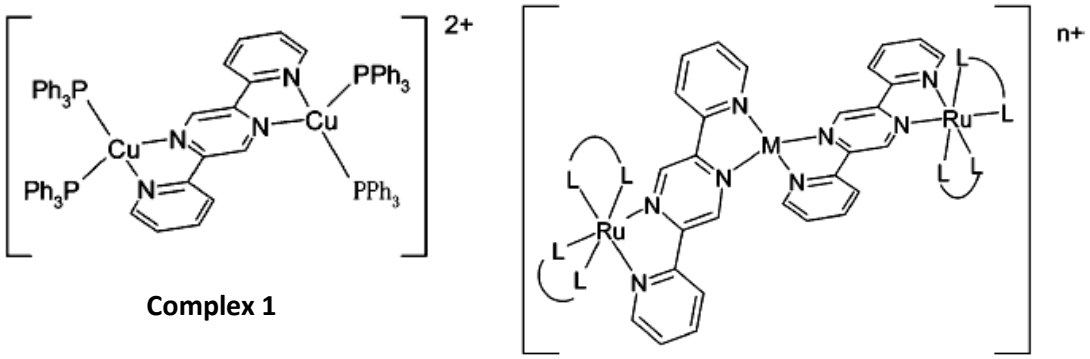

Complex 1

M = Cu(I), n = 3, Complex 2; M = Cu(II), n = 4, Complex 3

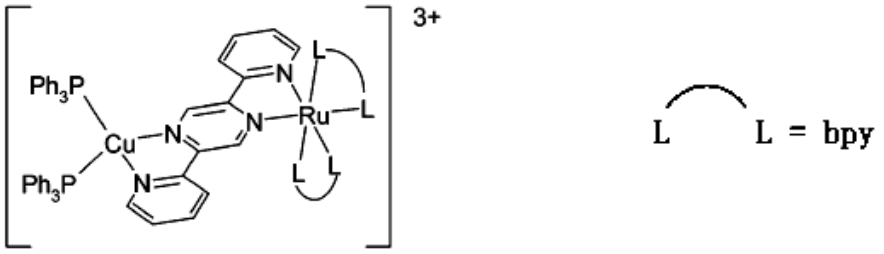

Complex 4

Figure 3.3: *Showing chemical structure of complexes reported by Tsubomura et al.*[58]

Visible light irradiation of complex 2 in CH_2Cl_2 causes a change in the absorption spectra of the complex. As shown in Figure 3.4, the absorption spectra of the photo-product are similar to that of complex 3 and therefore complex 2 can photochemically be oxidized to complex 3 using atmospheric oxygen as an oxidant.

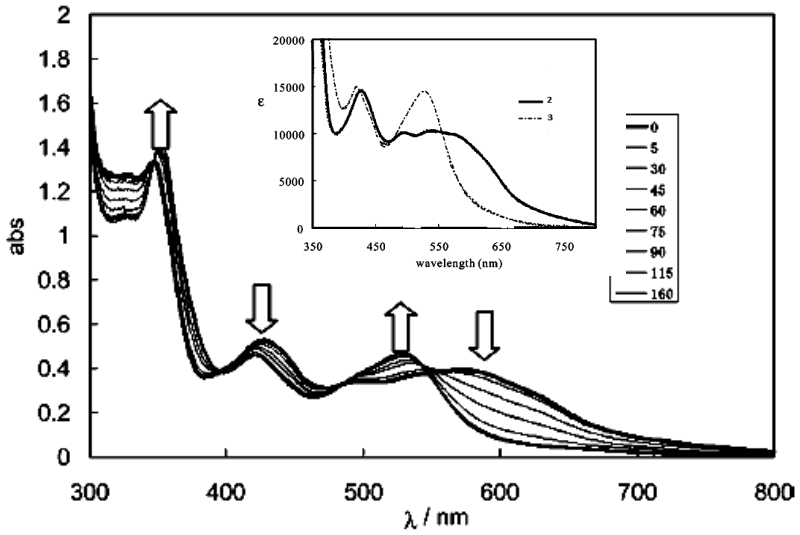

Figure 3.4: *Change in the absorption spectra of complex* ***2*** *with irradiation of light. The duration times after starting the photo-irradiation are shown in the small inset (minutes) and Comparison of absorption spectra (inserted) of complex 2 and 3 in DCM.*[58]

Our primary interests in these studies are to make effective photocatalytic hydrogen production catalysts. Tris(2,2'-bipyridine)ruthenium(II) ($[Ru(bpy)_3]^{2+}$, bpy=2,2'-bipyridine) and its derivatives have attracted considerable attention for many years due to their potential application as a photosensitizers in water splitting reactions.[59, 60, 61, 62] The fundamental concepts on the application of such photosensitizers have been well demonstrated.[63, 64, 65, 66] Studies showed that the photochemical hydrogen production is effectively promoted by visible light irradiation of an aqueous solution containing three key components in the presence of a sacrificial electron donor, such as EDTA (ethylenediaminetetra–acetic acid disodium salt) and TEOA (triethanolamine). The three components correspond to $[Ru(bpy)_3]^{2+}$, methylviologen (*N*,*N*'-dimethyl-4,40 bipyridinium, abbreviated as MV^{2+}), and an H_2 - evolving catalyst such as colloidal platinum (Figure 3.5).

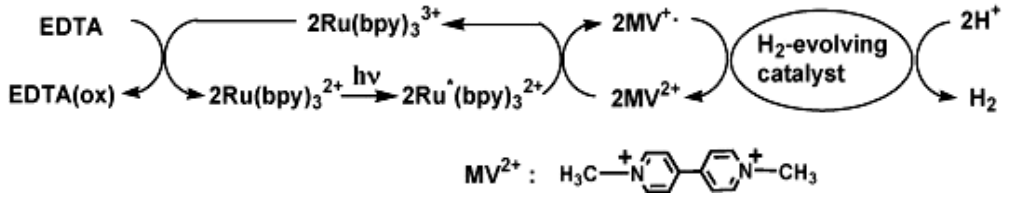

Figure 3.5: *A photochemical model system for the H_2-evolving half cell, which consists of $[Ru(bpy)_3]^{2+}$ as a photosensitizer, MV^{2+} (methylviologen) as an electron relay, and either colloidal platinum or a platinum(II) catalyst as an H_2-evolving catalyst. The overall reaction can be understood as a visible-light-induced reduction of water into molecular hydrogen using EDTA as a sacrifacial electron donor.*[66]

K. Sakai and coworkers developed photocatalytic hydrogen production systems based on photosensitizing $[Ru(bpy)_3]^{2+}$ derivatives and Pt(II) catalysts. A variety of heteronuclear Ru(II)Pt(II) complexes had been prepared and evaluated (see Figure 3.6).[67] In the earlier studies, relatively simple models (**1**–**4**) were developed and their photo-hydrogen-evolving activities were tested. However, it was found that these compounds do not preserve the important photochemical properties required to enhance the visible light induced charge separation process: the strong electronic coupling between the $[Ru(bpy)_3]^{2+}$- like moiety and the heavy Pt ion promotes the quenching of the ^{3}MLCT excited state of the $[Ru(bpy)_3]^{2+}$ - like moiety.[68]

In the later studies, the multinuclear Ru(II)Pt(II) compounds having luminescent $[Ru(bpy)_3]^{2+}$ - like moieties have been the major targets in their research.[62, 69] Although luminescent compounds **5** and **6** do not exhibit any desirable photo-hydrogen-evolving activity at all, compound **7** actually drives the reduction of water by EDTA into molecular hydrogen using visible light.[70] Importantly, a mixture of the two precursor compounds of **7** (e.g., a combination of $[Ru(bpy)_2$(5-amino-1,10-phenanthroline)$]^{2+}$ and $PtCl_2$(dcbpy); dcbpy = 4,4'-dicarboxy-2,2'-bipyridine) does not give rise to the photochemical H_2 generation, which is a possibility that a certain decomposed species, such as colloidal platinum, may not serves as a catalytically

active species in the H_2 formation. In spite of the structural similarity between compounds **5**–**7**, only compound **7** behaves as a photo hydrogen evolving molecular device.[62] This was interpreted in terms of the fact that only the bridging spacer connecting the Ru(II) and Pt(II) centers in **7** has sp^2-hybridized character, in sharp contrast with the aliphatic bridging spacer moieties involved in **5** and **6** (propylene units in **5** and methylene units in **6**).

The trinuclear $Ru(II)_2Pt(II)$ complex **8** and tetranuclear $Ru(II)_2Pt(II)_2$ complex **9** were successfully prepared and characterized.[61, 71] However, they were also found to be inactive as a photo-hydrogen evolving molecular device. It was suggested that the intramolecular energy transfer quenching among the two Ru(II) chromophores is strongly enhanced and therefore deactivation of the ^{3}MLCT excited state of the complex is fast in these systems. In the latter case, it was also suggested that the so-called metal–metal-to-ligand charge transfer transition at the di-platinum entity in **9** (the values of λ_{max} = 475 nm and $\varepsilon = 2110 M^{-1}\ cm^{-1}$ were reported for the analogous $Pt(II)_2$ dimer $[Pt_2(bpy)_2(\mu\text{-pivalamidato})_2]^{2+}$)[72] promotes the energy transfer quenching of the ^{3}MLCT excited state of the $[Ru(bpy)_3]^{2+}$ - unit.[65]

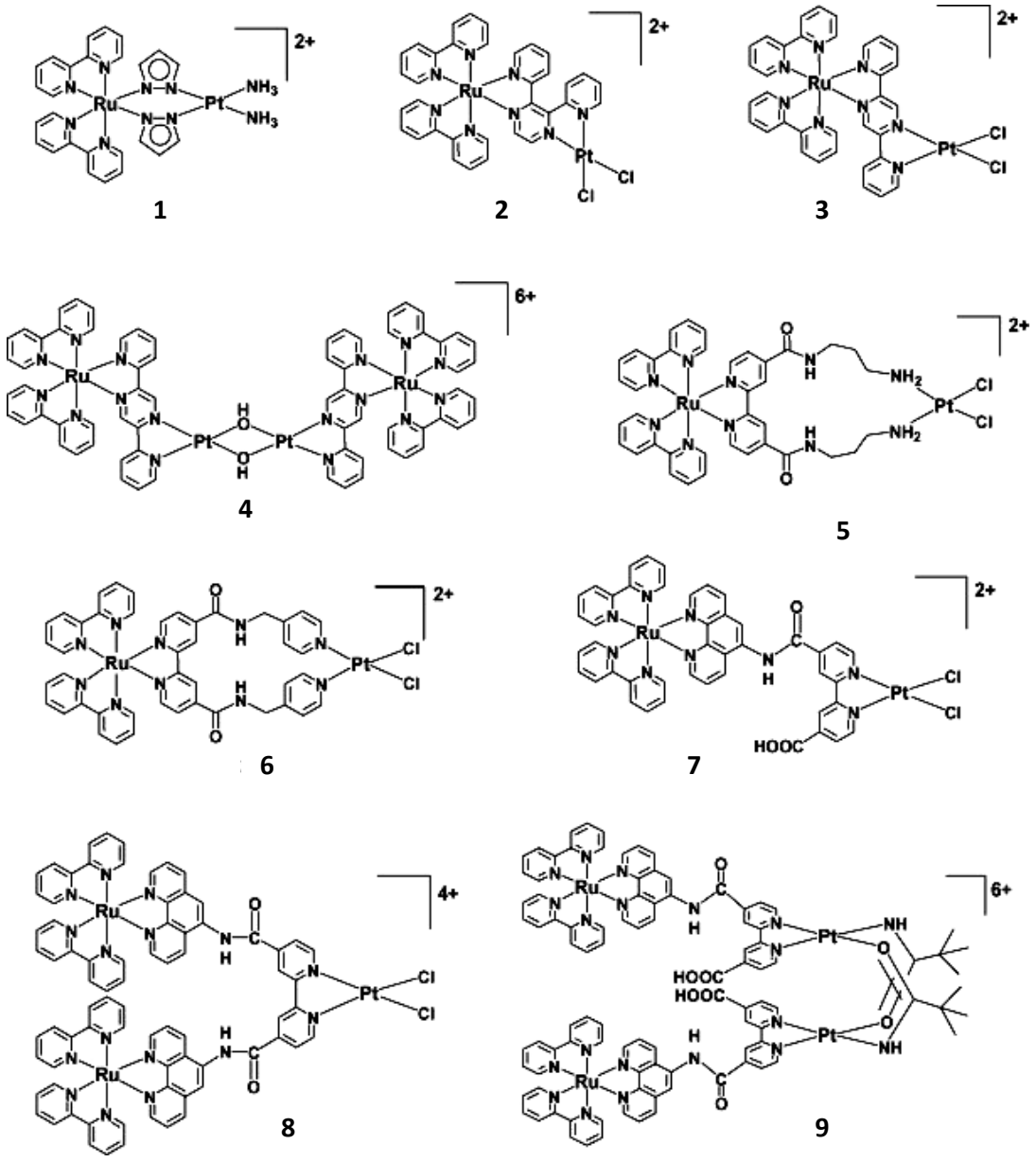

Figure 3.6: *Structures of multinuclear Ru(II)Pt(II) complexes.*[67]

The main aim of this work is to design novel ruthenium(II) based heterodinuclear complexes for the photocatalytic production of hydrogen by splitting of water using triethyl amine as a sacrificial donor and 470 nm as the light source. Characterization, photocatalytic and photophysical properties are discussed later in the chapter.

3.2 Experimental section.

3.2.1 Preparation of the ligand 2,5-dipyridylpyrazine (2,5-dpp).

The bridging ligand 2,5-dipyridylpyrazine (2,5-dpp) was prepared according to the literature with little modification.[73, 74] The complete synthesis has been reported in Chapter 2, Section 2.3.2.

Synthesis of 2,5-di(pyridine-2-yl)pyrazine (2,5-dpp).

This ligand was prepared as described in chapter 2 (section 2.3.2).[75]

Yield: 1.9 g, 0.0081 mol, 13 %.

^{1}H NMR ($CDCl_3$, 400 MHz): 9.59 (s, 2H, 3-H, 6-H), 8.68 (d, 2H, *J* = 4.7 Hz, 6”-H, 6’-H), 8.38 (d, 2H, *J* = 7.8 Hz, 3”-H, 3’-H), 7.91 (ddd, 2H, *J* = 7.6 Hz, *J* = 2.1 Hz, 4”-H, 4’-H), 7.80 (ddd, 2H, *J* = 5.0 Hz, *J* = 1.8 Hz, 5”-H, 5’-H).

^{1}H NMR (DMSO-d_6, 400 MHz): 9.63 (s, 2H, 3-H, 6-H), 8.79 (d, 2H, *J* = 5.0 Hz, 6”-H, 6’-H), 8.43 (d, 2H, *J* = 8.0 Hz, 3”-H, 3’-H), 8.04 (t, 2H, *J* = 8.0 Hz, *J* = 2.1 Hz, 4”-H, 4’-H), 7.57 (t, 2H, *J* = 5.0 Hz, *J* = 1.8 Hz, 5”-H, 5’-H).

3.2.2 Preparation of the deuteriated ligands.

In this chapter the deuteriated 2,5-di(pyridine-2-yl)pyrazine (2,5-dpp) and deuteriated 2,2’-bipyridine (bpy) were synthesised. The purpose of making the deuteriated complexes is to see the effect on lifetime of the excited state and aid in interpretating the ^{1}H-NMR.

Synthesis of D_8-2,2’-bipyridine (D_8-bpy).

This ligand was prepared as described in chapter 2 (section 2.3.3).

Yield: 1.33 g, 8.16 mmol, 85 %, deuteriated amount 98%.

^{1}H-NMR (400 MHz, $CDCl_3$): 8.63 (s, 2H, 6a-H), 8.36 (s, 2H, 3a-H), 7.77 (s, 2H, 4a-H), 7.26 (s, 2H, 5a-H).

Synthesis of D_{10}-2,5-di(pyridine-2-yl)pyrazine (D_{10}-2,5-dpp).

This ligand was prepared as described in chapter 2 (section 2.3.3).

Yield: 0.066 g, 2.7 mmol, 42 %, deuteriated amount 99%.

^{1}H NMR (400 MHz, $CDCl_3$): 9.59 (s, 3-H, 6-H), 8.68 (s, 2H, 6”-H, 6’-H), 8.38 (s, 2H, 3”-H, 3’-H), 7.80 (s, 2H, 4”-H, 4’-H), 7.31 (s, 2H, 5”-H, 5’-H).

Elemental analysis (CHN): calculated C = 68.85, H = 4.09, N = 22.95%, found C = 68.71, H = 4.32, N = 22.64 %.

3.2.3 Preparation of the ruthenium mononuclear complexes.

Synthesis of [Ru(bpy)$_2$(2,5-dpp)] (PF$_6$)$_2$ · H$_2$O (Complex 3.1).

[bis-(2,2'-bipyridine)(2,5-di(pyridin-2-yl)pyrazine)ruthenium(II)] (PF$_6$)$_2$ · H$_2$O

[Ru(2,2'-bipyridine)$_2$Cl$_2$]·2H$_2$O (0.339 g, 0.65 mmol) dissolved in 10 ml of ethanol was added drop-wise to a solution of 2,5-di(pyridin-2-yl)pyrazine (2,5-dpp) (0.187 g, 0.80 mmol) in 10 ml of ethanol/water (3:1 v/v). The reaction mixture was heated at reflux for 8 h. Subsequently, the mixture was allowed to cool to room temperature and the solvent was evaporated in vacuo. Then 2 ml of water was added to dissolve the red complex and filtered to remove unreacted 2,5-dpp. The red aqueous solution yielded a precipitate upon the addition of a saturated aqueous solution of NH_4PF_6 followed by filtration of the product and washing with 10 ml of diethyl ether. Recrystallization from acetone/water (3:1 v/v) afforded a red solid.

Yield: 0.439 g, 0.46 mmol, 71%. Anal. Calcd. for $C_{34}H_{26}F_{12}N_8P_2Ru \cdot H_2O$ (956.08 g/mol): C, 42.73; H, 2.95; N, 11.73%. Found: C, 43.11; H, 2.94; N, 11.46%. ^{1}H-NMR (Acetonitrile-d_3, 400 MHz): δ = 9.65 (d, *J* = 1.2 Hz, 1H, 3-H), 8.74 (d, *J* = 1.2 Hz, 1H, 6-H), 8.69 (d, *J* = 8.4 Hz, 1H, 3”-H), 8.57 – 8.52 (m, 4H, (3a-H) bpy), 8.51 (d, *J* = 4.8 Hz, 1H, 6’-H), 8.44 (d, *J* = 8.0 Hz, 1H, 3’-H), 8.19-8.08 (m, 4H, (4a-H) bpy), 8.14 (ddd, *J* = 8.0 Hz, *J* = 1.6 Hz, 1H, 4”-H), 7.97 (ddd, *J* = 8.0 Hz, *J* = 1.6 Hz, 1H, 4’-H), 7.81 (d, *J* = 5.6 Hz, 1H, 6”-H), 7.82-7.75 (m, 4H, (6a-H) bpy), 7.50-7.44 (m, 4H, (5a-H) bpy), 7.49 (m, 1H, 5”-H), 7.46 (m, 1H, 5’-H).

Also measured ^{1}H-NMR in (DMSO-d_6, 400MHz): 10.04 (s, 1H, 3-H), 9.04 (d, *J* = 8.4 Hz, 1H, 3”-H), 8.90-8.51 (m, 4H, (3a-H) bpy), 8.59 (s, 1H, 6-H), 8.53 (d, 1H, *J* = 4.8

Hz, 6'-H), 8.42 (d, 1H, *J* = 8.0 Hz, 3'-H), 8.28-8.19 (m, 4H, (4a-H) bpy), 8.25 (ddd, *J* = 8.0 Hz, *J* = 1.6 Hz, 1H, 4"-H), 8.08-7.72 (m, 4H, (6a-H) bpy), 8.03 (t, *J* = 8.0 Hz, *J* = 1.6 Hz, 1H, 4'-H), 7.80 (d, *J* = 5.6 Hz, 1H, 6"-H), 7.63-7.48 (m, 4H, (5a-H) bpy), 7.60 (ddd, *J* = 8.0 Hz, *J* = 1.6 Hz, 1H, 5"-H), 7.52 (m, 1H, 5'-H).

Synthesis of [Ru(dceb)$_2$(2,5-dpp)] (PF$_6$)$_2$ · 2H$_2$O (Complex 3.2).

[bis-(4,4'-dicarboxyethyl(2,2'-bipyridine))(2,5-di(pyridin-2-yl)pyrazine)ruthenium(II)] (PF$_6$)$_2$ · 2H$_2$O

[Ru(4,4'-dicarboxyethyl(2,2'-bipyridine)$_2$Cl$_2$]·2H$_2$O (0.339 g, 0.42 mmol) dissolved in 10 ml of ethanol was added drop-wise to a solution of 2,5-di(pyridin-2-yl)pyrazine (2,5-dpp) (0.120 g, 0.51 mmol) in 10 ml of ethanol/water (3:1 v/v). The reaction mixture was heated at reflux for 8 h. Subsequently, the mixture was allowed to cool to room temperature and the solvent was evaporated in vacuo. Then 2 ml of water was added to dissolve the red complex and filtered to remove unreacted 2,5-dpp. The red aqueous solution yielded a precipitate upon the addition of a saturated aqueous solution of NH_4PF_6 followed by filtration of the product and washing with 10 ml of diethyl ether. Recrystallization from acetone/water (3:1 v/v) afforded a red solid.

Yield: 0.416 g, 0.33 mmol, 78%. Anal. Calcd. for $C_{46}H_{42}F_{12}N_8O_8P_2Ru \cdot 2H_2O$ (1261.90 g/mol): C, 43.78; H, 3.67; N, 8.88%. Found: C, 43.53; H, 3.27; N, 8.49%. ^{1}H-NMR (Acetonitrile-d$_3$, 400 MHz): δ = 9.69 (s, 1H, 3-H), 9.12-9.07 (m, 4H, (3a-H) bpy) 8.71 (d, *J* = 8.3 Hz, 1H, 3"-H), 8.64 (s, 1H, 6-H), 8.50 (d, *J* = 4.8 Hz, 1H, 6'-H), 8.44 (d, *J* = 8.0 Hz, 1H, 3'-H), 8.20 (ddd, *J* = 8.0 Hz, *J* = 1.5 Hz, 1H, 4"-H), 8.13-7.84 (m, 8H, 6a-H, 5a-H, bpy) 7.97 (m, 1H, 4'-H), 7.74 (d, *J* = 5.6 Hz, 1H, 6"-H), 7.52 (m, 1H, 5"-H), 7.46 (m, 1H, 5'-H) 4.54-4.46 (m, 8H, CH_2), 1.50-1.40 (m, 12H, CH_3).

Synthesis of [Ru(D$_8$-bpy)$_2$(2,5-dpp)] (PF$_6$)$_2$ (Complex 3.3).

[bis-(D$_8$-2,2'-bipyridine)(2,5-di(pyridin-2-yl)pyrazine)ruthenium(II)] (PF$_6$)$_2$

[Ru(D$_8$-2,2'-bipyridine)$_2$Cl$_2$]·2H$_2$O (0.077 g, 0.14 mmol) dissolved in 10 ml of ethanol was added drop-wise to a solution of 2,5-di(pyridin-2-yl)pyrazine (D$_{10}$-2,5-dpp) (0.050 g, 0.21 mmol) in 10 ml of ethanol/water (3:1 v/v). The reaction mixture was heated at reflux for 8 h. Subsequently, the mixture was allowed to cool to room

temperature and the solvent was evaporated in vacuo. Then 2 ml of water was added to dissolve the red complex and filtered to remove unreacted 2,5-dpp. The red aqueous solution yielded a precipitate upon the addition of a saturated aqueous solution of NH_4PF_6 followed by filtration of the product and washing with 10 ml of diethyl ether. Recrystallization from acetone/water (3:1 v/v) afforded a red solid.

Yield: 0.064 mg, 0.067 mmol, 48%. Anal. Calcd. for $C_{34}H_{10}D_{16}F_{12}N_8P_2Ru$. H_2O (971.74 g/mol): C, 42.02; H, 2.90; N, 11.53%. Found: C, 42.14; H, 2.94; N, 11.63%. ^{1}H-NMR (DMSO-d_6): δ = 10.04 (s, 1H, 3-H), 9.04 (d, *J* = 8.4 Hz, 1H, 3"-H), 8.90 (s, 1H, (3a-H) bpy), 8.89 (s, 1H, (3a-H) bpy), 8.86 (s, 1H, (3a-H) bpy), 8.85 (s, 1H, (3a-H) bpy), 8.59 (s, 1H, 6-H), 8.53 (d, *J* = 4.8 Hz, 1H, 6'-H), 8.42 (d, *J* = 8.0 Hz, 1H, 3'-H), 8.28 (s, 1H, (4a-H) bpy), 8.25 (ddd, *J* = 8.0 Hz, *J* = 1.6 Hz, 1H, 4"-H), 8.23 (s, 1H, (4a-H) bpy), 8.20 (s, 1H, (4a-H) bpy), 8.19 (s, 1H, (4a-H) bpy), 8.08 (s, 1H, (6a-H) bpy), 8.03 (t, *J* = 8.0 Hz, *J* = 1.6 Hz, 1H, 4'-H), 7.83 (s, 1H, (6a-H) bpy), 7.80 (d, *J* = 5.6 Hz, 1H, 6"-H), 7.74 (s, 1H, (6a-H) bpy), 7.72 (s, 1H, (6a-H) bpy), 7.63 (s, 1H, (5a-H) bpy), 7.60 (ddd, *J* = 8.0 Hz, *J* = 1.6 Hz, 1H, 5"-H), 7.59 (s, 1H, (5a-H) bpy), 7.57 (s, 1H, (5a-H) bpy), 7.52 (m, 1H, 5'-H), 7.48 (s, 1H, (5a-H) bpy).

Synthesis of [Ru(bpy)$_2$(D_{10}-2,5-dpp)](PF_6)$_2$ (Complex 3.4).

[bis-(2,2'-bipyridine)(D_{10}-2,5-di(pyridin-2-yl)pyrazine)ruthenium(II)] (PF_6)$_2$

[Ru(2,2'-bipyridine)$_2$$Cl_2$]·$2H_2O$ (0.022 g, 0.04 mmol) dissolved in 10 ml of ethanol was added drop-wise to a solution of D_{10}-2,5-di(pyridin-2-yl)pyrazine (D_{10}-2,5-dpp) (0.015 g, 0.06 mmol) in 10 ml of ethanol/water (3:1 v/v). The reaction mixture was heated at reflux for 8 h. Subsequently, the mixture was allowed to cool to room temperature and the solvent was evaporated in vacuo. Then 2 ml of water was added to dissolve the red complex and filtered to remove unreacted D_{10}-2,5-dpp. The red aqueous solution yielded a precipitate upon the addition of a saturated aqueous solution of NH_4PF_6 followed by filtration of the product and washing with 10 ml of diethyl ether. Recrystallization from acetone/water (3:1 v/v) afforded a red solid.

Yield: 0.026 g, 0.027 mmol, 67%. Anal. Calcd. for $C_{34}H_{16}D_{10}F_{12}N_8P_2Ru$. H_2O (965.70 g/mol): C, 42.29; H, 2.93; N, 11.60%; found: C, 42.33; H, 3.05; N, 11.41%. ^{1}H-NMR (DMSO-d_6): δ = 10.04 (s, 3-H), 9.04 (s, 3”-H), 8.90-8.85 (m, 4H, (3a-H) bpy), 8.59 (s, 6-H), 8.53 (s, 6’-H), 8.42 (s, 3’-H), 8.28-8.19 (m, 4H, (4a-H) bpy), 8.25 (s, 4”-H), 8.08 (d, 1H, *J* = 8.0 Hz, (6a-H) bpy), 8.03 (s, 4’-H), 7.83 (d, 1H, *J* = 8.0 Hz, (6a-H) bpy), 7.80 (s, 6”-H), 7.72 (m, 2H, (6a-H) bpy), 7.63-7.57 (m, 3H, (5a-H) bpy), 7.60 (s, 5”-H), 7.52 (s, 5’-H), 7.48 (t, *J* = 7.0 Hz, 1H, (5a-H) bpy).

Synthesis of [Ru(D_8-bpy)$_2$(D_{10}-2,5-dpp)] (PF_6)$_2$ (Complex 3.5).

[bis-(D_8-2,2'-bipyridine)(D_{10}-2,5-di(pyridin-2-yl)pyrazine)ruthenium(II)] (PF_6)$_2$

[Ru(D_8-2,2'-bipyridine)$_2$$Cl_2$]·2$H_2O$ (0.022 g, 0.04 mmol) dissolved in 10 ml of ethanol was added drop-wise to a solution of D_{10}-2,5-di(pyridin-2-yl)pyrazine (D_{10}-2,5-dpp) (0.015 g, 0.06 mmol) in 10 ml of ethanol/water (3:1 v/v). The reaction mixture was heated at reflux for 8 h. Subsequently, the mixture was allowed to cool to room temperature and the solvent was evaporated in vacuo. Then 2 ml of water was added to dissolve the red complex and filtered to remove unreacted D_{10}-2,5-dpp. The red aqueous solution yielded a precipitate upon the addition of a saturated aqueous solution of NH_4PF_6 followed by filtration of the product and washing with 10 ml of diethyl ether. Recrystallization from acetone/water (3:1 v/v) afforded a red solid.

Yield: 0.024 g, 0.025 mmol, 61%. Anal. Calcd. for $C_{34}D_{26}F_{12}N_8P_2Ru$. H_2O (981.80 g/mol): C, 41.59; H, 2.88; N, 11.41%. Found: C, 41.83; H, 2.82; N, 11.29%. ^{1}H-NMR (DMSO-d_6): 10.04 (s, 1H, 3-H), 9.04 (s, 1H, 3”-H), 8.90 (s, 1H, (3a-H) bpy), 8.89 (s, 1H, (3a-H) bpy), 8.86 (s, 1H, (3a-H) bpy), 8.85 (s, 1H, (3a-H) bpy), 8.59 (s, 1H, 6-H), 8.53 (s, 1H, 6’-H), 8.42 (s, 1H, 3’-H), 8.28 (s, 1H, (4a-H) bpy), 8.25 (s, 1H, 4”-H), 8.23 (s, 1H, (4a-H) bpy), 8.20 (s, 1H, (4a-H) bpy), 8.19 (s, 1H, (4a-H) bpy), 8.08 (s, 1H, (6a-H) bpy), 8.03 (s, 1H, 4’-H), 7.83 (s, 1H, (6a-H) bpy), 7.80 (s, 1H, 6”-H), 7.72 (m, 2H, (6a-H) bpy), 7.63 (s, 1H, (5a-H) bpy), 7.60 (s, 1H, 5”-H), 7.59 (s, 1H, (5a-H) bpy), 7.57 (s, 1H, (5a-H) bpy), 7.52 (s, 1H, 5’-H), 7.48 (s, 1H, (5a-H) bpy).

3.2.4 Preparation of Ru-Pd / Ru-Pt Heterodinuclear complexes.

Synthesis of $[Ru(bpy)_2(2,5\text{-}dpp)PdCl_2](PF_6)_2 \cdot 2\ H_2O$ (Complex 3.6).

[Ruthenium(II)(2,2'-bipyridine)$_2$(μ-2,5-di(pyridin-2-yl)pyrazine)PdCl$_2$] $(PF_6)_2 \cdot 2\ H_2O$

The mononuclear precursor $[Ru(bpy)_2(2,5\text{-}dpp)](PF_6)_2 \cdot H_2O$ (0.100 g, 0.10 mmol) was dissolved in 5 ml of dichloromethane and added drop wise to a solution of $Pd(acetonitrile)_2Cl_2$ (0.026 g, 0.10 mmol) in 5 ml of dichloromethane. The reaction mixture was heated at reflux for 24 h. Subsequently the mixture was allowed to cool to room temperature. The product was precipitated by the addition of 10 ml of n-hexane. After filtration and washing with 10 ml of diethyl ether a reddish purple solid was obtained.

Yield: 0.107 g, 0.09 mmol, 90%. Anal. Calcd for $C_{34}H_{26}Cl_2F_{12}N_8P_2PdRu \cdot 2\ H_2O$ (1150.98): C, 35.48; H, 2.63; N, 9.74%. Found: C, 35.30; H, 2.22; N, 9.31%. ^{1}H-NMR (Acetonitrile-d_3, 400MHz): δ = 10.05 (s, 1H, 3-H), 8.91 (d, *J* = 4.8 Hz, 1H, 6'-H), 8.62 (d, *J* = 8.4 Hz, 1H, 3"-H), 8.57 – 8.52 (m, 4H, (3a-H) bpy), 8.42 (s, 1H, 6-H), 8.15 (ddd, *J* = 6.0 Hz, *J* = 1.8 Hz, 1H, 4"-H), 8.19-8.08 (m, 4H, (4a-H) bpy), 8.10 (ddd, *J* = 7.6 Hz, *J* = 1.2 Hz, 1H, 4'-H), 7.81 (d, *J* = 8.0 Hz, 1H, 6"-H), 7.82-7.75 (m, 4H, (6a-H) bpy), 7.66 (d, *J* = 7.6 Hz, 1H, 3'-H), 7.61 (m, 1H, 5'-H), 7.59 (m, 1H, 5"-H), 7.50-7.44 (m, 4H, (5a-H) bpy).

Synthesis of $[Ru(bpy)_2(2,5\text{-}dpp)PtCl_2](PF_6)_2 \cdot 2\ H_2O$ (Complex 3.7).

[Ruthenium(II)(2,2'-bipyridine)$_2$(μ-2,5-di(pyridin-2-yl)pyrazine)PtCl$_2$] $(PF_6)_2 \cdot 2\ H_2O$

The mononuclear precursor $[Ru(bpy)_2(2,5\text{-}dpp)](PF_6)_2 \cdot H_2O$ (0.100g, 0.10 mmol) was dissolved in 5 ml of dichloromethane and added drop wise to a solution of $Pt(dimethylsulphoxide)_2Cl_2$ (0.042 g, 0.10 mmol) in 5 ml of dichloromethane. The reaction mixture was heated at reflux for 24 h. Subsequently the mixture was allowed to cool to room temperature. The product was precipitated by the addition of 10 ml of

n-hexane. After filtration and washing with 10 ml of diethyl ether a reddish purple solid was obtained.

Yield: 0.115 g, 0.09 mmol, 90%. Anal. Calcd for $C_{34}H_{26}Cl_2F_{12}N_8P_2PtRu \cdot 2\ H_2O$ (1238.98): C, 32.93; H, 2.44; N, 9.04%. Found: C, 32.62; H, 2.19; N, 8.67%. ^{1}H-NMR (Acetonitrile-d_3, 400MHz): δ = 10.50 (s, 1H, 3-H), 9.39 (d, *J* = 4.8 Hz, 1H, 6'-H), 8.65 (d, *J* = 8.4 Hz, 1H, 3"-H), 8.57 – 8.48 (m, 4H, (3a-H) bpy), 8.34 (s, 1H, 6-H), 8.20 (ddd, *J* = 8.0 Hz, *J* = 1.6 Hz, 1H, 4"-H), 8.19 (ddd, *J* = 8.0 Hz, *J* = 1.8 Hz, 1H, 4'-H), 8.19-8.05 (m, 4H, (4a-H) bpy), 8.07-7.55 (m, 4H, (6a-H) bpy), 7.84 (d, *J* = 5.6 Hz, 1H, 6"-H), 7.73 (d, *J* = 8.0 Hz, 1H, 3'-H), 7.72 (m, 1H, 5'-H), 7.67-7.42 (m, 4H, (5a-H) bpy), 7.60 (m, 1H, 5"-H).

Synthesis of [Ru(dceb)$_2$(2,5-dpp)PdCl$_2$] (PF$_6$)$_2$ · 2H$_2$O (Complex 3.8).

[Ruthenium(II)(4,4'-dicarboxyethyl(2,2'-bipyridine))$_2$(μ-2,5-di(pyridin-2-yl)pyrazine)-PdCl$_2$] (PF$_6$)$_2$ · 2 H$_2$O

The mononuclear precursor [Ru(dceb)$_2$(2,5-dpp)] $(PF_6)_2 \cdot 2H_2O$ (0.100 g, 0.08 mmol) was dissolved in 5 ml of dichloromethane and added drop wise to a solution of Pd(acetonitrile)$_2$Cl$_2$ (0.026 g, 0.08 mmol) in 5 ml of dichloromethane. The reaction mixture was heated at reflux for 24 h. Subsequently the mixture was allowed to cool to room temperature. The product was precipitated by the addition of 10 ml of n-hexane. After filtration and washing with 10 ml of diethyl ether a reddish purple solid was obtained.

Yield: 0.101 g, 0.070 mmol, 88%. Anal. Calcd. for $C_{46}H_{42}F_{12}N_8O_8Cl_2PdP_2Ru \cdot 2H_2O$ (1439.23 g/mol): C, 38.39; H, 3.22; N, 7.79%. Found: C, 38.22; H, 2.89; N, 7.72%. ^{1}H-NMR (Acetonitrile-d_3, 400 MHz): δ = 10.13 (s, 1H, 3-H), 9.12-9.08 (m, 4H, (3a-H) bpy), 8.81 (d, *J* = 4.8 Hz, 1H, 6'-H), 8.68 (d, *J* = 8.4 Hz, 1H, 3"-H), 8.42 (s, 1H, 6-H), 8.25 (ddd, *J* = 8.0 Hz, *J* = 1.2 Hz, 1H, 4"-H), 8.10 (ddd, *J* = 8.0 Hz, *J* = 1.8 Hz, 1H, 4'-H), 7.92-7.83 (m, 8H, (6a-H, 5a-H) bpy), 7.82 (d, *J* = 5.6 Hz, 1H, 3'-H), 7.79 (d, *J* = 7.6 Hz, 1H, 6"-H), 7.61 (m, 1H, 5"-H), 7.59 (m, 1H, 5'-H), 4.54-4.46 (m, 8H, CH_2), 1.50-1.40 (m, 12H, CH_3).

Synthesis of [Ru(dceb)$_2$(2,5-dpp)PtCl$_2$] (PF$_6$)$_2$ · 2H$_2$O (Complex 3.9).

[Ruthenium(II)(4,4'-dicarboxyethyl(2,2'-bipyridine))$_2$(μ-2,5-di(pyridin-2-yl)pyrazine)-PtCl$_2$] (PF$_6$)$_2$ · 2 H$_2$O

The mononuclear precursor [Ru(dceb)$_2$(2,5-dpp)] (PF$_6$)$_2$ · H$_2$O (0.100g, 0.08 mmol) was dissolved in 5 ml of dichloromethane and added drop wise to a solution of Pt(dimethylsulphoxide)$_2$Cl$_2$ (0.035 g, 0.08 mmol) in 5 ml of dichloromethane. The reaction mixture was heated at reflux for 24 h. Subsequently the mixture was allowed to cool to room temperature. The product was precipitated by the addition of 10 ml of n-hexane. After filtration and washing with 10 ml of diethyl ether a reddish purple solid was obtained.

Yield: 0.116 g, 0.07 mmol, 88%. Anal. Calcd. for $C_{46}H_{42}F_{12}N_8O_8Cl_2PtP_2Ru \cdot 2H_2O$ (1527.06 g/mol): C, 36.14; H, 3.01; N, 7.34%. Found: C, 36.08; H, 2.62; N, 7.74%. ^{1}H-NMR (Acetonitrile-d$_3$, 400 MHz): δ = 10.58 (s, 1H, 3-H), 9.12-9.08 (m, 4H, (3a-H) bpy), 9.40 (d, *J* = 4.8 Hz, 1H, 6'-H), 8.68 (d, *J* = 8.4 Hz, 1H, 3"-H), 8.30 (s, 1H, 6-H), 8.25 (ddd, *J* = 8.0 Hz, *J* = 1.8 Hz, 1H, 4"-H), 8.18 (ddd, *J* = 8.0 Hz, *J* = 1.8 Hz, 1H, 4'-H), 7.92-7.83 (m, 8H, (6a-H, 5a-H) bpy), 7.81 (ddd, *J* = 8.0 Hz, *J* = 1.2 Hz, 1H, 3'-H), 7.79 (d, *J* = 5.6 Hz, 1H, 6"-H), 7.72 (m, 1H, 5'-H), 7.61 (d, *J* = 7.6 Hz, 1H, 5"-H), 4.45-4.30 (m, 8H, CH$_2$), 1.35-1.25 (m, 12H, CH$_3$).

Synthesis of [Ru(D$_8$-bpy)$_2$(2,5-dpp)PdCl$_2$] (PF$_6$)$_2$ (Complex 3.10).

[Ruthenium(II)bis-(D$_8$-2,2'-bipyridine)(μ-2,5-di(pyridin-2-yl)pyrazine)PdCl$_2$] (PF$_6$)$_2$

The mononuclear precursor [Ru(D$_8$-bpy)$_2$(2,5-dpp)] (PF$_6$)$_2$ (0.015 g, 0.016 mmol) was dissolved in 5 ml of dichloromethane and added drop wise to a solution of Pd(acetonitrile)$_2$Cl$_2$ (0.004 g, 0.016 mmol) in 5 ml of dichloromethane. The reaction mixture was heated at reflux for 24 h. Subsequently the mixture was allowed to cool to room temperature. The product was precipitated by the addition of 10 ml of n-hexane. After filtration and washing with 10 ml of diethyl ether a reddish purple solid was obtained.

Yield: 0.017 g, 0.015 mmol, 91%. ^{1}H-NMR (Acetonitrile-d$_3$, 400MHz): δ = 10.05 (s, 1H, 3-H), 8.91 (d, *J* = 4.8 Hz, 1H, 6'-H), 8.62 (d, *J* = 8.4 Hz, 1H, 3"-H), 8.57-8.52 (m, 4H, (3a-H) bpy), 8.42 (s, 1H, 6-H), 8.15 (ddd, *J* = 6.0 Hz, *J* = 1.8 Hz, 1H, 4"-H),

8.19-8.08 (m, 4H, (4a-H) bpy), 8.10 (ddd, *J* = 7.6 Hz, *J* = 1.2 Hz, 1H, 4'-H), 7.81 (d, *J* = 8.0 Hz, 1H, 6"-H), 7.82-7.75 (m, 4H, (6a-H) bpy), 7.66 (d, *J* = 7.6 Hz, 1H, 3'-H), 7.61 (m, 1H, 5'-H), 7.59 (m, 1H, 5"-H), 7.50-7.44 (m, 4H, (5a-H) bpy).

Synthesis of [Ru(D_8-bpy)$_2$(D_{10}-2,5-dpp)PdCl$_2$](PF_6)$_2$ (Complex 3.11).

[Ruthenium(II)bis-(D_8-2,2'-bipyridine)(μ-D_{10}-2,5-di(pyridin-2-yl)pyrazine)PdCl$_2$](PF_6)$_2$

The mononuclear precursor [Ru(D_8-bpy)$_2$(D_{10}-2,5-dpp)] (PF_6)$_2$ (0.010 g, 0.01 mmol) was dissolved in 5 ml of dichloromethane and added drop wise to a solution of Pd(acetonitrile)$_2$Cl$_2$ (0.003 g, 0.01 mmol) in 5 ml of dichloromethane. The reaction mixture was heated at reflux for 24 h. Subsequently the mixture was allowed to cool to room temperature. The product was precipitated by the addition of 10 ml of n-hexane. After filtration and washing with 10 ml of diethyl ether a reddish purple solid was obtained.

Yield: 0.011 g, 0.0098 mmol, 98%. ^{1}H-NMR (acetonitrile-d_3): Singlets aroused form the remaining protons in the molecule are listed as found. ^{1}H-NMR (Acetonitrile-d_3, 400MHz): δ = 10.05 (s, 1H, 3-H), 8.91 (s, 6'-H), 8.62 (s, 1H, 3"-H), 8.57 – 8.52 (m, 4H, (3a-H) bpy), 8.42 (s, 1H, 6-H), 8.15 (s, 1H, 4"-H), 8.19-8.08 (m, 4H, (4a-H) bpy), 8.10 (s, 1H, 4'-H), 7.81 (s, 1H, 6"-H), 7.82-7.75 (m, 4H, (6a-H) bpy), 7.66 (s, 1H, 3'-H), 7.61 (s, 1H, 5'-H), 7.59 (s, 1H, 5"-H), 7.50-7.44 (m, 4H, (5a-H) bpy).

3.3 Results and discussion

3.3.1 Synthesis of ligand, mononuclear and heterodinuclear complexes.

The synthesis of the mononuclear complexes $[Ru(bpy)_2(2,5\text{-}dpp)]^{2+}$, $[Ru(dceb)_2(2,5\text{-}dpp)]^{2+}$ and heterodinuclear complexes $[Ru(bpy)_2(2,5\text{-}dpp)PdCl_2]^{2+}$, $[Ru(bpy)_2(2,5\text{-}dpp)PtCl_2]^{2+}$, $[Ru(dceb)_2(2,5\text{-}dpp)PdCl_2]^{2+}$, $[Ru(dceb)_2(2,5\text{-}dpp)PtCl_2]^{2+}$ are represented schematically in Figure 3.7.[76]

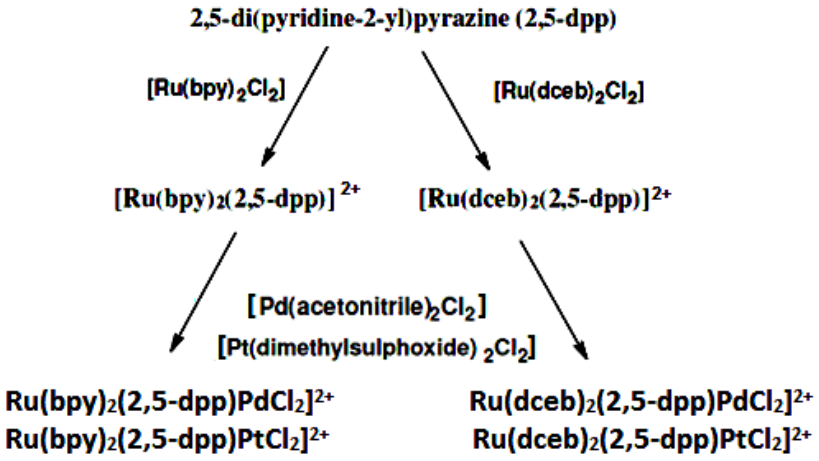

Figure 3.7: *Synthetic pathway for the formation of the mononuclear and heterodinuclear complexes.*

The maximum yield obtained for the 2,5-di(pyridin-2-yl)pyrazine (2,5-dpp) was ~ 10% by using inert atmospheres and anhydrous solvents. A different procedure was developed, and the yield increased marginally to 13% without using anhydrous solvents as an inert atmosphere (see chapter 2 for synthesis), synthesis detailed in Figure 3.8.

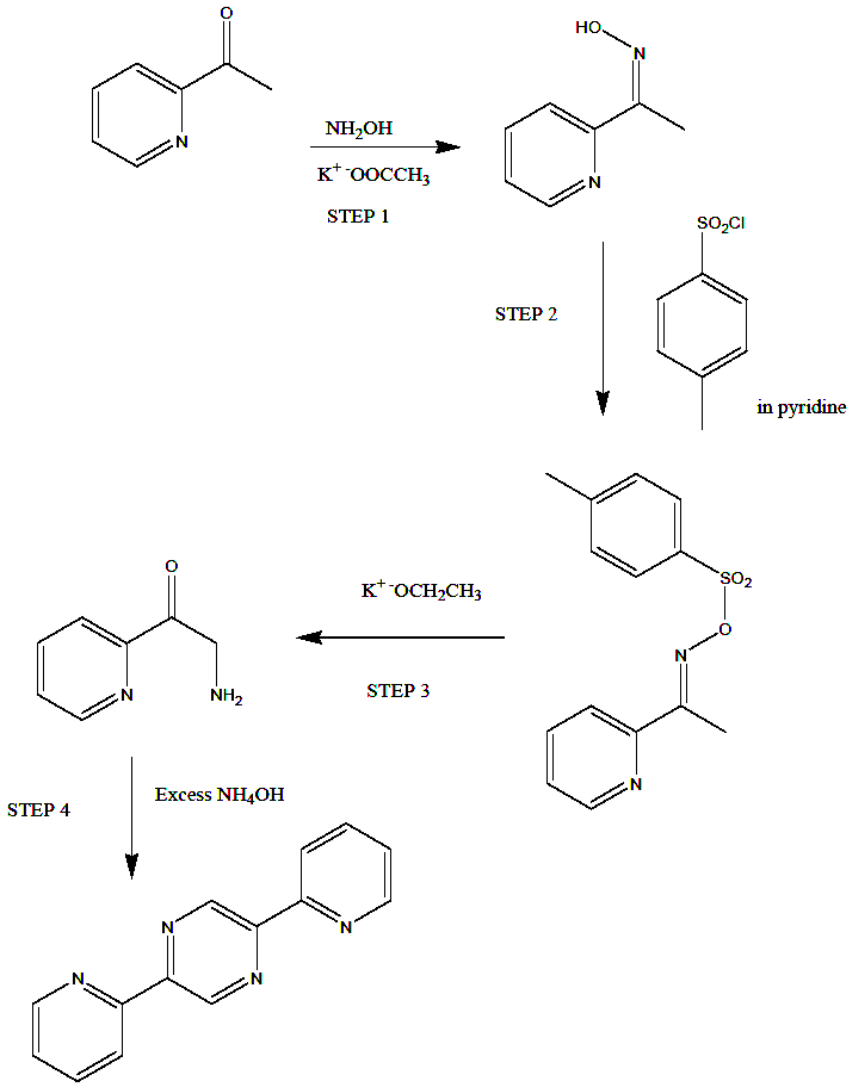

2,5-di(pyridine-2-yl)pyrazine (2,5-dpp)

Figure 3.8: *Stepwise synthesis of 2,5-di(pyridine-2-yl)pyrazine (2,5-dpp) .*

Step 1 in the synthesis provided a 98% yield using potassium acetate as a base in the reaction. Step 2 in the synthesis provided 89% yield by following the reported procedure.[73] The most important steps in the synthesis were step 3 and 4 which were combined. The reason for combining step 3 and 4 was because of intermediate (2-amino-1-pyridyl ethanone) which formed after step 3 was not isolated due to the formation of multiple hydrolysis products and solubility in water. After the complete precipitation of potassium p-toluenesulphonate salt, the reaction mixture was extracted with diethyl ether and 2 M HCl (100 cm^3 x 2). The organic layer which was

light yellow in colour became colourless and the aqueous layer becomes orange during extraction. After vacuo evaporation the organic layer gives the p-toluensulphonic acid as a precipitate. Treatment of the orange aqueous layer with excess of ammonium hydroxide solution (complete neutralisation of 2M HCl and also helped in condensation). The reaction mixture was stirred for 24 hours at room temperature to precipitate 2,5-dpp as an orange compound, recrystallised from ethanol/water (3:1), gave a yield = 13%, (see Figure 3.9 for ^{1}H-NMR in $CDCl_3$ solvent.)

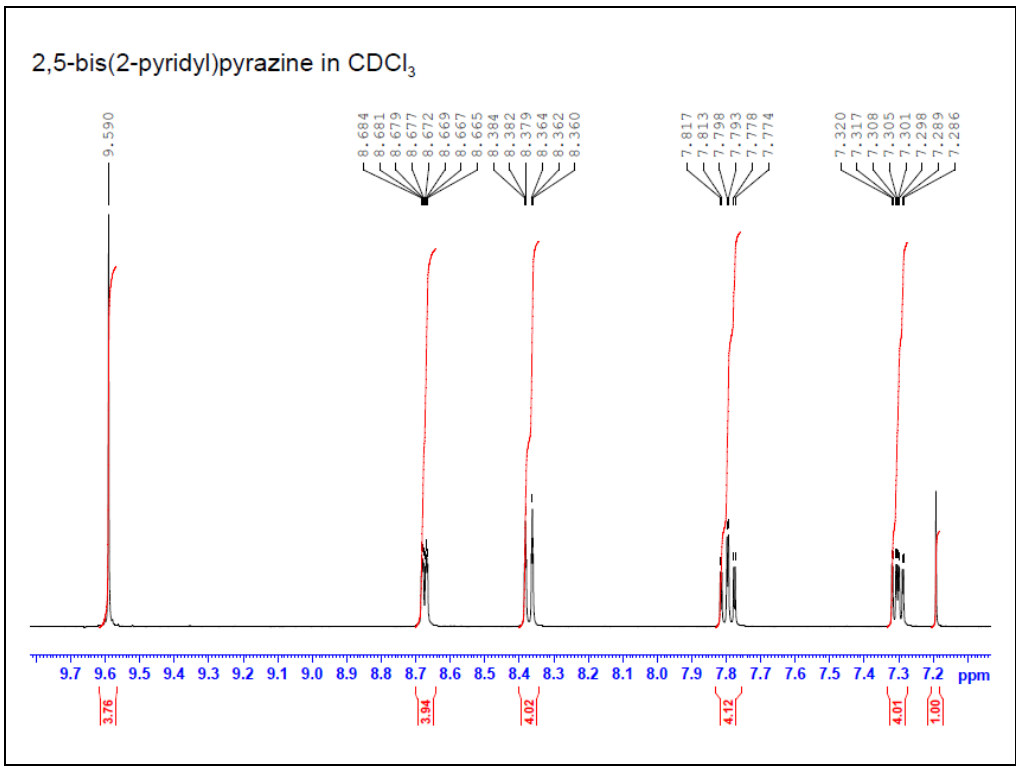

Figure 3.9: *^{1}H-NMR spectra of 2,5-dpp in $CDCl_3$.*

The preparation of the starting material $[Ru(bpy)_2Cl_2].2H_2O$ for the synthesis of the ruthenium bipyridyl complexes was carried out with a slight modification to the literature method.[77] This reaction can be problematic, sometimes leading to the formation of carbonyl containing complexes due to decomposition of the solvent DMF, which must be removed before the compound is used. The synthesis of the ester analogue of $[Ru(dceb)_2Cl_2].2H_2O$ is quite straightforward without any carbonyl decomposition products due to use of ethanol as a reaction solvent. From here the synthesis of all Ru(II) compounds was relatively straightforward using the classical synthetic strategy of "complexes as metals / complexes as ligands". The mononuclear

complexes $[Ru(bpy)_2(2,5\text{-dpp})]^{2+}$ and $[Ru(dceb)_2(2,5\text{-dpp})]^{2+}$ were formed by the addition of excess 2,5-dpp ligand to a refluxing solution of $[Ru(bpy)_2Cl_2]$ and $[Ru(dceb)_2Cl_2]$, respectively. Here it is necessary to dissolved the ligand completely before adding to $[Ru(bpy)_2Cl_2]$ and $[Ru(dceb)_2Cl_2]$, to limit the formation of any homodinuclear complex as a by-product. As the reaction proceeds, the deep violet colour of the $[Ru(bpy)_2Cl_2]$ and deep green colour of the $[Ru(dceb)_2Cl_2]$ solution are gradually replaced by an orange / a red colour, which indicates the presence of the $[Ru(bpy)_2(2,5\text{-dpp})]^{2+}$ and $[Ru(dceb)_2(2,5\text{-dpp})]^{2+}$ complexes respectively. The ethanol was removed at this stage and the chloride counter ion replaced by a PF_6^- counter ion which led to precipitation of the complexes from the aqueous solution. The PF_6^- salts of this type of complexes tend to be only sparingly water soluble and soluble in organic solvents which greatly eases the isolation and purification of these compounds. The yields for the monomer complexes $[Ru(bpy)_2(2,5\text{-dpp})]^{2+}$ was 71% and for $[Ru(dceb)_2(2,5\text{-dpp})]^{2+}$ was 78% after recrystallization in acetone/ water (3:1 v/v). This reaction does not require an inert conditions e.g. nitrogen or argon atmosphere. The mononuclear complexes were stable in visible light and at room temperature.[76]

The heterodinuclear Ru-Pd / Ru-Pt complexes were synthesised by the addition of a 1:1 ratio of the ruthenium(II) mononuclear complexes and the $[Pd(acetonitrile)_2Cl_2]$/ $[Pt(dimethylsulphoxide)_2Cl_2]$ complexes, and heating to reflux in dichloromethane. $Pd(acetonitrile)_2Cl_2$ / $Pt(dimethylsulphoxide)_2Cl_2$ was generally added first and allowed to completely dissolve in dichloromethane before adding the more soluble monomers $[Ru(bpy)_2(2,5\text{-dpp})]^{2+}$ and $[Ru(dceb)_2(2,5\text{-dpp})]^{2+}$. After 24 hours of reflux in dichloromethane, the complexes were precipitated by an addition of n-hexane. The yields of all the heterodinuclear complexes were from 88 – 98% after recrystallization in acetone/ water (3:1 v/v). These complexes were stable in visible light and room temperature, and also did not require any inert conditions for their synthesis.[76]

The synthesis of partial and fully deuteriated mononuclear ruthenium and heterodinuclear Ru – Pd complexes were the same as that mentioned for the non-deuteriated complexes. Instead of $[Ru(bpy)_2Cl_2]$ and (H_{10}-2,5-dpp), $[Ru(D_8\text{-bpy})_2Cl_2]$ and (D_{10}-2,5-dpp) were used for the synthesis of the mononuclear complexes [Ru(D_8-

bpy)$_2$(2,5-dpp)]$^{2+}$, [Ru(bpy)$_2$(D$_{10}$-2,5-dpp)]$^{2+}$ and [Ru(D$_8$-bpy)$_2$(D$_{10}$-2,5-dpp)]$^{2+}$. [Pd(acetonitrile)$_2$Cl$_2$] $_{was}$ used for the synthesis of the deuteriated heterodinuclear Ru – Pd complexes [Ru(D$_8$-bpy)$_2$(2,5-dpp)PdCl$_2$]$^{2+}$ and [Ru(D$_8$-bpy)$_2$(D$_{10}$-2,5-dpp)PdCl$_2$]$^{2+}$. The yields for the deuteriated monomer complexes were from 48 – 61% and for the heterodinuclear Ru – Pd, from 91 – 98% after recrystallization in acetone/ water (3:1 v/v).[75]

3.3.1.1 Deuteriation of the ligands

The polypyridine ligands were deuteriated according to the method developed by Browne et. al. at 200°C, and a 1 M solution of sodium deuterioxide in deuterium oxide (Figure 3.10).[78] After heating the ligands in a closed Teflon container under pressure for six days the deuteriated products were obtained. The isolated products contained 98% deuterium in case of the bpy ligand and 99% in the case of 2,5-dpp (for the calculation of amount of deuteriation see chapter 2).

By examination of the ^{1}H-NMR spectra of the deuteriated compounds it was observed that for both bpy and 2,5-dpp the extent of proton exchange in every position was almost equal. This could be seen by means of the integrals in the associated spectra (figure 3.11 and 3.12).

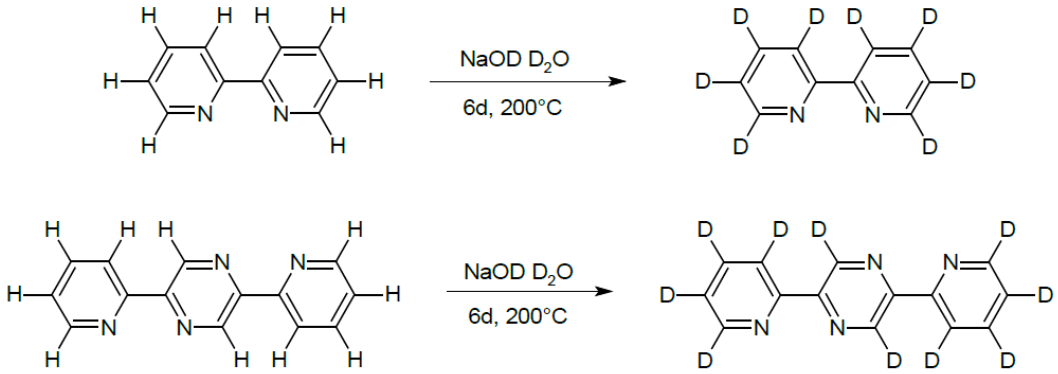

Figure 3.10: *Reaction schemes for the deuteriation of bipyridine (top) and 2,5-bis(2-pyridyl)pyrazine (bottom).*

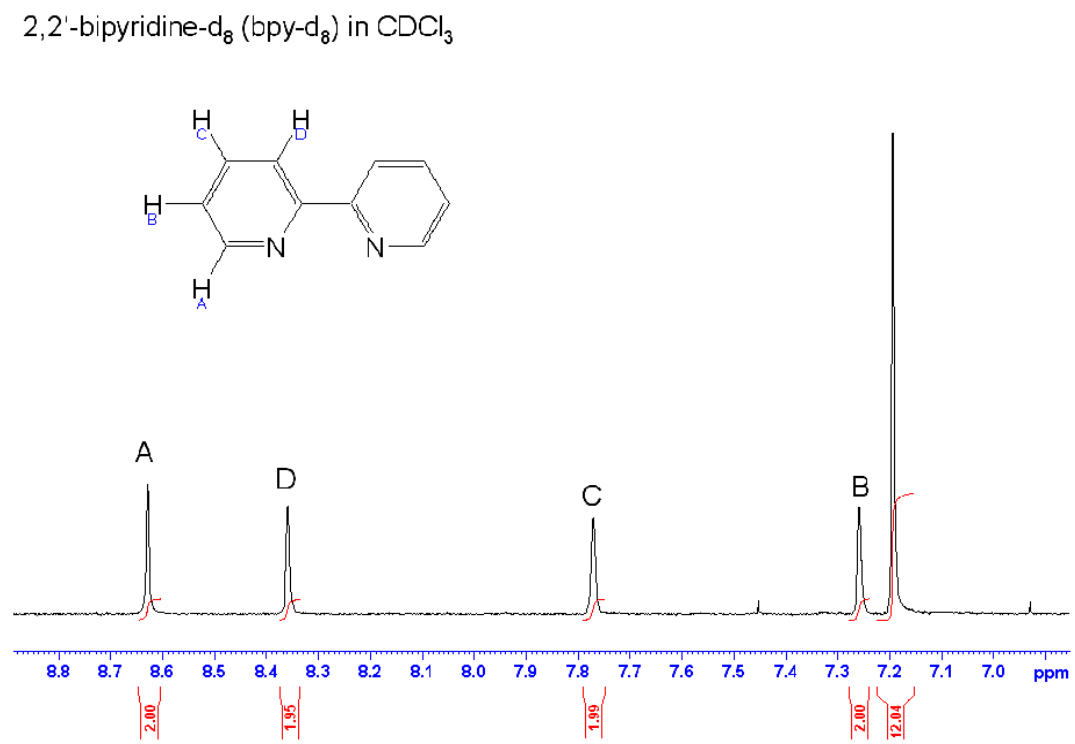

Figure 3.11: *^{1}H-NMR spectrum of deuteriated bpy recorded in $CDCl_3$ (19.9 mg bpy in 1.0 cm^3 of $CDCl_3$).*

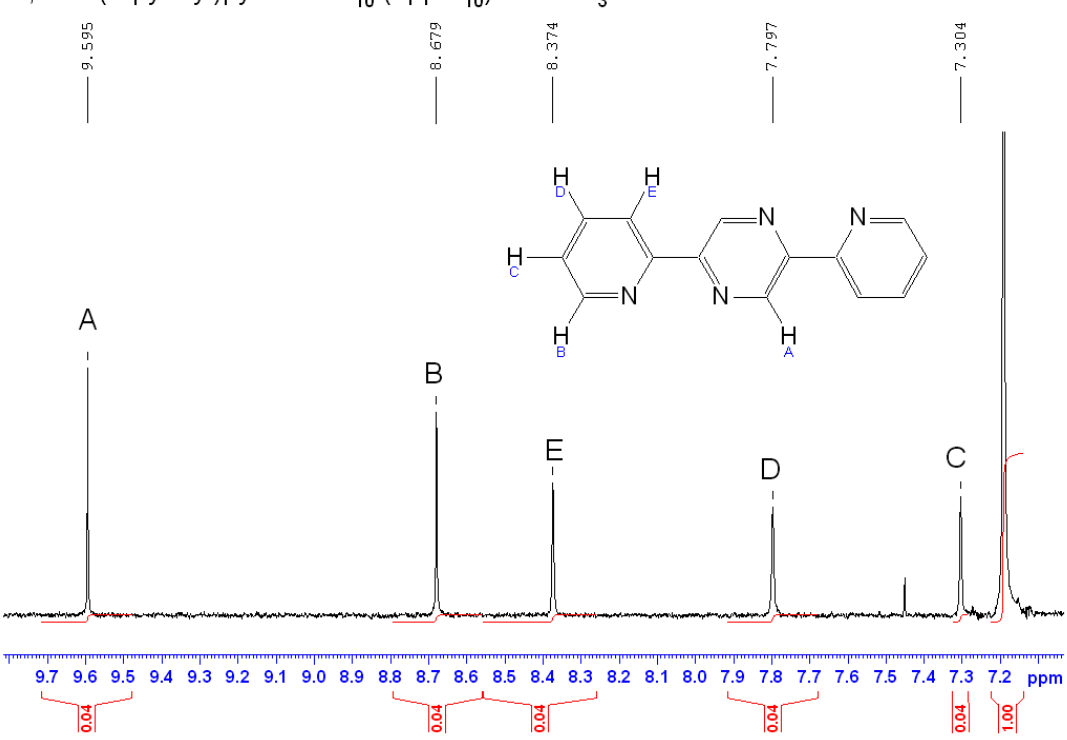

Figure 3.12: *^{1}H-NMR spectrum of deuteriated 2,5-dpp recorded in $CDCl_3$ (10.0 mg of deuteriated 2,5-dpp in 0.65 cm^3 of $CDCl_3$).*

The signals in both spectra appear as singlets. Although there are some protons left, no coupling is observed anymore. In case of the 2,5-dpp ligand, in which only 1% of protons are left, the probability of coupling is only 0.01%. Nevertheless, the chemical shifts of these signals are the same as for the centers of the multipletts in the protonated starting material (see figure 3.9). Therefore, the information about the chemical environment is conserved. By recording the IR spectra of the protonated ligands and their deuteriated analogues, the energetical difference between the C – H and C – D stretching modes can clearly be observed. For both ligands (bpy and 2,5-dpp) the C – D vibrations appear at lower wavenumbers. In case of the 2,2'-bipyridine (bpy) ligand the difference between the C – H (3055 cm^{-1}) and C – D (2266 cm^{-1}) stretching vibrations is about 789 cm^{-1} (Figure 3.13). A small alteration in the region of aromatic C – C stretching modes and out of plane C – H vibrations can be observed as well. However, the influence of the isotope exchange on these bands is of a lower extent compared to the effect on the C – H vibrations.

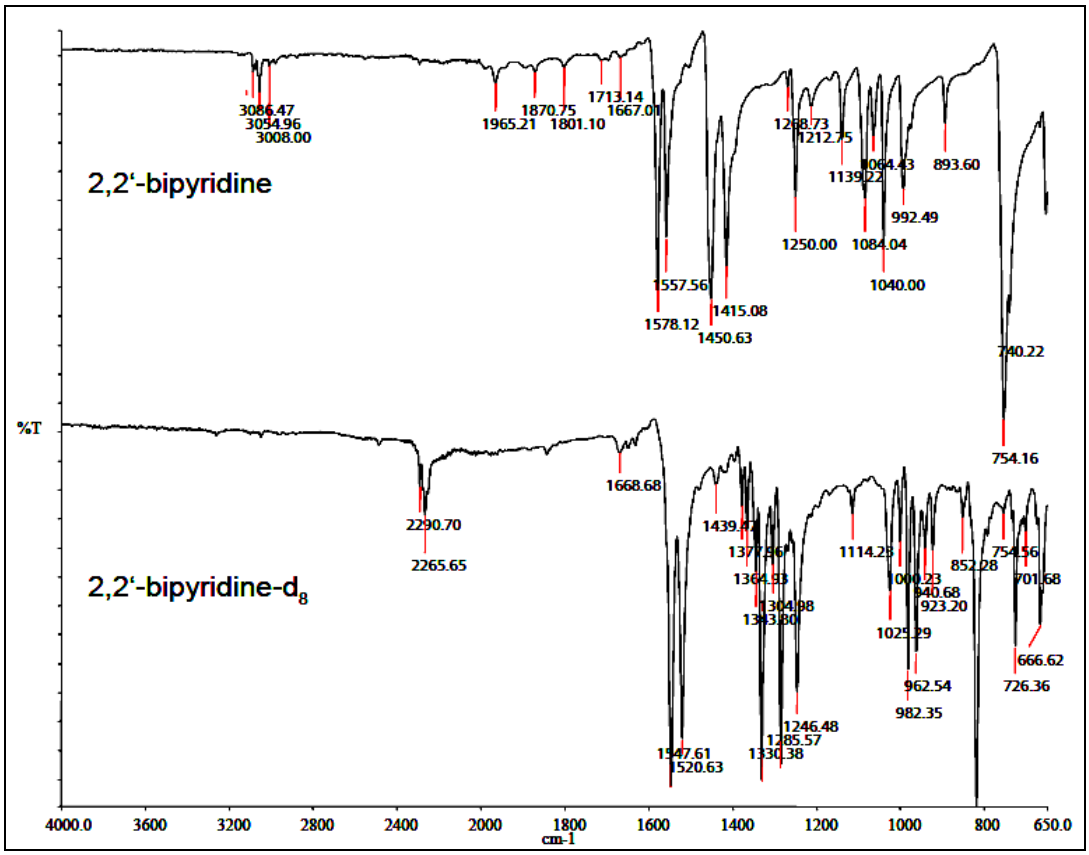

Figure 3.13: *Comparison of IR spectra of the protonated (top) and deuteriated bipyridine ligand (bottom).*

The IR spectra of the bridging ligand 2,5-dpp and its deuteriated analogue were compared accordingly. The spectra are depicted in Figure 3.14. The C – H stretching vibrations can be located as a small peak at 3054 cm^{-1}. By deuteriation, the resulting C – D vibrations appear at 2272 cm^{-1}. The energetic difference is in the same range as in the case of the bipyridine (bpy) ligand. The deuteriated 99.5% D_5-Pyridine C – D stretching vibration is about 2300 cm^{-1} which is same for bpy and 2,5-dpp on deuteriation.[79]

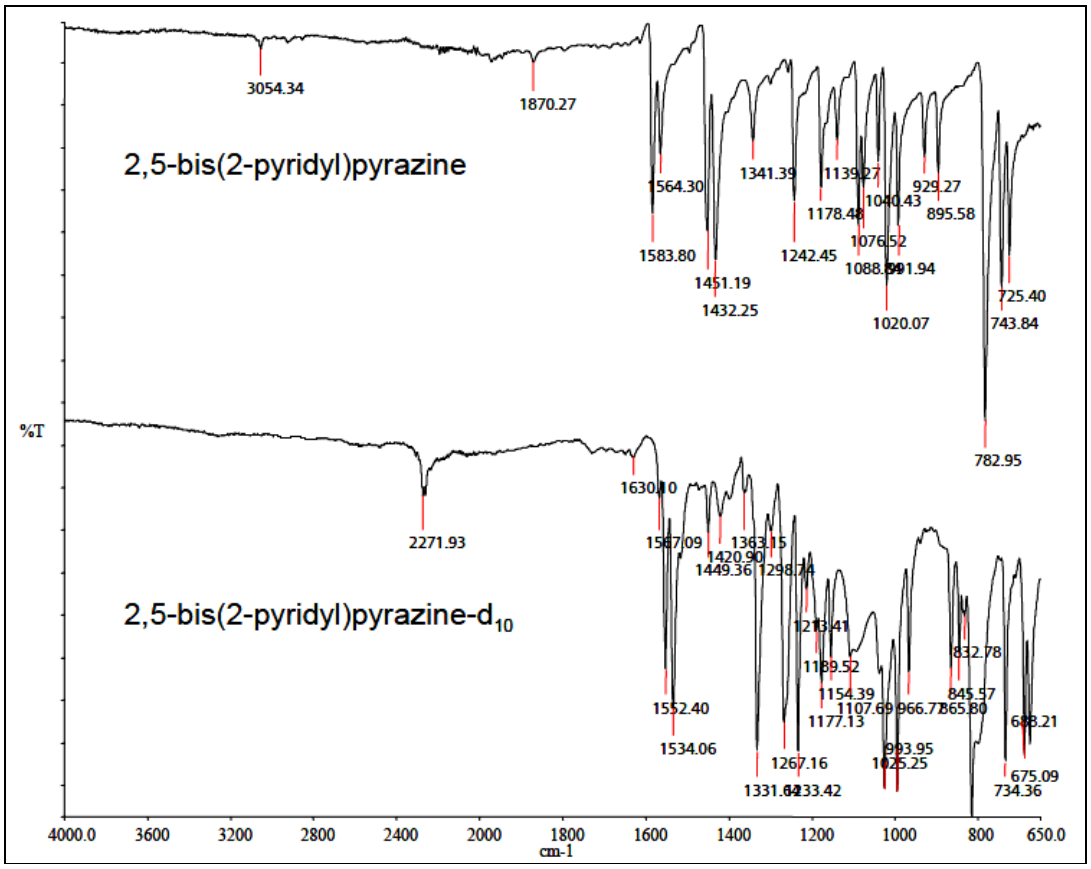

Figure 3.14: *Comparison of IR spectra of the protonated (top) and the deuteriated 2,5-dpp ligand (bottom).*

3.3.2 ^{1}H-NMR Spectroscopy

Proton NMR spectroscopy can provide useful information for elucidating the structure of the ruthenium complexes. NMR spectroscopy is an invaluable tool not only in the identification of the compounds but also in the monitoring of reactions and the determination of purity. It was used extensively in this thesis and where practical, full assignment of ^{1}H-NMR spectra have been made using a combination of 1-dimensional and 2-dimensional studies. In the present chapter the synthesis of mononuclear ruthenium (II) and mixed-metal Ru – Pd or Ru – Pt complexes will be described with 2,5-dpp as the bridging ligands.

In order to simply the ^{1}H-NMR spectra the deuteriated analogues of the complexes were synthesised and used as a tool to confirm peak assignment and the structures of complexes. For the non-symmetric mononuclear complexes, up to sixteen non-

equivalent protons may arise from the 2,2'-bipyridyl (bpy) moieties making complete unambiguous structural assignment difficult. Deuteriation of the 2,2'-bipyridyl (bpy) ligand led to the removal of a number of protons. As a result it only remained to assign the protons of the 2,5-di(pyridin-2-yl)pyrazine (2,5-dpp) ligands in the case of the mononuclear complexes as well as in the case of heterodinuclear complexes. Deuteriated D_{10}-2,5-di(pyridin-2-yl)pyrazine (D_{10}-2,5-dpp) was also used to see the remaining protons of 2,2'-bipyridine (bpy) in the case of the mononuclear and the heterodinuclear complexes.

3.3.2.1 ^{1}H-NMR of the mononuclear complex.

Figure 3.15 shows the numbering of the non-deuteriated and deuteriated ruthenium(II) mononuclear complexes. The chemical shifts of the ruthenium(II) mononuclear complex $[Ru(bpy)_2(2,5\text{-dpp}]^{2+}$ with 2,5-dpp ligand in d_6-dmso and d_3-acetonitrile are outlined in Table 3.2. For simplicity to distinguish between the protons of the pyridine rings (Ring C (free) (proton sign (H3' – H6') / Ring B (metal bound) (proton sign (H3" – H6")) and pyrazine ring (A) (proton sign (H3 – H6) of the 2,5-dpp ligand, and the bpy protons are number H(3a) – H(6a) (see figure 3.15). These bpy protons occur in the expected range and will not be discussed here. The same numbering system of the 2,5-dpp ligand for the $[Ru(bpy)2(2,5\text{-dpp})]^{2+}$ complex was used here and comparable chemical shifts was observed as reported by Ferrari et. al.[80]

In this section, the 2,5-dpp protons of the mononuclear complex $[Ru(bpy)_2(2,5\text{-dpp}]^{2+}$are discussed. As expected, due to the nature of coordination, there is a clear difference between the protons of the two pyridine rings (B and C) of the 2,5-dpp ligand, as shown in figure 3.16 (^{1}H-NMR comparison of complexes 3.1, 3.3, 3.4 and 3.5). The H6" protons of the metal bound pyridine (ring B) experience the ring current of an adjacent bpy and are strongly shifted upfield as a result. The proton H6' (ring B) is present at ~ 8.53 ppm while H6" is observed at 7.80 ppm in d_6-dmso as solvent (H6' = 8.51 ppm and H6" = 7.81 ppm in case of d_3-acetonitrile as a solvent [80]). This large difference between ring 1 and ring 2 for the H6" / H6' resonances demonstrates that the H6" protons present at 7.80 ppm / 7.81 ppm (in both solvents) must be assigned to the metal-bound pyridine as it is shifted over 1.30 ppm upfield. In addition

protons in close proximity to large atoms, such as a metal ion, are greatly shielded from the induced magnetic field of the NMR and therefore require a greater applied magnetic field strength for resonance.[81]

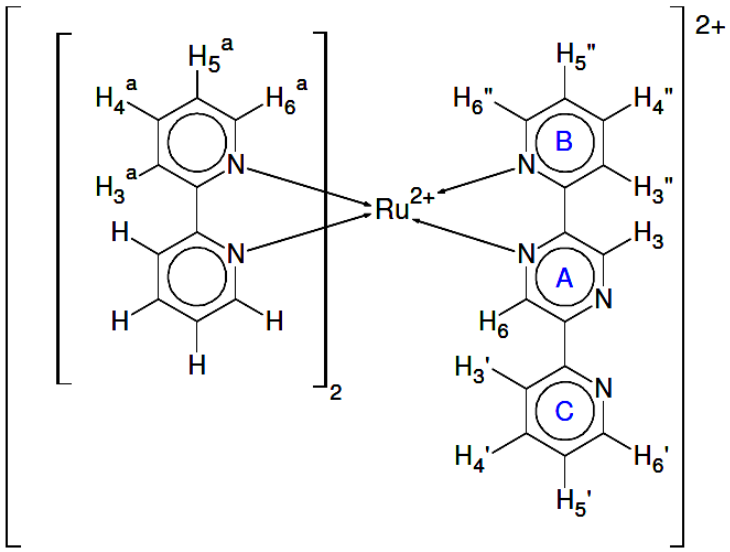

[Ru(bpy)$_2$(2,5-dpp)]$^{+2}$

Complex 3.1

[Ru(D$_8$-bpy)$_2$(2,5-dpp)]$^{+2}$

Complex 3.3

[Ru(bpy)$_2$(D$_{10}$-2,5-dpp)]$^{+2}$

Complex 3.4

[Ru(D$_8$-bpy)$_2$(D$_{10}$-2,5-dpp)]$^{+2}$

Complex 3.5

Figure 3.15: *Labelling of the chemical structures for non-deuteriated and deuteriated (partial/ full) analogues of ruthenium(II) mononuclear complexes.*

Ring C (free)	H6'(d)	H5'(t)	H4'(t)	H3'(d)
δ in (d_6-dmso)	8.53	7.52	8.03	8.42
δ in (d_3-acetonitrile)	8.51	7.46	7.97	8.44
δ in (d_6-dmso) for 2,5-dpp[a]	8.79	7.57	8.04	8.43
{Free ligand (2,5-dpp)}[b]	(+0.26)	(+0.05)	(+0.01)	(+0.01)

Ring B (Metal)	H6"(d)	H5"(t)	H4"(t)	H3"(d)
δ in (d_6-dmso)	7.80	7.60	8.25	9.04
δ in (d_3-acetonitrile)	7.81	7.49	8.14	8.69
δ in (d_6-dmso) for 2,5-dpp[a]	8.79	7.57	8.04	8.43
{Free ligand (2,5-dpp)}[b]	(+0.99)	(-0.03)	(-0.21)	(-0.61)

Pyrazine Ring (A)	H3(s)	H6(s)
δ in (d_6-dmso)	10.04	8.59
δ in (d_3-acetonitrile)	9.65	8.74
δ in (d_6-dmso) for 2,5-dpp[a]	9.63	9.63
{Free ligand (2,5-dpp)}[b]	(-0.41)	(+1.04)

Bpy ^{1}H of complex	H3a	H4a	H5a	H6a
δ in (d_6-dmso)	8.08-7.72	7.63-7.48	8.28-8.19	8.90-8.51
δ in (d_3-acetonitrile)	7.82-7.75	7.50-7.44	8.19-8.08	8.57-8.52

[a] *Protons shifts of H6' = H6", H5' = H5", H4' = H4", H3' = H3" are chemically equivalent due to i_2 symmetry element present in 2,5-dpp ligand.*

[b] *Chemical shifts direction for free ligand w.r.t. mononuclear complex: (free ligand – complexed ligand), (+ sign indicates downfield), (- sign indicates upfield); in d_6-dmso.*

Table 3.2: Chemical shifts in ppm (with multiplet) of the 2,5-dpp protons of the non-deuteriated $[Ru(bpy)2(2,5\text{-}dpp)]^{2+}$ as measured in d_6-dmso (red) and also measured in d_3-acetonitrile (blue). The other shifts present in the table represent the free 2,5-dpp ligand in d_6-dmso (green).

The H6' free pyridine (ring C) proton is shifted only 0.26 ppm upfield (low ppm) from free 2,5-dpp ligand in d_6-dmso (Table 3.2). For the free pyridine ring C, all

protons (H3' – H6') are slightly upfield / more or less same while metal bind pyridine ring B is a slight downfield (for H3", H4", H5") except H6" is 0.99 ppm upfield in comparison to free 2,5-dpp ligand. The explanation for H3 (10.04 ppm)/ H6 (8.59 ppm) is the same as for H6"/ H6' through space interaction of Ru-metal and bpy protons.

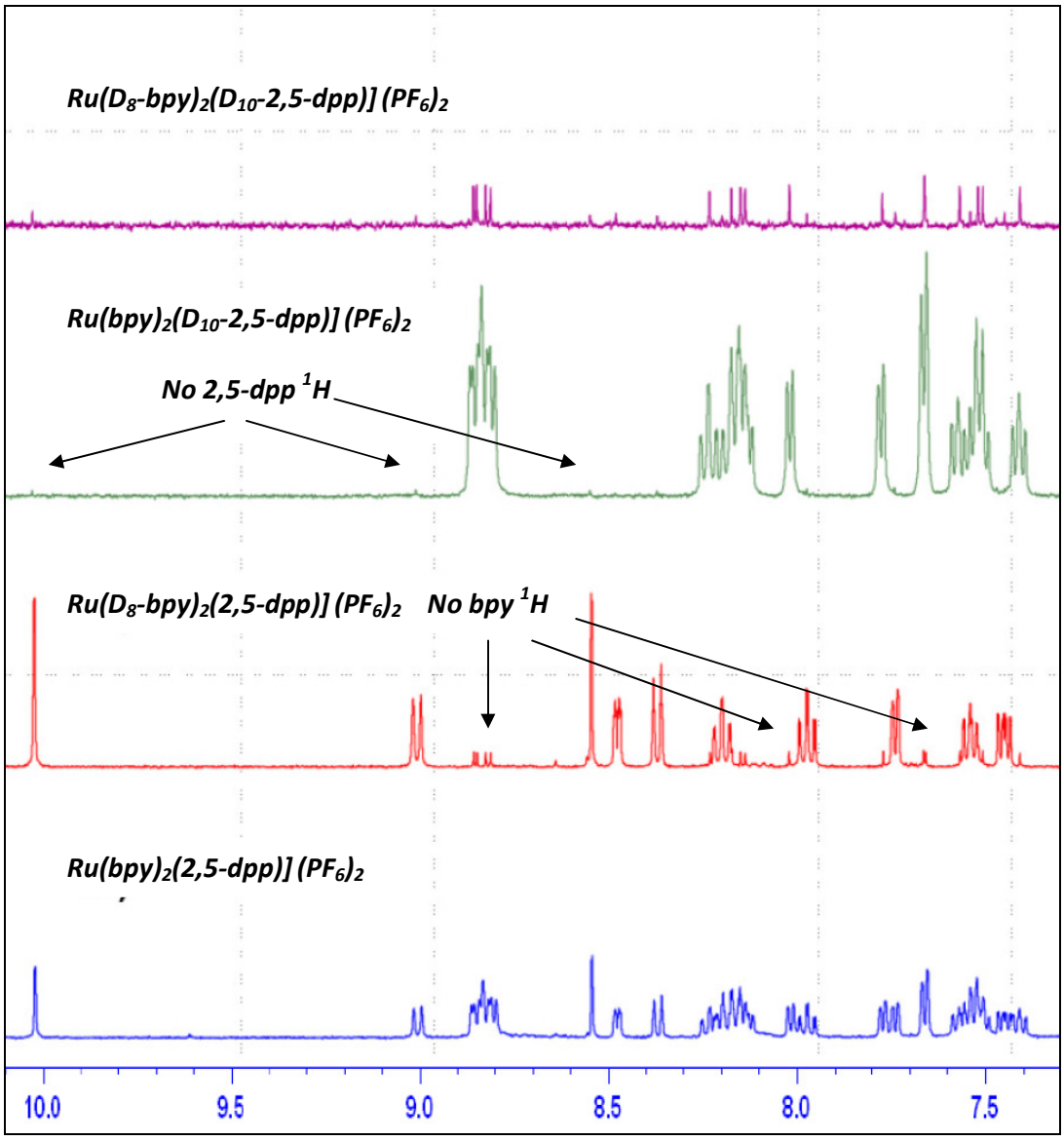

Figure 3.16: *Comparison of proton-NMR spectra of non-deuteriated and deuteriated analogous of ruthenium(II) monomers in DMSO-d_6.*

Using 2-D COSY and the analogous deuteriated complex $[Ru(D_8\text{-bpy})_2(2,5\text{-dpp})]^{2+}$, it became possible to assign the chemical shifts for the all 2,5-dpp protons of the two pyridine rings (B and C) and middle pyrazine ring (A). As can be seen from the

comparison between the deuteriated and non-deuteriated mononuclear complexes the deuteriated species has resulted in a simplification of the ^{1}H-NMR spectrum and therefore, assisted in the confirmation of the chemical shifts for the 2,5-dpp and bipyridine protons, which are documented above in Table 3.2. 2-D COSY ^{1}H-NMR spectra of the $[Ru(D_8\text{-bpy})_2(2,5\text{-dpp})]^{2+}$ is recorded in d_6-dmso (depicted in figure 3.17) and in d_3-acetonitrile (depicted in figure 3.18).

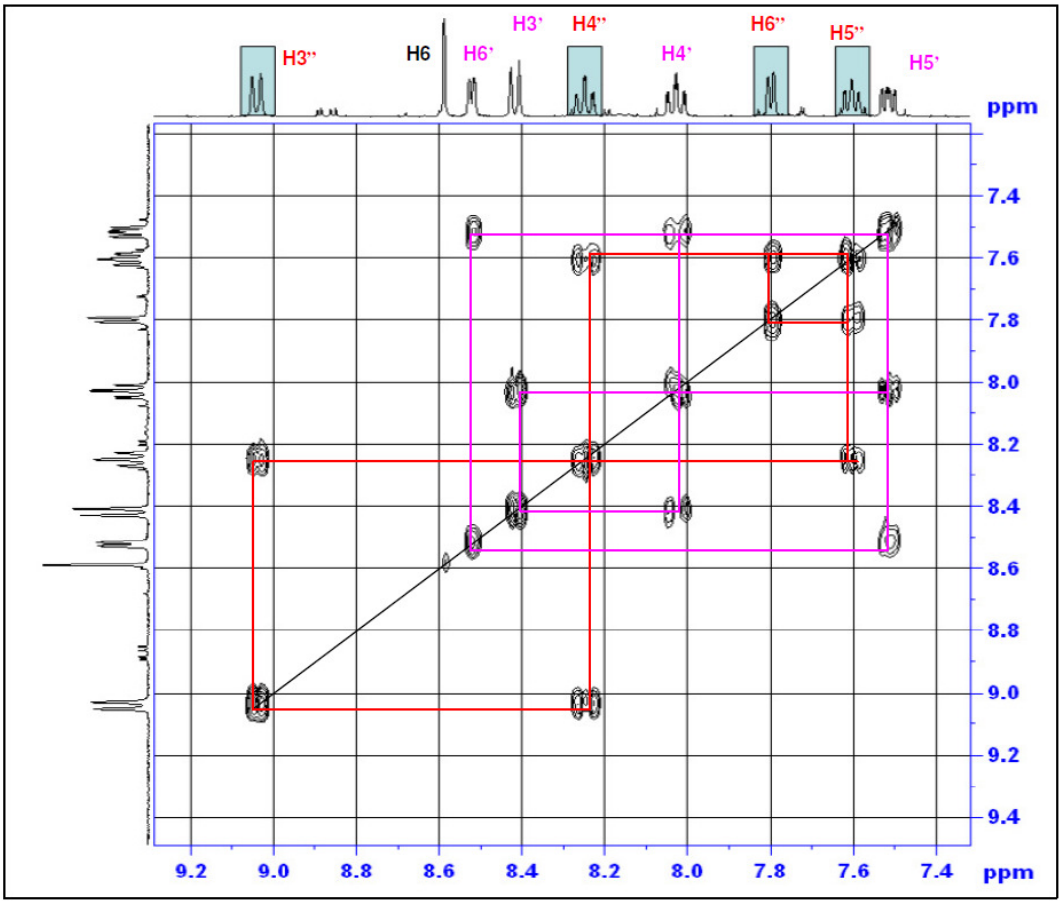

Figure 3.17: *2D-COSY NMR of the $[Ru(D_8\text{-bpy})_2(2,5\text{-dpp})]^{2+}$ in d_6-dmso.*

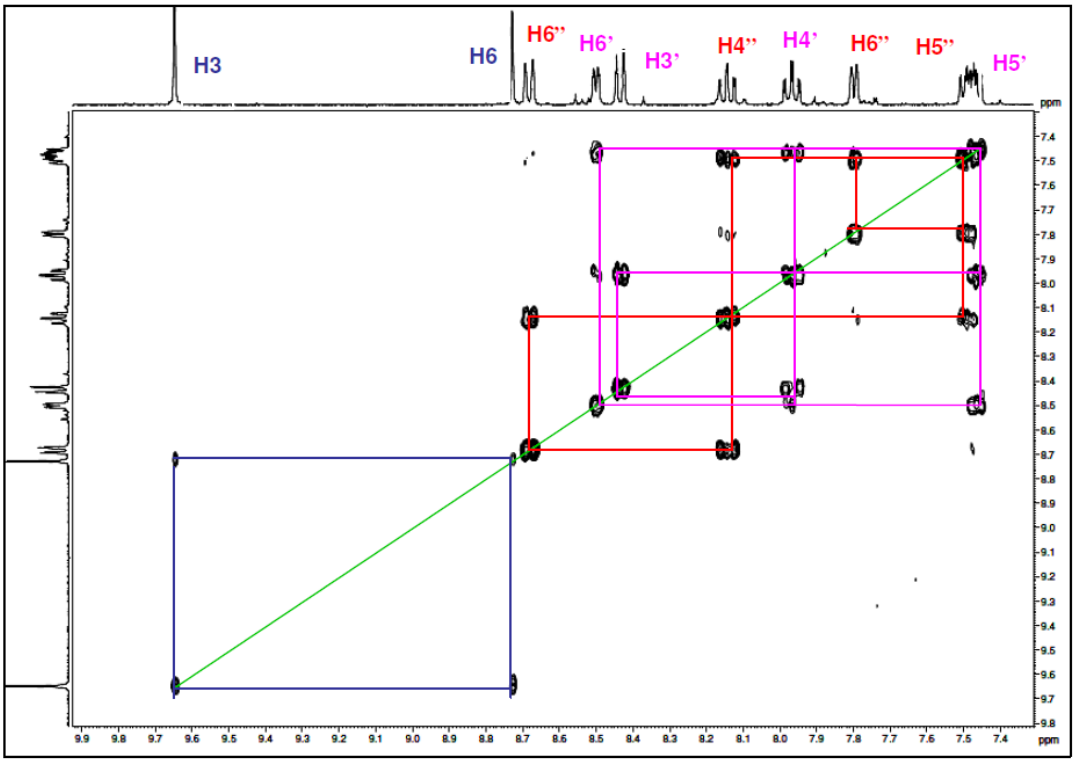

Figure 3.18: *2D-COSY NMR of the $[Ru(D_8\text{-bpy})_2(2,5\text{-dpp})]^{2+}$ in d_3-acetonitrile.*

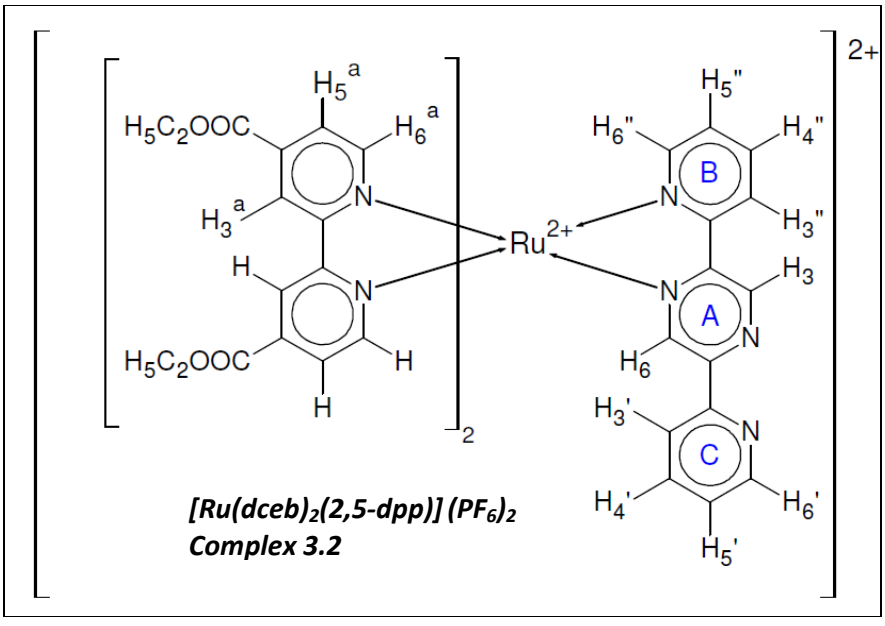

Figure 3.19: *Chemical structure of $[Ru(dceb)_2(2,5\text{-dpp})]\ (PF_6)_2$ with numbering.*

The numbering and ^{1}H-NMR chemical shifts for $[Ru(dceb)_2(2,5\text{-dpp})]^{2+}$ are shown in Figure 3.19 and Table 3.3. In general there is no change in the chemical shifts of the

2,5-dpp ligand (pyridine ring B, pyridine ring C and pyrazine middle ring A) when 4,4'-dicarboxyethyl-(2,2'-bipyridine) (dceb) was used as a peripheral ligand. The H3a protons of the peripheral ligand 'dceb' is shifted from 8.57-8.52 ppm to 9.12-9.07 ppm which is downfield due to the electron withdrawing carboxylic ester group present at H4a position in 2,2'-bpy. Also the same effect was observed for H6a and H5a on the dceb ligand (see table 3.3 below). Protons for the ethyl ester group occurs in the range at 4.54-4.46 ppm (m, 8H, CH_2) with four quartet signals that overlap in this region, similarly at 1.50-1.40 (m, 12H, CH_3) four triplet signals overlap. 2-D COSY ^{1}H-NMR & 1-D ^{1}H-NMR spectra of the $[Ru(dceb)_2(2,5\text{-}dpp)]^{2+}$ is recorded in d_3-acetonitrile, and in depicted in figure 3.20 & 3.21 respectively.

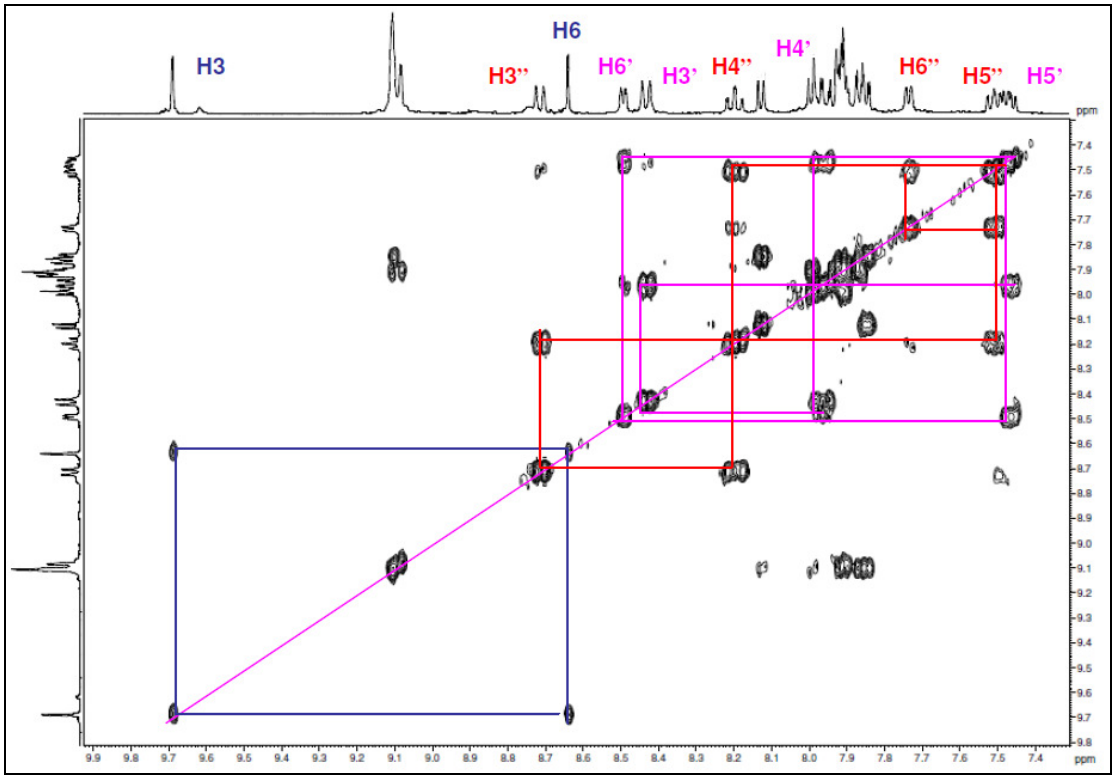

Figure 3.20: *2D-COSY NMR of the $[Ru(dceb)_2(2,5\text{-}dpp)]^{2+}$ in d_3-acetonitrile.*

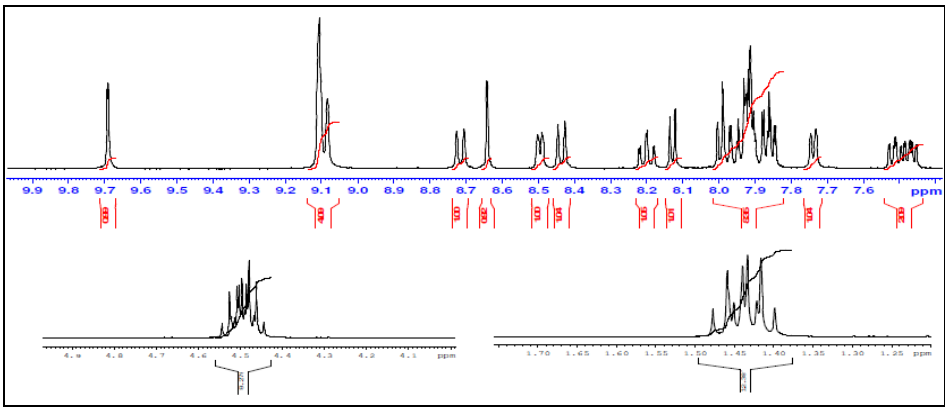

Figure 3.21: *^{1}H-NMR of the $[Ru(dceb)_2(2,5\text{-}dpp)]^{2+}$ in d_3-acetonitrile.*

Ring C (free)	***H6'(d)***	***H5'(t)***	***H4'(t)***	***H3'(d)***
δ in (d_3-acetonitrile) $[Ru(bpy)_2(2,5\text{-}dpp)]^{+2}$	*8.51*	*7.46*	*7.97*	*8.44*
δ in (d_3-acetonitrile) $[Ru(dceb)_2(2,5\text{-}dpp)]^{+2}$	*8.50*	*7.46*	*7.97*	*8.44*
Ring B (Metal)	***H6"(d)***	***H5"(t)***	***H4"(t)***	***H3"(d)***
δ in (d_3-acetonitrile) $[Ru(bpy)_2(2,5\text{-}dpp)]^{+2}$	*7.81*	*7.49*	*8.14*	*8.69*
δ in (d_3-acetonitrile) $[Ru(dceb)_2(2,5\text{-}dpp)]^{+2}$	*7.74*	*7.52*	*8.20*	*8.71*
Pyrazine Ring (A)	***H3(s)***	***H6(s)***		
δ in (d_3-acetonitrile) $[Ru(bpy)_2(2,5\text{-}dpp)]^{+2}$	*9.65*	*8.74*		
δ in (d_3-acetonitrile) $[Ru(dceb)_2(2,5\text{-}dpp)]^{+2}$	*9.69*	*8.64*		
Bpy 1H of complex	***H6a***	***H5a***	***H4a***	***H3a***
δ in (d_3-acetonitrile) $[Ru(bpy)_2(2,5\text{-}dpp)]^{+2}$	*7.82-7.75*	*7.50-7.44*	*8.19-8.08*	*8.57-8.52*
δ in (d_3-acetonitrile) $[Ru(dceb)_2(2,5\text{-}dpp)]^{+2}$	*8.13 - 7.84*		*NA*	*9.12-9.07*

Table 3.3: Chemical shifts in ppm comparison of the non-ester $[Ru(bpy)_2(2,5\text{-}dpp)]^{2+}$ and ester analogous $[Ru(dceb)_2(2,5\text{-}dpp)]^{2+}$ as measured in d_3-acetonitrile.

3.3.2.2 ^{1}H-NMR of the heterodinuclear complexes.

The numbering of the heterodinuclear complexes (non-deuteriated and deuteriated) is shown in figure 3.22 and 3.23. The chemical shifts of the 2,5-dpp ligand, 2,2'-bpy and 4,4'-carboxyethylester-2,2'-bpy in the Ru–Pd / Ru–Pt heterodinuclear complexes are outlined in Table 3.4. After complexation with $[Pd(CH_3CN)_2Cl_2]$ or $[Pt(dmso)_2Cl_2]$, the protons on the pyridine ring C and pyrazine ring A of the heterodinuclear complexes are shifted downfield due to the electro withdrawing effect of the Pd(II)/ Pt(II) metal centre, (see Table 3.4).

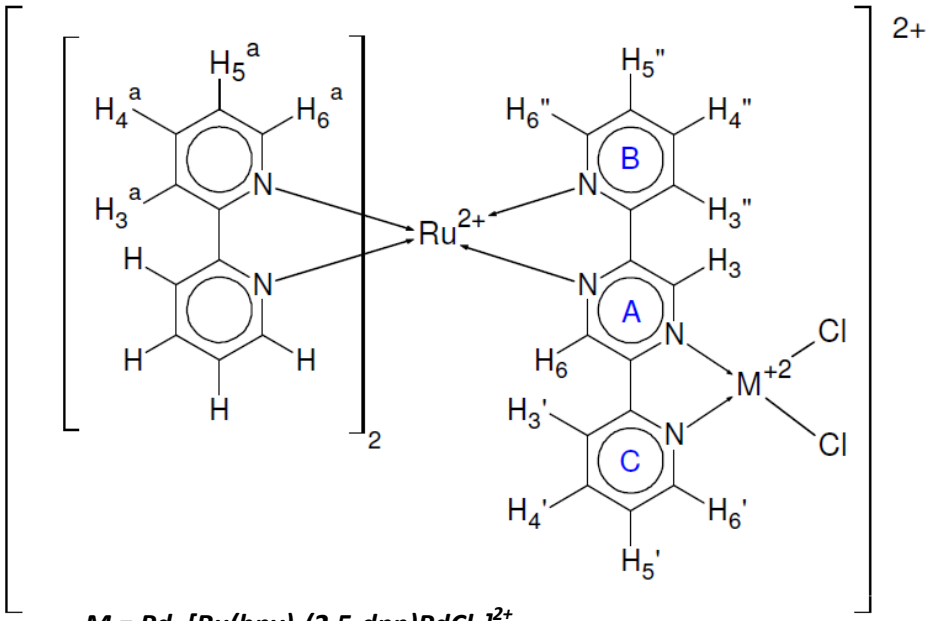

M = Pd, $[Ru(bpy)_2(2,5\text{-}dpp)PdCl_2]^{2+}$
Complex 3.6
M = Pt, $[Ru(bpy)_2(2,5\text{-}dpp)PtCl_2]^{2+}$
Complex 3.7
M = Pd, H [bpy] = D, $[Ru(D_8\text{-}bpy)_2(2,5\text{-}dpp)PdCl_2]^{2+}$
Complex 3.10
M = Pd, H [bpy and 2,5-dpp] = D, $[Ru(D_8\text{-}bpy)_2(D_{10}\text{-}2,5\text{-}dpp)PtCl_2]^{2+}$
Complex 3.11

Figure 3.22: *Chemical structure and numbering of Ru – Pd (for non-deuteriated and deuteriated) complexes.*

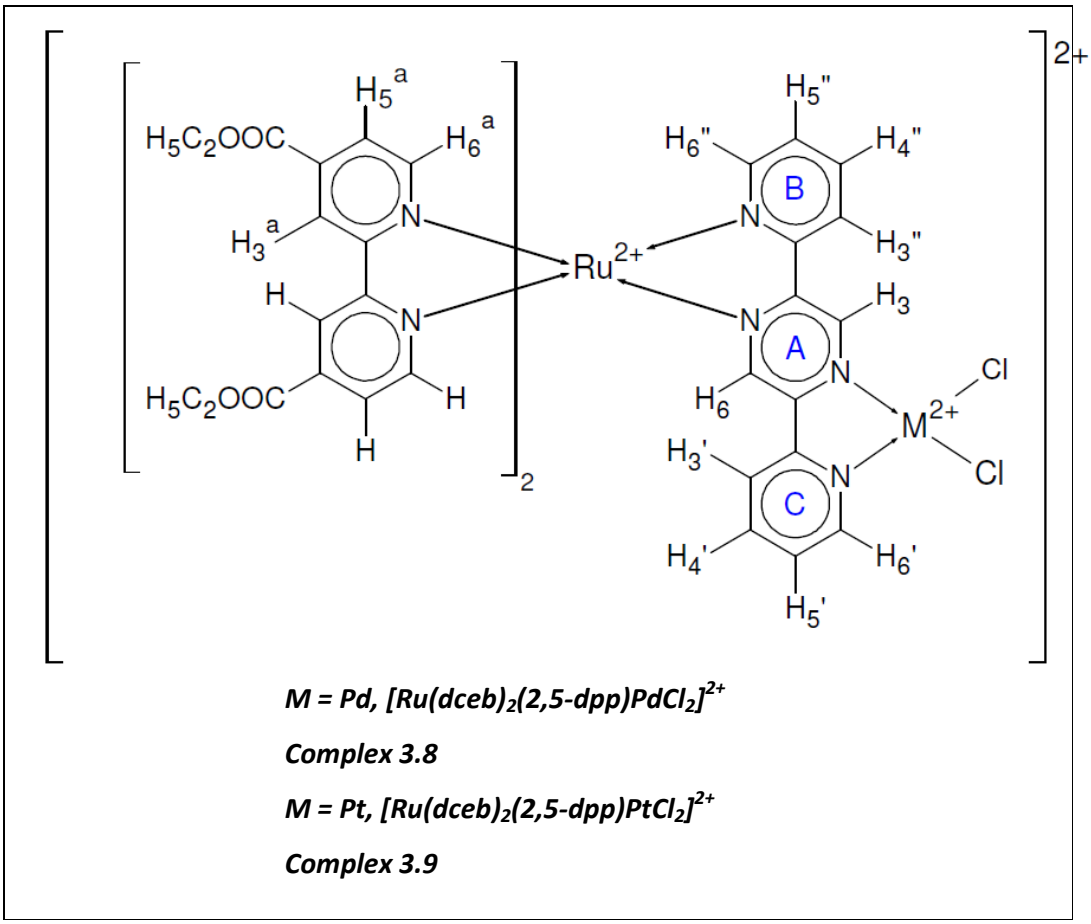

M = Pd, [Ru(dceb)$_2$(2,5-dpp)PdCl$_2$]$^{2+}$

Complex 3.8

M = Pt, [Ru(dceb)$_2$(2,5-dpp)PtCl$_2$]$^{2+}$

Complex 3.9

Figure 3.23: *Chemical structure and numbering of Ru – Pt complexes.*

In general, for the pyridine ring B, bpy ligands and dceb ligands, the protons were observed at the same chemical shift as observed as in the relevant mononuclear complexes, see Table 3.4. In the case of $[Ru(bpy)_2(2,5\text{-dpp})PdCl_2]^{2+}$ with bpy as the peripheral ligand, the H3, H6', H5' and H4' protons of the 2,5-dpp bridging ligand show a large shift from 0.40 ppm to 0.13 ppm downfield due to the electron withdrawing Pd metal centre while H3' proton undergoes a shift upfield by 0.78 ppm due to a combination of through space interactions between the two ligand species H3' / bpy ligand and the general shielding effects of the metal ion. A comparison of the non- deuteriated / bpy-deuteriated analogue of the $[Ru(bpy)_2(2,5\text{-dpp})PdCl_2]^{2+}$ shown in (figure 3.24) and 2D-COSY ^{1}H-NMR (figure 3.25), it is possible to assign the chemical shifts of all 2,5-dpp protons.

Ring C (free)	H6'(d)	H5'(t)	H4'(t)	H3'(d)
$[Ru(bpy)_2(2,5\text{-}dpp)PdCl_2]^{2+}$	8.91	7.61	8.10	7.66
$[Ru(bpy)_2(2,5\text{-}dpp)PtCl_2]^{2+}$	9.39	7.72	8.19	7.73
$[Ru(dceb)_2(2,5\text{-}dpp)PdCl_2]^{2+}$	8.81	7.61	8.10	7.82
$[Ru(dceb)_2(2,5\text{-}dpp)PtCl_2]^{2+}$	9.40	7.72	8.18	7.81
$[Ru(bpy)_2(2,5\text{-}dpp)]^{2+}$	8.51	7.46	7.97	8.44
$[Ru(dceb)_2(2,5\text{-}dpp)]^{2+}$	8.50	7.46	7.97	8.44
Ring B (Metal)	**H6"(d)**	**H5"(t)**	**H4"(t)**	**H3"(d)**
$[Ru(bpy)_2(2,5\text{-}dpp)PdCl_2]^{2+}$	7.81	7.59	8.15	8.62
$[Ru(bpy)_2(2,5\text{-}dpp)PtCl_2]^{2+}$	7.84	7.60	8.20	8.65
$[Ru(dceb)_2(2,5\text{-}dpp)PdCl_2]^{2+}$	7.79	7.61	8.25	8.68
$[Ru(dceb)_2(2,5\text{-}dpp)PtCl_2]^{2+}$	7.79	7.61	8.35	8.68
$[Ru(bpy)_2(2,5\text{-}dpp)]^{2+}$	7.81	7.49	8.14	8.69
$[Ru(dceb)_2(2,5\text{-}dpp)]^{2+}$	7.74	7.52	8.20	8.71
Pyrazine Ring (A)	**H3(s)**	**H6(s)**		
$[Ru(bpy)_2(2,5\text{-}dpp)PdCl_2]^{2+}$	10.05	8.42		
$[Ru(bpy)_2(2,5\text{-}dpp)PtCl_2]^{2+}$	10.50	8.34		
$[Ru(dceb)_2(2,5\text{-}dpp)PdCl_2]^{2+}$	10.13	8.42		
$[Ru(decb)_2(2,5\text{-}dpp)PtCl_2]^{2+}$	10.58	8.30		
$[Ru(bpy)_2(2,5\text{-}dpp)]^{2+}$	9.65	8.74		
$[Ru(dceb)_2(2,5\text{-}dpp)]^{2+}$	9.69	8.64		
Bpy ^{1}H of complex	**H6a**	**H5a**	**H4a**	**H3a**
$[Ru(bpy)_2(2,5\text{-}dpp)PdCl_2]^{2+}$	7.82-7.75	7.50-7.44	8.19-8.08	8.57-8.52
$[Ru(bpy)_2(2,5\text{-}dpp)PtCl_2]^{2+}$	8.07-7.55	7.67-7.42	8.19-8.05	8.57-8.48
$[Ru(dceb)_2(2,5\text{-}dpp)PdCl_2]^{2+}$	7.92 - 7.83		NA	9.12-9.08
$[Ru(dceb)_2(2,5\text{-}dpp)PtCl_2]^{2+}$	7.92 - 7.83		NA	9.12-9.08
$[Ru(bpy)_2(2,5\text{-}dpp)]^{2+}$	7.82-7.75	7.50-7.44	8.19-8.08	8.57-8.52
$[Ru(dceb)_2(2,5\text{-}dpp)]^{2+}$	8.13 - 7.84		NA	9.12-9.07

Table 3.4: Chemical shifts in ppm (with multipletts) of the 2,5-dpp protons, bpy and dceb of the different heterodinuclear complexes as measured in d_3-acetonitrile.

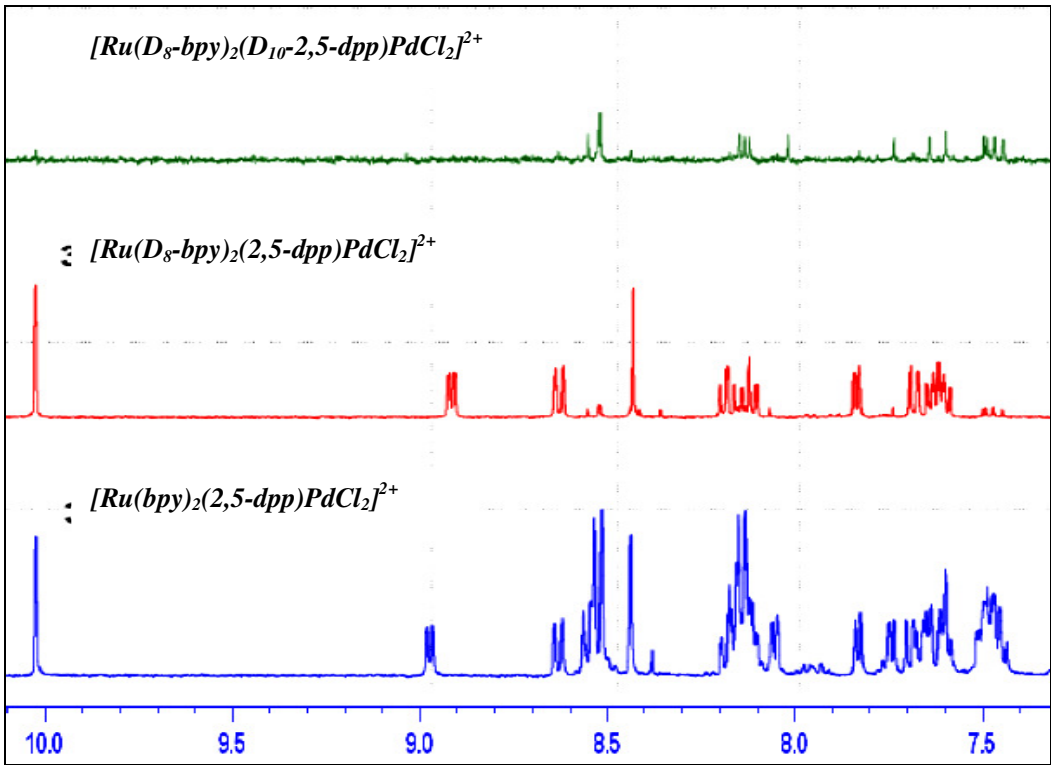

Figure 3.24: *Comparison between non-deuteriated* $[Ru(bpy)_2(2,5\text{-}dpp)PdCl_2]^{2+}$ complex*, D_8-bpy and D_8-bpy / D_{10}-2,5-dpp fully-deuteriated complex.*

Apart from deuteriation, the 2-dimensional-COSY proton-NMR spectra also provided invaluable information (figure 3.25). The proton-proton correlation of the $[Ru(D_8\text{-}bpy)_2(2,5\text{-}dpp)PdCl_2]^{2+}$ complex allows for the assignment of neighbouring protons without the hindrance of large bipyridine signals overshadowing other resonances. By connecting signals through the diagonal intercept an overall picture of the ^{1}H-NMR of the metal complex is obtained. By combining all the data from 1-dimensional and 2-dimensional NMR techniques a complete assignment of the protons within each complex was achieved.

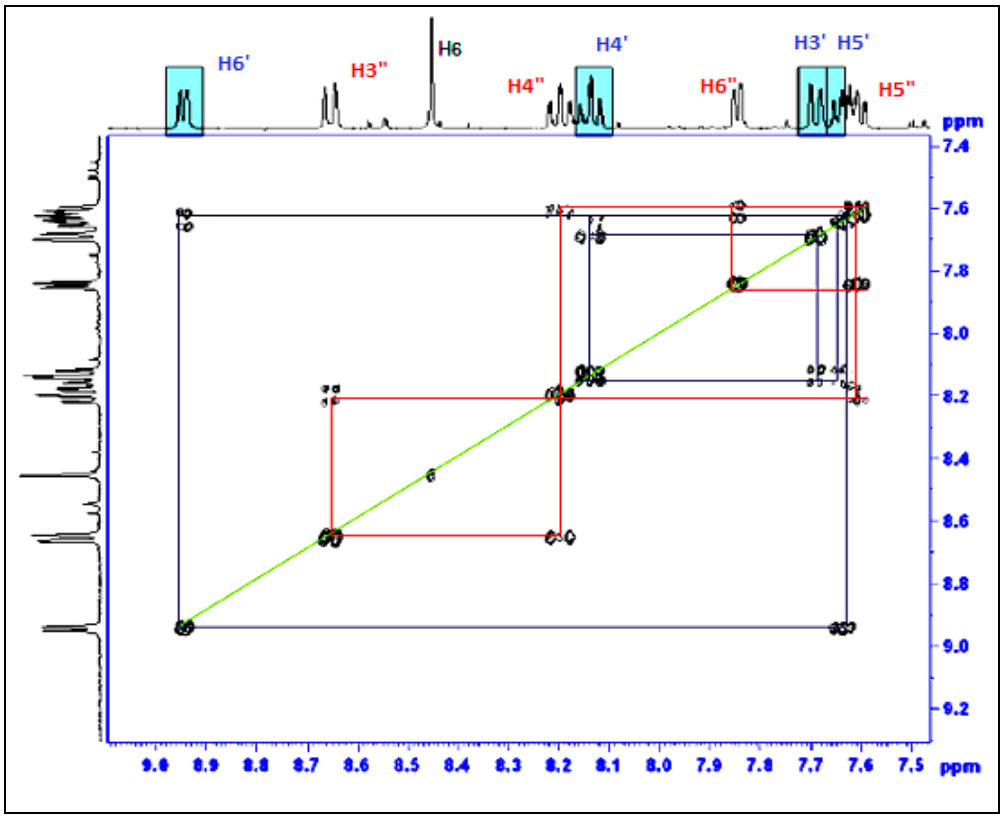

Figure 3.25: *2D-COSY NMR of the* $[Ru(D_8\text{-}bpy)_2(2,5\text{-}dpp)PdCl_2]^{2+}$ *in* d_3*-acetonitrile.*

Figure 3.26, the depicted 2D-COSY proton-NMR correlations of the 2,5-dpp ligand protons and dceb ligands protons of the $[Ru(dceb)_2(2,5\text{-}dpp)PdCl_2]^{2+}$, see structure in figure 3.23. In the $[Ru(dceb)_2(2,5\text{-}dpp)PdCl_2]^{2+}$ complex, the protons of the 2,5-dpp is more or less same w.r.t. the non-ester analogue $[Ru(bpy)_2(2,5\text{-}dpp)PdCl_2]^{2+}$ but protons H6' – H3' on ring C and H6" – H3" on ring B shift slightly downfield w.r.t. the ester mononuclear complex $[Ru(dceb)_2(2,5\text{-}dpp)]^{2+}$ due to the shielding effect of the Ru(II) ion and through space interaction of the peripheral ligands (see table 3.4). Due to the space interaction of ester group on dceb ligands and ruthenium metal shielding the proton H6 remains at the same chemical shift as in the non-ester analogue $[Ru(bpy)_2(2,5\text{-}dpp)PdCl_2]^{2+}$ but upfield shifts w.r.t. mononuclear complex $[Ru(dceb)_2(2,5\text{-}dpp)]^{2+}$ while the H3 proton shifts slight downfield w.r.t. both the complexes. The dceb ligand H3a protons undergo a shift downfield to 9.12-9.07 ppm (4 protons, $[Ru(dceb)_2(2,5\text{-}dpp)PdCl_2]^{2+}$) from 8.57-8.52 ppm (4 protons, $[Ru(bpy)_2(2,5\text{-}dpp)PdCl_2]^{2+}$) while there is not much effect on H6a but H5a moves in downfield region at 7.92-7.83 ppm from 7.50-7.44 ppm w.r.t. the non-ester analogue

$[Ru(bpy)_2(2,5\text{-dpp})PdCl_2]^{2+}$ due to electron-withdrawing effect of the ethyl ester group.

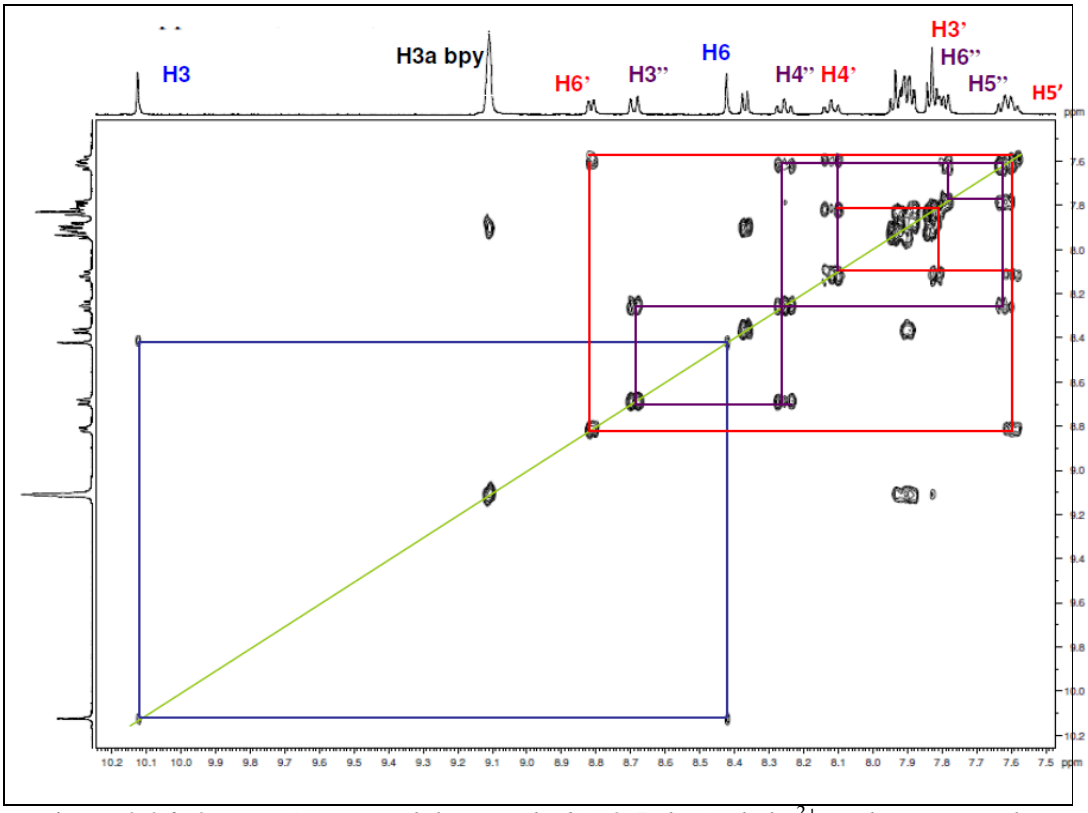

Figure 3.26: *2D-COSY NMR of the* $[Ru(dceb)_2(2,5\text{-dpp})PdCl_2]^{2+}$ *in* d_3*-acetonitrile.*

In the case of the $[Ru(bpy)_2(2,5\text{-dpp})PtCl_2]^{2+}$ complex, the protons H3, H6', H5' and H4' of the 2,5-dpp ligand are shifted to 10.50 ppm, 9.39 ppm, 7.72 ppm and 8.19 ppm respectively on compared to complex $[Ru(bpy)_2(2,5\text{-dpp})PdCl_2]^{2+}$ (H3 = 10.05 ppm, H6' = 8.91 ppm, H5' = 7.61 and H6' = 8.10 ppm) / complex $[Ru(bpy)_2(2,5\text{-dpp})]^{2+}$ (H3 = 9.69 ppm, H6' = 8.51 ppm, H5' = 7.46 and H4' = 7.97 ppm) (see table 3.4). The de-shielding effect of an electron deficient $PtCl_2$ metal is more compare to the shielding effect of an electron rich ruthenium metal on the protons H3, H6', H5' and H4', also the slightly distorted square planer geometry influence chemical shifts downfield. The protons H6'' – H3'' of the 2,5-dpp in $[Ru(bpy)_2(2,5\text{-dpp})PtCl_2]^{2+}$ are not effected to any great extent when compared to both $[Ru(bpy)_2(2,5\text{-dpp})PdCl_2]^{2+}$ and the mononuclear complex $[Ru(bpy)_2(2,5\text{-dpp})]^{2+}$.The 2D-COSY ^{1}H-NMR of the $[Ru(bpy)_2(2,5\text{-dpp})PtCl_2]^{2+}$ is depicted in figure 3.27.

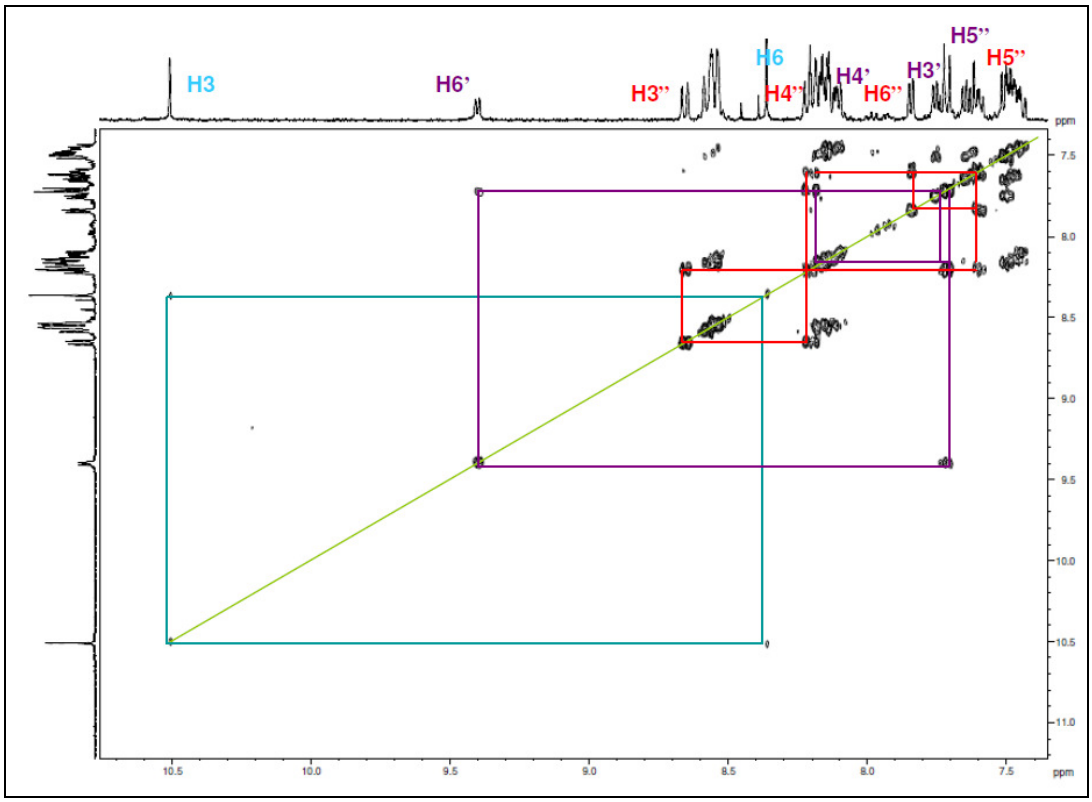

Figure 3.27: *2D-COSY NMR of the* $[Ru(bpy)_2(2,5\text{-}dpp)PtCl_2]^{2+}$ *in* d_3*-acetonitrile.*

Figure 3.28 represents the 2D-COSY proton-NMR for $[Ru(dceb)_2(2,5\text{-}dpp)PtCl_2]^{2+}$ complex. In the complex $[Ru(dceb)_2(2,5\text{-}dpp)PtCl_2]^{2+}$, the protons of the bridging ligand 2,5-dpp are more or less the same as in the non-ester analogue $[Ru(bpy)_2(2,5\text{-}dpp)PtCl_2]^{2+}$. As discussed earlier in the case of the ester-Pd analogue $[Ru(dceb)_2(2,5\text{-}dpp)PdCl_2]^{2+}$ only changes shift downfield of the dceb ligand protons H3a and H5a due to the electron-withdrawing effect of ethyl ester group. On comparing for $[Ru(dceb)_2(2,5\text{-}dpp)PtCl_2]^{2+}$ the proton H3 at 10.58 ppm and H6' at 9.40 ppm shift downfield w.r.t. $[Ru(dceb)_2(2,5\text{-}dpp)PdCl_2]^{2+}$ (H3 = 10.13 ppm; H6' = 8.81 ppm) and the mononuclear complex $[Ru(dceb)_2(2,5\text{-}dpp)]^{2+}$ (H3 = 9.69 ppm; H6' = 8.50 ppm) due to the de-shielding effect of electron-withdrawing $PtCl_2$ moiety from the 2,5-dpp bridging ligand. The rest of the protons in the $[Ru(dceb)_2(2,5\text{-}dpp)PtCl_2]^{2+}$ complex shift slightly downfield for protons H5'-H3' ; H6"-H3" w.r.t. the $[Ru(dceb)_2(2,5\text{-}dpp)PdCl_2]^{2+}$ complex while all the protons undergo a downfield shifts due to complexation with the $PtCl_2$ moiety to the mononuclear $[Ru(dceb)_2(2,5\text{-}dpp)]^{2+}$ complex.

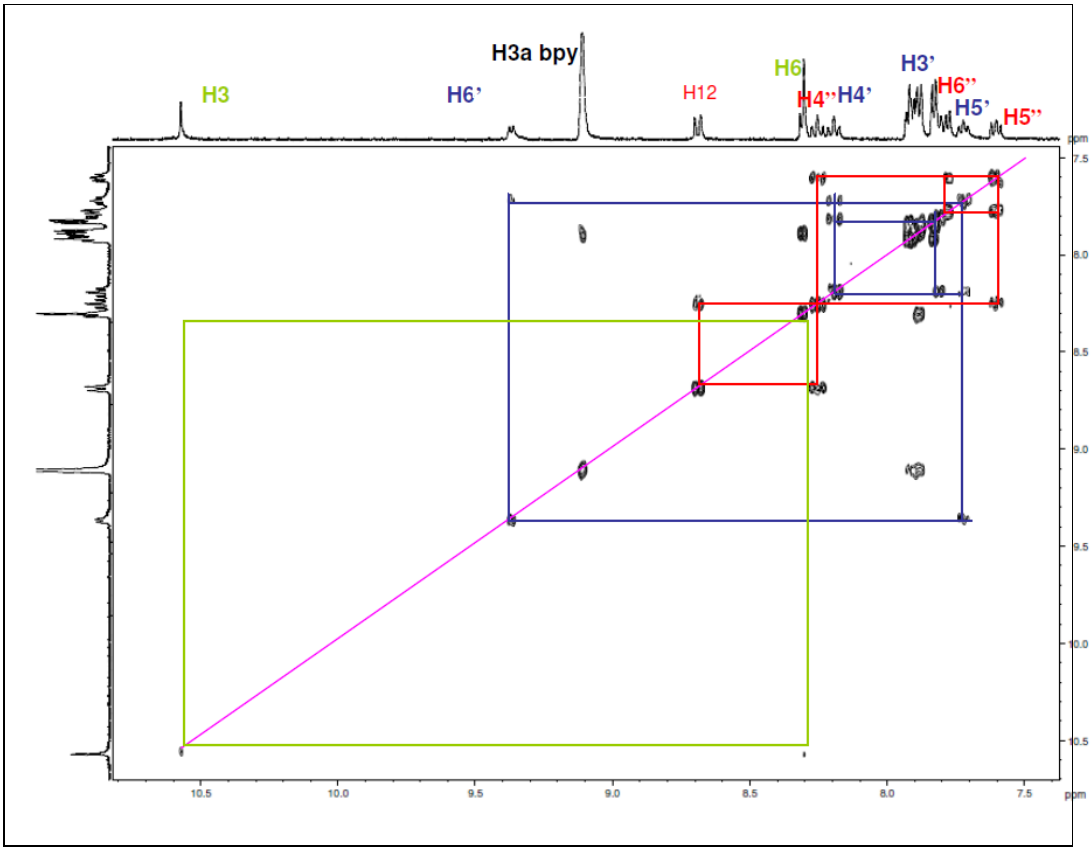

Figure 3.28: *2D-COSY NMR of the* $[Ru(dceb)_2(2,5\text{-}dpp)PtCl_2]^{2+}$ *in* d_3*-acetonitrile.*

3.3.3 UV-Vis absorption, emission and luminescence properties of the Ru(II) mononuclear and heterodinuclear complexes.

The photophysics and spectroscopy of the ruthenium(II) polypyridyl mononuclear and heterodinuclear complexes with 2,5-dpp as a bridging ligand have been studied.[75, 76] These studies provided information regarding intramolecular interactions between the ligands and the metals.

Complex	Absorption λ_{max} (nm) ($\varepsilon = 10^4\ M^{-1}cm^{-1}$)	Emission λ_{max} (nm) (at 293 K)	τ [a] (ns) (aerated) (at 293 K)	Φ [b] (deaerated) (at 293 K)
$[Ru(bpy)_3]^{2+}$	453 (1.3)	605	576	0.068 [c, 82]
$[Ru(bpy)_2(2,5\text{-dpp})]^{2+}$	483 (0.92)	695	266	0.034
$[Ru(dceb)_2(2,5\text{-dpp})]^{2+}$	467 (1.79)	630	564	0.039
$[Ru(bpy)_2(2,5\text{-dpp})PdCl_2]^{2+}$	539 (1.0) 403 (0.9)	807	< 0.5	-
$[Ru(bpy)_2(2,5\text{-dpp})PtCl_2]^{2+}$	565 (1.0) 424 (1.0)	813 630	< 0.5	-
$[Ru(dceb)_2(2,5\text{-dpp})PdCl_2]^{2+}$	444 (1.6) 526 (1.6)	778	< 0.5	-
$[Ru(dceb)_2(2,5\text{-dpp})PtCl_2]^{2+}$	444 (1.73) 540 (1.71)	778 630	< 0.5	-

[a] Determined by time correlated single photon counting in aerated acetonitrile solution, error ± 10 % ns.

[b] Quantum yield of an excited state emission (deaerated Acetonitrile at λ = 455 nm).

[c] Lifetime of the $[Ru(bpy)_3]^{2+}$ in deaerated acetonitrile using freeze-pump-thaw degassing.

Table 3.5: *Photophysical properties of all ruthenium monomer and heterodinuclear complexes synthesised carried out in spectroscopy grade aerated acetonitrile at 293 K.*

3.3.3.1 Absorption and emission spectra properties.

UV-Vis absorption data are collected in Table 3.5; spectra of the listed compounds in this Thesis are shown in Figure 3.29, 3.30, 3.31, 3.32, 3.33 and 3.34. The absorption spectra of all these compounds are essentially similar to that of other Ru(II) – based polypyridine complexes and can be accordingly interpreted. The high intensity absorption bands in the UV region can be ascribed to ^{1}LC transitions. In particular, the peak at 280 nm can be attributed to the bpy peripheral ligand and 320 nm attributed to the dceb peripheral ligand, the band around 350 – 360 nm are assigned to the 2,5-dpp bridging ligand. Moderately intense ^{1}MLCT bands are observed in the region 400 – 600 nm.[42, 75, 76]

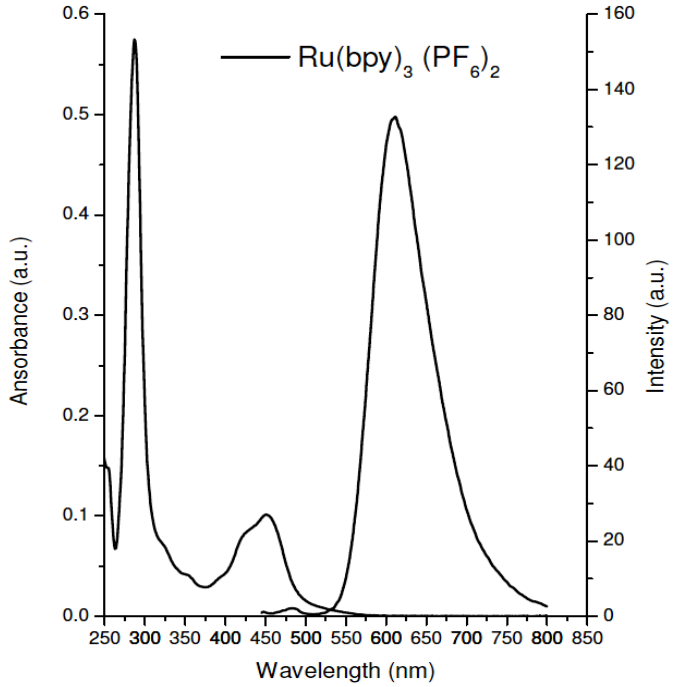

Figure 3.29: *Absorption and emission spectra of the $[Ru(bpy)_3]^{2+}$ at room temperature in acetonitrile solution (deaerated), excitation wavelength at 453 nm.*

One can note the non-chromophoric nature of the $PdCl_2$ / $PtCl_2$ fragments in the sense that there is no absorption band that clearly involves this unit. However, the absorption spectrum of the heterodinuclear complex differ somewhat to the ruthenium

mononuclear complex which may indicate complexation of $PdCl_2$ / $PtCl_2$ to the free end of the 2,5-dpp ligand. Both the ^{1}MLCT band in the visible region and the LC band around 330 nm are different before and after coordination of $PdCl_2$ / PtCl2 (see figure 3.33 and 3.34).

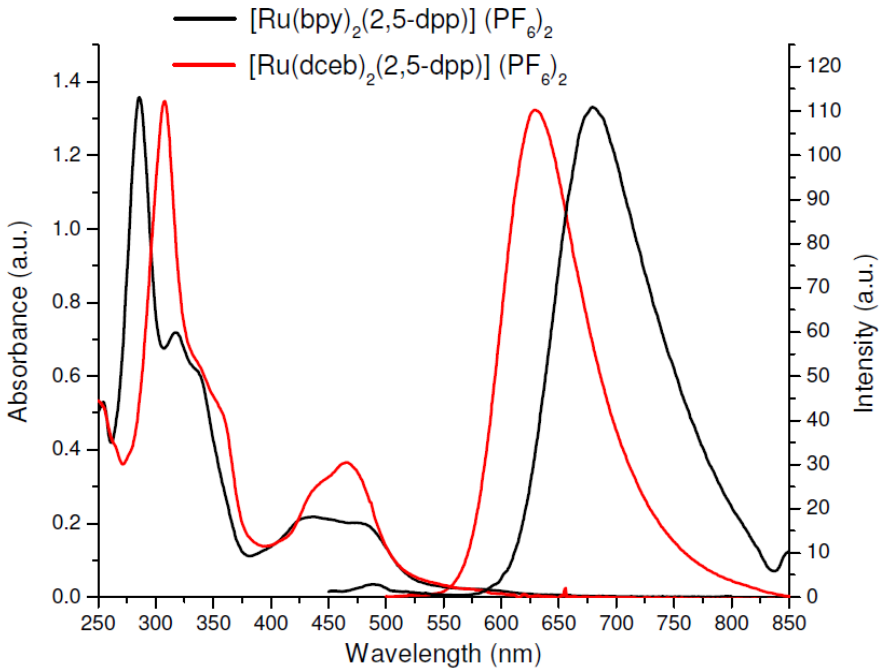

Figure 3.30: *Absorption and emission spectra (normalized) of the [Ru(bpy)$_2$(2,5-dpp)]$^{2+}$ (black) (λ_{ex} = 483 nm) and [Ru(dceb)$_2$(2,5-dpp)]$^{2+}$ (red) (λ_{ex} = 467 nm) at room temperature in acetonitrile solution.*

The obtained spectra of the complex [Ru(bpy)$_2$(2,5-dpp)]$^{2+}$ is in good agreement with the results of *Denti et al.* (see figure 3.30).[42, 75, 76] A comparison of the mononuclear [Ru(bpy)$_2$(2,5-dpp)]$^{2+}$ compound with the homoleptic [Ru(bpy)$_3$]$^{2+}$ complex (see figure 3.29) allows assignment of the bands at 318 and 337 nm to the 2,5-dpp ligand. Also the very intense peak at 285 nm can be assigned to bpy, due to its appearance in all the spectra. Transitions in the ultraviolet part of the spectrum belong to ligand centered absorptions.[42] In the visible region, the mononuclear compound [Ru(bpy)$_2$(2,5-dpp)]$^{2+}$ complex has a broad absorption peak with two shoulders. One shoulder is at 435 nm and the second shoulder is situated at lower energy at 483 nm. Those peaks in the visible area of light belong to d → π* metal to ligand charge transfer transitions. In contrast, the MLCT peak of the homoleptic [Ru(bpy)$_3$]$^{2+}$

complex shows only one clear maximum at 453 nm. The broad peak in case of the mixed ligand complex $[Ru(bpy)_2(2,5\text{-dpp})]^{2+}$ is explained by considering the contributions of Ru → bpy as well as Ru → 2,5-dpp MLCT transitions, whereas the shoulder at 483 nm can be assigned to a Ru → 2,5-dpp π* MLCT.[42] The superposition of those peaks results in the broad absorption features. The shift of the MLCT bands compared to $[Ru(bpy)_3]^{2+}$ is explained by the higher π-acceptor and weaker σ – donor properties of the 2,5-dpp ligand compared to bpy. Due to the weaker σ – donor strength the metal d-orbitals are stabilised. Therefore, the energy gap between the ruthenium t_{2g} orbitals and the bpy π* orbital increases, resulting in a blue shift of this transition (Ru→bpy MLCT) in comparison to $[Ru(bpy)_3]^{2+}$.

The ruthenium monomer complex $[Ru(bpy)_2(2,5\text{-dpp})]^{2+}$ exhibits luminescence at room temperature in the red region of the spectrum after excitation at 483 nm (figure 3.30). The emission maxima were observed at 695 nm, and are in agreement with those reported.[42, 75] In comparison, the emission maximum for $[Ru(bpy)_3]^{2+}$ is centered at 605 nm. Generally, in the case of ruthenium polypyridyl complexes, emission occurs from the lowest triplet MLCT excited state. Considering the homoleptic reference complex the originating level must be the π* orbital of the bipyridine ligands. In contrast, the emission maximum for the mixed chelate complex $[Ru(bpy)_2(2,5\text{-dpp})]^{2+}$ lies at lower energy. The difference is approximately 80 nm. This shift and the appearance of only one band leads to the assumption that the emission occurs from the Ru→2,5-dpp ^{3}MLCT excited state, which is in agreement with the literature.[42, 75] For confirmation, the luminescence measurements were carried out by exciting the samples at 435 nm. This wavelength was assigned to the Ru→bpy ^{3}MLCT transition in the absorption spectra. The same emission maxima at 695 nm were recorded as observed before. This implies that population of a Ru → bpy π* MLCT state is followed by a radiationless decay where the electron is transferred into the lower lying Ru → 2,5-dpp π* MLCT state. By recording the absorption and emission spectra of the heteroleptic ruthenium mononuclear $[Ru(bpy)_2(2,5\text{-dpp})]^{2+}$ complex and its deuteriated analogues, when comparing to $[Ru(bpy)_3]^{2+}$ it can be conclude that the luminescence is mainly governed by the relatively low lying Ru → 2,5-dpp ^{3}MLCT excited state. Therefore, by measuring the lifetimes of the mixed ligand compounds, the deuteriated complexes should have

significantly longer lifetimes [75] (see table 3.6, figure 3.31 and figure 3.32, emission spectra of the $[Ru(bpy)_2(2,5\text{-dpp})]^{2+}$ at 77 K glass matrix MeOH/ EtOH (4:1 vol. ration)).[75]

Complex	Absorption [a] λ_{max} (nm) [d] ($\varepsilon = 10^4\ M^{-1}cm^{-1}$)	Emission [a] λ_{max} (nm) at 293 K (at 77 K) [e]	Φ [b] (deaerated) (at 293 K)	τ [c] in ns [54] (aerated) at 293 K (at 77 K in µs) [e]
$[Ru(bpy)_2(2,5\text{-dpp})]^{2+}$	483 (0.92)	695 (638)	0.034	266 (3.6)
$[Ru(D_8\text{-bpy})_2(2,5\text{-dpp})]^{2+}$	483 (0.97)	695 (638)	0.040	271 (4.1)
$[Ru(bpy)_2(D_{10}\text{-}2,5\text{-dpp})]^{2+}$	483 (0.91)	695 (638)	0.041	296 (4.5)
$[Ru(D_8\text{-bpy})_2(D_{10}\text{-}2,5\text{-dpp})]^{2+}$	483 (1.05)	695 (638)	0.044	306 (4.7)
$[Ru(D_8\text{-bpy})_2(2,5\text{-dpp})PdCl_2]^{2+}$	539 (1.0) 403 (0.9)	807	-	< 0.5
$[Ru(D_8\text{-bpy})_2(D_{10}\text{-}2,5\text{-dpp})PdCl_2]^{2+}$	539 (1.0) 403 (0.91)	807	-	< 0.5

[a] Absorption and emission in acetonitrile solution (aerated).

[b] quantum yield (in deaerated acetonitrile at 293 K).

[c] Lifetime in ns not in brackets and lifetime in µs (at 77 K) in brackets (aerated acetonitrile), error ± 10 % ns or µs.

[d] Lowest energy maximum wavelength.

[e] MeOH/ EtOH (4:1 v/v) glass (aerated).

Table 3.6: *Photophysical properties of all deuteriated ruthenium monomer complexes and heterodinuclear complexes synthesised carried out in spectroscopy grade acetonitrile.*

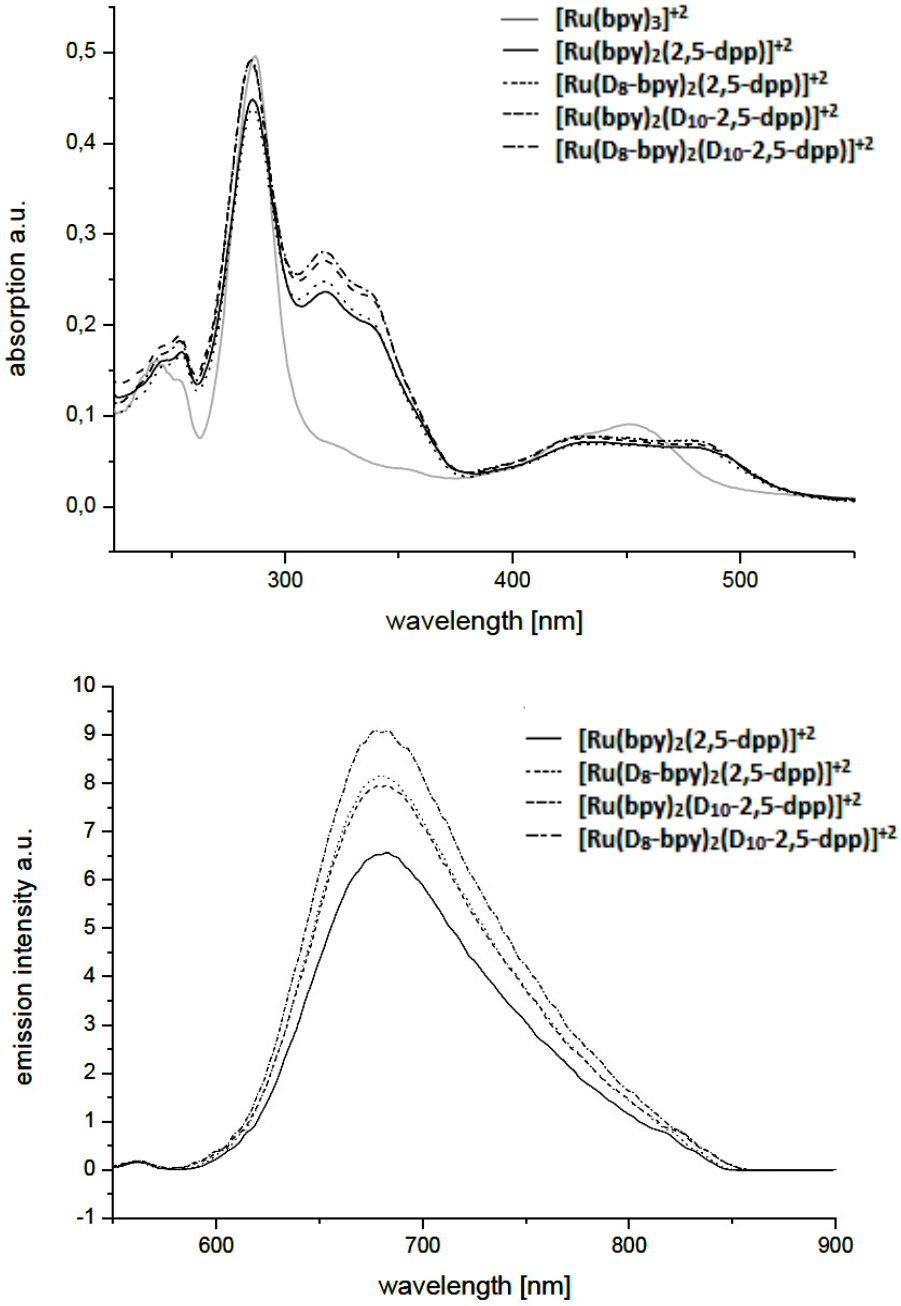

Figure 3.31: *Absorption and emission spectra for $[Ru(bpy)_3]^{2+}$, $[Ru(bpy)_2(2,5\text{-}dpp)]^{2+}$ and the deuteriated analogues of the $[Ru(bpy)_2(2,5\text{-}dpp)]^{2+}$ at 293 K in acetonitrile solution (concentration of the compounds were ~ 7.0×10^{-6} M). The samples were excited with a wavelength of 483 nm*

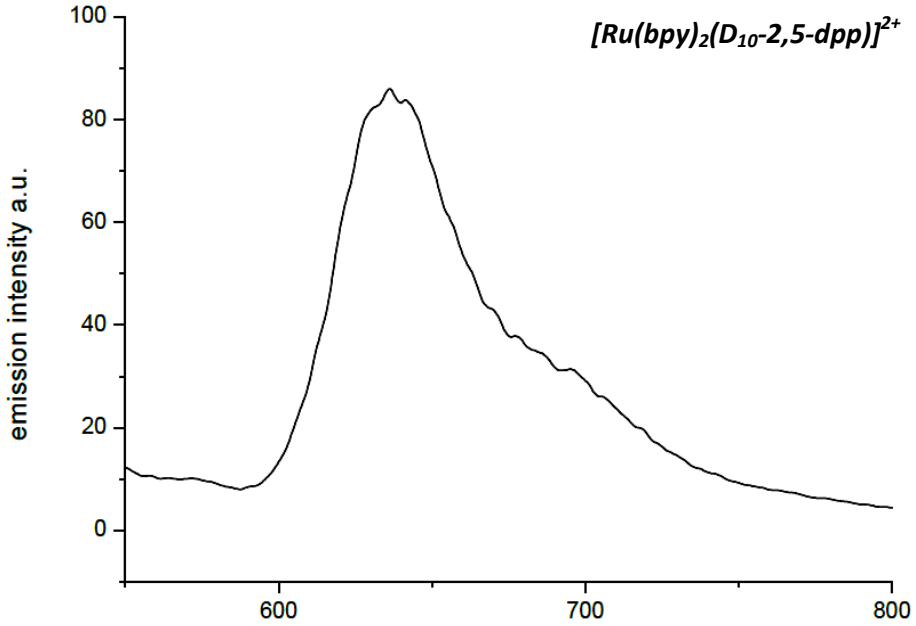

Figure 3.32: *Emission spectrum of $[Ru(bpy)_2(D_{10}\text{-}2,5\text{-}dpp)]^{2+}$ recorded at 77 K in a rigid matrix of MeOH/EtOH (4:1 volume ratio). The sample was excited with a wavelength of 483 nm.*

Additionally, emission spectra of the mononuclear complexes were recorded at low temperature (77K) in a rigid matrix of methanol and ethanol (4:1 volume ratio). Since all the monometallic deuteriated compounds emit at the same wavelength, only the emission spectrum of $[Ru(bpy)_2(D_{10}\text{-}2,5\text{-}dpp)]^{2+}$ which is representative for the whole class is shown (figure 3.32). The emission maximum at low temperatures was observed at 638 nm, and is in agreement with reported values.[42] The hypsochromic shift of the emission band in comparison to the emission spectra in acetonitrile can be explained by solvatochromic and temperature effects.[42]

A comparison of the mononuclear ester $[Ru(dceb)_2(2,5\text{-}dpp)]^{2+}$ compound (Figure 3.30) with the homoleptic $[Ru(bpy)_3]^{2+}$ complex (see figure 3.29) and $[Ru(bpy)_2(2,5\text{-}dpp)]^{2+}$ allows a assignment of the absorption bands at 357 nm to the 2,5-dpp ligand. Also the very intense peak at 307 nm can be assigned to dceb, due to its appearance in all the spectra. Transitions in the ultraviolet part of the spectrum belong to ligand centered absorptions (dceb and 2,5-dpp ligands). In the visible region, the mononuclear compound $[Ru(dceb)_2(2,5\text{-}dpp)]^{2+}$ feature a broad absorption peak with

two shoulders. One shoulder is at 444 nm (Ru → dceb; MLCT) and the second shoulder is situated at lower energy at 467 nm (Ru → 2,5-dpp; MLCT). Those peaks in the visible region to d → π* metal to ligand charge transfer transitions.[76]

In contrast, the MLCT peak of the homoleptic $[Ru(bpy)_3]^{2+}$ shows only one clear maximum at 453 nm. The broad peak in case of the mixed ligand complex $[Ru(dceb)_2(2,5\text{-dpp})]^{2+}$ is explained by considering the contributions of Ru → dceb as well as Ru → 2,5-dpp MLCT transitions, whereas the shoulder at 467 nm can be assigned to a Ru → 2,5-dpp π* MLCT which is blue shifted by 16 nm in comparison to the $[Ru(bpy)_2(2,5\text{-dpp})]^{2+}$ complex due to the electron withdrawing group present on the peripheral ligands, and the energy gap between the Ru (t_{2g}) orbitals and the 2,5-dpp π* orbital increase.[76] The superposition of those peaks results in broad absorption features. As discussed above for the $[Ru(bpy)_2(2,5\text{-dpp})]^{2+}$ complex, the energy gap between the ruthenium t_{2g} orbitals and the bpy π* orbital increases, resulting in a blue shift of this transition (Ru → bpy MLCT) in comparison to $[Ru(bpy)_3]^{2+}$. The MLCT band at 444 nm in $[Ru(dceb)_2(2,5\text{-dpp})]^{2+}$ is red-shifted by 9 nm compared to the analogue $[Ru(bpy)_2(2,5\text{-dpp})]^{2+}$ (λ_{max} at 435 nm). This red shift of the MLCT band occurs because of the presence of the carboxylic acid groups; the withdrawing nature of the carboxylic acid groups lowers the energy of the π* orbital of the ligand, causing the d to π* transition to occur at lower energy.[83, 84]

The ruthenium monomer complex $[Ru(dceb)_2(2,5\text{-dpp})]^{2+}$ exhibit luminescence at room temperature in the red region of the spectrum after excitation with 467 nm (figure 3.30). The emission maximum was observed at 630 nm.[76] Generally, in the case of ruthenium polypyridyl complexes, the emission occurs from the lowest triplet MLCT excited state. Considering the homoleptic reference complex $[Ru(bpy)_3]^{2+}$ the originating level must be the π* orbital of the bipyridine ligands. In contrast, the emission maximum for the mixed chelate complex $[Ru(dceb)_2(2,5\text{-dpp})]^{2+}$ lies at lower energies. The difference is approximately 15 nm. This is in a close proximity to $[Ru(bpy)_3]^{2+}$ whose luminescence occurs at 605 nm, indicating that the luminescence may be [Ru(bpy)] based. This shift and the appearance of only one band leads to the assumption that the emission is occurs from the Ru → 2,5-dpp ^{3}MLCT excited state. For confirmation, the luminescence measurements were carried out by exciting the

samples at 444 nm. This wavelength was assigned to the Ru → dceb ^{3}MLCT transition in the absorption spectra. Although the samples were excited with the energy of Ru → dceb ^{3}MLCT transitions, the same emission maxima at 630 nm, as observed before, were recorded. This implies that populating a Ru → dceb π* MLCT state is followed by a radiationless decay where the electron is transferred into the lower lying Ru → 2,5-dpp π* MLCT state. Thus both the possibility may happened in the case of the complex $[Ru(dceb)_2(2,5\text{-dpp})]^{2+}$.[76]

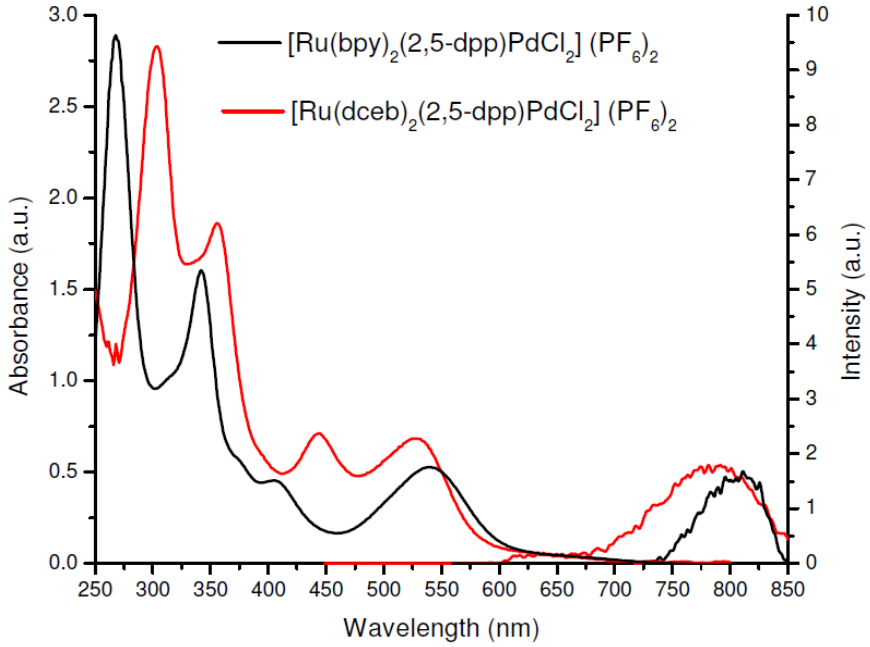

Figure 3.33: *Absorption and emission spectra of the $[Ru(bpy)_2(2,5\text{-dpp})PdCl_2]^{2+}$ (black) (λ_{ex} = 539 nm) and $[Ru(dceb)_2(2,5\text{-dpp})PdCl_2]^{2+}$ (red) (λ_{ex} = 526 nm) at room temperature in acetonitrile solution.*

Depicted in figure 3.33 depicted are the absorption and emission spectra for $[Ru(bpy)_2(2,5\text{-dpp})PdCl_2]^{2+}$ and $[Ru(dceb)_2(2,5\text{-dpp})PdCl_2]^{2+}$, and similar spectra were observed as seen in the two mononuclear complexes $[Ru(bpy)_2(2,5\text{-dpp})]^{2+}$ and $[Ru(dceb)_2(2,5\text{-dpp})]^{2+}$ (e.g. blue shifted of the Ru → 2,5-dpp π* ^{1}MLCT from ester analogue of bpy to non ester bpy). In the heterodinuclear Ru-Pd complexes, the peak at 270 nm can be attributed to the bpy peripheral ligand and 305 nm attributed to dceb peripheral ligand. The band around 340 – 360 nm is attributed to the 2,5-dpp bridging ligand.[76] Moderately intense ^{1}MLCT bands are observed in the region 400 – 600 nm.

Thus for the $[Ru(bpy)_2(2,5\text{-dpp})PdCl_2]^{2+}$ and $[Ru(dceb)_2(2,5\text{-dpp})PdCl_2]^{2+}$ complexes the lowest energy ^{1}MLCT transitions Ru → 2,5-dpp are observed at 539 and 526 nm. The lowest energy ^{1}MLCT transitions Ru → bpy / dceb are observed at 403 and 444 nm respectively.[76] This is due to progressive lowering of the π* orbital of the bridging ligand when the free chelating site connects to a formally uncharged unit ($PdCl_2$).[42]

The complexes $[Ru(bpy)_2(2,5\text{-dpp})PdCl_2]^{2+}$ and $[Ru(dceb)_2(2,5\text{-dpp})PdCl_2]^{2+}$ emit at room temperature but the emission is highly quenched compared to the ruthenium monomers. Both $[Ru(bpy)_2(2,5\text{-dpp})PdCl_2]^{2+}$ and $[Ru(dceb)_2(2,5\text{-dpp})PdCl_2]^{2+}$ complex exhibit luminescence at room temperature in the red region of the spectrum after excitation at 539 nm and 526 nm respectively (figure 3.33). The emissions maxima were observed at 807 nm and 778 nm respectively. This appearance of two band leads to the assumption that the emission originates from the Ru → 2,5-dpp ^{3}MLCT excited state when excited at 526 nm. The ^{1}MLCT band for Ru → 2,5-dpp π* in the complex $[Ru(dceb)_2(2,5\text{-dpp})PdCl_2]^{2+}$ is blue shifted by 13 nm compared to the $[Ru(bpy)_2(2,5\text{-dpp})PdCl_2]^{2+}$, and a similar effect was seen for the mononuclear non-ester and ester analogous.[76]

For the $PtCl_2$ containing dinuclear complexes (see Figure 3.34), $[Ru(bpy)_2(2,5\text{-dpp})PtCl_2]^{2+}$ and $[Ru(dceb)_2(2,5\text{-dpp})PtCl_2]^{2+}$ similar trends were observed, with absorption maxima at 424 nm / 565 nm and 444 nm/ 540 nm, and unusual emission at 630 nm / 813 nm when excited at 565 nm and 630 nm / 778 nm when excited at 540 nm for the two complexes respectively.

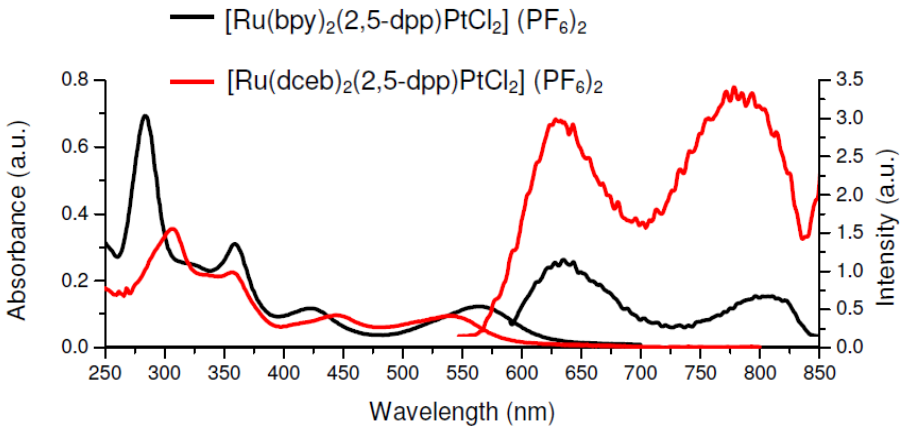

Figure 3.34: *Absorption and emission spectra of the* $[Ru(bpy)_2(2,5\text{-}dpp)PtCl_2]^{2+}$ *(black) (*λ_{ex} *= 565 nm) and* $[Ru(dceb)_2(2,5\text{-}dpp)PtCl_2]^{2+}$ *(red) (*λ_{ex} *= 540 nm) at room temperature in acetonitrile solution.*

3.3.3.2 Lifetime measurements.

The lifetime is the time it takes for a number of excited molecules to decay to 1/e of the original population.[85] In the case of one single fluorescence process the decay curve responds to the following equation 3.1.

$$I(t) = I_0 \cdot e^{-t/\tau} \ldots\ldots\ldots\ldots \text{(Eq. 3.1)}$$

Hereby I_0 resembles the fluorescence intensity at the time t equal to zero and τ is the lifetime of the fluorescence.

The time correlated single photon count (TCSPC) was used to determine the lifetime of the compounds. Hereby the time between excitation and the detection of the first emitted photon is measured repeatedly. The TCSPC measurements were carried out at room temperature in acetonitrile solution. All the deuteriated, non deuteriated and ester analogous of the $[Ru(bpy)_2(2,5\text{-}dpp)]^{2+}$ were excited with a wavelength of 360 nm and the time response of their emission was recorded. The results are shown in figure 3.35 and 3.36. The corresponding lifetimes were obtained using single exponential fits on the decay curves, and are as listed in table 3.5 and table 3.6 above.

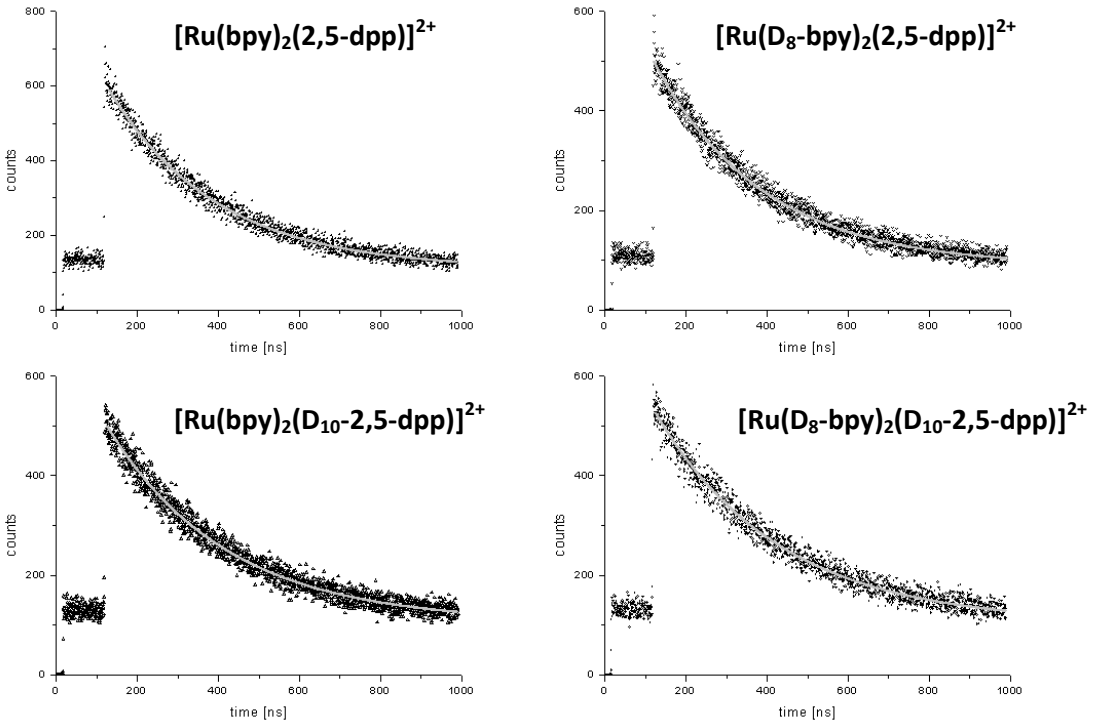

Figure 3.35: *TCSPC spectra of the mononuclear ruthenium(II) complexes. The spectra were recorded at room temperature in aerated acetonitrile solution, by exciting the samples with a wavelength of 360 nm and observing the emission at 695 nm. The graphs were fitted (grey line) using a single exponential decay function.*

The lifetime for compound $[Ru(bpy)_2(2,5\text{-}dpp)]^{2+}$ is in very good agreement with *Denti et al.*[42] The lifetimes of the excited states increase upon deuteriation. However, the extent of this effect for the investigated mononuclear compounds is different. By deuteriation of the peripheral bpy ligands $[Ru(D_8\text{-}bpy)_2(2,5\text{-}dpp)]^{2+}$ the increase of the lifetime at room temperature by 5 ns is marginal compared to the lifetime of the non-deuteriated complex $[Ru(bpy)_2(2,5\text{-}dpp)]^{2+}$. Deuteriation of the 2,5-dpp ligand however in the case of compound $[Ru(bpy)_2(D_{10}\text{-}2,5\text{-}dpp)]^{2+}$ shows a stronger effect. Compared to the mononuclear complexes $[Ru(bpy)_2(2,5\text{-}dpp)]^{2+}$ and $[Ru(D_8\text{-}bpy)_2(2,5\text{-}dpp)]^{2+}$ the lifetimes increased by 30 ns and 25 ns respectively, i.e. 11% (see table 3.6). As suggested by Keyes et al.[86], the emission lifetime of a compound should only increase when the excited state is situated on the deuteriated ligand. The observed data in addition to the preceding absorption and emission measurements suggest that the excited state is most likely situated on the 2,5-dpp ligand. The biggest

increase of emission lifetime was measured for the $[Ru(D_8\text{-bpy})_2(D_{10}\text{-2,5-dpp})]^{2+}$ complex, where all ligands are deuteriated. An extension of even 10 ns in comparison to $[Ru(bpy)_2(D_{10}\text{-2,5-dpp})]^{2+}$ could be detected. This leads to the assumption that the bpy ligands are involved in radiationless decay as well. Possibly, due to additional low energy bpy C-D stretching vibrations, internal conversion from the Ru → bpy π* to the lowest lying Ru → 2,5-dpp π* ^{3}MLCT state is de-accelerated, what has an effect on the lifetime, too.

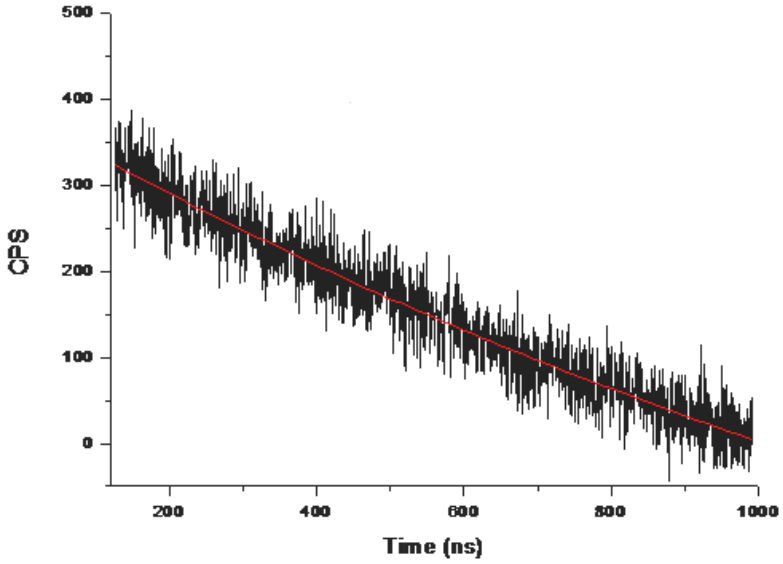

Figure 3.36: *TCSPC spectra of the mononuclear $[Ru(dceb)_2(2,5\text{-dpp})]^{2+}$ complexes. The spectra were recorded at room temperature in aerated acetonitrile solution, by exciting the samples with a wavelength of 360 nm and observing the emission at 630 nm. The graphs were fitted (red line) using a single exponential decay function.*

In case of the $[Ru(dceb)_2(2,5\text{-dpp})]^{2+}$ compound lifetimes doubled in comparison to the non ester analogue of the $[Ru(bpy)_2(2,5\text{-dpp})]^{2+}$ complex (see table 3.5), due to stabilisation of the ground state by the electron withdrawing ester group present on the bipyridine ligand in figure 3.36.

The TCSPC results were complemented by time dependent fluorescence measurements at 77 K in a rigid matrix. The excitation wavelength of the laser was 355 nm, and the emissions for the heteroleptic monometallic compounds were

recorded at 638 nm. The obtained time responses of emission and their associated exponential fits are plotted in figure 3.37.

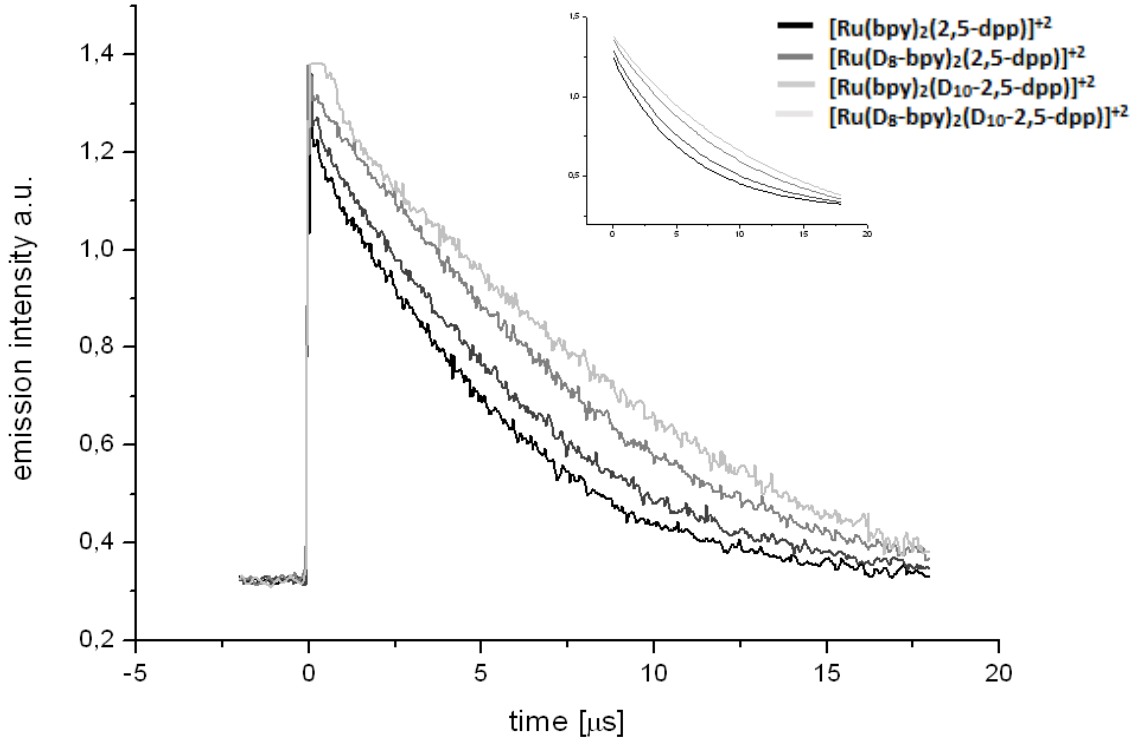

Figure 3.37: *Time dependent fluorescence spectra of the heteroleptic monometallic ruthenium(II) complexes and their associated exponential fits. The spectra were recorded at 77K in a rigid matrix of MeOH/EtOH (4:1 volume ratio), by exciting the samples with a wavelength of 360 nm and observing the emission at 638 nm.*

Compared to Denti et al. the value determined for the $[Ru(bpy)_2(2,5\text{-dpp})]^{2+}$ compound was the same.[42] Analogous to the TCSPS result, an increase in fluorescence lifetime due to deuteriation could be detected. Again, although not expected, the deuteriation of the bpy ligands seems to have an effect on the lifetime of the excited state as well. Compared to $[Ru(bpy)_2(2,5\text{-dpp})]^{2+}$ the lifetime of $[Ru(D_8\text{-}bpy)_2(2,5\text{-dpp})]^{2+}$ increased by approx. 0.5 μs (see table 3.6).

3.3.4 Photocatalytic hydrogen generation experiments.

The photocatalytic hydrogen generation activity of each intramolecular Ru – Pd / Ru – Pt heterodinuclear complex and the intermolecular Ru(II) mononuclear complexes with Pd(acetonitrile)$_2$Cl$_2$ were evaluated from water by photo-irradiation of an acetonitrile solution of each compounds in the presence of a sacrificial electron donor, triethyl amine (TEA), under a N_2 atmosphere (detailed experimental procedure discussed in chapter 2).

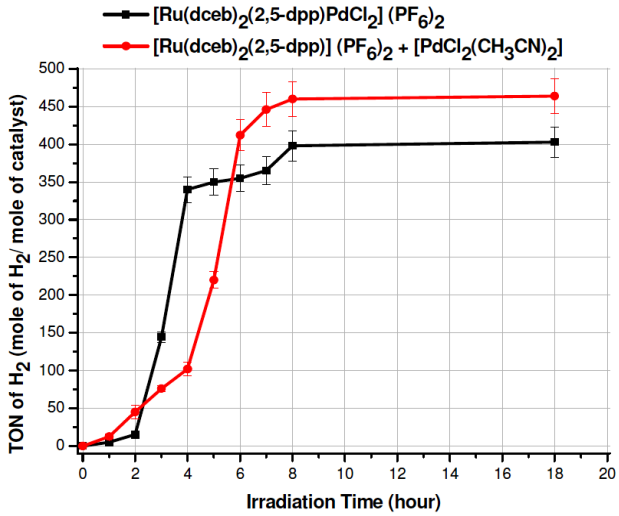

Figure 3.38: *Photocatalytic hydrogen produced determined by GC from an interval 0 – 8 hours. Photocatalytic reaction (under N_2) of the $[Ru(dceb)_2(2,5\text{-}dpp)PdCl_2]^{2+}$ (Blue) and $[Ru(dceb)_2(2,5\text{-}dpp)]^{2+}$ (Red) + $Pd(ACN)_2Cl_2$; c(cat.) = 4.08 × 10^{-5} M in anhyd. ACN as solvent, conc. of TEA = 2.15 M and 5% water (v/v); taken in a 5 ml clear glass vial with septa capped (2 ml solution with 3 ml head space). S.D. ± 10 TONs or less.*

As shown in Fig. 3.38 and Table 3.8, $[Ru(dceb)_2(2,5\text{-}dpp)PdCl_2]^{2+}$ and intermolecular reaction of the $[Ru(dceb)_2(2,5\text{-}dpp)]^{2+}$ with **[**Pd(acetonitrile)$_2$Cl$_2$] were found to be active as photocatalytic hydrogen generation molecular devices. The $[Ru(dceb)_2(2,5\text{-}dpp)PtCl_2]^{2+}$ (very low TONs of hydrogen), $[Ru(bpy)_2(2,5\text{-}dpp)PdCl_2]^{2+}$, $[Ru(bpy)_2(2,5\text{-}dpp)PtCl_2]^{2+}$ and other intermolecular reaction between mononuclear complexes with [Pt(acetonitrile)$_2$Cl$_2$] did not drive H_2 evolution by TEA in the presence of water at all. Time dependent hydrogen production along with the turn over frequency for complexes $[Ru(dceb)_2(2,5\text{-}dpp)PdCl_2]^{2+}$ and intermolecular

reaction $[Ru(dceb)_2(2,5\text{-}dpp)]^{2+}$ with palladium complex are given in the Table 3.9. A typical sample solution of complexes were prepared by mixing 0.1 ml of an 8.16×10^{-4} M catalyst solution in anhydrous acetonitrile (final concentration in 2 ml irradiation solution = $4.08 \cdot 10^{-5}$ M); 0.6 ml of triethylamine (2.15 M); 0.0 – 0.3 ml (0 – 15% v/v) of thoroughly degased water and rest fill with 1.0 – 1.4 ml of anhydrous acetonitrile. Subsequently, the GC vials were irradiated at 470 nm using light emitting diodes (LEDs, vide infra) for 18 h. Average of 3 samples were taken for calculating TONs for hydrogen.

Complexes	***TON {Water percentage}: (Stand. Deviation)***			
	{0 %}	***{5 %}***	***{10 %}***	***{15 %}***
$[Ru(dceb)_2(2,5\text{-}dpp)PdCl_2]^{2+}$	***0***	***403 (15)***	***313 (15)***	***94 (9)***
$[Ru(dceb)_2(2,5\text{-}dpp)PtCl_2]^{2+}$	***0***	***14 (1)***	***7 (0)***	***4 (1)***
$[Ru(bpy)_2(2,5\text{-}dpp)PdCl_2]^{2+}$	***0***	***0***	***0***	***0***
$[Ru(bpy)_2(2,5\text{-}dpp)PtCl_2]^{2+}$	***0***	***0***	***0***	***0***
$[Ru(dceb)_2(2,5\text{-}dpp)]^{2+}$	***0***	***0***	***-***	***-***
$[Ru(bpy)_2(2,5\text{-}dpp)]^{2+}$	***0***	***0***	***-***	***-***
$[Ru(dceb)_2(2,5\text{-}dpp)]^{2+}$ + $Pd(acetonitrile)_2Cl_2$	***0***	***464 (4)***	***-***	***-***
$[Ru(dceb)_2(2,5\text{-}dpp)]^{2+}$ + $Pt(acetonitrile)_2Cl_2$	***0***	***0***	***-***	***-***
$[Ru(bpy)_2(2,5\text{-}dpp)]^{2+}$ + $Pd(acetonitrile)_2Cl_2$	***0***	***0***	***-***	***-***
$[Ru(bpy)_2(2,5\text{-}dpp)]^{2+}$ + $Pt(acetonitrile)_2Cl_2$	***0***	***0***	***-***	***-***
$Pd(acetonitrile)_2Cl_2$ / $Pt(acetonitrile)_2Cl_2$	***0***	***0***	***-***	***-***
No Catalyst (only TEA) [a]	***0***	***0***	***-***	***-***

Table 3.8: *Turn over numbers for hydrogen for the above listed complexes.*

Time (hour)	TON / TOF {Water percentage (5%)}			
	$[Ru(dceb)_2(2,5\text{-}dpp)PdCl_2]^{2+}$		$[Ru(dceb)_2(2,5\text{-}dpp)]^{2+}$ + $[Pd(CH_3CN)_2Cl_2]$	
	TON	TOF (TON h^{-1})	TON	TOF (TON h^{-1})
0	0	0	0	0
1	5	5	13	13
2	15	7.5	45	22.5
3	144	48	76	25
4	340	85	102	25.5
5	350	70	220	44
6	355	59	412	69
7	365	52	446	64
8	398	50	460	58

Table 3.9: Photocatalytic hydrogen determined by GC from an interval 0 – 8 hours. Photocatalytic mixture (prepared under N_2) of the $[Ru(dceb)_2(2,5\text{-}dpp)PdCl_2]^{2+}$ (Blue) and $[Ru(dceb)_2(2,5\text{-}dpp)]^{2+}$ (Red) + $Pd(ACN)_2Cl_2$; c(cat.) = 4.08 x 10^{-5} M in anhydrous acetonitrile as solvent, TEA = 2.15 M and 5% water (v/v); taken in a 5 ml clear glass vial with septa capped (2 ml solution with 3 ml head space). S.D. = ± 10 TONs or less.

Importantly, it was also confirmed that $[Ru(bpy)_2(2,5\text{-}dpp)PtCl_2]^{2+}$ did not produce hydrogen photochemically.[67] Thus, the intramolecular electron transfer from the $[Ru(bpy)_2(2,5\text{-}dpp)]^{2+}$ moiety to the tethering $PtCl_2$ unit in $Ru(bpy)_2(2,5\text{-}dpp)PtCl_2]^{2+}$ complex was not promoted, which is considered the major reason for the ineffectiveness of $[Ru(bpy)_2(2,5\text{-}dpp)PtCl_2]^{2+}$ as a photocatalytic hydrogen generation molecular device. On the contrary, the photoinduced intramolecular electron transfer from the $[Ru(R_2\text{-}bpy)_2(2,5\text{-}dpp)]^{2+}$ (where, R = COOEt) unit tethering to the $PdCl_2$ or $PtCl_2$ unit in $[Ru(dceb)_2(2,5\text{-}dpp)PdCl_2]^{2+}$ and $[Ru(dceb)_2(2,5\text{-}dpp)PtCl_2]^{2+}$ is well enhanced by the introduction of an electron withdrawing group (R = COOEt) present on the bipyridine.

For the photocatalytic process described in this thesis (see chapter 2), the reaction mixture was excited at 470 nm and triethyl amine (TEA) was used as the sacrificial agent to re-reduce the Ru(III) centre formed. The presence of water was found to be an important factor for photocatalytic water splitting. However, the reasons for this observation are not straight forward, since the addition of water changes several parameters: (1) Water is assumed to be a reactant and hence an increasing concentration would accelerate kinetic process and / or shift its equilibria. (2) Proton-transfer is inevitable for hydrogen and is facilitated by the presence of water due to its excellent proton donor ability. (3) Solvent polarity increases with increasing water content, thus stabilising polar intermediates which may also lead to higher TONs. With the dinuclear catalyst $[Ru(dceb)_2(2,5\text{-}dpp)PdCl_2]^{2+}$ TONs up to 400, for $[Ru(dceb)_2(2,5\text{-}dpp)PtCl_2]^{2+}$ (only TONs = 12) were obtained, whereas $[Ru(bpy)_2(2,5\text{-}dpp)PdCl_2]^{2+}$ and $[Ru(bpy)_2(2,5\text{-}dpp)PtCl_2]^{2+}$ no hydrogen was detected with 5% water. An equimolar mixture of the mononuclear precursor $[Ru(dceb)_2(2,5\text{-}dpp)]^{2+}$ and $[Pd(acetonitrile)_2Cl_2]$ (TON = 460) gave slightly higher TONs then $[Ru(dceb)_2(2,5\text{-}dpp)PdCl_2]^{2+}$ when irradiated under the same conditions as the hetero-dinuclear species. Catalysis of the mononuclear species $[Ru(dceb)_2(2,5\text{-}dpp)]^{2+}$ and $[Pt(acetonitrile)_2Cl_2]$ and also $[Ru(bpy)_2(2,5\text{-}dpp)]^{2+}$ with $[Pd(acetonitrile)_2Cl_2]$ / or $[Pt(acetonitrile)_2Cl_2]$ yielded no hydrogen. For both experiments where the mononuclear precursors $[Ru(bpy)_2(2,5\text{-}dpp)]^{2+}$ and $[Ru(dceb)_2(2,5\text{-}dpp)]^{2+}$ were reacted with $[Pd(acetonitrile)_2Cl_2]$ / or $[Pt(acetonitrile)_2Cl_2]$ the formation of a black precipitate was observed. No precipitate was observed in the $[Ru(dceb)_2(2,5\text{-}dpp)PdCl_2]^{2+}$, $[Ru(dceb)_2(2,5\text{-}dpp)PtCl_2]^{2+}$, $[Ru(bpy)_2(2,5\text{-}dpp)PdCl_2]^{2+}$ and $[Ru(bpy)_2(2,5\text{-}dpp)PtCl_2]^{2+}$ cases. However, colloid formation has been discussed by several authors for Ru/Pd complexes.[87, 88] From a present viewpoint the question remain if electron transfer is intra- or intermolecular in nature. But even if catalytically active aggregates (i.e. Pd-colloids) may have formed under the applied conditions, it would still depend on the light harvesting moiety in the present case as shown by the TONs. The polypyridyl heterodinuclear complexes $[Ru(dceb)_2(2,5\text{-}dpp)PdCl_2]^{2+}$, $[Ru(dceb)_2(2,5\text{-}dpp)PtCl_2]^{2+}$, $[Ru(bpy)_2(2,5\text{-}dpp)PdCl_2]^{2+}$ and $[Ru(bpy)_2(2,5\text{-}dpp)PtCl_2]^{2+}$ reveal an interesting peripheral ligand effect for photo-catalytic hydrogen production. TONs of 400 were obtained for the $[Ru(dceb)_2(2,5\text{-}dpp)PdCl_2]^{2+}$ complex but the compound exhibits a very short excited state lifetime.

An experiment was performed by adding metallic mercury (Hg) to the photo-catalytic solution of the $[Ru(dceb)_2(2,5\text{-}dpp)PdCl_2]^{2+}$ and carrying out photocatalysis. After 18 hours of constant irradiation low hydrogen TONs of 38 were observed. This observation suggests decomposition of the complex $[Ru(dceb)_2(2,5\text{-}dpp)PdCl_2]^{2+}$ during irradiation. Another experiment was also performed with constant stirring with metallic mercury, and without irradiation of the photocatalytic solution. After 24 hours constant stirring, the photocatalytic solution colour change from deep red to light pink suggesting decomposition of the catalytic solution.

3.4 Summary and conclusion.

Chapter 3 detailed the synthetic method available for the generation of mononuclear and heterodinuclear metal complexes utilising the strategy of "complexes as metal / complexes as ligands". Initially the heterodinuclear complexes (Ru – Pd / Ru – Pt) and their deuteriated analogues where synthesised and their properties, such as absorption, emission and luminescence data were obtained (see table 3.5, 3.6 and 3.7).

These results were taken in conjunction with the characterization tools of ^{1}H-NMR and CHN to confirm the synthesis of the mononuclear and heterodinuclear complexes. Proton-NMR 1D proved invaluable in determining the binding of the $PdCl_2$ / $PtCl_2$ to the mononuclear complexes and then 2D-COSY proton-NMR to determine the coupling of the protons (see table 3.2, 3.3 and 3.4).

The main aim of this chapter is the synthesis of photosensitizers for the photocatalytic generation of hydrogen using water using 470 nm. For measuring the gaseous products during the photocatalytic experiments, gas chromatography was employed for the head space analysis. The non-ester analogues, i.e. mononuclear Ru(II) in both intermolecular or heterodinuclear Ru – Pd / Ru – Pt complexes were not produced hydrogen. The ester analogues proved to be very efficient for the photocatalytic of generation hydrogen. The ester-Ru – Pd intramolecular as well as ester-Ru + Pd intermolecular complexes shows higher TON hydrogen in the range 400 – 460. It has

been confirmed that water enhanced the production of hydrogen in the range 0 – 15 % but maximum at 5 %, then decrease little when 10 % and further to 15 % (see table 3.8 and 3.9).

3.5 Bibliography

[1] T.J. Meyer, Pure Appl. Chem., 1986, 58, 1193.

[2] A. Juris, V. Balzani, F. Barigelletti, S. Campagna, P. Belser, A. von Zelewsky, Coord. Chem. Rev., 1988, 84, 85.

[3] V. Balzani, A. Juris, Coord. Chem. Rev., 2001, 211, 97.

[4] M. K. De Armond, C. M. Carlin, Coord. Chem. Rev., 1981, 36, 325.

[5] (a) A. A. Vlcek, Coord. Chem. Rev., 1982, 43, 39; (b) A. A. Vlcek, Rev. Chim. Min., 1983, 20, 612.

[6] A. A. Vlcek, E. S. Dodsworth, W. J. Pietro, A. B. P. Lever, Inorg. Chem., 1995, 34, 1906.

[7] A. Vlcek, Jr., M. Heyrovsky, in: V. Balzani (Ed.), Electron Transfer in Chemistry, vol. 2 (Chapter 5), Wiley-VCH, Weinheim, 2001.

[8] V. Balzani, F. Scandola, Supramolecular Photochemistry, Ellis Horwood, Chichester, 1991.

[9] F. Scandola, M. T. Indelli, C. Chiorboli, C. A. Bignozzi, Top. Curr. Chem., 1990, 158, 73.

[10] V. Balzani, A. Juris, M. Venturi, S. Campagna, S. Serroni, Chem. Rev., 1996, 96, 759.

[11] D. Astruc, Electron Transfer and Radical Processes in Transition Metal Complexes, VCH, New York, 1995.

[12] F. L. Carter, L. E. Siatkowski, H. Wohltjen (Eds.), Molecular Electronic Devices, North Holland, Amsterdam, The Netherlands, 1988.

[13] J. -M. Lehn, Supramolecular Chemistry, VCH, Weinheim, 1995.

[14] P. F. Barbara, Acc. Chem. Res., 2001, 34, 409.

[15] (a) J. J. Hopfield, J. N. Onuchic, D. N. Beratan, Science, 1988, 241, 817; (b) J. J. Hopfield, J. N. Onuchic, D. N. Beratan, J. Phys. Chem., 1989, 93, 6350.

[16] L. De Cola, P. Belser, in: V. Balzani (Ed.), Electron Transfer in Chemistry, vol. 5 (Chapter 3), Wiley-VCH, Weinheim, 2001.

[17] J. G. Vos and J. M. Kelly, Dalton Trans., 2006, 4869.

[18] (a) B. O'Regan, M. Grätzel, Nature, 1991, 353, 737; (b) M. Grätzel, Comments Inorg. Chem., 1991, 12, 93.

[19] C. A. Bignozzi, J. R. Schoonover, F. Scandola, Prog. Inorg. Chem., 1997, 47, 1.

[20] A. Hagfeldt, M. Grätzel, Acc. Chem. Res., 2000, 33, 269.

[21] L. De Cola and P. Belser, Coord. Chem. Rev., 1998, 177, 301.

[22] (a) U. Knof and A. von Zelewsky, Angew. Chem., Int. Ed., 1999, 38, 302; (b) N. C. Fletcher, P. C. Junk, D. A. Reitsma and F. R. Keene, J. Chem. Soc., Dalton Trans., 1998, 133.

[23] L. Spiccia, G. B. Deacon and C. M. Kepert, Coord. Chem. Rev., 2004, 248, 1329.

[24] (a) D. A. Freedman, J. K. Evju, M. K. Pomije and K. R. Mann, Inorg. Chem., 2001, 40, 5711; (b) D. Mulhern, S. Brooker, H. Görls, S. Rau and J. G. Vos, Dalton Trans., 2006, 51.

[25] S. Campagna, G. Denti, S. Serroni, A. Juris, M. Venturi, V. Ricevuto, V. Balzani, Chem. Eur. J., 1995, 1, 211.

[26] V. Balzani, S. Campagna, G. Denti, A. Juris, S. Serroni, M. Venturi, Acc. Chem. Res., 1998, 31, 26.

[27] M. Marcaccio, F. Paolucci, C. Paradisi, S. Roffia, C. Fontanesi, L. J. Yellowlees, S. Serroni, S. Campagna, G. Denti, V. Balzani, J. Am. Chem. Soc., 1999, 121, 10081.

[28] M. Marcaccio, F. Paolucci, C. Paradisi, M. Carano, S. Roffia, C. Fontanesi, L. J. Yellowlees, S. Serroni, S. Campagna, V. Balzani, J. Electroanal. Chem., 2002, 532, 99.

[29] R. Amadelli, R. Argazzi, C. A. Bignozzi, F. Scandola, J. Am. Chem. Soc., 1990, 112, 7099.

[30] M. K. Nazeeruddin, P. Liska, J. Moser, N. Vlachopoulos, M. Grätzel, Helv. Chim. Acta, 1990, 73, 1788.

[31] S. Roffia, R. Casadei, F. Paolucci, C. Paradisi, C.A. Bignozzi, F. Scandola, J. Electroanal. Chem., 1991, 302, 157.

[32] M.G. Teixeira, S. Roffia, C.A. Bignozzi, C. Paradisi, F. Paolucci, J. Electroanal. Chem., 1993, 345, 243.

[33] S. Roffia, M. Marcaccio, C. Paradisi, F. Paolucci, V. Balzani, G. Denti, S. Serroni, S. Campagna, Inorg. Chem., 1993, 32, 3003.

[34] Y. Fuchs, S. Lofters, T. Dieter, W. Shi, R. Morgan, T. C. Strekas, H. D. Gafney, A. D. Baker, J. Am. Chem. Soc. 1987, 109, 2691.

[35] W. R. Murphy, K. J. Brewer, G. Gettliffe, J. D. Petersen, Inorg. Chem. 1989, 28, 81.

[36] S. Campagna, G. Denti, L. Sabatino, S. Serroni, M. Ciano, V. Balzani, J. Chem. Soc., Chem. Comm.. 1989, 1500.

[37] K. Kalyanasundaram, Md. K. Nazeeruddin, Chem. Phys. Lett. 1989, 158, 45.

[38] K. J. Brewer, W. R. Murphy, S. R. Spurlin, J. D. Petersen, Inorg. Chem. 1986, 25, 882.

[39] S. Ernst, V. Kasack, W. Kaim, Inorg. Chem. 1988, 27, 1146.

[40] S. Campagna, G. Denti, G. De Rosa, L. Sabatino, M. Ciano, V. Balzani, Inorg. Chem., 1989, 28, 2565.

[41] S. Campagna, G. Denti, L. Sabatino, S. Serroni, M. Ciano, V. Balzani, Gazz. Chim. Ital., 1989, 119, 415.

[42] G. Denti, S. Campagna, J. L. Sabatino, S. Serroni, M. Ciano and V. Balzani, Inorg. Chem. 1990, 29, 4750.

[43] C. Hicks, J. Fan, I. Rutenberg, H. D. Gafney, Coord. Chem. Rev., 1998, 171, 71.

[44] V. W. W. Yam, V. W. M. Lee, K. K. Cheung, Organometallics, 1997, 16, 2833.

[45] V. W. W. Yam, V. W. M. Lee, K. K. Cheung, J. Chem. Soc., Chem. Commun. 1994, 2075.

[46] A. Neel, H. Stoeckii-Evans, Chimica, 1993, 47, 198.

[47] G. Clemo, J. Chem. Soc., 1938, 753.

[48] E. C. Constable, H. Eriksson, C. E. Housecroft, B. M. Kariuki, E. Nordlander, J. Olsson, Inorg. Chem. Commun., 2001, 4, 749.

[49] E. C. Constable, M. J. Hannon, A. M. W. Cargill Thompson, D. A. Tocher and J. V. Walker, Supramol. Chem., 1993, 2, 243; R. Chotalia, E. C. Constable, M. J. Hannon and D. A. Tocher, J. Chem. Soc. Dalton Trans., 1995, 3571; E. C. Constable and A. M. W. Cargill Thompson, Inorg. Chim. Acta, 1994, 223, 177.

[50] E. C. Constable, Adv. Inorg. Chem., 1989, 34, 1.

[51] C. Kutal, Coord. Chem. Rev., 1990, 99, 213; D. R. McMillin, K. M. McNett, Chem. Rev., 1998, 98, 1201; N. Armaroli, Chem. Soc. Rev., 2001, 30, 113.

[52] D. G. Cuttell, S. -M. Kuang, P. E. Fanwick, D. R. McMillin, R. A. Walton, J. Am. Chem. Soc., 2002, 124, 6; S. -M. Kuang, D. G. Cuttell, D. R. McMillin, P. E. Fanwick, R. A. Walton, Inorg. Chem., 2002, 41, 3313.

[53] Y. -G. Ma, W. -H. Chan, X. -M. Zhou, C. -M. Che, New J. Chem. 1999, 263; S. Sakaki, T. Kuroki, T. Hamada, J. Chem. Soc., Dalton Trans., 2002, 840.

[54] M. H. W. Lam, S. T. C. Cheung, K. -M. Fung, W. -T. Wong, Inorg. Chem. 1997, 36, 4618; M. Riklin, D. Tran, X. Bu, L. E. Laverman, P. C. J. Ford, Chem. Soc., Dalton Trans., 2001, 1813; V. Grosshenny, R. J. Ziessel, Chem. Soc., Dalton Trans. 1993, 817; R. Ziessel, D. Matt, L. J. Toupet, Chem. Soc., Chem. Commun., 1995, 2033.

[55] S. M. Scott, K. C. Gordon, A. K. J. Burrel, Chem. Soc., Dalton Trans., 1999, 2669.

[56] Z. A. Siddique, T. Ohno, K. Nozaki, T. Tsubomura, Inorg. Chem., 2004, 43, 663; T. Tsubomura, M. Abe, M. Tarutani, H. Yamada, T. Tsukuda, Bull. Chem. Soc. Jpn., 2003, 76, 2151.

[57] T. Tsubomura, N. Takahashi, K. Saito, T. Tsukuda, Chem. Lett. 2004, 33, 678.

[58] T. Tsubomura, S. Enoto, S. Endo, T. Tamane, K. Matsumoto and T. Tsukuda, Inorg. Chem., 2005, 44, 18, 6373.

[59] V. Balzani, L. Moggi, M.F. Manfrin, F. Bolletta, M. Gleria, Science, 1975, 189, 852.

[60] J. R. Bolton, Science, 1978, 202, 705.

[61] N. Sutin, C. Creutz, Pure Appl. Chem., 1980, 52, 2717

[62] K. Kalyanasundaram, Coord. Chem. Rev., 1982, 46, 159.

[63] (a) J. -M. Lehn, J. -P. Sauvage, Nouv. J. Chim., 1977, 1, 449; (b) M. Kirch, J. -M. Lehn, J. -P. Sauvage, Helv. Chim. Acta, 1979, 62, 1345.

[64] (a) K. Kalyanasundaram, J. Kiwi, M. Grätzel, Helv. Chim. Acta, 1978, 61, 2720; (b) J. Kiwi, M. Grätzel, Nature, 1979, 281, 657; (c) M. Grätzel, Acc. Chem. Res., 1981, 14, 376; (d) E. Borgarello, J. Kiwi, E. Pelizzetti, M. Visca, M. Grätzel, Nature, 1981, 289, 158; (e) E. Borgarello, J. Kiwi, E. Pelizzetti, M. Visca, M. Grätzel, J. Am. Chem. Soc., 1981, 103, 6324.

[65] (a) A. Moradpour, E. Amouyal, P. Keller, H. B. Kagan, Nouv. J. Chim., 1978, 2, 547; (b) P. Keller, A. Moradpour, E. Amouyal, H. B. Kagan, Nouv. J. Chim., 1980, 4, 377; (c) O. Johansen, A. Launikonis, J. W. Loder, A. W. -H. Mau, W. H. F. Sasse, J. D. Swift, D. Wells, Aust. J. Chem., 1981, 34, 981; (d) E. Amouyal, D. Grand, A. Moradpour, P. Keller, Nouv. J. Chim., 1982, 6, 241.

[66] (a) G. M. Brown, B. S. Brunschwig, C. Creutz, J. F. Endicott, N. Sutin, J. Am. Chem. Soc., 1979, 101, 1298; (b) G. M. Brown, S. -F. Chan, C. Creutz, H. A. Schwarz, N. Sutin, J. Am. Chem. Soc., 1979, 101, 7638; (c) S. F. Chan, M. Chou, C.

Creutz, T. Matsubara, N. Sutin, J. Am. Chem. Soc., 1981, 103, 369; (d) C. V. Krishnan, B. S. Brunschwig, C. Creutz, N. Sutin, J. Am. Chem. Soc., 1985, 107, 2005; (e) H. A. Schwarz, C. Creutz, N. Sutin, Inorg. Chem., 1985, 24, 433.

[67] K. Sakai and H. Ozawa, Coordination Chemistry Reviews, 2007, 251, 2753.

[68] H. Ozawa, Y. Yokoyama, M. Haga and K. Sakai, Dalton Trans., 2007, 1197.

[69] (a) K. Sakai, T. Tsubomura, J. Inorg. Biochem., 1997, 67, 349; (b) K. Sakai, H. Ozawa, H. Yamada, T. Tsubomura, M. Hara, A. Higuchi, M. Haga, Dalton Trans., 2006, 3300.

[70] H. Ozawa, M. Haga, K. Sakai, J. Am. Chem. Soc., 2006, 128, 4926.

[71] H. Ozawa, Ph.D. Dissertation, Kyushu University, 2007.

[72] K. Yokokawa, K. Sakai, Acta Crystallogr., 2004, C60, m244.

[73] (a) G. R. Clemo, T. Holmes and G. C. Leitch, J. Chem. Soc., 1938, 753; (b) F. Case and E. Koft, J. Am. Chem. Soc., 1959, 81, 905.

[74] O. Vallat, A. Neels and H. Stoeckli-Evans, Journal of Chemical Crystallography, Vol. 33, 2003, 39.

[75] M. Schulz, J. Hirschmann, A. Draksharapu, G. Singh Bindra, S. Soman, A. Paul, R. Groarke, M. T. Pryce, S. Rau, W. R. Browne and J. G. Vos, Dalton Trans., DOI: 10.1039/c1dt10960j.

[76] G. Singh Bindra, M. Schulz, A. Paul, S. Soman, R. Groarke, J. Inglis, M. T. Pryce, W. R. Browne, S. Rau, B. J. Maclean and J. G. Vos, Dalton Trans., DOI: 10.1039/c1dt11241d.

[77] B. P. Sullivan, D. J. Salmon, T. J. Meyer, Inorg. Chem., 1978, 17, 3334.

[78] W. R. Browne, C. M. O'Connor, J. S. Killeen, A. L. Guckian, M. Burke, P. James, M.

Burke, J. G. Vos, Inorg. Chem., 2002, 41, 4245.

[79] http://www.sigmaaldrich.com/spectra/rair/RAIR002625.PDF

[80] M. B. Ferrari, G. G. Fava, G. Pelosi, G. Predieri, C. Vignali, G. Denti, S. Serroni, Inorg. Chimica Acta, 1998, 275-276, 320.

[81] J. McMurry, Organic Chemistry, 5th Edition, Brooks/ Cole, 2000.

[82] J. M. Calvert, J. V. Caspar, R. A. Binstead, T. D. Westmoreland and T. J. Meyer, J. Am. Chem. Soc., 1982, 104, 24, 6620.

[83] M. K. Nazeruddin, E. Muller, R. Humphry-Baker, N. Vlachopoulos, M. Grätzel, J. Chem. Soc., Dalton Trans., 1997, 4571.

[84] R. Ghanem, Y. Xu, J. Pan, T. Hoffmann, J. Andersson, T. Polivka, T. Pascher, S. Styring, L. Sun and V. Sundström, Inorg. Chem., 2002, Vol. 41, 24, 6258.

[85] G. Weber in D.M. Hercules, Fluorescence and Phosphorescence Analysis. Principles and Applications, 1966, Interscience Publishers (J. Wiley & Sons), New York, pp. 217-240.

[86] T. E. Keyes, F. Weldon, E. Muller, P. Pechy, M. Grätzel, Vos J. G., Dalton Trans., 1995, 16, 2750.

[87] P. Du, J. Schneider, L. Fan, W. Zhao, U. Patel, F. N. Castellano and R. Eisenberg, J. Am. Chem. Soc., 2008, 130, 5056.

[88] P. Lei, M, Hedlund, R. Lomoth, H. Rensmo, O. Johansson and L. Hammarström, J. Am. Soc., 2008, 130, 26.

Chapter 4: Synthesis, Characterisation and Photocatalytic Properties of Ruthenium(II) - Palladium(II) Hetero-Bimetallic Compounds with 2,2':5',2''-terpyridine (2,5-bpp) and 2,2':6',2''-terpyridine (2,6-bpp) as Bridging Ligands.

Abstract:

This chapter describes the synthesis of novel hetero-bimetallic cyclometallated complexes using the conventional "complexes as metal / complexes as ligands" strategy. The complexes synthesised in this chapter were designed for photocatalytic generation of hydrogen from water. In these dinuclear metal complexes 2,2':5',2''-terpyridine (2,5-bpp) and 2,2':6',2''-terpyridine (2,6-bpp) have been used as bridging ligands. This chapter is the starting point for the development of appropriate methods for the synthesis of multi-component metal based systems and includes their characterisation using nuclear magnetic resonance, deuteriation of peripheral ligands, elemental analysis and electronic properties. The photocatalytic production of hydrogen from water was also investigated using different photocatalytic conditions.

4.1 Introduction.

2,2'-Bipyridines (bpy) are undoubtedly among the most widely used ligands in coordination and supramolecular chemistry and the photophysical properties of their metal complexes are of special interest. [1] In particular, electroluminescent chelate complexes have been shown to be useful as organic light emitting diodes (OLEDs).[2] Ruthenium complexes of functionalized bipyridines are presently the most effective sensitizers for dye-sensitized solar cells (DSSCs).[3]

A critical element in designing and fabricating materials for OLEDs is to control their emission wavelength.[4] One such approach involve appending fluorescent chromophores to a polymeric backbone or to blend such dyes into inert polymeric matrices.[5, 6] Ideally, one would like to utilize one family of modular chromophores and tune their photophysical characteristics as required.[7] The parent oligopyridines (2,2'-bipyridine, 2,2':6',2''-terpyridine (2,6-bpp) and 1,10-phenanthroline) possess extremely low fluorescence quantum yields and undesirable short emission wavelengths. Introduction of conjugated electron donor moieties, e.g., pyrrolylethenyl,[8] phenylethynyl,[9] aminophenyl,[10] or manisyl (4-methoxy-2,6 dimethylphenyl)[11] leads to an increase in quantum yields and a shift in emission wavelength towards the visible area. Since the most intense electronic transition of the 2,2'- bipyridine skeleton is polarized along the 5,5' positions,[11] the 5-position of bipyridines is considered ideal for the introduction of aromatic substituents. As an example 5-manisyl-2,2'-bipyridines have been previously shown to exhibit higher emission quantum yields compared with the 2- and 4-manisyl analogs.[11] In addition, an aryl moiety at the β – position does not affect the coordination behavior of the ligand. The DSSCs are in principle the opposite of OLEDs, producing electrical energy from photonic energy. However, since a sensitizer in DSSC must effectively absorb sunlight, conjugated aromatic substituents in bipyridine are desirable at position 4 or 5. The 5-aryl 2,2'-bipyridines (arbpy) exhibit the best luminescent properties with emission quantum yields (ϕ_{em}) up to 0.80, due to the aromatic substituents making the bipyridines attractive as chromophores and 'antennae'.[11] Strong fungicidal activity of 5-aryl-2,2'-bipyridines against different plant diseases is another application

reported.[12] However, the study of these interesting and useful compounds is hampered by inefficient synthetic methods. The typical Kroehnke synthesis was modified to prepare 5-substituted-2,2'- bipyridines giving mixtures of isomers and poor yields.[12] Alternative cross-coupling [13] approaches are limited by inaccessible starting compounds.

Kozhevnikov *et. al.* [14, 15] reported (see Scheme 4.1) an efficient strategy for the synthesis of 5-(hetero)aryl-2,2'-bipyridines **1** based on the conversion of 3-(2-pyridyl)-1,2,4-triazines to substituted bpy's via an aza-Diels–Alder reaction.[16] The key-step of their strategy is the regiospecific and easy synthesis of 3-pyridyl-1,2,4-triazines bearing an aryl substituent at the 6-position of the 1,2,4-triazine ring. It should be noted that 3-pyridyl 1,2,4-triazines are interesting compounds in their own right due to their application in transition metal analysis[17] or in the separation of lanthanides and actinides in the management of nuclear waste.[18] A new method for the synthesis of 6-aryl-3-(2-pyridyl)-1,2,4-triazines **2** starts from readily available acylarenes **3** bearing various substituents on the aryl moiety, for example, fluoro-, chloro-, bromo-, methyl-, methoxy- or nitrophenyl. Nitrosation of **3** yielded the corresponding 1-aryl-2-oximino-1-ethanones **4**, and then treatment with hydrazine hydrate resulted in the formation of 1-aryl-1H-ydrazono-2 oximinoethanes **5** in good yields. Condensation of hydrazones **5** with pyridine-2-carboxaldehyde gave 1-aryl-2-oximino-1-(2-pyridylmethylenehydrazono)ethanes **6** in excellent yields. The open-chain compounds **6** exist in equilibrium with the cyclic 6-aryl-4H-ydroxy-3-(2-pyridyl)-3,4-dihydro-1,2,4-triazines **7** (the ring-chain isomerism of 4H-ydroxy-3,4-dihydro-1,2,4-triazines is described elsewhere[19]). Dehydration of the dihydrotriazines **7** after brief refluxing in acetic acid yielded the aromatic pyridyltriazines **2**. The aryl substituents of the starting ketones **3** appear at the defined 6-position of the 1,2,4-triazines **2** and not the 5-position as in 1,2,4-triazine synthesis from arylglyoxals.[20] Isolation of the intermediates **6** and **7** from the reaction mixtures can be omitted to make the synthetic procedure easier.[14, 15] Conversion of triazines **2** to arbpys **1** was achieved by aza-Diels–Alder reactions with a strained dienophile 2,5-norbornadiene following a typical procedure.[16] The reaction proceeded slowly and at high temperature (refluxing in xylene) to give 5-aryl-2,2'-bipyridines **1** in high yields (see Scheme 4.1).

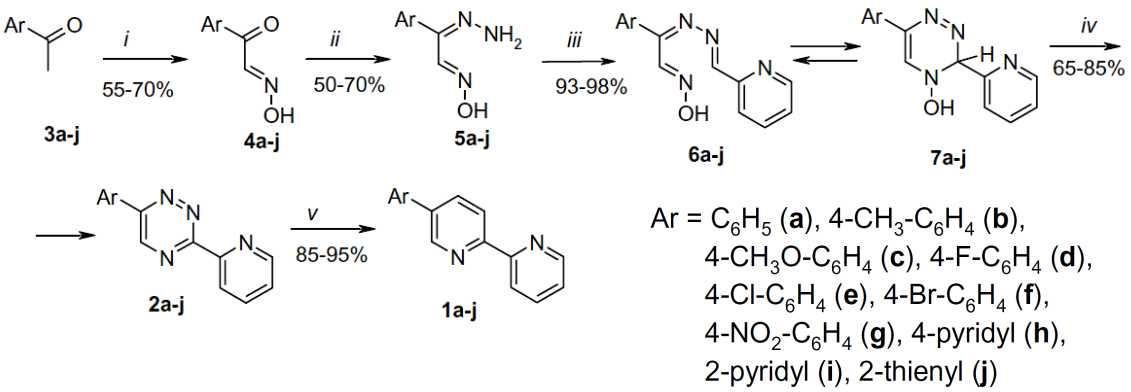

Reagents and conditions: (i) i-PrONO, EtONa, EtOH, 10°C, then AcOH; (ii) N_2H_4–H_2O, EtOH, rt; (iii) pyridine-2-carboxaldehyde, EtOH; (iv) AcOH, reflux; (v) 2,5-norbornadiene, xylene, reflux, 8–15 h.

Scheme 4.1: *Synthetic strategy for the preparation of 5-(hetero)aryl-2,2'-bipyridines by Kozhevnikov et. al.*[14, 15]

The use of 2,2':6',2''-terpyridine (2,6-bpp) as a ligand has been hindered by the short excited state lifetime and absence of emission at room temperature for $[Ru(2,6\text{-bpp})_2]^{2+}$.[21] It has been concluded that this behavior is due to the thermal population of a ligand field state giving rise to rapid non-radiative deactivation of the MLCT excited state.[21] The typical bridging ligand should possess at least two donor sites to bind the catalytically active metal centre and it is important to gain some insight into the photophysical properties of the compounds. Based on these concepts, Schwalbe *et. al.*[22] studied the bridging ligand tris(2-pyridyl)triazine (tpt) which is based on a terpyridine ligand. In which an electron storage capacity can be assigned to the central triazine ring allowing directed electron transfer processes based on earlier investigations.[23] The ligand tpt has the possibility of binding metals in different ways (Scheme 4.2). This is especially interesting in view of the fact that a comparison of structures III and IV shows that the central metal (M1) has the option of binding to a free pyridine moiety in IV to form III. Such behavior might stabilize the whole photo-molecular device (PMD) as a transiently formed reduced metal centre may bind the additional pyridine thus preventing colloid formation.

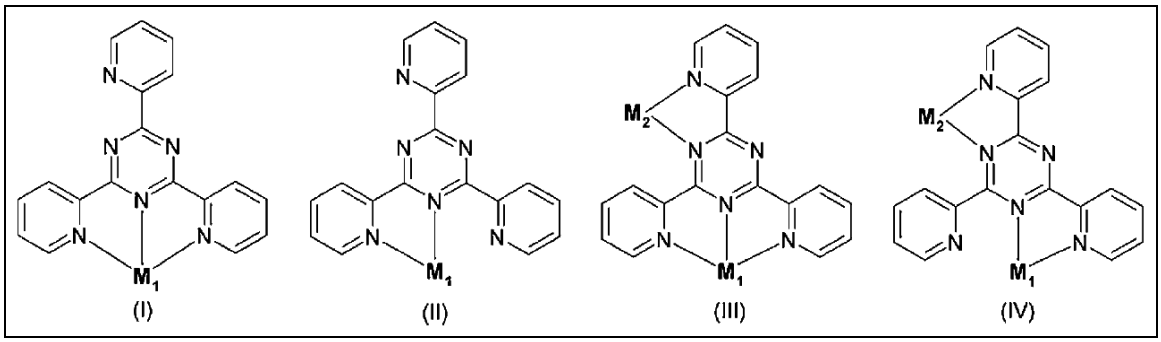

Scheme 4.2: *Different binding possibilities of the bridging ligand tpt.*[22]

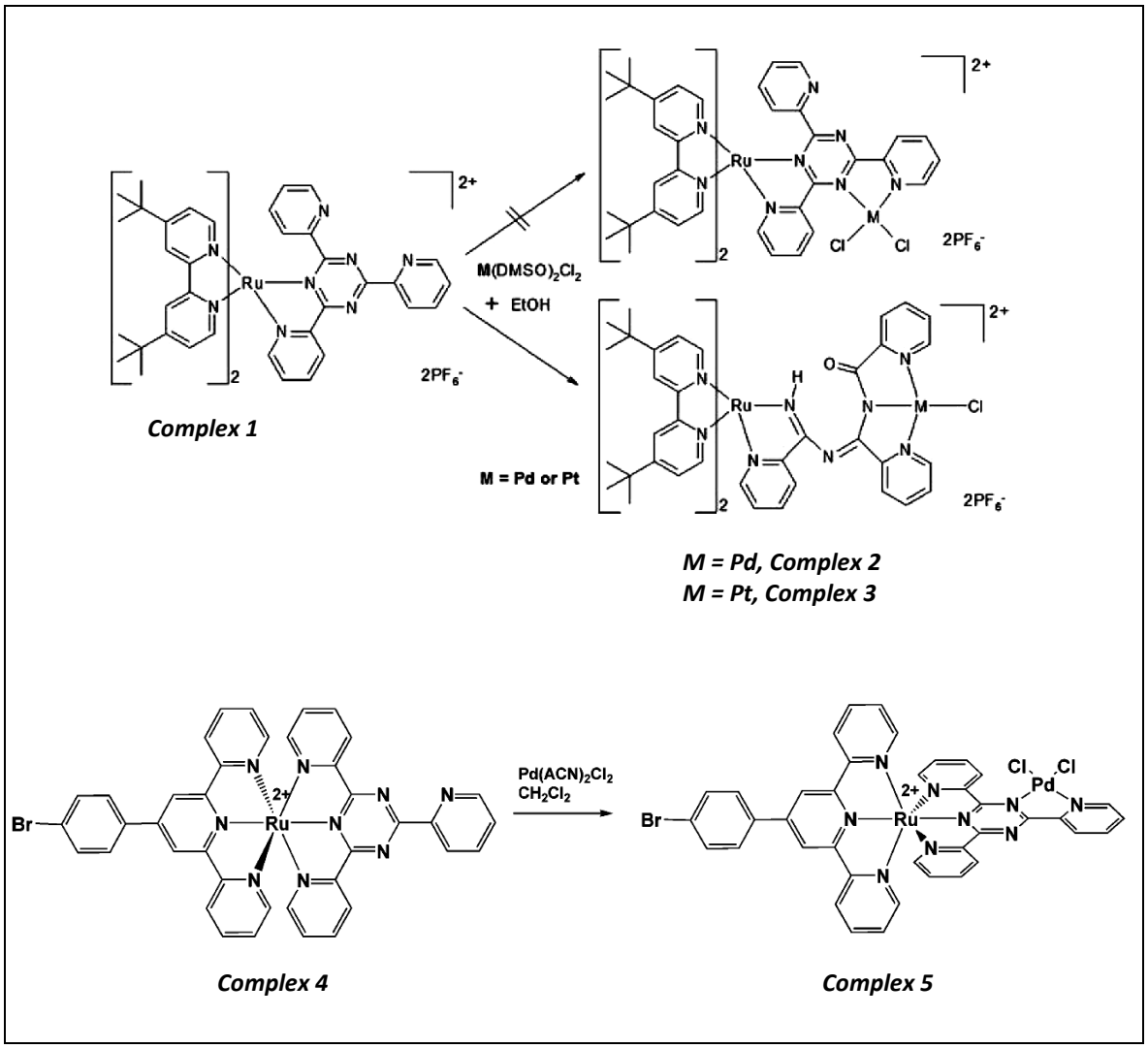

Figure 4.1: *The reaction of complex **1** to complex **2**, M = Pd / complex **3**, M = Pt and complex **4** to complex **5**.* [22]

The synthesis, structure and photophysical properties of three mononuclear complexes and one dinuclear complex with the bridging ligand tris(2-pyridyl)triazine (tpt) and two heterodinuclear supramolecular ruthenium–palladium and ruthenium–platinum complexes with the bridging ligand tptO (hydrolysis of triazine ring) (see figure 4.1) were reported by Rau *et. al.*[22] The latter ligand results from a ring-opening reaction and selective hydrolysis of the tpt ligand during the reaction. This hydrolysis reaction was not observed when a terpyridine-like ruthenium precursor complex **4** was used (tri-coordination complex, see also figure 4.1).[22] The hydrolysis of the tpt ligand can be monitored by both ^{1}H-NMR and UV-vis absorption spectroscopy. The increased reactivity of the tpt ligand towards nucleophiles confirms the electron deficient nature of triazine-based ligands in dinuclear complexes. The triazine ligand acts as an electron acceptor in this case and the complex is susceptible to nucleophilic attack. The ring-opening of the triazine ligand in the dinuclear complexes leads to the formation of the two complexes (based on complex **1**) leading to palladium and platinum complexes (see figure 4.1) where the metal centers are coordinated to three nitrogen donor sites. All three heterodinuclear complexes **2**, **3** and **5** are incapable of catalyzing photoinduced hydrogen production from aqueous solution. Under standard catalytic conditions,[24] these compounds show no activity as hydrogen evolving catalysts following irradiate in acetonitrile/water mixtures containing triethylamine as an electron donor. There are several potential explanations for these observations. On the one hand, the catalytic centers in complex **2** and **3** are coordinated by three nitrogen donors. Eisenberg and co-workers have shown that such a ligand environment in terpyridine platinum complexes is preventing any high catalytic activity in this reaction.[25] In addition, the electronic properties of the bridging ligand tptO may not facilitate efficient electron transfer and good storage capabilities as was observed for other bridging ligands. A very short lifetime of the charge separated excited state for compound **5** (shows no emission) might also be responsible.[22] The very short lifetimes of the exited states of the dinuclear compounds in general may limit the likelihood of photoinduced electron transfer between the excited ruthenium centre and the sacrificial electron donor.

The photocatalytic production of hydrogen is therefore a major challenge in converting

solar energy directly to chemical energy. One of the most promising approaches towards this goal is the use of molecular photocatalysts that utilise visible light to drive proton reduction and it can be envisaged that such systems comprise a light harvesting antenna (photosensitizer) that can donate electrons to a catalytically active centre to which it is connected via a bridging ligand. Due to their exceptional photophysical and redox properties ruthenium (II) polypyridyl complexes are an excellent choice as the light harvesting centre while Pd(II) or Pt(II) are the metal of choice for the catalytically active centres.[26] Alternative combinations already reported are the combinations of Re/Co, Ru/Pd, Ru/Pt, Os/Rh, Ru/Rh, Pt/Co, Ir/Rh.[27, 28, 29, 30, 31, 32, 33, 34] The intramolecular approach in which a bridging ligand facilitates photoinduced electron transfer from the light harvesting centre to the hydrogen forming centre, requires vectorial electron transfer to be mediated by the bridging ligand. This realisation has lead to the application of bridging ligands which are more electron deficient than the peripheral ligands. But subtle changes of the bridge or the peripheral ligand may turn the catalyst active or inactive.[35, 36] Moreover, the creation of an open coordination site was also found to be a crucial step for the photocatalytic water splitting of *cis*-Pd complexes and is accomplished by cleavage of one Pd – Cl bond. This was found to be a key step for light driven hydrogen generation of $[Ru(4,4'\text{-}tert\text{butyl-bpy})_2(tpphz)PdCl_2]\ (PF_6)_2$.[24]

4.2 Experimental section.

The compounds 2,2'-bipyridine (bpy), $RuCl_3.xH_2O$, $(NH_4)_2[PdCl_4]$ and 2,2':6',2''-terpyridine (2,6-bpp) were purchased from Aldrich and used without further purification. The deuteriated D_8-2,2'-bipyridine (D_8-bpy) ligand was prepared as reported [37] in the literature (and is described in chapter 2).

4.2.1 Preparation of the ligand 2,2':5',2''-terpyridine (2,5-bpp).

The bridging ligand 2,2':5',2''-terpyridine (2,5-bpp) was synthesised differently from that reported by V. N. Kozhevnikov *et. al.* [14, 15], using a slightly modified method to that reported by Hanan *et. al.* [38] The linear 2,2':5',2"-terpyridine ligand was prepared by Negishi coupling of 2,5-dibromopyridine with 2-pyridylzinc bromide following

published procedures.[14, 15] The complete synthesis has been described in Chapter 2 (Section 2.3.2).

Synthesis of bridging ligand (2,2':5',2''-terpyridine) (2,5-bpp)

This ligand was prepared as described in chapter 2.

Yield: 505 mg (2.15 mmol, 51%).

Anal. Calcd. for $C_{15}H_{11}N_3$. 0.1 $C_2H_5OOCCH_3$: C, 76.41; H, 4.91; N, 17.36%. Found: C, 76.60; H, 4.91; N, 17.31%. ^{1}H-NMR (DMSO-d_6, 400 MHz) δ: 9.40 (d, *J* = 2.4 Hz, 1H, H_6), 8.74 (m, 2H, $H_{6'}$, $H_{6''}$), 8.62 (dd, *J* = 8.4 Hz, *J* = 2.0 Hz, 1H, H_4), 8.52 (d, *J* = 8.4 Hz, 1H, H_3), 8.47 (d, *J* = 7.8 Hz, 1H, $H_{3''}$), 8.15 (d, *J* = 8.1 Hz, 1H, $H_{3'}$), 7.98 (m, 2H, $H_{4'}$, $H_{4''}$), 7.48 (m, 2H, $H_{5'}$, $H_{5''}$).

4.2.2 Preparation of the ruthenium mononuclear complexes.

Synthesis of [Ru(bpy)$_2$(2,5-bpp)] (PF$_6$)$_2$ · 0.5 (CH$_3$)$_2$CO (Complex 4.1).

[bis-(2,2'-bipyridine)(2,2':5',2''-terpyridine)ruthenium(II)](PF$_6$)$_2$·0.5(CH$_3$)$_2$CO

$[Ru(bpy)_2Cl_2]\cdot 2H_2O$ (0.339 g, 0.65 mmol) dissolved in 5 cm^3 of ethanol was added drop-wise to a solution of 2,2':5',2''-terpyridine (2,5-bpp) (0.152 g, 0.65 mmol) in 10 cm^3 of ethanol/water (3:1 v/v). The reaction mixture was heated at reflux for 8 hours. Subsequently, the mixture was allowed to cool to room temperature and the solvent was evaporated under vacuum. The obtained residue was precipitated in saturated aqueous solution of NH_4PF_6 followed by filtration of the product which was then washed with 10 cm^3 of diethyl ether. Recrystallization from acetone/water (3:1 v/v) afforded a red solid. Yield: 0.576 g (0.60 mmol, 92%). Anal. Calcd. for $C_{35}H_{27}F_{12}N_7P_2Ru$ · 0.5 $(CH_3)_2CO$ (965.67): C, 45.39; H, 3.13; N, 10.15%. Found: C, 45.06; H, 2.95; N, 9.88%. ^{1}H-NMR (Acetonitrile-d_3, 400 MHz): bridging ligand δ = 8.64 – 8.54 (m, 4H, bipy H_{3a}), 8.60-8.58 (m, 2H, H_3, H_4), 8.54-8.52 (m, 2H, $H_{3''}$, $H_{6'}$), 8.30 (s, 1H, H_6), 8.15 – 8.07 (m, 4H, bipy H_{4a}), 8.07 (t, 1H, *J* = 8.0 Hz, $H_{4''}$), 7.95 – 7.78 (m, 4H, bipy H_{6a}), 7.83 (t, 1H, *J* = 7.8 Hz, $H_{4'}$), 7.75 (d, 1H, *J* = 5.6 Hz, $H_{6''}$), 7.67 (d, 1H, *J* = 7.6 Hz, $H_{3'}$), 7.48 – 7.38 (m, 4H, bipy H_{5a}), 7.41 (m, 1H, $H_{5''}$), 7.36 (m, 1H, $H_{5'}$).

Synthesis of [Ru(bpy)$_2$(2,6-bpp)] (PF$_6$)$_2$ · 2 H$_2$O (Complex 4.2).

[bis-(2,2'-bipyridine)(2,2':6',2''-terpyridine)ruthenium(II)](PF$_6$)$_2$· 2 H$_2$O

[Ru(bpy)$_2$Cl$_2$]·2H$_2$O (0.500 g, 0.96 mmol) dissolved in 6 cm^3 ethanol was added drop-wise to a solution of 2,2';6',2"-terpyridine (0.224 g, 0.96 mmol) in 40 cm^3 ethanol/water (3:1). The reaction mixture was heated at reflux for 6 hours. Subsequently, the mixture was allowed to cool to room temperature and the solvent was evaporated under vacuum. The obtained residue was precipitated in saturated aqueous solution of NH_4PF_6 followed by filtration of the product which was then washed with 10 cm^3 of diethyl ether. Recrystallization from acetone/water (3:1 v/v) afforded a red solid. Yield: 0.510 g (0.52 mmol, 54%). Anal. Calcd for $C_{35}H_{27}F_{12}N_7P_2Ru \cdot 2\ H_2O$ (972.67): C, 43.22; H, 3.21; N, 10.08 %. Found: C, 43.15; H, 2.82; N, 9.99 % ^{1}H-NMR (Acetonitrile-d$_3$, 400 MHz): δ = 8.75 (br s, 1H, bipy H_{3a}), 8.63 (m, 2H, H_5, $H_{3"}$), 8.48 (d, 1H, J = 7.5 Hz, bipy H_{3a}), 8.42-8.39 (m, 2H, bipy H_{3a}), 8.17-8.07 (m, 6H, H_4, $H_{4"}$, $H_{3'}$, bipy H_{4a} (3H)), 7.96 (t, 1H, J = 7.8 Hz, bipy H_{4a}), 7.67 (d, 1H, J = 6.0 Hz, bipy H_{6a}), 7.62 (t, 1H, J = 7.5 Hz, bipy H_{5a}), 7.58-7.53 (m, 2H, $H_{6"}$, bpy H_{6a} (1H)), 7.41-7.28 (m, 5H, H_3, $H_{5"}$, $H_{5'}$, bipy H_{6a} (1H), bipy H_{5a} (1H)), 7.21 (t, 1H, J = 7.6 Hz, bipy H_{5a}), 6.99 (t, 1H, J = 7.5 Hz, $H_{4'}$), 6.88 (d, 1H, J = 7.6 Hz, bipy H_{6a}), 6.85-6.76 (m, 2H, $H_{6'}$, bipy H_{5a} (1H)).

4.2.3 Preparation of Ru-Pd Heterodinuclear complexes.

Synthesis of [Ru(bpy)$_2$(2,5-bpp)PdCl(CH$_3$CN)]$_2$ (PF$_6$)$_2$ (Complex 4.3).

[Ruthenium(II)(2,2'-bipyridine)$_2$(μ-2,2':5',2''-terpyridine)PdCl(acetonitrile)] (PF$_6$)$_2$

[Ru(bpy)$_2$(2,5-bpp)] (PF$_6$)$_2$ (0.100 mg, 0.11 mmol) was dissolved in 5 cm^3 of methanol and added drop wise to a solution of $(NH_4)_2PdCl_4$ (0.027 g, 0.10 mmol) in 10 cm^3 of methanol. The reaction mixture was heated at reflux for 48 hours. Subsequently the mixture was allowed to cool at room temperature. The product was precipitated by the addition of 20 cm^3 of n-Hexane. After filtration and washing with 10 cm^3 of diethyl ether, a red solid product was recrystallised from acetonitrile / acetone (1:3). Yield: 0.101 g (0.09 mmol, 90%). Anal. Calcd for $C_{35}H_{26}ClF_{12}N_7P_2PdRu \cdot CH_3CN$ (1118.55 g/mol): C, 39.73; H, 2.61; N, 10.02%. Found: C, 39.49; H, 2.82; N, 10.04%. ^{1}H-NMR (Acetonitrile-d$_3$, 400 MHz): bridging ligand δ = 9.51 (d, *J* = 6.0 Hz, 1H, $H_{6'}$), 9.13 (s, 1H, H_3), 8.64 –

8.54 (m, 4H, bipy H_{3a}), 8.45 (d, *J* = 8.4 Hz, 1H, $H_{3''}$), 8.15 – 8.07 (m, 4H, bipy H_{4a}), 8.01 (m, 1H, $H_{4''}$), 7.95 – 7.78 (m, 4H, bipy H_{6a}), 7.86 (m, 1H, $H_{4'}$), 7.67 (d, *J* = 5.6 Hz, 1H, $H_{6''}$), 7.46 (s, 1H, H_6), 7.48 – 7.38 (m, 4H, bipy H_{5a}), 7.39 (m, 1H, $H_{5'}$), 7.34 (m, 1H, $H_{5''}$), 7.18 (d, *J* = 7.6 Hz, $H_{3'}$), 2.06 (s, 3H, CH_3CN).

Synthesis of [Ru(bpy)$_2$(2,6-bpp)PdCl(CH$_3$CN)] (PF$_6$)$_2$ · H$_2$O (Complex 4.4).

[Ruthenium(II)(2,2'-bipyridine)$_2$(μ-2,2':6',2''-terpyridine)PdCl(acetonitrile)] (PF$_6$)$_2$ · H$_2$O

[Ru(bpy)$_2$(2,6-bpp)] $(PF_6)_2$ (0.100 mg, 0.11 mmol) was dissolved in 5 cm^3 of methanol and added drop wise to a solution of $(NH_4)_2PdCl_4$ (0.027 g, 0.10 mmol) in 10 cm^3 of methanol. The reaction mixture was heated at reflux for 48 hours. Subsequently the mixture was allowed to cool to room temperature. The product was precipitated by addition of 20 cm^3 of n-Hexane. After filtration and washing with 10 cm^3 of diethyl ether, a red solid product was recrystallised from acetonitrile / acetone (1:3). Yield: 0.110 g (0.096 mmol, 96%). Anal. Calcd for $C_{35}H_{26}ClF_{12}N_7P_2PdRu \cdot CH_3CN \cdot H_2O$ (1136.55): C, 39.10; H, 2.75; N, 9.86%. Found: C, 38.96; H, 2.49; N, 9.84%. ^{1}H-NMR (Acetonitrile-d_3, 400 MHz): δ = 9.12 (br s, 1H, $H_{6'}$), 9.01(br s, 1H, bipy H_{3a}), 8.75(d, 1H, *J* = 7.5 Hz, bipy H_{3a}), 8.66(d, 1H, *J* = 7.5 Hz, bipy H_{3a}), 8.42 (d, 1H, *J* = 7.8 Hz, $H_{3''}$), 8.40(d, 1H, *J* = 7.5 Hz, bipy H_{3a}), 8.24 (ddd, 1H, *J* = 7.5 Hz, J = 1.5 Hz, bipy H_{4a}), 8.12 -8.00 (m, 4H, $H_{4''}$, bipy H_{4a}), 7.93 (d, 1H, *J* = 7.5 Hz, H_4), 7.88(d, 1H, *J* = 7.6 Hz, bipy H_{6a}), 7.80 (d, 1H, *J* = 7.7 Hz, $H_{3'}$), 7.70 (d, 1H, *J* = 7.5 Hz, H_3), 7.69-7.59 (m, 3H, bipy H_{6a}), 7.55 (d, 1H, *J* = 7.5 Hz, bipy H_{5a}), 7.50 (t, 1H, *J* = 7.8 Hz, $H_{4'}$), 7.46 (d, 1H, *J* = 7.8 Hz, $H_{6''}$), 7.29 (t, 1H, *J* = 7.5 Hz, bipy H_{5a}), 7.27(t, 1H, *J* = 7.8 Hz, $H_{5''}$), 7.18 (t, 1H, *J* = 7.5 Hz, bipy H_{5a}), 7.09 (t, 1H, *J* = 7.4 Hz, bipy H_{5a}), 7.02 (t, 1H, *J* = 7.8 Hz, $H_{5'}$), 2.07 (s, 3H, CH_3CN).

4.2.4 Preparation of the partial deuteriated complexes.

Synthesis of [Ru(D$_8$-bpy)$_2$(2,5-bpp)] (PF$_6$)$_2$ (Complex 4.5).

[bis-(D_8-2,2'-bipyridine)(2,2':5',2''-terpyridine)ruthenium(II)] (PF_6)$_2$

[Ru(D_8-bpy)$_2$Cl$_2$]·2H$_2$O (0.155 g, 0.29 mmol) dissolved in 5 cm^3 of ethanol was added drop-wise to a solution of 2,2':5',2"-terpyridine (2,5-bpp) (0.068 g, 0.29 mmol) in 10 cm^3 of ethanol/water (3:1 v/v). The reaction mixture was heated at reflux for 8 hours. Subsequently, the mixture was allowed to cool to room temperature and the solvent was evaporated under vacuum. The obtained residue was precipitated in saturated aqueous solution of NH_4PF_6 followed by filtration of the product which was then washed with 10 cm^3 of diethyl ether. Recrystallization from acetone/water (3:1 v/v) afforded a red solid. Yield: 0.265 g (0.28 mmol, 96%). Anal. Calcd. for $C_{35}H_{11}D_{16}F_{12}N_7P_2Ru$ (953.17): C, 44.12; H, 2.83; N, 10.29%. Found: C, 44.06; H, 2.95; N, 10.11%. ^{1}H-NMR (Acetonitrile-d_3, 400 MHz): bridging ligand δ = 8.65-8.52 (m, 4H, H-3, H-4, H-3", H-6'), 8.59 (s, 1H, bpy H-3a), 8.58 (m, 2H, bpy H-3a), 8.57 (s, 1H, bpy H-3a), 8.34 (s, 1H, H-6), 8.10-8.08 (m, 4H, bpy H-4a), 8.10 (ddd, 1H, J = 8.0 Hz, J = 1.6 Hz, H-4"), 7.95 (s, 1H, bpy H-6a), 7.86 (ddd, 1H, J = 7.8 Hz, J = 1.6 Hz, H-4'), 7.80 (s, 1H, bpy H-6a), 7.79 (s, 1H, bpy H-6a), 7.78 (d, 1H, J = 5.6 Hz, H-6"), 7.74 (s, 1H, bpy H-6a), 7.69 (d, 1H, J = 7.6 Hz, H-3'), 7.45-7.40 (m, 4H, bpy H-5a), 7.43 (m, 1H, H-5"), 7.39 (m, 1H, H-5').

Synthesis of [Ru(D_8-bpy)$_2$(2,6-bpp)] (PF_6)$_2$. H_2O (Complex 4.6).

[bis-(D_8-2,2'-bipyridine)(2,2':6',2''-terpyridine)ruthenium(II)] (PF_6)$_2$. H_2O

[Ru(D_8-bpy)$_2$Cl$_2$]·2H$_2$O (0.155 g, 0.29 mmol) dissolved in 5 cm^3 of ethanol was added drop-wise to a solution of 2,2':6',2"-terpyridine (2,6-bpp) (0.068 g, 0.29 mmol) in 10 cm3 of ethanol/water (3:1 v/v). The reaction mixture was heated at reflux for 8 hours. Subsequently, the mixture was allowed to cool to room temperature and the solvent was evaporated under vacuum. The obtained residue was precipitated in saturated aqueous solution of NH_4PF_6 followed by filtration of the product which was then washed with 10 cm^3 of diethyl ether. Recrystallization from acetone/water (3:1 v/v) afforded a red solid. Yield: 0.260 g (0.27 mmol, 95%). Anal. Calcd. for $C_{35}H_{11}D_{16}F_{12}N_7P_2Ru$. H_2O (971.18): C, 43.40; H, 2.78; N, 10.10%. Found: C, 43.33; H, 2.89; N, 10.04%. ^{1}H-NMR (Acetonitrile-d_3, 400 MHz): δ = 8.63 (m, 2H, H-5, H-3"), 8.48 (s, 1H, bpy H-3a), 8.42-

8.39 (m, 2H, bpy H-3a), 8.17-8.07 (m, 6H, H-4, H-11, H-18, bpy H-3a (1H), bpy H-4a (2H)), 7.96 (s, 1H, bpy H-4a), 7.67 (s, 1H, bpy H-4a), 7.62 (s, 1H, bpy H-6a), 7.58-7.53 (m, 2H, H-6", bpy H-6a), 7.41-728 (m, 6H, H-3, H-5", H-5', bpy H-6a (2H), bpy H-5a (1H)), 7.21 (s, 1H, bpy H-5a), 6.99 (ddd, J = 7.5 Hz, J = 1.0 Hz, 1H, H-4'), 6.88 (s, 1H, bpy H-5a), 6.85-6.76 (m, 2H, H-6', bpy).

Synthesis of [Ru(D_8-bpy)$_2$(2,5-bpp)PdCl(CH_3CN)] (PF_6)$_2$ · Pd (Complex 4.7).

[Ruthenium(II)(D_8-2,2'-bipyridine)$_2$(μ-2,2':5',2''-terpyridine)PdCl(acetonitrile)] (PF_6)$_2$ · Pd

[Ru(D_8-bpy)$_2$(2,5-bpp)] (PF_6)$_2$ (0.104 mg, 0.11 mmol) was dissolved in 5 cm^3 of methanol and added drop wise to a solution of $(NH_4)_2PdCl_4$ (0.028 g, 0.10 mmol) in 10 cm^3 of methanol. The reaction mixture was heated at reflux for 48 hours. Subsequently the mixture was allowed to cool to room temperature. The product was precipitated by addition of 20 cm^3 of n-Hexane. After filtration and washing with 10 cm^3 of diethyl ether a red solid was obtained, a red solid product was recrystallised from acetonitrile/acetone (1:3). Yield: 0.091 g (0.08 mmol, 80%). Anal. Calcd for $C_{35}H_{11}D_{16}ClF_{12}N_7P_2PdRu \cdot CH_3CN \cdot Pd$ (1240.97 g/mol): C, 35.78; H, 2.09; N, 9.02%. Found: C, 35.49; H, 2.01; N, 8.89%. ^{1}H-NMR (Acetonitrile-d_3, 400MHz): bridging ligand δ = 9.54 (d, 1H, J = 6.0 Hz, H-6'), 9.16 (s, 1H, H-3), 8.59 (s, 1H, bpy H-3a), 8.58 (m, 2H, bpy H-3a), 8.57 (s, 1H, bpy H-3a), 8.48 (d, 1H, J = 8.4 Hz, H-3"), 8.10-8.08 (m, 4H, bpy H-4a), 8.04 (m, 1H, bpy H-4"), 7.95 (s, 1H, bpy H-6a), 7.89 (m, 1H, H-4'), 7.80 (s, 1H, H-6a), 7.79 (s, 1H, bpy H-6a), 7.74 (s, 1H, bpy H-6a), 7.70 (d, 1H, J = 5.6 Hz, H-6"), 7.49 (s, 1H, H-6), 7.45-7.40 (m, 4H, bpy H-5a), 7.41 (m, 1H, H-5'), 7.37 (m, 1H, H-5"), 7.20 (d, 1H, J = 7.6 Hz, H-3'), 2.06 (s, 3H, CH_3CN).

Synthesis of [Ru(D_8-bpy)$_2$(2,6-bpp)PdCl(CH_3CN)] (PF_6)$_2$ · Pd (Complex 4.8).

[Ruthenium(II)(D_8-2,2'-bipyridine)$_2$(μ-2,2':6',2''-terpyridine)PdCl(acetonitrile)] (PF_6)$_2$ · Pd

[Ru(D_8-bpy)$_2$(2,6-bpp)] (PF_6)$_2$ (0.104 mg, 0.11 mmol) was dissolved in 5 cm^3 of methanol and added drop wise to a solution of $(NH_4)_2PdCl_4$ (0.028 g, 0.10 mmol) in 10 cm^3 of methanol. The reaction mixture was heated at reflux for 48 hours. Subsequently the mixture was allowed to cool to room temperature. The product was precipitated by addition of 20 cm^3 of n-Hexane. After filtration and washing with 10 cm^3 of diethyl ether a red solid was obtained, a red solid product was recrystallised from acetonitrile/acetone (1:3). Yield: 0.089 g (0.08 mmol, 80%). Anal. Calcd for $C_{35}H_{11}D_{16}ClF_{12}N_7P_2PdRu$ · CH_3CN · Pd (1240.97 g/mol): C, 35.78; H, 2.09; N, 9.02%. Found: C, 35.39; H, 2.29; N, 8.77%. ^{1}H-NMR (Acetonitrile-d_3, 400 MHz): δ = 9.12 (br s, 1H, H-6'), 9.01 (s, 1H, bpy H-3a), 8.75 (s, 1H, bpy H-3a), 8.66 (s, 1H, bpy H-3a), 8.42 (d, J = 7.8 Hz, 1H, H-3''), 8.40 (s, 1H, bpy H-3a), 8.24 (s, 1H, bpy H-4a), 8.12-8.00 (m, 4H, H-4'', bpy H-4a (3H)), 7.93 (d, 1H, J = 7.5 Hz, H-4), 7.88 (s, 1H, bpy H-6a), 7.80 (d, 1H, J = 7.7 Hz, H-3'), 7.70 (d, 1H, J = 7.5 Hz, H-3), 7.69-7.59 (m, 3H, bpy H-6a), 7.55 (s, 1H, bpy H-5a), 7.50 (t, J = 7.8 Hz, 1H, H-4'), 7.46 (d, J = 7.8 Hz, 1H, H-6''), 7.29 (s, 1H, bpy H-5a), 7.27 (t, J = 7.8 Hz, 1H, H-5''), 7.18, (s, 1H, bpy H-5a), 7.09 (s, 1H, bpy H-5a), 7.02 (t, 1H, J = 7.8 Hz, H-5'), 2.06 (s, 3H, CH_3CN).

Synthesis of [Ru(bpy)$_2$(2,5-bpp)PtCl(CH_3CN)] (PF_6)$_2$ (Complex 4.9).

[Ruthenium(II)(2,2'-bipyridine)$_2$(μ-2,2':5',2''-terpyridine)PtCl(acetonitrile)] (PF_6)$_2$

[Ru(bpy)$_2$(2,5-bpp)] (PF_6)$_2$ (0.104 mg, 0.11 mmol) was dissolved in 5 cm^3 of methanol and added drop wise to a solution of K_2PtCl_4 (0.018 g, 0.10 mmol) in 10 cm^3 of methanol. The reaction mixture was heated at reflux for 48 hours. Subsequently the mixture was allowed to cool at room temperature. The product was precipitated by addition of 20 cm^3 of n-Hexane. After filtration and washing with 10 cm^3 of diethyl ether a red solid was obtained. A red solid product was recrystallised from acetonitrile/acetone (1:3). The product was analysed by proton-NMR.

The desired product was not obtained.

4.3 Results and discussion

4.3.1 Synthesis of ligand, mononuclear and heterodinuclear complexes.

The linear 2,2':5',2"-terpyridine ligand was prepared by Negishi coupling reactions with modifications to published procedures. The ligand was obtained in moderate yields following the method reported by Hanan *et. al.*, (reaction pathway shown in figure 4.2).[38] The Negishi Coupling, published in 1976 (see reaction mechanism in Figure 4.3),[39] was the first reaction that allowed the preparation of unsymmetrical bi-aryls in good yields. The versatile nickel- or palladium-catalyzed coupling of organozinc compounds with various halides (aryl, vinyl, benzyl, or allyl) has broad scope, and is not restricted to the formation of bi-aryls.

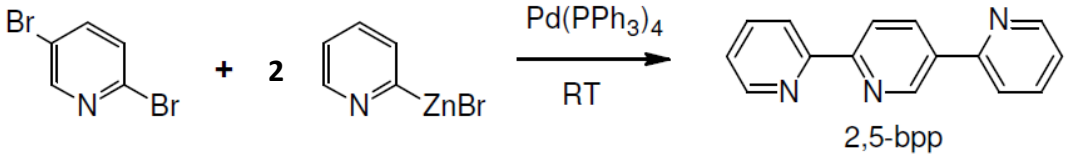

Figure 4.2: *Synthetic strategy for the preparation of 2,5-bpp ligand using Negishi's coupling.*

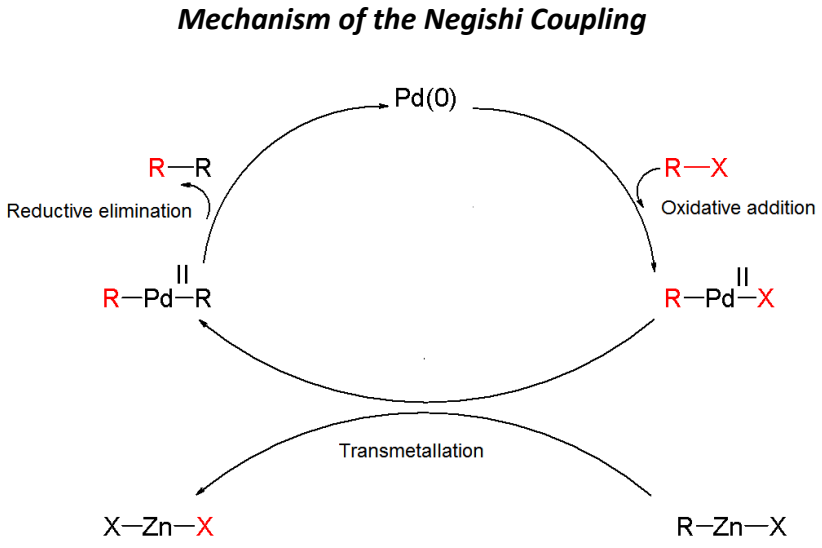

Figure 4.3: *Mechanism involved for the Negishi coupling.*[39]

The synthesis required complete inert conditions and low temperatures (0^o C – 21^o C). All glassware was dried in an oven at 120^o C. The palladium catalyst and reactant 2,5-dibromobipyridine were added to a dry two neck round bottom flask under a stream of nitrogen. The temperature of this reaction mixture was maintained at 0^oC. During the addition of 2-pyridylzinc bromide in THF, the reaction became exothermic, for this reason the reaction mixture was maintained at 0^o C. At this point the reaction mixture turned a brown colour. The reactant 2-pyridylzinc bromide is very sensitive to moisture and is kept at -4^o C for further use. This reaction can be problematic, sometimes leading to the formation of a hydrolysis product of 2-pyridylzinc bromide. A 6% mole equivalent of the $[Pd(PPh_3)_4]$ catalyst was taken (0.258 mmol, 0.06 eq.) with respect to 2,5-dibromobipyridine (4.22 mmol, 1.00 eq.) and 2-pyridylzinc bromide (8.44 mmol, 2.00 eq.) used for nucleophilic attack on 2,5-dibromobipyridine. The reaction mixture was then stirred at room temperature for 12 hours under a constant stream of nitrogen. After 12 hour of constant stirring the reaction mixture was precipitated as a white solid. Then the reaction mixture was poured into a saturated solution of EDTA / Na_2CO_3 (200 cm^3) to dissolve the white precipitate, with the formation of a yellow precipitate. The saturated basic EDTA solution formed a water soluble chelate complex with Zn^{2+} metal ion. The aqueous solution and the yellow precipitate were extracted with dichloromethane (DCM) (3 x 50 cm^3). The DCM layer was dried and evaporated under vacuum. This crude product was purified on an activated neutral alumina (150 mesh size) column using hexane / ethylacetate (9.5:0.5 v/v). The second spot in TLC plate (R_f = 0.15) was collected as the desired ligand 2,2':5',2''-terpyridine (2,5-bpp) with a yield of 50 % (see Figure 4.4). An undesired by-product (5-bromo-2,2'-bipyridine) (R_f = 0.18) (yield = 9 %) also formed. From the synthesis point of view another by product may form (2-bromo-5-(2'-pyridyl)pyridine) but this was not found during the purification process because of better coupling between 2-pyridyl carbocation than 5-pyridyl carbocation with 2-pyridylzinc bromide.

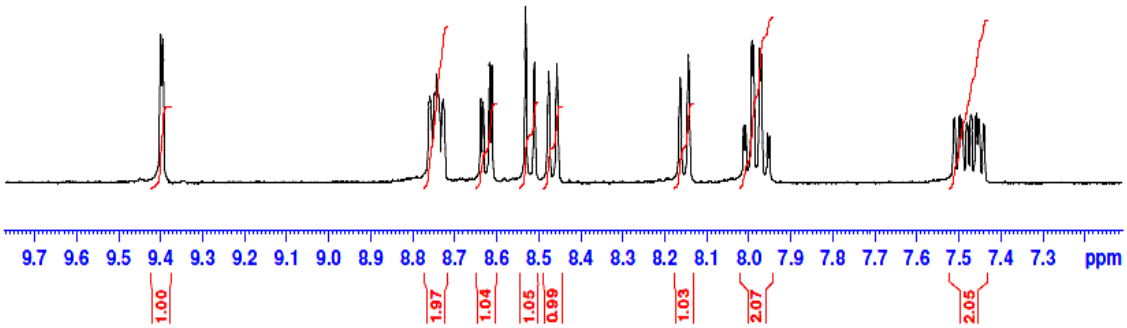

Figure 4.4: *^{1}H-NMR of bridging ligand (2,2':5',2''-terpyridine) (2,5-bpp) in d_6-dmso.*

The synthetic strategies of the mononuclear complexes $[Ru(bpy)_2(2,5\text{-bpp})]^{2+}$, $[Ru(bpy)_2(2,6\text{-bpp})]^{2+}$ and heterodinuclear complexes $[Ru(bpy)_2(2,5\text{-bpp})PdCl(CH_3CN)]^{2+}$, $[Ru(bpy)_2(2,6\text{-bpp})PdCl(CH_3CN)]^{2+}$ are depicted in Figure 4.5. Similarly the deuteriated mononuclear complexes $[Ru(D_8\text{-bpy})_2(2,5\text{-bpp})]^{2+}$, $[Ru(D_8\text{-bpy})_2(2,6\text{-bpp})]^{2+}$ and deuteriated heterodinuclear complexes $[Ru(D_8\text{-bpy})_2(2,5\text{-bpp})PdCl(CH_3CN)]^{2+}$, $[Ru(D_8\text{-bpy})_2(2,6\text{-bpp})PdCl(CH_3CN)]^{2+}$ were synthesised under identical conditions.

The mononuclear complexes $[Ru(bpy)_2(2,5\text{-bpp})]^{2+}$ and $[Ru(bpy)_2(2,6\text{-bpp})]^{2+}$ were formed by the addition of equimolar ratio of 2,5-bpp and 2,6-bpp ligand to $[Ru(bpy)_2Cl_2]$, and heating at reflux in ethanol / water (3:1 v/v). As the reaction proceeded, the deep violet colour of the $[Ru(bpy)_2Cl_2]$ solution gradually was replaced by an orange / red colour, which indicates the presence of the $[Ru(bpy)_2(2,5\text{-bpp})]^{2+}$ and $[Ru(bpy)_2(2,6\text{-bpp})]^{2+}$ complex. The ethanol was removed at this stage and the chloride counter ion was replaced by a PF_6^- counter ion which led to precipitation of the complexes from the aqueous solution. The PF_6^- salts of this type of complexes tend to be only sparingly water soluble and soluble in organic solvents which greatly eases the isolation, purification and analysis of these compounds. The yields for the monomer complexes $[Ru(bpy)_2(2,5\text{-bpp})]^{2+}$ was 92% and for $[Ru(bpy)_2(2,6\text{-bpp})]^{2+}$ was 54%.

The heterodinuclear Ru-Pd cyclometallated complexes were synthesised by the addition of a mononuclear ruthenium starting material to $(NH_4)_2(PdCl_4)$ and heating to reflux in methanol. $(NH_4)_2(PdCl_4)$ was generally added first and allowed to dissolved completely

in methanol before adding the more soluble monomers $[Ru(bpy)_2(2,5\text{-bpp})]^{2+}$ or $[Ru(bpy)_2(2,6\text{-bpp})]^{2+}$ drop by drop.

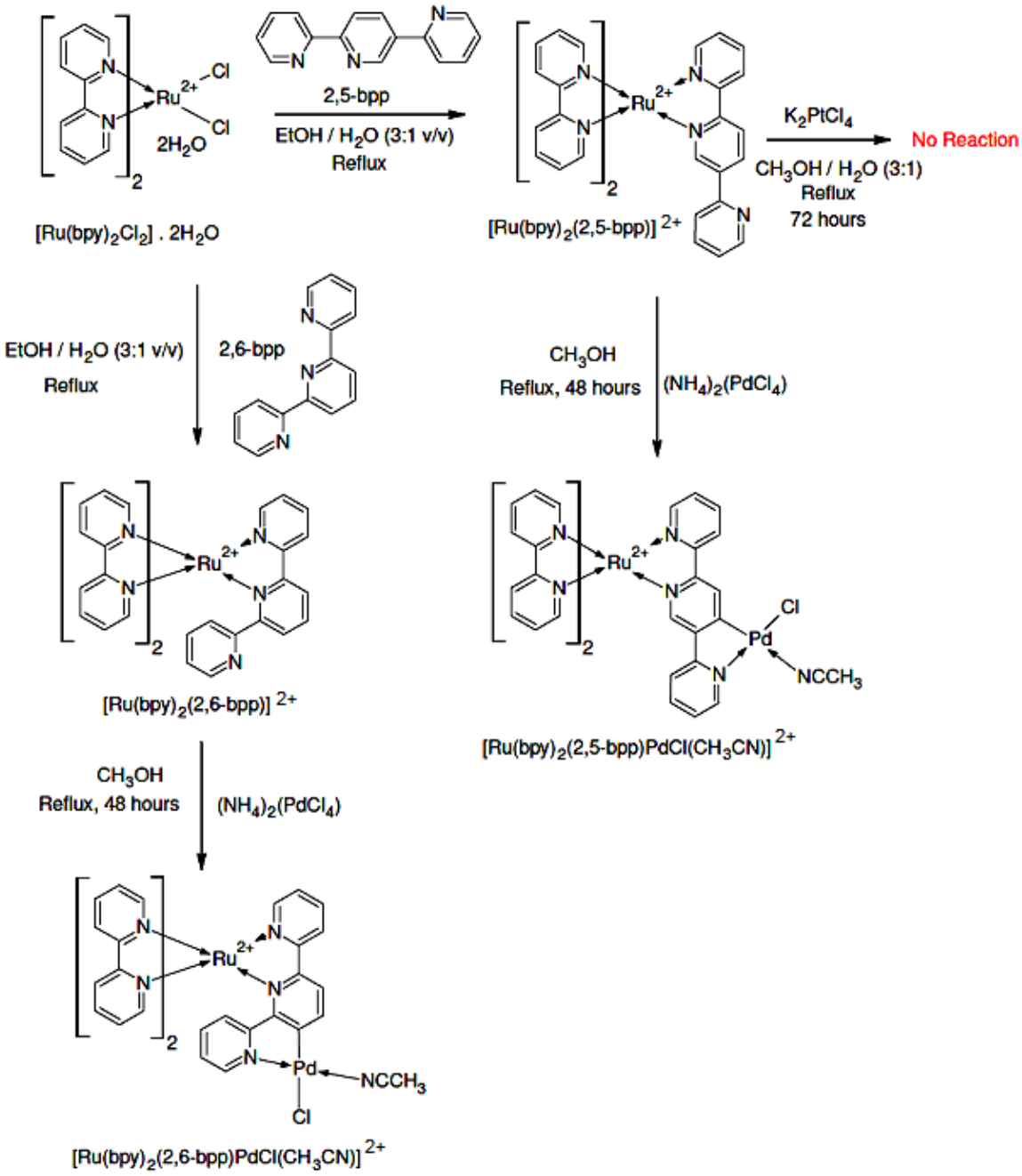

Figure 4.5: *Synthesis pathways of the mononuclear and heterodinuclear complexes.*

After 48 hours of reflux in methanol, the complexes were precipitated by the addition of n-hexane and recrystallised in acetonitrile/acetone (3:1 v/v). The yields of the

heterodinuclear complexes $[Ru(bpy)_2(2,5\text{-bpp})PdCl(CH_3CN)]^{2+}$ and $[Ru(bpy)_2(2,6\text{-bpp})PdCl(CH_3CN)]^{2+}$ were from 95 – 98 %. These complexes were stable in sunlight and at room temperature.

The platinum based heterodinuclear complex with 2,5-bpp as a bridging ligand does not form by following the above method shown in Figure 4.5. The K_2PtCl_4 salt does not dissolve in CH_3OH so for dissolving the platinum salt small amounts of deionised water was added. The reason may also be that bond formation energy between Pt metal and carbon is high 598 KJ mol^{-1} and not feasible for cyclometalation. The partially deuteriated monomers $[Ru(D_8\text{-bpy})_2(2,5\text{-bpp})]^{2+}$ / $[Ru(D_8\text{-bpy})_2(2,6\text{-bpp})]^{2+}$ and partially deuteriated heterodinuclear complexes $[Ru(bpy)_2(2,5\text{-bpp})PdCl(CH_3CN)]^{2+}$ / $[Ru(bpy)_2(2,6\text{-bpp})\text{-}PdCl(CH_3CN)]^{2+}$ complexes were synthesised by the same method as the non-deuteriated complexes. The yields for deuteriated monomer complexes with 2,5-bpp and 2,6-bpp were from 95 – 96%. The heterodinuclear Ru – Pd cyclometalated complexes were from 79 – 80%.

4.3.2 ^{1}H-NMR Spectroscopy.

In order to simplify the ^{1}H-NMR spectra the deuteriated analogues of the complexes were synthesised and used as a tool to confirm peak assignment and the structures of complexes. For the non-symmetric mononuclear complexes, up to sixteen non-equivalent protons may arise from the 2.2'-bipyridyl (bpy) moieties making complete unambiguous structural assignment difficult. Deuteriation of 2.2'-bipyridyl led to the removal of these protons. As a result it only remains to assign the protons of 2,2':5',2''-terpyridine (2,5-bpp) and 2,2':6',2''-terpyridine (2,6-bpp) ligands in the case of the mononuclear complexes as well as in the case of heterodinuclear complexes.

4.3.2.1 ^{1}H-NMR of the mononuclear complex.

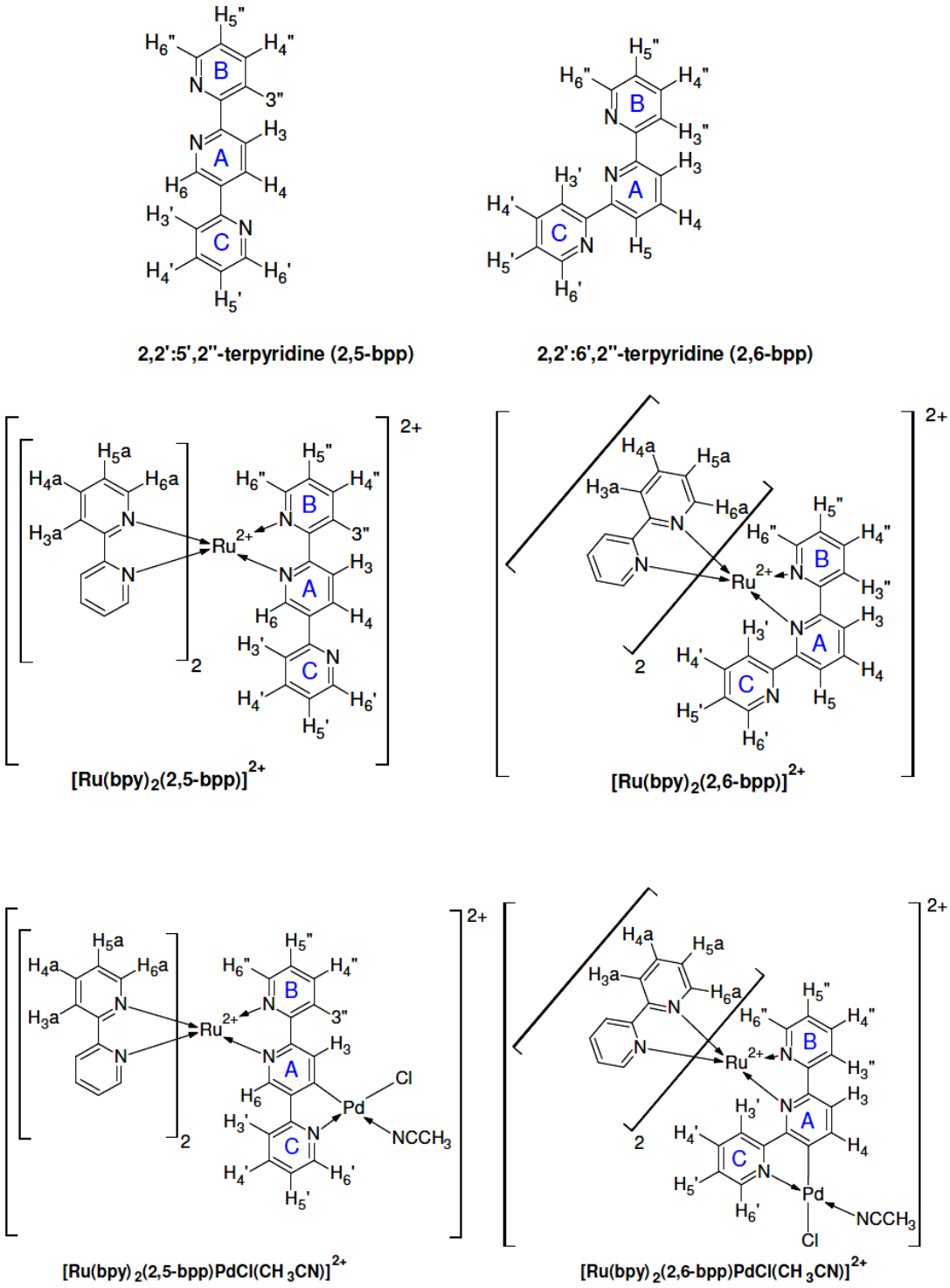

Figure 4.6: Structures and numbering of ligands, mononuclear and heterodinuclear complexes (in deuteriated analogues, H_8-bpy replaced with D_8-bpy).

Figure 4.6 show the numbering of the non-deuteriated and deuteriated (bpy = D_8-bpy) ruthenium(II) mononuclear complexes $[Ru(bpy)_2(2,5\text{-bpp})]^{2+}$ and $[Ru(bpy)_2(2,6\text{-bpp})]^{2+}$ and their ^{1}H-NMR spectrum are shown in Figure 4.7 and 4.8. The chemical shifts of the ruthenium(II) monomers with 2,5-bpp and 2,6-bpp ligands in d_3-acetonitrile are given in table 4.1. For simplicity to distinguish between the protons of the pyridine rings (ring B (metal) complexed (H3" – H6") and ring C (free) non-complexed (H3' – H6')) and the pyrazine (middle) ring A (H3 – H6) of the 2,5-bpp or 2,6-bpp ligands and the bpy protons are number H3a – H6a shown in Figure 4.6. In case of the ligand mononuclear 2,5-bpp complex, all bpy protons occur in the expected range while in the case of ligand 2,6-bpp mononuclear complex, all bpy's protons spread in the region of 8.75 – 6.8 ppm and will be discussed in detail. In this section the signals the 2,5-bpp and 2,6-bpp protons of the mononuclear complexes $[Ru(bpy)_2(2,5\text{-bpp})]^{2+}$ and $[Ru(bpy)_2(2,6\text{-bpp})]^{2+}$ are discussed. As expected, due to the shape of the ligands, there is a clear difference between the protons of the two pyridine rings of the 2,5-bpp and 2,6-bpp ligands, as shown in table 4.1.

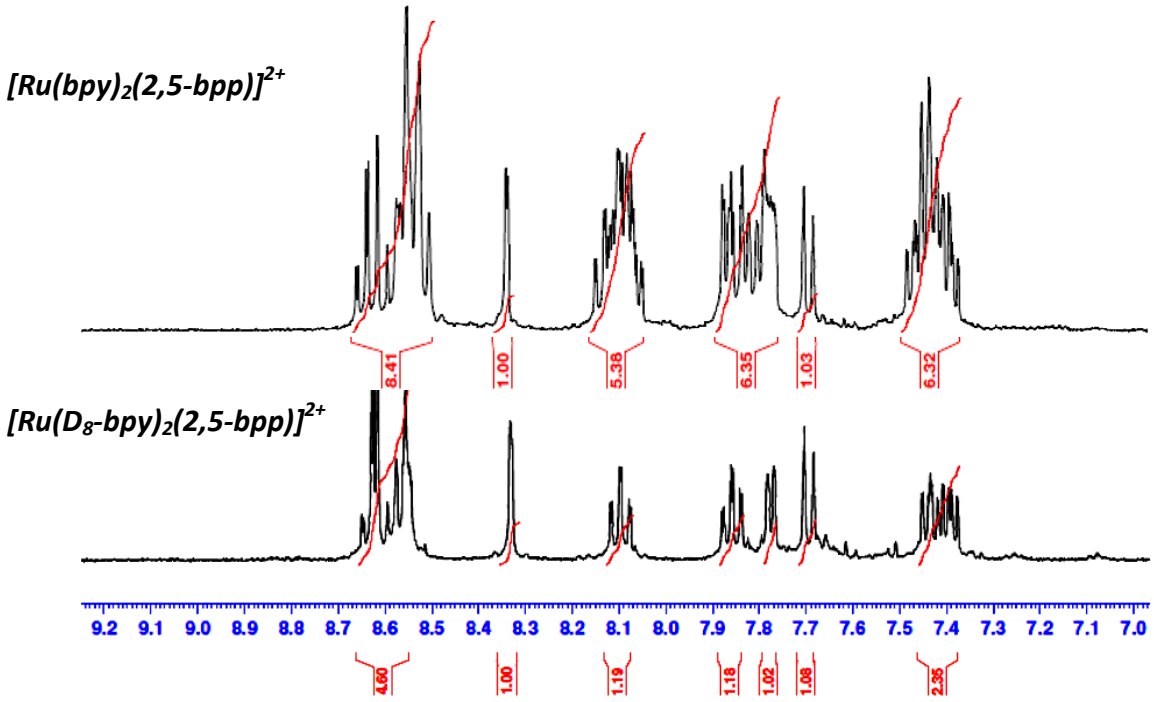

Figure 4.7: *Comparison between non-deuteriated and deuteriated complex of $[Ru(bpy)_2(2,5\text{-bpp})]^{2+}$ in d_3-acetonitrile.*

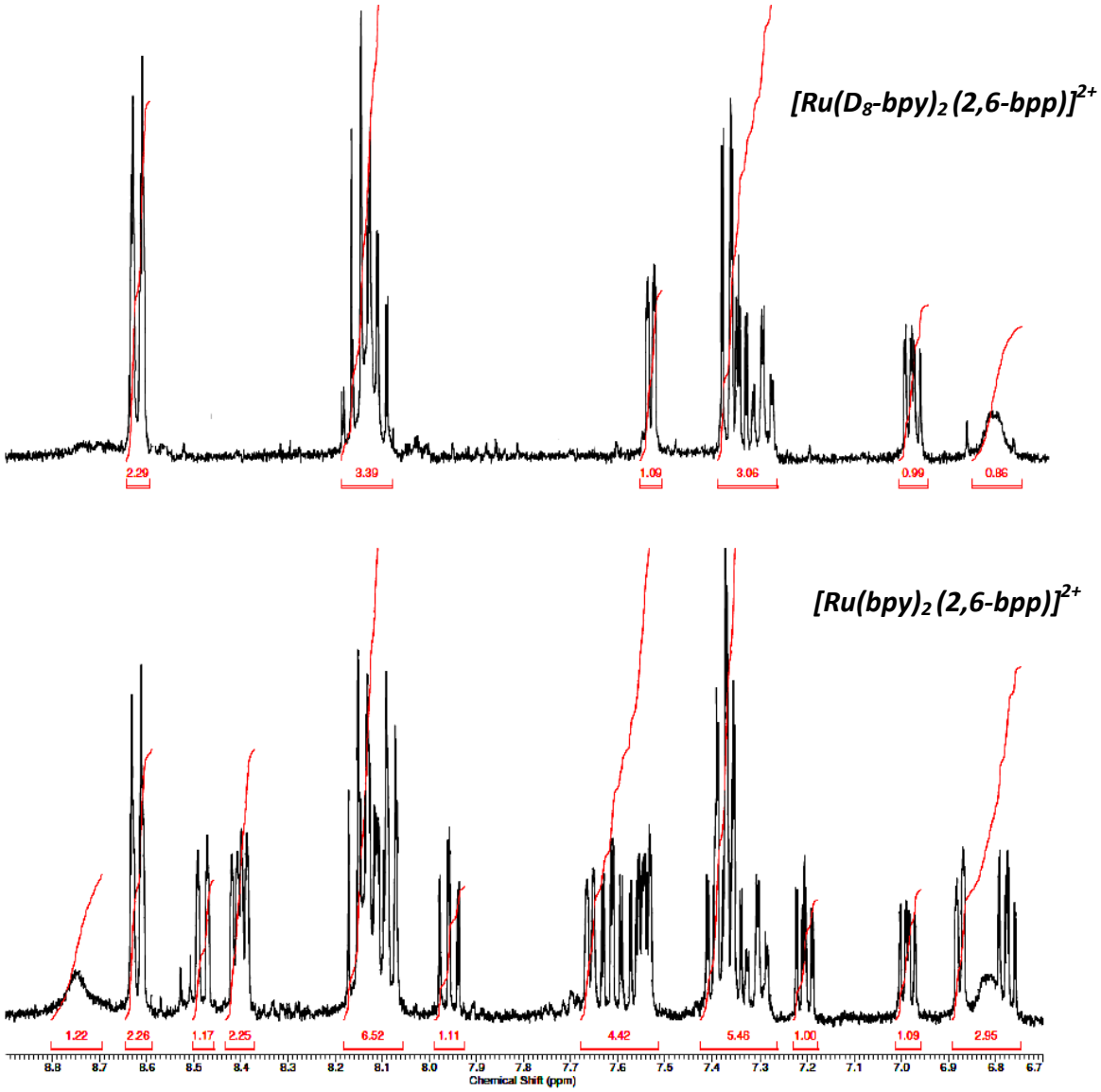

Figure 4.8: *Comparison between non-deuteriated and deuteriated complex of* $[Ru(bpy)_2(2,6\text{-}bpp)]^{2+}$ *in* d_3*-acetonitrile.*

In case of $[Ru(bpy)_2(2,5\text{-}bpp)]^{2+}$, the proton H6' (ring C) is present at ~ 8.52 ppm while H6" (ring B) was observed at 7.78 ppm in d_3-acetonitrile as a solvent. This large difference between ring B and ring C for the H6" / H6' resonances indicates that the H6" protons present at 7.78 ppm are assigned to the metal-bound pyridine as it is shifted over 1.26 ppm upfield. This is due to through space interactions occurring between H6" and adjacent bpy ring. In addition protons in close proximity to such large atoms, such as a

metal ion, are more shielded from the induced magnetic field of the NMR and therefore require a greater applied magnetic field strength for resonance.[40]

In the case of $[Ru(bpy)_2(2,6\text{-bpp})]^{2+}$, the H6" proton of the metal bound pyridine (ring B) experiences the strongly upfield effect as observed for $[Ru(bpy)_2(2,5\text{-bpp})]^{2+}$. The proton H6' (ring C) is present at 6.85 ppm with broadening of the peak while H6" (ring B) is observed at 7.52 ppm. Again interaction of this proton with the bpy rings is responsible for this shift. The proton H6' (ring C) (un-complexed) in strongly shifted upfield due to through space interactions occurring between H6' and the adjacent bpy ligand. The ring C of 2,6-bpp ligand is in the influence of aromatic ring current of bpy ligand. The H6' proton has broadened due to the sterically hindered rotation of the ring C, as shown in the Figure 4.9, (see **Appendix A** for 3D structure calculation for heterodinuclear complexes with Gaussian 09 suite done by Dr. Martin Schulz)

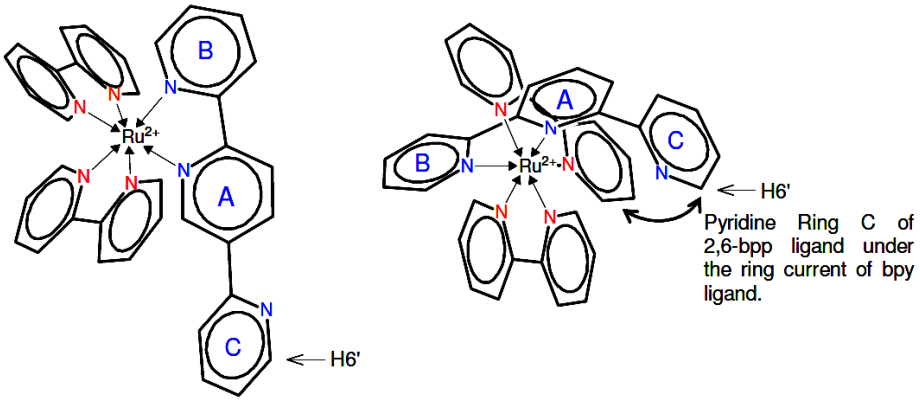

Figure 4.9: *3D – model of* $[Ru(bpy)_2(2,5\text{-bpp})]^{2+}$ and $[Ru(bpy)_2(2,6\text{-bpp})]^{2+}$ *represent space interaction between bridging ligands and peripheral bpy ligands.*

Due the to 5-subsituted and 6-subsituted pyridyl-bipyridine in the ligand 2,5-bpp and 2,6-bpp, ^{1}H-NMR of the respective mononuclear complexes are not much different from each other. The chemical shifts in ring B (H3" – H6") and ring C protons H5', H4' and H3' were comparable for the two mononuclear complexes. The protons marked as H3, H4, H5, H6, H6" and H6' in the two mononuclear complexes were under the influence of magnetic field of the adjacent bpy ligands and the Ru(II) metal ion. The chemical shifts are depicted in table 4.1.

Ring C (free)	H6'(d)	H5'(t)	H4'(t)	H3'(d)
δ in (d_3-acetonitrile)	8.52	7.39	7.86	7.69
$[Ru(bpy)_2(2,5\text{-bpp})]^{2+}$				
δ in (d_3-acetonitrile)	6.85	7.31	6.99	8.09
$[Ru(bpy)_2(2,6\text{-dpp})]^{2+}$				
δ in (d_6-dmso)	8.74	7.48	7.98	8.15
Free ligand 2,5-bpp				
δ in (d_1-$CDCl_3$)	8.68	7.30	7.83	8.61
Free ligand 2,6-bpp				
Ring B (Metal)	**H6"(d)**	**H5"(t)**	**H4"(t)**	**H3"(d)**
δ in (d_3-acetonitrile)	7.78	7.43	8.10	8.65
$[Ru(bpy)_2(2,5\text{-bpp})]^{2+}$				
δ in (d_3-acetonitrile)	7.52	7.34	8.14	8.63
$[Ru(bpy)_2(2,6\text{-bpp})]^{2+}$				
δ in (d_6-dmso)	8.74	7.48	7.98	8.47
Free ligand 2,5-bpp				
δ in (d_1-$CDCl_3$)	8.68	7.30	7.83	8.61
Free ligand 2,6-bpp				
Pyridine Ring A (Middle)	**H3(d)**	**H4(d)/(t)**	**H5(d)**	**H6(s)**
δ in (d_3-acetonitrile)	8.60	8.55	–	8.33
$[Ru(bpy)_2(2,5\text{-bpp})]^{2+}$				
δ in (d_3-acetonitrile)	7.36	8.15	8.63	–
$[Ru(bpy)_2(2,6\text{-bpp})]^{2+}$				
δ in (d_6-dmso)	8.52	8.62	–	9.40
Free ligand 2,5-bpp				
δ in (d_1-$CDCl_3$)	8.45	7.93	8.45	–
Free ligand 2,6-bpp				
Bpy ^{1}H of complex	**H6a**	**H5a**	**H4a**	**H3a**
δ in (d_3-acetonitrile)	7.95-7.78	7.48-7.38	8.15-8.07	8.64-8.54
$[Ru(bpy)_2(2,5\text{-bpp})]^{2+}$				
δ in (d_3-acetonitrile)	7.67, 7.55	7.62, 7.33	8.15-8.05	8.75
$[Ru(bpy)_2(2,6\text{-bpp})]^{2+}$	7.40, 6.88	7.21, 6.77	7.96	8.48-8.40

Table 4.1: *Chemical shifts in ppm comparison of the $[Ru(bpy)_2(2,5\text{-bpp})]^{2+}$, $[Ru(bpy)_2(2,6\text{-bpp})]^{2+}$, 2,5-bpp ligand and 2,6-bpp ligand in respective solvents.*

It was possible to assign the chemical shifts for the all 2,5-bpp and 2,6-bpp protons of the two pyridine rings and middle pyridine ring using 2-D COSY NMR, the deuteriated complexes $[Ru(D_8\text{-bpy})_2(2,5\text{-bpp})]^{2+}$ and $[Ru(D_8\text{-bpy})_2(2,6\text{-bpp})]^{2+}$. As can be seen from a comparison between the deuteriated and non-deuteriated mononuclear complexes the deuteriation results in simplification of the ^{1}H-NMR spectrum and therefore, assisted in the confirmation of the chemical shifts for the 2,5-bpp and 2,6-bpp and bipyridine protons, which are documented above in table 4.1. 2-D COSY-NMR spectra of the $[Ru(D_8\text{-bpy})_2(2,5\text{-bpp})]^{2+}$ and $[Ru(D_8\text{-bpy})_2(2,6\text{-bpp})]^{2+}$ were recorded in d_3-acetonitrile (depicted in figure 4.10 and 4.11).

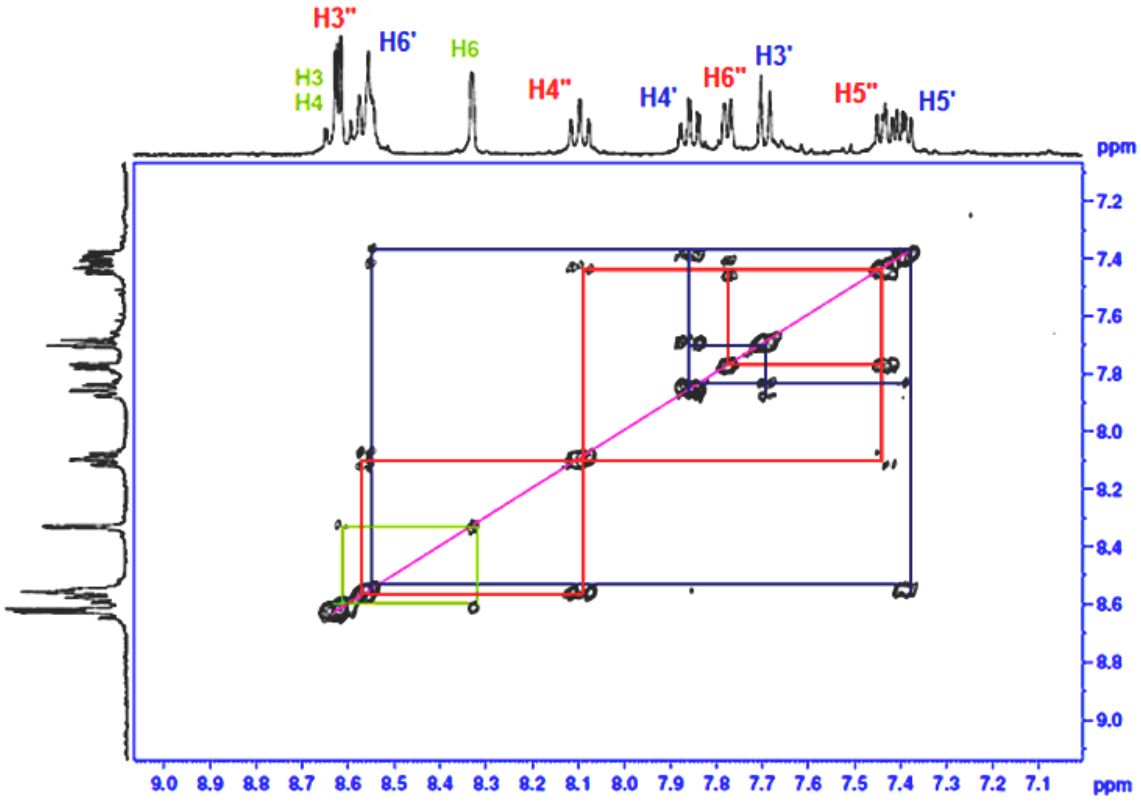

Figure 4.10: *2D-COSY NMR spectra of the $[Ru(D_8\text{-bpy})_2(2,5\text{-bpp})]^{2+}$ in d_3-acetonitrile.*

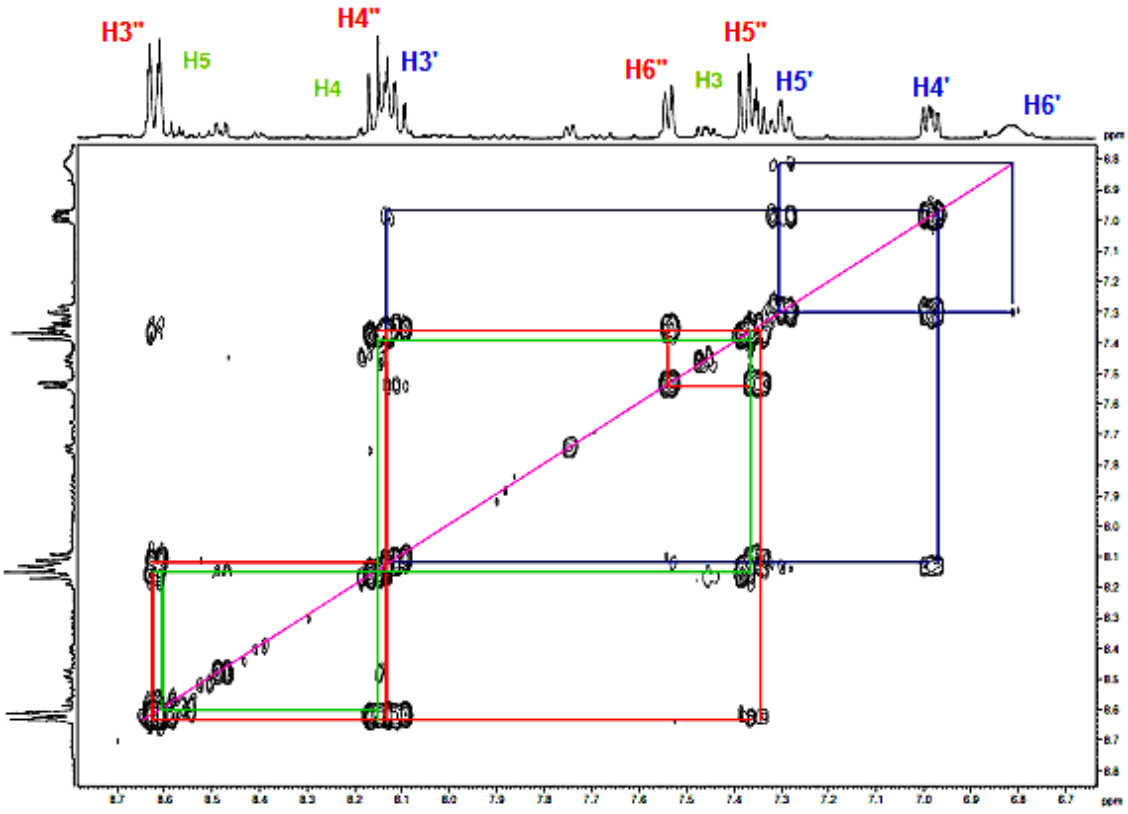

Figure 4.11: *2D-COSY NMR spectra of the* $[Ru(D_8\text{-bpy})_2(2,6\text{-bpp})]^{2+}$ *in* d_3*-acetonitrile.*

4.3.2.2 ^{1}H-NMR spectra of heterodinuclear cyclometallated Ru – Pd complexes.

The chemical shifts and assignment of the 2,5-bpp, 2,6-bpp and 2,2'-bpy ligands of the Ru – Pd heterodinuclear cyclometallated complexes are outlined in Table 4.2. The structure of the non-deuteriated and deuteriated analogues of the heterodinuclear cyclometallated complexes are depicted in Figure 4.6. Following formation of the Ru-Pd compounds, the protons in the pyridine ring C and those in the middle pyridine ring A are shifted downfield with respect to the other protons present in the molecule, due to the electron withdrawing effect of Pd(II) metal centre as depicted in Table 4.2.

Ring 1 (free)	H6'(d)	H5'(t)	H4'(t)	H3'(d)
$[Ru(bpy)_2(2,5\text{-}bpp)PdCl]_2^{4+}$	9.54	7.41	7.89	7.20
$[Ru(bpy)_2(2,6\text{-}bpp)PdCl]_2^{4+}$	9.12	7.02	7.50	7.80
$[Ru(bpy)_2(2,5\text{-}bpp)]^{2+}$	8.52	7.39	7.86	7.69
$[Ru(bpy)_2(2,6\text{-}dpp)]^{2+}$	6.85	7.31	6.99	8.09
Free ligand 2,5-bpp[a]	8.74	7.48	7.98	8.15
Free ligand 2,6-bpp[b]	8.68	7.30	7.83	8.61

Ring 2 (Metal)	H6"(d)	H5"(t)	H4"(t)	H3"(d)
$[Ru(bpy)_2(2,5\text{-}bpp)PdCl]_2^{4+}$	7.70	7.37	8.04	8.48
$[Ru(bpy)_2(2,6\text{-}bpp)PdCl]_2^{4+}$	7.46	7.27	8.12	8.42
$[Ru(bpy)_2(2,5\text{-}bpp)]^{2+}$	7.78	7.43	8.10	8.65
$[Ru(bpy)_2(2,6\text{-}bpp)]^{2+}$	7.52	7.34	8.14	8.63
Free ligand 2,5-bpp[a]	8.74	7.48	7.98	8.47
Free ligand 2,6-bpp[b]	8.68	7.30	7.83	8.61

Pyridine Ring (Middle)	H3(d)/(s)	H4(d)/(t)	H5(d)	H6(s)
$[Ru(bpy)_2(2,5\text{-}bpp)PdCl]_2^{4+}$	9.16	–	–	7.49
$[Ru(bpy)_2(2,6\text{-}bpp)PdCl]_2^{4+}$	7.70	7.93	–	–
$[Ru(bpy)_2(2,5\text{-}bpp)]^{2+}$	8.60	8.55	–	8.33
$[Ru(bpy)_2(2,6\text{-}bpp)]^{2+}$	7.36	8.15	8.63	–
Free ligand 2,5-bpp[a]	8.52	8.62	–	9.40
Free ligand 2,6-bpp[b]	8.45	7.93	8.45	–

Bpy ^{1}H of complex	H6a	H5a	H4a	H3a
$[Ru(bpy)_2(2,5\text{-}bpp)PdCl]_2^{4+}$	7.95-7.79	7.45-7.40	8.10-8.08	8.59-8.57
$[Ru(bpy)_2(2,6\text{-}bpp)PdCl]_2^{4+}$	7.88-7.59	7.55-7.09	8.24-8.00	9.01-8.10
$[Ru(bpy)_2(2,5\text{-}bpp)]^{2+}$	7.95-7.78	7.48-7.38	8.15-8.07	8.64-8.54
$[Ru(bpy)_2(2,6\text{-}bpp)]^{2+}$	7.67, 7.55	7.62, 7.33	8.15-8.05	8.75
	7.40, 6.88	7.21, 6.77	7.96	8.48-8.40

[a] *in d_6-dmso solvent.*
[b] *in $CDCl_3$ solvent.*

Table 4.2: Chemical shifts in ppm of heterodinuclear cyclometallated Ru – Pd complexes (in d_3-acetonitrile) compared to mononuclear complexes $[Ru(bpy)_2(2,5\text{-}bpp)]^{2+}$/$[Ru(bpy)_2(2,6\text{-}bpp)]^{2+}$ (in d_3-acetonitrile) and free ligands 2,5-bpp/2,6-bpp.

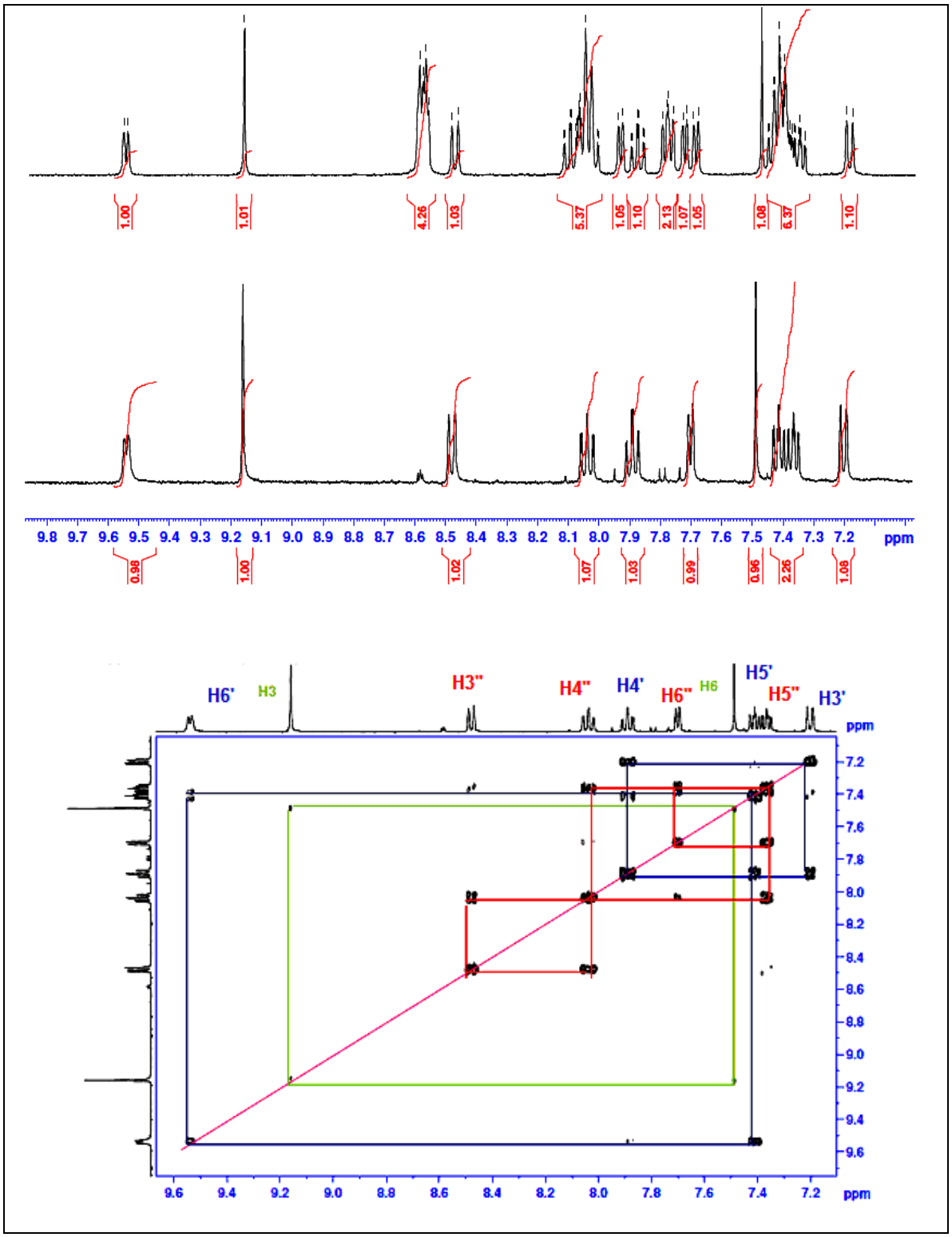

Figure 4.12: *Comparison between non-deuteriated and deuteriated complexes of* $[Ru(bpy)_2(2,5\text{-}bpp)PdCl(CH_3CN)]^{2+}$ *(top) and 2D-COSY 1H-NMR of the* $[Ru(D_8\text{-}bpy)_2(2,5\text{-}bpp)PdCl(CH_3CN)]^{2+}$ *(bottom).*

The ^{1}H-NMR spectrum of $[Ru(D_8\text{-bpy})_2(2,5\text{-bpp})PdCl(CH_3CN)]^{2+}$ in CD_3CN at room temperature displays 10 non-equivalent proton resonances, without the interference of bpy protons (see figure 4.12). The numbering scheme used for the assignments of the protons is given in figure 4.6. The H4 proton disappeared due to cyclometallation with the Pd metal (see figure 4.12). The H6' proton is distinct due to palladium attached to the adjacent nitrogen atom and appears as a doublet at δ 9.54 ppm. Upon assignment of H6', the H5' at δ 7.41 ppm can be easily correlated using 2D-COSY ^{1}H-NMR. The remaining protons on the pyridine ring C were identified based on the 2D-COSY correlations. The resonances at δ 7.89 and 7.20 display the expected splitting pattern for H4' and H3'. The individual assignments of the pyridine ring B (H3" – H6") component in $[Ru(bpy)_2(2,5\text{-bpp})PdCl(CH_3CN)]^{2+}$, are comparable with those of the pyridine ring B component in $[Ru(bpy)_2(2,5\text{-bpp})]^{2+}$ (see table 4.2). Coordination of a Pd center to the middle pyrazine ring A in $[Ru(bpy)_2(2,5\text{-bpp})PdCl(CH_3CN)]^{2+}$, leads to a significant downfield shift in H3 (δ 9.16 ppm). Using 2D-COSY, the resonances at δ 7.49 were assigned to H6 in $[Ru(bpy)_2(2,5\text{-bpp})PdCl(CH_3CN)]^{2+}$. By contrast, the upfield shift of H6 in $[Ru(bpy)_2(2,5\text{-bpp})PdCl(CH_3CN)]^{2+}$ (δ 7.49) relative to $[Ru(bpy)_2(2,5\text{-bpp})]^{2+}$ (δ 8.33) is caused by pronounced shielding of H6 when ring C is complexed to Pd in $[Ru(bpy)_2(2,5\text{-bpp})PdCl(CH_3CN)]^{2+}$ relative to the free pyridine ring of $[Ru(bpy)_2(2,5\text{-bpp})]^{2+}$. This shielding is imposed by ring current effects as H6 lies directly above the π-cloud of bpy ring in $[Ru(bpy)_2(2,5\text{-bpp})PdCl(CH_3CN)]^{2+}$. The coordinated acetonitrile ligand attached to the Pd metal is observed at 2.06 ppm as shown Figure 4.13.

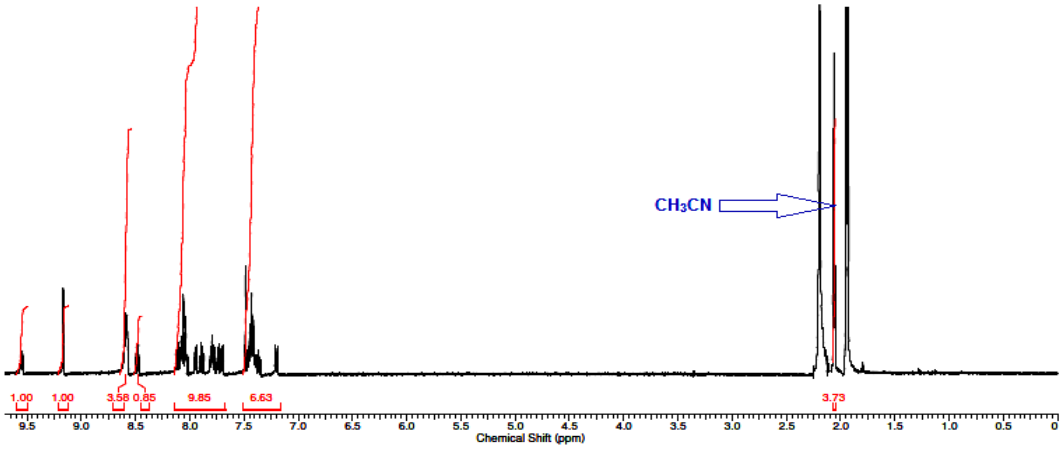

Figure 4.13: *^{1}H-NMR of $[Ru(bpy)_2(2,5\text{-bpp})PdCl(CH_3CN)]^{2+}$ in CD_3CN.*

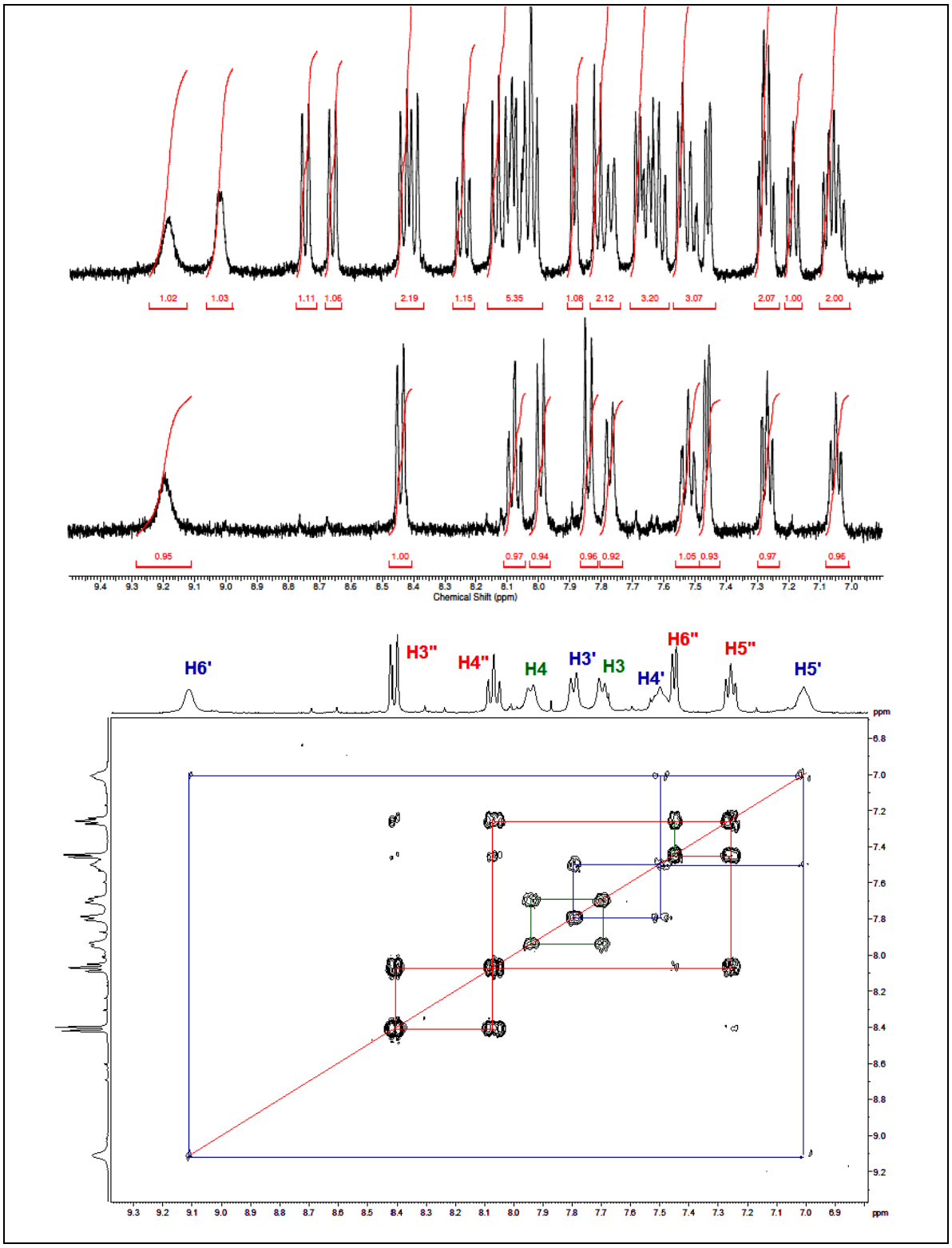

Figure 4.14: *Comparison between non-deuteriated & deuteriated complex of* $[Ru(bpy)_2(2,6\text{-}bpp)PdCl(CH_3CN)]^{2+}$ *(top) and 2D-COSY* ^{1}*H-NMR of the* $[Ru(D_8\text{-}bpy)_2(2,6\text{-}bpp)PdCl(CH_3CN)]^{2+}$ *(bottom) in* CD_3CN.

The ^{1}H-NMR spectrum of $[Ru(D_8\text{-bpy})_2(2,6\text{-bpp})PdCl(CH_3CN)]^{2+}$ in CD_3CN at room temperature displays 10 nonequivalent proton resonances as shown in figure 4.14. The H5 proton is absent due to cyclometallation with the Pd metal (see figure 4.14). The H6' proton is distinct due coordinate of palladium to the adjacent nitrogen atom and appears as a broad peak at δ 9.12 due to hindered rotation or steric strained of ring C. The other protons of the dine ring C,were identified based on the 2D-COSY coupling patterns.

Coordination of a Pd center to the middle pyrazine ring A in $[Ru(bpy)_2(2,6\text{-bpp})PdCl(CH_3CN)]^{2+}$, leads to a slight upfield shift in H4 (δ 7.93 ppm). Using 2D-COSY, the resonances at δ 7.70 ppm were assigned to H3 in $[[Ru(bpy)_2(2,6\text{-bpp})PdCl(CH_3CN)]^{2+}$ as shown in Figure 4.14. By contrast, the upfield shift of H4 in $[Ru(bpy)_2(2,6\text{-bpp})PdCl]_2^{4+}$ (δ 7.93) relative to $[Ru(bpy)_2(2,6\text{-bpp})]^{2+}$ (δ 8.15) is caused by pronounced shielding of H4 by the ruthenium centre. The individual assignments of the pyridine ring B (H3" – H6") component of $[Ru(bpy)_2(2,6\text{-bpp})PdCl(CH_3CN)]^{2+}$are comparable with those of the pyridine ring B component of $[Ru(bpy)_2(2,5\text{-bpp})]^{2+}$ as shown in Table 4.2. The coordinated acetonitrile ligand attached to Pd metal resonance at 2.06 ppm is shown in Figure 4.15.

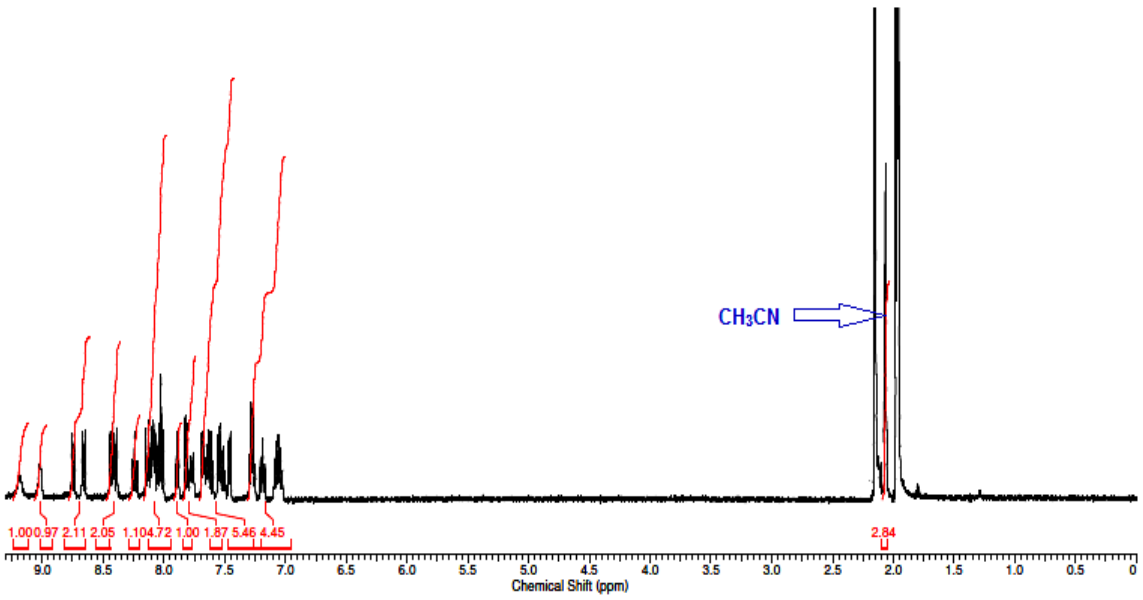

Figure 4.15: *^{1}H-NMR of $[Ru(bpy)_2(2,6\text{-bpp})PdCl(CH_3CN)]^{2+}$ in CD_3CN.*

4.3.3 UV-Vis absorption and luminescence properties of the Ru(II) mononuclear and heterodinuclear complexes.

The absorption and emission data of the complexes $[Ru(bpy)_2(2,5\text{-}bpp)PdCl(CH_3CN)]^{2+}$ and $[Ru(bpy)_2(2,6\text{-}bpp)PdCl(CH_3CN)]^{2+}$ and their monometallic synthons, $[Ru(bpy)_2(2,5\text{-}bpp)]^{2+}$ and $[Ru(bpy)_2(2,6\text{-}bpp)]^{2+}$ are shown in Figure 4.16. Table 4.3 lists the photophysical parameters of the non-deuteriated Ru(II) monomers and heterodinuclear complexes. The life time studies were carried out by Mr. Suraj Soman.

Complex	Absorption λ_{max} (nm) ($\varepsilon = 10^4\ M^{-1}cm^{-1}$)	Emission λ_{max} (nm) (at 293 K)	τ [a] (ns) (deaerated) (at 293 K)	Φ [b] (deaerated) (at 293 K)
$[Ru(bpy)_3]^{2+}$	453 (1.3)	605	576	0.068 [41]
$[Ru(bpy)_2(2,5\text{-}bpp)]^{2+}$	455 (1.18)	630	442	0.047
$[Ru(bpy)_2(2,6\text{-}dpp)]^{2+}$	467 (1.79)	630	564	0.039
$[Ru(bpy)_2(2,5\text{-}bpp)PdCl(CH_3CN)]^{2+}$	449 (1.88)	627	33	0.003
$[Ru(bpy)_2(2,6\text{-}dpp)PdCl(CH_3CN)]^{2+}$	449 (1.72)	635	-	0.001 [42]

[a] *Determined by time correlated single photon counting at 293 K in deaerated acetonitrile solution using freeze-pump-thaw degassing.*

[b] *Quantum yield of an excited state emission at 293 K, excited at λ = 455 nm (in deaerated acetonitrile).*

Table 4.3: *Photophysical properties of all ruthenium monomer and heterodinuclear non-deuteriated (in black) / deuteriated (in red) complexes synthesised carried out in spectroscopy grade deaerated acetonitrile at 293 K.*

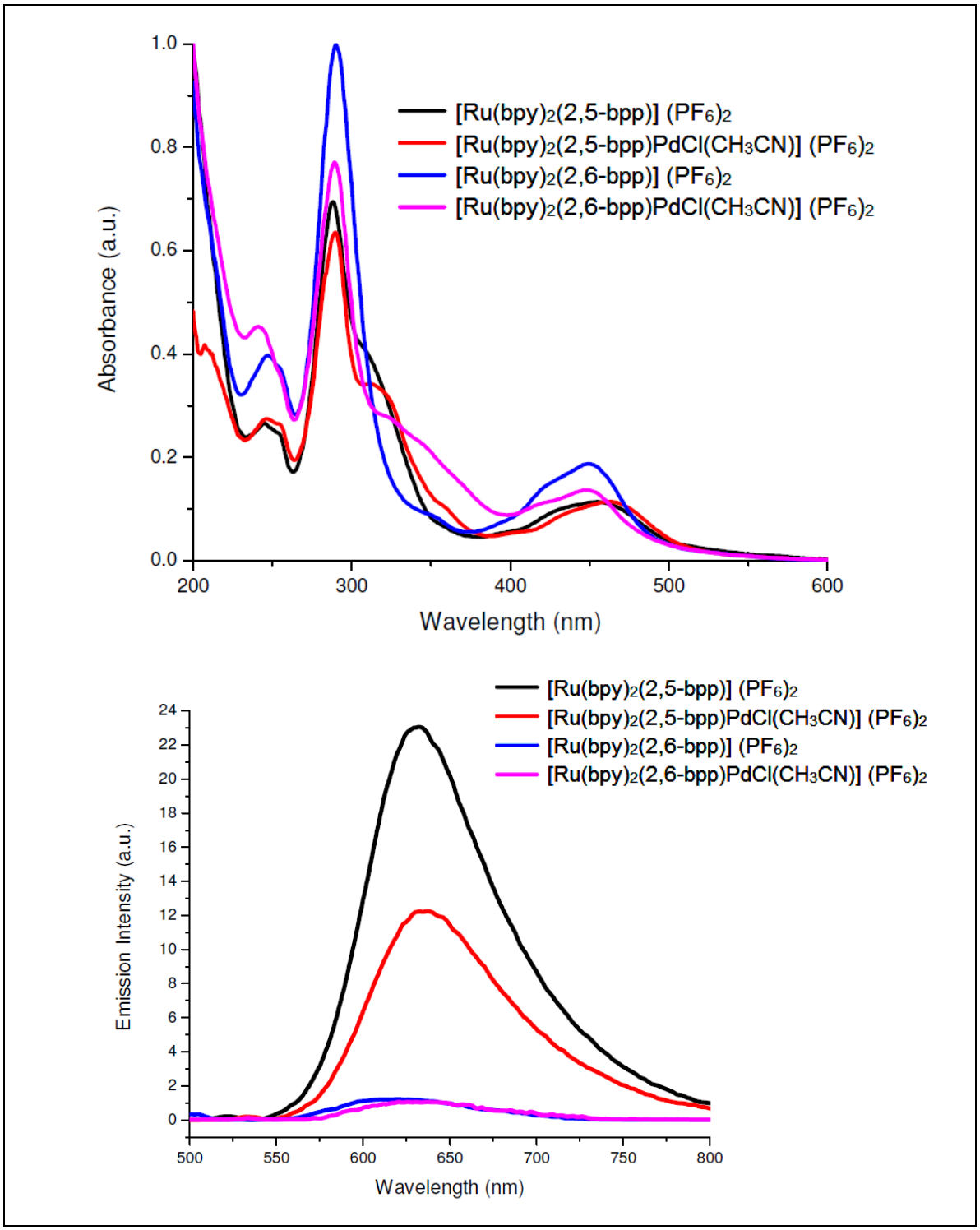

Figure 4.16: *Absorption (above) and emission (below) spectra of the listed non-deuteriated Ru(II) complexes in Table 4.3 at 293 K in deaerated acetonitrile solution. The excitation wavelength corresponds to ^{1}MLCT wavelength of the complexes.*

Time correlated single photon count (TCSPC) was used to determine the lifetime of the compounds (described in chapter 2). TCSPC measurements were carried out at room temperature for all non-deuteriated complexes $[Ru(bpy)_2(2,5\text{-bpp})]^{2+}$, $[Ru(bpy)_2(2,6\text{-bpp})]^{2+}$ and $[Ru(bpy)_2(2,5\text{-bpp})PdCl(CH_3CN)]^{2+}$. The complexes were excited at 360 nm and the time response of their individual emission at a particular wavelength in deaerated acetonitrile using freeze-pump-thaw method was recorded, the results are shown in figure 4.17. Only very weak signals were observed for $[Ru(bpy)_2(2,6\text{-bpp})PdCl(CH_3CN)]^{2+}$ and hence were not recorded. The luminescence decay was mono-exponential in all cases. The corrected maxima of the luminescence bands, the luminescence lifetimes, and the luminescence quantum yields are given in Table 4.3.

The high intensity absorption bands in the UV region can be ascribed to ^{1}LC transitions. In particular, the peak at 280 nm can be attributed to the bpy peripheral ligand and the band in the region 330 – 360 nm is attributed to the 2,5-bpp / 2,6-bpp bridging ligand.[22, 35, 42] Moderately intense ^{1}MLCT bands are observed in the 400 – 600 nm regions (see figure 4.16). Upon Pd coordination, the Ru(dπ) → 2,5-bpp(π^*) MLCT transitions is red-shifted in $[Ru(bpy)_2(2,5\text{-bpp})PdCl(CH_3CN)]^{2+}$ (λ_{max} (abs) = 463 nm) relative to the monometallic synthons $[Ru(bpy)_2(2,5\text{-bpp})]^{2+}$ (λ_{max} (abs) = 455 nm) due to stabilisation of the ground state.[35] The spectroscopic properties of $[Ru(bpy)_2(2,5\text{-bpp})PdCl(CH_3CN)]^{2+}$ suggests that upon light absorption, electron transfer is promoted toward the coordinated Pd center via 2,5-bpp bridging ligand from ruthenium(II) center.[35] In the case of the 2,6-bpp ligand there is no change in the absorption spectra of the heterodinuclear complexes $[Ru(bpy)_2(2,6\text{-bpp})PdCl(CH_3CN)]^{2+}$ (λ_{max} (abs) = 449 nm) upon Pd coordination compared to the monometallic synthons $[Ru(bpy)_2(2,6\text{-bpp})]^{2+}$ (λ_{max} (abs) = 449 nm) [22, 42], which suggests no stabilisation of the ground state upon light absorption and charge transfer is not promoted toward the coordinated Pd center. There is no marked difference in the absorption behaviour between the mononuclear and the dinuclear complex suggesting that the coordinated palladium centre doesn't disturb the electronic ground state of the ruthenium core.[22] The absorption spectra for the complexes $[Ru(bpy)_2(2,5\text{-bpp})PdCl(CH_3CN)]^{2+}$/ $[Ru(bpy)_2(2,6\text{-bpp})PdCl(CH_3CN)]^{2+}$shows a broad peak from 320 – 380 nm in the UV region upon Pd coordination compared to the mononuclear

complexes $[Ru(bpy)_2(2,5\text{-bpp})]^{2+}$/ $[Ru(bpy)_2(2,6\text{-bpp})]^{2+}$, assigned to a MLCT band Pd(dπ) → 2,5-bpp(π*)/ Pd(dπ) → 2,6-bpp(π*) as expected because the palladium(II) center is much more difficult to oxidize.[22, 43]

Ruthenium polyazine complexes often possess lowest-lying ^{3}MLCT states that are typically emissive.[22, 41, 42] The prototypical tris complex $[Ru(bpy)_3]^{2+}$ is emissive.[41] This is attributed to the presence of low-lying ligand centered (LC) states that are thermally accessible at room temperature leading to emission because of stabilization of the Ru(dπ) → bpy(π*) ^{3}MLCT state, which limits thermal population of the ^{3}LC state. Ruthenium complexes of the bi-dentate 2,5-bpp have been shown to be emissive because of stabilization of the Ru(dπ) → 2,5-bpp (π*) ^{3}MLCT state, which limits thermal population of the ^{3}LC state.[42] The room temperature emission spectra recorded in deoxygenated acetonitrile solution of the monometallic complexes $[Ru(bpy)_2(2,5\text{-bpp})]^{2+}$ and the heterodinuclear complex, $[Ru(bpy)_2(2,5\text{-bpp})PdCl(CH_3CN)]^{2+}$, are shown in Figure 4.16. The complex $[Ru(bpy)_2(2,5\text{-bpp})]^{2+}$ emits at 630 nm with an excited-state lifetime (τ) of 442 ns and a Φ_{em} = 0.047 in deaerated acetonitrile.[35] The heterodinuclear complex $[Ru(bpy)_2(2,5\text{-bpp})PdCl(CH_3CN)]^{2+}$ displays a Ru(dπ) → 2,5-bpp (π*) ^{3}MLCT emission centered at 635 nm with an excited-state lifetime (τ) of 105 ns and a Φ_{em} = 0.032 in deaerated acetonitrile. The Ru(dπ) → 2,5-bpp (π*) ^{3}MLCT emission of complex $[Ru(bpy)_2(2,5\text{-bpp})PdCl]_2^{4+}$ is slightly red shifted relative to $[Ru(bpy)_2(2,5\text{-bpp})]^{2+}$, also quenching of the emission intensity relative to the mononuclear analogue, consistent with the stabilized ground state upon Pd(II) coordination was observed (see figure 4.16).[22, 35]

By contrast, $[Ru(bpy)_2(2,6\text{-bpp})]^{2+}$ and $[Ru(bpy)_2(2,6\text{-bpp})PdCl(CH_3CN)]^{2+}$ display less intense emission under the same conditions. This difference in excited-state properties of Ru(II) complexes containing either the 2,5-bpp and 2,6-bpp bridging ligand is an interesting result imparted by the difference in their structures. When an acetonitrile solution of $[Ru(bpy)_2(2,6\text{-bpp})]^{2+}$ and $[Ru(bpy)_2(2,6\text{-bpp})PdCl(CH_3CN)]^{2+}$ are diluted to below 1.0×10^{-5} M, an extremely weak emission was observed at 630 nm with an excited-state lifetime (τ) of 33 ns (Φ_{em} = 0.003) in deaerated acetonitrile,[22, 42] while very weak signals were observed for complex $[Ru(bpy)_2(2,6\text{-bpp})PdCl(CH_3CN)]^{2+}$ and hence

a lifetime was not calculated. A possible reason may be that the $[Ru(bpy)_2(2,6\text{-}bpp)PdCl(CH_3CN)]^{2+}$ complex undergoes intermolecular Pd ⋯ Pd interactions that lead to quenching of the otherwise emissive ^{3}MLCT excited states. Similar UV-Vis spectroscopic properties were obtained for the deuteriated complexes but due to the presence of small amounts of Pd(0) impurities, lifetimes were not recorded.

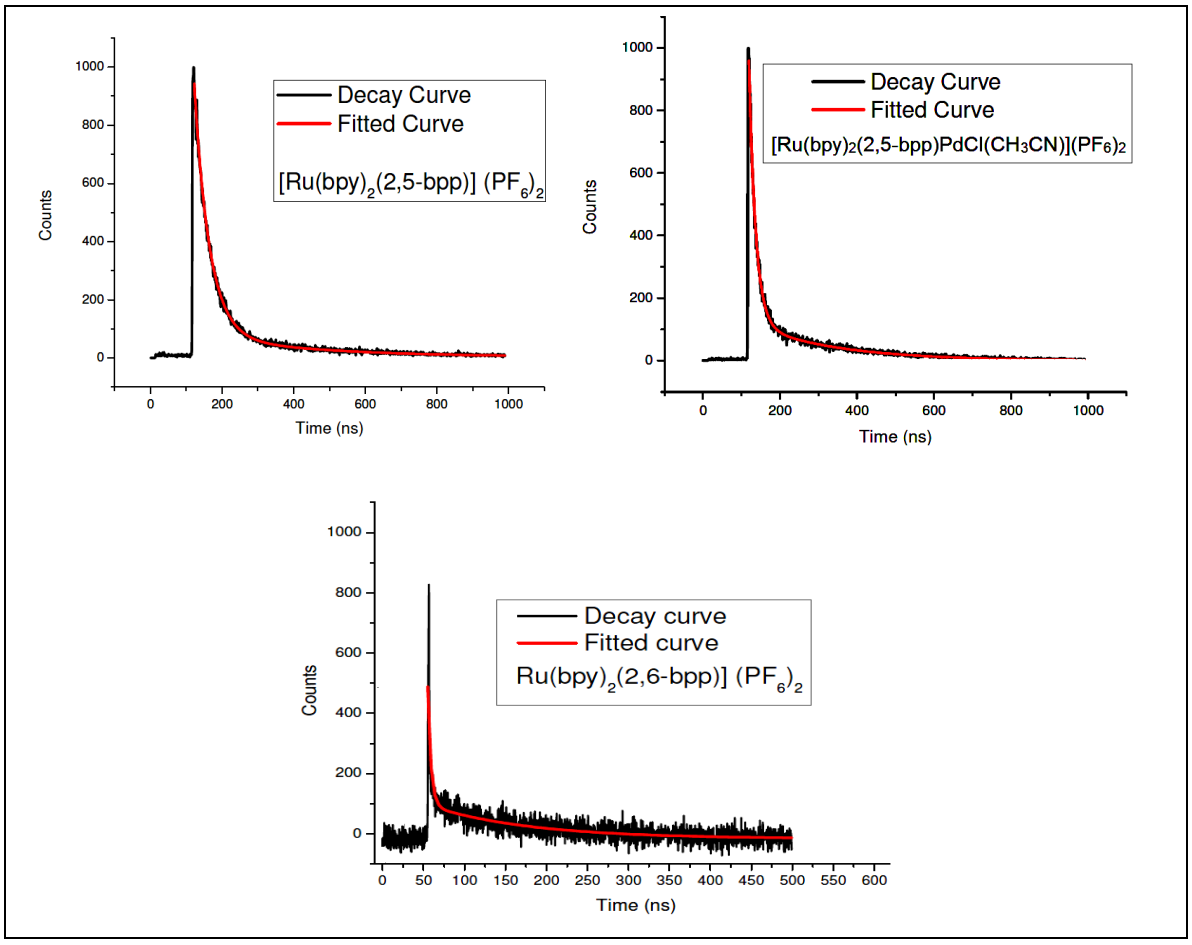

Figure 4.17: *TCSPC spectra of the ruthenium(II) complexes (in black) and their associated exponential fits (in red). The spectra were recorded at 293 K in a deaerated acetonitrile by using freeze-pump-thaw three times. The samples were excited at 360 nm and the emission decay curves were observed at emission wavelengths, depending on the complexes, see Table 4.3.*

4.3.4 Photocatalytic hydrogen generation experiments.

Run	Complexes	TON {Water percentage} (Standard Deviation)			
		{0 %}	{5 %}	{10 %}	{15 %}
1	$[Ru(bpy)_2(2,5\text{-}bpp)PdCl]_2^{4+}$	0	108 (2)	130 (1)	94 (2)
2	$[Ru(bpy)_2(2,6\text{-}bpp)PdCl]_2^{4+}$	0	0	0	0
3	$[Ru(bpy)_2(2,5\text{-}bpp)]^{2+}$	0	0	0	-
4	$[Ru(bpy)_2(2,6\text{-}bpp)]^{2+}$	0	0	0	-
5	$[Ru(bpy)_2(2,5\text{-}bpp)]^{2+}$ + $Pd(acetonitrile)_2Cl_2$	0	79 (3)	70 (2)	-
6	$[Ru(bpy)_2(2,6\text{-}bpp)]^{2+}$ + $Pd(acetonitrile)_2Cl_2$	0	0	0	-
7	$[Ru(bpy)_2(2,5\text{-}bpp)]^{2+}$ + $(NH_4)_2(PdCl_4)$	0	50 (5)	48 (3)	-
8	$[Ru(bpy)_2(2,6\text{-}bpp)]^{2+}$ + $(NH_4)_2(PdCl_4)$	0	0	0	-
9	$(NH_4)_2(PdCl_4)$	0	0	-	-
10	$Pd(acetonitrile)_2Cl_2$	0	0	-	-
11	No Catalyst (only TEA)	0	0	-	-

Table 4.4: *Evaluation of heterodinuclear Ru-Pd complexes (intramolecular catalysis) and mononuclear complexes Ru + $[Pd(CH_3CN)_2Cl_2]$ (intermolecular catalysis) for photocatalytic hydrogen evolution reactions (6×10^{-5} M of catalyst / $[Pd(CH_3CN)_2Cl_2]$ in 2 cm^3 of 2.15 M TEA in ACN-H_2O (0%, 5%, 10% and 15% H_2O (v/v)), λ_{exc} = 470 nm, 18 hours irradiation). Averages of 3 samples were taken for calculating TONs.*

A typical sample solution was prepared by mixing 0.1 ml of a $1.2 \cdot 10^{-3}$ M catalyst solution in acetonitrile, 0.6 ml of triethylamine, 0.1 ml (5 vol. %) or {(0.2 ml for 10 vol. %), (0.3 ml for 15 vol. %)} of thoroughly degased water and 1.2 ml (5 vol. %) or {(1.1 ml for 10 vol. %), (1.0 ml for 15 vol. %)} of anhydrous acetonitrile. Final Concentration

of photocatalysts is $6.0 \cdot 10^{-5}$ M. The photocatalytic hydrogen generation activity of each intramolecular cyclometallated heterodinuclear complexes (Ru–Pd) and the intermolecular Ru(II) mononuclear complexes of 2,5-bpp / 2,6-bpp with [Pd(acetonitrile)$_2$Cl$_2$] were evaluated with various percentages of water, by irradiation at 470 nm in an acetonitrile solution in the presence of a sacrificial electron donor, triethyl amine (TEA), under a N_2 atmosphere. As shown in table 4.4, $[Ru(bpy)_2(2,5\text{-bpp})PdCl]_2^{4+}$ (run 1), the intermolecular reaction of the $[Ru(bpy)_2(2,5\text{-bpp})]^{2+}$ with [Pd(acetonitrile)$_2$Cl$_2$] (run 5) / $(NH_4)_2(PdCl_4)$ (run 7) were found to be active as a photocatalytic hydrogen generation molecular devices in the presence of 5 – 10% water, while $[Ru(bpy)_2(2,6\text{-bpp})PdCl]_2^{4+}$ (not effective as photocatalyst; no hydrogen (run 2)) and $[Ru(bpy)_2(2,5\text{-bpp})]^{2+}$ (run 3), $[Ru(bpy)_2(2,6\text{-dpp})]^{2+}$ (run 4) and other intermolecular reactions between the mononuclear complex $[Ru(bpy)_2(2,6\text{-dpp})]^{2+}$ with [Pd(acetonitrile)$_2$Cl$_2$] (run 6) / $(NH_4)_2(PdCl_4)$ (run 8) did not result in H_2 evolution.

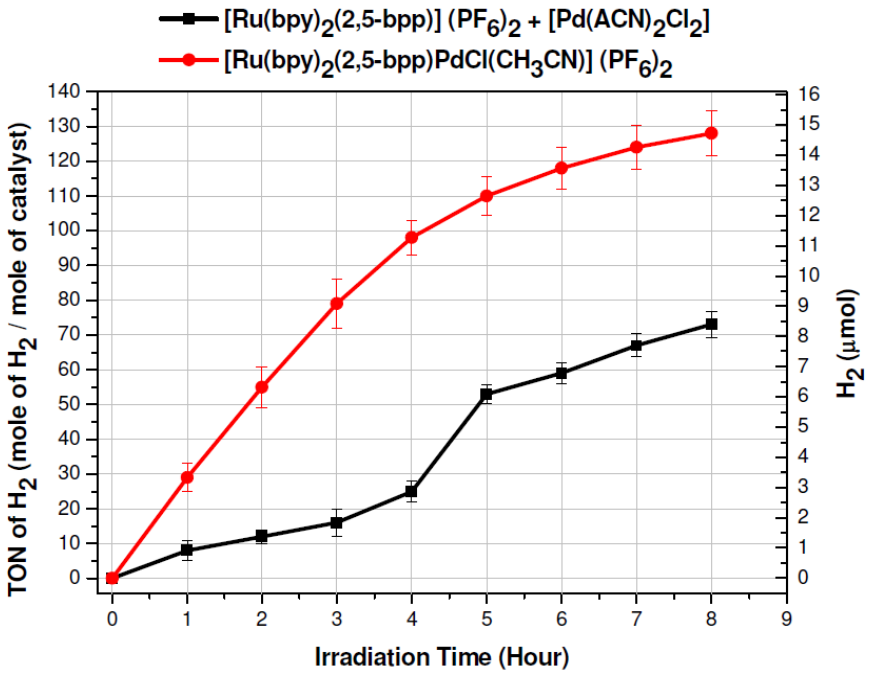

Figure 4.18: *Evaluation of $[Ru(bpy)_2(2,5\text{-bpp})PdCl(CH_3CN)]^{2+}$ (intramolecular catalysis) and $[Ru(bpy)_2(2,5\text{-bpp})]^{2+}$ + $[Pd(CH_3CN)_2Cl_2]$ (intermolecular catalysis) in photocatalytic hydrogen evolution reactions (6×10^{-5} M of catalyst /[Pd(CH3CN)$_2$Cl$_2$] in 2 cm^3 of 2.15 M TEA in ACN-H_2O (5% H_2O v/v), λ_{exc} = 470 nm, 0 – 8 hours irradiation). 3 samples were taken for calculating TONs. S.D.= ± 10 TONs or less.*

Time dependent hydrogen production is shown in Table 4.5, along with a turn over frequency (TOF = TON h^{-1}) graph for the complex $[Ru(bpy)_2(2,5\text{-bpp})PdCl(CH_3CN)]^{2+}$ (intramolecular) and the intermolecular photocatalytic reaction of $[Ru(bpy)_2(2,5\text{-bpp})]^{2+}$ with $[Pd(CH_3CN)_2Cl_2]$ in figure 4.18. The TOF curve for $[Ru(bpy)_2(2,5\text{-bpp})PdCl(CH_3CN)]^{2+}$ shows a smooth exponentially curve which reaches a maximum TON = 120 after 6 – 8 hours. The intermolecular reaction is less efficient (shows an induction period from 0 – 3 h) than the intramolecular reaction. Possibly in the intermolecular approach, electron transfer is slower as it relies on collision induced processes between several species. The TOF (TON h^{-1}) calculated for the intramolecular reaction is 15.5 per hour, while for the intermolecular reaction it decreases to 9.8 per hour.

Time ***(hour)***	***TON {Water percentage (5%)}***	
	$[Ru(bpy)_2(2,5\text{-bpp})PdCl(CH_3CN)]^{2+}$	$[Ru(bpy)_2(2,5\text{-bpp})]^{2+}$ + $[Pd(CH_3CN)_2Cl_2]$
0	***0***	***0***
1	***29***	***8***
2	***55***	***12***
3	***79***	***16***
4	***98***	***25***
5	***110***	***53***
6	***118***	***59***
7	***124***	***67***
8	***128***	***73***

Table 4.5: *Evaluation of $[Ru(bpy)_2(2,5\text{-bpp})PdCl(CH_3CN)]^{2+}$ (intramolecular catalysis) and $[Ru(bpy)_2(2,5\text{-bpp})]^{2+}$ + $[Pd(CH_3CN)_2Cl_2]$ (intermolecular catalysis) in photocatalytic hydrogen reactions (6×10^{-5} M of catalysts / $[Pd(CH_3CN)_2Cl_2]$ in 2 cm^3 of 2.15 M TEA in ACN-H_2O (5% H_2O v/v), λ_{exc} = 470 nm, 0 – 8 hours irradiation). 3 samples were taken for calculating TONs (see figure 4.18). S.D. ± 10 TONs or less.*

The intermolecular shows a sigmoidal curve with an induction period for the first three hours and after that gradually increases to the maximum TON = 79 (see figure 4.18). It is possible that the intermolecular reaction can behave as an intramolecular reaction[35] during photocatalysis but the efficiency is low due to the cyclometallation of the bridging ligand with the palladium metal. The turnover numbers (TONs) obtained for photocatalytic hydrogen production are listed in Table 4.4. While TONs up to 130 were obtained for $[Ru(bpy)_2(2,5\text{-bpp})PdCl(CH_3CN)]$ $(PF_6)_2$, the angular complex $[Ru(bpy)_2(2,6\text{-bpp})PdCl(CH_3CN)](PF_6)_2$ did not produce hydrogen. TONs were calculated per Pd atom although the complexes may exist as μ-chloro bridged dimers [44] as $[Ru(bpy)_2(2,5\text{-bpp})PdCl]_2$ $(PF_6)_4$ and $[Ru(bpy)_2(2,6\text{-bpp})PdCl]_2$ $(PF_6)_4$ in solution / solid state. The CHN analysis and ^{1}H-NMR confirmed that the one acetonitrile ligand coordinate with each Pd metal centre. For the photocatalytic process described in this chapter, the reaction mixture was excited at 470 nm and triethylamine (TEA) was used as the sacrificial agent to re-reduce the Ru(III) centre formed. The presence of water was found to be an important factor for photocatalytic water-splitting. Increasing turnover numbers were obtained with increasing water concentration (see table 4.5).[35, 45] However, the reasons for these observations are not straightforward, since its addition changes several parameters as discussed in chapter 3. Lower TONs were obtained when an equimolar mixture of the mononuclear precursor $[Ru(bpy)_2(2,5\text{-bpp})]^{2+}$ and $(NH_4)_2[PdCl_4]$ and $[Pd(CH_3CN)_2Cl_2]$ were irradiated under the same conditions as the dinuclear species while the complex $[Ru(bpy)_2(2,6\text{-bpp})]^{2+}$ did not produce hydrogen. Control experiments with the mononuclear precursors $[Ru(bpy)_2(2,5\text{-bpp})]^{2+}$ and $[Ru(bpy)_2(2,6\text{-bpp})]^{2+}$, without Pd yielded no hydrogen. Colloid formation has been discussed by several authors for Ru/Pd complexes.[46, 47] Since both complexes have comparable binding properties for Pd it seems unlikely that one should act as a precursor for catalytically active colloids while the other does not. However, black precipitates were found for $[Ru(bpy)_2(2,5\text{-bpp})]^{2+}$ and $[Ru(bpy)_2(2,5\text{-bpp})PdCl(CH_3CN)](PF_6)_2$ under photocatalysis conditions and with rapid decomposition of the complexes. No precipitates were found for $[Ru(bpy)_2(2,6\text{-bpp})PdCl(CH_3CN)](PF_6)_2$ under the same conditions, however, the solution slightly change in colour from yellow to light pink.

4.4 Summary and conclusion.

Chapter 4 details the synthetic method used for the generation of mononuclear and heterodinuclear metal complexes utilising the method of "complexes as metal / complexes as ligands" strategy. The heterodinuclear cyclometallated complexes (Ru – Pd) and their deuteriated analogues were synthesised and their properties, such as absorption and luminescence data were obtained (see table 4.3 and 4.4). These results were taken in conjunction with the characterization tools of ^{1}H-NMR and CHN to confirm the synthesis of these mononuclear and heterodinuclear complexes with properties similar to other families of ruthenium(II) complexes. Proton-NMR proved invaluable in determining the binding of the cyclometallated Pd moiety to the mononuclear complexes and then 2D-COSY ^{1}H-NMR was applied to obtain the correlation of the other protons present in the molecule (see table 4.1 and 4.2).

The main aim of this thesis is to determine the photocatalytic activity of the synthesised complexes for the generation of hydrogen using water and a sacrificial agent (TEA) and 470 nm as the irradiation wavelength. The gaseous products produced during the photocatalytic experiments were measured using gas chromatography and head space analysis. The results obtained showed that 2,6-bpp based complexes such as the mononuclear $[Ru(bpy)_2(2,6\text{-bpp})]^{2+}$ or cyclometallated heterodinuclear $[Ru(bpy)_2(2,6\text{-bpp})PdCl(CH_3CN)]^{2+}$ produced no hydrogen. However, the 2,5-bpp analogues proved very efficient at photocatalytic hydrogen generation. The $[Ru(bpy)_2(2,5\text{-bpp})PdCl(CH_3CN)]^{2+}$ intramolecular process yields higher TON of hydrogen at 130 for a 10% water content. By contrast the intermolecular reaction involving $[Ru(bpy)_2(2,6\text{-bpp})]^{2+}$ and $[Pd(CH_3CN)_2Cl_2]$ or $(NH_4)_2[PdCl_4]$ showed less hydrogen with a TONs of 70 / 48 for a 10% water which indicates that intermolecular electron transfer processes are less efficient. The results were complimentary with the time dependent hydrogen production for calculating turn over frequency (TOF). The TOF provides the rate of TON per hour and stability of catalyst during irradiation. The TOF for the intramolecular complex $[Ru(bpy)_2(2,5\text{-bpp})PdCl(CH_3CN)]^{2+}$ (TOF = 15.5 h^{-1}) compared to intermolecular reactions involving $[Ru(bpy)_2(2,6\text{-bpp})]^{2+}$ and $[Pd(CH_3CN)_2Cl_2]$ (TOF =

9.8 h^{-1}) shows good efficiency for the intramolecular electron transfer process. For the complex $[Ru(bpy)_2(2,5\text{-bpp})PdCl(CH_3CN)]^{2+}$, when the amount of water was increased from 0% (TON = 0) to 5% (TON = 108), the maximum TON = 130 for solution containing 10% water and drops for solution containing 15% (TON = 94) (see table 4.5). These results will be discussed further in chapter 6 where they will be compared with those obtained for the photocatalytic results obtained in chapter 3 and chapter 5.

4.5 Bibliography

[1] (a) A. von Zelewsky, Stereochemistry of Coordination Compounds; Wiley: Chichester, UK, 1996; (b) E, C. Constable, In Comprehensive Supramolecular Chemistry; J. Lehn, M., Ed.; Pergamon: 1996; Vol. 9, pp 213–252.

[2] (a) R. C. Evans, P. Douglas, C. J. Winscom, Coord. Chem. Rev. 2006, 250, 2093; (b) Q. Wu, M. Esteghamatian, N. -X. Hu, Z. Popovic, G. Enright, Y. Tao, M. D'Iorio, S. Wang, Chem. Mater., 2000, 12, 79.

[3] (a) M. K. Nazeeruddin, C. Klein, P. Liska, M. Grätzel, Coord. Chem. Rev. 2005, 249, 1460; (b) A. S. Polo, M. K. Itokazu, N. Yukie, M. Iha, Coord. Chem. Rev., 2004, 248, 1343; (c) K. Kalyanasundaram, M. Grätzel, Coord. Chem. Rev., 1998, 77, 347.

[4] A. Kraft, A. C. Grimsdale, A. B. Holmes, Angew. Chem., Int. Ed., 1998, 37, 402.

[5] (a) M. Berggren, O. Inganas, G. Gustafsson, J. Rasmusson, M. R. Andersson, T. Hjertberg, O. Wennerstrom, Nature, 1994, 372, 444; (b) E. M. Girotto, M. -A. De Paoli, Adv. Mater, 1998, 10, 790.

[6] W. R. Dawson, M. W. Windsor, J. Phys. Chem., 1968, 72, 3251.

[7] H. S. Joshi, R. Jamshidi, Y. Tor, Angew. Chem. Int. Ed., 1999, 38, 2722.

[8] A. Ajayaghosh, P. Carol, S. Sreejith, J. Am. Chem. Soc., 2005, 127, 14962.

[9] S. A. Raw, R. J. K. Taylor, Chem. Commun., 2004, 508.

[10] W. Goodall, J. A. G. Williams, Chem. Commun. 2001, 2514.

[11] J. C. Loren, J. S. Siegel, Angew. Chem. Int. Ed., 2001, 40, 754.

[12] B. M. Kelly-Basetti, D. J. Cundy, S. M. Pereira, W. H. F. Sasse, G. P. Savage, G. W. Simpson, Bioorg. Med. Chem. Lett., 1995, 5, 2989.

[13] A. C. Thompson, Coord. Chem. Rev., 1997, 160, 1.

[14] V. N. Kozhevnikov, D. N. Kozhevnikov, O. V. Shabunina, V. L. Rusinov and O. N. Chupakhin, Tetrahedron Letters, 2005, 46, 1791.

[15] V. N. Kozhevnikov, O. V. Shabunina, D. S. Kopchuk, M. M. Ustinova, B. König, D. N. Kozhevnikov, Tetrahedron, 2008, 64, 8963.

[16] G. R. Pabst, O. C. Pfüller, J. Sauer, Tetrahedron 1999, 55, 8045.

[17] P. L. Croot, K. A. Hunter, Anal. Chim. Acta, 2000, 406, 289.

[18] Z. Kolarik, U. Mullich, F. Gassner, Solvent Extr. Ion Exch., 1999, 17, 23.

[19] D. N. Kozhevnikov, V. L. Rusinov, O. N. Chupakhin, In Adv. Heterocycl. Chem.; A. R. Katritzky, Ed.; Academic, 2002; Vol. 82, pp 261–305.

[20] H. Neunhoeffer, In Comp. Heterocycl. Chem. II; A. R. Katrizky, C. W. Rees, E. F. V. Scriven, Eds.; Pergamon: Oxford, 1996; Vol. 6, pp 50–574.

[21] (a) J. R. Winkler, T. L. Netzel, C. Creutz, N. Sutin, J. Am. Chem. Soc., 1987, 109, 2381. (b) Hecker, Gushurst, McMillin., Inorg. Chem., 1991, 30, 538. (c) R. M. Berger, D. R. McMillin, J. Am. Chem. Soc., 1988, 109, 2381. (d) R. M. Berger, D. R. McMillin, Inorg. Chem. 1988, 27, 4245. (e) R. C. Young, J. K. Nagle, T. J. Meyer, D. G. Whitten, J. Am. Chem. Soc. 1978, 100, 4773.

[22] M. Schwalbe, M. Karnahl, H. Görls, D. Chartrand, F. Laverdiere, G. S. Hanan, S. Tschierlei, B. Dietzek, M. Schmitt, J. Popp, J. G. Vos and S. Rau, Dalton Trans., 2009, 4012.

[23] R. M. Berger and D. D. Ellis, Inorg. Chim. Acta, 1996, 241, 1; P. Paul, B. Tyagi, A. K. Bilakhiya, P. Dastidar and E. Suresh, Inorg. Chem., 2000, 39(1), 14; R. M. Berger and J. R. Holcombe, Inorg. Chim. Acta, 1995, 232, 217; R. M. Berger, Inorg. Chem., 1990, 29, 1920.

[24] S. Rau, B. Schäfer, D. Gleich, E. Anders, M. Rudolph, M. Friedrich, H. Görls, W. Herny and J. G. Vos, Angew. Chem., Int. Ed., 2006, 45, 6215.

[25] E. Amouyal, Sol. Energy Mater. Sol. Cells, 1995, 38, (1–4), 249–276.

[26] P. Chen and T. J. Meyer, Chem. Rev. 1998, 98, 1439; B. S. Brunschwig, C. Creutz and N. Sutin, Chem. Soc. Rev. 2002, 31, 168; K. D. Demadis, C. M. Hartshorn, and T. J. Meyer, Chem. Rev. 2001, 101, 2655; W. R. Browne, R. Hage and J. G. Vos, Coord. Chem. Rev. 2006, 250, 1653.

[27] H. Ozawa, Y. Yokoyama, M. Haga and K. Sakai, Dalton Trans., 2007, 1197.

[28] S. A. Arachchige, J. Brown and K. J. Brewer, J. Photochem. Photobiol., A, 2008, 197, 13.

[29] E. D. Cline, S. E. Adamson and S. Bernhard, Inorg. Chem., 2008, 47, 10378.

[30] P. W. Du, K. Knowles and R. Eisenberg, J. Am. Chem. Soc., 2008, 130, 12576.

[31] A. Fihri, V. Artero, M. Razavet, C. Baffert, W. Leibl and M. Fontecave, Angew. Chem., Int. Ed., 2008, 47, 564.

[32] C. Li, M. Wang, J. X. Pan, P. Zhang, R. Zhang and L. C. Sun, J. Organomet. Chem., 2009, 694, 2814.

[33] Y. Miyake, K. Nakajima, K. Sasaki, R. Saito, H. Nakanishi and Y. Nishibayashi, Organometallics, 2009, 28, 5240.

[34] B. Probst, C. Kolano, P. Hamm and R. Alberto, Inorg. Chem., 2009, 48, 1836.

[35] G. Singh Bindra, M. Schulz, A. Paul, S. Soman, R. Groarke, J. Inglis, M. T. Pryce, W. R. Browne, S. Rau, B. J. Maclean and J. G. Vos, Dalton Trans., 2011, DOI: 10.1039/c1dt11241d.

[36] H. Ozawa and K. Sakai, Chem. Commun., 2011, 47, 2227.

[37] W. R. Browne, C. M. O'Connor, J. S. Killeen, A. L. Guckian, M. Burke, P. James, M. Burke and J. G. Vos, Inorg. Chem., 2002, 41, 4245.

[38] Y. Q. Fang and G. S. Hanan, Synlett, 2003, 6, 852.

[39] (a) E. Negishi, S. Baba, J. Am. Chem. Soc. Chem Comm., 1976, 596 (b) E. Negishi, Aspects of Mechanism and Organometallic Chemistry, J. H. Brewster, Ed.: Plenum Press: New York, 1978, 285.

[40] J. McMurry, Organic Chemistry, 5th Edition, Brooks/ Cole, 2000.

[41] J. M. Calvert, J. V. Caspar, R. A. Binstead, T. D. Westmoreland and T. J. Meyer, J. Am. Chem. Soc., 1982, 104, 24, 6620.

[42] (a) C. Metcalfe, S. Spey, H. Adams and J. A. Thomas, J. Chem. Soc., Dalton Trans., 2002, 4732; (b) R. M. Berger and D. D. Ellis, Inorg. Chim. Acta, 1996, 241, 1.

[43] F. Neve, A. Crispini and S. Campagna, Inorg. Chem., 1997, 36, 6150.

[44] K. Sakai, H. Ozawa, Coord. Chem. Rev., 2007, 251, 2753.

[45] E. D. Cline, S. E. Adamson and S. Bernard, Inorg. Chem., 2008, 47, 10378

[46] P. Du, J. Schneider, L. Fan, W. Zhao, U. Patel, F. N. Castellano and R. Eisenberg, J. Am. Chem. Soc., 2008, 130, 5056.

[47] P. Lei, M. Hedlund, R. Lomoth, H. Rensmo, O. Johansson and L. Hammarström, J. Am. Chem. Soc., 2008, 130, 26.

Chapter 5: Synthesis, Characterisation and Photocatalytic Properties of Ruthenium(II) and Palladium(II) / Platinum(II) Hetero-Bimetallic compounds with 2,2':5',5":2",2"'-quaterpyridine (bisbpy) as bridging ligand.

Abstract:

The complexes synthesised in this chapter were designed for photocatalytic generation of hydrogen from water. In these hetero-dinuclear metal complexes 2,2':5',5":2",2"'-quaterpyridine (bisbpy) has been used as bridging ligand. The application of these metal complexes as photocatalyst was investigated. This chapter includes characterisation of the complexes synthesised using nuclear magnetic resonance, elemental analysis and UV-Vis spectroscopy studies. The photocatalytic production of hydrogen from water was investigated using different photocatalytic conditions. The photocatalytic reduction of water was performed both using intermolecular and intramolecular approaches.

5.1 Introduction

The tuneable photophysical, photochemical and electrochemical properties constitute the primary basis of interest in ruthenium polypyridyl metal complexes and have led to widespread use for application such as artificial antenna systems, charge separation devices for photochemical solar energy conversion, and molecular electronics.[1] The development of such applications is greatly dependent on the availability of a synthetic approach capable of delivering organized structures of metal based molecular components with specific supramolecular properties.[2] The challenges encountered in the preparation of pure, structurally well-defined metal complexes increases with the size of the compound. Although the complexes as metals/complexes as ligands approaches have proven remarkably effective there remains a need for the development of alternative synthetic approaches.[3]

2,2'-Bipyridines are among the most widely used ligand structure motifs in metal coordination compounds.[4] In particular, transition metal-bipyridine complexes exhibit many interesting characteristics, which have resulted in numerous studies of, for example, their photochemical[5] and electrochemical behavior,[6] as well as their application in catalysis.[7] About two decades ago, however, a new and exciting field emerged; bipyridine and oligopyridine metal complexes serve as important structure determining units in self-assembled supramolecular architectures, an area of study that has seen tremendous development since.[8]

Although existing methods for the synthesis of symmetrically functionalized 2,2'-bipyridines permit the elaboration of many different derivatives,[9] the synthesis of bipyridine with differently functionalized pyridine subunits is still not common. In principle, this can mainly be achieved through two different pathways: a) mono functionalization of 2,2'-bipyridine, which often involves multi-step procedures and/ or requires rather harsh conditions,[10] or b) coupling of two different pyridine components by use of palladium- and nickel-catalyzed cross-coupling procedures such as the Stille, Suzuki, or Negishi reactions coupling reactions generally employed for the synthesis of

biaryls.[11] Most of these reactions, however, require bromides, iodides, or triflates as coupling components, and these are often not easily accessible but necessary in order to provide satisfying yields.

Thummel *et. al.*[12] reported the syntheses of four bi-1,10-phenanthrolines (Figure 5.1) and their mononuclear Ru(II) complexes (**Ru-1 – Ru-2**) for sensor applications (Figure 5.2). The spectroscopic properties of these complexes was investigated in response to various metal ions. Ligands **1** and **2** involve two 1,10-phenanthroline (phen) subunits joined at the 2,2'- and 3,3'-positions. The transoid conformation of **1** will be favored to avoid a putative H3,-H3'-interaction[13] while the cisoid and transoid forms of **2** should be of approximately equal energy. Ligand **3** is a 2,2'-dimethylene bridged derivative of **2** wherein the cisoid conformation is enforced. Ligand **4** is a 2,3'-biphen with a 3,2'-dimethylene bridge which enforces a transoid conformation. In **1**-**3**, the bidentate binding sites are equivalent while in **4** one site is more sterically encumbered.

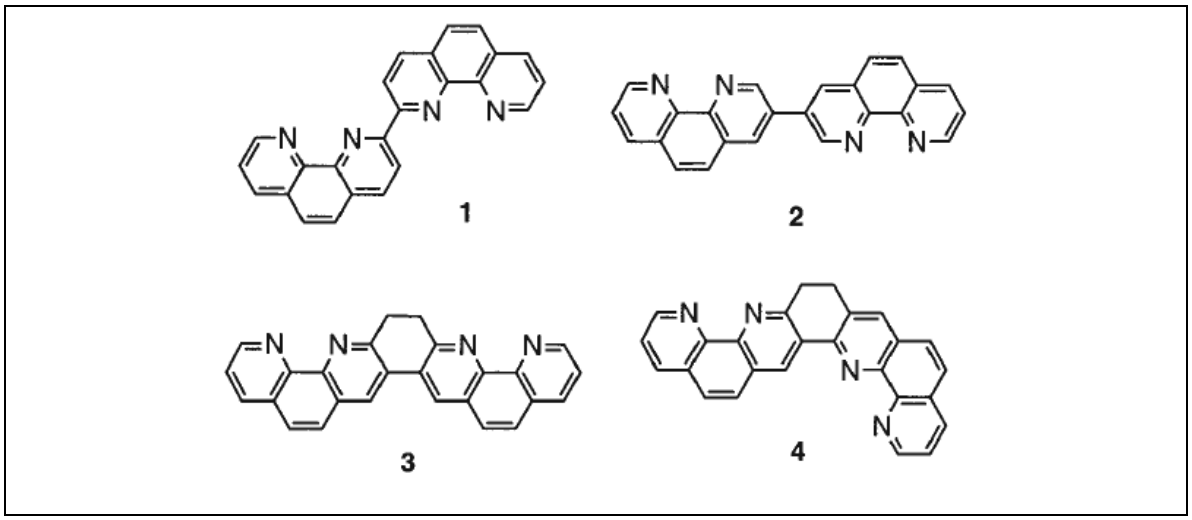

Figure 5.1: *Chemical structure of ligands reported by Thummel et. al.*[12]

For the mononuclear Ru(II) complexes of these four ligands (Figure 5.2), the luminescent metal center is located near a vacant bidentate coordination site that remains accessible to added cations. Thus, these complexes fit the general model of a sensor system, and it had been demonstrated that for certain cations luminescence is enhanced, for some, it remains nearly unchanged, and for others, it is diminished or quenched.

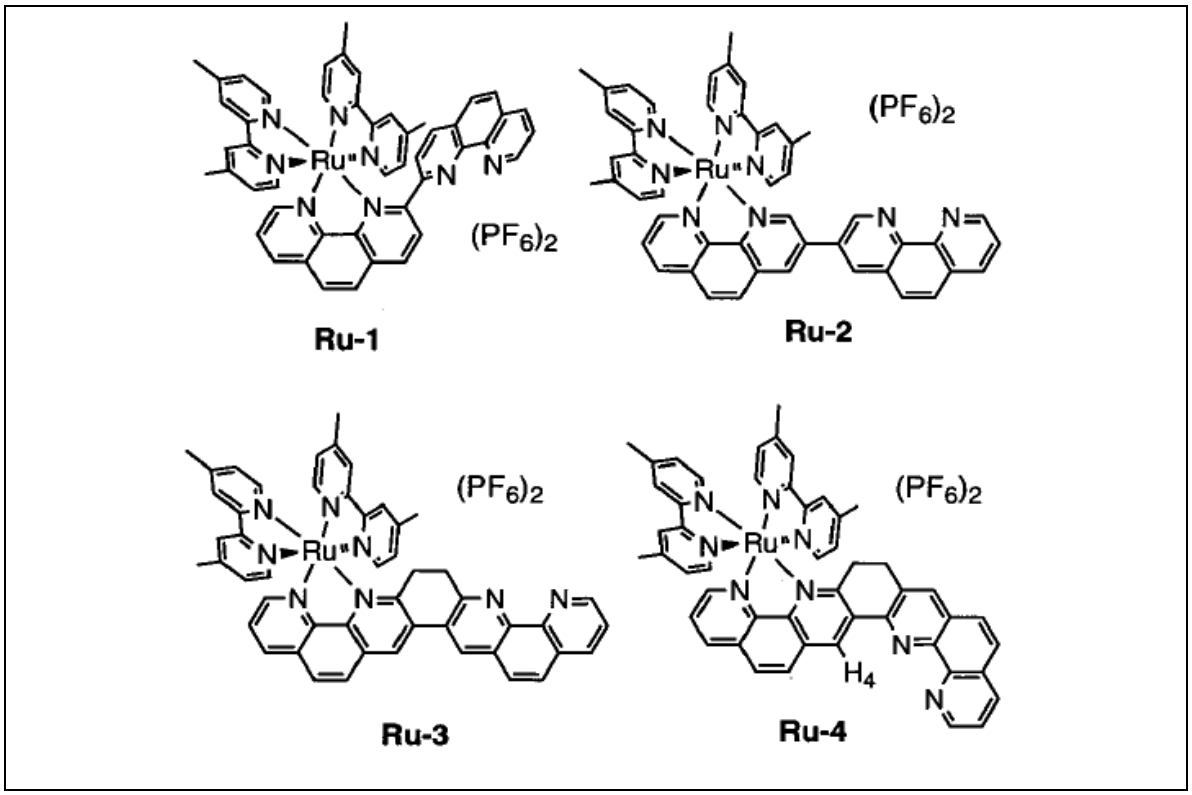

Figure 5.2: *Chemical structure of Ru(II) mononuclear complexes reported by Thummel.*[12]

The two non-bridged biphenthroline ligands **1** and **2** were synthesized in 70% - 80% yields by Ni(0) coupling of 2-chlorophen (**5**) [13, 14] or 3-bromophen (**6**) (see Scheme 5.1).[15] The reaction initially yielded a Ni(II) complex which may be demetalated by treatment with NaCN, thereby liberating the free ligand. Although 3,3'-biphen **2** was previously unknown, 2,2'-biphen **1** had earlier been prepared by Case in 24% yield, using Ullmann coupling with 2-chlorophen.[16] When care is taken to remove the complexed nickel, Ni(0) coupling dramatically improved the yield.[13, 17] The bridged biphens **3** and **4** were synthesized by the Friedländer condensation[18] of 8 amino- 7-quinolinecarbaldehyde (**8**) with 1,4-cyclohexanedione (**7**) or 1,3-cyclohexanedione (**10**).[19] The condensation of **7** and **8** in a 1:1 or 1:2 molar ratio with piperidine as the catalyst gave only the doubly condensed product **3**; the mono-condensed product was not obtained. This is understandable if one realizes that the condensations with **8** occur in a stepwise fashion. Only one mono-condensation product is available from **7**, thus activating the methylene group closest to the phen ring in **9** and directing the formation of **3** (Scheme 5.1). In 1,3-

cyclohexanedione, **10**, the methylene group at the 2-position is activated by two carbonyl groups and hence is more reactive than the other methylene groups.[20] Thus, the condensation of **8** and **10** in a 1:1 molar ratio using a mildly basic catalyst such as piperidine only gave 5,6,7,8-tetrahydro- [2,3:*b*]pyridoacrid- 8-one (**11**) in 94% yield. The condensation of **11** with 1 equiv of **8** in the presence of ethanolic KOH provided the doubly condensed species, 2,3'-dimethylene-3,2'-biphen (**4**) (see scheme 5.1). However, the condensation of **8** with 2 equiv of **10** using ethanolic KOH or piperidine as the catalyst did not readily afford **4**.

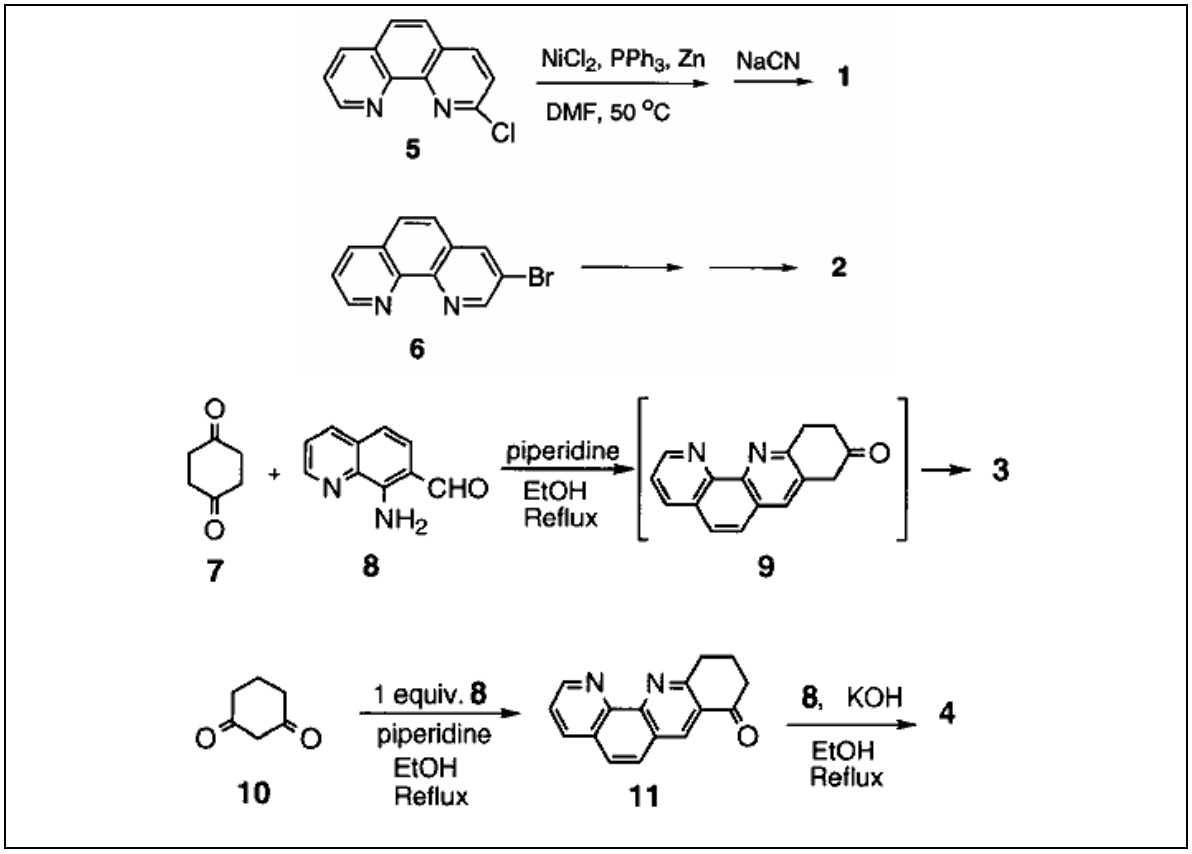

Scheme 5.1: *Synthetic chemical procedure for bridging ligands **1**, **2**, **3** and **4**.*[12]

Advances in inorganic photochemistry over the past two decades have driven the diversification of model systems under investigation.[21] As interest in energy and electron transfer studies in mono- and polymetallic complexes grew, so did the synthetic approaches to obtain these complexes. Homodimetallic complexes are readily

synthesized by first preparing symmetric dinucleating ligands followed by the direct synthesis of their dimetallic complexes. However, more elaborate energy and electron transfer studies require the preparation of the synthetically more challenging heterodimetallic complexes.

Most synthetic approaches to heterodimetallic complexes make use of symmetric dinucleating ligands.[22] The monometallic complexes of dinucleating ligands are usually obtained in moderate yield as a statistical mixture from the reaction of the ligand with 1 equiv of metal ion, followed by the introduction of the second metal ion. Protection deprotection methodology has also been developed to build up polymetallic complexes, whereby one metal-binding site is protected by methylation, followed by metal ion complexation, deprotection, and subsequent heterometal ion binding.[23] The "chemistry-on-the-complex" approach, in which classic organic and organometallic reactions are performed directly on metal complexes, has shown significant versatility and promise.[24, 3a] Typically, this approach simplifies the purification of products, increases the overall yields, and, in some cases, proves to be the only method to obtain the desired products.

The "chemistry-on-the-complex" approach is even more powerful when a new binding site is created in the complex, which allows further metal ion complexation (Figure 5.3).[25] The first metal ion binds selectively to a complete chelating site as opposed to an incomplete binding site (Figure 5.3 (a)). A catalytic reaction, in this case the Negishi reaction, creates a new binding site in the metal complex (Figure 5.3 (b)). A second and different metal ion is introduced into the newly created binding site, thus allowing the straightforward synthesis of heterodimetallic complexes (Figure 5.3 (c)).

Hanan and coworkers,[26] used 2-pyridylzinc bromide to create a new bidentate coordination site on both ligands and metal complexes by using the Pd-catalyzed Negishi reaction. The Negishi reaction affords a facile method to prepare new binding sites. 2,2'-dibromo-4,4'-bipyridine [27] (0.75 mmol) readily reacts with 2-pyridylzinc bromide (1.5 mmol) at room temperature in THF with $[Pd(PPh_3)_4]$ (0.025 mmol, 3%) $[Pd(PPh_3)_4]$ [tetrakis(triphenylphosphine)-palladium(0)] as catalyst to afford a mixture of terpyridine

1a and quaterpyridine **1b** (Scheme 5.2). It is noteworthy that, even with an excess of 2-pyridylzinc bromide, **1a** forms selectively because of its precipitation from the reaction mixture, which disfavors the formation of dinucleating ligand **1b**. The mono-halogenated ligand is obtained in high yield by avoiding reactions that generate statistical mixtures of products.

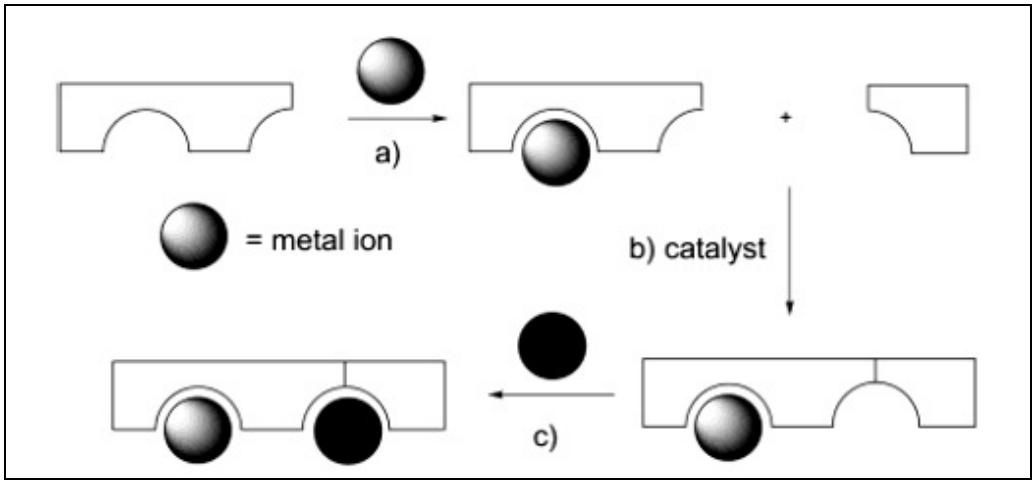

Figure 5.3*: Strategy for the synthesis of heterodimetallic complexes: (a) the first metal ion binds to a complete chelating site; (b) a new binding site is created in a reaction on the metal complex; (c) the second metal ion is then introduced giving a heterodimetallic complex.*

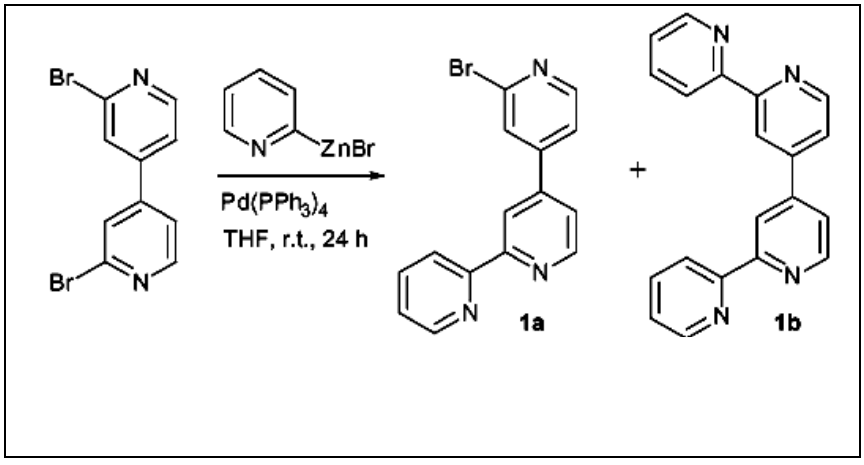

Scheme 5.2: *Synthesis of Polypyridyl Ligands (**1a** and **1b**).* [26]

As an example of a heterodimetallic complex, a mixed Ru-Os dimetallic complex was made in high overall yield using this methodology (Scheme 5.3).

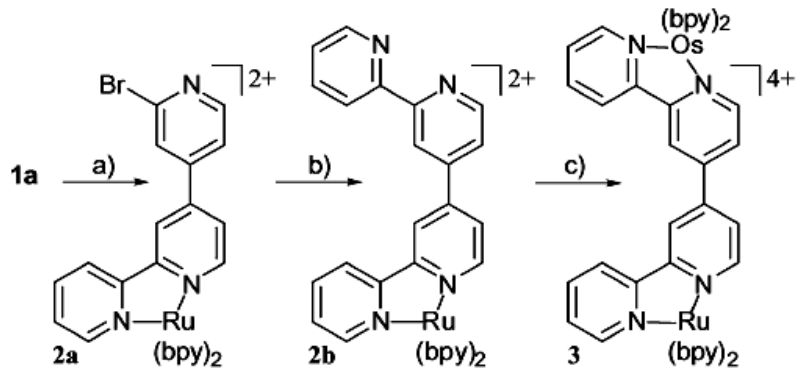

Reaction conditions: (a) $Ru(bpy)_2Cl_2$, $AgNO_3$, EtOH, 93% yield; (b) 2-pyridylzinc bromide, $Pd(PPh_3)_4$, DMF, r.t., 97% yield; (c) $Os(bpy)_2Cl_2$, $HOCH_2CH_2OH$, 43% yield.

Scheme 5.3*: Preparation of heterodimetallic ruthenium-osmium complex* ***3***. [26]

Allowing ligand **1a** to react with an equimolar amount of $[Ru(bpy)_2Cl_2]$ (bpy) 2,2'-bipyridine) in EtOH at reflux temperature in the presence of $AgNO_3$ gives the monometallic complex **2a** in 93% yield (Scheme 5.3 (a)). The $[Ru(bpy)_2]^{2+}$ moiety binds much more effectively to the bpy-like site in **1a** as opposed to the monodentate 2-bromopyridyl site because of the chelate effect. In addition, the bromine atom hinders the pyridyl nitrogen's ability to bind to the metal ion. The 2-bromopyridyl site in **2a** is readily converted into a chelating bpy like site using the Negishi reaction (Scheme 5.5 (b)). The reaction of **2a** (0.10 mmol) with an excess of 2-pyridylzinc bromide (0.50 mmol) under mild Negishi cross coupling conditions, stirring at room temperature in DMF with $[Pd(PPh_3)_4]$ as catalyst (20 mol % based on **2a**), affords **2b** in 97% yield. Thus, the conversion of 2,2'-dibromo-4,4'- bipyridine to **2b** occurs in 69% overall yield. Because of the hydration of **2a**, excess organozinc reagent (5 equiv) is required for the Negishi reaction to proceed. The crude product is purified by sequestering excess zinc halides formed in the transmetalation step with EDTA, followed by column chromatography on silica gel. These cross-coupling conditions are considerably milder than those required for cross coupling stannyl or borane reagents with metal complexes.[24a- 24e] The newly formed ligand **1b** in complex **2b** is not isolated in its metal-

free state. Indeed, the reaction of the metal-free ligand **1b** with $[Ru(bpy)_2Cl_2]$ would require difficult purification steps as both bpy sites could react with $[Ru(bpy)_2Cl_2]$. The newly created bpy site in **2b** is then allowed to react with *cis*-$[Os(bpy)_2Cl_2]$ in ethylene glycol to yield the heterodimetallic complex **3** in 43% yield (Scheme 5.3 (c)). The lower yield in the last step is typical for the synthesis of osmium bpy complexes.

Vos and coworkers [28] reported intramolecular processes in asymmetric homodinuclear metal complexes, containing two $[M(bipy)_2]$ units, where M is Ru(II) or Os(II), incorporating bridging ligands consisting of two different chelating moieties, bipy or triazole, as shown in Figure 5.4.

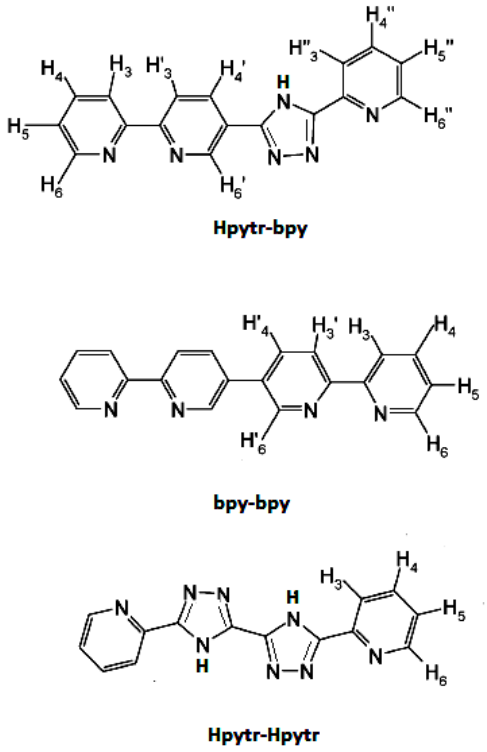

Figure 5.4: *Structure of targeted bridging ligands Hpytr-bipy, bpy-bpy and Hpytr-Hpytr using homo-coupling reaction reported by Vos et. al.* [28]

In this contribution they reported the syntheses, separation and characterization of the target hetero and homo-dinuclear complexes using a homo-coupling reaction. The decision to utilize a nickel catalyzed [29] homogeneous coupling approach for the synthesis

of asymmetric homodinuclear complexes seems, in the first instance, counterintuitive. The results obtained show, however, that such an approach can prove to be fruitful provided that the mixture of products obtained can be separated in a facile manner. Coupling was carried out employing the ruthenium and osmium precursors $[Ru(bpy)_2(bipy\text{-}Br)]^{2+}$ / $[Os(bpy)_2(bipy\text{-}Br)]^{2+}$ (**1a/1b**), $[Ru(bpy)_2(pytr\text{-}Br)]^{+}$ / $[Os(bpy)_2(pytr\text{-}Br)]^{+}$ (**2a/2b**)**.** With this method binuclear complexes of the types $[Ru(bpy)_2(bpy\text{-}bpy)Ru(bpy)_2]^{4+}$ / $[Os(bpy)_2(bpy\text{-}bpy)Os(bpy)_2]^{4+}$ (**3/4**), $[Ru(bpy)_2(pytr\text{-}pytr)Ru(bpy)_2]^{2+}$ / $[Os(bpy)_2(pytr\text{-}pytr)Os(bpy)_2]^{2+}$ (**5/6**), and $[Ru(bpy)_2(pytr\text{-}bpy)Ru(bpy)_2]^{3+}$ **7**, $[Os(bpy)_2(pytr\text{-}bpy)Ru(bpy)_2]^{3+}$ **8**, $[Ru(bpy)_2(pytr\text{-}bpy)Os(bpy)_2]^{3+}$ **9**, where (bpy-bpy) is 2,2'-bis(pyridin-2"-yl)-5,5'-bis(pyridin-3"-yl), (Hpytr-Hpytr) is 5,5'-bis(pyridin-2"-yl)-3,3'-bis(1,2,4-triazole) and (Hpytr-bpy) is [5-(5'-bipyridin-2',2"-yl)-3-(pyridin-2-yl)]-1,2,4-triazole and M is either Ru(II) or Os(II) were isolated (Figure 5.5).

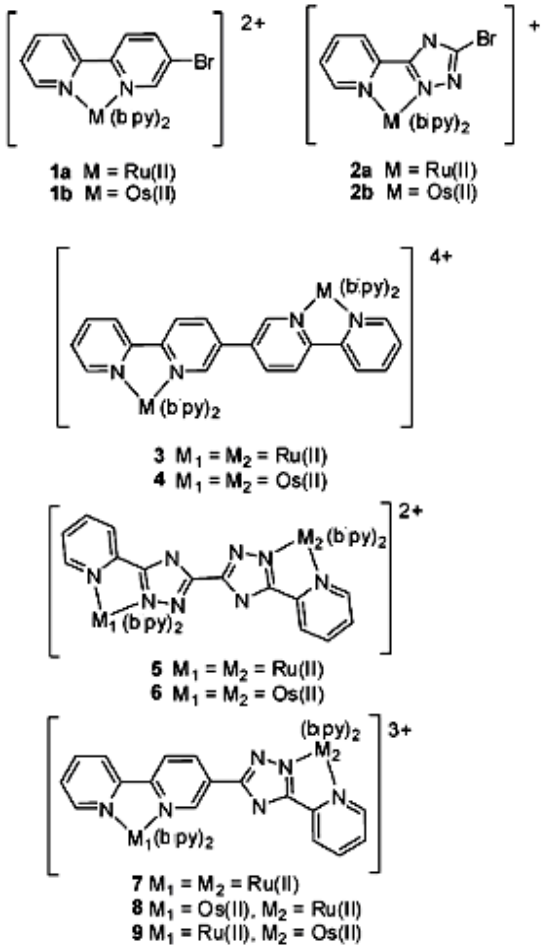

Figure 5.5: *Structures of the dinuclear complexes and their precursor complexes.* [28]

With triazole based systems, in addition, two positional coordination isomers can be expected also, since the metal ions may coordinate at the N2 or the N4 atom of the triazole ring. For example, direct reaction of Hpytr-Hpytr to form dinuclear compounds leads to the formation of up to eight isomers.[30] The $[M(bpy)_2]$-type precursor complexes $[M(bpy)_2(bipy\text{-}Br)]^{2+}$ **1** and $[M(bpy)_2(pytr\text{-}Br)]^{+}$ **2** (Figure 5.5) were used as bromo-precursors where M = Ru(II) or Os(II). Importantly, such compounds are readily accessible. The results obtained show that the bromine functional group allows for efficient coupling of the mononuclear complexes using this Ni(0) catalysed reaction. Furthermore, the presence of the bromine substituent at the 3'-position of the triazole ring results in the preferential formation of the N2 isomer (>95%) of complexes $[Ru(bpy)_2(pytr\text{-}Br)]^{+}$ **2a** and $[Os(bpy)_2(pytr\text{-}Br)]^{+}$ **2b**. This reduces the number of isomers that may be obtained for the mononuclear precursors and hence the dinuclear complexes formed in subsequent reactions.

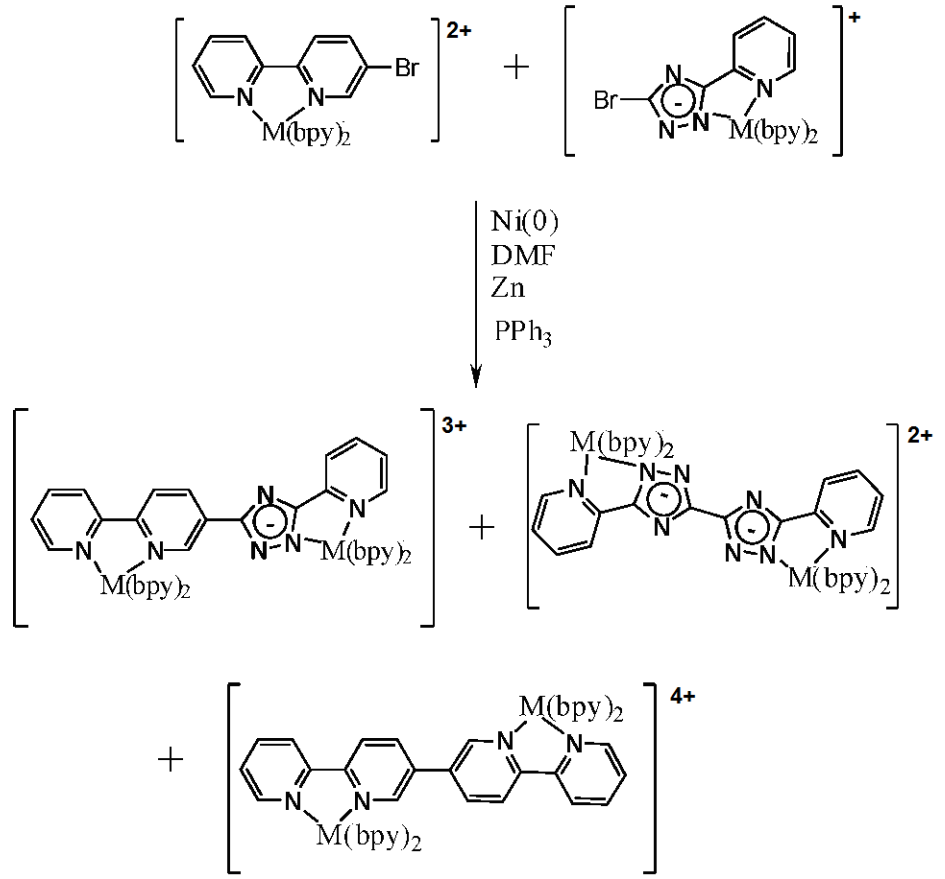

Figure 5.6: *Synthetic approach used for the synthesis of the homodinuclear complexes.*[30]

One disadvantage of this method is that, since the Ni(0) catalyzed coupling reaction is in essence a homogeneous cross-coupling reaction, three different compounds will be obtained, each containing a different bridging ligand as shown in Figure 5.6. The compounds obtained were separated using silica and Sephadex based column chromatography based on their respective charges with the di-cationic complex as the first fraction, the target tri-cationic complex as the second fraction, and finally the tetra-cationic complex.

All complexes reported by Vos and coworkers,[28] exhibit absorption and emission properties which are characteristic of Ru(II) and Os(II) based polypyridyl complexes with triazole and/or bipyridyl bridging ligands.[3] The characteristic dπ–π* metal to ligand charge transfer (^{1}MLCT) absorption bands are observed in the visible region (350–520 nm). For the bis-1,2,4-triazolato containing complex $[Ru(bpy)_2(pytr\text{-}pytr)Ru(bpy)_2]^{2+}$ **5** the ^{1}MLCT absorption bands are red shifted compared with those complexes containing one ($[Ru(bpy)_2(pytr\text{-}bpy)Ru(bpy)_2]^{3+}$ **7**) or no ($[Ru(bpy)_2(bpy\text{-}bpy)Ru(bpy)_2]^{4+}$ **3**) 1,2,4-triazolato units due to the increased σ-donor capacity of this moiety. Similar spectral features are observed for the corresponding Os(II) complexes ($[Os(bpy)_2(bpy\text{-}bpy)Os(bpy)_2]^{4+}$ **4**, $[Os(bpy)_2(pytr\text{-}pytr)Os(bpy)_2]^{2+}$ **6** and $[Os(bpy)_2(pytr\text{-}bpy)Ru(bpy)_2]^{3+}$ **8**). However additional absorption bands are observed in the 500–700 nm region characteristic of ^{3}MLCT absorption bands typical of Os(II) polypyridyl compounds.[28]

All complexes exhibit the expected ^{3}MLCT based luminescence at room temperature in acetonitrile solution.[3, 31] As observed for the absorption spectra there is a general shift to lower energy with increasing number of σ-donor triazolato moieties. For the heteronuclear complexes, $[Os(bpy)_2(pytr\text{-}bpy)Ru(bpy)_2]^{3+}$ **8** and $[Ru(bpy)_2(pytr\text{-}bpy)Os(bpy)_2]^{3+}$ **9**, emission is observed only from the osmium centre. This indicates that in the excited state interaction between the two metal centres is significant. For the compounds based either on the Hpytr-Hpytr bridging ligand the emissive ^{3}MLCT state was thought to be based on peripheral bpy ligands.[3a, 3b]

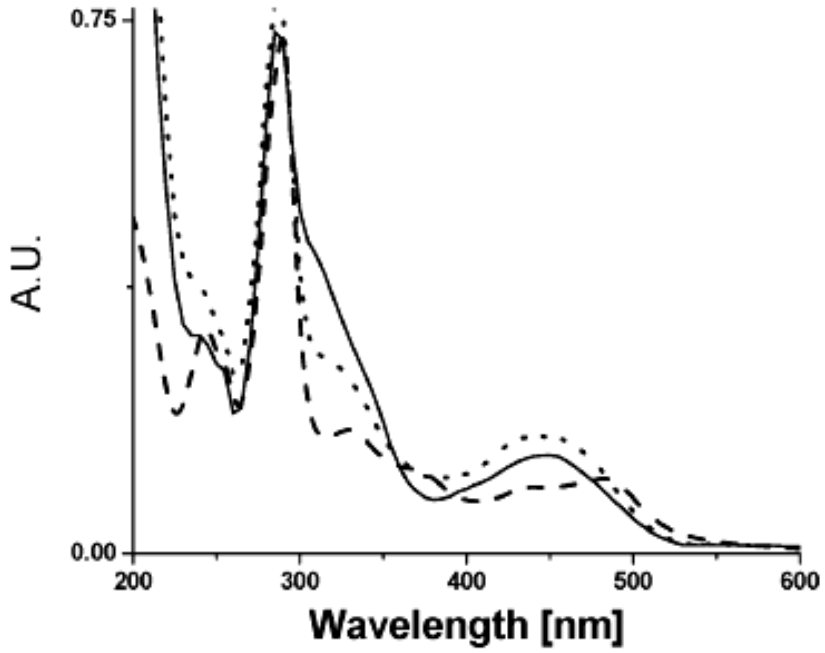

Figure 5.7: *UV/Vis absorption spectra of* $[(bpy)_2Ru(bpy\text{-}bpy)Ru(bpy)_2]^{4+}$ (***3***) *(solid line),* $[(bpy)_2Ru(pytr\text{-}pytr)Ru(bpy)_2]^{2+}$ (***5***) *(dashed line) and* $[(bpy)_2Ru(pytr\ bipy)Ru(bpy)_2]^{3+}$ (***7***) *(dotted line) in acetonitrile. Spectral intensities were adjusted for comparison.*[28]

In the bpy-pytr and bpy-bpy bridged complexes, the emitting state may be based on the bridging ligand or on the peripheral bipyridyl ligands. The absorption spectrum shown for $[(bpy)_2Ru(bpy\text{-}bpy)Ru(bpy)_2]^{4+}$ **3** is given in Figure 5.7. For this compound a strong shoulder in the UV region is shown at 330 nm. This feature is not present in the other compounds and may indicate a lower energy π–π* transitions in the bridging ligand.[28]

The main aim of this chapter is to design novel Ru – Pd/Pt based heterodinuclear complexes containing 2,2':5',5":2",2"'-quaterpyridinem (bisbpy) as a bridging ligand for photocatalytic production of hydrogen by splitting of water using triethyl amine as sacrificial donor and 470 nm as the light source. The complete characterization, photocatalytic, electrochemical and photophysical properties are discussed in the sections.

5.2 Experimental section.

The compounds 2,2'-bipyridine (bpy), $RuCl_3.xH_2O$ and [Pd(acetonitrile)$_2Cl_2$] were purchased from Aldrich and used without further purification. The synthesis of ruthenium precursors [Ru(bpy)$_2Cl_2$].$2H_2O$, [Ru(dceb)$_2Cl_2$].$2H_2O$ and [Pt(dmso)$_2Cl_2$] are reported in chapter 2. The structure with numbering of ligand 2,2':5',5":2",2"'-quaterpyridine (bisbpy), mononuclear complexes and hetero-dinuclear complexes discussed in this chapter are depicted in Figure 5.8, 5.9, 5.10 respectively.

5.2.1 Preparation of ligand 2,2':5',5":2",2"'-quaterpyridine (bisbpy).

The bridging ligand 2,2':5',5":2",2"'-quaterpyridine (bisbpy) was prepared according to the literature with little modification.[28] The complete synthesis of the ligand in two steps was described in Chapter 2, Section 2.3.2.

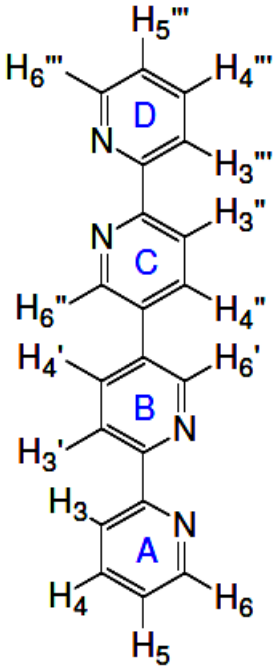

2,2':5',5":2",2"'-quaterpyridine (bisbpy)

Figure 5.8: *Structures and numbering of ligand 2,2':5',5":2",2"'-quaterpyridine (bisbpy).*

Synthesis of bridging ligand 2,2':5',5":2",2"'-quaterpyridine (bisbpy)

This ligand was prepared as described in chapter 2, section 2.3.2.

Yield: 0.205 mg (0.66 mmol, 78 %).

^{1}H-NMR (DMSO-d_6, 400 MHz): δ = 7.50 (ddd, 2H, *J* = 7.4 Hz, *J* = 2.5 Hz, *J* = 1.1 Hz, H-5, H-5"'), 8.00 (ddd, 2H, *J* = 7.8 Hz, *J* = 2.0, H-4, H-4"'), 8.43 (dd, 2H, *J* = 8.3 Hz, *J* = 2.5 Hz, H-4', H-4"), 8.46 (dd, 2H, *J* = 7.8 Hz, *J* = 1.0 Hz, H-3, H-3"'), 8.54 (dd, 2H, *J* = 8.0 Hz, *J* = 1.0 Hz, H-3', H-3"), 8.72 (dd, 2H, *J* = 4.8 Hz, *J* = 1.0 Hz, H-6, H-6"'), 9.18 (d, 2H, *J* = 2.5 Hz, H-6', H-6").

5.2.2 Preparation of the ruthenium mononuclear complexes.

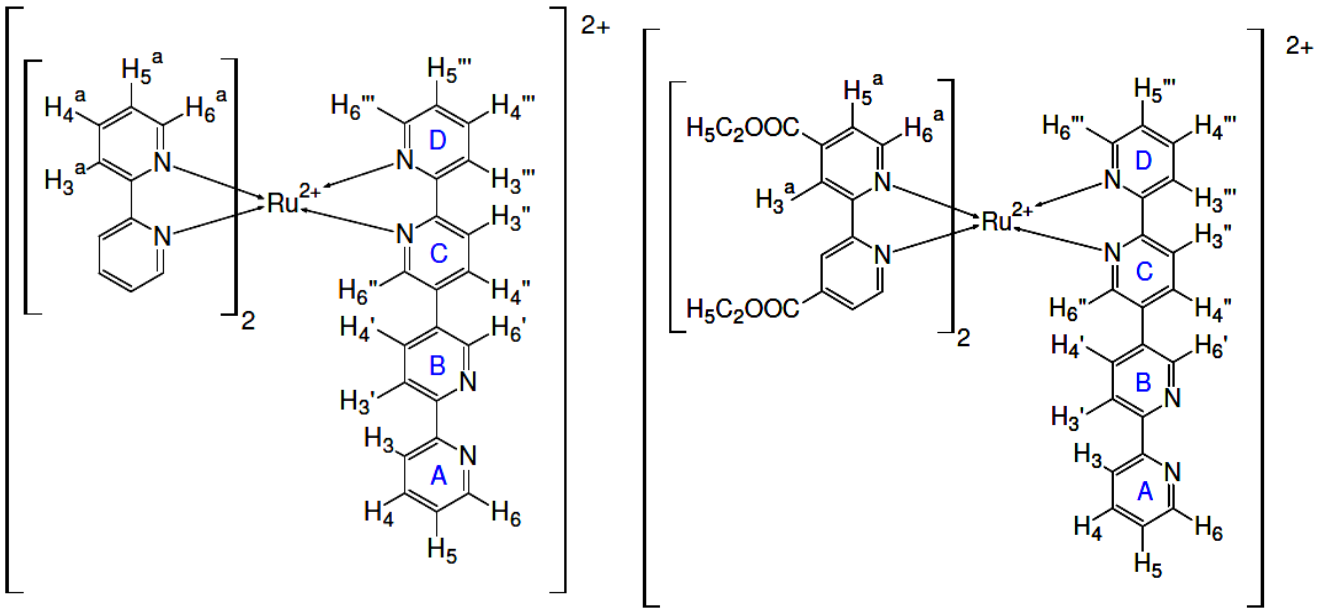

[Ru(bpy)$_2$(bisbpy)]$^{2+}$
Complex 5.1

[Ru(dceb)$_2$(bisbpy)]$^{2+}$
Complex 5.2

Figure 5.9: *Structures and numbering of the mononuclear non-ester and ester analogues of Ru(II)-(bisbpy) complexes.*

Synthesis of [Ru(bpy)$_2$(bisbpy)] (PF$_6$)$_2$ · 2 H$_2$O (Complex 5.1).

[bis-(2,2'-bipyridine)(2,2':5',5'',2'',2'''-quaterpyridine)ruthenium(II)](PF$_6$)$_2$· 2H$_2$O

[Ru(bpy)$_2$Cl$_2$]·2H$_2$O (0.339 g, 0.65 mmol) dissolved in 5 cm^3 of ethanol was added drop-wise to a solution of 2,2':5',5'',2'',2'''-quaterpyridine (bisbpy) (0.264 g, 0.85 mmol) in 10 cm^3 of ethanol/water (3:1 v/v). The reaction mixture was heated at reflux temperature for 8 hours. Subsequently, the mixture allowed cooling to room temperature and the solvent was evaporated under vacuum. To the residue was added 2 cm^3 of distilled water to dissolve the product and the excess ligand (bisbpy) filtered. The KPF_6 was added to the filtered solution to precipitate the product, which was washed with 5 cm^3 of water and 10 cm^3 of diethylether. Recrystallization from acetone/water (3:1 v/v) afforded a red solid. Yield: 0.588 g (0.56 mmol, 86%). Anal. Calcd. for $C_{40}H_{30}F_{12}N_8P_2Ru \cdot 2H_2O$ (1049.75): C, 45.77; H, 3.26; N, 10.67%. Found: C, 46.15; H, 2.86; N, 10.29%. ^{1}H-NMR (Acetonitrile-d$_3$, 400 MHz): δ = 8.72-8.68 (m, 2H, H-6, H-6'), 8.65 (d, 1H, *J* = 8.0 Hz, H-3"), 8.58 (d, 1H, *J* = 7.8 Hz, H-3"'), 8.62-8.50 (m, 4H, bpy (H-3a)), 8.45- 8.39 (m , 2H, H-3', H-4"), 8.15-8.05 (m, 5H, bpy (H-4a), H-4"'), 7.97-7.89 (m, 4H, H-3, H-4, H-4', H-6"), 7.83 (d, 1H, *J* = 4.8 Hz, bpy (H-6a), 7.79-7.72 (m, 4H, bpy (H-6a), H-6"'), 7.47-7.39 (m , 6H, bpy (H-5a), H-5, H-5"').

Synthesis of [Ru(dceb)$_2$(bisbpy)] (PF$_6$)$_2$ · 2 CH$_3$COCH$_3$ (Complex 5.2).

[bis-(4,4'-dicarboxyethyl-2,2'-bipyridine)(2,2':5',5'',2'',2'''-quaterpyridine)ruthenium-(II)](PF$_6$)$_2$· 2 CH$_3$COCH$_3$

[Ru(dceb)$_2$Cl$_2$]·2H$_2$O (0.525 g, 0.65 mmol) dissolved in 5 cm^3 of ethanol was added drop-wise to a solution of 5,5'-bisbipyridine (bis-bpy) (0.264 g, 0.85 mmol) in 10 cm^3 of ethanol/water (3:1 v/v). The reaction mixture was heated at reflux temperature for 8 hours. Subsequently, the mixture allowed cooling to room temperature and the solvent was evaporated under vacuum. To the residue was added 2 cm^3 of distilled water to dissolve the product and the excess ligand (bisbpy) filtered. The KPF_6 was added to the filtered solution to precipitate the product, which was washed with 5 cm^3 of water and 10 cm^3 of diethylether. Recrystallization from acetone/water (3:1 v/v) afforded a red solid.

Yield: 0.765 g (0.54 mmol, 83%). Anal. Calcd. for $C_{52}H_{46}F_{12}N_8P_2Ru \cdot 2(CH_3COCH_3)$ (1418.26): C, 49.12; H, 4.12; N, 7.90%. Found: C, 49.42; H, 4.14; N, 7.84%. ^{1}H-NMR (Acetonitrile-d_3, 400 MHz): δ = 9.13-9.08 (m, 4H, bpy (H-3a)), 8.74-8.66 (m, 3H, H-3", H-6, H-6'), 8.61 (d, 1H, *J* = 8.0 Hz, H-3"'), 8.46 (m, 1H, H-4"), 8.42 (d, 1H, *J* = 7.8 Hz, H-3'), 8.16 (ddd, 1H, *J* = 7.8 Hz, *J* = 2.0, H-4"'), 8.12 (d, 1H, *J* = 4.8 Hz, bpy (H-6a)), 8.00-7.82 (m, 11H, bpy (H-6a, H-5a), H-3, H-4, H-4', H-6"), 7.69 (d, 1H, *J* = 4.8 Hz, H-6"'), 7.48-7.42 (m, 2H, H-5, H-5"'), 4.52-4.43 (m, 8H, CH_2), 1.46-1.40 (m, 12H, CH_3), 2.10 (s, 12H, CH_3, acetone).

5.2.3 Preparation of Ru-Pd / Ru-Pt Heterodinuclear complexes.

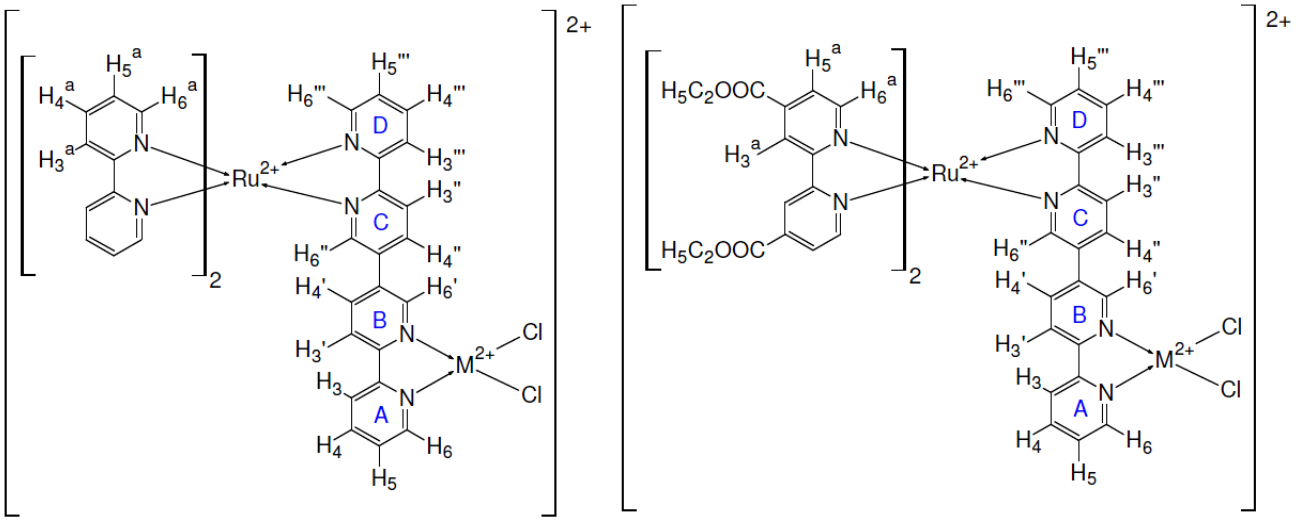

[Ru(bpy)$_2$(bisbpy)PdCl$_2$]$^{2+}$
Complex 5.3

[Ru(bpy)$_2$(bisbpy)PtCl$_2$]$^{2+}$
Complex 5.4

[Ru(dceb)$_2$(bisbpy)PdCl2]$^{2+}$
Complex 5.5

[Ru(dceb)$_2$(bisbpy)PtCl2]$^{2+}$
Complex 5.6

Figure 5.10: *Structures with numbering of the non- ester and ester analogues of Ru – Pd / Ru – Pt heterodinuclear complexes.*

Synthesis of $[Ru(bpy)_2(bisbpy)PdCl_2](PF_6)_2 \cdot 2\ H_2O$ (Complex 5.3).

[Ruthenium(II)(2,2'-bipyridine)$_2$(μ-2,2':5',5'',2'',2'''-quaterpyridine)$PdCl_2$] $(PF_6)_2 \cdot 2\ H_2O$

$[Ru(bpy)_2(bisbpy)]\cdot 2H_2O$ (0.100 g, 0.095 mmol) dissolved in 5 cm^3 of dichloromethane was added drop-wise to a solution of $[Pd(CH_3CN)_2Cl_2]$ (0.025 g, 0.095 mmol) in 5 cm^3 of dichloromethane. The reaction mixture was heated at reflux temperature for 24 hours. Subsequently, the mixture was allowed to cool to room temperature and 5 cm^3 of diethylether was added to precipitate the product. The obtained precipitate was filtered and washed with 10 cm^3 of diethylether. Recrystallization from acetone/water (3:1 v/v) afforded a red solid. Yield: 0.115 g (0.094 mmol, 99%). Anal. Calcd. for $C_{40}H_{30}F_{12}Cl_2N_8P_2RuPd \cdot 2H_2O$ (1226.5): C, 39.14; H, 2.70; N, 9.13; Found: C, 39.29; H, 2.50; N, 8.83. ^{1}H-NMR (Acetonitrile-d_3, 400 MHz): δ = 9.21 (d, 1H, *J* = 4.8 Hz, H-6), 9.17 (d, 1H, *J* = 2.5 Hz, H-6'), 8.67 (d, 1H, *J* = 8.0 Hz, H-3"), 8.63-8.57 (m, 3H, bpy (H-3a), H-3"'), 8.54-8.50 (m, 2H, bpy (H3a)), 8.43-8.37 (m, 2H, H-4', H-4"), 8.30 (d, 1H, *J* = 7.8 Hz, H-3'), 8.26-8.21 (m, 2H, H-3, H-4), 8.13-8.05 (m, 5H, bpy (H-4a), H-4"'), 8.02 (d, 1H, *J* = 2.3 Hz, H-6"), 7.89 (d, 1H, *J* = 4.8 Hz, bpy (H-6a)), 7.79-7.74 (m, 4H, bpy (H-6a), H-6"'), 7.70 (m, 1H, H-5), 7.48-7.39 (m, 5H, bpy (H-5a), H-5"').

Synthesis of $[Ru(bpy)_2(bisbpy)PtCl_2](PF_6)_2 \cdot 3\ H_2O$ (Complex 5.4).

[Ruthenium(II)(2,2'-bipyridine)$_2$(μ-2,2':5',5'',2'',2'''-quaterpyridine)$PtCl_2$] $(PF_6)_2 \cdot 3\ H_2O$

$[Ru(bpy)_2(bisbpy)]\cdot 2H_2O$ (0.100 g, 0.095 mmol) dissolved in 5 cm^3 of dichloromethane was added drop-wise to a solution of $[Pt(dmso)_2Cl_2]$ (0.042 g, 0.095 mmol) in 5 cm^3 of dichloromethane. The reaction mixture was heated at reflux temperature for 24 hours. Subsequently, the mixture was allowed to cool to room temperature and 5 cm^3 of diethylether was added to precipitate the product. The obtained precipitate was filtered and washed with 10 cm^3 of diethylether. Recrystallization from acetone/water (3:1 v/v) afforded a red solid. Yield: 0.109 g (0.082 mmol, 86%). Anal. Calcd. for $C_{40}H_{30}F_{12}Cl_2N_8P_2RuPt \cdot 3H_2O$ (1334.2): C, 35.97; H, 2.60; N, 8.30; Found: C, 35.70; H, 2.35; N, 7.95. ^{1}H-NMR (Acetonitrile-d_3, 400 MHz): δ = 9.54 (d, 1H, *J* = 2.5 Hz, H-6'),

9.51 (d, 1H, *J* = 4.8 Hz, H-6), 8.69 (d, 1H, *J* = 8.0 Hz, H-3"), 8.63-8.58 (m, 3H, bpy (H-3a), H-3"'), 8.55-8.51 (m, 2H, bpy (H-3a)), 8.47-8.40 (m, 2H, H-4', H-4"), 8.30-8.23 (m, 2H, H-3', H-4), 8.19 (d, 1H, *J* = 7.8 Hz, H-3), 8.14-8.04 (m, 6H, bpy (H-4a), H-4"', H-6"), 7.92 (d, 1H, *J* = 4.8 Hz, bpy (H-6a)), 7.79-7.74 (m, 4H, bpy (H-6a), H-6"'), 7.70 (m, 1H, H-5), 7.48-7.39 (m, 5H, bpy (H-5a), H-5"').

Synthesis of [Ru(dceb)$_2$(bisbpy)PdCl$_2$] (PF$_6$)$_2$ · 0.5 C$_6$H$_{14}$ · CH$_2$Cl$_2$ (Complex 5.5).

[Ruthenium(II)(4,4'-dicarboxyethyl-2,2'-bipyridine)$_2$(μ-2,2':5',5'',2'',2'''-quarter-pyridine)PdCl$_2$] (PF$_6$)$_2$ · 0.5 C$_6$H$_{14}$ · CH$_2$Cl$_2$

[Ru(dceb)$_2$(bisbpy)]·2(CH_3COCH_3) (0.100 g, 0.071 mmol) dissolved in 5 cm^3 of dichloromethane was added drop-wise to a solution of [Pd(CH_3CN)$_2$Cl$_2$] (0.018 g, 0.071 mmol) in 5 cm^3 of dichloromethane. The reaction mixture was heated at reflux temperature for 24 hours at 50º C. Subsequently, the mixture was allowed to cool to room temperature and 5 cm^3 of diethylether was added to precipitate the product. The obtained precipitate was filtered and washed with 10 cm^3 of diethylether and 10 cm^3 of n-hexane. Recrystallization from acetone/water (3:1 v/v) afforded a red solid. Yield: 0.112 g (0.070 mmol, 98.5%). Anal. Calcd. for $C_{52}H_{46}F_{12}O_8Cl_2N_8P_2RuPd$ · (0.3 C_6H_{14}) (CH_2Cl_2) (1590.08): C, 41.39; H, 3.30; N, 7.04; Found: C, 41.12, H, 3.22, N, 6.67. ^{1}H-NMR (Acetonitrile-d$_3$, 400 MHz): δ = 9.23 (d, 1H, *J* = 4.8 Hz, H-6), 9.20 (d, 1H, *J* = 2.5 Hz, H-6'), 9.13-9.10 (m, 2H, bpy (H-3a), 9.08-9.05 (m, 2H, bpy (H-3a), 8.67 (d, 1H, *J* = 8.0 Hz, H-3"), 8.62 (m, 1H, *J* = 7.8 Hz, H-3"'), 8.47-8.43 (m, 2H, H-4', H-4"), 8.27 (d, 1H, *J* = 8.0 Hz, H-3'), 8.26-8.21 (m, 2H, H-3, H-4), 8.16 (ddd, 1H, *J* = 7.8 Hz, *J* = 2.4 Hz, H-4"'), 8.11 (d, 1H, *J* = 4.8 Hz, bpy (H-6a)), 8.00 (d, 1H, *J* = 2.3 Hz, H-6"), 7.97-7.90 (m, 7H, bpy (H-6a, H-5a)), 7.72-7.66 (m, 2H, H-5, H-6"'), 7.48 (ddd, 1H, *J* = 4.8 Hz, *J* = 1.0 Hz H-5"'), 5.40 (s, 2H, CH_2, CH_2Cl_2), 4.52-4.44 (m, 8H, CH_2, ethyl-ester), 1.46-1.41 (m, 12H, CH_3, ethyl-ester), 1.25 (m, 4H, CH_2, ½ mole of n-hexane), 0.90 (m, 3H, CH_3, ½ mole of n-hexane).

Synthesis of $[Ru(dceb)_2(bisbpy)PtCl_2](PF_6)_2 \cdot 0.5\ C_6H_{14} \cdot CH_2Cl_2$ (Complex 5.6).

[Ruthenium(II)(4,4'-dicarboxyethyl-2,2'-bipyridine)$_2$(μ-2,2':5',5'',2'',2'''-quarter-pyridine)$PtCl_2$] $(PF_6)_2 \cdot 0.5\ C_6H_{14} \cdot CH_2Cl_2$

$[Ru(dceb)_2(bisbpy)]\cdot 2(CH_3COCH_3)$ (0.100 g, 0.071 mmol) dissolved in 5 cm^3 of dichloromethane was added drop-wise to a solution of $[Pt(DMSO)_2Cl_2]$ (0.030 g, 0.071 mmol) in 5 cm^3 of dichloromethane. The reaction mixture was heated at reflux temperature for 24 hours. Subsequently, the mixture was allowed to cool to room temperature and 5 cm^3 of diethylether was added to precipitate the product. The obtained precipitate was filtered and washed with 10 cm^3 of diethylether and 10 cm^3 of n-hexane. Recrystallization from acetone/water (3:1 v/v) afforded a red solid. Yield: 0.115 g (0.068 mmol, 96%). Anal. Calcd. for $C_{52}H_{46}F_{12}O_8Cl_2N_8P_2RuPt \cdot (0.5\ C_6H_{14})\ (CH_2Cl_2)$ (1696.5): C, 39.66; H, 3.27; N, 6.60; Found: C, 39.97, H, 3.24; N, 6.25. ^{1}H-NMR (Acetonitrile-d_3, 400 MHz): δ = 9.57 (d, 1H, *J* = 2.5 Hz, H-6'), 9.49 (d, 1H, *J* = 4.8 Hz, H-6), 9.13-9.10 (m, 2H, bpy (H-3a)), 9.08-9.02 (m, 2H, bpy (H-3a)), 8.72 (d, 1H, *J* = 8.0 Hz, H-3"), 8.63 (m, 1H, *J* = 7.8 Hz, H-3"'), 8.47-8.40 (m, 2H, H-4', H-4"), 8.23 (t, 1H, *J* = 7.8 Hz, H-4), 8.19-8.09 (m, 4H, bpy (H-6a), H-3, H-4"', H-6"), 8.05 (d, 1H, *J* = 2.5 Hz, H-6"), 7.95-7.81 (m, 7H, bpy (H-6a, H-5a), 7.71-7.66 (m, 2H, H-5, H-6"'), 7.48 (ddd, 1H, *J* = 4.8 Hz, *J* = 1.0 Hz, H-5"'), 5.40 (s, 2H, CH_2, CH_2Cl_2), 4.52-4.44 (m, 8H, CH_2, ethyl-ester), 1.46-1.41 (m, 12H, CH_3, ethyl-ester), 1.25 (m, 4H, CH_2, ½ mole of n-hexane), 0.90 (m, 3H, CH_3, ½ mole of n-hexane).

5.3 Results and discussion

5.3.1 Synthesis of ligand, mononuclear and heterodinuclear complexes.

The Negishi Coupling, published in 1976,[32] was the first reaction that allowed the preparation of unsymmetrical bi-aryls in good yields. The versatile nickel- or palladium-catalyzed coupling of organozinc compounds with various halides (aryl, vinyl, benzyl, or allyl) has broad scope, and is not restricted to the formation of bi-aryls. The 2,2':5',5":2",2"'-quaterpyridine (bisbpy) ligand was prepared in two steps by Negishi

coupling reaction of 2,5-dibromopyridine with 2-pyridylzinc bromide (see figure 5.11). In the first step formation of 5-bromo-2,2'-bipyridine in which coupling reaction preferentially occurs at 2-position following reported procedure by Hanan *et. al.*[33]

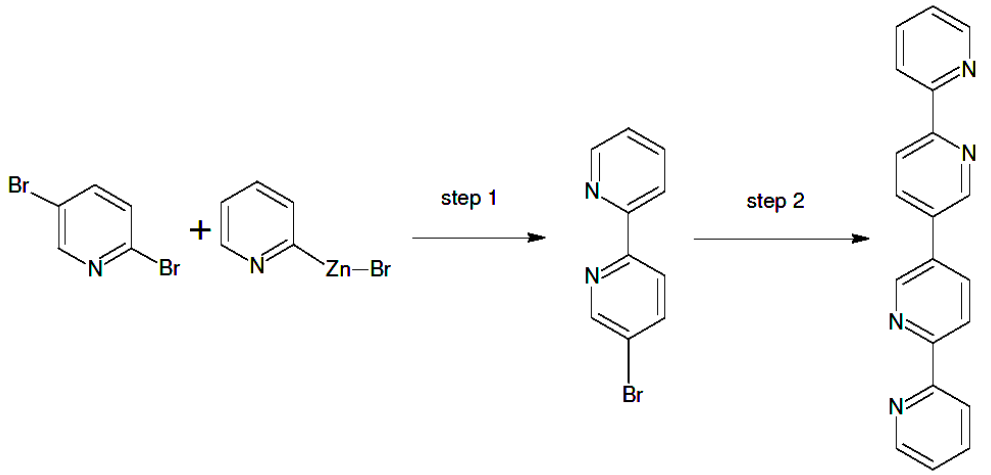

Figure 5.11: *Synthetic pathway for the formation of 2,2':5',5":2",2"'-quaterpyridine (bisbpy) ligand.*

The yield in the first step is higher (81%) with selectivity at 2-position than direct bromination of 2,2'-bpyridine gives 15 % yield.[34] The synthesis required an inert atmosphere and low temperature. In a dried two neck round bottom flask $Pd(PPh_3)_4$ (0.3 g, 0.26 mmol) and 2,5-dibromobipyridine (2.0 g, 8.44 mmol) were added under a nitrogen atmosphere. During the addition of 2-pyridylzinc bromide in THF (19.4 cm^3, 8.44 mmol) to the reaction mixture, the temperature was kept at 0^0C. At this point the reaction mixture turned brown in colour. The reaction mixture was then stirred over night at room temperature under a nitrogen atmosphere and a white precipitate formed. The reaction mixture was poured in to 200 cm^3 of a saturated aqueous solution of equimolar EDTA and Na_2CO_3 and stirred until the white precipitate dissolved and a yellow precipitate formed. The saturated basic EDTA solution formed a water soluble chelate complex with the Zn^{2+} metal ion. The aqueous solution as well as the yellow precipitate was extracted with dichloromethane (DCM) (3 x 50 cm^3). The DCM layer was dried and evaporated by vacuum. This crude product was purified on an activated neutral alumina (150 mesh size) column using hexane / ethylacetate (9.5:0.5 v/v). The second spot on the

TLC plate (R_f = 0.2) was collected as the desired compound 5-bromo-2,2'-bipyridine (5-brbpy) with a yield of 81 % (see ^{1}H-NMR in Figure 5.12).

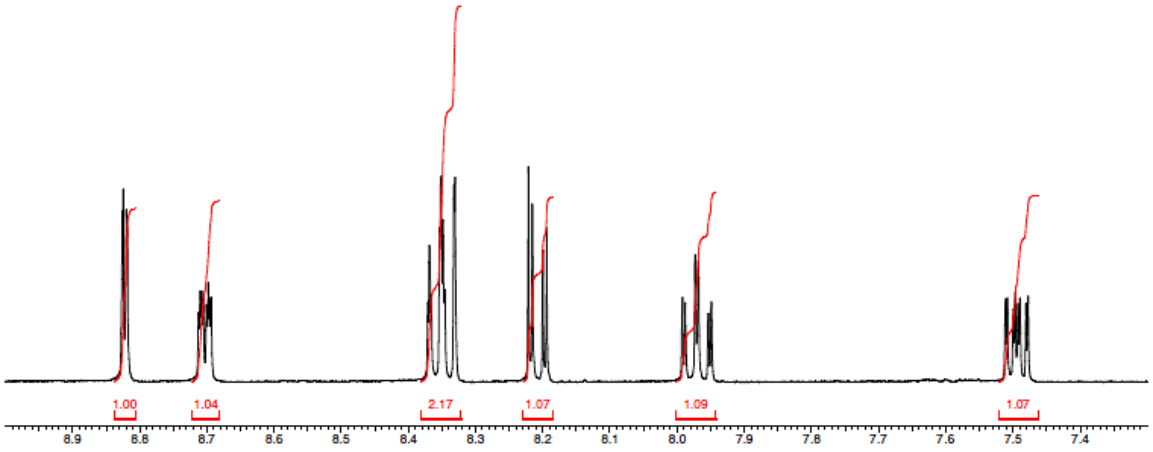

Figure 5.12: *^{1}H-NMR of 5-bromo-2,2'-bipyridine (5-brbpy) in d_6-dmso.*

In the second step 5-brbpy was used as a reactant for the Negishi's homo-coupling. A solid $[Ni(PPh_3)_2Cl_2]$ (0.557 g, 0.85 mmol) was added in to 10 cm^3 of anhydrous DMF and stirred for few minutes at room temperature under nitrogen, until the reaction mixture turned blue. Then zinc powder (Zn) (0.056 g, 0.85 mmol) was added and stirring continued at room temperature under nitrogen. The reaction mixture turned green and ultimately deep brown after 30 to 45 minutes which is the $Ni(PPh_3)_4$ catalyst (see Figure 5.13 for mechanism). Now 5-bromo-2,2'-bipyridine (5-brbpy) (0.200 g, 0.85 mmol) was added and the reaction mixture was stirred at room temperature 10 hours. The reaction mixture was poured in 150 cm^3 of 3 molar aqueous NH_4OH solution to form the water soluble chelate complexes with Ni^{2+} and Zn^{2+}. A greyish white product was precipitated out. The precipitate was extracted with ethyl acetate (3 x 50 cm^3) and the combined organic phases were dried over $MgSO_4$. Removal of the solvent in vacuo yielded the crude product which was purified by column chromatography (neutral alumina, hexane/ethyl acetate (9 : 1 v/v), TLC: R_f = 0.1) to obtain 2,2':5',2"-quaterpyridine (bisbpy) in 78 % yield, see proton-NMR in Figure 5.14.

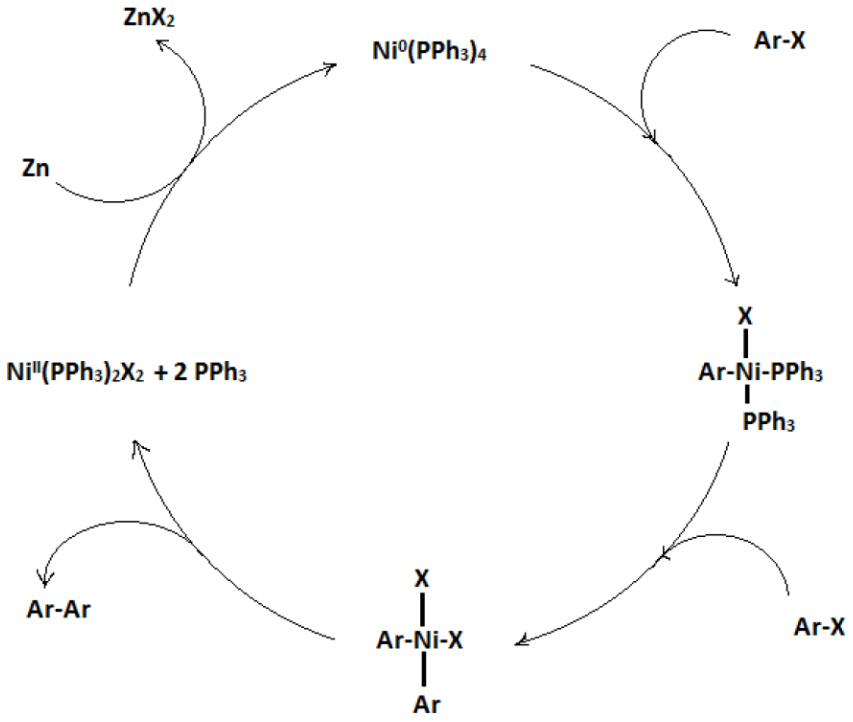

Figure 5.13: *Mechanism involved for the Negishi homo- coupling reaction.*

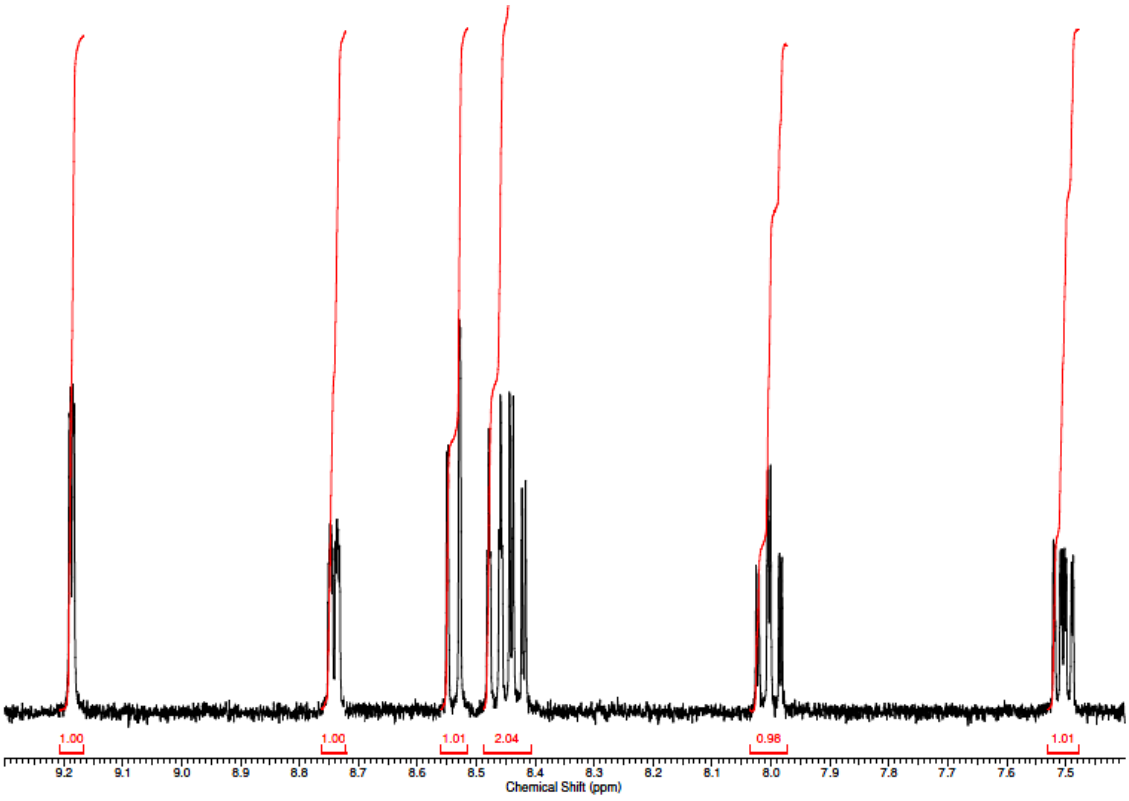

Figure 5.14: *^{1}H-NMR of 2,2':5',2"-quaterpyridine (bisbpy) ligand in d_6-dmso.*

The synthesis of the mononuclear complexes $[Ru(bpy)_2(bisbpy)]^{2+}$, $[Ru(dceb)_2(bisbpy)]^{2+}$ and heterodinuclear complexes $[Ru(bpy)_2(bisbpy)PdCl_2]^{2+}$, $[Ru(bpy)_2(bisbpy)PtCl_2]^{2+}$, $[Ru(dceb)_2(bisbpy)PdCl_2]^{2+}$, $[Ru(dceb)_2(bisbpy)PtCl_2]^{2+}$ are represented schematically in Figure 5.15.

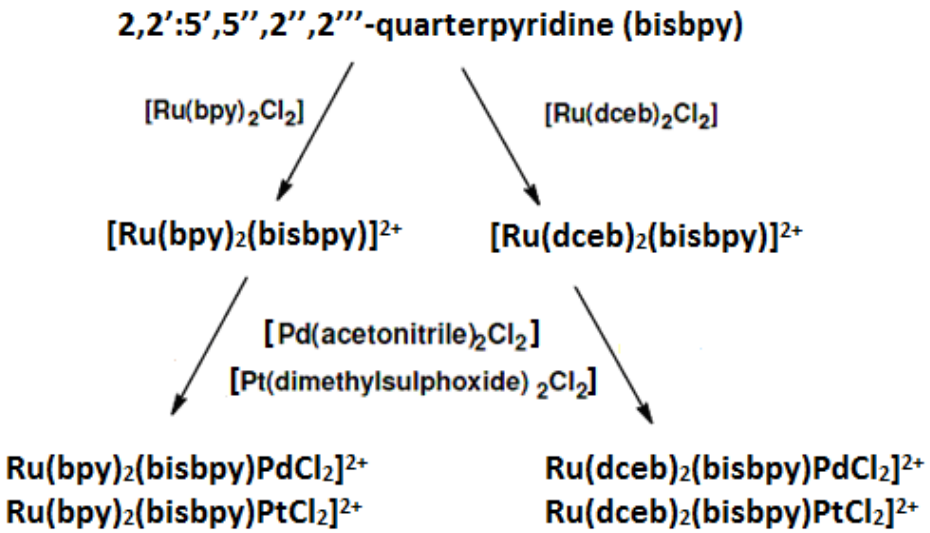

Figure 5.15: *Synthetic pathway for the formation of the mononuclear and heterodinuclear complexes of bisbpy as bridging ligand.*

From here the synthesis of all Ru(II) compounds was relatively straightforward using classical synthetic strategy of "complexes as metals / complexes as ligands". The mononuclear complexes $[Ru(bpy)_2(bisbpy)]^{2+}$ and $[Ru(dceb)_2(2,6\text{-dpp})]^{2+}$ was formed by the addition of a 1:1.5 ratio of bisbpy ligand to $[Ru(bpy)_2Cl_2]$ / $[Ru(dceb)_2Cl_2]$, and heating to reflux temperature in ethanol / water (3:1 v/v). It is necessary to dissolve the ligand completely before the slow addition of Ru(II) precursors. As the reaction proceeds, the deep violet colour of the $[Ru(bpy)_2Cl_2]$ / green colour of $[Ru(dceb)_2Cl_2]$ solution is gradually replaced by an orange-red colour, which indicates the presence of the $[Ru(bpy)_2(bisbpy)]^{2+}$ and $[Ru(dceb)_2(bisbpy)]^{2+}$ complex. The ethanol was removed at this stage and the chloride counter ion replaced by a PF_6^- counter ion which led to precipitation of the complexes from the aqueous solution. The PF_6^- salts of these type of complexes tend to be only sparingly water soluble and soluble in organic solvents which greatly eases the isolation, purification and analysis of these compounds. The yields for

the monomer complex $[Ru(bpy)_2(bisbpy)]^{2+}$ was 86% and for $[Ru(dceb)_2(bisbpy)]^{2+}$ was 83%. The monomers were stable in sunlight and at room temperature.

The heterodinuclear Ru-Pd / Ru-Pt complexes were synthesised by the addition of a 1:1 ratio of the ruthenium(II) mononuclear complexes and the $[Pd(acetonitrile)_2Cl_2]$/ $[Pt(dimethylsulphoxide)_2Cl_2]$ complexes, followed by heating to reflux in dichloromethane as a solvent. $[Pd(acetonitrile)_2Cl_2]$ / $[Pt(dimethylsulphoxide)_2Cl_2]$ was generally added first and allowed to dissolved completely in dichloromethane before adding the more soluble monomers $[Ru(bpy)_2(bisbpy)]^{2+}$ and $[Ru(dceb)_2(bisbpy)]^{2+}$. After 24 hours of reflux in dichloromethane, the complexes were precipitated by addition of n-hexane. The yields of all the heterodinuclear complexes were from 88 – 98% after recrystallization in acetone/water (3:1 v/v). These complexes were stable in visible light and at room temperature also did not require any inert conditions for their synthesis.

5.3.2 ^{1}H-NMR Spectroscopy

An important feature of low-spin d^6 system is that the complexes are diamagnetic and sharp NMR spectra are obtained easily. In this section the effects of coordination on the chemical shifts of the protons are discussed. [35] When comparing the proton NMR spectrum of $[Ru(bpy)_3]^{+2}$ with the spectrum of free bpy, a number of differences are apparent. After coordination to the metal ion, the ligand is force to adopt a cis conformation, whereas the free bpy ligand is presumed to have a *trans* structure.[35(g), 35(h)] The steric crowding of the H3 protons in $[Ru(bpy)_3]^{+2}$ gives rise to a strong Van der Waals interaction and a downfield shift of 0.33 ppm is observed.[35(j)] The second important effect is that in the complex $[Ru(bpy)_3]^{+2}$ the H6 proton is directed just above a pyridine ring of an adjacent bpy ligand.[35(i), 35(j)] This diamagnetic anisotropic effect causes an upfield shift of approximately 1 ppm. The third effect is the influence of the metal ion itself: due to the σ-donor behaviour, the electron density at the ligand atoms diminishes and a general downfield shift is present. A similar trend was observed in the proton-NMR resonance of H3 and H6 protons of the heteroleptic Ru(II) complexes containing 2,2':5',5":2", 2"'-quaterpyridine (bisbpy) as bridging ligand.

5.3.2.1 ^{1}H-NMR of the mononuclear complexes.

Figure 5.9 shows the numbering of the ruthenium(II) mononuclear complexes $[Ru(bpy)_2(bisbpy)]^{2+}$ and $[Ru(dceb)_2(bisbpy)]^{2+}$ and their ^{1}H-NMR spectra are shown in Figure 5.16. The chemical shifts of the ruthenium(II) monomers with the 2,2':5',5":2", 2"'-quaterpyridine (bisbpy) ligand in d_3-acetonitrile are outlined in table 5.1. For simplicity to distinguish between the protons of the pyridine rings {[(Ring A (proton sign (H3 – H6) and Ring B (proton sign (H3' – H6'): (free) non-complexed] and [Ring C (proton sign (H3" – H6") and Ring D (proton sign (H3"' – H6"'): (metal) complexed)]} of the bisbpy ligand and the bpy / dceb ligands protons are numbered H3a – H6a. These bpy's / dceb's protons occur in the expected range and will not be discussed here. The same numbering system of the bisbpy ligand for the homodinuclear $[Ru(bpy)_2(bisbpy)Ru(bpy)_2]^{4+}$ complex was used here and comparable chemical shifts were observed for metal complexed bisbpy ligand protons as reported by Vos and coworkers.[28]

In this section, the bisbpy protons of the mononuclear complexes $[Ru(bpy)_2(bisbpy)]^{2+}$ and $[Ru(dceb)_2(bisbpy)]^{2+}$ are discussed. As expected, due to coordination, there is a clear difference between the protons of the two bipyridine systems (Ring A/B and Ring C/D) of the bisbpy ligand, as shown in Figure 5.9. The H6" and H6"' protons of the metal bound (ring C/D) experience the ring current of an adjacent bpy and are strongly shifted upfield as a result (H6" = 7.96 ppm and H6"' = 7.77 ppm).[28] The protons H6 and H 6' (ring A/B) are both present at around 8.70 ppm in d_3-acetonitrile. This large difference between ring A/B and ring C/D for the H6/H6' and H6"/H6"' resonances demonstrates that the H6"/H6"' must be assigned to the metal-bound bipyridine system as it is shifted 0.74 ppm upfield. This is due to through space interactions occurring between H6"/H6"' and bpy ring. In addition protons in close proximity to such large atoms, such as a metal ion, are greatly shielded from the induced magnetic field of the NMR and therefore require a greater applied magnetic field strength for resonance.[36] The steric crowding of the H3, H3', H3" and H3"' protons in complexes $[Ru(bpy)_2(bisbpy)]^{2+}$ and $[Ru(dceb)_2(bisbpy)]^{2+}$ of the bisbpy ligand gives rise to a strong Van der Waals

interaction and a significant downfield shift is observed. In general the resonance of bisbpy protons in the complexes $Ru(bpy)_2(bisbpy)]^{2+}$ and $[Ru(dceb)_2(bisbpy)]^{2+}$ are approximately the same (see Table 5.1).

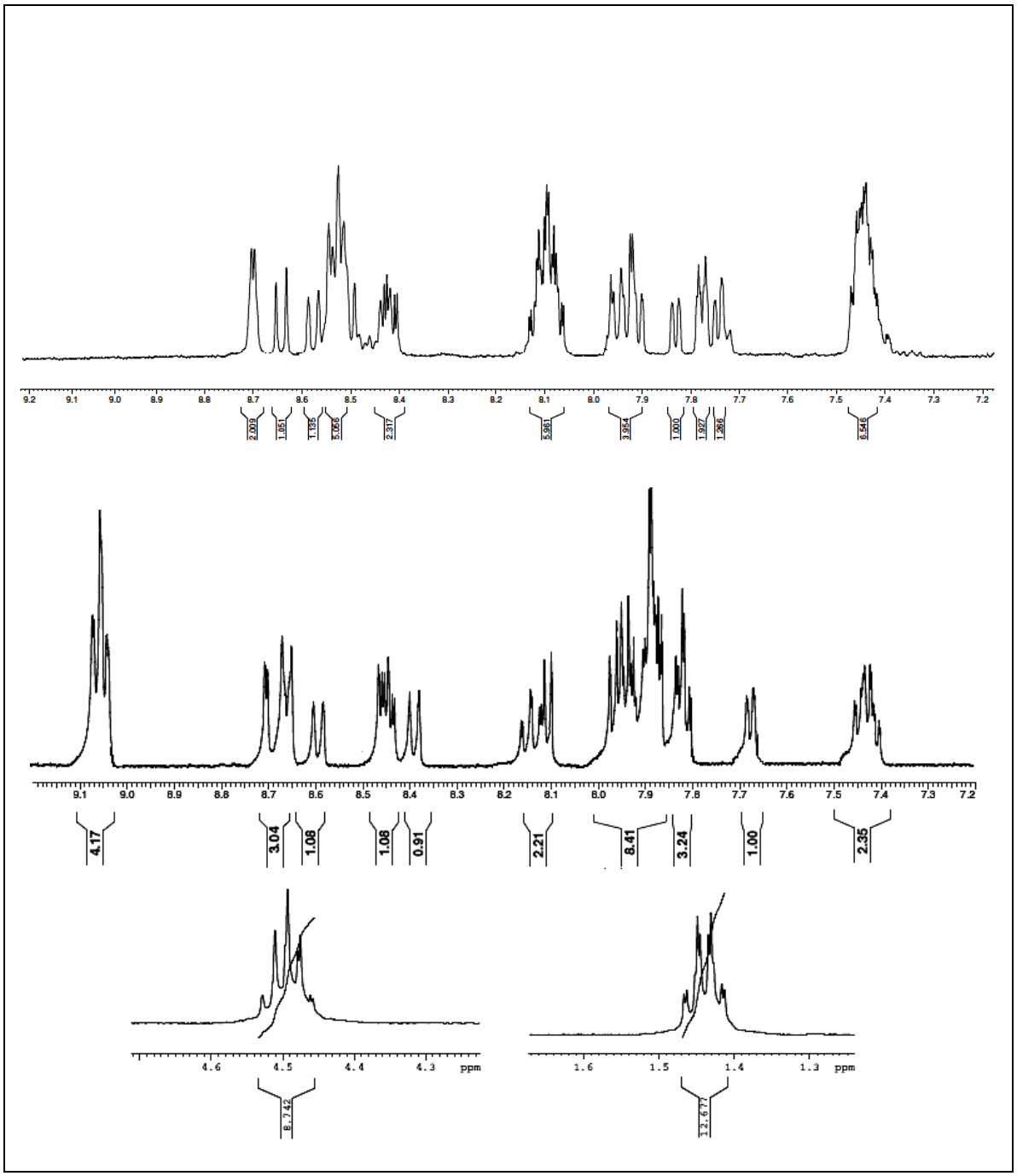

Figure 5.16: *^{1}H-NMR spectra of $Ru(bpy)_2(bisbpy)]^{2+}$ (top) and $[Ru(dceb)_2(bisbpy)]^{2+}$ (bottom) in Acetonitrile-d_3.*

Ring A	**H6(d)**	**H5(t)**	**H4(t)**	**H3(d)**
$[Ru(bpy)_2(bisbpy)]^{2+}$	8.71	7.46	7.92	7.92
$[Ru(dceb)_2(bisbpy)]^{2+}$	8.68	7.47	7.90	7.90
$[Ru(bpy)_2(bisbpy)PdCl_2]^{2+}$	9.21	7.70	8.23	8.23
$[Ru(dceb)_2(bisbpy)PdCl_2]^{2+}$	9.23	7.70	8.23	8.23
$[Ru(bpy)_2(bisbpy)PtCl_2]^{2+}$	9.51	7.70	8.27	8.18
$[Ru(dceb)_2(bisbpy)PtCl_2]^{2+}$	9.49	7.71	8.25	8.13
Ring B	**H6'(d)**	**H5'(t)**	**H4'(t)**	**H3'(d)**
$[Ru(bpy)_2(bisbpy)]^{2+}$	8.71	-	7.96	8.43
$[Ru(dceb)_2(bisbpy)]^{2+}$	8.73	-	7.96	8.40
$[Ru(bpy)_2(bisbpy)PdCl_2]^{2+}$	9.17	-	8.43	8.30
$[Ru(dceb)_2(bisbpy)PdCl_2]^{2+}$	9.20	-	8.44	8.27
$[Ru(bpy)_2(bisbpy)PtCl_2]^{2+}$	9.54	-	8.45	8.24
$[Ru(dceb)_2(bisbpy)PtCl_2]^{2+}$	9.57	-	8.45	8.18
Ring C	**H6"(d)**	**H5"(t)**	**H4"(t)**	**H3"(d)**
$[Ru(bpy)_2(bisbpy)]^{2+}$	7.96	-	8.41	8.64
$[Ru(dceb)_2(bisbpy)]^{2+}$	7.97	-	8.46	8.67
$[Ru(bpy)_2(bisbpy)PdCl_2]^{2+}$	8.02	-	8.41	8.67
$[Ru(dceb)_2(bisbpy)PdCl_2]^{2+}$	8.00	-	8.48	8.70
$[Ru(bpy)_2(bisbpy)PtCl_2]^{2+}$	8.06	-	8.42	8.69
$[Ru(dceb)_2(bisbpy)PtCl_2]^{2+}$	8.05	-	8.49	8.72
Ring D	**H6"'(d)**	**H5"'(t)**	**H4"'(t)**	**H3"'(d)**
$[Ru(bpy)_2(bisbpy)]^{2+}$	7.74	7.44	8.11	8.58
$[Ru(dceb)_2(bisbpy)]^{2+}$	7.68	7.45	8.16	8.61
$[Ru(bpy)_2(bisbpy)PdCl_2]^{2+}$	7.78	7.46	8.12	8.61
$[Ru(dceb)_2(bisbpy)PdCl_2]^{2+}$	7.69	7.48	8.16	8.62
$[Ru(bpy)_2(bisbpy)PtCl_2]^{2+}$	7.78	7.46	8.12	8.61
$[Ru(dceb)_2(bisbpy)PtCl_2]^{2+}$	7.69	7.48	8.17	8.63
Bipyridine protons	**H6a(d)**	**H5a(t)**	**H4a(t)**	**H3a(d)**
$[Ru(bpy)_2(bisbpy)]^{2+}$	7.83, 7.79 - 7.72	7.47 - 7.39	8.15 - 8.05	8.62 - 8.50
$[Ru(dceb)_2(bisbpy)]^{2+}$	8.13 – 7.84		-	9.13 – 9.08
$[Ru(bpy)_2(bisbpy)PdCl_2]^{2+}$	7.83, 7.79 - 7.72	7.47 - 7.39	8.15 - 8.05	8.62 - 8.50
$[Ru(dceb)_2(bisbpy)PdCl_2]^{2+}$	8.13 – 7.84		-	9.13 – 9.08
$[Ru(bpy)_2(bisbpy)PtCl_2]^{2+}$	7.83, 7.79 - 7.72	7.47 - 7.39	8.15 - 8.05	8.62 - 8.50
$[Ru(dceb)_2(bisbpy)PtCl_2]^{2+}$	8.13 – 7.84		-	9.13 – 9.08

Table 5.1: *Chemical shifts (in ppm) of all synthesised complexes in d_3-acetonitrile.*

Using 2-D COSY spectra of the mononuclear complexes $Ru(bpy)_2(bisbpy)]^{2+}$ and $[Ru(dceb)_2(bisbpy)]^{2+}$, it was possible to assign the chemical shifts for the all bisbpy ligand protons of the four pyridine rings (A, B, C and D), which are documented in Table 5.1. In the case of $[Ru(dceb)_2(bisbpy)]^{2+}$, the H3a protons of the peripheral ligand 'dceb' is shifted from a range of 8.57 – 8.52 ppm (in bpy) to a range of 9.12-9.07 ppm (in dceb) downfield due to the electron withdrawing carboxylic ester group present at H4a position. Also the same effect caused a slight downfield shift for H6a and H5a protons of the dceb ligand (see Table 5.1 below). The ethyl ester groups are present at 4.54 – 4.46 (m, 8H, CH_2) four quartet signals and similarly resonance at 1.50 – 1.40 (m, 12H, CH_3) four triplet signals overlap in this region. 2-D COSY ^{1}H-NMR spectra of the complexes $[Ru(bpy)_2(bisbpy)]^{2+}$ and $[Ru(dceb)_2(bisbpy)]^{2+}$ are recorded in d_3-acetonitrile and are depicted in Figure 5.17 and Figure 5.18, respectively.

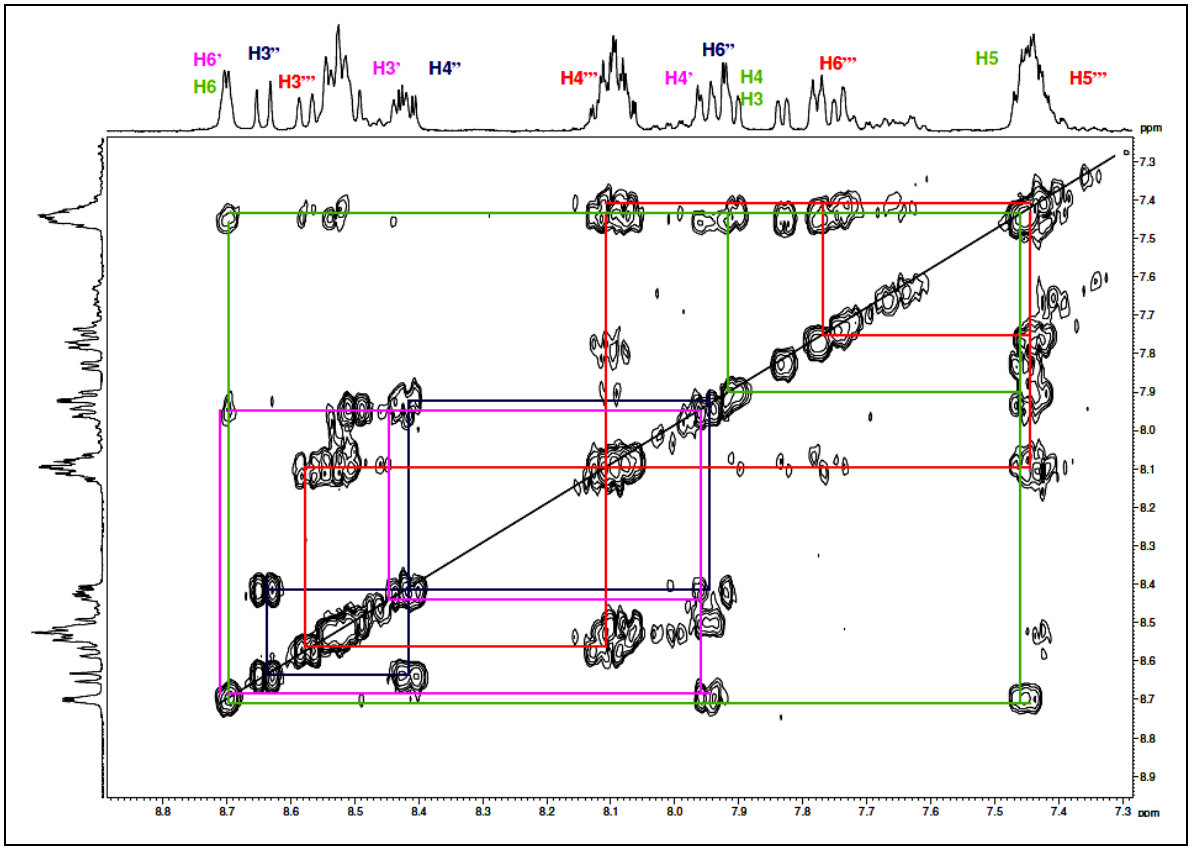

Figure 5.17: *2D-COSY ^{1}H-NMR of the $[Ru(bpy)_2(bisbpy)]^{2+}$ in d_3-acetonitrile.*

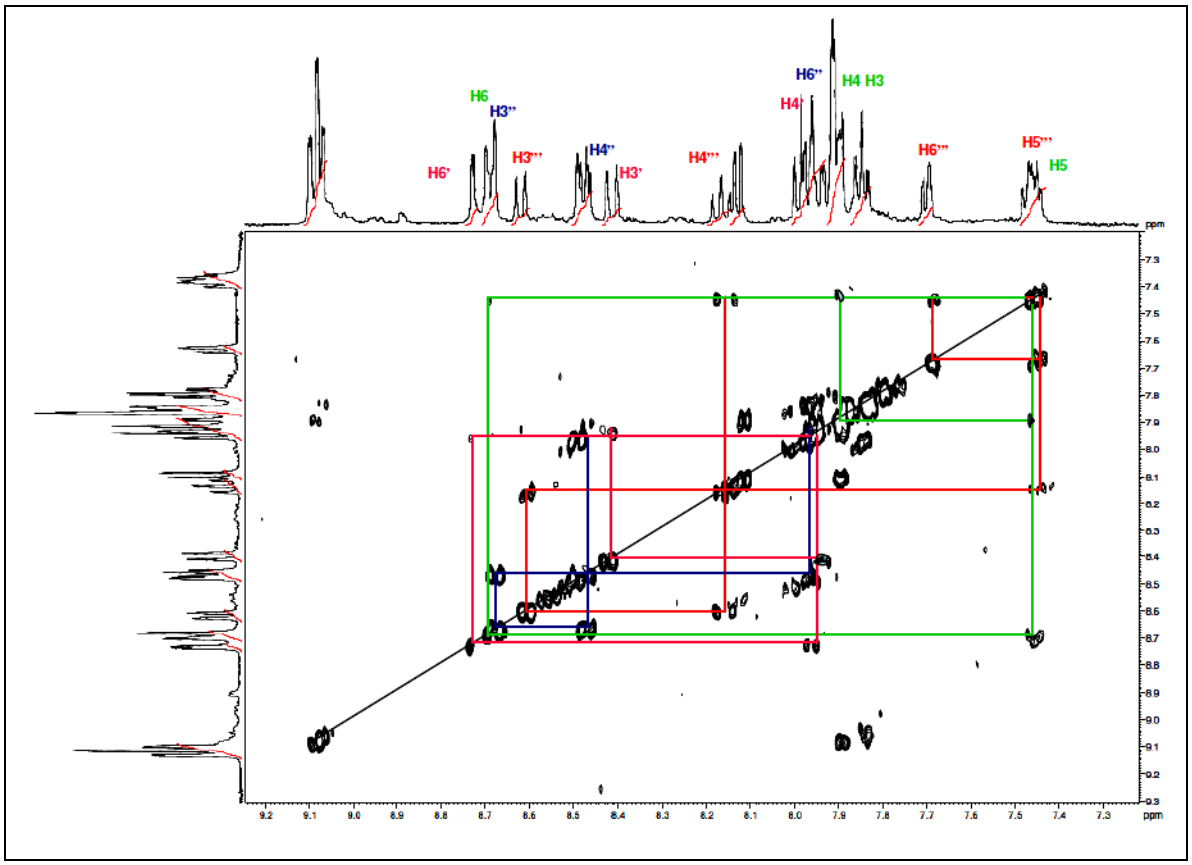

Figure 5.18: *2D-COSY ^{1}H-NMR of the $[Ru(bpy)_2(bisbpy)]^{2+}$ in d_3-acetonitrile.*

5.3.2.2 ^{1}H-NMR of the heterodinuclear complexes.

Figure 5.10, shows the numbering of the ruthenium(II) heterodinuclear complexes $[Ru(bpy)_2(bisbpy)PdCl_2]^{2+}$, $[Ru(bpy)_2(bisbpy)PtCl_2]^{2+}$, $[Ru(dceb)_2(bisbpy)PdCl_2]^{2+}$ and $[Ru(dceb)_2(bisbpy)PtCl_2]^{2+}$ and their ^{1}H-NMR spectra are shown in Figure 5.19. The bpy and dceb ligands protons have similar chemical shifts as mentioned above for mononuclear complexes. Following complexation of the relevant Ru(II) mononuclear with $[Pd(acetonitrile)_2Cl_2]$ and $[Pt(dmso)_2Cl_2]$, the pyridine ring A/B protons of the heterodinuclear complexes are shifted downfield due to the Pd(II)/ Pt(II) metal centre (see in Table 5.1).

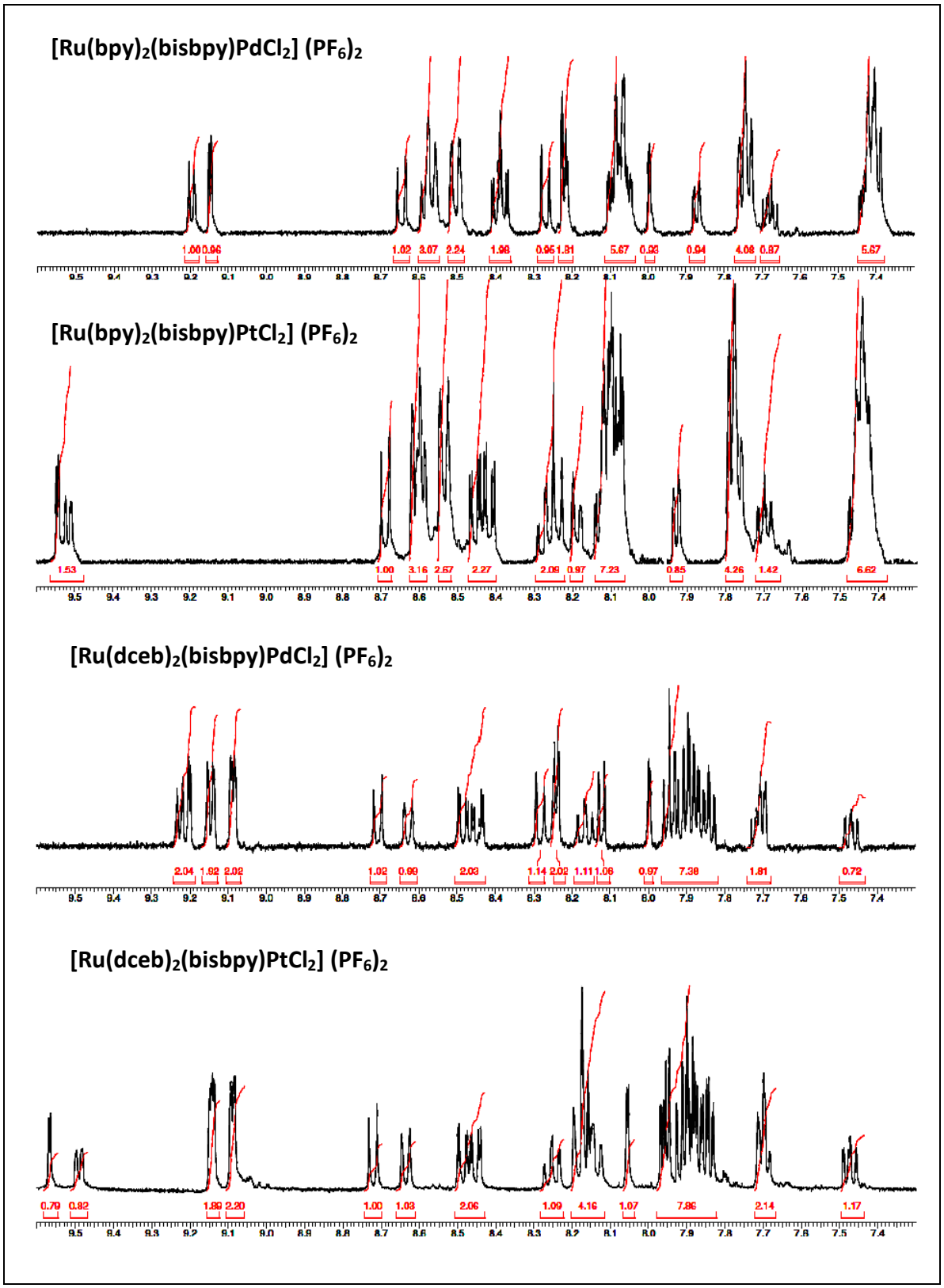

Figure 5.19: *^{1}H-NMR spectra of heterodinuclear complexes in Acetonitrile-d_3.*

In all heterodinuclear complexes, the pyridine ring C/D (complexed) protons (H3" – H6") / H3"' – H6"') are shifted slight downfield (0.01 – 0.05 ppm) as shown in Table 5.1. There is a large downfield shift 0.40 – 0.70 ppm for the pyridine ring A/B of all the heterodinuclear complexes compared to the mononuclear complexes. The H6 is the most deshielded proton due to Pd / Pt complexation. The two Pd complexes $[Ru(bpy)_2(bisbpy)PdCl_2]^{2+}$ and $[Ru(dceb)_2(bisbpy)PdCl_2]^{2+}$ undergo upfield shifts for H6 / H6' compared to the two Pt complexes $[Ru(bpy)_2(bisbpy)PtCl_2]^{2+}$ and $[Ru(dceb)_2(bisbpy)PtCl_2]^{2+}$. This is attributed to the less efficient metal deshielding effect of the Pd metal (4d orbital) with compared to the Pt metal (5d orbital) as depicted in Table 5.1. In these four heterodinuclear complexes (two Ru-Pd and two Ru-Pt complexes), the H3 – H5 and H3' – H5' observed have similar chemical shifts but for proton H6 and H6' observed different chemical shifts when complexed with Pd metal compared to Pt metal. This is attributed to the metal deshielding properties of Pd and Pt metal as shown in Table 5.1. 2D-COSY ^{1}H-NMR provides useful information for the correlation of the rest of the protons; the four complexes 2D-COSY ^{1}H-NMR spectra are depicted in Figure 5.20, 5.21, 5.22 and 5.23.

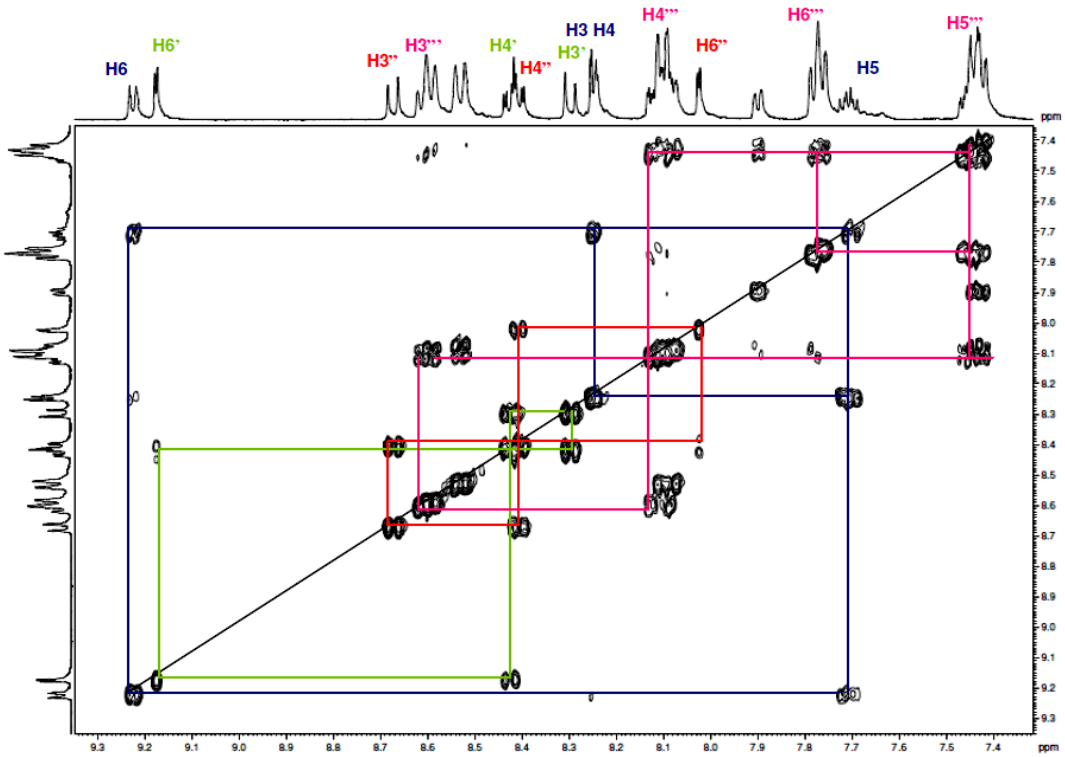

Figure 5.20: *2D-COSY NMR of the $[Ru(bpy)_2(bisbpy)PdCl_2]^{2+}$ in d_3-acetonitrile.*

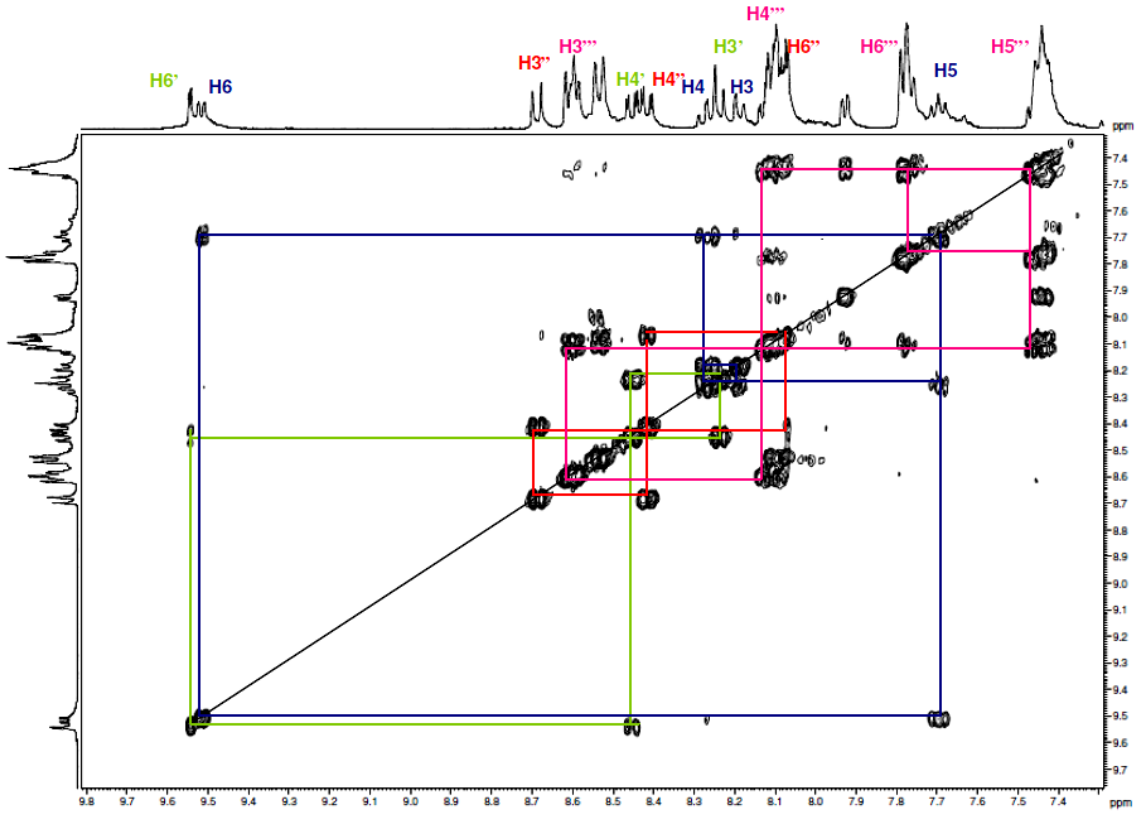

Figure 5.21: *2D-COSY NMR of the* $[Ru(bpy)_2(bisbpy)PtCl_2]^{2+}$ *in* d_3*-acetonitrile.*

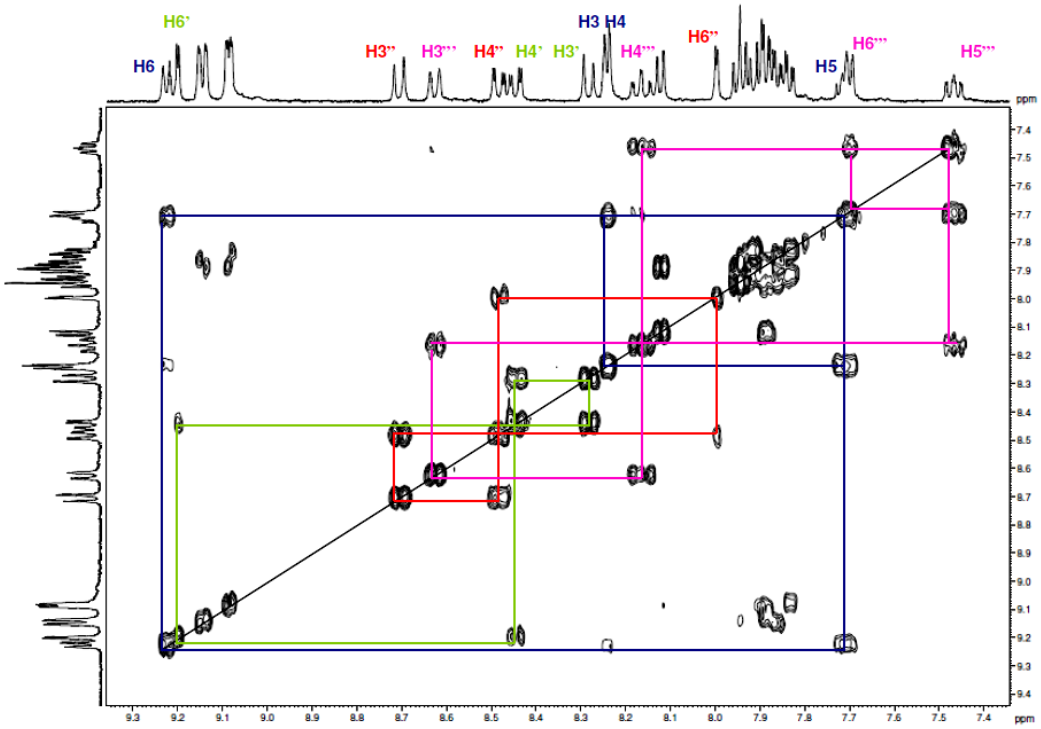

Figure 5.22: *2D-COSY NMR of the* $[Ru(dceb)_2(bisbpy)PdCl_2]^{2+}$ *in* d_3*-acetonitrile.*

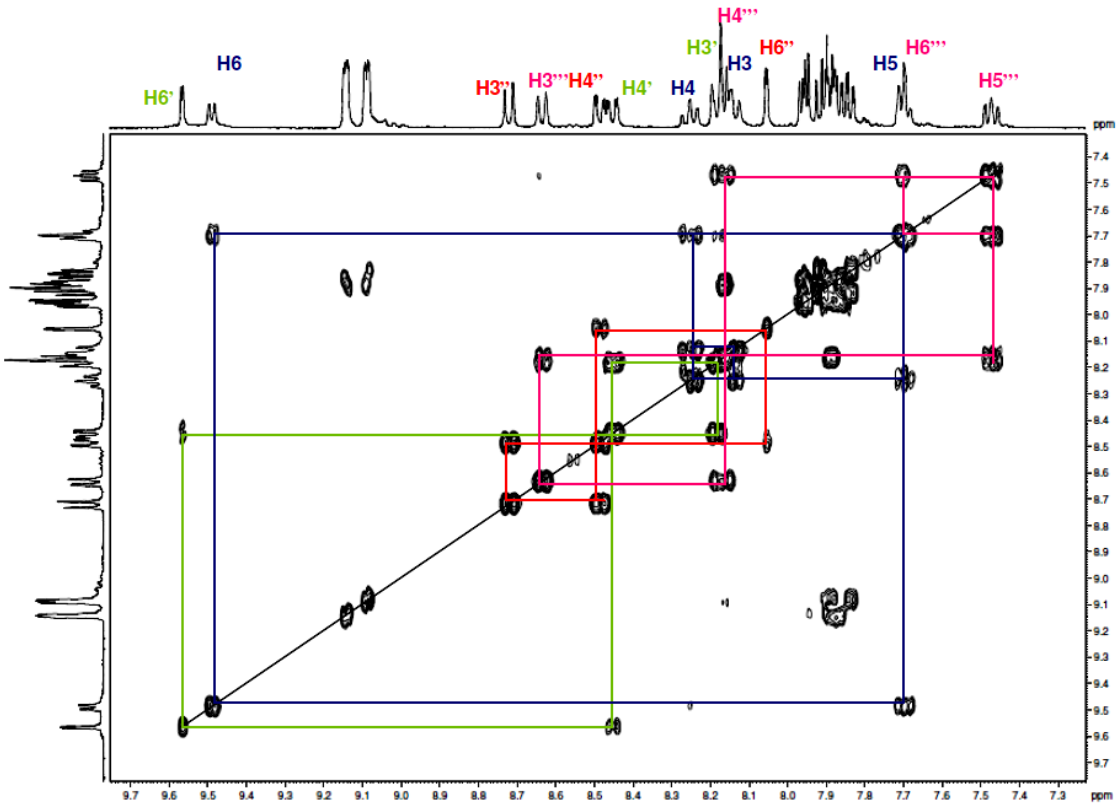

Figure 5.23: *2D-COSY NMR of the [Ru(dceb)$_2$(bisbpy)PtCl$_2$]$^{2+}$ in d$_3$-acetonitrile.*

The complexes [Ru(dceb)$_2$(bisbpy)PdCl$_2$]$^{2+}$ and [Ru(dceb)$_2$(bisbpy)PtCl$_2$]$^{2+}$ contained dichloromethane and n-hexane which is shown in the ^{1}H-NMR (Figure 5.25) and also confirmed by CHN analysis.

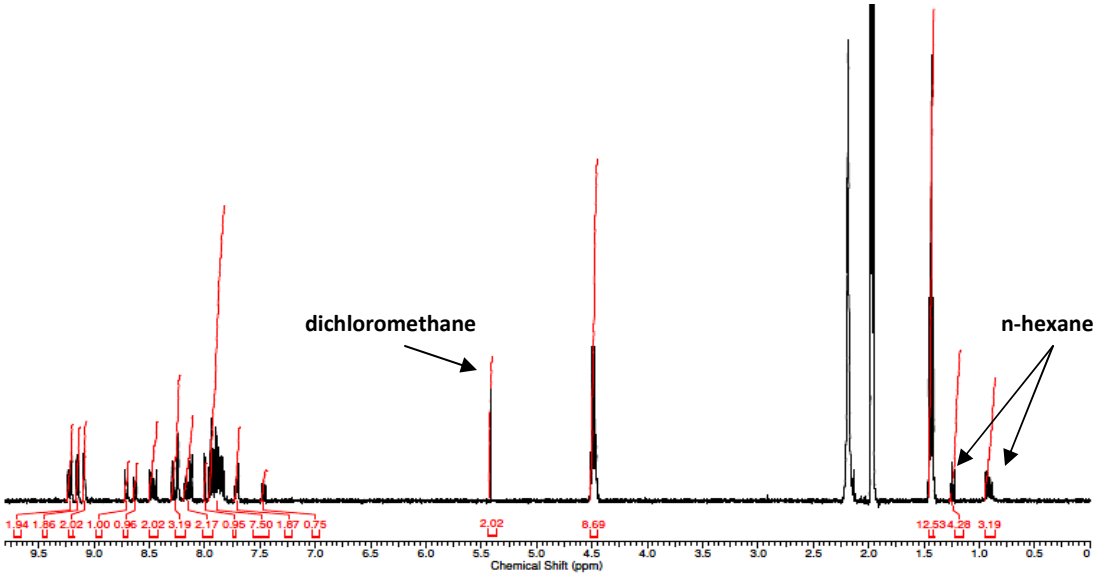

Figure 5.25: ^{1}H-NMR of [Ru(dceb)$_2$(bisbpy)PdCl$_2$]$^{2+}$ in CD$_3$CN.

5.3.3 UV-Vis absorption, emission and luminescence properties of the Ru(II) mononuclear and heterodinuclear complexes.

The photophysics and spectroscopy of the ruthenium(II) polypyridyl homodinuclear complexes with bisbpy as a bridging ligand and Ru heterodinuclear complexes have been studied.[28] These studies provided information of the intramolecular interaction between the ligands and the metal centre present.

Complex	Absorption λ_{max} (nm) ($\varepsilon = 10^4\ M^{-1}cm^{-1}$)	Emission λ_{max} (nm) at 293 K	τ [a] (ns) (deaerated) at 293 K	Φ [b] (deaerated) at 293 K
$[Ru(bpy)_3]^{2+}$ [37]	453 (1.3)	605	576	0.068 [c, 37]
$[Ru(dcmb)_3]^{2+}$ [38]	467 (1.97)	631	1174	-
$[Ru(bpy)_2(bisbpy)Ru(bpy)]^{4+}$ [28, 39]	450 (2.53)	663	215 [d]	0.040
$[Ru(bpy)_2(bisbpy)]^{2+}$	448 (1.16)	633	755	0.040
$[Ru(dceb)_2(bisbpy)]^{2+}$	475 (1.13)	647	825	0.101
$[Ru(bpy)_2(bisbpy)PdCl_2]^{2+}$ [e]	447 (1.02)	655	τ_1 = 17 (37 %) τ_2 = 218 (63%)	0.044
$[Ru(bpy)_2(bisbpy)PtCl_2]^{2+}$	447 (1.15)	664	331	0.017
$[Ru(dceb)_2(bisbpy)PdCl_2]^{2+}$ [e]	475 (1.76)	647	τ_1 = 42 (60 %) τ_2 = 325 (40 %)	0.033
$[Ru(dceb)_2(bisbpy)PtCl_2]^{2+}$	475 (1.63)	644	534	0.054

[a] *Lifetime determined by time correlated single photon counting at 293 K in deaerated acetonitrile solution.*

[b] *Quantum yield of an excited state emission (deaerated Acetonitrile at λ = 455 nm).*

[c] *Lifetime of the $[Ru(bpy)_3]^{2+}$ in deaerated acetonitrile using freeze-pump-thaw degassing.*

[d] *Lifetime in aerated acetonitrile at 293 K temperature.*

[e] *Bi-exponential decay fits curve (relative percentage in bracket).*

Table 5.2: *Photophysical properties of all ruthenium monomer and heterodinuclear complexes synthesised carried out in spectroscopy grade aerated acetonitrile at 293 K.*

Time correlated single photon counting (TCSPC) was used to determine the emission lifetime of the compounds, as described in chapter 2, these were carried out by Mr. Suraj Soman. The TCSPC measurements were carried out at room temperature in deaerated acetonitrile solution. All complexes were excited at wavelength of 360 nm and the time response of their emission at the appropriate wavelength was recorded. The results are shown in figure 5.29, 5.30 and 5.31. The corresponding lifetimes for mononuclear and heterodinuclear Ru – Pt complexes were obtained using single exponential fits on the decay curves, and bi-exponential fits for heterodinuclear Ru – Pd complexes with relative percentage are as listed in Table 5.2.

UV-Vis absorption data are shown in Table 5.2; with spectra of are shown in Figure 5.26, 5.27 and 5.28. The absorption spectra of all these compounds are essentially similar to that of other Ru(II) – based polypyridine complexes and can be accordingly interpreted.[3, 28, 39] The high intensity absorption bands in the UV region can be ascribed to ^{1}LC transitions. In particular, the peak at 280 nm can be attributed to the bpy peripheral ligand and 320 nm attributed to the dceb peripheral ligand. The band around 330 – 360 nm is assigned to the bisbpy bridging ligand. Moderately intense ^{1}MLCT bands were observed in the 400 – 550 nm regions. One can note the non-chromophoric nature of the $PdCl_2$ / $PtCl_2$ fragments in the sense that there is no absorption band that clearly involves this unit. However, following coordination with $PdCl_2$ / $PtCl_2$ changes in the UV-Vis spectra are indicated at 330 nm as shown in Figure 5.27 and 5.28.

The spectra obtained for the complex $[Ru(bpy)_2(bisbpy)]^{2+}$ (see Figure 5.26) is in good agreement with the results of homodinuclear compound $[Ru(bpy)_2(bisbpy)Ru(bpy)_2]^{4+}$ reported by Vos and coworkers.[28, 39] A comparison of the mononuclear $[Ru(bpy)_2(bisbpy)]^{2+}$ compound with the homoleptic $[Ru(bpy)_3]^{2+}$ complex suggests that the absorption bands at 325 nm is based on the bisbpy ligand. The very intense peak at 285 nm is assigned to bpy, due to its appearance in all the spectra. [28, 39] In the visible region, the mononuclear compound $[Ru(bpy)_2(bisbpy)]^{2+}$ has a broad absorption peak with two shoulders. One shoulder is at 425 nm and the second shoulder is situated at lower energy, at 448 nm. Those peaks in the visible region belong to metal to ligand

charge transfer transitions. In contrast, the MLCT peak of the homoleptic $[Ru(bpy)_3]^{2+}$ shows only one clear maximum at 453 nm.[37] The broad peak in the mixed ligand complex $[Ru(bpy)_2(bisbpy)]^{2+}$ is explained by considering the contributions of Ru → bpy as well as Ru → bisbpy MLCT transitions, whereas the shoulder at 448 nm can be assigned to a Ru → bisbpy π* MLCT.[28] The superposition of those peaks results in the broad absorption features. The energy shift of the MLCT bands compared to $[Ru(bpy)_3]^{2+}$ are explained by the higher π-acceptor and weaker σ – donor properties of bisbpy compared to bpy. Due to the weaker σ – donor strength the metal d-orbitals are stabilised. Therefore, the energy gap between the ruthenium t_{2g} orbitals and the bpy π* orbital increases, resulting in a blue shift of this transition (Ru → bpy ^{1}MLCT) in comparison to $[Ru(bpy)_3]^{2+}$.

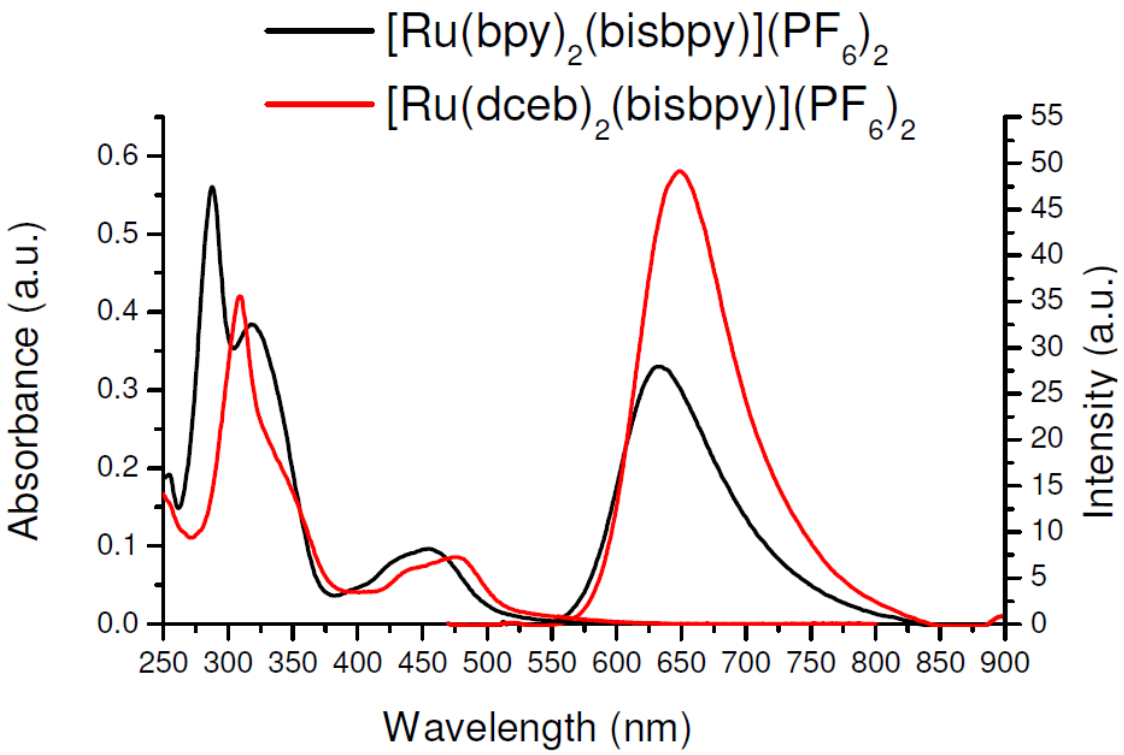

Figure 5.26: *Absorption and emission spectra of the $[Ru(bpy)_2(bisbpy)]^{2+}$ (black) (λ_{ex} = 448 nm) and $[Ru(dceb)_2(bisbpy)]^{2+}$(red) ($\lambda_{ex}$ = 475 nm) at room temperature in acetonitrile solution (deaerated).*

The ruthenium monomer complex $[Ru(bpy)_2(bisbpy)]^{2+}$ exhibit luminescence at room temperature in the red region of the spectrum following excitation with 448 nm (Figure 5.26). The complex $[Ru(bpy)_2(bisbpy)]^{2+}$ emits at 633 nm with an excited state lifetime (τ) of 755 ns and Φ_{em} of 0.04 in deaerated acetonitrile. The emission maxima were observed at 633 nm, indicates a bipyridine based emission, and is 33 nm blue shifted compared to homodinuclear complex $[Ru(bpy)_2(bisbpy)Ru(bpy)_2]^{4+}$ (τ = 215 ns in aerated acetonitrile).[28] In $[Ru(bpy)_2(bisbpy)\text{-}Ru(bpy)_2]^{4+}$ compounds the emitting state may be based on the bisbpy bridging ligand or on the peripheral bipyridyl ligands but the absorption spectrum of $[(bpy)_2Ru(bisbpy)Ru(bpy)_2]^{4+}$ shows a strong shoulder in the UV region at 330 nm which may indicate lower energy $\pi - \pi^*$ transitions in the bridging ligand.[28] In comparison, the emission maximum for $[Ru(bpy)_3]^{2+}$ is situated at 605 nm. Considering the homoleptic complex $[Ru(bpy)_3]^{2+}$ the originating level must be the π^*-orbital of the bipyridine ligands (τ = 860 ns, Φ_{em} = 0.068 deaerated acetonitrile).[37]

In case of the 4,4'-Diethoxycarbonyl-2,2'-bipyridine (dceb) mononuclear analogue complex $[Ru(dceb)_2(bisbpy)]^{2+}$ (see figure 5.26), The comparison of the mononuclear ester $[Ru(dceb)_2(bisbpy)]^{2+}$ compound with the homoleptic $[Ru(dcmb)_3]^{2+}$ (dcmb = 4,4'-Dimethoxycarbonyl-2,2'-bipyridine)[38] complex allows the allocation of the absorption bands at 350 nm to the bisbpy ligand. Also the very intense peak at 307 nm can be assigned to dceb, due to their appearance in all the spectra and better π-acceptor. Transitions in the ultraviolet part of the spectrum belong to ligand centered absorptions (dceb and bisbpy ligands). In the visible region, a mononuclear compound $[Ru(dceb)_2(bisbpy)]^{2+}$ feature a broad absorption peak with two shoulders. One shoulder is at 430 nm (Ru $\rightarrow$ dceb; MLCT) and the second shoulder is situated at lower energy at 475 nm (Ru $\rightarrow$ bisbpy; MLCT). These peaks in the visible area of the light belong to metal to ligand charge transfer transitions. In case of homoleptic $[Ru(dcmb)_3]^{2+}$ a single absorption with maximum at 467 nm (Ru $\rightarrow$ dcmb; ^{1}MLCT) was observed.[38] The absorption maxima was red shifted in the case of the heteroleptic compound $[Ru(dceb)_2(bisbpy)]^{2+}$ probably occurs as a result of a decrease in symmetry and an effect of electron-withdrawing properties. The superposition of those peaks results in the broad absorption features. The shift of the MLCT bands compared to $[Ru(dcmb)_3]^{2+}$ is

explained by the higher π-acceptor and weaker σ – donor properties of bisbpy compared to dceb. Due to the weaker σ – donor strength the metal d-orbitals are stabilised. Therefore, the energy gap between the ruthenium t_{2g} orbitals and the dceb π* orbital increases, resulting in a blue shift of this transition (Ru → dceb ^{1}MLCT) in comparison to $[Ru(dcmb)_3]^{2+}$.[38]

The ruthenium mononuclear complex $[Ru(dceb)_2(bisbpy)]^{2+}$ exhibit luminescence at room temperature in the red region of the spectrum after excitation with 475 nm (Figure 5.26). The complex $[Ru(dceb)_2(bisbpy)]^{2+}$ emits at 647 nm with an excited state lifetime (τ) of 825 ns and Φ_{em} of 0.101 in deaerated acetonitrile. In comparison, the emission maximum for $[Ru(dcmb)_3]^{2+}$ is situated at 631 nm (τ = 825 ns in deaerated acetonitrile).[38] Generally, in the case of ruthenium polypyridyl complexes, the emission occurs from the lowest triplet MLCT excited state.[3] Considering the homoleptic reference complex $[Ru(dcmb)_3]^{2+}$ the originating level must be the π* orbital of the dcmb ligands. In contrast, the emission maximum for the mixed chelate complex $[Ru(dceb)_2(bisbpy)]^{2+}$ lies at lower energies. The difference is ~16 nm. This is in close proximity to $[Ru(dcmb)_3]^{2+}$ whose luminescence occurs at 631 nm, indicating that the luminescence may be [Ru(dcmb)] based. This shift and the appearance of only one band leads to the assumption that the emission may occur from the Ru → dceb ^{3}MLCT excited state shown in Figure 5.26.[38]

In figure 5.27 and 5.28 the absorption and emission spectra for complexes $[Ru(bpy)_2(bisbpy)PdCl_2]^{2+}$, $[Ru(dceb)_2(bisbpy)PdCl_2]^{2+}$, $[Ru(bpy)_2(bisbpy)PtCl_2]^{2+}$ and $[Ru(dceb)_2(bisbpy)PtCl_2]^{2+}$ shows similar effects as seen in the two mononuclear complexes $[Ru(bpy)_2(bisbpy)]^{2+}$ and $[Ru(dceb)_2(bisbpy)]^{2+}$. In all the heterodinuclear complexes, the peak at 285 nm is attributed to the bpy peripheral ligand and 310 nm assigned to the dceb peripheral ligand, the band around 340 – 360 nm is assigned to the bisbpy bridging ligand.[28, 39] Moderately intense ^{1}MLCT bands are observed in the 400 – 500 nm regions. Thus for the heterodinuclear complexes $[Ru(bpy)_2(bisbpy)PdCl_2]^{2+}$, $[Ru(dceb)_2(bis\text{-}bpy)PdCl_2]^{2+}$, $[Ru(bpy)_2(bisbpy)PtCl_2]^{2+}$ and $[Ru(dceb)_2(bisbpy)PtCl_2]^{2+}$ lowest energy ^{1}MLCT transitions Ru → bisbpy are observed at 447 nm, 447 nm, 475 nm

and 475 nm respectively; small shoulder of lowest energy ^{1}MLCT transitions Ru → bpy / dceb are observed at 403 nm, 403, 444 nm and 444 nm respectively. There is no such effect observed due to progressive lowering of the π* orbital of the bridging ligand when the free chelating site connects to a formally uncharged unit ($PdCl_2$) and ($PtCl_2$).[40]

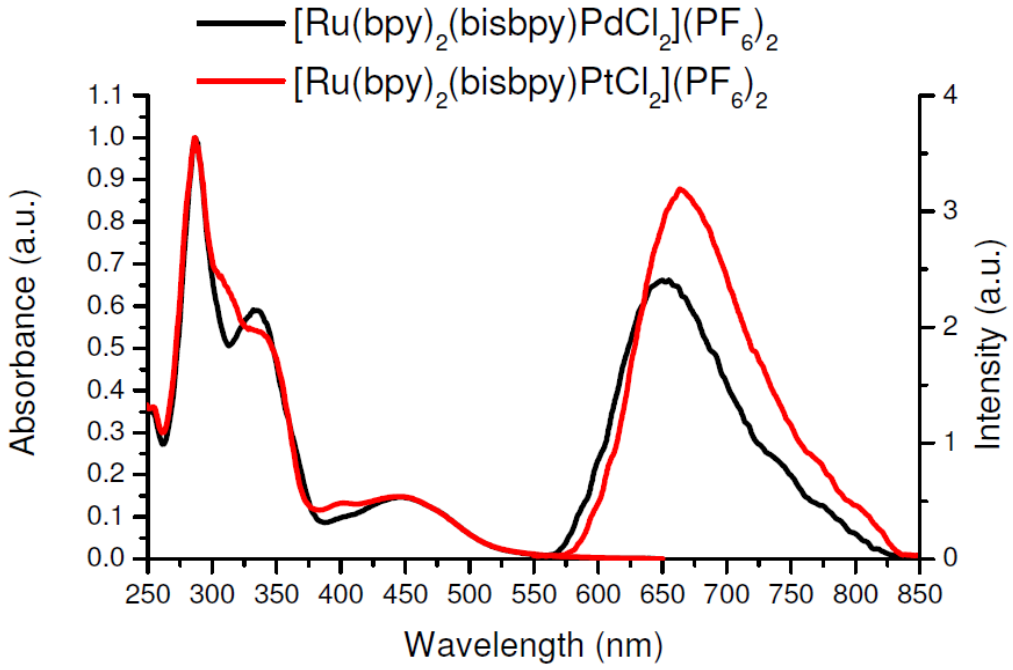

Figure 5.27: *Absorption and emission spectra of the $[Ru(bpy)_2(bisbpy)PdCl_2]^{2+}$ (black) (λ_{ex} = 447 nm) and $[Ru(bpy)_2(bisbpy)PtCl_2]^{2+}$(red) ($\lambda_{ex}$ = 447 nm) at room temperature in acetonitrile solution (deaerated).*

The ^{1}MLCT band Ru → bisbpy π* in the complex $[Ru(dceb)_2(bisbpy)PdCl_2]^{2+}$ is blue shifted by 8 nm compared to $[Ru(bpy)_2(bisbpy)PdCl_2]^{2+}$ and $[Ru(dceb)_2(bis\text{-}bpy)PtCl_2]^{2+}$ is blue shifted by 20 nm compared to $[Ru(bpy)_2(bisbpy)PtCl_2]^{2+}$, and similar effects were seen above for the mononuclear $[Ru(bpy)_2(bisbpy)]^{2+}$ and $[Ru(dceb)_2(bisbpy)]^{2+}$ due to the π-acceptor properties of the peripheral ligands. The ^{1}MLCT band Ru → bisbpy π* is blue shifted by 9 nm for $[Ru(bpy)_2(bisbpy)PdCl_2]^{2+}$ complexes compared to $[Ru(bpy)_2(bisbpy)PtCl_2]^{2+}$ as expected because the palladium(II) center is much more difficult to oxidize than the platinum(II) center. Therefore, ^{1}MLCT transitions should occur at higher energy in palladium complexes than in the platinum complexes.[41]

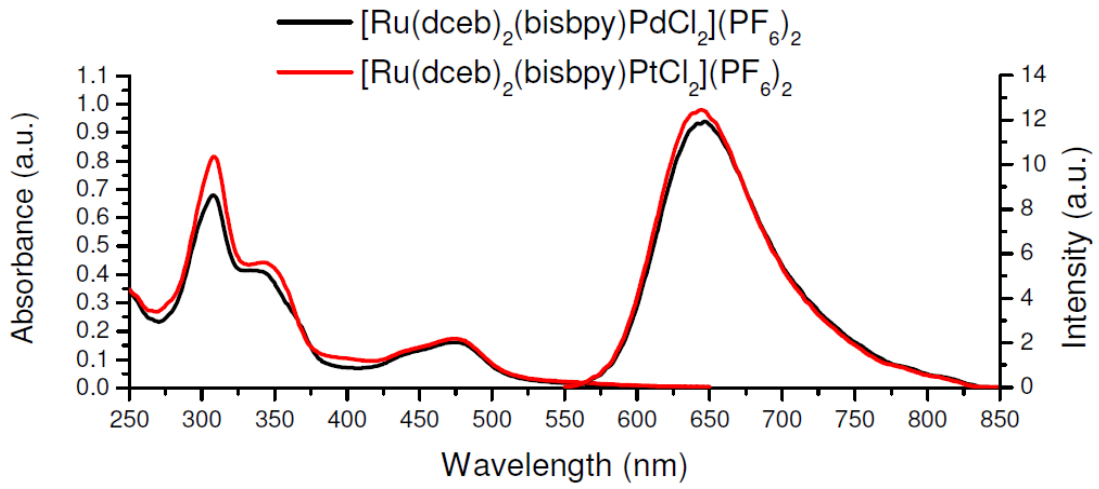

Figure 5.28: *Absorption and emission spectra of the $[Ru(dceb)_2(bisbpy)PdCl_2]^{2+}$ (black) (λ_{ex} = 475 nm) and $[Ru(dceb)_2(bisbpy)PtCl_2]^{2+}$(red) ($\lambda_{ex}$ = 475 nm) at room temperature in acetonitrile solution (deaerated).*

The complexes $[Ru(bpy)_2(bisbpy)PdCl_2]^{2+}$, $[Ru(dceb)_2(bisbpy)PdCl_2]^{2+}$, $[Ru(bpy)_2(bisbpy)PtCl_2]^{2+}$ and $[Ru(dceb)_2(bisbpy)PtCl_2]^{2+}$ emit at room temperature and their emission is quenched compared to mononuclear complexes with similar concentrations (compared Figure 5.26 to Figure 5.27 and 5.28). The complexes $[Ru(bpy)_2(bisbpy)\text{-}PtCl_2]^{2+}$ and $[Ru(dceb)_2(bisbpy)PtCl_2]^{2+}$ emits at 664 nm and 644 nm with an excited state lifetimes of decay τ = 331 ns, (ϕ_{em} = 0.017) and τ = 534 ns, (ϕ_{em} = 0.054), respectively, in deaerated acetonitrile. The complexes $[Ru(bpy)_2(bisbpy)PdCl_2]^{2+}$ and $[Ru(dceb)_2(bisbpy)PdCl_2]^{2+}$ emits at 655 nm and 647 nm with bi-exponential decays with τ_1 = 17 ns (rel. % = 37 %), τ_2 = 218 ns (rel. % = 63 %), ϕ_{em} = 0.044 and τ_1 = 42 ns (rel. % = 60 %), τ_2 = 325 ns (rel. % = 40 %), ϕ_{em} = 0.033, respectively, in deaerated acetonitrile.This appearance of single band leads to the assumption that the emission is occurs from the Ru → bisbpy ^{3}MLCT excited state for the complexes $[Ru(bpy)_2(bisbpy)PdCl_2]^{2+}$ and $[Ru(bpy)_2(bis\text{-}bpy)PtCl_2]^{2+}$ because the bisbpy ligand is a better π-acceptor (lowest π* orbital) than bpy, ^{3}MLCT excited state is red shifted compared to $[Ru(bpy)_3]^{2+}$. By following the mononuclear complex $[Ru(dceb)_2(bisbpy)]^{2+}$, the emission state is assumed to be from the Ru → dceb ^{3}MLCT excited state as

discussed earlier for both complexes $[Ru(dceb)_2(bisbpy)PtCl_2]^{2+}$ and $[Ru(dceb)_2(bis\text{-}bpy)PtCl_2]^{2+}$.[38]

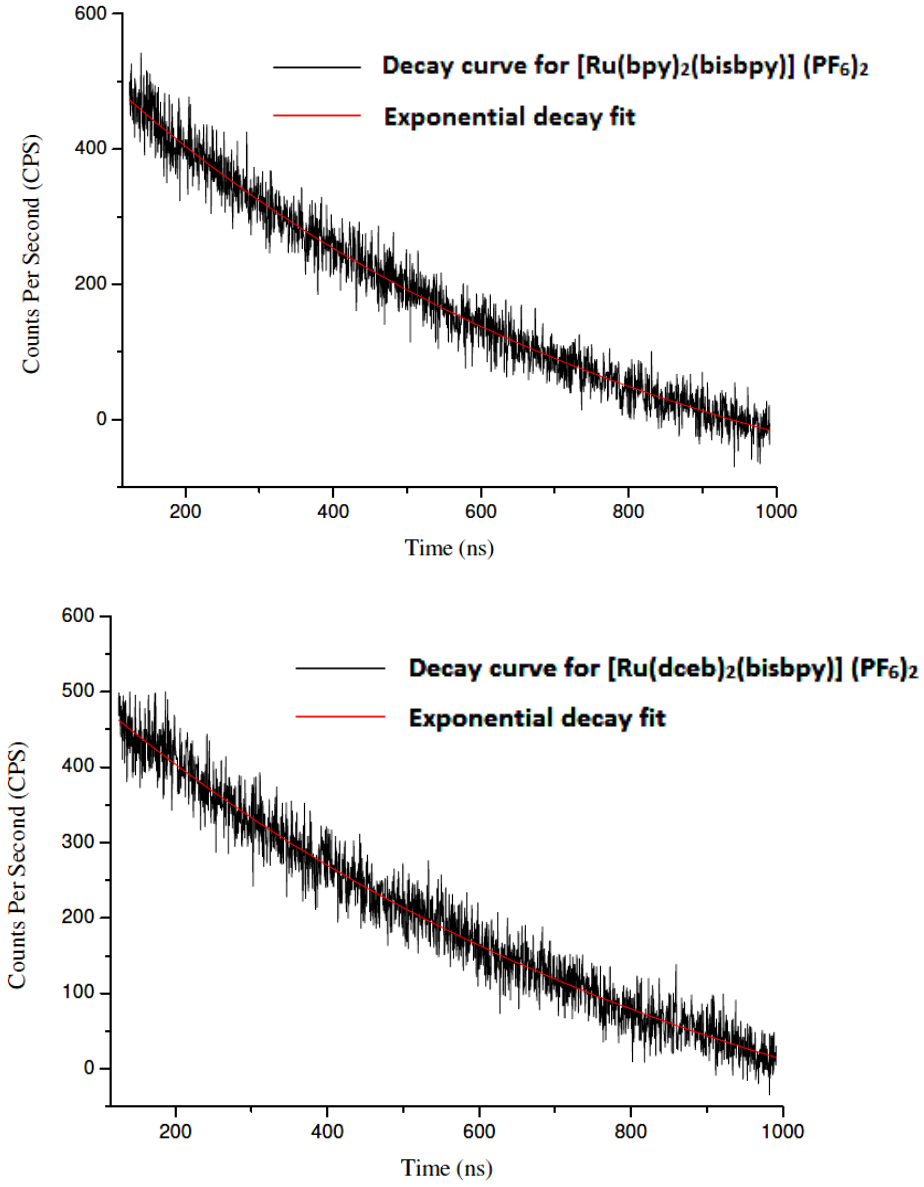

Figure 5.29: *TCSPC spectra of the mononuclear complexes. The spectra were recorded at room temperature in deaerated acetonitrile solution, by exciting the samples with a wavelength of 360 nm and observing the emission at 633 nm (above) and 647 nm (below). The graphs were fitted (red line) using a single exponential decay function.*

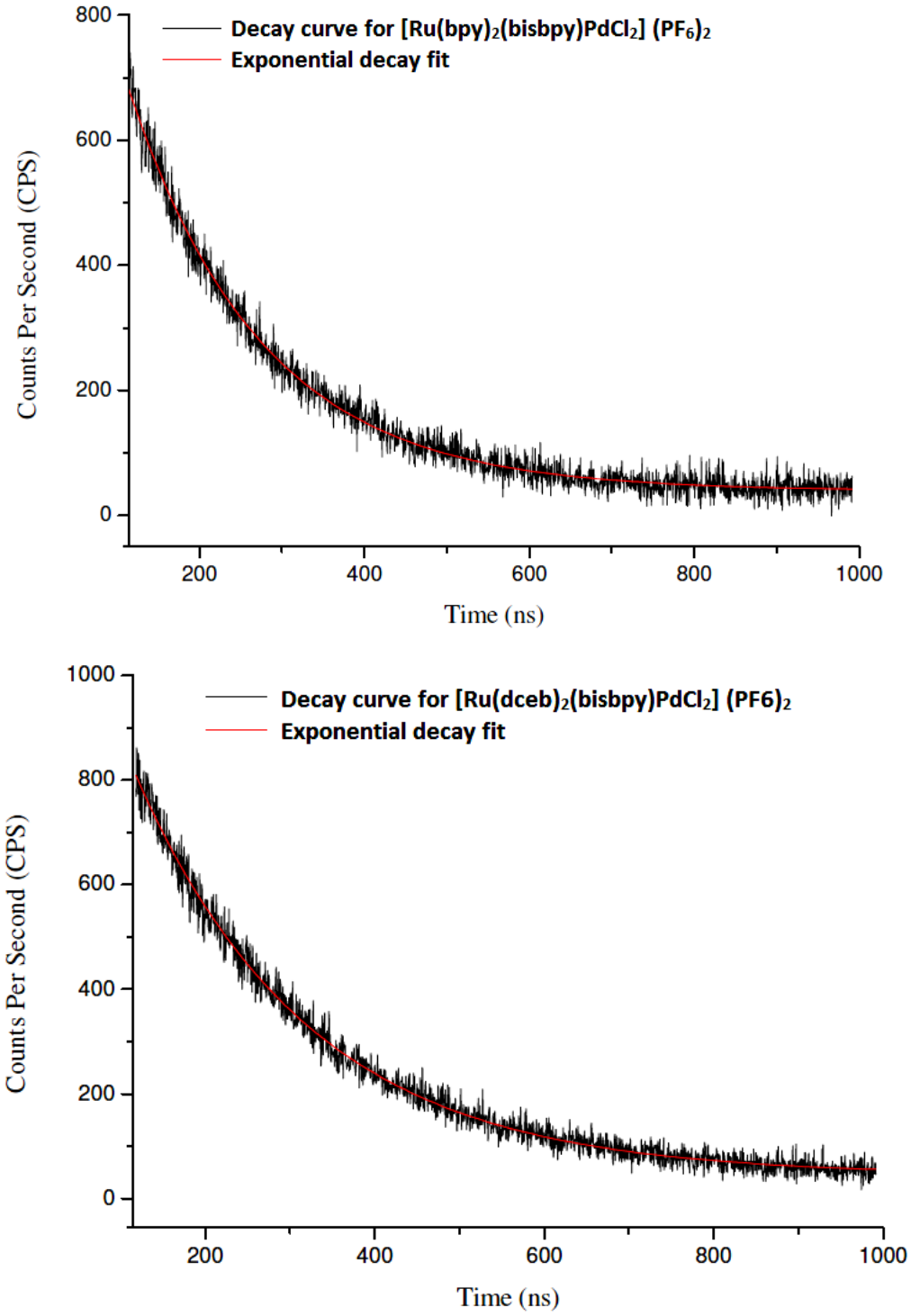

Figure 5.30: *TCSPC spectra of the heterodinuclear Ru – Pd complexes. The spectra were recorded at room temperature in deaerated acetonitrile solution, by exciting the samples with a wavelength of 360 nm and observing the emission at 655 nm (above) and 647 nm (below). The graphs were fitted (red line) using a bi- exponential decay function.*

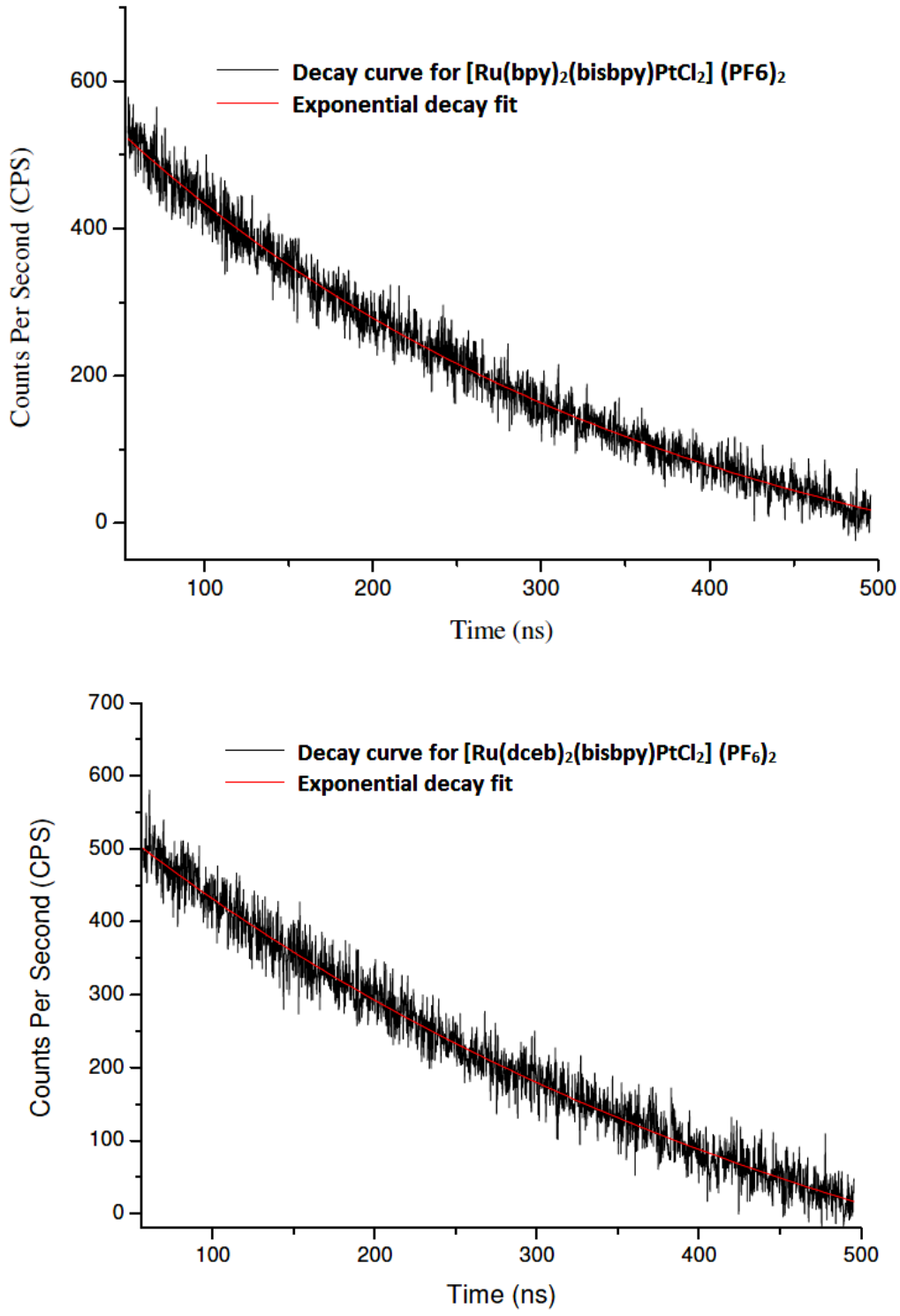

Figure 5.31: *TCSPC spectra of the heterodinuclear Ru – Pd complexes. The spectra were recorded at room temperature in deaerated acetonitrile solution, by exciting the samples with a wavelength of 360 nm and observing the emission at 664 nm (above) and 644 nm (below). The graphs were fitted (red line) using a single exponential decay function.*

5.3.4 Photocatalytic hydrogen generation experiments.

Table 5.3 represented the TONs of photocatalytical hydrogen generation intermolecular or intramolecular photochemical reaction of the listed complexes in this chapter.

Run	Complexes	TON {Water percentage} (Standard Deviation)			
		{0 %}	{5 %}	{10 %}	{15 %}
1	$[Ru(bpy)_2(bisbpy)PdCl_2]^{2+}$	0	5 (1)	16 (3)	13 (1)
2	$[Ru(bpy)_2(bisbpy)PtCl_2]^{2+}$	29 (2)	75 (8)	92 (4)	85 (4)
3	$[Ru(dceb)_2(bisbpy)PdCl_2]^{2+}$	23 (1)	513 (2)	360 (10)	198 (12)
4	$[Ru(dceb)_2(bisbpy)PtCl_2]^{2+}$	13 (1)	258 (6)	286 (5	45 (1)
5	$[Ru(dceb)_2(bisbpy)]^{2+}$ + $[Pd(acetonitrile)_2Cl_2]$	-	489 (7)	321 (10)	-
6	$[Ru(bpy)_2(bisbpy)]^{2+}$	0	0	0	0
7	$[Ru(dceb)_2(bisbpy)]^{2+}$	0	0	0	0
8	$[Pd(acetonitrile)_2Cl_2]$	0	0	0	0
9	No Catalyst (only TEA)	0	0	0	0

Table 5.3: *Evaluation of heterodinuclear Ru-Pd / Ru-Pt complexes (intramolecular catalysis) and mononuclear complexes* $[Ru(dceb)_2(bisbpy)]^{2+}$ + $[Pd(CH_3CN)_2Cl_2]$ *(intermolecular catalysis) in photocatalytic hydrogen evolution reactions (*4.08×10^{-5} *M of catalysts and* $[Pd(CH_3CN)_2Cl_2]$ *in 2* cm^3 *containing 2.15 M TEA in ACN-*H_2O *(0%, 5%, 10% & 15%* H_2O *(v/v)), 470 nm, 18 hours). Averages of 3 samples were taken for calculating TONs.*

The photocatalytic hydrogen generation activity of each intramolecular Ru – Pd / Ru – Pt heterodinuclear complex and the intermolecular Ru(II) mononuclear complex $[Ru(dceb)_2(bisbpy)]^{2+}$ with $[Pd(acetonitrile)_2Cl_2]$ were evaluated. The complexes were irradiated in acetonitrile with vary percentages of water, presence of a sacrificial electron donor, triethyl amine (TEA), under N_2 atmosphere (detailed procedure mentioned in chapter 2).

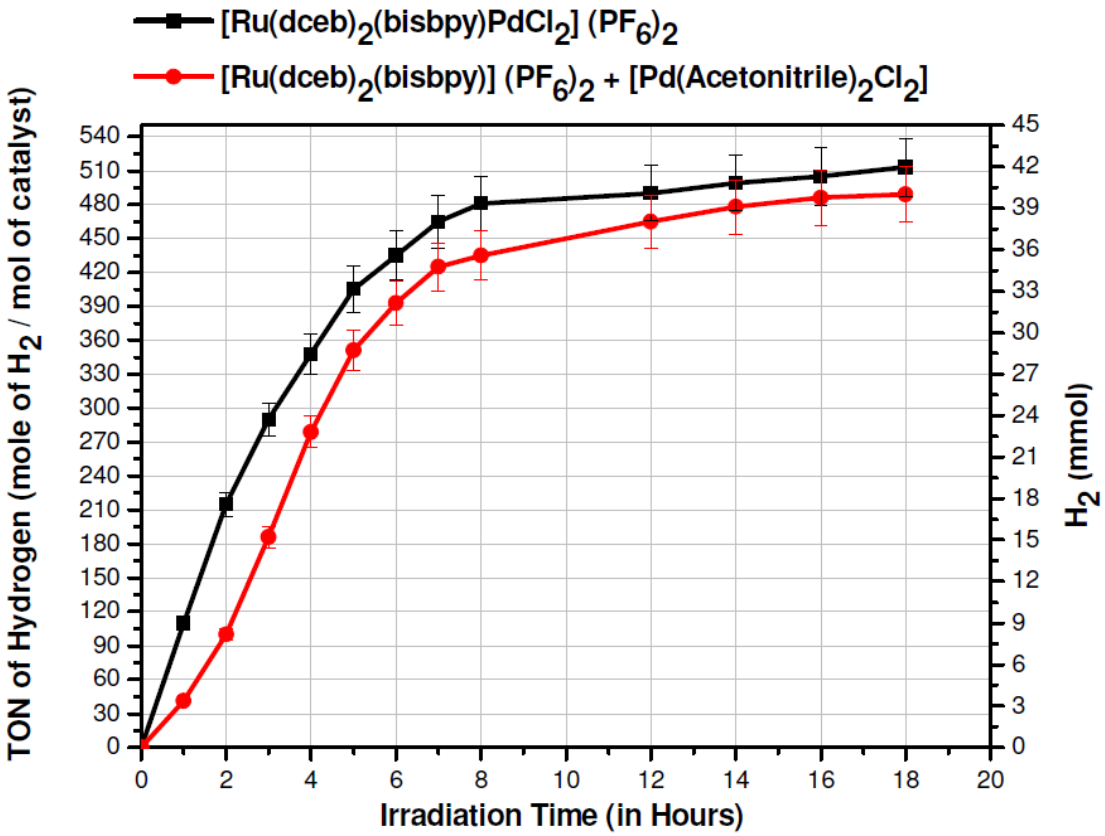

Figure 5.32: *Evaluation of $[Ru(dceb)_2(bisbpy)PdCl_2]^{2+}$ (intramolecular catalysis) and $[Ru(dceb)_2(bisbpy)]^{2+}$ + $Pd(CH_3CN)_2Cl_2$ (intermolecular catalysis) in photocatalytic reactions (4.08×10^{-5} M of catalysts and $Pd(CH_3CN)_2Cl_2$ in 2 cm^3 containing of 2.15 M TEA in ACN-H_2O (5% H_2O v/v), 470 nm, 0 – 18 hours). S.D. ± 10 TONs or less.*

The photocatalytic hydrogen generation activity for each intramolecular heterodinuclear complex (Ru–Pd / Ru–Pt) and the intermolecular ester analogue of the Ru(II) mononuclear complex with $[Pd(acetonitrile)_2Cl_2]$ were evaluated using water over 18 hours photo-irradiation at 470 nm in an acetonitrile solution containing triethyl amine. As

shown in table 5.3, $[Ru(dceb)_2(bisbpy)PdCl_2]^{2+}$ (run 3), intermolecular photocatalysis of $[Ru(dceb)_2(bisbpy)]^{2+}$ with **[**$Pd(acetonitrile)_2Cl_2$] (run 5) gave the highest TONs for photocatalytic hydrogen generation with TONs of 513 and 489 respectively. In intermolecular reaction suggested that the formation of intramolecular system when mixing the $[Ru(dceb)_2(bisbpy)]^{2+}$ with **[**$Pd(acetonitrile)_2Cl_2$] (run 5), while without adding palladium precursor to the complexes $[Ru(bpy)_2(bisbpy)]^{2+}$ (run 6) and $[Ru(dceb)_2(bisbpy)]^{2+}$ (run 7) were not drive H_2 evolution by TEA in the presence of water suggested that the Pd metal as catalytic centre is important to drive hydrogen. $[Ru(bpy)_2(bisbpy)PdCl_2]^{2+}$ is not as effective a photocatalyst as the ester analogue $[Ru(dceb)_2(bisbpy)PdCl_2]^{2+}$. All the heterodinuclear complexes show maximum TONs at 10% water content except $[Ru(dceb)_2(bisbpy)PdCl_2]^{2+}$ which shows maximum TONs of 513 at 5% water content as depicted in Table 5.3.[42, 43]

As shown in Table 5.3, all heterodinuclear complexes $[Ru(bpy)_2(bisbpy)PdCl_2]^{2+}$, $[Ru(dceb)_2(bisbpy)PdCl_2]^{2+}$, $[Ru(bpy)_2(bisbpy)PtCl_2]^{2+}$, $[Ru(dceb)_2(bis\text{-}bpy)PtCl_2]^{2+}$ and also intermolecular photocatalysis of $[Ru(dceb)_2(bisbpy)]^{2+}$ with **[**$Pd(acetonitrile)_2Cl_2$] produced hydrogen photocatalytically. Time dependent hydrogen efficiencies are shown in the Figure 5.32, for $[Ru(dceb)_2(bisbpy)PdCl_2]^{2+}$ and intermolecular photocatalysis of $[Ru(dceb)_2(bisbpy)]^{2+}$ with **[**$Pd(acetonitrile)_2Cl_2$]. The turn over frequency (TOF) provides the rate of TON of hydrogen per hour and stability of catalyst during irradiation. The TOF experiment for $[Ru(dceb)_2(2,5\text{-}dpp)PdCl_2]^{4+}$ shows a smooth exponentially growing curve with an increment of hydrogen TON and amount of hydrogen in the head space which reached a maximum TON = 481 in 8 hours (TOF = 60 h^{-1}) with 470 nm irradiation (see Table 5.4). The intramolecular reaction reached close to the maximum TON after 8 hours with only a slight increase on increasing irradiation time to 18 hours. The intermolecular reaction was slightly less efficient in early stages compared to the intramolecular reaction with a TONs 435 after 8 hours (TOF = 54.3 h^{-1}). This value is close in efficiency to the intramolecular reaction (see Table 5.4). One explanation for the similarity in efficiency is due to the formation of heterodinuclear complex in situ during intermolecular photocatalysis of $[Ru(dceb)_2(bisbpy)]^{2+}$ with **[**$Pd(acetonitrile)_2Cl_2$].[43] It

has been seen from figure 5.32 that the both systems still produce hydrogen after 18 hour of irradiation.

Time ***(hour)***	***TON {Water percentage (5%)}*** ***(mole of H_2 / mole of catalyst)***	
	$[Ru(dceb)_2(bisbpy)PdCl_2)]^{2+}$	$[Ru(dceb)_2(bisbpy)]^{2+}$ + $[Pd(CH_3CN)_2Cl_2]$
0	*0*	*0*
1	*110*	*41*
2	*215*	*100*
3	*290*	*186*
4	*348*	*279*
5	*405*	*351*
6	*435*	*393*
7	*465*	*425*
8	*481*	*435*
12	*490*	*465*
14	*499*	*478*
16	*505*	*486*
18	*513*	*489*

Table 5.4: *Evaluation of $[Ru(dceb)_2(bisbpy)PdC_2]^{2+}$ (intramolecular catalysis) and $[Ru(dceb)_2(bisbpy)]^{2+}$ + $[Pd(CH_3CN)_2Cl_2]$ (intermolecular catalysis) in photocatalytic hydrogen evolution reactions (4.08×10^{-5} M of catalysts and $[Pd(CH_3CN)_2Cl_2]$ in 2 cm^3 of 2.15 M TEA in ACN-H_2O (5% H_2O v/v), 470 nm, 0 – 18 hours). 3 samples were taken for calculating TONs (see figure 5.32). S.D. ± 10 TONs or less.*

5.4 Summary and conclusion

Chapter 5 details the synthetic methods available for the generation of mononuclear and heterodinuclear metal complexes utilising the method of "complexes as metal / complexes as ligands" strategy. Initially the heterodinuclear complexes (Ru – Pd) / (Ru – Pt) were synthesised and their properties, such as absorption, emission and luminescence were obtained (see Table 5.2). These results were taken in conjunction with the characterization tools of ^{1}H-NMR and CHN to confirm the synthesis of these mononuclear and heterodinuclear complexes with properties similar to other families of ruthenium(II) complexes. ^{1}H-NMR proved invaluable in determining the binding of the cyclometallated Pd moiety to the mononuclear complexes and then 2D-COSY proton-NMR to determine coupling between protons in the molecule (see Table 5.1).

The objective of this thesis is photocatalytic generation of hydrogen for the complexes discussed using water and sacrificial agent (TEA) by irradiation at 470 nm wavelength. Gas chromatography was used for measuring the gaseous products during the photocatalytic experiments. The compounds containing bridging ligand, bisbpy, in the mononuclear Ru(II) ($[Ru(bpy)_2(bisbpy)]^{2+}$/ $[Ru(dceb)_2(bisbpy)]^{2+}$) complexes did not produced hydrogen. The bisbpy analogues heterodinuclear complexes proved to be very efficient photocatalysts for hydrogen generation. The $[Ru(dceb)_2(bisbpy)PdCl_2]^{2+}$ intramolecular gave the highest TONs of 513 with 5% water content. The intermolecular reaction using $[Ru(bpy)_2(bisbpy)]^{2+}$ and $[Pd(ACN)_2Cl_2]$ show more or less the same TONs of 489 with 5% water for hydrogen generation. The results were complimentary with the time dependent hydrogen production for calculating turn over frequency (TOF). The TOF provides the rate of TON of hydrogen per hour and stability of catalyst during irradiation. It was confirmed that water enhanced the production of hydrogen (0 – 15 %) and was at a maximum with 5% water for $[Ru(dceb)_2(bisbpy)PdCl_2]^{2+}$, and solution containing 10 % water gave the highest amount of hydrogen for all other heterodinuclear complexes (see table 5.3).

5.5 Bibliography

[1] (a) V. Balzani, A. Juris, A. Venturi, S. Campagna and S. Serroni, Acc. Chem. Rev., 1998, 31, 26; (b) Molecular Wires and Electronics, Top. Curr. Chem., ed. L. De Cola, Springer, Berlin, 2005, vol. 257, p. 63; (c) J. G. Vos and J. M. Kelly, Dalton Trans., 2006, 4869; (d) V. Balzani, M. Venturi and A. Credi, Molecular Devices and Machines, Wiley-VCH, Weinheim, 2003; (e) L. Sun, L. Hammarström, B. Åkermark and S. Styring, Chem. Soc. Rev., 2001, 30, 36; (f) S. Rau, D. Walther and J. G. Vos, Dalton Trans., 2007, 915.

[2] (a) G. Denti, S. Campagna, S. Serroni, M. Ciano and V. Balzani, J. Am. Chem. Soc., 1992, 114, 2944; (b) V. Balzani, S. Campagna, G. Denti, A. Juris, S. Serroni and M. Venturi, Acc. Chem. Res., 1998, 31, 26; (c) C. Chiorboli, M. T. Indelli and F. Scandola, Molecular Wires, Top. Curr. Chem., 2005, 257; (d) L. Flamigni, J. P. Collin and J. P. Sauvage, Acc. Chem. Res., 2008, 41, 857; (e) D. M. D'Alessandro and F. R. Keene, Chem. Rev., 2006, 106, 2270.

[3] (a) S. Fanni, C. Di Pietro, S. Serroni, S. Campagna and J. G. Vos, Inorg. Chem. Commun., 2000, 42; (b) C. Di Pietro, S. Serroni, S. Campagna, T. Gandolfi, R. Ballardini, S. Fanni, W. R. Browne and J. G. Vos, Inorg. Chem., 2002, 41, 2871; (c) D. Tzalis and Y. Tor, J. Am. Chem. Soc., 1997, 119, 852; (d) M. I. J. Polson, J. A. Lotoski, K. O. Johansson, N. J. Taylor, G. S. Hanan, B. Hasenknopf, R. Thouvenot, F. Loiseau, R. Passalaqua and S. Campagna, Eur. J. Inorg. Chem., 2002, 2549; (e) B. Schafer, H. Görls, M. Presselt, M. Schmitt, J. Pop, W. Henry, J. G. Vos and S. Rau, Dalton Trans., 2006, 2225; (f) M. Polson, C. Chiorboli, S. Fracasso and F. Scandola, Photochem. Photobiol. Sci., 2007, 6, 438; (g) W. R. Browne, N. M. O'Boyle, W. Henry, A. L. Guckian, S. Horn, T. Fett, C. M. O'Connor, M. Duati, L. De Cola, C. G. Coates, K. L. Ronayne, J. J. McGarvey and J. G. Vos, J. Am. Chem. Soc., 2005, 127, 1229; (h) P. Passaniti, W. R. Browne, F. C. Lynch, D. Hughes, M. Nieuwenhuyzen, P. James, M. Maestri and J. G. Vos, J. Chem. Soc., Dalton Trans., 2002, 1740.

[4] C. Kaes, A. Katz, M. W. Hosseini, Chem. Rev., 2000, 100, 3553.

[5] (a) A. Juris, V. Balzani, F. Barigelletti, S. Campagna, P. Belser, A. von Zelewsky, Coord. Chem. Rev., 1988, 84, 85; (b) V. Balzani, F. Barigelletti, L. De Cola, Top. Curr.

Chem., 1990, 158, 31; (c) F. Barigelletti, L. Flamigni, Chem. Soc. Rev., 2000, 29, 1; (d) I. M. Dixon, J. -P. Collin, J. -P. Sauvage, L. Flamigni, S. Encinas, F. Barigelletti, Chem. Soc. Rev., 2000, 29, 385; (e) H. Le Bozec, T. Renouard, Eur. J. Inorg. Chem., 2000, 229; (f) R. D. Gerardi, N. W. Barnett, S. W. Lewis, Anal. Chim. Acta, 1999, 378, 1.

[6] P. L. Boulas, M. Gomez-Kaifer, L. Echegoyen, Angew. Chem. Int. Ed. 1998, 37, 216.

[7] (a) C. J. Elsevier, Coord. Chem. Rev., 1999, 185_186, 809. (b) A. von Zelewsky, Coord. Chem. Rev., 1999, 190-192, 811.

[8] (a) E. C. Constable, Tetrahedron, 1992, 48, 10013; (b) C. Piguet, G. Bernardinelli, G. Hopfgartner, Chem. Rev., 1997, 97, 2005; (c) R. Ziessel, Synthesis, 1999, 1839; (d) U. Knof, A. von Zelewsky, Angew. Chem. Int. Ed., 1999, 38, 302; (e) S. Leininger, B. Olenyuk, P. J. Stang, Chem. Rev., 2000, 100, 853; (f) G. F. Swiegers, T. J. Malefetse, Chem. Rev., 2000, 100, 3483; (g) J. -P. Sauvage, (Ed.) Perspectives in Supramolecular Chemistry, Vol. 5, John Wiley & Sons, Chichester, 1999; (h) L. Fabbrizzi, A. Poggi, (Eds.) Transition Metals in Supramolecular Chemistry, Kluwer Academic Publishers, Dordrecht, 1994.

[9] (a) F. H. Case, J. Am. Chem. Soc., 1946, 68, 2574; (b) G. Maerker, F. H. Case, J. Am. Chem. Soc., 1958, 80, 2745; (c) G. R. Newkome, W. E. Puckett, G. E. Kiefer, V. K. Gupta, Y. Xia, M. Coreil, M. A. Hackney, J. Org. Chem., 1982, 47, 4116; (d) U. Neumann, F. Vögtle, Chem. Ber., 1989, 122, 589; (e) L. Della Ciana, W. J. Dressick, A. von Zelewsky, J. Heterocyclic Chem., 1990, 27, 163; (f) N. Garelli, P. Vierling, J. Org. Chem., 1992, 57, 3046; (g) K. Nakashima, S. Shinkai, Chem. Lett., 1994, 1267; (h) V. Grosshenny, F. M. Romero, R. Ziessel, J. Org. Chem., 1997, 62, 1491; (i) C. L. Fraser, N. R. Anastasi, J. J. S. Lamba, J. Org. Chem., 1997, 62, 9314; (j) V. Penicaud, F. Odobel, B. Bujoli, Tetrahedron Lett., 1998, 39, 3689; (k) C. Janiak, S. Deblon, H. -P. Wu, Synth. Commun., 1999, 29, 3341; (l) A. El-ghayoury, R. Ziessel, J. Org. Chem., 2000, 65, 7757.

[10] (a) F. Kröhnke, Synthesis 1976, 1; (b) N. H. Pirzada, P. M. Pojer, L. A. Summers, Z. Naturforsch., B: Anorg. Chem. Org. Chem., 1976, 31 B, 115; (c) G. R. Newkome, V. K. Gupta, F. R. Fronczek, Inorg. Chem., 1983, 22, 171; (d) L. Della Ciana, I. Hamachi, T. J. Meyer, J. Org. Chem., 1989, 54, 1731; (e) F. M. Romero, R. Ziessel, Tetrahedron Lett. 1995, 36, 6471; (f) G. R. Newkome, J. Gross, A. K. Patri, J. Org. Chem. 1997, 62, 3013;

(g) R. Ziessel, A. El-ghayoury, Synthesis, 2000, 2137; (h) B. M. Bishop, D. G. McCafferty, B. W. Erickson, Tetrahedron 2000, 56, 4629.

[11] (a) S. P. Stanforth, Tetrahedron 1998, 54, 263; (b) F. Diederich, P. J. Stang, (Eds.) Metal-catalyzed Cross-coupling Reactions, Wiley-VCH, Weinheim, 1998; (c) E. -i. Negishi, A. O. King, N. Okukado, J. Org. Chem. 1977, 42, 1821; (d) E. -i. Negishi, T. Takahashi, A. O. King, Org. Synth. 1988, 66, 67.

[12] Y. Z. Hu, Q. Xiang and R. P. Thummel, Inorganic Chemistry, Vol. 41, No. 13, 2002, 3423.

[13] C. R. Rice, K. M. Anderson, Polyhedron, 2000, 19, 495.

[14] B. E. Halcrow, W. O. Kermack, J. Chem. Soc. 1946, 155.

[15] D. Tzalis, Y. Tor, S. Failla, J. S. Siegel, Tetrahedron Lett., 1995, 36, 3489.

[16] F. H. Case, J. Heterocycl. Chem. 1964, 1, 112.

[17] E. C. Constable, S. M. Elder, J. Healy, D. A. Tocher, J. Chem. Soc., Dalton Trans. 1990, 1669.

[18] (a) R. P. Thummel, R. P. Synlett 1992, 1. (b) C. -C. Cheng, S. -J. Yan, Org. React. 1982, 28, 37. (c) C. -Y. Hung, T. -L. Wang, Z. Shi, R. P. Thummel, Tetrahedron 1994, 50, 10685.

[19] R. P. Thummel, C. M. Chamchoumis, In Advances in Nitrogen Heterocycles, Vol. 4; C. J. Moody, Ed.; JAI Press: Stamford, CT, 2000; p 107.

[20] T. Majewicz, P. Caluwe, J. Org. Chem., 1979, 44, 531.

[21] (a) V. Balzani, A. Juris, M. Venturi, S. Campagna, G. Denti, S. Serroni, Chem. Rev., 1996, 96, 759; (b) V. Balzani, F. Scandola, Supramolecular Photochemistry; Ellis Horwood: Chichester, U.K., 1991.

[22] (a) M. D. Ward, F. Barigelletti, Coord. Chem. Rev., 2001, 216-217, 127. (b) S. Encinas, F. Barigelletti, A. M. Barthram, M. D. Ward, S. Campagna, Chem. Commun., 2001, 277.

[23] (a) G. Denti, S. Serroni, S. Campagna, A. Juris, M. Ciano, V. Balzani, Perspect. Coord. Chem. 1992, 153; (B) G. Denti, S. Campagna, L. Sabatino, S. Serroni, M. Ciano, V. Balzani, Inorg. Chem. 1990, 29, 4750.

[24] (a) C. J. Aspley, J. A. Gareth Williams, New J. Chem. 2001, 25, 1136; (b) P. M. Griffiths, F. Loiseau, F. Puntoriero, S. Serroni, S. Campagna, Chem. Commun. 2000, 2297; (c) G. R. Pabst, O. C. Pfuller, J. Sauer, Tetrahedron, 1999, 55, 8045; (d) S. J. Dunne, E. C. Constable, Inorg. Chem. Commun. 1998, 1, 167; (e) C. Patoux, J. -P. Launay, M. Beley, S. Chodorowski-Kimmes, J. -P. Collin, S. James, J. P. Sauvage, J. Am. Chem. Soc. 1998, 120, 3717; (f) E. C. Constable, A. M. W. Cargill Thompson, S. Greulich, J. Chem. Soc., Chem. Commun., 1993, 1444; (g) M. Beley, J. P. Collin, R. Louis, B. Metz, J. P. Sauvage, J. Am. Chem. Soc. 1991, 113, 8521.

[25] (a) K. O. Johansson, J. A. Lotoski, C. C. Tong, G. S. Hanan, Chem. Commun. 2000, 819; (b) Y. Tomohiro, A. Satake, Y. Kobuke, J. Org. Chem. 2001, 66, 8442.

[26] Y, -Q, Fang, M. I. J. Polson and G. S. Hanan, Inorg. Chem., 2003, Vol. 42, 5.

[27] T. R. Kelly, Y. -J. Lee, R. J. Mears, J. Org. Chem. 1997, 62, 2774.

[28] L. Cassidy, S. Horn, L. Cleary, Y. Halpin, W. R. Browne and Johannes G. Vos, Dalton Trans., 2009, 3923.

[29] M. Tiecco, M. Tingoli, L. Testaferri, D. Chianelli and E. Wenkert, Tetrahedron, 1986, 42, 1475.

[30] (a) R. Wang, J. G. Vos, R. H. Schmehl and R. Hage, J. Am. Chem. Soc., 1992, 114, 1964; (b) S. Fanni, T. E. Keyes, C. M. O'Connor, H. Hughes, R. Wang and J. G. Vos, Coord. Chem. Rev., 2000, 3, 42.

[31] (a) J. C. Curtis, J. S. Bernstein and T. J. Meyer, Inorg. Chem., 1985, 24, 385; (b) K. S. Schanze and T. J. Meyer, Inorg. Chem., 1985, 24, 2122.

[32] (a) E. Negishi, S. Baba, J. Am. Chem. Soc. Chem Comm., 1976, 596 (b) E. Negishi, Aspects of Mechanism and Organometallic Chemistry, J. H. Brewster, Ed.: Plenum Press: New York, 1978, 285.

[33] Y. Q. Fang and G. S. Hanan, Synlett, 2003, 6, 852.

[34] F. M. Romero, R. Ziessel, Tetrahedron Lett., 1995, 36, 6471.

[35] (a) P. J. Steel, F. Lahouse, D. Lerner, C. Marzin, Inorg. Chem., 1983, 22, 1488; (b) C. Marzin, F. Budde, P. J. Steel, D. Lerner, Nouv. J. Chim., 1987, 11, 33; (c) P. J. Steel, E. C. Constable, J. Chem. Soc., Dalton Trans, 1990, 1389; (d) R. Hage, A. H. J. Dijkhuis, J. G. Haasnoot, R. Prins, J. Reedijk, B. E. Buchanan, J. G. Vos, Inorg. Chem., 1988, 27,

2185: (e) R. Hage, R. Prins, J. G. Haasnoot, J. Reedijk, J. G. Vos, Dalton Trans., 1987, 1389: (f) R. Hage, J. G. Haasnoot, D. J. Stufkens, T. L. Snoeck, J. G. Vos, J. Reedijk, Inorg. Chem., 1989, 28, 1413; (g) G. M. Bryant, J. E. Fergusson, Aust. J. Chem., 1971, 24, 441; (h) F. E. Lytle, L. M. Petrosky, L. R. Carlson, Anal. Chim. Acta, 1971, 57, 239; (i) P. Belsar, A. von Zelewsky, Helv. Chim. Acta, 1980, 63, 1675; (j) E. C. Constable, J. Lewis, Inorg. Chim. Acta, 1983, 70, 251.

[36] J. McMurry, Organic Chemistry, 5th Edition, Brooks/ Cole, 2000.

[37] J. M. Calvert, J. V. Caspar, R. A. Binstead, T. D. Westmoreland and T. J. Meyer, J. Am. Chem. Soc., 1982, 104, 24, 6620.

[38] M. Schwalde, B. Schäfer, H. Görls, S. Rau, S. Tschierlei, M. Schmitt, J. Popp, G. Vaughan, W. Henry, J. G. Vos, Eur. J. Inorg. Chem., 2008, 3310.

[39] Y. Halpin, L. Cleary, L. Cassidy, S. Horne, D. Dini, W. R. Browne and J. G. Vos, Dalton Trans., 2009, 4146.

[40] G. Denti, S. Campagna, J. L. Sabatino, S. Serroni, M. Ciano and V. Balzani, Inorg. Chem. 1990, 29, 4750.

[41] F. Neve and A. Crispini, Inorg. Chem., 1997, 36, 6150.

[42] E. D. Cline, S. E. Adamson and S. Bernard, Inorg. Chem., 2008, 47, 10378

[43] G. S. Bindra, M. Schulz, A. Paul, S. Soman, R. Groarke, J. Inglis, M. T. Pryce, W. R. Browne, S. Rau, B. J. Maclean and J. G. Vos, Dalton Trans., 2011, DOI: 10.1039/c1dt11241d.

Chapter 6: Photocatalytic Properties of Heterodinuclear Supramolecular Photocatalysts for the Production Hydrogen

Abstract:

The complexes synthesised in the previous chapters were designed for the photocatalytic generation of hydrogen from water. The results obtained in this chapter are compared and explained taking into account the reaction conditions and nature of the components of the photocatalytic compounds. The dependences of the H_2-evolving activity on the peripheral ligands, bridging ligand, the Pd/Pt(II) d_z^2 orbital energy and the steric factors are discussed. On the basis of this comparison a possible mechanism for the generation of hydrogen is proposed.

6.1 Introduction

- The most important aspect of a catalytic system is the catalyst's ability to turn over, or perform the same reaction multiple times. The turnover number (TON) reflects a catalyst's stability and efficiency under the employed conditions and describes its ability to generate a product. In photochemical reactions, light absorption and charge transport are essential components. Full operating efficiency is therefore determined by;
- a system's molar absorptivity at the useful wavelengths,
- its quantum yield, or the reaction's competence at making the desired product once a photon is absorbed, and
- its longevity. The monetary expense of a photosynthetic operation is equal in importance to its functionality.

For this reason, great emphasis has fallen on the development of catalysts derived from inexpensive starting materials, maximizing the power output per cost of fabrication. Accordingly, the final measure of a system's success is the ratio of its full operating efficiency to its inherent costs. Bearing in mind these considerations, the development of a complete photosynthetic system becomes complicated by the need to simultaneously address many criteria.

Owing to the inevitable complexity of both powering and directing multiple charge transfers during water photolysis, as discussed in Chapter 1, researchers separate the overall water cleavage reaction into two half cells, allowing an independent study of water oxidation and reduction, as shown in Scheme 6.1. Separating the two halves of the process is made possible by introducing sacrificial electron donors or acceptors as surrogates for the missing complementary half reaction. The specific choice of these sacrificial agents dictates the energetic potential of the net reaction and this choice is therefore important in developing a system that truly converts photonic energy into a chemical fuel. Typical sacrificial reductants for the formation of dihydrogen are tertiary amines such as 1,4-diazabicyclo[2.2.2]-octane (DABCO), triethylamine (TEA), N,N-

dimethyl aniline (DMA), Ethylenediaminetetraacetic acid (EDTA) and triethanolamine (TEOA), which decompose after a one electron oxidation, allowing for maximal cage escape yield.[1]

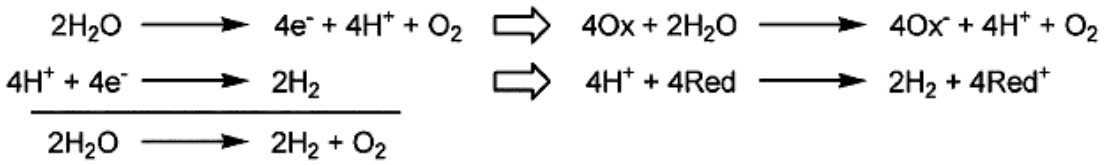

Scheme 6.1: *Left: separation of water splitting reaction into independent half reactions. Right: introduction of sacrificial reductant (Red) and oxidant (Ox), allowing an independent study of water reduction and oxidation catalysis.*

Typically, chosen oxidants include persulfate, cobalt(III), and cerium(IV), all of whose oxidative potentials are strong enough to be considered irreversible. There are few examples of molecular catalysts that have been successfully employed in photochemical oxygen production.[2] Rotzinger *et. al.*[2a] reported controlled-potential electrolysis of cis-$[Ru^{II}L_2(OH_2)]^{2+}$ (where L is 2,2'-bipyridyl-5,5'-dicarboxylic acid) in 0.5 M H_2SO_4 solutions leads to the formation of a relatively durable and active molecular water-oxidation catalyst. Detailed analyses by UV-visible absorption spectrophotometry, resonance Raman spectrophotometry, electrochemical measurements, HPLC, and elemental analysis indicate that the water-oxidation catalyst is an oxo-bridged dimer, $[L_2(H_2O)Ru\text{-}O\text{-}Ru(OH_2)L_2]$. The effectiveness of the oxo-bridged complex as a water-oxidation catalyst has been evaluated by electrochemical and spectrophotometric analyses and by determining oxygen production.[2a] This homogeneous catalyst is highly effective in mediating the thermal and visible-light-induced generation of oxygen from water. The presence of the COOH groups at the 5,5'-positions of the bipyridyl ligands correlates with the unusual and favorable properties of cis-$[RuL_2(OH_2)_2]$ and $[L_2(OH_2)Ru\text{-}O\text{-}Ru(OH_2)L_2]$.[2a] Nocera and coworkers,[2b] reported a high surface area electrode functionalized with a cobalt-based oxygen evolving catalysts (Co-OEC = electrodeposited from pH 7 phosphate, Pi, pH 8.5 methylphosphonate, MePi, and pH 9.2

borate electrolyte, Bi).[2b] Co-OEC prepared from MePi and operated in Pi and Bi achieves a current density of 100 mA cm^{-2} for water oxidation at 442 and 363 mV overpotential, respectively. The catalyst retains activity in near-neutral pH buffered electrolyte in natural waters and seawater.[2b] Fundamentally, photosynthesis is the two step process of absorbing light and forming a fuel/oxidant pair. By independently developing species capable of absorption or catalysis, it becomes possible to fine tune each component individually before reassembling them into a complete catalytic cycle.

Light-driven water photolysis starts with photoinduced charge separation. A molecular photosensitizer (PS) may absorb a photon to generate a vibrationally and electronically excited state, which quickly relaxes to the lowest-lying excited state, PS*. This excited state may then be quenched by another species via electron transfer, provided PS* is sufficiently long-lived. While conjugated organic molecules have been used as photosensitizers,[3, 4, 5] the majority of employed molecular dyes rely on metal to ligand charge transfer (MLCT) transitions that exhibit strong absorbance in the visible part of the spectrum and relatively long excited state lifetimes. Some of the most studied molecular architectures in solar energy absorption are polypyridyl complexes of ruthenium(II). Tris(2,2'-bipyridine) ruthenium(II) ($[Ru(bpy)_3]^{2+}$) possesses strong absorbance in the visible spectrum (ε = 14000 $M^{-1}cm^{-1}$, λ_{max} = 450 nm) and microsecond lifetimes at room temperature.[6] However, it was found that the emission energy of ruthenium(II) tris-diimine complexes can be adjusted through ligand modification due to the presence of a low lying triplet metal centered (^{3}MC) excited state.[7] The detrimental effect of this short-lived and accessible ^{3}MC state (see Chapter 1) is that the populating this anti-bonding, e_g* molecular orbital (MO) weakens the metal–ligand bond, promoting degradation through ligand dissociation. In an effort to alleviate the constraint of the ^{3}MC state, third row transition metals such as iridium[11] have been targeted as alternative photosensitizers, since their greater ligand field splitting allows for a broader range of populated/unpopulated MO gap energies.[11] Additionally, the absolute energies corresponding to the highest populated and lowest unpopulated MOs of heteroleptic iridium complexes incorporating 2 phenylpyridine (ppy) and one bpy can be adjusted independently of each other through chemical substitution on the peripheries of the ppy

and bpy ligands, respectively.[8, 9, 10] This ability to selectively tune the critical MOs may prove useful in reuniting the PS with a pair of optimized catalysts. One disadvantage of the Ir(III) however is that most absorption bands observed for these type of complexes are in the UV region of the spectrum.

Therefore, because its favorable absorption in the visible part of the spectrum, the luminescent excited state of tris(2,2'-bipyridine)ruthenium(II) ($*[Ru(bpy)_3]^{2+}$) has attracted most attention.[11, 12, 13] This excited state, a strong reductant rapidly reduces even mild oxidants [14, 15, 16] and is thermodynamically capable of reducing water to hydrogen. However there is no evidence that the latter reaction occurs rapidly in homogeneous solution. In the strategy employed here, the short-lived reductant $*[Ru(bpy)_3]^{2+}$ is transformed into the longer-lived, more strongly reducing ion, $[Ru(bpy)_3]^{+}$. It is proposed that $[Ru(bpy)_3]^{+}$ subsequently reduces a metal complex such as $[Co^{II}(Me_6[14]dieneN_4)(H_2O)_2]^{2+}$ [18] which in turn reacts rapidly with H_3O^+ or H_2O to form an unstable hydride. For example, it has been noted that metal hydrides can be useful intermediates in the catalyzed photodissociation of water.[17]

In 1979, Sutin *et. al.*,[18] reported the success of two such systems for the photochemically initiated evolution of H_2 from aqueous solution. Europium(II) [19, 20] and the ascorbate ion [22] react with $*[Ru(bpy)_3]^{2+}$ in aqueous solution to form high transient concentrations of $[Ru(bpy)_3]^{+}$. Macrocyclic cobalt(I) complexes such as $[Co^{I}(Me_6[14]dieneN_4)]^{+}$ have been shown by pulse-radiolysis studies [21] to react rapidly with H_3O^+. The related cobalt(I) complex, $[Co^{I}(Me_6[14]tetraeneN_4)]^{+}$, reacts with H_2O and other protic solvents with the evolution of H_2, [22] From electrochemical data in CH_3CN, [23, 24] the $[Ru(bpy)_3]^{+}$ ion is thermodynamically capable of reducing $[Co^{II}(Me_6[14]dieneN_4)(H_2O)_2]^{2+}$ ($Co^{II}L$) to the corresponding Co(I) complex. A system consisting of $[Ru(bpy)_3]^{2+}$, $Co^{II}L$, and either ascorbate ion or Eu(II) is therefore a rationally designed system in which to attempt the catalyzed photoreduction of water using visible light.

Recently, there has been a considerable amount of recent work invested in linking a photosensitizing unit to a water reduction catalyst. Such bridged systems may result in

increased electron transfer rates, while the adjustment of orbital energies and overlap allows for a long-lived charge-separated state. Many systems use the same catalyst and photosensitizer prototypes that have been discussed in chapters 1.[25] Connecting the photosensitizer to a water reducing catalyst might prove to be advantageous, but knowing for certain the nature of the *active* catalyst can be difficult. Since several recent examples of bridged systems use Pt(II) or Pd(II) based catalysts for proton reduction, the formation of a metallic colloid by reduction of the catalytic site is a concern and needs to be addressed. Specifically since the formation of a potentially more efficient colloidal catalysts must be considered. Recently, the photoinduced decomposition of a catalyst similar to structures reported in chapter 1 was shown by ESI-MS, while the formation of the Pd colloids was observed by TEM and XPS during hydrogen production.[26] In addition, the possibility of dissociation of the catalytic centre from the bridge in intramolecular photocatalysts needs to be investigated. Therefore, such systems must be studied in detail with carefully selected conditions to determine the nature of the catalytic species.

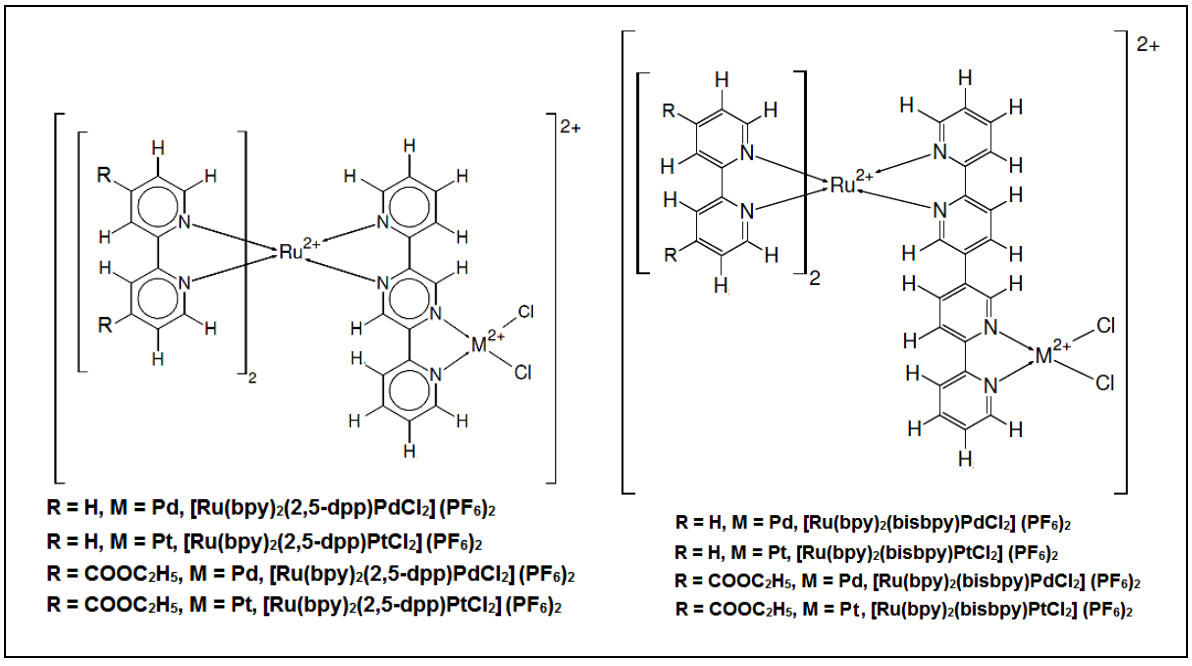

Figure 6.1: *Chemical structures of the photocatalysts synthesised in this thesis (contd. to next page).*

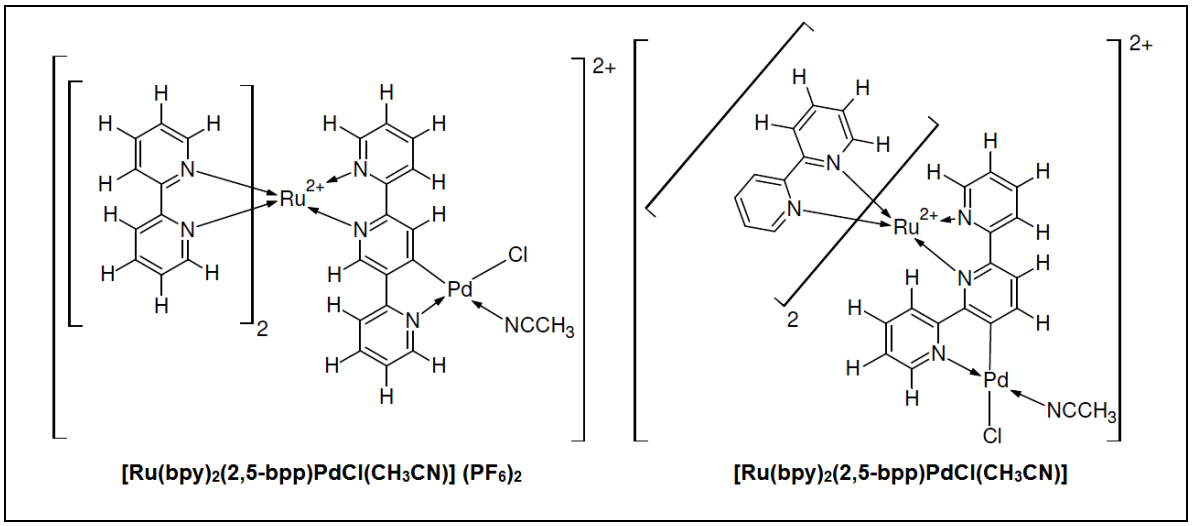

Figure 6.1: *Chemical structures of the photocatalysts synthesised in this thesis.*

Chapters 3, 4 and 5 reported the synthesis and the photocatalytic properties of the number of new photocatalysts (Figure 6.1) which have some similar with structures reported in to literature,[25, 26] The photocatalytic properties of these compounds will be discussed and compared in detail in this chapter.

6.2 Result and discussions.

The name of the heterodinuclear complexes used in this chapter is the same as that listed in chapters 3, 4 and 5, as shown in figure 6.1.

6.2.1 Comparative analysis of photocatalytic properties.

6.2.1.1 Effect of an electron-withdrawing group attached to the peripheral ligand and deuteriation of peripheral / bridging ligands.

Since the absorption features of the compound are important from a photocatalytic point of view, the electronic spectra of the compounds are discussed briefly. The photophysical and photochemical properties of mixed-ligand polypyridyl ruthenium(II) model

complexes $[Ru(tbbpy)_3]^{2+}$, $[Ru(tbbpy)_2(dcmb)]^{2+}$ and $[Ru(dcmb)_3]^{2+}$ (where ligands tbbpy; 4,4'-di-tert-butyl-2,2'-bipyridine and dcmb; 4,4'-dimethoxycarbonyl-2,2'-bipyridine) were studied by Rau. *et. al.*[27] The absorption spectra of the homoleptic compounds $[Ru(dcmb)_3]^{2+}$ and $[Ru(tbbpy)_3]^{2+}$ in dichloromethane show a single maximum at 464 nm and 461 nm, respectively. The heteroleptic compound $[Ru(tbbpy)_2(dcmb)]^{2+}$ shows two maxima at 424 nm and 488 nm (see Figure 6.2), which can be assigned to the two possible MLCT states of the two different ligands, corresponding to a transition from the d orbital of the ruthenium centre to the π* orbital of tbbpy or dcmb. The red shift in the absorption maxima in the case of the heteroleptic compounds probably occurs as a result of a decrease in symmetry and a cumulative effect of electron withdrawing and electron-donating properties which is supported by resonance Raman and electrochemical data.[27, 28, 29]

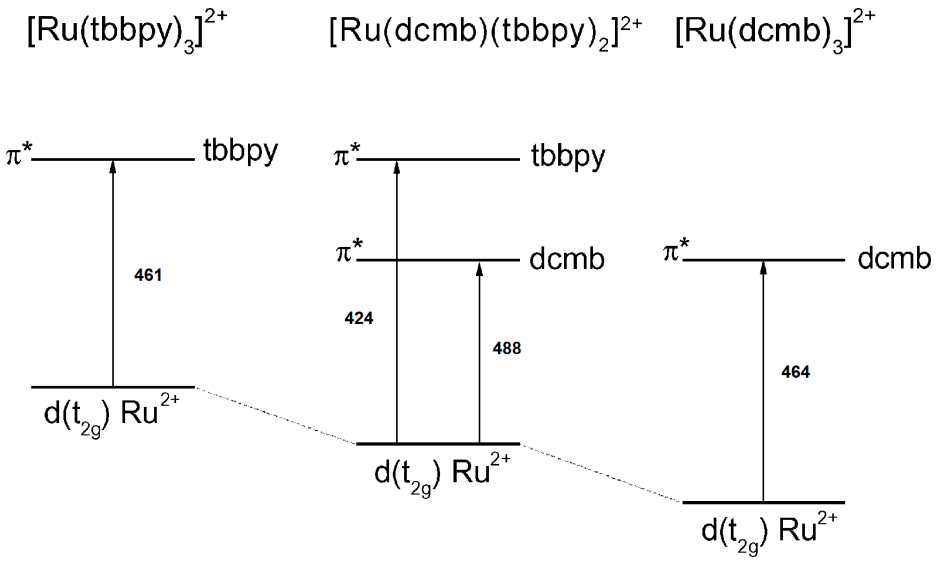

Figure 6.2: *Schematic representation of the [1]MLCT transitions (in dichloromethane) of the compounds $[Ru(tbbpy)_3]^{2+}$, $[Ru(tbbpy)_2(dcmb)]^{2+}$ and $[Ru(dcmb)_3]^{2+}$ (in nm).*[27]

Similarly, when comparing the complexes containing 2,5-dpp/ bisbpy as bridging ligands and dceb as peripheral ligands, the [1]MLCT absorption maxima of $[Ru(dceb)_3]^{2+}$ [27, 28], $[Ru(dceb)_2(2,5\text{-}dpp)]^{2+}$ [30] and $[Ru(dceb)_2(bisbpy)]^{2+}$ are observed at 467 nm, 467 nm and 475 nm in acetonitrile. The position of the lowest energy [1]MLCT transition Ru → ligand

changes when one dceb unit in $[Ru(dceb)_3]^{2+}$ is replaced with 2,5-dpp or the bisbpy bridging ligands. There is not much change in the absorption maxima when 2,5-dpp was used as a bridging ligand, but the maximum is red shifted when the more conjugated π-electron bisbpy ligand was used. There is a lowering of the π* orbital of the bridging ligand when the free chelating site is coordinated by $PdCl_2$ or $PtCl_2$ units.[30]

For the complex $[Ru(dceb)_2(2,5\text{-dpp})PdCl_2]^{2+}$, the lowest energy ^{1}MLCT transition Ru → 2,5-dpp is observed at 526 nm,[30] however for the complex $[Ru(dceb)_2(bisbpy)PdCl_2]^{2+}$, the lowest energy ^{1}MLCT transition, Ru → bisbpy is observed at 475 nm. There was no change in absorption maxima for this complex when compared to the mononuclear complex, suggesting limited interaction between the two metal centres. The similar trend has been observed for $PtCl_2$ containing complexes for $[Ru(dceb)_2(2,5\text{-dpp})PdCl_2]^{2+}$ (^{1}MLCT = 540 nm) and $[Ru(dceb)_2(bisbpy)PdCl_2]^{2+}$ (^{1}MLCT = 475 nm) (*see chapter 3 and 5*).

Sakai and coworkers reported that the photoinduced hydrogen generation via intramolecular electron transfer from the $[Ru^*(bpy)_2(phen)]^{2+}$ (Ru* = absorb light) unit to the $PtCl_2$(R-bpy) unit in complexes **B**, $\mathbf{B_1}$ and $\mathbf{B_2}$ as shown in Figure 6.3, is enhanced by the introduction of an electron withdrawing group (R = COOH or COOEt) on the Pt bound polypyridyl ligand. These results are in agreement with the difference observed in the first reduction potential ($E_{½}$ = -1.20 V (**B**), -1.23 V ($\mathbf{B_1}$) and -1.39 V ($\mathbf{B_2}$)) and DFT analysis for these compounds.[31]

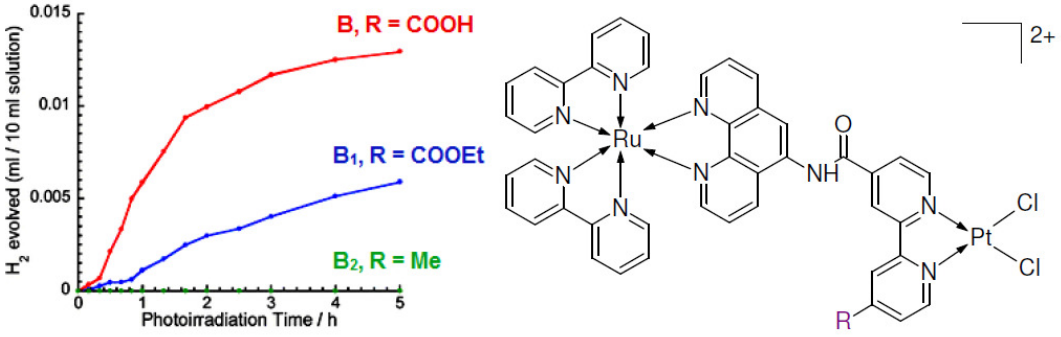

Figure 6.3: *Electron withdrawing group effects on photochemical hydrogen production by Sakai et. al.*[25c]

Since the energy level of the π* orbital of the bpy ligand bound to the *cis*-$PtCl_2$ unit largely affects the photoinduced electron transfer efficiency together with the photo-hydrogen generation of these molecular devices, two structural analogues of **B** in figure 6.3 (*i.e.*, **B_1: R = COOEt** and **B_2: R = CH_3**; see Figure 6.3) were developed by substituting the carboxyl group of **B** (**R = COOH**) with either the ethoxycarbonyl group in **B_1** (**R = $COOC_2H_5$**) or the methyl group in **B_2** (**R = CH_3**). As illustrated in Figure 6.4, the energy level of the LUMO, corresponding to the π* orbital of the $PtCl_2$(bpy) unit, gradually increases with increasing electron-donating character of the substituent group **R**.[31] Since the energies of the ^{3}MLCT exited states of these complexes are not greatly affected upon changing the group **R** substituent, the driving force for the intramolecular photo-electron transfer is primarily governed by the first reduction potential at the bpy ligand ($E_{½}$ = -1.20 V (**B**), -1.23 V (**B_1**) and -1.39 V (**B_2**)) bound to the *cis*-$PtCl_2$ unit.[31]

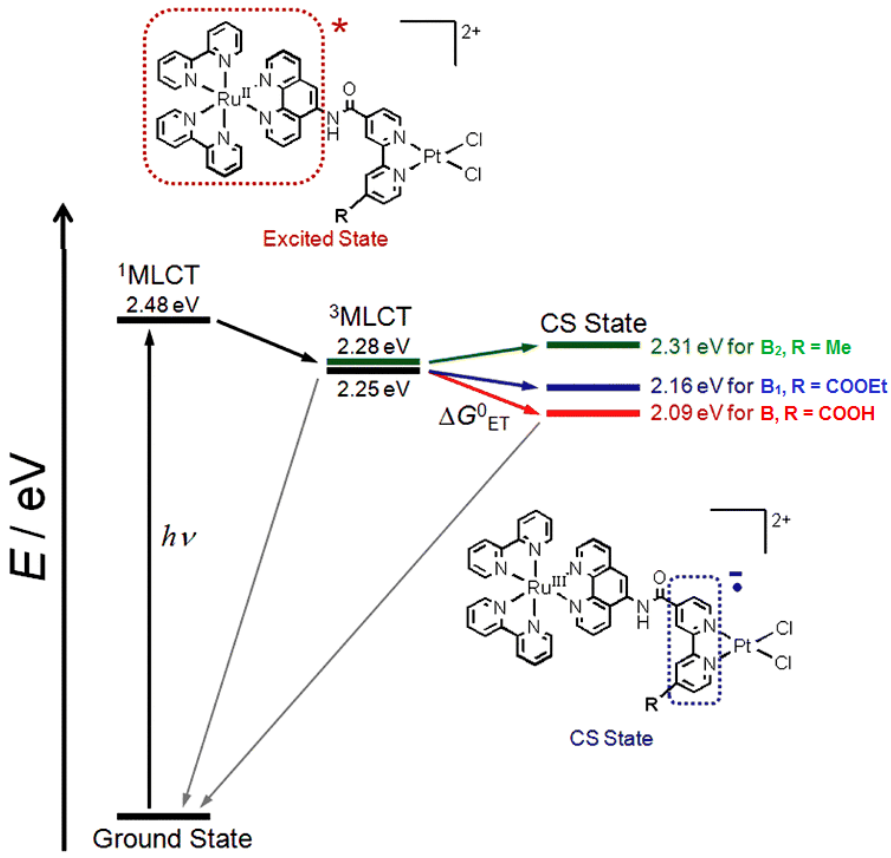

Figure 6.4: *Energy level diagram of the photochemical events for the Ru(II)Pt(II)-based photo-molecular devices by sakai et. al.*[31]

The driving forces for the photo-electron transfer were estimated as –0.16 eV for **B**, –0.09 eV for $\mathbf{B_1}$, and 0.06 eV for $\mathbf{B_2}$ as shown in Figure 6.4, clearly indicating that the photoinduced electron transfer in $\mathbf{B_2}$ is an uphill process.[31] As expected from these results, strong platinum induced quenching of the emission was observed in $\mathbf{B_1}$ and for **B**, but not for $\mathbf{B_2}$.[31] In accord with these results, the photo-hydrogen activity of $\mathbf{B_1}$ was lower than that observed for **B**, while $\mathbf{B_2}$ did not show any detectable photo-hydrogen activity as shown in Figure 6.3.[31] The observed clear relationship between the photo-hydrogen activity and the driving force for the photoinduced electron transfer can be regarded as an important guideline for the structural design of more highly active photo-molecular devices.

Run	Complexes	TON (with 5 % water) {S.D.}	TOF / h^{-1} (with 5 % water)
1.	$[Ru(bpy)_2(bisbpy)PdCl_2]^{2+}$	5 {1}	1
2.	$[Ru(bpy)_2(bisbpy)PtCl_2]^{2+}$	75 {8}	9
3.	$[Ru(dceb)_2(bisbpy)PdCl_2]^{2+}$	513 {2}	64
4.	$[Ru(dceb)_2(bisbpy)PtCl_2]^{2+}$	258 {6}	32
5.	$[Ru(bpy)_2(2,5\text{-}dpp)PdCl_2]^{2+}$	0	0
6.	$[Ru(bpy)_2(2,5\text{-}dpp)PtCl_2]^{2+}$	0	0
7.	$[Ru(dceb)_2(2,5\text{-}dpp)PdCl_2]^{2+}$	403 {15}	50
8.	$[Ru(dceb)_2(2,5\text{-}dpp)PtCl_2]^{2+}$	14{1}	2
9.	$[Ru(D_8\text{-}bpy)_2(2,5\text{-}dpp)PdCl_2]^{2+}$	0	0
10.	$[Ru(D_8\text{-}bpy)_2(D_{10}\text{-}2,5\text{-}dpp)PdCl_2]^{2+}$	0	0
11.	$[Ru(bpy)_2(2,5\text{-}bpp)]^{2+} + (NH_4)_2[PdCl_4]$	50 {3}	6
12.	$[Ru(D_8\text{-}bpy)_2(2,5\text{-}bpp)]^{2+} + (NH_4)_2[PdCl_4]$	49{3}	6

Table 6.1: *Photocatalytic activity of the listed complexes, ((Conc. of catalyst = 4.08×10^{-5} M and TEA (conc.) = 2.15 M in anhydrous acetonitrile with 5 % water), 18 hours irradiation at 470 nm); TOF = TON per hour.*

In table 6.1, a comparison of non-ester and ester analogues containing 2,5-dpp and bisbpy bridging ligands shows that the ester analogues are more efficient photocatalysts then the non-ester analogues. The exact reason for this behaviour of ester complexes is still in processes but may be due to their photophysical properties. The non-ester analogues $[Ru(bpy)_2(bisbpy)PdCl_2]^{2+}$ (run 1), $[Ru(bpy)_2(bisbpy)PtCl_2]^{2+}$ (run 2), $[Ru(bpy)_2(2,5\text{-}dpp)PdCl_2]^{2+}$ (run 5) and $[Ru(bpy)_2(2,5\text{-}dpp)PdCl_2]^{2+}$ (run 1) are not good photocatalysts for the reduction of water compared to the ester-analogues as shown in run 3, 4, 7 and 8. The photocatalytic generation of hydrogen of the heterodinuclear complexes listed in Figure 6.1, increased when an electron-withdrawing group was attached at the peripheral ligands (see table 6.1), due to stabilisation of the ground state, as the energy gap between orbital Ru^{2+} $d(t_2^g)$ – π^*(dceb) orbital decreases.[27] This demonstrate that the energetic separation between the ^{3}MLCT state and the reactive ^{3}MC state can be controlled by designing complexes having a ligand with a low-energy π^* level.

Run 9 and 10 in table 6.1, the D_8-bpy complexes, $[Ru(D_8\text{-}bpy)_2(2,5\text{-}dpp)PdCl_2]^{2+}$ and $[Ru(D_8\text{-}bpy)_2(D_{10}\text{-}2,5\text{-}dpp)PdCl_2]^{2+}$ show no hydrogen activity. Deuterium is a stable isotope of hydrogen and has an increased molar mass of 2 g/mol. When bound to carbon, due to the higher mass, a reduction in amplitude and frequency of the vibrational stretching modes is observed. This results in a slower vibrational relaxation which causes an increase of the lifetime of the excited state. However, an increase of lifetime due to deuteriation is only observable when there is a significant contribution of the C-H stretching to the radiationless decay.[32, 33, 34, 35, 36] The complexes $[Ru(D_8\text{-}bpy)_2(2,5\text{-}dpp)PdCl_2]^{2+}$ and $[Ru(D_8\text{-}bpy)_2(D_{10}\text{-}2,5\text{-}dpp)PdCl_2]^{2+}$ observed no increase in lifetime compared to the non-deuteriated complexes (see table 3.5 and 3.6, chapter 3) because of the very short emission lifetimes observed for both non-deuteriated and deuteriated complexes (τ = < 0.5 ns). It was expected that the hydrogen TON may increase with an increase in lifetime following deuteriation of the peripheral and bridging ligands in the complexes. Experiments 11 and 12 indicate that an intermolecular reaction of non-deuteriated mononuclear complex $[Ru(bpy)_2(2,5\text{-}bpp)]^{2+}$ (TON = 50) (τ = 442 ns) and deuteriated mononuclear complex $[Ru(D_8\text{-}bpy)_2(2,5\text{-}bpp)]^{2+}$ (TON = 49) (τ = 525 ns)

with a palladium precursor $(NH_4)_2[PdCl_4]$ shows the same amount of hydrogen was produced.

6.2.1.2 Effects of the amount of water on the photocatalytic properties.

Table 6.2, shows the effect that various quantities of water had on the hydrogen turn over number. When the water concentration increases, from 0-5% the amount of hydrogen increases for all complexes however upon further addition of water to the photocatalytic solution, the TON decreases for runs 4,6 and 7 but increases for the others. At 15% water H_2 production decreases for all the complexes. This may be due to insolubility of catalyst in the solution as shown in run 1-7 with 15 % water. The activating effect of water might be the result from altered solvent polarity, increased proton mobility, or the propensity of water molecules to act as ligands at the Pd / Pt center.[37, 38] Run 3, shows formation of black precipitates for the cyclometallated complex $[Ru(bpy)_2(2,5\text{-bpp})PdCl(CH_3CN)]^{2+}$ (intermolecular as well as intramolecular reaction), possibly due to Pd colloids, which act as active catalytic species,[26] however the remaining complexes in Table 6.2, showed no black precipitates.

Run	Complexes	TON with H_2O %			
		0%	5%	10%	15%
1.	$[Ru(bpy)_2(bisbpy)PdCl_2]^{2+}$	0	5	16	13
2.	$[Ru(bpy)_2(bisbpy)PtCl_2]^{2+}$	29	75	92	85
3.	$[Ru(bpy)_2(2,5\text{-bpp})PdCl(CH_3CN)]^{2+}$	0	108	130	94
4.	$[Ru(dceb)_2(bisbpy)PdCl_2]^{2+}$	23	513	360	198
5.	$[Ru(dceb)_2(bisbpy)PtCl_2]^{2+}$	13	258	286	45
6.	$[Ru(dceb)_2(2,5\text{-dpp})PdCl_2]^{2+}$	0	403	313	94
7.	$[Ru(dceb)_2(2,5\text{-dpp})PtCl_2]^{2+}$	0	14	7	4

Table 6.2: *Photocatalytic activity of the listed complexes, ((Conc. of catalyst = 4.08×10^{-5} M, except for $[Ru(bpy)_2(2,5\text{-bpp})PdCl(CH_3CN)]^{2+}$ = 6.0×10^{-5} M and TEA (conc.) = 2.15 M in anhydrous acetonitrile with 0-15 % water (v/v)), 18 hours irradiation at 470 nm light). S.D. ± 15 TONs or less.*

6.2.1.3 Time and wavelength dependent studies on the photocatalytic properties.

The TON-spectra discussed in this contribution refer to the integrated amount of hydrogen produced over the course of 8 hours irradiation, while Table 6.3 and Fig. 6.6 reflect the entire time-course of the catalytic reaction in terms of the irradiation-time dependence of the TON, called turnover frequency (TOF = TON per hour). Time dependent studies of the complexes shown in figure 6.5, illustrate the photocatalytic activity for hydrogen production for the different compounds. $[Ru(dceb)_2(2,5\text{-}dpp)PdCl_2]^{2+}$ and $[Ru(dceb)_2(bisbpy)PdCl_2]^{2+}$ produce hydrogen much more efficiently (TON = 390 and 481, respectively) under the stated conditions while the TON reduces to 124 for $[Ru(bpy)_2(2,5\text{-}bpp)PdCl(CH_3CN)]^{2+}$. The turnover frequency measured for the complex $[Ru(dceb)_2(2,5\text{-}dpp)PdCl_2]^{2+}$ is TOF = 49 h^{-1} with an induction period for the first 2 hours. After 1 hour irradiation of $[Ru(dceb)_2(2,5\text{-}dpp)PdCl_2]^{2+}$, a TON of 5.0, reflects a small amount hydrogen-produced followed by a sudden rise in the amount of hydrogen until 4 hours (TON = 341) and a further small increase to reach maximum TON after 8 hours (TON = 390). The catalytic activity of the complexes $[Ru(dceb)_2(bisbpy)PdCl_2]^{2+}$ (TOF = 60 h^{-1}) and $[Ru(bpy)_2(2,5\text{-}bpp)PdCl(CH_3CN)]^{2+}$ (TOF = 16 h^{-1}) show a constant increase in hydrogen generation which reached the maximum turnover at 8 hours. No photocatalytic activity was observed for the complex $[Ru(bpy)_2(2,6\text{-}bpp)PdCl(CH_3CN)]^{2+}$, which is attributed to steric hindrance and its electronic properties.

The compounds $[Ru(dceb)_2(2,5\text{-}dpp)PdCl_2]^{2+}$ and $[Ru(dceb)_2(bis\text{-}bpy)PdCl_2]^{2+}$ produce hydrogen with 5 % water after 18 hours TON = 403 and 513, respectively while the compound $[Ru(bpy)_2(2,5\text{-}bpp)PdCl(CH_3CN)]^{2+}$ generated a TON = 108 after 18 hours of irradiation. Hence, the observed time-dependence of the catalytic reaction is in agreement with the general trend observed in supramolecular catalytic systems.[25, 38]

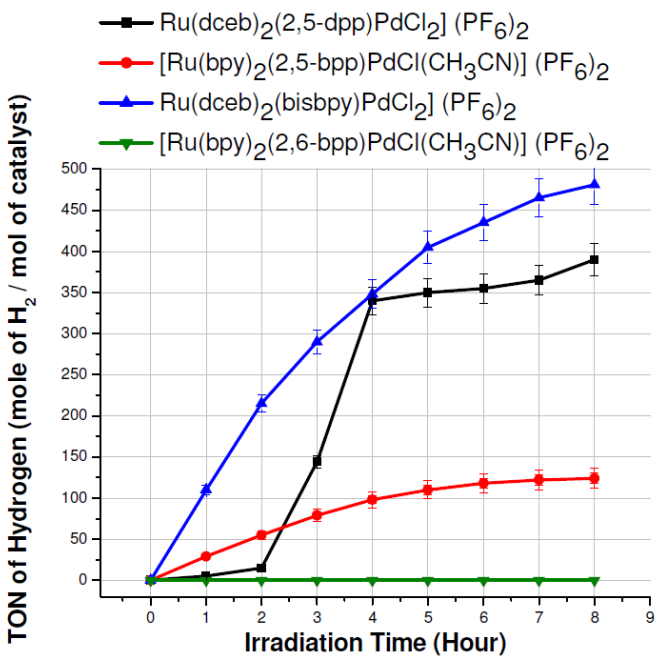

Figure 6.5: *Photocatalytic TON vs. Time (= TOF) of the listed complexes, ((Conc. of catalyst (in blue and black) = 4.08×10^{-5}M; (Conc. of catalyst (in red and green) = 6.0×10^{-5} M) and TEA (conc.) = 2.15 M in anhydrous acetonitrile with 5 % water (v/v)), 8 hours irradiation at 470 nm); TOF = TON h^{-1}. S.D. ± 10 TONs or less.*

Time / h	$[Ru(dceb)_2(2,5\text{-}dpp)PdCl_2]^{2+}$		$[Ru(bpy)_2(2,5\text{-}bpp)PdCl(CH_3CN)]^{2+}$		$[Ru(dceb)_2(bisbpy)PdCl_2]^{2+}$		$[Ru(bpy)_2(2,6\text{-}bpp)PdCl(CH_3CN)]^{2+}$	
	TON	TOF / h^{-1}	TON	TOF / h^{-1}	TON	TOF / h^{-1}	TON	TOF / h^{-1}
0	0	0	0	0	0	0	0	0
1	5	5	29	29	110	110	0	0
2	15	7.5	55	27.5	215	107.5	0	0
3	144	48	79	26.3	290	96.7	0	0
4	340	85	98	24.5	348	87	0	0
5	350	70	110	22	405	81	0	0
6	355	59.2	118	19.7	435	72.5	0	0
7	365	52.1	122	17.4	465	66.4	0	0
8	390	48.8	124	15.5	481	60.2	0	0

Table 6.3: *Summary of the turnover number (TON) and the turnover frequency (TOF) during the time-course of the catalytic reaction for the listed complexes. The reaction was driven by irradiation of the sample at 470 nm.*

The complexes $[Ru(bpy)_2(2,5\text{-}bpp)PdCl(CH_3CN)]^{2+}$ and $[Ru(dceb)_2(bisbpy)PdCl_2]^{2+}$ show a maximum rate of 29 h^{-1} and 110 h^{-1} after 1 hour irradiation, respectively. The complex $[Ru(dceb)_2(2,5\text{-}dpp)PdCl_2]^{2+}$ shows a maximum rate of 85 h^{-1} after 4 hours with a sharp increase from 2 – 4 hours of irradiation, and after that the rate of hydrogen production leveled off. The complexes $[Ru(bpy)_2(2,5\text{-}bpp)PdCl(CH_3CN)]^{2+}$, $[Ru\text{-}(dceb)_2(bisbpy)PdCl_2]^{2+}$ and $[Ru(dceb)_2(2,5\text{-}dpp)PdCl_2]^{2+}$ shows maximum catalytic activity within the first four hours. In all these complexes the rate of production of hydrogen decreases strongly after reaching to the maximum value of TOF, possibly suggesting that photocatalytic activity is dropping constantly due to the decomposition of the photocatalysts as shown in Figure 6.6. In relation to decomposition of the photocatalysts, time dependent UV-Vis spectroscopy experiments were performed (see figure 6.15, later section) with $[Ru(dceb)_2(2,5\text{-}dpp)PdCl_2]^{2+}$, and the mononuclear $[Ru(dceb)_2(2,5\text{-}dpp)]^{2+}$ precursor mixed with $[Pd(CH_3CN)_2Cl_2]$ (intermolecular reaction) under photocatalytic conditions.

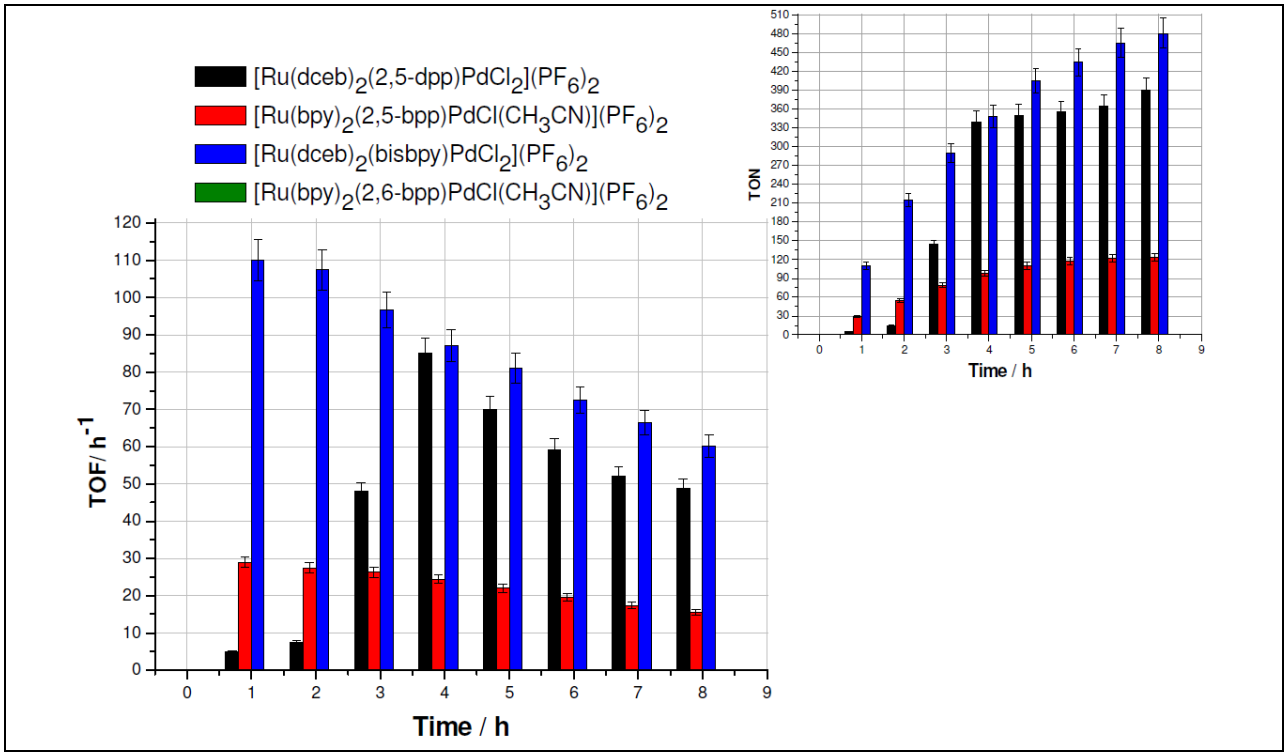

Figure 6.6: *The turnover frequency (TOF) for the listed complexes at 470 nm irradiation shown in dependence on the reaction time. The values obtained up to 8 hours in increments of 1 hour. The inset presents the TON dependence on the reaction time. S.D. ± 10 TONs or less.*

The amount of hydrogen produced for compound $[Ru(bpy)_2(2,5\text{-bpp})PdCl(CH_3CN)]^{2+}$ was measured at various irradiation wavelengths as shown in Figure 6.7. This experiment was performed by Prof. Sven Rau, University of Erlangen, Germany. A maximum TON of 130 with 10 % water was obtained close to the absorption extinction maximum at λ = 463 nm when photo-excitation using visible light at 470 nm for 18 hours was used as shown in Figure 6.7. For other excitation energies the TON values decreased according to the absorption spectrum. For the varying wavelength experiment, the turn over numbers of hydrogen were observed as follow; for green light, λ = 520 nm (TON = 51), yellow light, λ = 590 nm (TON = 5) and red light, λ = 630 nm (TON = 0). Rau and coworkers, observed similar behaviour for wavelength dependent intramolecular photocatalytic hydrogen generation experiments for the complex $[Ru(tbbpy)_2(tpphz)PdCl_2]$ $(PF_6)_2$ noting that the catalytic activity did not strictly follow the absorption spectrum. [37] On the other hand for the heterogeneous photocatalytic hydrogen production with graphitic C_3N_4 (g-C_3N_4) where the catalytic activity strictly follows the absorption spectrum. [39, 40]

In Figure 6.7, the maximum TON observed for $[Ru(bpy)_2(2,5\text{-bpp})PdCl(CH_3CN)]^{2+}$ was 130 following irradiation at 470 nm (where the compound has an extinction coefficient = 1.28×10^4 M^{-1} cm^{-1}) which is close to the ^{1}MLCT absorption band (λ = 463 nm, $\varepsilon = 1.33 \times 10^4$ M^{-1} cm^{-1}). For the other wavelengths used, observed TON decreased as expected with the extinction coefficients and are: at λ = 520 nm (TON = 51, $\varepsilon = 0.21 \times 10^4$ M^{-1} cm^{-1}), λ = 590 nm (TON = 5, $\varepsilon = 0.03 \times 10^4$ M^{-1} cm^{-1}) and λ = 630 nm (TON = 0, ε = 0 M^{-1} cm^{-1}). However, for the photocatalyst $[Ru(bpy)_2(2,5\text{-bpp})PdCl(CH_3CN)]^{2+}$ some differences between the absorption spectrum and TON become evident as shown in Figure 6.7. The extinction coefficient tails off much more steeply in the range of 470 to 525 nm than the TON values. This finding raises the question whether the absorption of photons of any wavelength within the MLCT band of $[Ru(bpy)_2(2,5\text{-bpp})PdCl(CH_3CN)]^{2+}$ yield identical catalysis results.

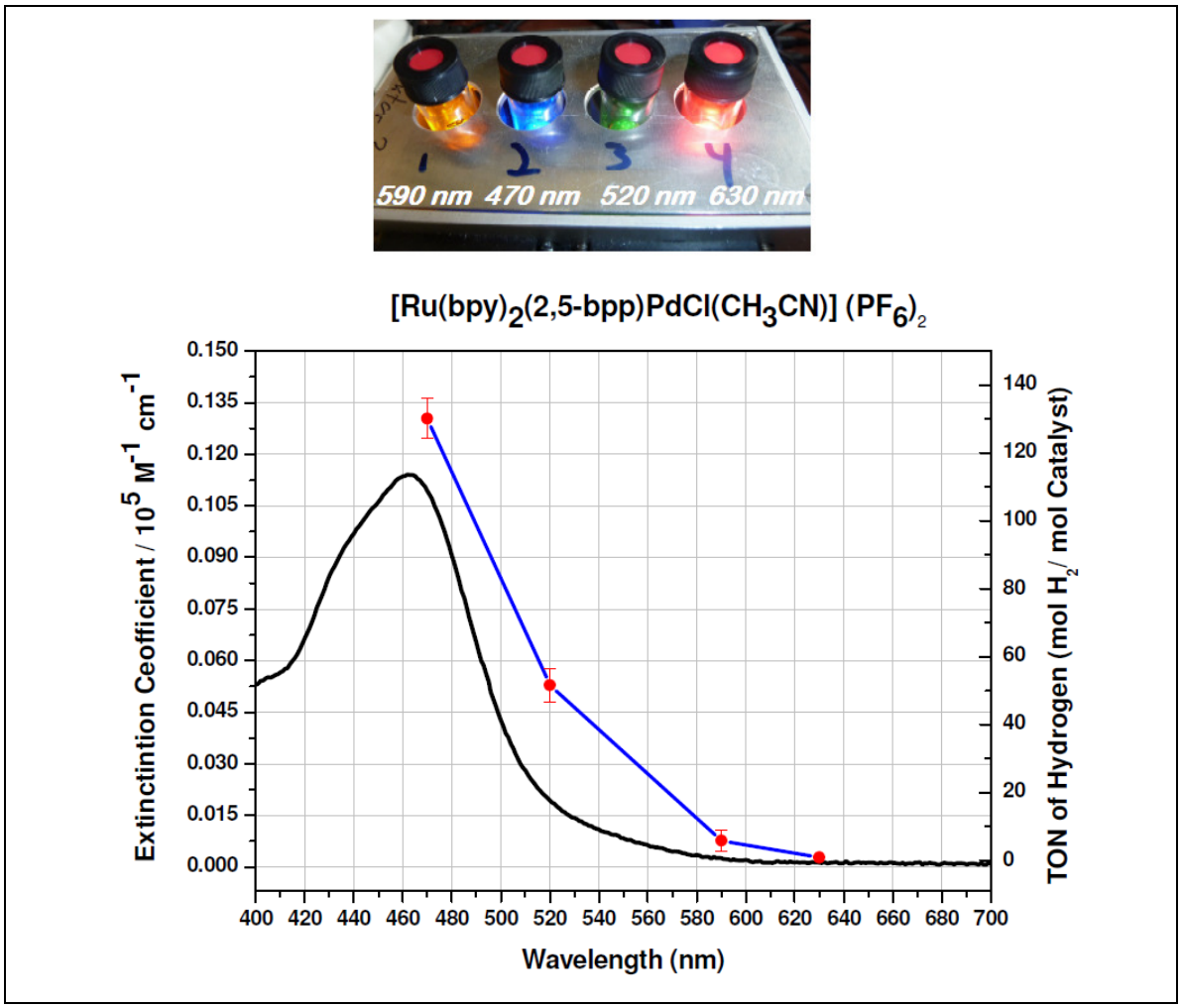

Figure 6.7: *Wavelength dependent studies of complex [Ru(bpy)$_2$(2,5-bpp)PdCl(CH$_3$CN)]$^{2+}$ at wavelength 470 nm, 520 nm, 590 nm and 630 nm: picture of catalytic solutions with different wavelength light (above) and dependence of molar extinction coefficient of the catalyst on the TON of hydrogen (below). ((Conc. of catalyst = 6.0×10^{-5} M) and TEA (conc.) = 2.15 M in anhydrous acetonitrile with 10 % water), 18 hours irradiation. S.D. ± 10 TONs or less.*

To address this question the TON values were converted into an efficiency spectrum Φ(λ) of the catalyst, which was calculated from the ratio of the TON values / the extinction coefficient of [Ru(bpy)$_2$(2,5-bpp)PdCl(CH$_3$CN)]$^{2+}$ normalized to a constant photon flux as shown in Figure 6.8.[37] The efficiency spectrum Φ(λ) calculated by {(TON/extinction coefficient) × Conversion factor (wavelength)} [C. F. value (λ (470) = 1), λ (520) =

2.67), λ (590) = 5.16]. The factors are calculated from the different power of the LEDs: 470 LED: P = 0.08 W, 520 LED: P = 0.03 W and 590 LED: P = 0.0155 W. Figure 6.8 shows that Φ(λ) increases with increasing wavelength in the range between 470 – 520 nm and then afterward decreases to zero. The efficiency spectrum Φ(λ) (Figure 6.8) shows that also for the present compound the extinction coefficient does not perfectly correlate with the TON (Figure 6.7).[37] The absorption of low-energy photons leads to higher catalytic efficiency. The spectral dependence of hydrogen production in the present study shows that excitation of the compound $[Ru(bpy)_2(2,5\text{-}bpp)PdCl(CH_3CN)]^{2+}$ at shorter wavelengths (at 470 nm) leads to a higher integrated hydrogen production than excitation at, for example, λ = 520 nm. However, the photon-to-hydrogen conversion efficiency Φ(λ) shows the opposite trend (Figure 6.8).[37] Rau and coworkers [37] had explained this kind of behaviour of efficiency Φ(λ) curve by means of resonance Raman (rR) spectroscopy. The authors suggested that when the excitation wavelength is shifted to lower energy, the electron density of the excited state shifts from the terminal to the bridging ligand thereby increasing the efficiency of hydrogen formation.[37]

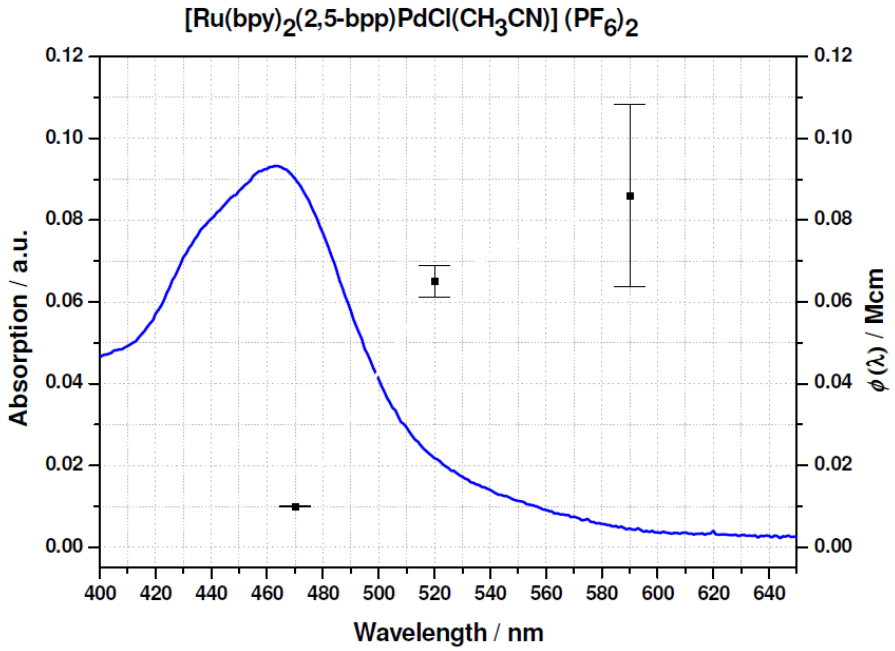

Figure 6.8: *Absorption and efficiency spectrum Φ(λ) of complex* $[Ru(bpy)_2(2,5\text{-}bpp)PdCl(CH_3CN)]^{2+}$ *shows the photon-to-hydrogen conversion of the catalytic process calculated as the ratio of the TON values and the extinction coefficient, normalized to a constant photon flux.*

6.2.1.4 Effects of the steric bulk for the H_2-evolving properties.

Sakai and coworkers [25b] reported how steric factors may affect the catalytic efficiency in H_2 formation at the axial site of the Pt(II) ion in complexes **B**, $\mathbf{B_1}$ and $\mathbf{B_2}$ as shown in figure 6.3 and 6.4. As illustrated in Figure 6.9, when a hydrogen atom attached to the coordinated pyridyl ligand is closely located near the filled Pt(II) d_z^2 orbital, approach of a hydrogen ion towards the d_z^2 orbital is sterically hindered due to the steric repulsion between the two H atoms (Figure 6.9, left). On the other hand, hydrogen activation at the axial site of the Pt(II) ion is sterically allowed when the pyridyl ligand bound to the Pt(II) ion is coplanar with the Pt(II) coordination plane (see Figure 6.9, right).[25b]

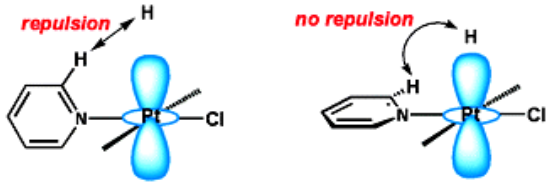

Figure 6.9: *Steric factors on photochemical hydrogen production by Sakai et. al.*[25b]

The synthesis of the sterically strained molecule $[Ru(bpy)_2(2,6\text{-}bpp)PdCl(CH_3CN)]^{2+}$ is straight forward with high yield, but the compound does not show photocatalytic hydrogen activity. This can possibly be explained by the observation that the cyclometallated site (middle pyridine ring) and pyridyl unit (Pd coordinated) in $[Ru(bpy)_2(2,6\text{-}bpp)PdCl(CH_3CN)]^{2+}$ are rigid (*i.e.*, not freely rotating) and therefore the hydrogen atom on the 6-position of the Pd coordinated pyridine and 4-position of the middle pyridine ring prohibit the approach of an H^+ ion (or $H^\bullet$) to the axial site of the Pd(II) ion. However, the planar geometries around the Pd(II) units containing linear terpyridine bridging ligand in the complex $[Ru(bpy)_2(2,5\text{-}bpp)PdCl(CH_3CN)]^{2+}$ sterically allows the approach of an H^+ ion (or $H^\bullet$) to the axial site of the Pd(II) ion. This is illustrated in Figure 6.10 showing the fully optimized structure of $[Ru(bpy)_2(2,5\text{-}bpp)PdCl(CH_3CN)]^{2+}$ (see Figure 6.10, above). The X-ray structure of $[Ru(bpy)_2(2,5\text{-}bpp)PdCl(CH_3CN)]^{2+}$ and $[Ru(bpy)_2(2,6\text{-}bpp)PdCl(CH_3CN)]^{2+}$ have not been reported. The figure shows that the hydrogen atoms at the coordinated α-positions of the pyridines ring are indeed closely located with regard to the filled Pd(II) d_z^2 orbital in $[Ru(bpy)_2(2,6\text{-}$

bpp)PdCl(CH_3CN)]$^{2+}$.[25b] The approach of an H^+ ion (or $H^\bullet$) at the axial site of the Pd(II) ion in [Ru(bpy)$_2$(2,6-bpp)PdCl(CH_3CN)]$^{2+}$ is unfavorable due to the steric contact between the H (α-position of coordinated site) atoms, neighbouring bpy rings and the H^+ ion (or $H^\bullet$) approaching the axial site (see figure 6.10, bottom).[25b]

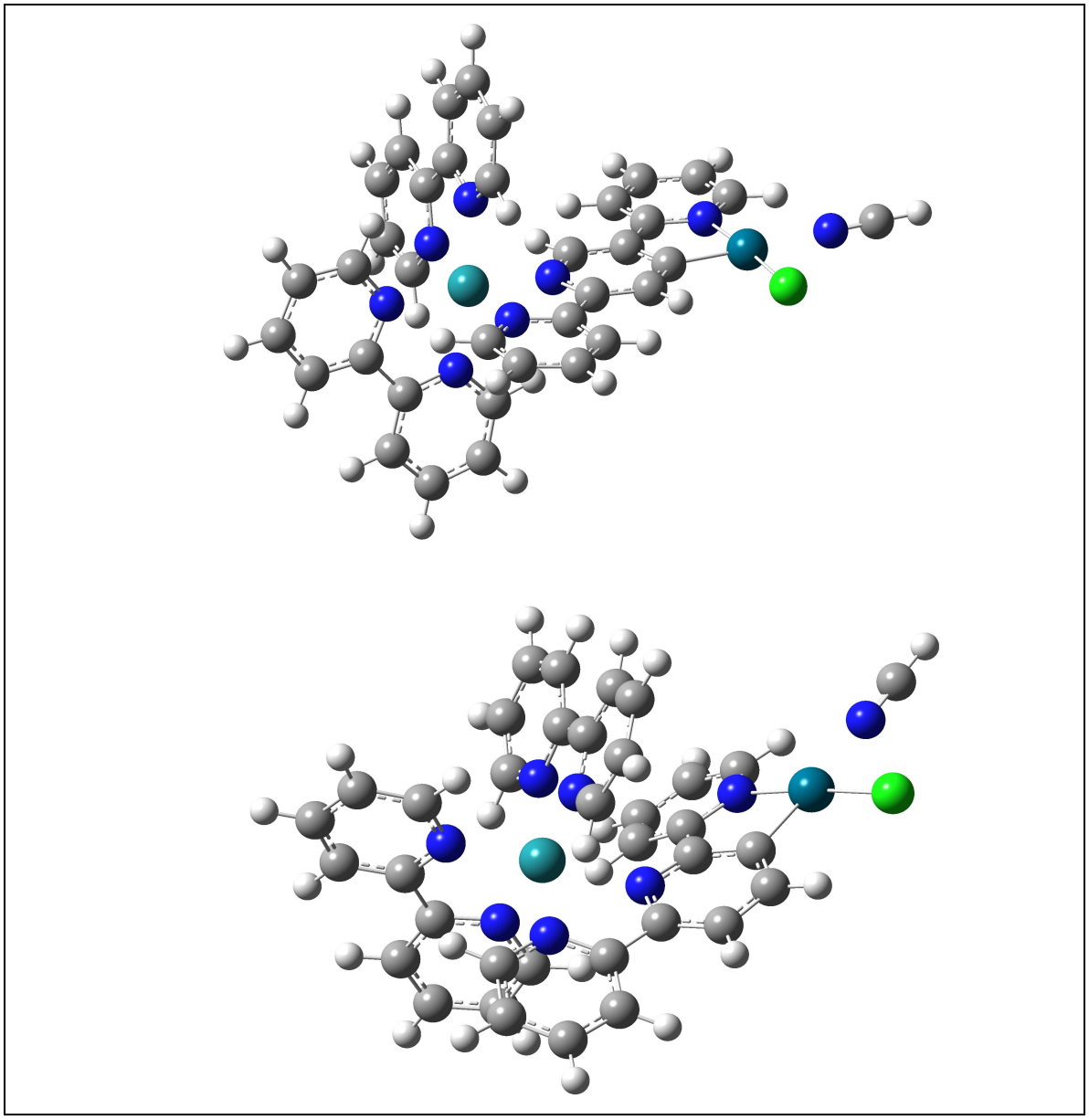

Figure 6.10: *A fully optimized structure for [Ru(bpy)$_2$(2,5-bpp)PdCl(CH_3CN)]$^{2+}$ (**above**) and [Ru(bpy)$_2$(2,6-bpp)PdCl(CH_3CN)]$^{2+}$ (**bottom**) obtained at the B3LYP level of DFT calculation by using Gaussian 09 (see also appendix I).*

Another possible reason why the complex $[Ru(bpy)_2(2,6\text{-bpp})PdCl(CH_3CN)]^{2+}$ does not produce hydrogen may be related to the photophysical properties. The compound does not have the important photochemical properties required to enhance the visible-light-induced charge separation process, as strong electronic coupling between the $[Ru(bpy)_3]^{2+}$-like moiety and the heavy Pd ion promotes quenching of the ^{3}MLCT excited state of the $[Ru(bpy)_3]^{2+}$-like moiety (refer to Chapter 4, Figure 4.17 for UV-Vis properties).[25b] In both the mononuclear and heterodinuclear complex of the 2,6-bpp bridging ligand, a ^{3}MLCT excited state with a short lifetime is observed. For the mononuclear complex $[Ru(bpy)_2(2,6\text{-bpp})]^{2+}$ a lifetime of τ = 33 ns was obtained, and a quantum efficiency of Φ_{em} = 0.003 while for the heterodinuclear complex $[Ru(bpy)_2(2,6\text{-bpp})PdCl(CH_3CN)]^{2+}$, lifetime data indicate a lifetime < 0.5 ns. This very short excited state lifetime and the steric consideration are likely factors for the inefficiency of the 2,6-bpp complex as a photocatalyst for hydrogen production.

6.2.1.5 Effects of the bridging ligand and catalytic centre (Pd/Pt) to the photocatalytic properties.

The results obtained in this study are summarized in Table 6.4. The complexes $[Ru(bpy)_2(2,5\text{-dpp})PdCl_2]^{2+}$, $[Ru(bpy)_2(2,5\text{-dpp})PtCl_2]^{2+}$ and $[Ru(bpy)_2(2,6\text{-bpp})PdCl(CH_3CN)]^{2+}$ (run 3, 4 and 6) do not produce hydrogen due to stronger coupling between the ruthenium(II) mononuclear species and Pd / Pt unit which results in quenching of the ^{3}MLCT excited states. The effect on the TON of conjugated π-electron systems (i.e 2,5-dpp, 2,5-bpp, 2,6-bpp and bisbpy) [30, 41, 42, 43] are shown in Table 6.4. It is assumed that the bisbpy ligand contains the lowest energy π* orbital due to the more electronically conjugated π-electron system[44a] and similarly for 2,5-dpp contained pyrazine based system.[44b] The increasing order of the bridging ligands containing the lowest energy π* orbital are proposed to be the following 2,6-bpp < 2,5-bpp < 2,5-dpp < bisbpy.[44] The runs 1 – 6 in Table 6.4, shows the catalytic activity of the bipyridine based heterodinuclear complexes with different bridging ligands (i.e. 2,5-bpp, 2,6-bpp, 2,5-dpp and bisbpy). The complexes containing bisbpy (runs 1, 2) and 2,5-bpp (run 5) bridging ligands with bpy as peripheral ligand promote hydrogen efficiently from water over the

range 0 – 15% (v/v). The bridging ligands bisbpy and 2,5-bpp control vectorial photoelectron transfer by precise tuning of the physical properties and orientation of the molecular components.[25c] As discussed earlier the effect of electron withdrawing nature of peripheral ligand (dceb), lowers the energy of the π* orbital and electron transfer is easy from ^{1}MLCT to ^{3}MLCT (bridging ligand) via intersystem crossing because the energy gap between the singlet excited state to the triplet excited state decreases.[30] At 0% water some of the complexes produce hydrogen (runs 2, 7 and 8) with a lower TON. It is assumed that TEA acts as a proton source in the absence of water as shown in equations 6.1 – 6.4.

Aliphatic tertiary amines have traditionally been employed as the sacrificial reductants in photocatalytic systems for water reduction, and their oxidation and subsequent degradation (Eq. 6.1 – 6.4) have been studied previously.[45] Following the initial one-electron oxidation, the TEA^+ radical cation is rapidly deprotonated and undergoes a radical shift to the α-carbon. This neutral carbon radical species is expected to be highly reducing, and a second oxidation forms the iminium cation, which is hydrolyzed to form DEA (diethylamine) and acetaldehyde. Thus, each TEA is capable of donating two electrons and two protons. Rapid conversion of the oxidized TEA species, as outlined in Eq. 6.2 and Eq. 6.4, avoids possible back reactions between the oxidized TEA species and the reduced ruthenium and catalytic center.

$$Et_3N \rightarrow Et_2N^{\bullet+}CH_2CH_3 + e^- \quad \text{(Eq. 6.1)}$$

$$Et_2N^{\bullet+}CH_2CH_3 \rightarrow Et_2NC^{\bullet}HCH_3 + H^+ \quad \text{(Eq. 6.2)}$$

$$Et_2NC^{\bullet}HCH_3 \rightarrow Et_2N^+{=}CHCH_3 + e^- \quad \text{(Eq. 6.3)}$$

$$Et_2N^+{=}CHCH_3 + H_2O \rightarrow Et_2NH + CH_3CHO + H^+ \quad \text{(Eq. 6.4)}$$

The effect of the nature of the catalytic Pd / Pt centre on the production of hydrogen is at present not completely understood. Run 2 for complex $[Ru(bpy)_2(bisbpy)PtCl_2]^{2+}$ is the only Pt and bpy based heterodinuclear complex producing hydrogen efficiently while for dceb based heterodinuclear complexes (runs 7 and 9), the Pd complexes yield the higher TON for H_2 production. It is possible that the Pd metal centre is difficult to oxidized but more easily reduced than the Pt metal centre.[46]

Run	Complexes	TON with H_2O %			
		0%	5%	10%	15%
1.	$[Ru(bpy)_2(bisbpy)PdCl_2]^{2+}$	0	5	16	13
2.	$[Ru(bpy)_2(bisbpy)PtCl_2]^{2+}$	29	75	92	85
3.	$[Ru(bpy)_2(2,5\text{-}dpp)PdCl_2]^{2+}$	0	0	0	0
4.	$[Ru(bpy)_2(2,5\text{-}dpp)PtCl_2]^{2+}$	0	0	0	0
5.	$[Ru(bpy)_2(2,5\text{-}bpp)PdCl(CH_3CN)]^{2+}$	0	108	130	94
6.	$[Ru(bpy)_2(2,5\text{-}bpp)PdCl(CH_3CN)]^{2+}$	0	0	0	0
7.	$[Ru(dceb)_2(bisbpy)PdCl_2]^{2+}$	23	513	360	198
8.	$[Ru(dceb)_2(bisbpy)PtCl_2]^{2+}$	13	258	286	45
9.	$[Ru(dceb)_2(2,5\text{-}dpp)PdCl_2]^{2+}$	0	403	313	94
10.	$[Ru(dceb)_2(2,5\text{-}dpp)PtCl_2]^{2+}$	0	14	7	4

Table 6.4: *Photocatalytic activity of the listed complexes, ((Conc. of catalyst = 4.08×10^{-5} M, Conc. of catalysts $[Ru(bpy)_2(2,5\text{-}bpp)PdCl(CH_3CN)]^{2+}$ and $[Ru(bpy)_2(2,6\text{-}bpp)PdCl(CH_3CN)]^{2+}$ = 6.0×10^{-5} M and TEA (conc.) = 2.15 M in anhydrous acetonitrile with 0-15 % water (v/v)), 18 hours illumination at 470 nm). S.D. ± 15 TONs or less.*

6.2.1.6 Effects of the photosensitizer used (Ru^{2+}/Ir^{3+}) to the photocatalytic properties.

In an attempt to rapidly develop diverse photocatalysts, our group also developed iridium cyclometallated ppy complexes which act as a light absorbing unit (detailed work has been reported in the Ph.D. Thesis of Mr. Suraj Soman, Dublin City University, 2011). A number of iridium complexes containing the bridging ligand 2,5-bpp were synthesised, and the same bridging ligand was used here for the case of Ru – Pd/Pt complexes as shown in Figure 6.11.

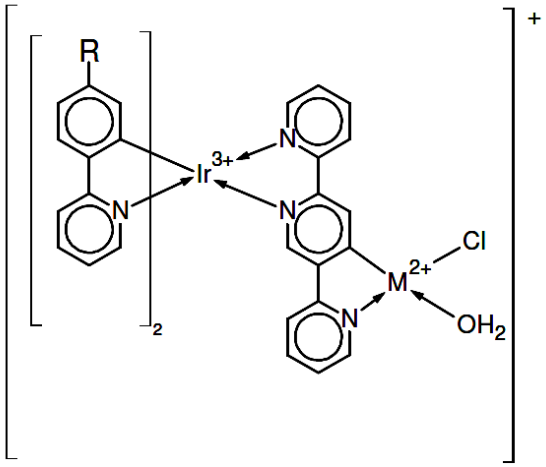

R = H, M = Pd, $[Ir(ppy)_2(2,5\text{-}bpp)PdCl(H_2O)]^+$

R = H, M = Pt, $[Ir(ppy)_2(2,5\text{-}bpp)PdCl(H_2O)]^+$

R = COOMe, M = Pd, $[Ir(COOMe\text{-}ppy)_2(2,5\text{-}bpp)PdCl(H_2O)]^+$

R = COOMe, M = Pt, $[Ir(COOMe\text{-}ppy)_2(2,5\text{-}bpp)PdCl(H_2O)]^+$

Figure 6.11: *Chemical structure of heterodinuclear Ir(III) complexes.*

Run	Complexes	TON {with H_2O %} (Standard deviation)			
		{0%}	{5%}	{10%}	{15%}
1.	$[Ru(bpy)_2(2,5\text{-}bpp)PdCl(CH_3CN)]^{2+}$	0	108 (2)	130 (1)	94 (2)
2.	$[Ir(ppy)_2(2,5\text{-}bpp)PdCl(H_2O)]^+$	73 (7)	245 (12)	253 (14)	242 (0)
3.	$[Ir(ppy)_2(2,5\text{-}bpp)PtCl(H_2O)]^+$	256 (7)	364 (12)	308 (16)	287 (2)
4.	$[Ir(COOMe\text{-}ppy)_2(2,5\text{-}bpp)PdCl(H_2O)]^+$	125 (4)	468 (9)	494 (5)	447 (8)
5.	$[Ir(COOMe\text{-}ppy)_2(2,5\text{-}bpp)PtCl(H_2O)]^+$	285 (22)	452 (12)	449 (21)	383 (11)
6.	$[Ru(bpy)_2(2,5\text{-}bpp)]^{2+} + [Pd(CH_3CN)_2Cl_2]$	-	79 (3)	70 (2)	-
7.	$[Ru(bpy)_2(2,5\text{-}bpp)]^{2+} + [Pt(CH_3CN)_2Cl_2]$	-	0.5 (0)	0.2 (0)	-
8.	$[Ir(ppy)_2(2,5\text{-}bpp)]^+ + [Pd(CH_3CN)_2Cl_2]$	-	280 (9)	64 (14)	-
9.	$[Ir(ppy)_2(2,5\text{-}bpp)]^+ + [Pt(CH_3CN)_2Cl_2]$	-	193 (9)	166 (22)	-
10.	$[Ir(COOMe\text{-}ppy)_2(2,5\text{-}bpp)]^+ + [Pd(CH_3CN)_2Cl_2]$	-	350 (16)	330 (13)	-
11.	$[Ir(COOMe\text{-}ppy)_2(2,5\text{-}bpp)]^+ + [Pt(CH_3CN)_2Cl_2]$	-	313 (8)	301 (15)	-

Table 6.5: *Photocatalytic activity of the listed complexes, ((Conc. of catalyst = 4.08×10^{-5} M, and TEA (conc.) = 2.15 M in anhydrous acetonitrile with 0-15 % water (v/v)), 18 hours of irradiation at 470 nm).*

For comparison, the TON for H_2 production from $[Ru(bpy)_2(2,5\text{-bpp})PdCl(CH_3CN)]^{2+}$ together with the iridium complexes are given in Table 6.5. This table shows that the Ir(III) heterodinuclear complexes produced hydrogen more efficiently than the Ru(II) heterodinuclear complex containing the 2,5-bpp bridging ligand. The presence of the ester groups on the peripheral ligand in both the iridium and ruthenium complexes led to an increase in hydrogen production.

Ir(III) complexes exhibit a wide range of photophysical and electrochemical properties.[47] The efficiency of these complexes as photosensitizers in a homogeneous photocatalytic water reduction system with $[Co(bpy)_3]^{2+}$ was studied, yet no direct correlation exists between the photophysics or electrochemistry and catalytic activity.[48, 49] This emphasizes the difficulties associated with improving such complex catalytic systems based on physical properties because differences in catalyst activity can be from any combination of changes in light absorption, electron transfer rates, or catalyst stability. Figure 6.11 represent a Ir(III) heterodinuclear complex which transfers an electron towards catalytic centre (Pd / Pt metal) by absorbing visible light photons. The intramolecular Ir(III) complexes (in runs 2 and 3) (Table 6.4) promotes higher TON for hydrogen formation than the complexes containing Ru(II) (in run 1). It has been noted that the electron withdrawing ester group attached to the ppy ligands in the intramolecular Ir(III) complexes (runs 4 and 5) produced four times the amount of hydrogen, compared to the analogous Ru(II) complex (run 1) as shown in Table 6.4. Surprisingly the Ir(III) complexes have lower extinction coefficient (ε = 600 – 2000 M^{-1} cm^{-1}) [50] in the visible region (400-600 nm) compared to Ru(II) complexes (ε = 10,000 – 16000 M^{-1} cm^{-1}) but produce higher TON for H_2 compared to the analogous Ru(II) complexes.

The intermolecular reaction between Ir(III) mononuclear complexes {$[Ir(ppy)_2(2,5\text{-bpp})]^+$, $[Ir(COOMe\text{-}ppy)_2(2,5\text{-bpp})]^+$} with Pd / Pt (runs 8 – 11) complexes promotes higher TONs for hydrogen compared to the Ru(II) mononuclear complexes with Pd / Pt {$[Ru(bpy)_2(2,5\text{-bpp})]^{2+}$ + ($[Pd(CH_3CN)_2Cl_2]$ / $[Pt(CH_3CN)_2Cl_2]$) (runs 6 and 7) (see Table 6.4). The photophysical and electrochemical properties are currently being carried out within the research group.

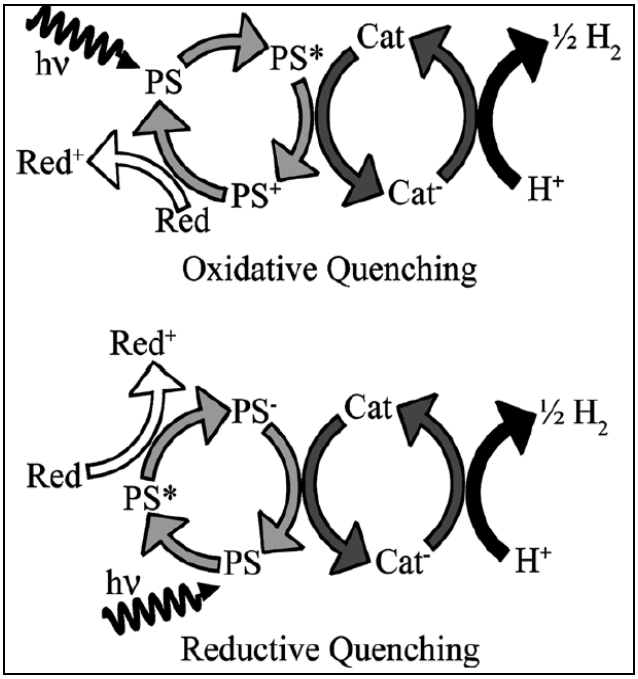

Figure 6.12: *Quenching pathways for the photoreduction of water. Top: oxidative quenching pathway, in which the excited photosensitizer (PS*) donates an electron to the catalyst (Cat) to produce* PS^+*. Bottom: reductive quenching pathway, in which PS* accepts an electron from a sacrificial reductant (Red) to produce* PS^-*.*[51]

Bernard and coworkers, have reported that the heteroleptic cyclometalated iridium(III) complexes significantly outperform ruthenium(II) tris-diimine photosensitizers in photocatalytic systems that utilize a $[Co(bpy)_3]^{2+}$ catalyst and TEOA as a sacrificial reductant.[49] The thermodynamics of charge transfer between PS* (light absorb by the photosensitizer) and sacrificial reductant were determined by fluorimetry and electrochemistry to be identical for the parent dyes ($E^{0'}$ $*M^{n+}/M^{(n-1)+}$ = + 0.68 V vs. SCE for $[Ir(ppy)_2bpy]^+$ and $[Ru(bpy)_3]^{2+}$).[49] However, the authors demonstrated that a reductive quenching mechanism, as shown in Fig. 6.12, is exclusively available to the iridium complexes, with a large excess of sacrificial agent, oxidative quenching may occur.

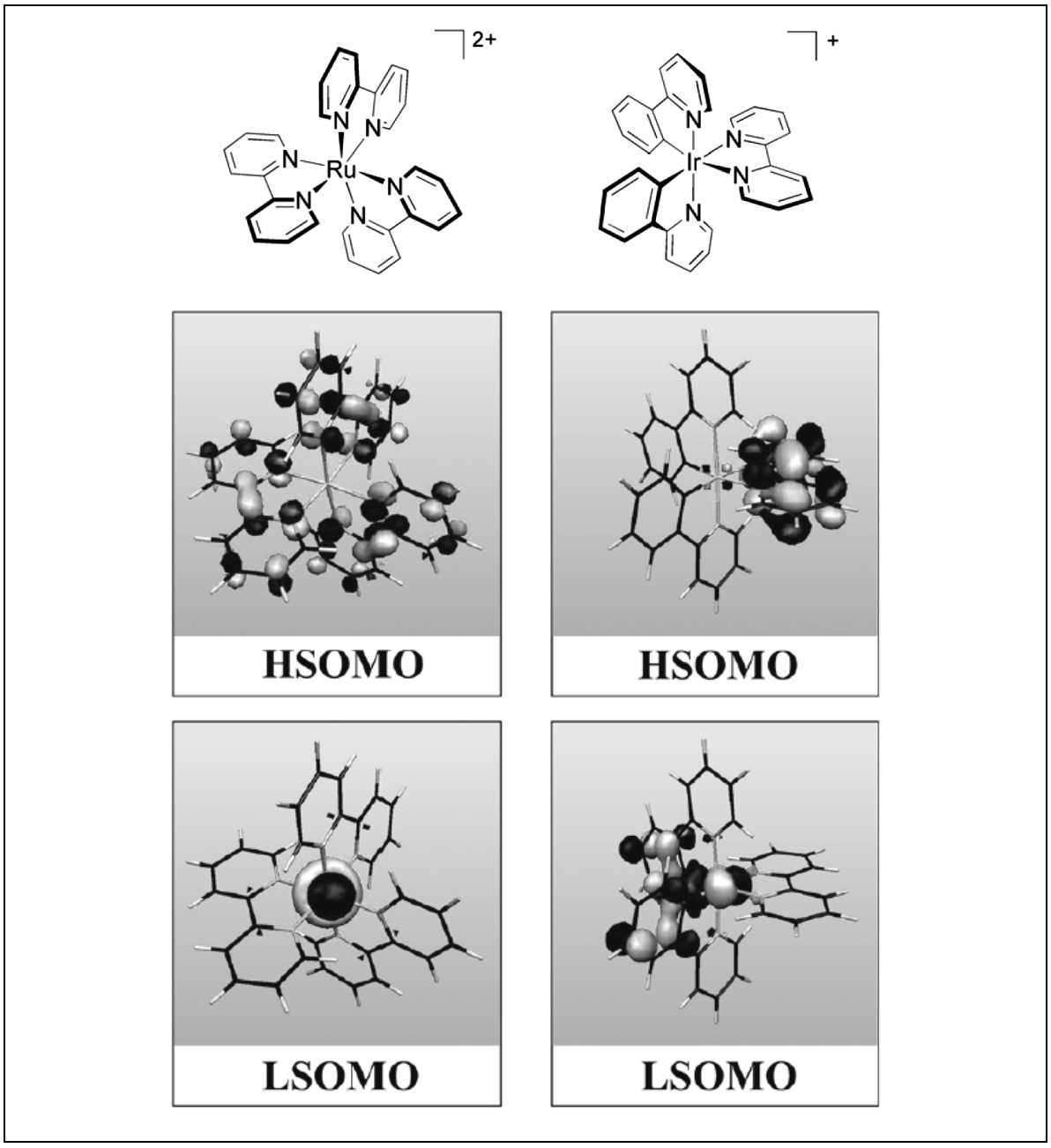

Figure 6.13: *Frontier orbitals of $[Ru(bpy)_3]^{2+}$ (left) and $[Ir(ppy)_2(bpy)]^{+}$ (right) in the triplet excited state obtained through DFT calculations (B3LYP/LANL2DZ). The lowest singly occupied molecular orbital (LSOMO) is exclusively metal centered in $[Ru(bpy)_3]^{2+}$ (95 percentile), while the analogous orbital of the Ir(III) complex exhibits mixed metal-based 5d and ppy-based π character. The highest singly occupied molecular orbitals (HSOMO) of both complexes are exclusively localized on the bpy ligand(s) reported by Bernard et. al.*[51]

$[Ir(ppy)_2bpy]^+$ complex was first substantiated through flash photolysis quenching experiments, and also justified by computational methods. By observing the orbital density of the highest singly occupied molecular orbital (HSOMO) and the lowest singly occupied molecular orbital (LSOMO) of each complexes $[Ru(bpy)_3]^{2+}$ and $[Ir(ppy)_2bpy]^+$ obtained through DFT calculations (Figure 6.13),[52] the difference in quenching susceptibilities between the two luminophores was rationalized: in the triplet state of $[Ir(ppy)_2bpy]^+$, significant LSOMO orbital density lies along the phenylpyridine-defined periphery of the complex, whereas the LSOMO of $[Ru(bpy)_3]^{2+}$ is almost exclusively metal centered, and is thus guarded by the nonparticipating ligand framework.[52] Bernard and coworkers concluded that the differing availability of the PS*'s LSOMO to the surrounding environment explains the observed variation in quenching behavior and increased photocatalytic efficiency.[52]

6.2.1.7 Effects of the intermolecular and intramolecular photocatalysis to the photocatalytic efficiency.

Table 6.6 and Figure 6.14, represents the TONs after 18 hours irradiation for the intermolecular photocatalysts and time dependent studies on these listed complexes from 0 – 8 hours irradiation at 470 nm, respectively. With 5% of water, equimolar ratios of the mononuclear complexes of either $[Ru(dceb)_2(2,5\text{-}dpp)]^{2+}$ (TON = 464) and $[Ru(dceb)_2(bisbpy)]^{2+}$ (TON = 489) with $[Pd(CH_3CN)_2Cl_2]$ (runs 3 and 4) gave higher TONs compared to the monomers $[Ru(bpy)_2(2,5\text{-}bpp)]^{2+}$ (TON = 79) and $[Ru(bpy)_2(2,6\text{-}bpp)]^{2+}$ (TON = 0) as shown in Table 6.6.

It is possible that both $[Ru(dceb)_2(2,5\text{-}dpp)]^{2+}$ and $[Ru(dceb)_2(bisbpy)]^{2+}$ may form heterodinuclear complexes in situ with $[Pd(CH_3CN)_2Cl_2]$, which will be discussed later in this section. The TON for H_2 production for these intermolecular complexes is comparable with their respective heterodinuclear complexes under similar photocatalytic conditions (i.e. $[Ru(dceb)_2(2,5\text{-}dpp)PdCl_2]^{2+}$ (TON = 403) and $[Ru(dceb)_2(bisbpy)PdCl_2]^{2+}$ (TON = 513) with 5% water and 18 hours irradiation) (Figure 6.14).[30] It is proposed that the complex $[Ru(bpy)_2(2,5\text{-}bpp)]^{2+}$ (TON = 79) with

$[Pd(CH_3CN)_2Cl_2]$ is unable to react *in situ* to form the cyclometallated heterodinuclear complex $[Ru(bpy)_2(2,5\text{-bpp})PdCl(CH_3CN)]^{2+}$ (TON = 108) under the stated photocatalytic conditions. For complex $Ru(bpy)_2(2,6\text{-bpp})]^{2+}$, the intermolecular reaction with the palladium precursor also did not produce hydrogen from water as discussed earlier due steric bulk and the quenching of the state (see Table 6.6).

Run	Complexes	TON with H_2O %	
		5%	10%
1.	$[Ru(bpy)_2(2,5\text{-bpp})]^{2+} + [Pd(CH_3CN)_2Cl_2]$	79	70
2.	$[Ru(bpy)_2(2,6\text{-bpp})]^{2+} + [Pd(CH_3CN)_2Cl_2]$	0	0
3.	$[Ru(dceb)_2(2,5\text{-dpp})]^{2+} + [Pd(CH_3CN)_2Cl_2]$	464	-
4.	$[Ru(dceb)_2(bisbpy)]^{2+} + [Pd(CH_3CN)_2Cl_2]$	489	321

Table 6.6: *Photocatalytic activity of the listed intermolecular complexes, ((Conc. of catalyst = 4.08×10^{-5} M, and TEA (conc.) = 2.15 M in anhydrous acetonitrile with 5-10 % water (v/v)), 18 hours of irradiation at 470 nm). S.D. ± 10 TONs or less.*

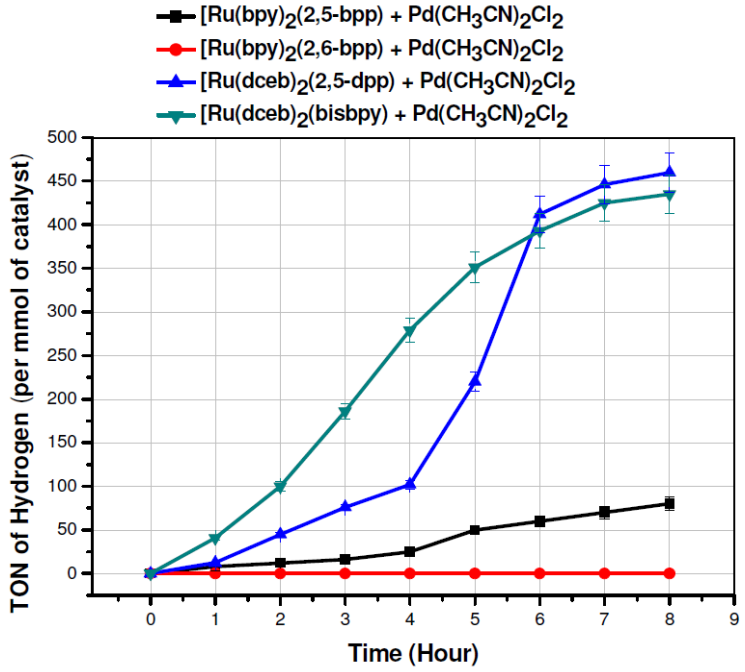

Figure 6.14: *Time dependent studies of intermolecular complexes, ((Conc. of catalyst = 4.08×10^{-5} M, conc. of $[Pd(CH_3CN)_2Cl_2]$ = 4.08×10^{-5} M, TEA (conc.) = 2.15 M in anhyd. ACN with 5 % water (v/v)), 0-8 hours of irrad. at 470 nm). S.D. ± 10 TONs or less.*

Control experiments with the mononuclear precursor compounds (non-ester)-Ru and ester-Ru confirmed the necessity of the presence of the Pd(II) centre for H_2 prodcution. The time-dependence for H_2 formation is shown in Fig. 6.14. Different behaviour was observed for the heterodinuclear complexes as shown in Figure 6.5, and the *in situ* formed complexes (self assembled systems) as shown in figure 6.14 (*i.e.* mononuclear complexes + $[Pd(CH_3CN)_2Cl_2]$, 1 : 1 molar ratio). Figure 6.5 and 6.14, show a sigmoidal time profile eventually reached a plateau that indicates deactivation of the catalyst.[30] Dihydrogen production, reaching a maximum after *ca.* 4 hour for the $[Ru(dceb)_2(2,5\text{-}dpp)PdCl_2]^{2+}$ (from figure 6.5) [30] and *ca.* 6.0 hour for $[Ru(dceb)_2(2,5\text{-}dpp)]^{2+}$ + $[Pd(CH_3CN)_2Cl_2]$ mixture as shown in Figure 6.14.[30] The longer induction period for the *in situ* formed binuclear complex supports the hypothesis that the active catalyst forms in situ and is a binuclear complex. The complexes $[Ru(dceb)_2(bisbpy)PdCl_2]^{2+}$ and $[Ru(dceb)_2(bisbpy)]^{2+}$ plus $[Pd(CH_3CN)_2Cl_2]$ show similar behaviour and the amount of hydrogen produced started to level off after 7 hours. The complex $[Ru(bpy)_2(2,5\text{-}bpp)PdCl(CH_3CN)]^{2+}$ show a constant increase in TON until 8 hours (TON = 124), while the intermolecular reaction mixture of $[Ru(bpy)_2(2,5\text{-}bpp)]^{2+}$ plus $[Pd(CH_3CN)_2Cl_2]$ shows an induction period of *ca.* 5 hours and reached a maxima for H_2 production after 8 hours with a TON = 79 (see figure 6.5 for comparison).

Figure 6.15, represents the absorption spectra for the time dependent irradiation of solutions containing the mononuclear $[Ru(dceb)_2(2,5\text{-}dpp)]^{2+}$ only, heterodinuclear $[Ru(dceb)_2(2,5\text{-}dpp)PdCl_2]^{2+}$ and mononuclear $[Ru(dceb)_2(2,5\text{-}dpp)]^{2+}$ plus palladium (1:1) complex mixture in the presence of sacrificial reductant (TEA) in the dark and after 24 hour continuous irradiation at 470 nm. The absorption spectra at 0 minute irradiation (dark reaction) in the presence of TEA and 5 % (v/v) water, the three individual reaction contained equal concentration of the complexes as shown in Figure 6.15 (upper). The absorption spectra of the solution containing the mononuclear complex $[Ru(dceb)_2(2,5\text{-}dpp)]^{2+}$ and the mixture of $[Ru(dceb)_2(2,5\text{-}dpp)]^{2+}$ + $[Pd(CH_3CN)_2Cl_2]$ both show ^{1}MLCT at 470 nm. This suggested that in the dark reaction no complexation between $[Ru(dceb)_2(2,5\text{-}dpp)]^{2+}$ and $[Pd(CH_3CN)_2Cl_2]$ occurs over a period of 2 hours. The heterodinuclear complex shows two ^{1}MLCT bands at 460 nm and 500 nm. After 30, 60,

120 and 1440 hours of irradiation at 470 nm, all three reactions absorption spectra changes for all the three reactions. Interestingly the heterodinuclear complex $[Ru(dceb)_2(2,5\text{-}dpp)PdCl_2]^{2+}$ and intermolecular reaction mixture of $[Ru(dceb)_2(2,5\text{-}dpp)]^{2+}$ + $[Pd(CH_3CN)_2Cl_2]$ show similarity in their absorption spectra with absorption maxima at 530 nm while the mononuclear complex $[Ru(dceb)_2(2,5\text{-}dpp)]^{2+}$ only shows ^{1}MLCT at 510 nm as shown in Figure 6.15. These results suggest that the complex $[Ru(dceb)_2(2,5\text{-}dpp)PdCl_2]^{2+}$ and the 1:1 complex mixture of $[Ru(dceb)_2(2,5\text{-}dpp)]^{2+}$ and $[Pd(CH_3CN)_2Cl_2]$ form an common intermediate species which efficiently reduced protons from water using visible light as shown in figure 6.15.[30]

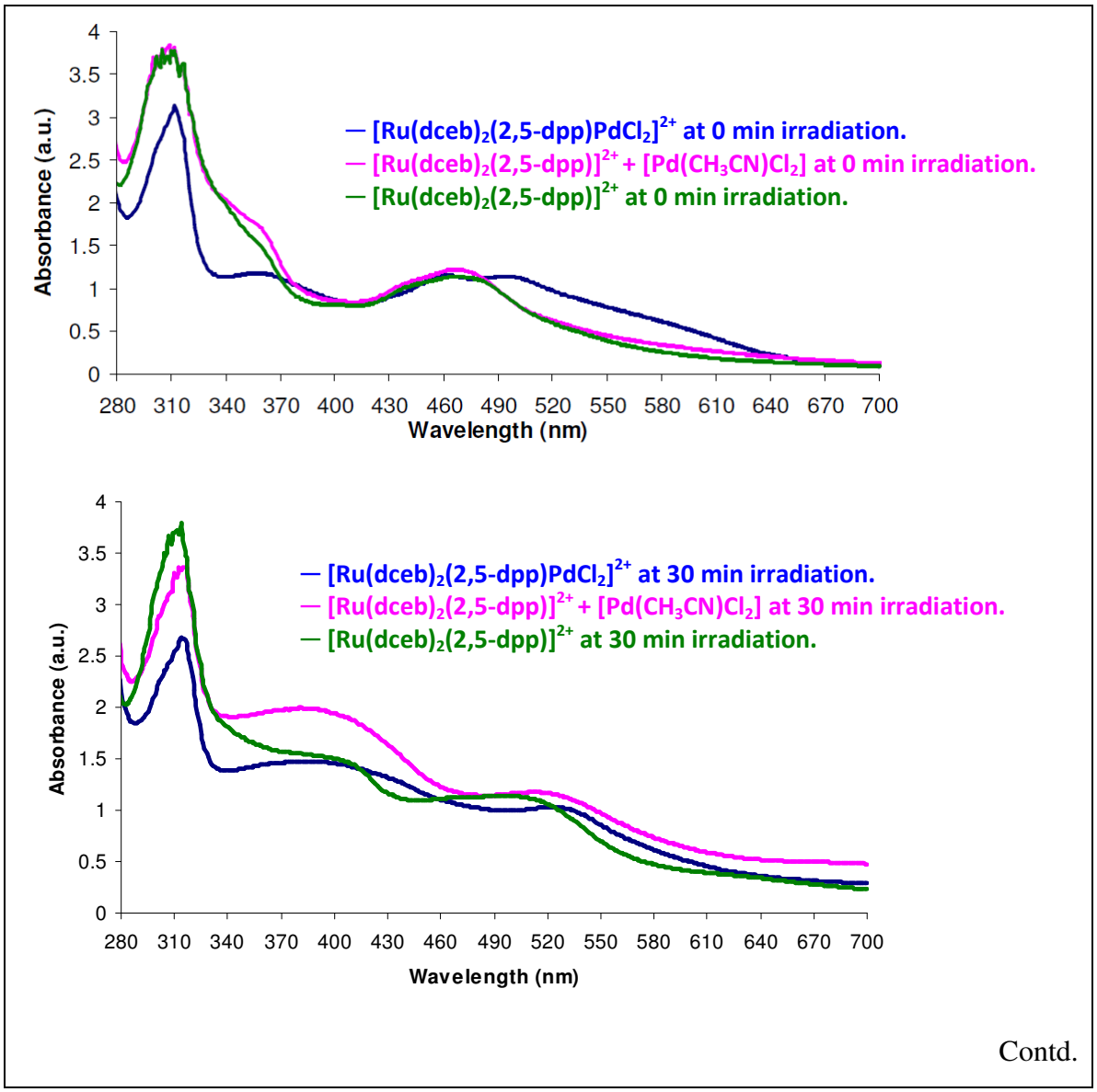

Contd.

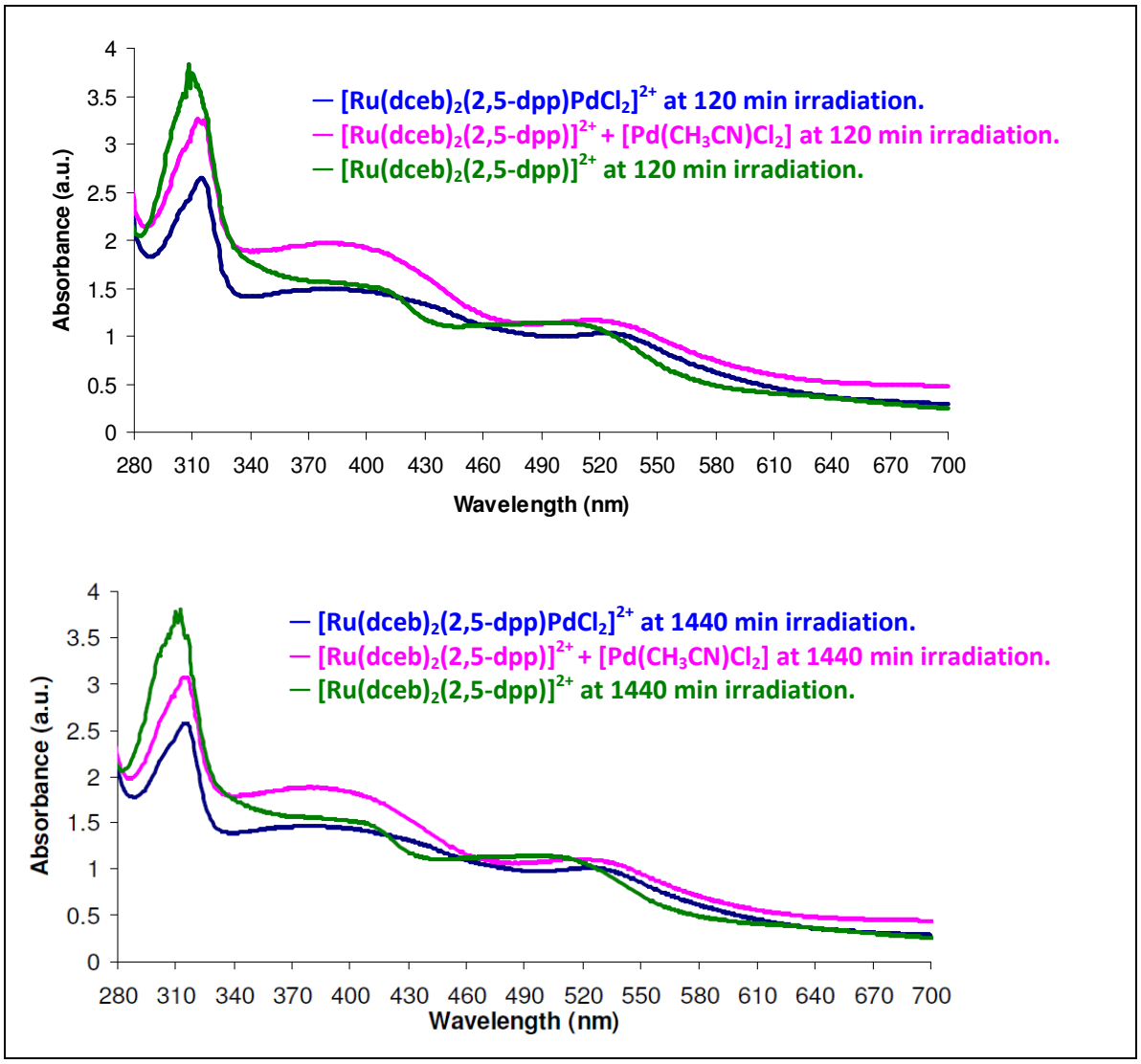

Figure 6.15: *Absorption spectra of time dependent irradiation of complexes listed are constant irradiation at 470 nm under N_2 atmosphere, conc. of complexes = 4.08 x 10^{-5} M dissolved in anhydrous acetonitrile, conc. of TEA = 2.15 M, conc. of water = 5 % (v/v) for time 0 – 1440 min (bottom).*

An experiment was performed by mixing equimolar solutions of $[Ru(dceb)_2(2,5\text{-}dpp)]^{2+}$ and $[Pd(CH_3CN)_2Cl_2]$ (1:1 molar ratio v/v, 5.3×10^{-3} M) in acetonitrile under a nitrogen atmosphere without adding TEA. This reaction mixture was irradiated at 470 nm for 10 minutes. The experimental data was analyzed by UV-Vis spectroscopy as shown in Figure 6.16. The absorption spectra show that the formation of the heterodinuclear

complex after 10 minutes of irradiation as shown in Figure 6.16. A similar experiment was performed in the dark and the complex also formed under these conditions.

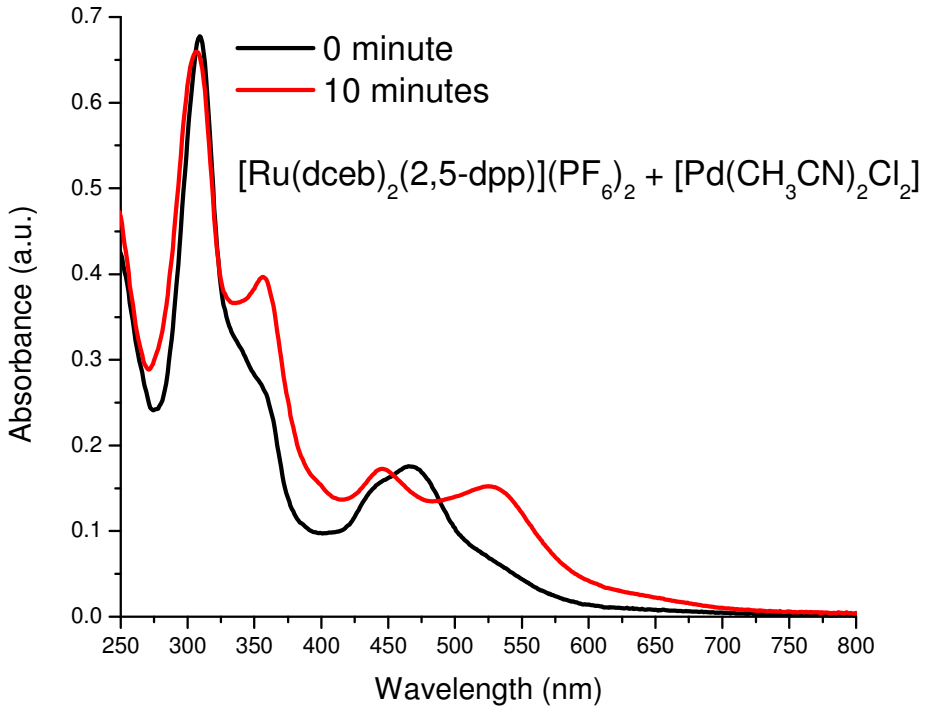

Figure 6.16: *The time dependent studies of the reaction between $[Ru(dceb)_2(2,5\text{-}dpp)](PF_6)_2$ and $[Pd(CH_3CN)_2Cl_2]$ (Conc. = 5.3 x 10^{-3} M, 1:1 molar ratio v/v), irradiated at 470 nm for 10 minutes without stirring under nitrogen atmosphere.*

The reaction mixture was also analyzed by ^{1}H-NMR. The equimolar solutions of $[Ru(dceb)_2(2,5\text{-}dpp)]^{2+}$ and $[Pd(CH_3CN)_2Cl_2]$ (1:1 molar ratio v/v, 5.3 × 10^{-3} M) were prepared in deuteriated acetonitrile and irradiated at 470 nm for 10 minutes. The NMR spectra showed that the formation of the heterodinuclear $[Ru(dceb)_2(2,5\text{-}dpp)PdCl_2]^{2+}$ complex in 100 % yield as shown in Figure 6.17. The ^{1}H-NMR of this intermolecular reaction is shown with the heterodinuclear $[Ru(dceb)_2(2,5\text{-}dpp)PdCl_2]^{2+}$ and mononuclear $[Ru(dceb)_2(2,5\text{-}dpp)]^{2+}$ complexes for comparison (see Figure 6.17).

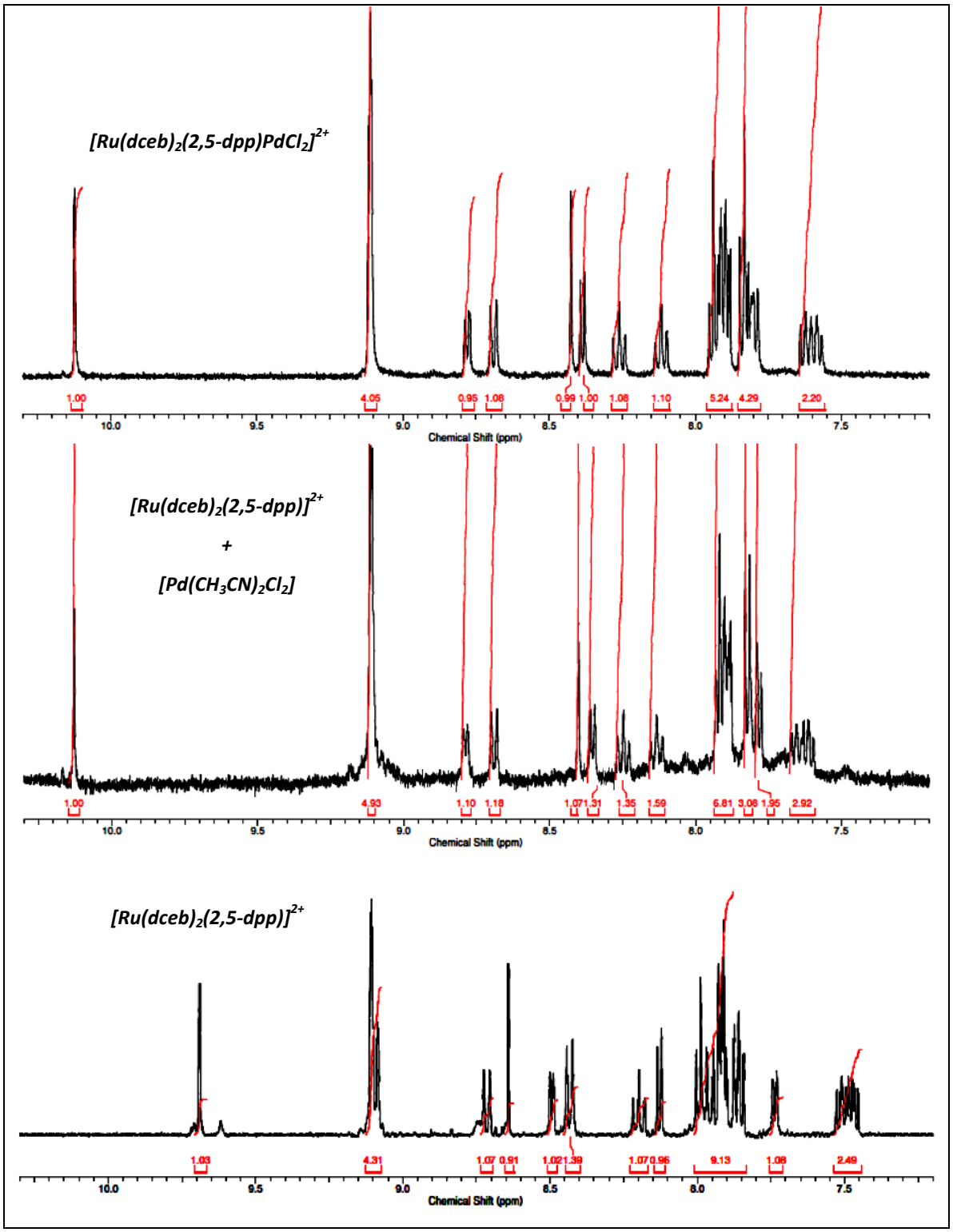

Figure 6.17: *^{1}H-NMR spectra of the intermolecular reaction between the $[Ru(dceb)_2(2,5\text{-}dpp)]^{2+}$ complex and $[Pd(CH_3CN)_2Cl_2]$ complex (Conc. = 5.3 x 10^{-3} M) in deuteriated CD_3CN and irradiated at 470 nm for 10 minutes.*

A similar experiment was carried out with the bpy derivates performed by mixing equimolar solutions of $[Ru(bpy)_2(2,5\text{-dpp})]^{2+}$ and $[Pd(CH_3CN)_2Cl_2]$ (1:1 molar ratio v/v, 5.3×10^{-3} M) in acetonitrile under nitrogen and without adding of TEA (see Figure 6.18). The reaction mixture changed colour from red (mononuclear complex) to purple (heterodinuclear complex) after 10 minutes irradiation at 470 nm (see Figure 6.18). This reaction mixture was also analyzed by ^{1}H-NMR as shown in Figure 6.19, which indicated the formation of the heterodinuclear complex in 100 % yield. This experiment was also performed using constant stirring as well as via sonication method in the dark. The formation of the heterodinuclear compound was the final product seen after 10 minutes in the case of stirring and 5 minutes in the case of sonication.

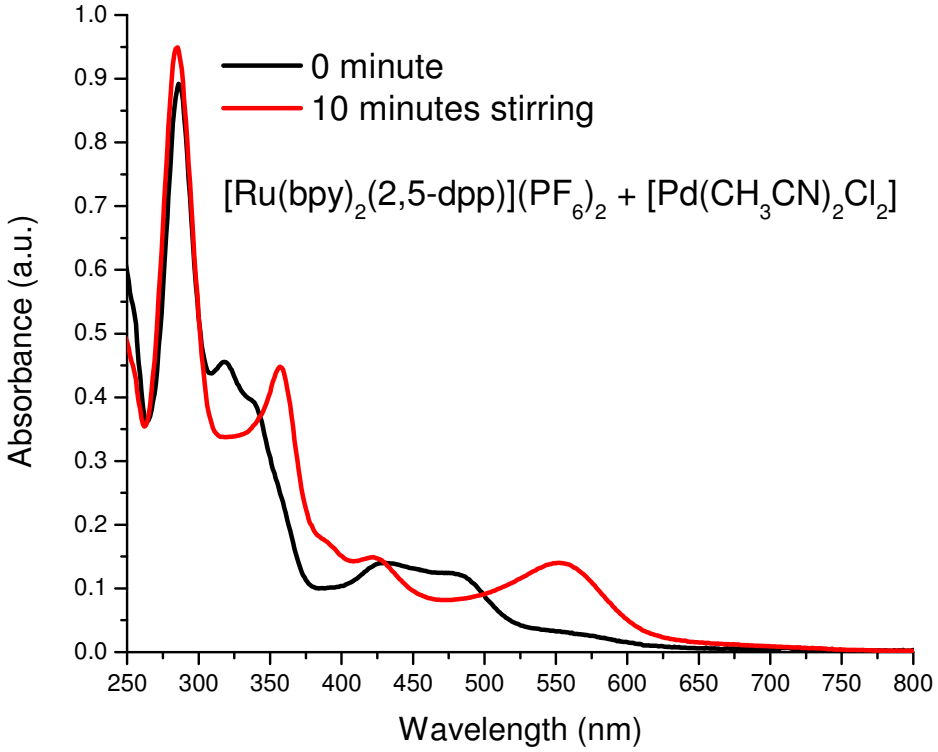

Figure 6.18: *The time dependent studies of the reaction between $[Ru(bpy)_2(2,5\text{-dpp})](PF_6)_2$ and $[Pd(CH_3CN)_2Cl_2]$ (Conc. = 5.3 x 10^{-3} M, 1:1 molar ratio v/v), irradiated at 470 nm for 10 minutes without stirring under nitrogen atmosphere.*

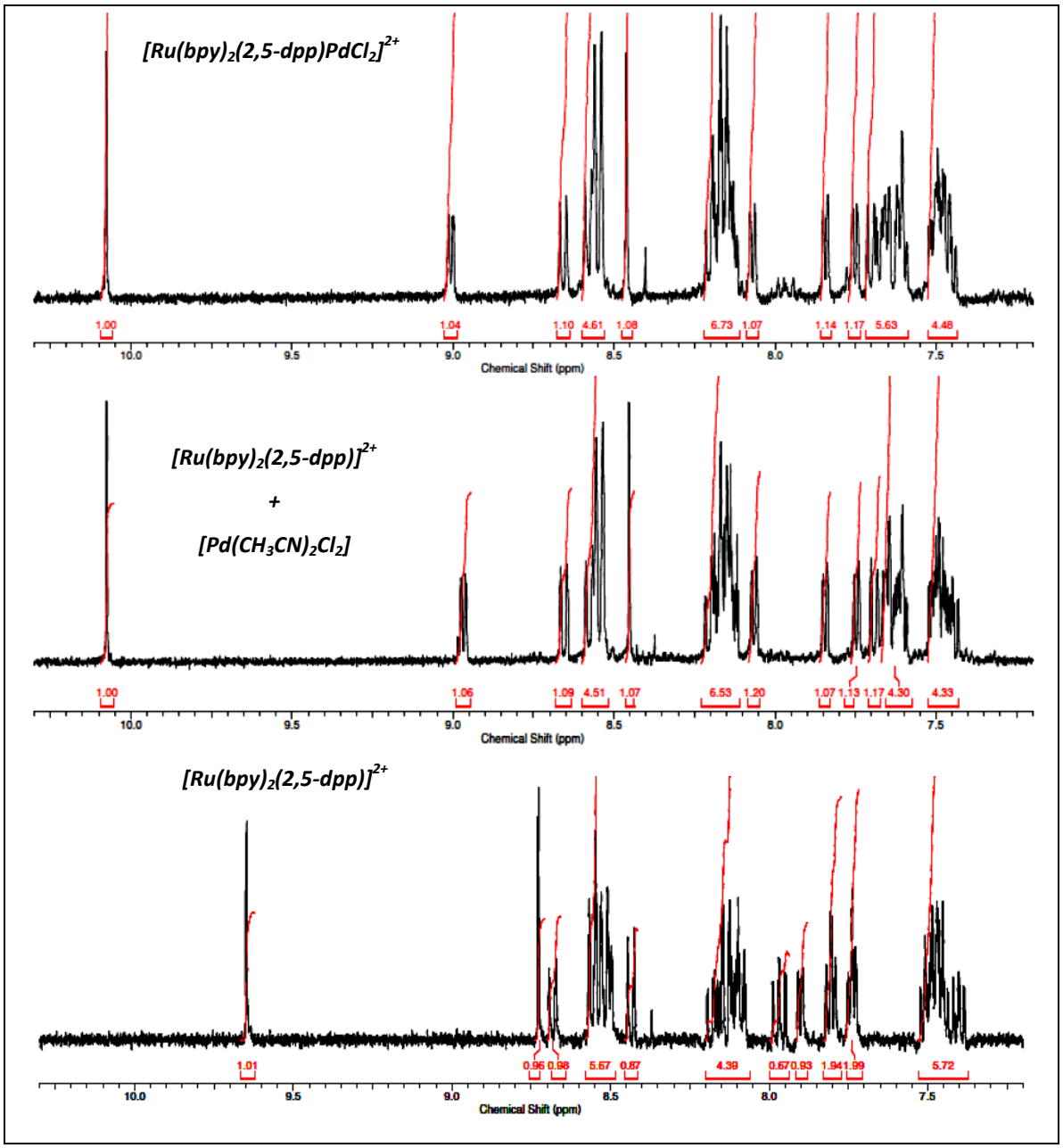

Figure 6.19: *^{1}H-NMR spectra of the intermolecular reaction between the $[Ru(bpy)_2(2,5\text{-}dpp)]^{2+}$ complex and $[Pd(CH_3CN)_2Cl_2]$ complex (Conc. = 5.3 x 10^{-3} M) in deuteriated CD_3CN and irradiated at 470 nm for 10 minutes.*

Figure 6.20 shows a comparison of the absorption spectra of the intermolecular reaction after 10 minutes of irradiation at 470 nm without stirring under nitrogen atmosphere with their respective mono- and heterodinuclear complexes. The above observations show that

the intermolecular reaction between monomer and Pd precursor may form heterodinuclear complex during the photocatalytic reaction which explains the similarity of the TONs.

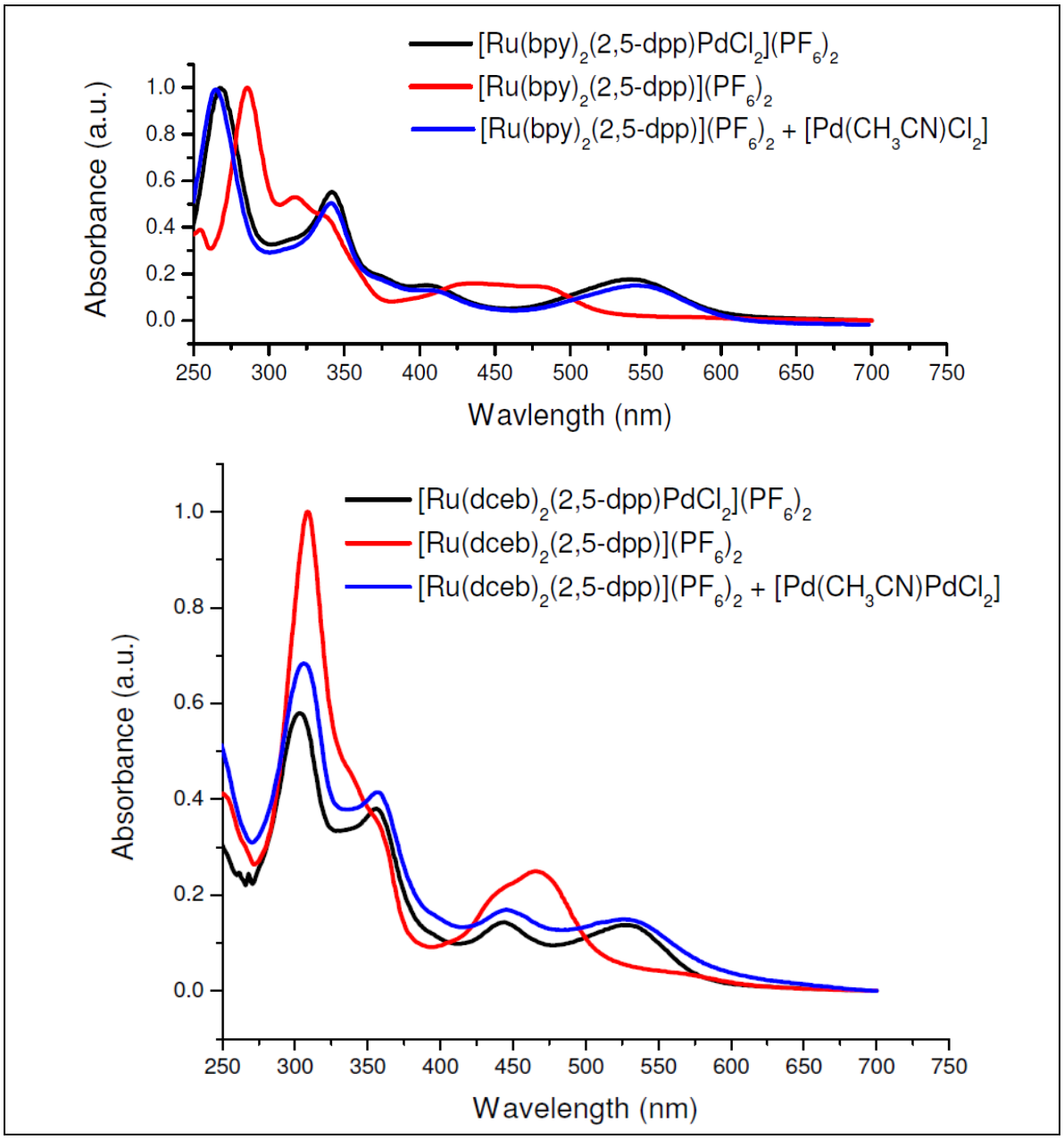

Figure 6.20: *Absorption spectra of the intermolecular reaction between the* $[Ru(bpy)_2(2,5\text{-}dpp)]^{2+}$ / $[Ru(dceb)_2(2,5\text{-}dpp)]^{2+}$ *and* $[Pd(CH_3CN)_2Cl_2]$ *complexes (Conc. =* 5.3×10^{-3} *M, 1:1 molar ratio v/v) in acetonitrile after 10 minutes of irradiation at 470 nm, plotted with respective mononuclear and heterodinuclear complexes.*

6.2.1.8 Plausible mechanism of an intramolecular photocatalysis of heterodinuclear complexes.

The photocatalytic water reduction processes reported in this thesis involve three critical components: the photosensitizer, the sacrificial reductant, and catalytic centre. In the photocatalytic cycle, the photosensitizer is responsible for the absorption of visible light to provide the energy necessary for the endothermic water reduction process to occur. In the catalytic dark cycle, the catalytic centre collects the high-energy electrons from the light cycle and protons from water to produce hydrogen.[25] The sacrificial reductant provides the electrons necessary for water reduction by replenishing the lowest singly occupied molecular orbital of PS* or PS^+, depending on the mechanism of quenching.[25] The excited-state can be quenched through two different pathways: reductive quenching by the sacrificial reductant (TEA) (see figure 6.12) or oxidative quenching by the components of the catalytic centre. As the sacrificial reductant used, is in a large excess, the excited state is quenched via reductive quenching pathways. The interactions of all three components and their corresponding redox intermediates determine the mechanism and energetics of the process. At this stage no detailed mechanistic data are available, but a likely reaction pathway may include the following steps: a twofold photoreduction of the Ru(II) photocatalyst by TEA (NEt_3) [43], and the subsequent reduction of the protons at the Pd/Pt center as shown according to Figure 6.21.[25]

Figure 6.21, shows a general reaction pathways for photocatalytic hydrogen production in the presence of water for the complex $[Ru(dceb)_2(2,5\text{-dpp})PdCl_2]^{2+}$. The complex $[Ru(dceb)_2(2,5\text{-dpp})PdCl_2]^{2+}$ resembles the pyrazine based bridging ligand used by Sven and coworkers [25c, 37] for the generation of hydrogen form water. It is proposed that the reaction pathways follow the reported mechanism.[25c] The first photoelectron transfer occurs in step 1 (see figure 6.21), and results in the generation of the Ru^{3+} – 2,5-dpp($^{-}$) – Pd^{2+}.[53] The sacrificial reductant (TEA) reduced Ru^{3+} to Ru^{2+} so that the Ru^{2+} centre became photoactive to absorb light. The TEA can also be used as a proton source (see also the decomposition of TEA under photocatalytic conditions in Eq. 6.1 – 6.4 above).[1, 25c, 45]

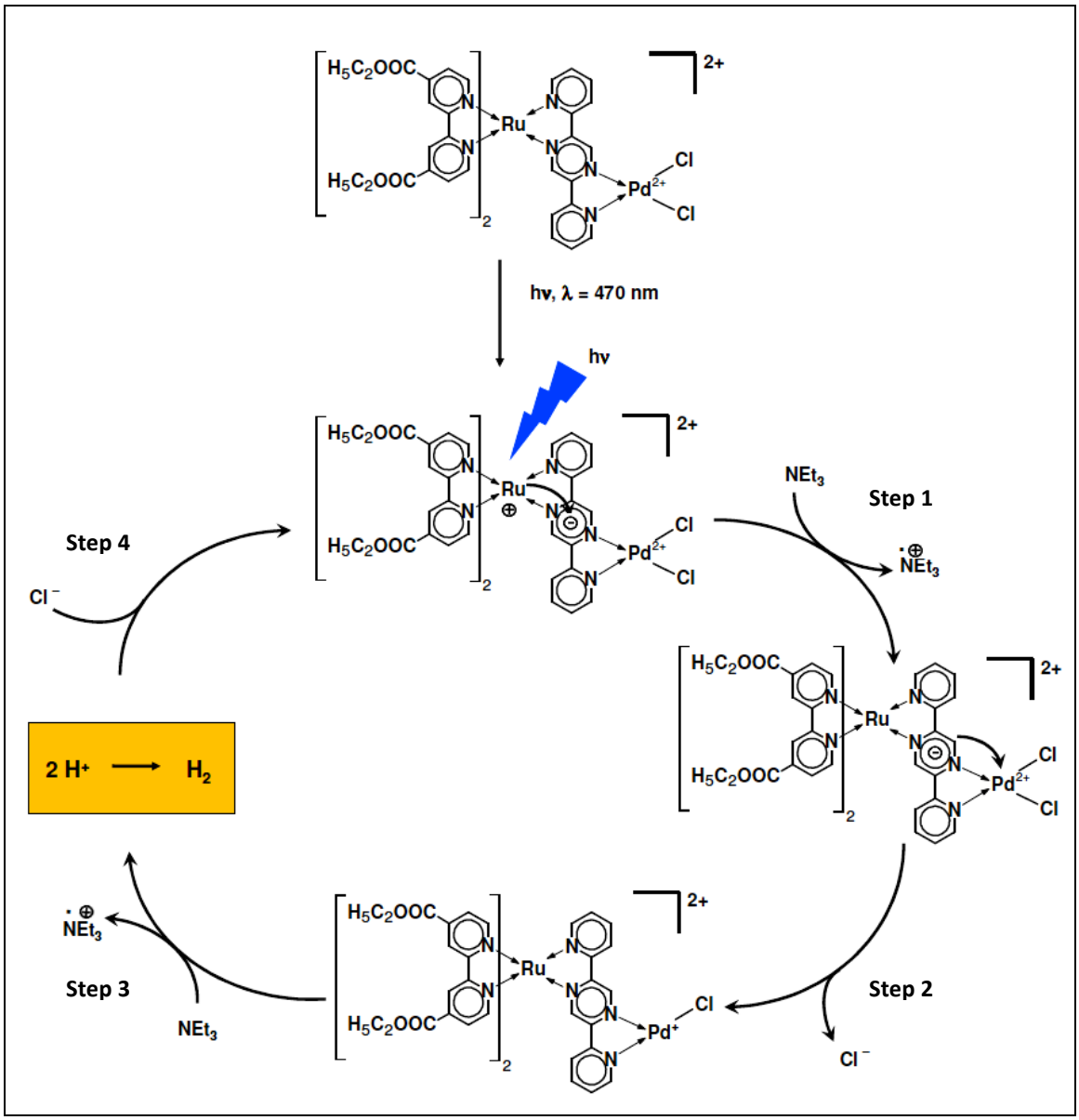

Figure 6.21: *General reaction mechanism for the photocatalytic production of hydrogen by the intramolecular route for* $[Ru(dceb)_2(2,5\text{-}dpp)PdCl_2]^{2+}$.

In step 2, loss of the chloride from the Pd^{2+} center leaves a vacant site at the metal centre which may be coordinated with solution, acetonitrile or H_2O from the solution. Electron transfer from 2,5-dpp(⁻) to the Pd^{2+} center then takes place yielding a Pd^{1+} moiety. The deprotonated, photo-oxidized triethylamine can also transfer another electron to the singly reduced catalyst in step 3. When this sequence of steps is repeated, two electrons

are stored in the molecule. These electrons are then utilized to reduce two protons [37] originating from oxidized TEA (step 3). The free chloride ion in solution is again coordinated to the Pd centre to complete the photocatalytic cycle. It is stated that the Cl^- atom removed from the Pd centre is assumed to be an important step for reduction of proton to hydrogen.[25c] Sven and coworkers reported, the DFT optimized structure of $[Ru(tbbpy)(tpphz)PdCl_2]^{2+}$ with a chloride ion removed, and indicated not only the relocation of the SOMO to the Pd center, but also the regeneration of the photoredox-active fragment, which can once again enter into a photocatalytic cycle with TEA plays an important roles.[25c] It is assumed that the all synthesised intermolecular photocatalysts listed in this thesis have similar photocatalytic pathways.

6.3 Summary and conclusions

This chapter deals with comparative studies of the photocatalytic properties of the heterodinuclear complexes reported in the previous chapters. It has been shown that the effect of an electron withdrawing group on the peripheral ligand and the nature of the aromatic conjugated bridging ligands influence the TON for hydrogen production. In general, the effect of increasing the amount of water from 0 – 10 % increases the TON value, but with a further increase in water (15 %) content, the amount of hydrogen forms begin to decrease. It has been suggested that the increase in polarity of the solvent increases the mobility of H^+ in the solution.[25c] There is no increase in TON when partial and fully deuteriated heterodinuclear complexes are used. It has been reported that effect on TON increases when Pd is used as the photocatalytic reduction centre, as opposed to Pt, as the former is more easily reduced. The use of Ir(III) metal centres as a light absorbing unit in the heterodinuclear photocatalyst containing 2,5-bpp as a bridging ligand and Pd or Pt as catalytic centre produces much more hydrogen production than the ruthenium analogues. The time dependent irradiation studies show that the intermolecular reaction of $[Ru(dceb)_2(2,5\text{-}dpp)]^{2+}$ + $[Pd(CH_3CN)_2Cl_2]$ complexed after illumination at 470 nm under catalytic condition. The intermolecular reaction suggested that the formation of common intermediate species as it was formed during precomplexed compound $[Ru(dceb)_2(2,5\text{-}dpp)PdCl_2]^{2+}$ shows more or less same TONs of hydrogen.

The time dependent studies of intermolecular reaction between $[Ru(dceb)_2(2,5\text{-}dpp)]^{2+}$ + $[Pd(CH_3CN)_2Cl_2]$ (Conc. = 5.3 x 10^{-3} M, 1:1 molar ratio v/v) suggested that the heterodinuclear complex formed when the mixture was irradiated at 470 nm for 10 minutes without TEA. However, these is no evidence for formation of the heterodinuclear complex following the in situ reaction $[Ru(bpy)_2(2,5\text{-}bpp)]^{2+}$ + $[Pd(CH_3CN)_2Cl_2]$ which may explain the lower TON = 70 for the production of hydrogen for the mixture as opposed to that observed for the heterodinuclear $[Ru(bpy)_2(2,5\text{-}bpp)Pd(CH_3CN)Cl]^{2+}$ complex TON = 130 with 10% water. It is assumed that the all synthesised intramolecular photocatalysts listed in this thesis are based on the photocatalytic pathway as shown in Figure 6.21.

6.4 Bibliography

[1] S. D. Ross, Tetrahedron Lett., 1973, 14, 1237.

[2] (a) F. P. Rotzinger, S. Munavalli, P. Comte, J. K. Hurst, M. Gratzel, F. J. Pern and A. J. Frank, J. Am. Chem. Soc., 1987, 109, 6619; (b) A. J. Esswein, Y. Surendranath, S. Y. Reece and D. G. Nocera, Energy Environ. Sci., 2011, 4, 499.

[3] K. Kalyanasundaram and M. Grätzel, J. Chem. Soc., Chem. Commun., 1979, 1137.

[4] D. Gust, T. A. Moore and A. L. Moore, Acc. Chem. Res., 2001, 34, 40.

[5] H. Kotani, K. Ohkubo, Y. Takai and S. Fukuzumi, J. Phys. Chem. B, 2006, 110, 24047.

[6] A. Juris, V. Balzani, F. Barigelletti, S. Campagna, P. Belser and A. Von Zelewsky, Coord. Chem. Rev., 1988, 84, 85.

[7] K. Kalyanasundaram, Photochemistry of Polypyridine and Porphyrin Complexes, Academic Press, New York, NY, 1992, pp. 105–164.

[8] P. J. Hay, J. Phys. Chem. A, 2002, 106, 1634–1641.

[9] M. G. Colombo, A. Hauser and H. U. Güdel, Top. Curr. Chem., 1994, 171, 143–171.

[10] M. G. Colombo, A. Hauser and H. U. Güdel, Inorg. Chem., 1993, 32, 3088.

[11] C. Creutz, N. Sutin, Proc. Natl. Acad. Sci. U.S.A. 1975, 72, 2858.

[12] G. Sprintschnik, H. W. Sprintschnik, P. P. Kirsch, D. G. Whitten, J. Am. Chem. Soc., 1975, 98, 2337; 1977, 99, 4947.

[13] C. -T, Lin, N. Sutin, J. Phys. Chem. 1976, 80, 77.

[14] T. J. Meyer, Isr. J. Chem., 1977, 75, 200.

[15] N. Sutin, C. Creutz, Adv. Chem. Ser., 1978, 168, 1.

[16] N. Sutin, J. Photochem., 1979, 10, 19.

[17] V. Balzani, L. Moggi, M. F. Manfrin, F. Bolletta, M. Gleria, Science, 1975, 189, 852

[18] C. Creutz, N. Sutin, B. S. Brunschwig, J. Am. Chem. Soc., 1979, 101, 1298.

[19] C. Creutz, N. Sutin, J. Am. Chem. Soc., 1976, 98, 6384.

[20] C. Creutz, Inorg. Chem., 1978, 77, 1046.

[21] A. M. Tait, M. Z. Hoffman, E. Hayon, J. Am. Chem. Soc. 1976, 98, 86.

[22] D. P. Rillema, J. F. Endicott, Inorg. Chem., 1976, 75, 1459.

[23] D. Rillema, J. F. Endicott, E. Papaconstantinou, Inorg. Chem. 1971, 10, 1739.

[24] N. E. Tokel-Takvoryan, R. E. Hemingway, A. J. Bard, J. Am. Chem. Soc., 1973, 95, 6562.

[25] (a) M. Elvington, J. Brown, S. M. Arachchige and K. J. Brewer, J. Am. Chem. Soc., 2007, 129, 10644; (b) H. Ozawa, M. Haga and K. Sakai, J. Am. Chem. Soc., 2006, 128, 4926; (c) S. Rau, B. Schäfer, D. Gleich, E. Anders, M. Rudolph, M. Friedrich, H. Görls, W. Henry and J. G. Vos, Angew. Chem., Int. Ed., 2006, 45, 6215; (d) A. Fihri, V. Artero, M. Razavet, C. Baffert, W. Leibl and M. Fontecave, Angew. Chem. Int. Ed., 2008, 47, 564; (e) A. F. Heyduk, D. G. Nocera, Science, 2001, 293, 1639.

[26] P. Lei, M. Hedlund, R. Lomoth, H. Rensmo, O. Johansson and L. Hammarström, J. Am. Chem. Soc., 2008, 130, 26.

[27] M. Schwalbe, B. Schäfer, H. Görls, S. Rau, S. Tschierlei, M. Schmitt, J. Popp, G. Vaughan, W. Henry and J. G. Vos, Eur. J. Inorg. Chem., 2008, 3310.

[28] W. F. Wacholtz, R. A. Auerbach, R. H. Schmehl, Inorg. Chem. 1986, 25, 227.

[29] S. G. Sun, X. J. Peng, Y. Q. Xu, L. Shi, Z. Guo, L. C. Sun, Chinese Chem. Letters, 2004, 5, 8, 969.

[30] G. S. Bindra, M. Schulz, A. Paul, S. Soman, R. Groarke, J. Inglis, M. T. Pryce, W. R. Browne, S. Rau, B. J. Maclean and J. G. Vos, Dalton Trans., 2011, DOI: 10.1039/c1dt11241d.

[31] S. Masaoka, Y. Mukawa and K. Sakai, Dalton Trans., 2010, 39, 5868.

[32] W. R. Browne, J. G. Vos, Coord. Chem. Rev., 2001, 219, 761.

[33] J. L. Kropp, M. W. Windsor, J. Chem. Phys., 1963, 39, 2769.

[34] J. Van Houten, R. J. Watts, J. Am. Chem. Soc., 1975, 97, 3843.

[35] C. A. Hutchinson, B. W. Mangum, J. Chem. Phys., 1960, 32, 1261.

[36] M. R. Wright, R. P. Frosch, G. W. Robinson, J. Chem. Phys., 1960, 33, 934.

[37] S. Tschierlei, M. Karnahl, M. Presselt, B. Dietzek, J. Guthmüller, L. Gonzalez, M. Schmitt, S. Rau and J. Popp, Angew. Chem., Int. Ed., 2010, 49, 3981.

[38] E. D. Cline, S. E. Adamson and S. Bernhard, Inorg. Chem., 2008, 47, 22, 10378.

[39] H. Ozawa, M. Haga, K. Sakai, J. Am. Chem. Soc. 2006, 128, 4926.

[40] X. Wang, K. Maeda, A. Thomas, K. Takanabe, G. Xin, J. M. Carlsson, K. Domen, M. Antonietti, Nat. Mater. 2009, 8, 76.

[41] B. Dietzek, W. Kiefer, J. Blumhoff, L. BMttcher, S. Rau, D. Walther, U. Uhlemann, M. Schmitt, J. Popp, Eur. J. Chem., 2006, 12, 5105.

[42] C. Chiorboli, M. A. J. Rodgers, F. Scandola, J. Am. Chem. Soc., 2003, 125, 483.

[43] R. Konduri, H. Ye, F. M. MacDonnell, S. Serroni, S. Campagna, K. Rajeshwar, Angew. Chem. 2002, 114, 3317; Angew. Chem. Int. Ed., 2002, 41, 3185.

[44] (a) L. Cassidy, S. Horn, L. Cleary, Y. Halpin, W. R. Browne and Johannes G. Vos, Dalton Trans., 2009, 3923; Y. Halpin, L. Cleary, L. Cassidy, S. Horne, D. Dini, W. R. Browne and J. G. Vos, Dalton Trans., 2009, 4146; (b) M. Sommovigo, G. Denti, S. Serroni, S. Campagna, C. Mingazzini, C. Mariotti and A. Juris, Inorg. Chem., 2001, 40, 3318.

[45] S. G. Cohen, A. Parola, G. H. Parsons, Chem. Rev., 1973, 73, 141; P. J. DeLaive, T. K. Foreman, C. Giannotti, D. G. Whitten, J. Am. Chem. Soc., 1980, 102, 5627; Y. L. Chow, W. C. Danen, S. F. Nelsen, D. H. Rosenblatt, Chem. ReV. 1978, 78, 243.

[46] F. Neve and A. Crispini, Inorg. Chem., 1997, 36, 6150.

[47] M. S. Lowry, W. R. Hudson, R. A. Pascal, S. Bernhard, J. Am. Chem. Soc., 2004, 126, 14129.

[48] J. I. Goldsmith, W. R. Hudson, M. S. Lowry, T. H. Anderson, S. Bernhard, J. Am. Chem. Soc. 2005, 127, 7502.

[49] M. S. Lowry, J. I. Goldsmith, J. D. Slinker, R. Rohl, A. Robert, J. Pascal, G. G. Malliaras, S. Bernhard, Chem. Mater., 2005, 17, 5712.

[50] F. Gärtner, D. Cozzula, S. Losse, A. Boddien, G. Anilkumar, H. Junge, T. Schulz, N. Marquet, A. Spannenberg, S. Gladiali, and M. Beller, Chem. Eur. J., 2011, 17, 6998.

[51] L. L. Tinker , N. D. McDaniel and S. Bernhard, J. Mater. Chem., 2009, 19, 3328.

[52] L. L. Tinker, N. D. McDaniel, P. N. Curtin, C. K. Smith, M. J. Ireland and S. Bernhard, Chem. Eur. J., 2007, 13, 8726.

[53] S. Tschierlei, M. Presselt, C. Kuhnt, A. Yartsev, T. Pascher, V. Sundström, M. Karnahl, M. Schwalbe, B. Schäfer, S. Rau, M. Schmitt, B. Dietzek, J. Popp, Chem. Eur. J., 2009, 15, 7678.

Chapter 7: Conclusions and Future Work

Abstract:

This chapter gives a brief overview o the results obtained following the syntheses, characterization and photocatalytic properties in the development of novel hetero-dinuclear transition metal complexes for the generation of hydrogen. Although there was a discussed detailed conclusion at the end of each chapter, now we will summarize our results and propose future work within this area.

7.1 Conclusions and future work

This thesis deals with the development of synthetic techniques, characterization and photocatalytic properties in the production of novel hetero-dinuclear ruthenium, palladium and platinum supramolecular systems for the generation of hydrogen from water. These complexes are promising photocatalysts for the dissociation of water using solar energy. The general composition of these supramolecular photocatalysts is a light absorber, bridging ligand and catalytic centre. This work has also focused on the intramolecular electron transfer processes, compared to the intermolecular electron transfer processes.

Chapter 3, 4 and 5 showed that the traditional method for the synthesis of inorganic transition metal complexes containing the bridging ligands 2,5-dpp, 2,5-bpp, 2,6-bpp and bisbpy are very successful for both mononuclear and hetero-dinuclear complexes. However, the synthesis of cyclometallated heterodinuclear complexes with 2,5-bpp and 2,6-bpp in chapter 4 required stirring for 48 hours at refluxing conditions. It has reported that the μ-bis-chloro complexes dissociates and coordinate with acetonitrile ligand after recrystallisation which is shown in the ^{1}H-NMR and CHN analyses. The anchoring ester group analogues of these complexes were also synthesised. The synthesis of platinum coordinated cyclometallated complexes with 2,5-bpp as the bridging ligand was not successful. The synthesis of the bridging ligands was based on a literature method with little modification. The overall percentage yield after purification of the mononuclear and heterodinuclear complexes containing the above bridging ligands ranged from 56 – 98 %. These complexes were characterized by using ^{1}H-NMR and 2D-COSY ^{1}H-NMR. The absorption, luminescence and lifetimes of these supramolecular photocatalysts have also measured. For the simplicity in the ^{1}H-NMR spectra and to see the effects on the lifetime decay of the complex, the partial and fully deuteriated analogues of these complexes were prepared. The results in chapter 3 suggests that the increment in the lifetime for the deuteriated mononuclear complex $[Ru(bpy)_2(D_{10}\text{-}2,5\text{-}dpp)]^{2+}$ compared to non-deuteriated mononuclear complex $[Ru(bpy)_2(2,5\text{-}dpp)]^{2+}$ indicates that the excited state ^{3}MLCT is based on the bridging ligand 2,5-dpp.

The photocatalytic properties of these supramolecular complexes were studied in chapters 3, 4 and 5. A comparison of their photocatalytic properties was also discussed in chapter 6. The headspace analysis of the photocatalytic reaction was performed using Gas chromatography. The compound containing 2,5-dpp as a bridging ligand with dceb as peripheral ligand $[Ru(dceb)_2(2,5\text{-}dpp)PdCl_2]^{2+}$ is a very promising photochemical molecular device for the generation of hydrogen with TON = 403 after 18 hours irradiation at 470 nm with 5% water while the platinum analogue generates only, TON = 14. The bpy analogues of the 2,5-dpp ligand with $PdCl_2$ and $PtCl_2$ moiety do not produce hydrogen. Interestingly, It was found that intermolecular photocatalysis between the mononuclear complex $[Ru(dceb)_2(2,5\text{-}dpp)]^{2+}$ and $[Pd(ACN)Cl_2]$ generates a TON = 464 with 5% water, which is explained by the formation of the intramolecular complex during photocatalysis, as discussed in chapter 6. It was shown in chapter 3 that the increase in water also increases the TON of hydrogen up to 5 %. $[Ru(dceb)_2(bisbpy)PdCl_2]^{2+}$ is the most effective and a promising photocatalyst for the generation of hydrogen using water and solar energy. A TON of 513 was observed after 18 hours irradiation at 470 nm with 5% water. $[Ru(dceb)_2(bisbpy)PtCl_2]^{2+}$ gave a TON = 256 under similar conditions. The effectiveness of the ester analogues as efficient photocatalysts is attributed to their excited states photophysical properties and the stabilisation of the ground state of dceb ligand compare to the bpy ligand.

In chapter 4, The photocatalytic activity of the heterodinuclear complex $[Ru(bpy)_2(2,5\text{-}bpp)PdCl(CH_3CN)]^{2+}$ (TON = 130 with 10% water) showed promising results with the production of hydrogen under visible light irradiation. Interestingly, the mononuclear complex $[Ru(bpy)_2(2,5\text{-}bpp)]^{2+}$ mixed with $[Pd(CH_3CN)_2Cl_2]$ shows a TON = 70 with 10% water which is half the TON compared to heterodinuclear complex $[Ru(bpy)_2(2,5\text{-}bpp)PdCl(CH_3CN)]^{2+}$. It is possible that the active intramolecular complex is not formed in situ due to cyclometallation of the complex. The heterodinuclear complex $[Ru(bpy)_2(2,6\text{-}bpp)PdCl(CH_3CN)]^{2+}$ and mononuclear complex with the palladium precursor shows no activity to produce hydrogen from water using visible light illumination. It has been suggested in chapter 6 that the steric repulsion between the Pd

d_z^2 orbital and neighboring α-hydrogen atom present on the pyridine ring, and the incoming H^+ found steric hindrance to reduce by Pd(I) species.

Chapter 6 deals with a comparative study of the photocatalytic properties of the listed heterodinuclear complexes in the previous chapters. It has been shown that the effect of an electron withdrawing group on the peripheral ligand and aromatic conjugated bridging ligands increases the TON of hydrogen. In general, increasing the amount of water increases the TON from 0 – 10% and then drops. It is possible that the increase in polarity of the solvent increases the mobility of H^+ in the solution and further increases in the polarity and decreases the solubility of the photocatalysts. There is no increase in TON when partial and fully deuteriated heterodinuclear complexes were used. The TON increases when a Pd centre was used as a photocatalytic reduction centre due to ease of oxidation compared to the Pt metal centre. The use of the Ir(III) metal centre as a light absorbing unit in the heterodinuclear photocatalyst containing 2,5-bpp as a bridging ligand and Pd or Pt as a catalytic centre produces much more hydrogen than the ruthenium analogues. It is assumed that the all synthesised intermolecular photocatalyst listed in this thesis are based on the photocatalytic pathway mentioned in Figure 6.13.

The future work in this area will involve further exploration in to the optimal conditions for the photocatalytic water reduction to proceed. The ester analogues of these heterodinuclear complexes will be in mobilized on nickel oxide surfaces to perform experiments for photocatalysis without using sacrificial electron donors. Further investigations will also be carried out into the photoelectrochemical reduction of water using these complexes.

Appendix A

A.1 Gaussian Calculation

All calculations were carried out with the Gaussian 09 program suite.[1] The compounds $[Ru(bpy)_2(2,5\text{-}bpp)PdCl(CH_3CN)]^{2+}$ and $[Ru(bpy)_2(2,6\text{-}bpp)PdCl(CH_3CN)]^{2+}$ (figure I.1 and I.2) were optimized using Becke's three parameter functional B3LYP[2]. The MWB28[3] basis was used for the heavy Ru and Pd atoms while Pople's 6-31G(d)[4] was used for the remainder. Tight convergence criteria were applied for the geometry optimization process and local minima were confirmed by a frequency calculation (absence of imaginary frequencies). All calculations were carried out in the presence of a solvent sphere which was modeled by the IEF-PCM[5] method in acetonitrile (ε = 35.688000). Although the maximum displacement value did not converge for Ru-Bpp-PdCl(ACN) a stationary point was found on the basis of negligible forces (< 1/100 of the threshold value).

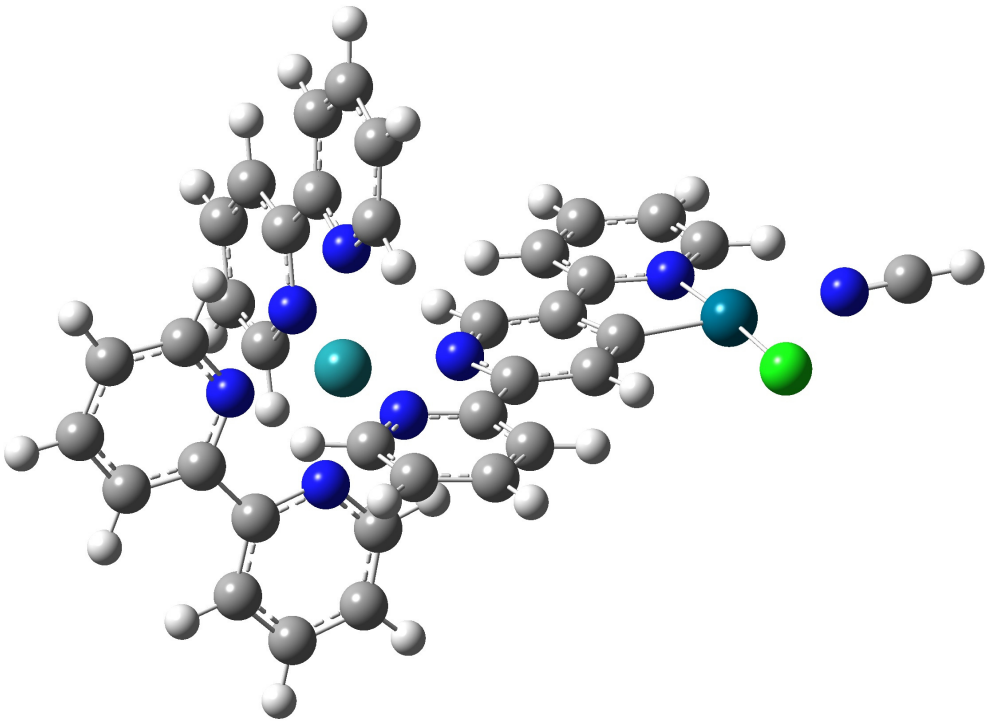

Figure I.1: *3D structure calculation for* $[Ru(bpy)_2(2,5\text{-}bpp)PdCl(CH_3CN)]^{2+}$ *with Gaussian 09 programme.*

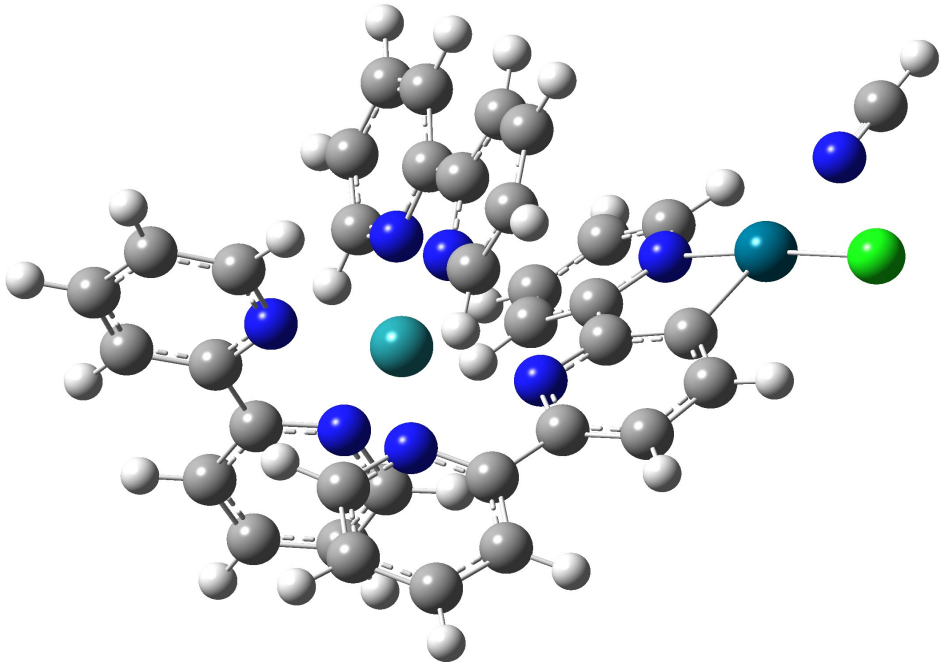

Figure I.2: *3D structure calculation for* $[Ru(bpy)_2(2,6\text{-}bpp)PdCl(CH_3CN)]^{2+}$ *with Gaussian 09 programme.*

A.2 Bibliography

[1] Frisch, M. J.; Trucks, G. W.; Schlegel, H. B.; Scuseria, G. E.; Robb, M. A.; Cheeseman, J. R.; Scalmani, G.; Barone, V.; Mennucci, B.; Petersson, G. A.; Nakatsuji, H.; Caricato, M.; Li, X.; Hratchian, H. P.; Izmaylov, A. F.; Bloino, J.; Zheng, G.; Sonnenberg, J. L.; Hada, M.; Ehara, M.; Toyota, K.; Fukuda, R.; Hasegawa, J.; Ishida, M.; Nakajima, T.; Honda, Y.; Kitao, O.; Nakai, H.; Vreven, T.; J. A. Montgomery, J.; Peralta, J. E.; Ogliaro, F.; Bearpark, M.; Heyd, J. J.; Brothers, E.; Kudin, K. N.; Staroverov, V. N.; Kobayashi, R.; Normand, J.; Raghavachari, K.; Rendell, A.; Burant, J. C.; Iyengar, S. S.; Tomasi, J.; Cossi, M.; Rega, N.; Millam, J. M.; Klene, M.; Knox, J. E.; Cross, J. B.; Bakken, V.; Adamo, C.; Jaramillo, J.; Gomperts, R.; Stratmann, R. E.; Yazyev, O.; Austin, A. J.; Cammi, R.; Pomelli, C.; Ochterski, J. W.; Martin, R. L.; Morokuma, K.; Zakrzewski, V. G.; Voth, G. A.; Salvador, P.; Dannenberg, J. J.; Dapprich, S.; Daniels, A. D.; Farkas, O.; Foresman, J. B.; Ortiz, J. V.; Cioslowski, J. & Fox, D. J. Gaussian 09, Revision A.02, 2009.

[2] Becke, A. D. J. Chem. Phys., 1993, 98, 5648-5652; Lee, C. T.; Yang, W. T. & Parr, R. G. Phys. Rev. B: Condens. Matter Mater. Phys., 1988, 37, 785-789; Miehlich, B.; Savin, A.; Stoll, H. & Preuss, H. Chem. Phys. Lett., 1989, 157, 200-206.

[3] Fuentealba, P.; Preuss, H.; Stoll, H. & Vonszentpaly, L. Chem. Phys. Lett., 1982, 89, 418-422; Vonszentpaly, L.; Fuentealba, P.; Preuss, H. & Stoll, H. Chem. Phys. Lett., 1982, 93, 555-559; Fuentealba, P.; Stoll, H.; Vonszentpaly, L.; Schwerdtfeger, P. & Preuss, H. J. Phys. B, 1983, 16, L323-L328; Stoll, H.; Fuentealba, P.; Schwerdtfeger, P.; Flad, J.; Vonszentpaly, L. & Preuss, H. J. Chem. Phys., 1984, 81, 2732-2736; Fuentealba, P.; Vonszentpaly, L.; Preuss, H. & Stoll, H. J. Phys. B, 1985, 18, 1287-1296; Wedig, U.; Dolg, M.; Stoll, H. & Preuss, H. Veillard, A. (Ed.) Quantum Chemistry: The Challenge of Transition Metals and Coordination Chemistry Reidel and Dordrecht, 1986; Dolg, M.;

Wedig, U.; Stoll, H. & Preuss, H. J. .Chem. Phys., 1987, 86, 866-872; Igelmann, G.; Stoll, H. & Preuss, H. Mol. Phys., 1988, 65, 1321-1328; Dolg, M.; Stoll, H. & Preuss, H. J. Chem. Phys., 1989, 90, 1730-1734; Schwerdtfeger, P.; Dolg, M.; Schwarz, W. H. E.; Bowmaker, G. A. & Boyd, P. D. W. J. .Chem. Phys., 1989, 91, 1762-1774; Dolg, M.; Stoll, H.; Savin, A. & Preuss, H. Theo. Chim. Acc., 1989, 75, 173-194; Andrae, D.; Haussermann, U.; Dolg, M.; Stoll, H. & Preuss, H. Theo. Chim. Acc., 1990, 77, 123-141; Dolg, M.; Fulde, P.; Kuchle, W.; Neumann, C. S. & Stoll, H. J. Chem. Phys., 1991, 94, 3011-3017; Kaupp, M.; Schleyer, P. V.; Stoll, H. & Preuss, H. J. Chem. Phys., 1991, 94, 1360-1366; Kuchle, W.; Dolg, M.; Stoll, H. & Preuss, H. Mol. Phys., 1991, 74, 1245-1263; Dolg, M.; Stoll, H.; Flad, H. J. & Preuss, H. J. Chem. Phys., 1992, 97, 1162-1173; Bergner, A.; Dolg, M.; Kuchle, W.; Stoll, H. & Preuss, H. Mol. Phys., 1993, 80, 1431-1441; Dolg, M.; Stoll, H. & Preuss, H. Theo. Chim. Acc., 1993, 85, 441-450; Haussermann, U.; Dolg, M.; Stoll, H.; Preuss, H.; Schwerdtfeger, P. & Pitzer, R. M. Mol. Phys., 1993, 78, 1211-1224; Dolg, M.; Stoll, H.; Preuss, H. & Pitzer, R. M. J. .Phys. Chem., 1993, 97, 5852-5859; Kuchle, W.; Dolg, M.; Stoll, H. & Preuss, H. J. Chem. Phys., 1994, 100, 7535-7542; Nicklass, A.; Dolg, M.; Stoll, H. & Preuss, H. J. Chem. Phys., 1995, 102, 8942-8952; Leininger, T.; Nicklass, A.; Kuchle, W.; Stoll, H.; Dolg, M. & Bergner, A. Chem. Phys. Lett., 1996, 255, 274-280; Cao, X. Y. & Dolg, M. J. Chem. Phys., 2001, 115, 7348-7355; Cao, X. Y. & Dolg, M. J. Mol. Struc. (Theochem), 2002, 581, 139-147.

[4] Ditchfield, R.; Hehre, W. J. & Pople, J. A. J. Chem. Phys., 1971, 54, 724; Hehre, W. J.; Ditchfield, R. & Pople, J. A. J. Chem. Phys., 1972, 56, 2257; Harihara, P. C. & Pople, J. A. Theor. Chem. Acc., 1973, 28, 213-222; Harihara, P. C. & Pople, J. A. Mol. Phys., 1974, 27, 209-214; Gordon, M. S. Chem. Phys. Lett., 1980, 76, 163-168; Francl, M. M.; Pietro, W. J.; Hehre, W. J.; Binkley, J. S.; Gordon, M. S.; Defrees, D. J. & Pople, J. A. J. Chem. Phys., 1982, 77, 3654-3665; Binning, R. C. & Curtiss, L. A. J. Comput. Chem., 1990, 11, 1206-1216; Blaudeau, J. P.; McGrath, M. P.; Curtiss, L. A. & Radom, L. J. Chem. Phys., 1997, 107, 5016-5021; Rassolov, V. A.; Pople, J. A.; Ratner, M. A. & Windus, T. L. J. Chem.

Phys., 1998, 109, 1223-1229; Rassolov, V. A.; Ratner, M. A.; Pople, J. A.; Redfern, P. C. & Curtiss, L. A. J. Comput. Chem., 2001, 22, 976-984.

[5] Miertus, S.; Scrocco, E. & Tomasi, J. Chem. Phys., 1981, 55, 117-129; Miertus, S. & Tomasi, J. Chem. Phys., 1982, 65, 239-245; Pascualahuir, J. L.; Silla, E. & Tunon, I. J. Comput. Chem., 1994, 15, 1127-1138; Cossi, M.; Barone, V.; Cammi, R. & Tomasi, J. Chem. Phys. Lett., 1996, 255, 327-335; Barone, V.; Cossi, M. & Tomasi, J. J. Chem. Phys., 1997, 107, 3210-3221; Barone, V.; Cossi, M. & Tomasi, J. J. Chem. Phys., 1997, 107, 3210-3221; Mennucci, B. & Tomasi, J. J. Chem. Phys., 1997, 106, 5151-5158; Mennucci, B.; Cances, E. & Tomasi, J. J. Phys. Chem. B, 1997, 101, 10506-10517; Barone, V. & Cossi, M. J. Phys. Chem. A, 1998, 102, 1995-2001; Cossi, M.; Barone, V.; Mennucci, B. & Tomasi, J. Chem. Phys. Lett., 1998, 286, 253-260; Barone, V.; Cossi, M. & Tomasi, J. J. Comput. Chem., 1998, 19, 404-417; Cammi, R.; Mennucci, B. & Tomasi, J. J. Phys. Chem. A, 1999, 103, 9100-9108; Cossi, M.; Barone, V. & Robb, M. A. J. Chem. Phys., 1999, 111, 5295-5302; Tomasi, J.; Mennucci, B. & Cances, E. J. Mol. Struct., 1999, 464, 211-226; Cammi, R.; Mennucci, B. & Tomasi, J. J. Phys. Chem. A, 2000, 104, 5631-5637; Cossi, M. & Barone, V. J. Chem. Phys., 2000, 112, 2427-2435; Cossi, M. & Barone, V. J. Chem. Phys., 2001, 115, 4708-4717; Cossi, M.; Rega, N.; Scalmani, G. & Barone, V. J. Chem. Phys., 2001, 114, 5691-5701; Cossi, M.; Scalmani, G.; Rega, N. & Barone, V. J. Chem. Phys., 2002, 117, 43-54; Cossi, M.; Rega, N.; Scalmani, G. & Barone, V. J. Comput. Chem., 2003, 24, 669-681.

Appendix B

Publications

1) "Reinvestigating 2,5-di(pyridin-2-yl)pyrazine ruthenium complexes: selective deuteration and Raman spectroscopy as tools to probe ground and excited-state electronic structure in homo- and heterobimetallic complexes"
Martin Schulz, Johannes Hirschmann, Appu Draksharapu, **Gurmeet Singh Bindra**, Suraj Soman, Avishek Paul, Robert Groarke, Mary. T. Pryce, Sven Rau, Wesley R. Browne and Johannes. G. Vos, *Dalton Trans.*, **2011**, 40, 10545–10552.

2) "The effect of peripheral bipyridine ligands on the photocatalytic hydrogen production activity of Ru/Pd catalysts"
Gurmeet Singh Bindra, Martin Schulz, Avishek Paul, Suraj Soman, Robert Groarke, Jane Inglis, Mary T. Pryce, Wesley R. Browne, Sven Rau, Brian J. Maclean and Johannes G. Vos, *Dalton Trans.*, **2011**, 40, 10812–10814.

3) *"The role of bridging ligand in hydrogen generation by photocatalytic Ru/Pd assemblies"*
Gurmeet Singh Bindra, Martin Schulz, Avishek Paul, Robert Groarke, Suraj Soman, Jane Inglis, W. R. Browne, Michael Pfeffer, Sven Rau, Brian J. Maclean, Mary T. Pryce and Johannes G. Vos, *Dalton Trans.*, **2012**, *DOI: 10.1039/C2DT30948C*.

4) *"Effect of bridging ligand on photocatalytic hydrogen production by Ru-Pd complexes incorporated by 5-bisbipyridine as a bridging ligand"*
Gurmeet Singh Bindra, Suraj Soman, Jane Inglis, Mary T. Pryce, Brian J. Maclean and Johannes G. Vos, (manuscript under preparation).

5) "Novel iridium-Pt/Pd complexes for photocatalytic hydrogen generation from water using blue light (470nm) and UV light (350nm)"

Suraj Soman, **Gurmeet Singh Bindra**, Jane Inglis, Avishek Paul, Martin Schulz, Mary T. Pryce and Johannes G. Vos, (manuscript under preperation).

6) "High yield synthesis for the preparation of heteroleptic Ir(III) polypyridyl complexes"

Suraj Soman, Hamid M. Y. Ahmed, Laura Cleary, **Gurmeet Singh Bindra**, Wesley R. Browne, Mary T. Pryce, Johannes G. Vos, (manuscript under preparation)

Posters Presented

1) The Design of new photocatalytic systems for the generation of hydrogen from H_2O using solar energy.

Gurmeet Singh Bindra, Michael Pfeffer, Suraj Soman, Jane Inglis, Avishek Paul, Martin Schulz, Mary Pryce, Johannes G. Vos and Sven Rau presented at University of Groningen, March 2011, Netherlands.

2) The novel photocatalytic systems for the generation of hydrogen from water using solar energy.

Gurmeet Singh Bindra, Suraj Soman, Jane Inglis, Martin Schulz, Avishek Paul, Mary Pryce, Johannes G. Vos, and Brian J. MacLean will be presenting at ISACS4 July 2011 at MIT, Boston, USA.

3) Dinuclear photocatalysts for hydrogen production from water.

Gurmeet Singh Bindra, Avishek Paul, Suraj Soman, Robert Groarke, Martin Schulz, Mary Pryce, Sven Rau, and Johannes G. Vos will be presenting at ISACS4 July 2011 at MIT, Boston, USA.

4) Harvesting Solar Energy for the generation of H_2.

Suraj Soman, **Gurmeet Singh Bindra**, Avishek Paul, Danilo Dini, Mary T. Pryce and Johannes G. Vos, **2010** Annual EPA Conference held at Cork Park, Dublin, Ireland.

5) Novel Iridium-Pt/Pd Photocatalysts for Intramolecular & Intermolecular Catalytic H2 Generation from H_2O.

Suraj Soman, **Gurmeet Singh Bindra**, Avishek Paul, Martin Schulz, Mary T. Pryce and Johannes G. Vos, Photochemistry and Photochemical Techniques 16-18th May **2011**, University College Dublin, Trinity College Dublin, Ireland.

6) Temperature dependent and solvent dependent photophysics of novel Ir-Pt/Pd dinuclear complexes.

Suraj Soman, Robert Goarke, **Gurmeet Singh Bindra**, Jane Inglis, Mary T. Pryce and Johannes G. Vos, Photochemistry and Photochemical Techniques 16-18th May **2011**, UCD, Ireland (also presented in International Symposia on Advancing the Chemical Sciences: Challenges in Renewable Energy (ISACS4), MIT, Boston, USA, **2011** July).

7) Novel Iridium-Pt/Pd Photocatalysts for Intramolecular & Intermolecular Catalytic H_2 Generation from H2O using Blue Light (470nm) & UV Light (350nm).

Suraj Soman, **Gurmeet Singh Bindra**, Jane Inglis, Avishek Paul, Martin Schulz, Mary T. Pryce and Johannes G. Vos, International Symposia on Advancing the Chemical Sciences: Challenges in Renewable Energy (ISACS4), MIT, Boston, USA, **2011** July.

8) Effect of metal centers on spectroscopic and catalytic properties of metal complexes.

Robert Groarke, Suraj Soman, **Gurmeet Singh Bindra**, Martin Schulz, Mary T. Pryce and Jonannes G. Vos, 19th International Symposium on the Photophysics and Photochemistry of Coordination Compounds, Strasbourg, France, **2011** July.

Dalton
Transactions

View Online
Dynamic Article Links

Cite this: DOI: 10.1039/c1dt11241d

www.rsc.org/dalton

COMMUNICATION

The effect of peripheral bipyridine ligands on the photocatalytic hydrogen production activity of Ru/Pd catalysts†

Gurmeet Singh Bindra,[a] Martin Schulz,[a] Avishek Paul,[a] Suraj Soman,[a] Robert Groarke,[a] Jane Inglis,[a] Mary T. Pryce,[a] Wesley R. Browne,[b] Sven Rau,[c] Brian J. Maclean[d] and Johannes G. Vos*[a]

Received 29th June 2011, Accepted 23rd August 2011
DOI: 10.1039/c1dt11241d

Dalton
Transactions

View Online
Dynamic Article Links

Cite this: DOI: 10.1039/c1dt10960j

www.rsc.org/dalton

PAPER

Reinvestigating 2,5-di(pyridin-2-yl)pyrazine ruthenium complexes: selective deuteration and Raman spectroscopy as tools to probe ground and excited-state electronic structure in homo- and heterobimetallic complexes†

M. Schulz,[a] J. Hirschmann,[b] A. Draksharapu,[c] G. Singh Bindra,[a] S. Soman,[a] A. Paul,[a] R. Groarke,[a] M. T. Pryce,[a] S. Rau,[b] W. R. Browne*[c] and J. G. Vos*[a]

Received 22nd May 2011, Accepted 26th July 2011
DOI: 10.1039/c1dt10960j

This text redacted due to 3rd party copyright
This text redacted due to 3rd party copyright
This text redacted due to 3rd party copyright
This text redacted due to 3rd party copyright
This text redacted due to 3rd party copyright
This text redacted due to 3rd party copyright
This text redacted due to 3rd party copyright
This text redacted due to 3rd party copyright
This text redacted due to 3rd party copyright
This text redacted due to 3rd party copyright
This text redacted due to 3rd party copyright
This text redacted due to 3rd party copyright
This text redacted due to 3rd party copyright
This text redacted due to 3rd party copyright
This text redacted due to 3rd party copyright
This text redacted due to 3rd party copyright
This text redacted due to 3rd party copyright
This text redacted due to 3rd party copyright
This text redacted due to 3rd party copyright
This text redacted due to 3rd party copyright
This text redacted due to 3rd party copyright
This text redacted due to 3rd party copyright
This text redacted due to 3rd party copyright
This text redacted due to 3rd party copyright
This text redacted due to 3rd party copyright

This text redacted due to 3rd party copyright
This text redacted due to 3rd party copyright
This text redacted due to 3rd party copyright
This text redacted due to 3rd party copyright
This text redacted due to 3rd party copyright
This text redacted due to 3rd party copyright
This text redacted due to 3rd party copyright
This text redacted due to 3rd party copyright
This text redacted due to 3rd party copyright
This text redacted due to 3rd party copyright
This text redacted due to 3rd party copyright
This text redacted due to 3rd party copyright
This text redacted due to 3rd party copyright
This text redacted due to 3rd party copyright
This text redacted due to 3rd party copyright
This text redacted due to 3rd party copyright
This text redacted due to 3rd party copyright
This text redacted due to 3rd party copyright
This text redacted due to 3rd party copyright
This text redacted due to 3rd party copyright
This text redacted due to 3rd party copyright
This text redacted due to 3rd party copyright
This text redacted due to 3rd party copyright
This text redacted due to 3rd party copyright
This text redacted due to 3rd party copyright

This text redacted due to 3rd party copyright
This text redacted due to 3rd party copyright
This text redacted due to 3rd party copyright
This text redacted due to 3rd party copyright
This text redacted due to 3rd party copyright
This text redacted due to 3rd party copyright
This text redacted due to 3rd party copyright
This text redacted due to 3rd party copyright
This text redacted due to 3rd party copyright
This text redacted due to 3rd party copyright
This text redacted due to 3rd party copyright
This text redacted due to 3rd party copyright
This text redacted due to 3rd party copyright
This text redacted due to 3rd party copyright
This text redacted due to 3rd party copyright
This text redacted due to 3rd party copyright
This text redacted due to 3rd party copyright
This text redacted due to 3rd party copyright
This text redacted due to 3rd party copyright
This text redacted due to 3rd party copyright
This text redacted due to 3rd party copyright
This text redacted due to 3rd party copyright
This text redacted due to 3rd party copyright
This text redacted due to 3rd party copyright
This text redacted due to 3rd party copyright

This text redacted due to 3rd party copyright
This text redacted due to 3rd party copyright
This text redacted due to 3rd party copyright
This text redacted due to 3rd party copyright
This text redacted due to 3rd party copyright
This text redacted due to 3rd party copyright
This text redacted due to 3rd party copyright
This text redacted due to 3rd party copyright
This text redacted due to 3rd party copyright
This text redacted due to 3rd party copyright
This text redacted due to 3rd party copyright
This text redacted due to 3rd party copyright
This text redacted due to 3rd party copyright
This text redacted due to 3rd party copyright
This text redacted due to 3rd party copyright
This text redacted due to 3rd party copyright
This text redacted due to 3rd party copyright
This text redacted due to 3rd party copyright
This text redacted due to 3rd party copyright
This text redacted due to 3rd party copyright
This text redacted due to 3rd party copyright
This text redacted due to 3rd party copyright
This text redacted due to 3rd party copyright
This text redacted due to 3rd party copyright
This text redacted due to 3rd party copyright

This text redacted due to 3rd party copyright
This text redacted due to 3rd party copyright
This text redacted due to 3rd party copyright
This text redacted due to 3rd party copyright
This text redacted due to 3rd party copyright
This text redacted due to 3rd party copyright
This text redacted due to 3rd party copyright
This text redacted due to 3rd party copyright
This text redacted due to 3rd party copyright
This text redacted due to 3rd party copyright
This text redacted due to 3rd party copyright
This text redacted due to 3rd party copyright
This text redacted due to 3rd party copyright
This text redacted due to 3rd party copyright
This text redacted due to 3rd party copyright
This text redacted due to 3rd party copyright
This text redacted due to 3rd party copyright
This text redacted due to 3rd party copyright
This text redacted due to 3rd party copyright
This text redacted due to 3rd party copyright
This text redacted due to 3rd party copyright
This text redacted due to 3rd party copyright
This text redacted due to 3rd party copyright
This text redacted due to 3rd party copyright

Cite this: DOI: 10.1039/c0xx00000x

www.rsc.org/xxxxxx

ARTICLE TYPE

The role of bridging ligand in hydrogen generation by photocatalytic Ru/Pd assemblies

Gurmeet. S. Bindra,[a] Martin Schulz,[a,b] Avishek Paul,[a] Robert Groarke,[a] Suraj Soman,[a] Jane L. Inglis,[a] Wesley R. Browne,[c] Michael Pfeffer,[d] Sven Rau,[d] Brian J. MacLean,[e] Mary.T. Pryce[a] and Johannes. G. Vos[a,*]

Received (in XXX, XXX) Xth XXXXXXXXX 20XX, Accepted Xth XXXXXXXXX 20XX
DOI: 10.1039/b000000x

This text redacted due to 3rd party copyright
This text redacted due to 3rd party copyright
This text redacted due to 3rd party copyright
This text redacted due to 3rd party copyright
This text redacted due to 3rd party copyright
This text redacted due to 3rd party copyright
This text redacted due to 3rd party copyright
This text redacted due to 3rd party copyright
This text redacted due to 3rd party copyright
This text redacted due to 3rd party copyright
This text redacted due to 3rd party copyright
This text redacted due to 3rd party copyright
This text redacted due to 3rd party copyright
This text redacted due to 3rd party copyright
This text redacted due to 3rd party copyright
This text redacted due to 3rd party copyright
This text redacted due to 3rd party copyright
This text redacted due to 3rd party copyright
This text redacted due to 3rd party copyright
This text redacted due to 3rd party copyright
This text redacted due to 3rd party copyright
This text redacted due to 3rd party copyright
This text redacted due to 3rd party copyright
This text redacted due to 3rd party copyright
This text redacted due to 3rd party copyright

This text redacted due to 3rd party copyright
This text redacted due to 3rd party copyright
This text redacted due to 3rd party copyright
This text redacted due to 3rd party copyright
This text redacted due to 3rd party copyright
This text redacted due to 3rd party copyright
This text redacted due to 3rd party copyright
This text redacted due to 3rd party copyright
This text redacted due to 3rd party copyright
This text redacted due to 3rd party copyright
This text redacted due to 3rd party copyright
This text redacted due to 3rd party copyright
This text redacted due to 3rd party copyright
This text redacted due to 3rd party copyright
This text redacted due to 3rd party copyright
This text redacted due to 3rd party copyright
This text redacted due to 3rd party copyright
This text redacted due to 3rd party copyright
This text redacted due to 3rd party copyright
This text redacted due to 3rd party copyright
This text redacted due to 3rd party copyright
This text redacted due to 3rd party copyright
This text redacted due to 3rd party copyright
This text redacted due to 3rd party copyright
This text redacted due to 3rd party copyright

This text redacted due to 3rd party copyright
This text redacted due to 3rd party copyright
This text redacted due to 3rd party copyright
This text redacted due to 3rd party copyright
This text redacted due to 3rd party copyright
This text redacted due to 3rd party copyright
This text redacted due to 3rd party copyright
This text redacted due to 3rd party copyright
This text redacted due to 3rd party copyright
This text redacted due to 3rd party copyright
This text redacted due to 3rd party copyright
This text redacted due to 3rd party copyright
This text redacted due to 3rd party copyright
This text redacted due to 3rd party copyright
This text redacted due to 3rd party copyright
This text redacted due to 3rd party copyright
This text redacted due to 3rd party copyright
This text redacted due to 3rd party copyright
This text redacted due to 3rd party copyright
This text redacted due to 3rd party copyright
This text redacted due to 3rd party copyright
This text redacted due to 3rd party copyright
This text redacted due to 3rd party copyright
This text redacted due to 3rd party copyright
This text redacted due to 3rd party copyright

This text redacted due to 3rd party copyright
This text redacted due to 3rd party copyright
This text redacted due to 3rd party copyright
This text redacted due to 3rd party copyright
This text redacted due to 3rd party copyright
This text redacted due to 3rd party copyright
This text redacted due to 3rd party copyright
This text redacted due to 3rd party copyright
This text redacted due to 3rd party copyright
This text redacted due to 3rd party copyright
This text redacted due to 3rd party copyright
This text redacted due to 3rd party copyright
This text redacted due to 3rd party copyright
This text redacted due to 3rd party copyright
This text redacted due to 3rd party copyright
This text redacted due to 3rd party copyright
This text redacted due to 3rd party copyright
This text redacted due to 3rd party copyright
This text redacted due to 3rd party copyright
This text redacted due to 3rd party copyright
This text redacted due to 3rd party copyright
This text redacted due to 3rd party copyright
This text redacted due to 3rd party copyright
This text redacted due to 3rd party copyright
This text redacted due to 3rd party copyright

This text redacted due to 3rd party copyright
This text redacted due to 3rd party copyright
This text redacted due to 3rd party copyright
This text redacted due to 3rd party copyright
This text redacted due to 3rd party copyright
This text redacted due to 3rd party copyright
This text redacted due to 3rd party copyright
This text redacted due to 3rd party copyright
This text redacted due to 3rd party copyright
This text redacted due to 3rd party copyright
This text redacted due to 3rd party copyright
This text redacted due to 3rd party copyright
This text redacted due to 3rd party copyright
This text redacted due to 3rd party copyright
This text redacted due to 3rd party copyright
This text redacted due to 3rd party copyright
This text redacted due to 3rd party copyright
This text redacted due to 3rd party copyright
This text redacted due to 3rd party copyright
This text redacted due to 3rd party copyright
This text redacted due to 3rd party copyright
This text redacted due to 3rd party copyright
This text redacted due to 3rd party copyright
This text redacted due to 3rd party copyright
This text redacted due to 3rd party copyright